Edited by
Andreas Athienitis and William O'Brien

Modeling, Design, and Optimization of Net-Zero Energy Buildings

CONTENTS

List of Tables

List of Illustrations

Related Titles

Hadorn, J. (ed.)

Solar and Heat Pump Systems for Residential Buildings

2015

Print ISBN: 978-3-433-03040-0

Donn, M., Garde, F., Aelenei, D., Aelenei, L., Røstvik, H.N., Tardiff, M., Scognamiglio, A., and Waldren, D.

Solution Sets for Net Zero Energy Buildings

Feedback from 30 Buildings worldwide

2015

Print ISBN: 978-3-433-03072-1

Hens, H.S.

Performance Based Building Design 1

From Below Grade Construction to Cavity Walls

2012

Print ISBN: 978-3-433-03022-6

Hens, H.S.

Performance Based Building Design 2

From Timber-framed Construction to Partition Walls.

2013

Print ISBN: 978-3-433-03023-3

Hootman, T.

Net Zero Energy Design

A Guide for Commercial Architecture

2013

Modeling, Design, and Optimization of Net-Zero Energy Buildings

Edited by
Andreas Athienitis
William O'Brien

Ernst & Sohn
A Wiley Brand

About the Editors

Dr. Andreas K. Athienitis is a Professor of Building Engineering and holds a Research Chair in Integration of Solar Energy Systems into Buildings and a NSERC/Hydro Quebec Industrial Chair at Concordia University, Montreal. He is the Scientific Director of the Canadian NSERC Smart Net-zero Energy Buildings Strategic Research Network (2011–2016) and the founding Director of the NSERC Solar Buildings Research Network (2005–2010). He was a sub-task co-leader for IEA SHC Task 40/EBC Annex 52 ("Towards Net-Zero Energy Solar Buildings"). He is author of more than 200 refereed papers and several books and book chapters in solar buildings and building energy systems. Prof. Athienitis is a Fellow of the Canadian Academy of Engineering and a contributing author of the Intergovernmental Panel for Climate Change (IPCC).

Dr. William O'Brien is an Assistant Professor in the Architectural Conservation and Sustainability Engineering program at Carleton University, Ottawa. He is the principal investigator of the Human

Building Interaction Laboratory, which consists of a multidisciplinary team of researchers that are designing buildings and building controls that incorporate human factors. He has published over 40 peer-reviewed papers. He was a sub-task co-leader for IEA SHC Task 40/EBC Annex 52 ("Towards Net-Zero Energy Solar Buildings") and now, IEA EBC Annex 66 ("Definition and Simulation of Occupant Behavior in Buildings").

Production Editor

Samson Yip is a Senior Architect at Saia Barbarese Topouzanov Architects in Montreal specializing in institutional architecture. He is completing a Master of Applied Science (Building Engineering) degree at Concordia University, Montreal, within the Canadian NSERC Smart Net-zero Energy Buildings Strategic Research Network. He was a participant in the IEA SHC Task 40/EBC Annex 52 ("Towards Net-Zero Energy Solar Buildings"). Prior to that, he was an Adjunct Professor at the School of Architecture, McGill University, Montreal.

List of Contributors

Andreas K. Athienitis

Concordia University

1455 de Maisonneuve Blvd. West

Montreal, QC H3G 1M8

Canada

Shady Attia

Université de Liège

Sustainable Buildings Design Lab

1 Chemin des Chevreuils

Sart Tilman B52/3

4000 Liège

Belgium

Josef Ayoub

CanmetENERGY

Natural Resources Canada

Government of Canada

1615 Lionel-Boulet Blvd.

Varennes, QC J3X 1S6

Canada

Paul Bourdoukan

Sorane France

25 B Quai Jean Baptiste Simon

69270 Fontaines sur Saone

France

Scott Bucking

McMaster University

1280 Main Street West

Hamilton, ON L8S 4L8

Canada

José A. Candanedo

CanmetENERGY

Natural Resources Canada

Government of Canada

1615 Lionel-Boulet Blvd.

Varennes, QC J3X 1S6

Canada

Salvatore Carlucci

NTNU Norwegian University of Science and Technology

Høgskoleringen 7A

7491 Trondheim

Norway

Maurizio Cellura

University of Palermo

Viale delle Scienze, Building 9

90128 Palermo

Italy

Yuxiang Chen

Concordia University

1455 de Maisonneuve Blvd. West

Montreal, QC H3G 1M8

Canada

Véronique Delisle

CanmetENERGY

Natural Resources Canada

Government of Canada

1615 Lionel-Boulet Blvd.

Varennes, QC J3X 1S6

Canada

Francois Garde

University of La Réunion

PIMENT Laboratory

117, rue Général Ailleret

97430 Le Tampon

Reunion Island

France

Francesco Guarino

University of Palermo

Viale delle Scienze, Building 9

90128 Palermo

Italy

Ala Hasan

VTT Technical Research Centre of Finland

Tekniikantie 4A

02044 Espoo

Finland

Mohamed Hamdy Hassan

Eindhoven University of Technology

Department of the Built Environment, Building Physics and Services

P.O. Box 513

5600 MB Eindhoven

The Netherlands

and

Aalto University School of Engineering

Department of Energy Technology

P.O. Box 14400

FI-00076 Aalto

Finland

Konstantinos Kapsis

Concordia University

1455 de Maisonneuve Blvd. West

Montreal, QC H3G 1M8

Canada

Aurélie Lenoir

University of Reunion Island

PIMENT Laboratory

117, rue du Général Ailleret

97430 Le Tampon

Reunion Island

France

Davide Nardi Cesarini

Loccioni Group

Via Fiume 16

60030 Angeli di Rosora

Italy

William O'Brien

Carleton University

1125 Colonel By Drive

3432 Mackenzie Building

Ottawa, ON K1S 5B6

Canada

Lorenzo Pagliano

Politecnico di Milano

end-use Efficiency Research Group (eERG)

via Lambruschini, 4

20156 Milano

Italy

Jaume Salom

Catalonia Institute for Energy Research, IREC

Jardins de les Dones de Negre, 1

8930 Sant Adrià de Besòs

Spain

Joakim Widén

Uppsala University

Department of Engineering Sciences

Lagerhyddsvagen 1

75121 Uppsala

Sweden

Samson Yip

Concordia University

Dept. of Building, Civil and Environmental Engineering

1455 de Maisonneuve West

EV 6.159

Montréal, QC H3G 1M8

Canada

Preface

Andreas Athienitis and WilliamO' Brien

Just over five years ago, approximately 60 international experts of the International Energy Agency – Solar Heating and Cooling Task 40/Energy in Buildings and Communities (EBC) Annex 52: Towards Net-zero Energy Solar Buildings ("T40A52") met in Montreal at Concordia University for the first official experts meeting. Many of the experts were in for a surprise as they discovered the diversity of international perspectives on net-zero energy buildings (Net ZEBs) – including definitions, official building standards, business and legal aspects, and design strategies. Over the following five years, the experts traveled to an additional nine meeting destinations and became immersed in the local building design cultures, providing us with a valuable international perspective on Net ZEBs and giving us the pleasure of meeting in several Net ZEBs (several of which were meeting venues and are discussed in depth in this book).

The objective of this book is to present a wide perspective on Net ZEB modeling, design, and related issues, while also providing substantial depth for designers and graduate students. The book was written by a total of 22 authors from seven countries of diverse climates with experts from both industry and academia/research. The book begins with fundamentals of modeling, strategies and technologies required to reach net-zero energy including many methods to quantify performance. As emphasized by T40A52, comfort is a fundamental aspect of Net ZEB and not an afterthought; therefore, a full chapter was devoted to thermal, visual, and acoustic comfort and indoor air quality. The following two chapters are devoted to design, modeling, simulation, and optimization of Net ZEBs with several examples. It was realized early in T40/A52 that research on Net ZEBs must encapsulate interactions with electrical grids since net-zero energy definitions are primarily focused on energy balances; thus, a whole chapter is devoted to this issue. In the second to last chapter, four detailed Net ZEB case studies are described in detail and linked to earlier fundamental chapters, including energy performance, comfort, design intent versus real

operation, and lessons learned. Finally, redesign of archetypes based on the case studies are presented.

Andreas Athienitis, Ph. D., P. Eng., FCAE
NSERC/Hydro Quebec Industrial
Chair & Concordia Research Chair
Scientific Director, NSERC Smart Net-zero Energy
Buildings Strategic Research Network &
Director, Concordia Centre for Zero Energy Building Studies
Concordia University, Montreal, Canada

William O'Brien, PhD
Civil and Environmental Engineering
Carleton University, Ottawa, Canada

Foreword

Josef Ayoub

This book was produced in the context of the collaboration between approximately 75 national experts from 19 nations in Europe, North America, Oceania, and Southeast Asia of the International Energy Agency (IEA), in the framework of the programs on Solar Heating and Cooling (SHC Task 40) and Energy in Buildings and Communities (EBC Annex 52), under the title "Towards Net-Zero Energy Solar Buildings." T40A52 sought to study current net-zero, near-net-zero and very low energy buildings and to develop a common understanding of a harmonized international definitions framework, tools, innovative solutions, and industry guidelines to support the conversion of the Net ZEB concept from an idea into practical reality in the marketplace.

This Task/Annex pursued optimal integrated design solutions that provided a good indoor environment for both heating and cooling situations. The process recognized the importance of optimizing a design to meet the functional requirement, reducing loads, and designing energy systems that pave the way for seamless incorporation of renewable energy innovations, as they become cost effective. To achieve these results, the National Experts met twice annually at a hosting member country to coordinate the R&D activities and advance the work plan comprised of the following four major activities:

1. Subtask A dealt with establishing an internationally agreed understanding on Net ZEBs based on a common methodology. This was done by reviewing and analyzing existing Net ZEB definitions and data with respect to the demand and the supply side; studying grid interaction (power/heating/cooling) and time-dependent energy mismatch analysis; developing a harmonized international definition framework for the Net ZEB concepts considering large-scale implications, exergy, and credits for grid interaction (power/heating/cooling); and, developing a monitoring, verification and compliance guide for checking the

annual balance in practice (energy, emissions, and costs) harmonized with the definition;

2. Subtask B aimed to identify and refine design approaches and tools to support industry adoption. This was done by conducting work along four major R&D streams: (i) in documenting and analyzing processes and tools currently being used to design Net ZEBs and under development by participating countries; (ii) assessing gaps, needs, and problems to inform simulation engine and detailed design tool developers of priorities for Net ZEBs; (iii) qualitative and quantitative benchmarking of selected tools; and (iv) selecting four case study buildings to conduct a detailed analysis of simulated/designed vs. actual performance, and proposing the redesign/optimization of these buildings;

3. Subtask C focused on developing and testing innovative, whole building net-zero solution sets for cold, moderate, and hot climates with exemplary architecture and technologies that would be the basis for demonstration projects and international collaboration. This was achieved by documenting and analyzing current Net ZEBs designs and technologies, benchmarking with near Net ZEBs and other very low energy buildings (new and existing), for cold, moderate, and hot climates considering sustainability, economy, and future prospects using a projects database, literature review, and practitioner input (workshops); developing and assessing case studies and demonstration projects in close cooperation with practitioners; investigating advanced integrated design concepts and technologies in support of the case studies, demonstration projects, and solution sets; and developing Net ZEB solution sets and guidelines with respect to building types and climate, and to document design options in terms of market application;

4. Subtask D was crosscutting work that focused on dissemination to support knowledge transfer and market adoption of Net ZEBs on a national and international level. This was accomplished by establishing a Net ZEB webpage within the IEA SHC/EBC Programmes' framework and a database that can be expanded and updated with the latest projects and experiences; transferring the outputs (reports, sourcebooks, guidelines, other) to national

policy groups, industry associations, utilities, academia, and funding programs; participating in national and international workshop, seminars, and industry exhibitions highlighting the results and activities of the Task/Annex contributing high-quality technical articles and features in journals to stimulate market adoption; and, establishing an education network of highly qualified people that will continue the work in the field for their future endeavors.

I am pleased to present the research results of Subtask B compiled in this volume of work entitled "*Modeling, Design, and Optimization of Net-Zero Energy Buildings*," as a major accomplishment in this field of research. Building energy design is currently going through a period of major changes driven largely by three key factors and related technological developments: (i) the increasingly widespread adoption in most OECD member countries and by influential engineering societies, such as ASHRAE, of net-zero energy as a long-term goal for new buildings; (ii) the need to reduce the peak electricity demand for buildings through optimal operation; and (iii) the need to efficiently integrate advanced energy technologies into buildings, such as photovoltaic/thermal systems, windows with semitransparent photovoltaic glazing, controlled shading/daylighting devices, and integrated thermal storage. It encapsulates the many and varied concepts of designing and optimizing net-zero energy buildings by government research organizations, international and regional research centers, academia, and industry. I am confident this book will find many interested readers.

Josef Ayoub
Operating Agent, IEA SHC Task 40/EBC Annex 52
Senior Planning Advisor, Energy Science & Technology
CanmetENERGY | Natural Resources Canada Government of Canada
task40.iea-shc.org/

Acknowledgments

Funding

1
Introduction

Andreas Athienitis, William O'Brien, and Josef Ayoub

1.1 Evolution to Net-Zero Energy Buildings

Buildings have evolved over time from largely passive systems into structures with increasingly high levels of environmental control, partly through the addition of man-made insulation materials, such as fiberglass and polystyrene. The adoption of electric lighting in early twentieth century buildings, contributed to a reduction in window areas and reliance on artificial lighting, particularly in the period from 1950 to 1970. But in the 1980s, the development and acceptance of sealed double-glazed windows with an insulating airspace, or insulating windows with special coatings to reduce heat transfer and optimize transmission of solar radiation (Athienitis and Santamouris, 2002), led to the adoption of larger fenestration areas (up to 60% of the façade area) in both the residential and commercial buildings. These large fenestration areas – as much as 90% of the façade area – lead to high heating and cooling energy consumption. Thus, fenestration and daylighting significantly influence the design of commercial buildings. The drivers of the design of residential buildings are shifting from space conditioning to appliances, lighting, and integrated energy systems, as building envelopes and HVAC become more efficient and passive techniques are employed.

Since the early 1990s the potential of solar radiation incident on building surfaces to satisfy all their energy needs has contributed to the idea of net-zero energy buildings gaining widespread acceptance as a technically feasible long-term goal (for most regions). *A net-zero energy building (Net ZEB) is normally defined as one that, in an average year, produces as much energy (electrical plus thermal) from renewable energy sources as it consumes*. When the energy production is on-site the Net ZEB definition is most strict.

The visible part of the solar spectrum (nearly half of total solar radiation) is useful as daylight. Almost all of solar radiation can be converted to useful heat for space heating, as well as other useful purposes, such as heating water and drying clothes, or even solar cooling using passive and active solar systems (International Solar Energy Society (ISES), 2001). Another solar technology – photovoltaic (PV) – that converts solar radiation to electricity has recently experienced significant advances and dramatic reductions in cost (almost 90% cost reduction per watt of generating capacity in the last 10 years). Both technologies can be integrated and optimized for combined heat and power generation to advance buildings toward net-zero energy consumption.

Most inhabited areas receive significant amounts of sunshine that enable the design of technically feasible Net ZEBs with current solar and energy efficiency technologies. For example, in Canada between latitudes 40–53 °N where most of Canada's population lives, a suitably oriented façade or roof on a typical building receives up to ~6 kWh/m² per day, and the incident solar energy often exceeds total building energy consumption. Photovoltaic panels integrated on the roof and façade can typically convert 6–20% of the sun's energy into electricity, and 50–70% of the remainder can be extracted as heat from the PV panels, while 10 to 30% can be utilized for daylighting in semitransparent systems. Combined solar energy utilization efficiencies on the order of 80% can be achieved if proper integration strategies are implemented and nearly the full spectrum of solar radiation can be utilized as daylight, useful heat, or electricity.

The energy generation function in Net ZEBs using solar energy – as *daylight, useful heat, and electricity* – requires a transformation of the way buildings are designed and operated so as to be cost effective and affordable. The key challenges for smart Net ZEBs to overcome are summarized in Table 1.1 for each of the four major building subsystems where the current situation is contrasted with the expected characteristics of Net ZEBs. In addition, the integration of design with operation is considered.

Table 1.1 Challenges for smart Net ZEBs

Building systems, design and operation	Current buildings	Smart Net ZEBs
Building fabric/envelope	Passive, not designed as an energy system	Optimized for passive design and integration of active solar systems
Heating, ventilation and air conditioning (HVAC)	Large oversized systems	Small HVAC systems optimally controlled; integrated with solar systems, combined heat and power; communities: seasonal storage and district energy
Solar systems/renewables, generation	No systematic integration – an afterthought	Fully integrated: daylighting, solar thermal, photovoltaics, hybrid solar, geothermal systems, biofuels, linked with smart microgrids
Building automation systems	Building automation systems not used effectively	Predictive building control to optimize comfort and energy performance; online demand prediction/peak demand reduction
Design and operation	The design and operation of buildings are typically not considered together	Design and operation of buildings fully integrated and optimized together subject to satisfying comfort; integrated design of the above four building subsystems

1.1.1 Net ZEB Concepts

The convergence of the need for innovation and the requirement for drastic reductions in energy use and greenhouse gas (GHG) emissions in the building sector provides a unique opportunity to

transform the way buildings and their energy systems are conceived. Demand abatement through passive design, energy efficiency, and conservation measures needs to be simultaneously considered with integration of solar systems and on-site generation of useful heat and electricity using a whole building approach.

Building energy design is currently undergoing a period of major changes driven largely by three key factors and related technological developments:

1. The adoption in many developed countries, and by influential professional societies, such as ASHRAE, of net-zero energy [3] as a long-term goal for new buildings;

2. The need to reduce the peak electricity demand from buildings through optimal operation, thus reducing the need to build new central power plants that often use fossil fuels; and,

3. The decreasing cost of energy-generating technologies, such as photovoltaics, which enables building-integrated energy systems to be more affordable and competitive. This is coupled with increasing costs of energy from traditional energy sources (e.g., fossil fuels).

A key requirement of high performance building design is *the need for rigorous design and operation of a building as an integrated energy system that must have a good indoor environment suited to its functions.* In addition to the extensive array of HVAC, lighting, and automation technologies developed over the last 100 years, many new building envelope technologies have been established, such as vacuum insulation panels and advanced fenestration systems (e.g., electrochromic coatings for so-called smart windows), as well as solar thermal technologies for heating and cooling, and solar electric or hybrid systems and combined heat and power (CHP) technologies. A high-performance building may be designed with optimal combinations of traditional and advanced technologies depending on its function and on climate.

Solar gain and daylight control through smart window systems, in which the transmission of solar radiation can be actively controlled, remain a challenge in building design and operation because of the

simultaneous effects on instantaneous and delayed heating/cooling loads, and on thermal and visual comfort. Solar gains may be controlled through a combination of passive and active measures – with the passive measures employed during design and active measures, such as positioning of motorized venetian blinds during operation. Since solar gains have delayed effects because of building thermal mass, there is significant benefit in predictive control and optimal operation of passive and active storage that utilizes real-time weather prediction (Athienitis, Stylianou, and Shou, 1990).

New building technologies, such as phase change materials (PCM), active façades with advanced daylighting devices, and building-integrated solar systems, open up new challenges and possibilities to improve comfort and reduce energy use and peak loads, and they need to be taken into account in developing optimal control strategies. The energy requirements and control needs of commercial and residential buildings are usually quite different. For example, in commercial buildings, cooling and lighting play major roles, while in houses, especially in cold climate regions, space heating and domestic hot water heating dominate energy consumption.

Plug loads (e.g., due to appliances and office equipment) represent a large portion of building energy consumption and their share is increasing, as HVAC and lighting systems become more energy efficient. Demand response strategies, such as scheduling of appliances, are becoming more popular as a way to significantly reduce the impact of plug loads on peak electric demand.

1.1.2 Design of Smart Net ZEBs and Modeling Issues

The design of smart net-zero energy buildings requires the following three key approaches:

1. An integrated approach to energy efficiency and passive design;
2. An integrated approach to building design and operation. Optimized net-zero energy buildings need to be designed based on anticipated operation so as to have a largely predictable and manageable impact on the grid. Smart buildings optimally linked with smart grids will enable a reduction in the need to build new power plants; and,

3. The concept of solar optimization requires optimal design of building form and orientation so as to provide the maximum capture of solar energy from near-equatorial facing façades and roofs for conversion to solar electricity, useful heat, and daylight.

To design a Net ZEB efficiently in an optimal manner, a rigorous quantitative approach is required in all stages of design starting from the conceptual phase. One of the unique challenges is how to handle the interaction and integration between the energy generating systems (such as building-integrated photovoltaic/thermal systems), the heating, cooling, and ventilating systems, and the building envelope in the different design stages. Model resolution and complexity is a key issue addressed in this book (Chapter 2) and gaps in simulation are also discussed, particularly in relation to four in-depth case studies (Chapter 7).

1.2 Scope of this Book

Chapter 2 discusses fundamental concepts, such as building thermal dynamics and different modeling approaches, design strategies (passive solar and energy efficiency measures), and technologies (renewable energy systems, heating and cooling technologies, and thermal storage) required to achieve net-zero energy in buildings. Because net-zero energy is an ambitious goal, the combination of systems and their integration is fundamentally important from the start of the design process to detailed design and building operation. This chapter discusses not only the individual technologies, but also effective integration strategies. It provides links to the application case studies that further exemplify the modeling techniques and technologies presented in the chapter.

Chapter 3 focuses on comfort considerations and models for different climates. Thermal comfort models are discussed, together with visual and acoustic comfort, as well as indoor air quality. Because of the highly efficient building envelopes in Net ZEBs, greater reliance on passive approaches, and a general trend toward higher glazing areas, comfort is particularly important for Net ZEBs. For example, in Net ZEBs with hybrid/natural ventilation systems there is a strong link between visual, thermal, and acoustic comfort.

Chapter 4 discusses different design processes and tools to support the design of Net ZEBs. Unlike other types of high-performance buildings, the net-zero energy target necessarily requires a high degree of accuracy in performance predictions, an integrated design process, and a combination of energy efficiency measures and renewable energy technologies. This chapter demonstrates the value of building performance simulation in design from conception to detailed design by providing accurate predictions for energy performance.

Chapter 5 presents different approaches, techniques, and considerations for Net ZEB optimization, including cost minimization and comfort. Examples from different countries, such as Finland and Italy, are presented.

Chapter 6 introduces matching of load with generation, grid interaction, and advanced control issues for Net ZEBs. Since the load profile of such buildings often peaks at different times from the generation peak, it is important to study this mismatch and how it can be addressed in order to optimize the interaction with electricity grids by shifting and reducing peak demand.

Chapter 7 provides detailed information about four diverse Net ZEBs (Figure 1.1), which are summarized in Table 1.2. These high-quality case studies were selected because they have at least one year of high-resolution measured data and the authors were intimately involved in all of them from conception to operation. The aim of this chapter is to draw lessons from the case studies, the design and simulation tools used and their gaps, and finally the technologies used and their integration. The last section of each of the case studies examines the redesign of archetype buildings based on additional information, new technologies, and lower material and component costs since they were built.

Fig. 1.1 The four Net ZEB case studies. Clockwise from top left: ÉcoTerra (Image courtesy of Agnieszka Koziol), Leaf House (Image courtesy of Loccioni Group), ENERPOS (Image courtesy of Jérôme Balleydier), and NREL RSF (Image courtesy of Dennis Schroeder, NREL)

Table 1.2 Summary of four in-depth case studies presented in Chapter 7

Case Study	Description	Location and Climate
ÉcoTerra House *Detailed monitored data available – partly designed by some of the authors; related scientific publications also by authors (Athienitis, O'Brien, Chen)*	Canada's first near net-zero energy demonstration house. Completed in 2007, commissioned for 2 years, now occupied with feedback from occupants; 200 m² rural detached house with building-integrated thermal/photovoltaic roof, ventilated concrete slab, passive solar optimized, and a ground source heat pump	Eastman, Quebec, Canada Cold, relatively sunny climate
Leaf House *Detailed monitored data available – engineers who participated in design provided input; related scientific publications also by authors (Cellura, Guarino, Cesarini)*	6-unit low-rise multiunit residential building with passive solar features, both solar thermal and photovoltaic collectors, and a heat pump	Ancona, Italy Mediterranean climate – hot summers, mild-cold winters

Case Study	Description	Location and Climate
National Renewable Energy Laboratory – Research Support Facility (RSF) *Detailed monitored data available – task participants work in the building; task meeting was held in the building; related scientific publications also by authors (Chen, Yip, Athienitis)*	A large institutional building consisting of offices, laboratories, and a large server room. Energy features include good natural ventilation and advanced daylighting design using fixed louvers and high, reflective ceilings; radiant cooling, a large photovoltaic array; and a transpired solar collector to preheat fresh air	Golden, Colorado, USA Cold sunny – mountain climate
ENERPOS *Detailed monitored data available – task participants work in the building; related scientific publications also by authors (Lenoir, Kapsis, Garde)*	A medium-sized energy-positive academic building with natural ventilation, daylighting, solar shading, and a large photovoltaic array	St-Pierre, Reunion Island, France Tropical climate

Chapter 8 concludes with a discussion on challenges and future directions in the design of Net ZEBs.

This book was written primarily by Subtask B of the International Energy Agency Solar Heating and Cooling Program Task 40/Energy in Buildings and Communities Annex 52. Subtask B, titled *Net ZEB Design Processes and Tools*, was focused on studying modeling methodologies and design processes for the state-of-the-art Net

ZEBs. Subtask B participants used carefully selected high-quality Net ZEB case studies to form a greater understanding of practical and technical challenges, including modeling considerations. Members of Subtask B were a diverse group of researchers and designers. Readers are encouraged to explore the products of five years of in-depth studies by the 50 IEA Task/Annex researchers world-wide on the Web site task40.iea-shc.org.

References

Athienitis, A.K. and Santamouris, M. (2002) *Thermal Analysis and Design of Passive Solar Buildings*, James & James, London.

Athienitis, A.K., Stylianou, M., and Shou, J. (1990) A methodology for building thermal dynamics studies and control applications. *ASHRAE Transactions*, **96**, 839–848.

International Solar Energy Society (ISES) (2001) *Solar Energy: State of the Art*, James & James, London, UK.

Marszal, A.J., Heiselberg, P., Bourrelle, J.S., Musall, E., Voss, K., Sartori, I., and Napolitano, A. (2011) Zero energy building – A review of definitions and calculation methodologies. *Energy and Buildings*, **43**, 971–979.

Voss, K. and Musall, E. (2011) *Net Zero Energy Buildings*, Detail Green Books – IEA SHC Task 40/EBC Annex 52, sponsored publication, Munich, Germany.

2
Modeling and Design of Net ZEBs as Integrated Energy Systems

Andreas Athienitis, Maurizio Cellura, Yuxiang Chen, Véronique Delisle, Paul Bourdoukan, and Konstantinos Kapsis

2.1 Introduction

Net-zero energy buildings (Net ZEBs) are emerging as a *quantifiable design concept* and a promising solution to minimizing the environmental impact of buildings. This is the main concept that we will focus on in this chapter with emphasis on dynamic modeling and examples of technological approaches to achieve net-zero energy. Net ZEBs, which minimize energy consumption and optimally use incident solar radiation, both passively and actively, are usually defined as those that export as much energy as they import, over the course of a year (also known as net-zero site energy (Torcellini *et al.*, 2006)). A review of international work on Net ZEBs was undertaken by the International Energy Agency Solar Heating and Cooling Program (IEA SHC) Task 40/Energy in Buildings and Communities (EBC) Annex 52 and its Subtask A studied several alternative definitions and calculation methodologies. Modeling, design, and optimization of such buildings have been studied by Subtask B (STB), which identified key issues that need to be addressed as follows:

– What is the appropriate model resolution for each stage of the design of Net ZEBs?

– What is the role of simple spreadsheet-based tools (e.g., RETScreen (NRCan, 2010) and PHPP (iPHA, 2013)) versus more advanced detailed simulation (such as ESP-r (ESRU, 2013) and EnergyPlus (EERE, 2013)) and optimization tools?

– What other tool capabilities are needed to model new technologies, such as building fabric-integrated phase-change

materials (PCMs)?

A three-dimensional conceptual problem space has been developed (Figure 2.1) to represent the framework being used by STB to define the role of modeling in Net ZEB design. Different simulation tools include different technologies and simulate building fabric energy transfer with different levels of detail. They also utilize different techniques to model the transient response of buildings and their systems to changes in internal and external thermal loads.
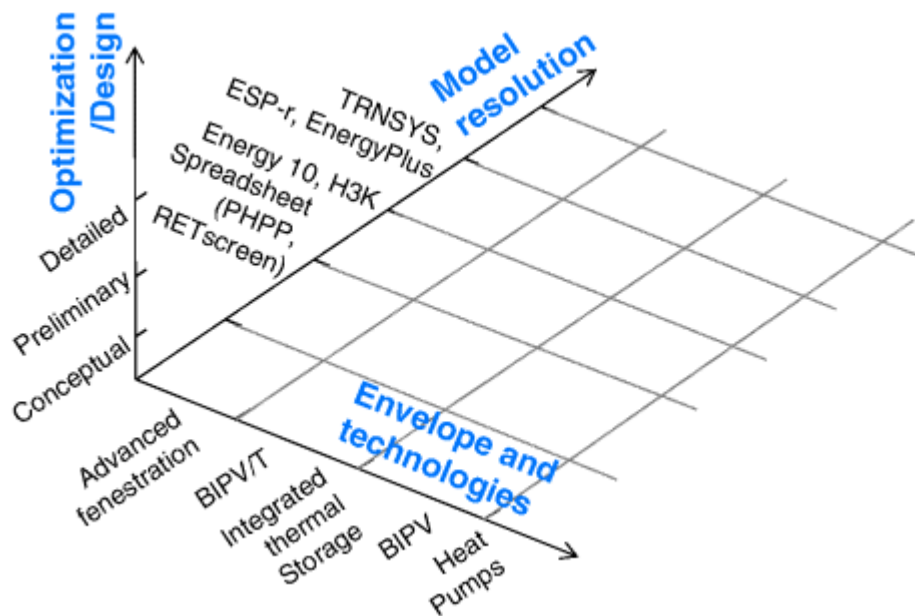
Fig. 2.1 The 3D matrix representing model resolution, technologies, and design stage

Appropriate modeling of building-integrated solar energy systems (thermal, electric, hybrid, and daylighting) is essential for the design of Net ZEBs and the study of optimal control strategies. These systems will play a major role in achieving the net-zero energy goal and need to be carefully selected, modeled, and sized for an accurate design. At the early stage of design, a simplified software tool, such as RETScreen, may provide enough accuracy to size a building-integrated photovoltaic (BIPV) or a solar thermal system as it provides monthly estimates of energy generated. However, a BIPV/thermal system (BIPV/T) that generates both electricity and heat requires estimation of the heat recovered and how it can potentially be used – to heat ventilation air, to heat water, or space

heating (directly or through a heat pump). To properly simulate these systems, there is a need for tools characterized by a high integrity representation of the dynamic and connected processes.

It is also recognized that the optimal interaction between a Net ZEB and a smart grid can facilitate reductions in peak electricity demand and under conditions of high photovoltaic (PV) penetration rates in neighborhoods, the use of energy storage in the building can reduce the peak renewable electricity supplied to the grid.

Figure 2.2a shows a typical demand and generation profile for a Canadian net-zero energy house on a cold sunny day. As can be seen in the figure, there is a high demand (negative) for heating in the early morning, so that if the weather of the previous day was similar, building-integrated thermal mass could be used to reduce this peak through collected solar gains. The net-zero energy balance may be achieved through a combination of passive and active solar technologies, heat pumps, combined heat and power (possibly using biofuels/biomass), and energy efficiency measures to reduce energy consumption for lighting and appliances as shown in Figure 2.2b. A plug-in hybrid electric vehicle (PHEV) may possibly be used as an electricity storage/backup device.
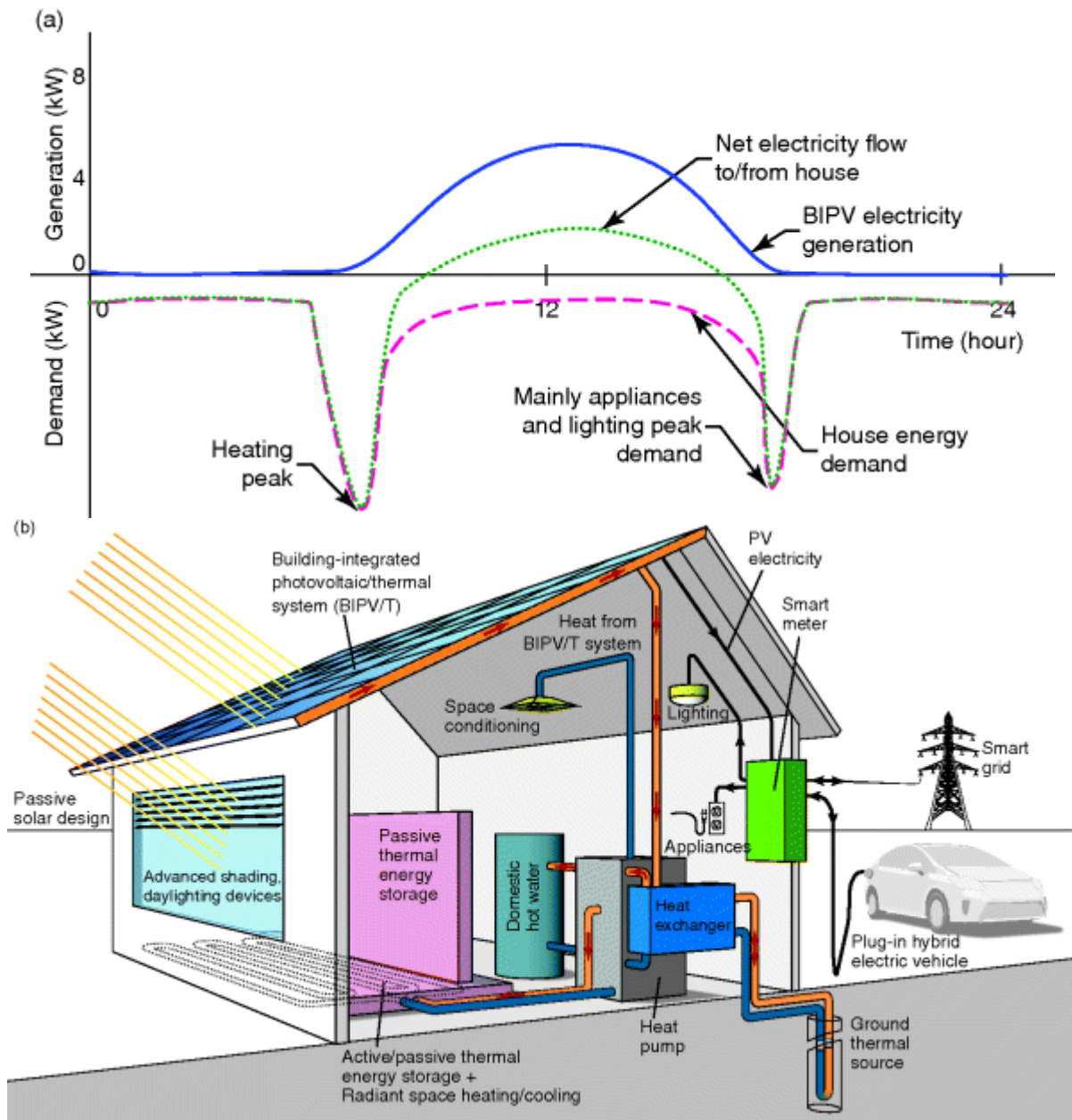
Fig. 2.2 (a) Schematic of demand and generation profile for a Canadian net-zero energy house (cold sunny day); (b) Net-zero energy solar home concept (Illustration: Samson Yip)

2.1.1 Passive Design, Energy Efficiency, Thermal Dynamics, and Comfort

There are two principal categories of building solar heating and cooling systems: passive and active. Passive systems integrate into the structure of the building technologies that admit, absorb, store,

and release solar energy, thereby reducing the need for electricity use to transport fluids. In contrast, active systems include fans and pumps controlled to move air and heat transfer fluids respectively for space heating and/or cooling and domestic hot water (DHW) heating.

Current international trends in net-zero energy building design are expected to continue and will increasingly rely on a combination of active and passive solar systems as enabling technologies for net-zero energy solar buildings – solar buildings that produce as much energy as they consume over a year. Similarly, hybrid systems – active/passive and thermal/electric – will gain popularity, such as the photovoltaic/thermal systems that are described later in this document.

This section presents approaches that are primarily used for modeling and simulating passive solar systems and some building-integrated solar systems.

Passive solar technologies generally do not use fans or pumps in the collection and usage of solar heat. Instead, these technologies use the natural modes of heat transfer to distribute solar gains among different spaces. When applied to buildings, this generally refers to passive energy flows among rooms and envelope, such as the redistribution of absorbed direct solar gains or night cooling. Buildings that primarily use these technologies to reduce heating and/or cooling energy consumption are commonly described as "*passive solar buildings*."[1] The major driving forces for thermal energy transfer within a passive solar building are longwave thermal radiation exchanges and natural convection.

Passive technologies are integrated within the building and may include the following:

1. *Near-equatorial-facing windows* with high solar transmittance and high thermal resistance. These properties maximize the amount of direct solar gains into the living space, while reducing envelope heat losses and gains in the heating and cooling seasons, respectively. Skylights are often employed for daylighting in office buildings and in sunspaces-solaria.

2. *Building-integrated thermal energy storage*. Thermal energy storage, which is commonly referred to as thermal mass, may consist of sensible heat storage materials, such as concrete or brick, or PCMs. Two design options are *isolated thermal storage* (not directly thermally coupled to the living space) or solarium/sunspace and *collector-storage walls*. A *collector-storage wall* – known as a Trombe wall – consists of thermal mass that is placed directly in front of the glazing; however, this system has not gained much acceptance since it limits the views to the outdoor environment. Direct gain systems are the most common implementation of thermal storage because of their simultaneous benefits for providing passive heating, daylight, and views to the exterior.

3. *Airtight insulated opaque envelope*. Such an envelope reduces heat transfer to/from the outdoor environment, but must be chosen to be appropriate for the local climate. In most climates, this energy efficiency aspect is an essential part of the passive design. A solar technology that may be employed in conjunction with opaque envelopes is transparent insulation combined with thermal mass to store solar gains in a wall to turn it into an energy positive thermal element. In addition to optimized thermal response, the envelope should control air and moisture transfer between the indoor and outdoor environments.

4. *Daylighting technologies and advanced solar control systems*. These technologies provide passive daylight transmission. They include electrochromic and thermochromic coatings, motorized shading (internal and external) that may be automatically controlled, and fixed shading devices, particularly for daylighting applications in the workplace. Newer technologies, such as transparent photovoltaics, can also generate electricity while transmitting daylight. Such technologies introduce a new level of complexity in building design since they generate electricity, have direct and indirect impacts on cooling loads, as well as electricity consumption for lighting (reducing the need for electric lighting through daylight). During the cooling season the need to provide daylight, while preventing excessive solar gains that raise cooling loads, should be carefully considered.

5. *Building-integrated photovoltaics*. Photovoltaic panels can serve as exterior cladding or roof shingles while producing electricity with no moving parts. Thus, they can be considered a passive element. In some cases, active heat recovery from BIPV through closed loop (e.g., water pipes as in solar collector absorber plates) or open loop (flowing air in a cavity behind the PV panels) can also be used to produce useful heat; these BIPV/T systems are hybrid building elements.

Simulation and analysis of the thermal and energy fluxes in a building facilitate the choice of materials and subsystems for the local climatic characteristics and building function. Many thermal processes are relevant in the assessment of building thermal behavior, such as

– heat conduction through exterior walls, roofs, ceilings, floors, and interior partitions;

– solar radiation through transparent surfaces;

– latent or sensible heat generated in the space by occupants, lights, and appliances;

– heat transfer through ventilation and infiltration of outdoor air and other miscellaneous heat gains (ASHRAE, 2009a).

One of the most important of these thermal processes is thermal conduction through a multilayered wall that is calculated in several ways, such as

– Finite difference methods

– Finite element methods

– Transform methods (frequency domain and time domain), including time series methods (such as those using *z*-transfer functions described below and used in Chapter 6).

During the thermal analysis of a building, it is necessary to determine heating loads and room temperature fluctuations either for design days or with given typical annual weather data. For sizing equipment and components, it is desirable to evaluate the building

response under extreme weather conditions for many design options, each time changing only a few of the building parameters, until an optimum or acceptable response is obtained. For a solar building that includes direct gain as a major solar energy utilization mechanism, it is also useful to study the free (passive) response of the building as this enables the designer to determine the relation between room temperature fluctuation and storage of passive solar gains. This relationship is an important consideration for thermal comfort studies, for which room temperature swings outside the comfort range are to be minimized. Thermal comfort is further discussed in [Chapter 3](#).

There are two main steps in creating a *mathematical model* that describes the energy transfer processes in a building. First, the thermal exchanges must be modeled as accurately as is necessary; while an acceptable level of precision is desired, too much complexity can limit the model usefulness in analysis and design. Second, an *appropriate method of solution* must be chosen to determine the room temperature and auxiliary energy loads. The type of solution may be *numerical or analytical*, as long as the variables of interest can be determined. As an optional third step, a *method of analyzing the system without simulation* can be developed; this is particularly important for comparison of design options on a relative basis, for optimal control studies and peak electricity demand reduction (see [Chapter 6](#)).

The degree of detail and *model resolution* required during the energy and thermal analysis of a building depends on the design stage. For the early stages of design, when the geometry of the building surfaces is not fully fixed, a steady-state or an approximate dynamic model is often adequate. However, more detail is required for a preliminary design, taking into account all objectives of building thermal design and the specific characteristics of the HVAC and solar systems considered.

Modeling the longwave radiant heat exchanges of the zone interior is more important with direct gain systems compared to indirect gain systems and generally requires more modeling detail, particularly if a floor heating system is integrated. In designing solar buildings, a key objective is to store energy in the walls during the daytime for release

at night without having uncomfortable temperature swings. If PCMs are integrated in the room interior layers the room mean radiant temperature variation is expected to be reduced.

A basic characteristic of a passive solar building is the strong convective and conductive coupling between adjacent thermal zones. This coupling is very important between equatorial-facing rooms receiving a significant amount of solar radiation transmitted through large windows and adjacent rooms that receive very little solar radiation. For example, heat transfer by natural convection through a doorway connecting a warm direct gain room or a solarium and a cool north facing room, can be an effective way of heating the cool room. The transfer of heat can be controlled so as to avoid backflow to the solarium at night by having motorized inlets that close.

Periodic conditions are usually assumed (explicitly or implicitly) in dynamic building thermal analysis and load calculations. Heating or cooling load, that is, the auxiliary heat energy input/removal required to maintain comfort conditions, is usually calculated for a design day. The peak heating load is used to size heating equipment and the peak cooling load is used to size cooling equipment.

The following three types of *approximations* are commonly introduced in mathematical and physical models to facilitate the characterization of the building thermal behavior:

1. *Linearization of heat transfer*. Convective and radiative heat transfer are inherently nonlinear processes and the respective heat transfer coefficients are usually linearized so that the system energy balance equations can be solved by direct linear algebra techniques and possibly represented by a linear thermal network. Linearization generally introduces less error for longwave radiant exchanges between surfaces than convection between room surfaces and room air.[2] In some cases heat flow reversal can occur, such as between a cold floor and warm air, where the convective heat transfer coefficient can be of the order of 1 W/m² K compared to 3 W/m² K for a heated floor and cold air.

2. *Spatial and/or temporal discretization*. Transient heat conduction is described by a parabolic, diffusion type partial differential equation. Thus, when using finite difference methods,

a conducting medium with significant thermal capacity, such as concrete or brick, must be discretized into a number of regions, commonly known as control volumes, which may be modeled by lumped network elements (thermal resistances and capacitances). Also, time domain discretization is required with an appropriate time step employed. In response factor methods only time discretization is necessary. For frequency domain analysis none of these approximations are required; in periodic models however, the number of harmonics employed must be kept within reasonable limits. It should be noted that when thermal storage undergoes phase change (e.g., PCMs) a linear approximation may not be possible in some cases and specialized modeling is required.

3. *Approximations for reduction in model complexity – establishing appropriate model resolution.* These approximations are employed in order to reduce both the number of simultaneous equations to be solved and the required data input or to enable the derivation of closed form analytical solutions. They are by far the most important approximations. Examples include combining radiative and convective heat transfer coefficients (so-called film coefficients commonly employed in building energy analysis), assuming that many surfaces are at the same temperature, or considering certain heat exchanges as negligible. Such approximations need to be carefully selected and applied by taking into consideration the expected temperature variations (spatial and temporal) in a zone. For example, a zone with large windows and floor heating may exhibit large spatial temperature variations, in which case the use of combined film coefficients would result in high errors in room operative temperature and floor heating rate calculations.

A major part of the modeling process considers transient heat conduction in the building envelope. In most cases relating to heating or cooling load estimations, energy savings calculations, and thermal comfort analysis, it is generally accepted that *one-dimensional heat conduction* may be assumed. Thermal bridges, such as those present around corners and at the structure, are generally accounted for in calculating the effective thermal resistance

of building envelope elements by using a more detailed spatial model or simplified techniques, such as the parallel heat flow path method. However, the thermal storage process may usually be adequately modeled as one-dimensional for well-insulated buildings. For steady state calculation of thermal bridge effects, a 2D or 3D calculation of thermal conductance is sometimes desirable (e.g., parallel heat flow method (ASHRAE, 2009a)).

Direct gain zone modeling (i.e., a zone with high interior solar gains) includes certain important requirements in addition to those required for traditional building modeling. In particular, there is an increased need to address thermal comfort requirements and to allow the room temperature to fluctuate so as to enable storage of direct solar gains in building integrated exposed thermal mass. In addition, for an office environment, daylighting considerations will dominate, such as the need to uniformly distribute daylight and to prevent glare.

Peak heating/cooling load calculations are a major aspect of heating/cooling equipment sizing and need to take into account building thermal storage capacity and dynamic variation of both solar radiation and outdoor temperature, in order to avoid over-sizing of HVAC systems. For most mild temperate climates, a heat pump will provide an efficient auxiliary heating and cooling system. Well-insulated buildings with effective shading systems and natural ventilation have a reduced need for auxiliary cooling. Similarly, appropriate sizing of the near-equatorial facing fenestration systems will satisfy most heating requirements on sunny days.

Frequency domain analysis techniques with complex variables may be employed for steady periodic analysis of multilayered walls and zones. They provide a convenient means for periodic analysis, in which parameters, such as magnitude and phase angle of room temperatures, and heat flows are obtained. The well-known cooling load temperature differential (CLTD) method proposed for many years by ASHRAE (McQuiston, Parker, and Spitler, 2005) for cooling load calculations is essentially an admittance-based technique, with magnitudes and phase lags of important frequency domain transfer functions. In the United Kingdom, an admittance-based technique is used to calculate room temperature swings and time lags between

cause (e.g., sol-air temperature peak) and effect (peak of room temperature rise).[3]

2.1.2 Detailed Frequency Domain Wall Model and Transfer Functions

Building heat exchanges may be represented by a *thermal network*, and transfer functions are obtained by performing an energy balance at all nodes in the Laplace domain. Both lumped and distributed elements can be considered using this approach. Simple models that do not represent in detail infrared radiation heat exchanges between room interior surfaces can usually be solved analytically. Transient heat conduction (assumed to be one-dimensional) in walls can be accurately represented without discretization using the approach that follows.

2.1.2.1 Distributed Parameter Model for Multilayered Wall

Consider a slab and assume one-dimensional transient conduction with uniform properties k, ρ, c. We have

$$\alpha \cdot \frac{\partial^2 T}{\partial x^2} = \frac{\partial T}{\partial t} \tag{2.1}$$

where $\alpha = k/(\rho c)$ is the thermal diffusivity

The boundary conditions will include convective heat transfer, absorbed solar radiation (a heat source), and longwave radiation exchange with other surfaces.

After taking the Laplace transform of Eq. (2.1) and some algebra, the equations for the conditions at the two surfaces may be expressed in the so-called cascade equation matrix form (Beccali *et al.*, 2005b) as follows (assuming heat flux q is positive into the wall on both sides):

$$\begin{bmatrix} T_1 \\ q'_1 \end{bmatrix} = \underbrace{\begin{bmatrix} \cosh(\gamma L) & \sinh(\gamma L)/k\gamma \\ k\gamma \sinh(\gamma L) & \cosh(\gamma L) \end{bmatrix}}_{\text{two port cascade matrix}} \cdot \begin{bmatrix} T_2 \\ -q'_2 \end{bmatrix} \tag{2.1a}$$

The parameter k is the thermal conductivity, L is thickness, γ is equal to $(s/\alpha)^{1/2}$ and s is the Laplace transform variable. For frequency

domain analysis, including admittance calculations, s is set equal to $j\omega$ ($s = j\omega$) where $j = \sqrt{-1}$ and $\omega = 2\pi/P$. For diurnal analysis, the period $P = 86{,}400$ s. For a multilayered wall we can multiply the cascade matrices for each successive layer to get an equivalent wall cascade matrix that relates conditions at one surface of the wall to those at the other surface, thus eliminating *all intermediate nodes with no approximation required and no discretization:*

$$\begin{bmatrix} T_1 \\ q'_2 \end{bmatrix} = \begin{bmatrix} A_1 & B_1 \\ C_1 & D_1 \end{bmatrix} \cdot \begin{bmatrix} A_2 & B_2 \\ C_2 & D_2 \end{bmatrix} \cdots \begin{bmatrix} A_N & B_N \\ C_N & D_N \end{bmatrix} \cdot \begin{bmatrix} T_N \\ -q'_N \end{bmatrix} \tag{2.1b}$$

The effective cascade matrix of the wall is expressed as

$$\begin{bmatrix} T_1 \\ q'_1 \end{bmatrix} = \begin{bmatrix} \bar{A} & \bar{B} \\ \bar{C} & \bar{D} \end{bmatrix} \cdot \begin{bmatrix} T_N \\ -q'_N \end{bmatrix} \tag{2.1c}$$

The cascade matrix for a simple conductance (per unit area), u, can be shown to be given by $\begin{bmatrix} 1 & 1/u \\ 0 & 1 \end{bmatrix}$

Usually, the interior surface temperatures of the room are of primary interest. Consider for example a wall made up of an inner (room side) storage mass layer and insulation on the exterior as shown in Figure 2.3. The effective cascade matrix can be represented by

$$\begin{bmatrix} T_1 \\ q'_1 \end{bmatrix} = \underbrace{\begin{bmatrix} D & B \\ C & D \end{bmatrix}}_{\substack{\text{mass} \\ \text{cascade} \\ \text{matrix}}} \cdot \underbrace{\begin{bmatrix} 1 & 1/u_o \\ 0 & 1 \end{bmatrix}}_{\substack{\text{insulation} \\ \text{and air cascade} \\ \text{matrix}}} \cdot \begin{bmatrix} T_2 \\ -q'_2 \end{bmatrix} = \underbrace{\begin{bmatrix} D & D/u_o + B \\ C & C/u_o + D \end{bmatrix}}_{\text{wall cascade matrix}} \cdot \begin{bmatrix} T_2 \\ -q'_2 \end{bmatrix} \tag{2.1d}$$
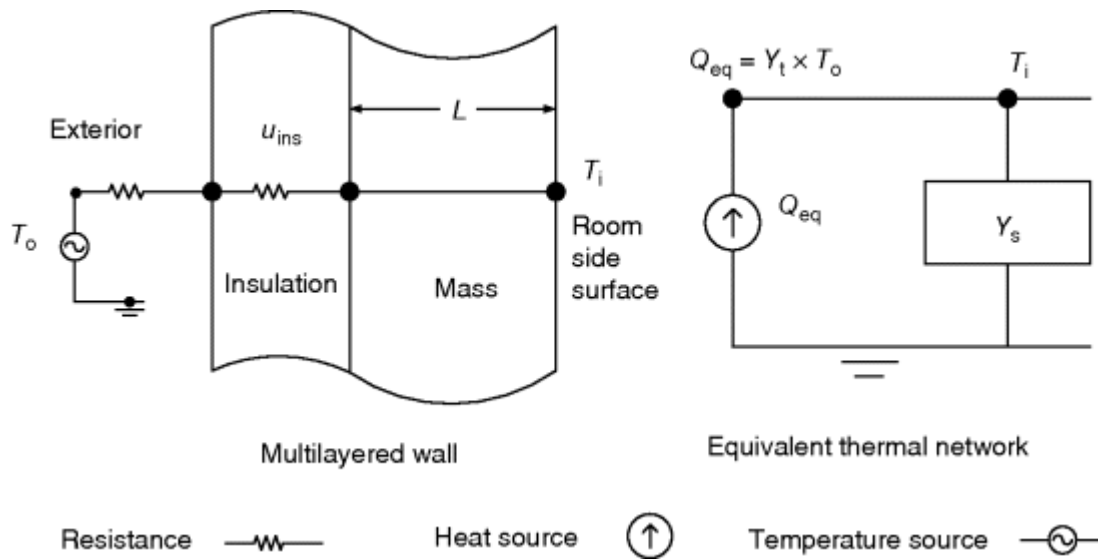
Fig. 2.3 Exterior wall with massive interior layer, and equivalent thermal network (for a wall with incident solar radiation replace T_o with the sol-air temperature T_{eo})

2.1.2.2 Admittance Transfer Functions for Walls

The above cascade equations for walls may be utilized to obtain frequency domain (admittance or impedance) transfer functions for walls and zones that can be used for steady periodic analysis or controls and system dynamics studies.

Simple Fourier series models consisting of a few harmonics (e.g., 3–12) for outside temperature or sol-air temperature and solar radiation are used for steady-periodic thermal analysis of wall heat flow. Frequency domain transfer functions, such as the wall admittance, are studied in terms of magnitude and phase lag and are then used together with Fourier series models for the weather variables to determine steady periodic thermal response of walls. The technique is applied for passive solar analysis and design.

Significant insight into wall dynamic thermal behavior may be obtained by studying the admittance transfer functions (magnitude and phase angle) as a function of frequency, thermal properties, and geometry. For inputs with more than one harmonic, the total response may be obtained by superposition of the response harmonics.

The thermal admittance of a wall is a transfer function parameter useful for analysis of the effects on room temperature of cyclic variations in weather variables, such as solar radiation, outside temperature, and dynamic heat flows under steady periodic conditions.

There are two transfer functions of primary interest, namely, the self-admittance Y_s relating the effect of a heat source at one surface to the temperature of that surface, and the transfer admittance Y_t relating the effect of an outside temperature variation to the resulting heat flow at the inside surface.

These two transfer functions are determined as demonstrated in the following model. The wall in Figure 2.3 consists of insulation and thermally nonmassive layers (low thermal capacity) with conductance value u per unit area, and a thermally massive layer of thickness L.

The Norton equivalent network for a wall with a specified temperature on one side (such as basement temperature or sol-air temperature) is obtained from the cascade form of the wall equations, which relates temperature and heat flow at one surface to those at the other surface. The cascade form of the equations is derived by first taking the Laplace transform of the one-dimensional heat diffusion equation to obtain an ordinary differential equation, which can then be readily solved to relate heat flux and temperature at one surface of a one-dimensional medium to those at the other surface in the following form (based on Eq. (2.1)):

$$\begin{bmatrix} T_1 \\ q_1' \end{bmatrix} = \begin{bmatrix} D & B \\ C & D \end{bmatrix} \begin{bmatrix} T_2 \\ -q_2' \end{bmatrix} \tag{2.1e}$$

where

$$D = \cosh(\gamma x)$$

$$B = \sinh(\gamma x)/k\gamma$$

$$C = k\gamma \sinh(\gamma x)$$

and q' is assumed positive into the slab (on both sides). As described previously, the cascade matrix for a multilayered wall is obtained by multiplying the cascade matrices of consecutive layers. Usually the temperatures of interest are either the inside or the outside temperatures. In this way, wall intermediate layer nodes and their temperatures are eliminated and a simplified but accurate model is obtained. A linear subnetwork connected to a network at only two terminals (surfaces) can be represented by its Norton equivalent network, consisting of a heat source and an admittance connected in parallel between the terminals (Athienitis, Sullivan, and Hollands, 1986).

The admittance is the subnetwork equivalent admittance as seen from the virtual connection port (the two terminals) and the heat source is the short-circuited heat flow at the port. Consider for example the wall in Figure 2.3, assumed to be made up of an inner layer of storage mass of uniform thermal properties and an insulation layer with negligible thermal capacity, also of uniform thermal properties. The region behind the thermal mass may be represented by equivalent conductance U in series with the outside temperature T_o (for exterior walls the sol-air temperature T_{eo}). The conductance U combines the insulation resistance and a film coefficient. The determination of Y_s (called the wall self-admittance) and the equivalent heat source Q_{sc} produced by the transformation, is as follows: Firstly, the total cascade matrix is obtained by multiplying the cascade matrix for the storage mass layer by the matrix for u (note: $u = U/A$):

$$\begin{bmatrix} T_s \\ q_s \end{bmatrix} = \begin{bmatrix} D & B \\ C & D \end{bmatrix} \begin{bmatrix} 1 & 1/u \\ 0 & 1 \end{bmatrix} \begin{bmatrix} T_o \\ -q_o \end{bmatrix} \tag{2.1f}$$

After multiplying, we temporarily set $T_S = 0$ (i.e., consider a short-circuit) to get the Norton equivalent heat source as

$$Q_{eq} = -Y_t T_o \tag{2.1g}$$

where the transfer admittance Y_t is given by

$$Y_t = \frac{-A}{\left[\dfrac{A \cosh(\gamma x)}{u_o} + \dfrac{\sinh(\gamma x)}{k\gamma}\right]} \qquad (2.1h)$$

The transfer admittance has been multiplied by the area A to obtain its total value. To obtain Y_s we temporarily set $T_0 = 0$ and obtain the admittance as seen from the interior surface, yielding (after multiplying by A):

$$Y_s = \frac{A\left(\dfrac{u_o}{A} + k\gamma \tanh(\gamma x)\right)}{\left[\dfrac{u_o}{k\gamma A}\tanh(\gamma x) + 1\right]} \qquad (2.1i)$$

If there is no thermal mass (zero thermal capacity) then we obtain the simple equality $Y_s = -Y_t = Au_o$. A similar result is obtained for windows by eliminating all nodes exterior to the inner glazing. An important result is obtained for an infinitely thick wall or a wall with no heat loss at the back (adiabatic surface, or high amount of insulation $u_o \approx 0$); in this case Y_s is given by

$$Y_s = A\, k\, \gamma \tanh(\gamma x) \qquad (2.1j)$$

Walls with thick massive layers have admittance that is close to that given by Eq. (2.1j). When the penetration depth, given by

$$d = \sqrt{2k/(c_p\rho\omega)} = \sqrt{(2\alpha/\omega)} \qquad (2.1k)$$

is significantly less than the wall thickness then the wall behaves like a semi-infinite solid. The magnitude and phase angle (and time lag/lead) of a transfer function, such as Y_s and Y_t, are computed by means of complex variables.

Substantial insight into wall and building thermal behavior may be gained by studying the magnitude and phase angle of key transfer functions, such as Y_s and Y_t. The time lead d_s of Y_s is the time difference between the peak of a sinusoidal input function, such as solar radiation in the case of the room interior surface, and the resulting peak of the interior surface temperature T_i. Now, we consider the variation of wall thermal admittance with thermal mass

thickness L for the fundamental frequency (one cycle per day, $n = 1$) for unit wall area. Note that the diurnal ($n = 1$) frequency is important in the analysis of variables with a dominant diurnal harmonic, such as solar radiation. High frequencies are important in analyzing the effect of varying heat inputs such as those due to the on/off cycling of a furnace.

For comparison, two walls, one with concrete and the other with softwood, are compared. The interior wall is assumed to be either concrete or wood. The exterior insulating layer has insignificant thermal capacity and its thermal resistance is equal to 2.5 RSI. The concrete is assumed to have a specific heat capacity of 800 J/kg °C, a density of 2200 kg/m³, and a thermal conductivity of 1.7 W/m K. The wood material has a specific heat capacity of 1360 J/kg °C, a density of 630 kg/m³, and a thermal conductivity of 0.13 W/m K.

The results presented here are specific to this type of concrete, but they generally indicate the expected trends for concrete, brick, and masonry type materials. Note that the thermal conductivity of these materials increases with moisture content and density. Figure 2.4 shows an extremely important result in steady-periodic analysis of building thermal response – the fact that there is a wall thermal mass thickness that will minimize room temperature fluctuations (in this case, $L = 0.2$ m of concrete) and this corresponds to the maximum admittance. Therefore, this is the optimum thermal mass thickness for passive solar design since the dominant harmonic component of solar radiation corresponds to one cycle per day. The figure also shows results for softwood, with the peak admittance at a thickness of 0.07 m.
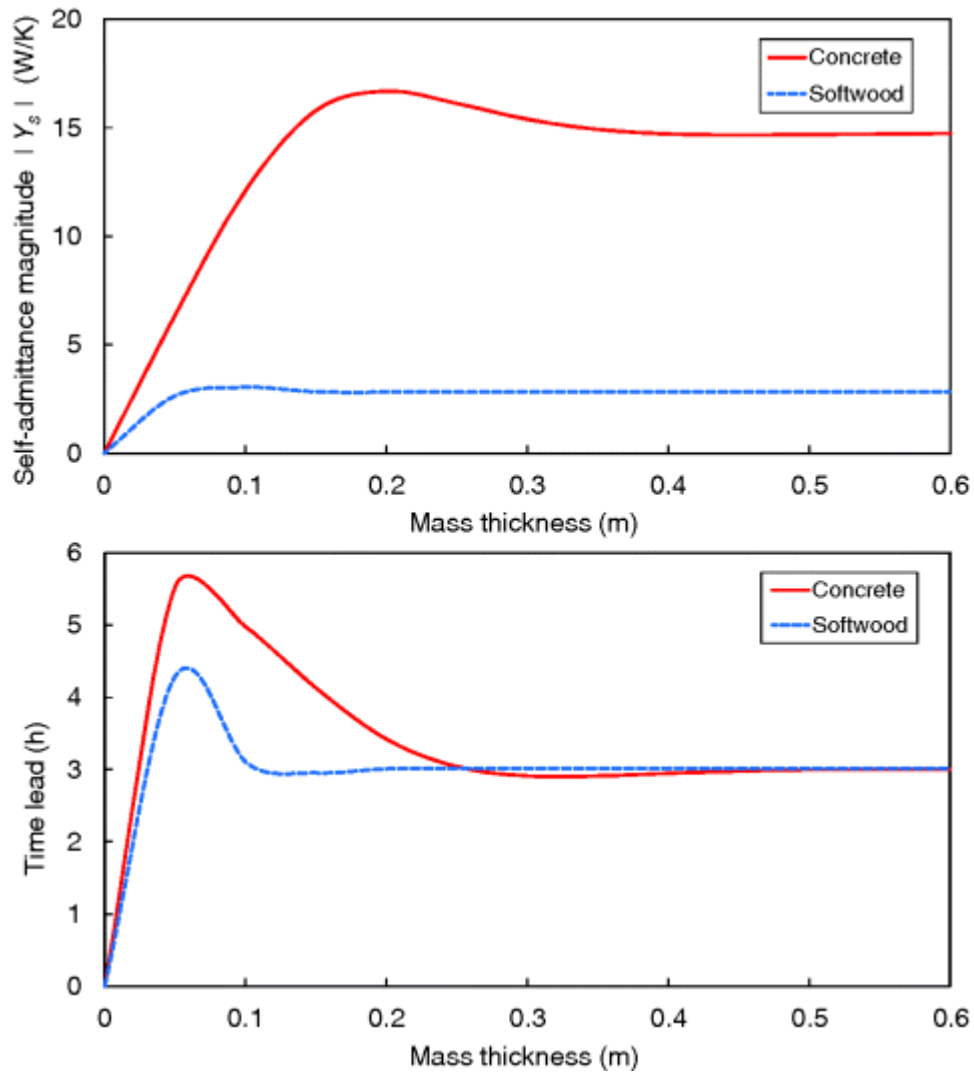
Fig. 2.4 Variation of the self-admittance and its time lead with mass thickness and material type for a period of one day (Figure courtesy of Ali Saberi Derakhtenjani)

As indicated in Figure 2.4, the magnitude of wall admittance (for mass thickness of 20 cm) increases with frequency (decreases with period). The magnitude of the wall admittance is also higher for concrete compared to softwoods. Thus, the inside room temperature fluctuations are smaller for high-frequency fluctuations in internal heat gains for the concrete wall construction. For harmonic numbers higher than about 8 – that is, for periods less than 3 h – the wall behaves like an infinitely thick solid; in this case the phase angle is 45°.

2.1.3 Z-Transfer Function Method

Software for thermal dynamic simulation of buildings often employ the so-called transfer function method (TFM) or conduction transfer functions (CTFs)[4], both of which provide a set of time domain coefficients relating the current conductive heat fluxes to past surface temperatures and past heat fluxes. TFM has been selected for the procedure recommended by ASHRAE, called heat balance method (HB) (ASHRAE, 2009a), mainly due to

- the computational time advantage compared to detailed numerical methods, and

- input or output data (such as hourly climatic data) being discrete in the time domain.

This method replaces the earlier CLTD method. Accurate simulations of thermal systems in the built environment can be performed using detailed modeling techniques, and are available in many software packages. Some of the most used building simulation software, such as TRNSYS (TRNSYS, 2013), and EnergyPlus (EERE, 2013), which are employed to perform design thermal load calculations, use mathematical models based on transform methods such as the response factor method, and the *z*-transfer function method (referred to as TFM) (Beccali *et al.*, 2003, 2005a, 2005b; Cellura *et al.*, 2010).

The TFM developed by Stephenson and Mitalas (1971) uses CTFs to calculate the transient one-dimensional heat conduction through the building wall and roof elements.

Mitalas described the wall transfer function $G(z)$ as the ratio between the *z*-transform (ZT) of the output $O(z)$ and the ZT of the input $I(z)$. $I(z)$ was directly calculated by means of Laplace transform (LT) while, to evaluate $O(z)$, Mitalas used the time response obtained from the differential equations of the wall, solved through LT; he used as input a linear ramp of temperature and obtained a set of values capable of identifying the system behavior; this set has been adopted by ASHRAE. According to the Mitalas procedure we need the system time-response related to the specific elementary input $I(z)$. The response can be evaluated exactly only by performing the

sum of the infinite number of terms that are related to the poles of the wall transfer function. When we limit the computations to the first N poles, an error is introduced, which will affect the system response for the following time. Stephenson and Mitalas (1971) applied ZT to non–steady-state heat transfer and showed how the physical behavior of walls can be properly described by using few numerical coefficients that decrease fast in magnitude (with time) after applying the input.

The walls in the TRNSYS software ([Figure 2.5](#)) are modeled based on the transfer function relationships defined from surface to surface. The evaluation of CTFs can be performed with an approximate mathematical approach because the exact solution requires an infinite number of calculations. The CTF method identifies the relationship between the signal that is input to the system (a multilayered wall) called the "input" and the response of the system (the temperature of the wall surfaces or a thermal flux through the wall) called the "output." This relation is called the Transfer Function of the system (a time domain transfer function).

Following the approach developed by Stephenson and Mitalas (1971), based on the use of the Z-transform (ZT) (Jury, 1964), consider a wall in which $u(t)$ is the input signal and $y(t)$ is the correlated output signal.
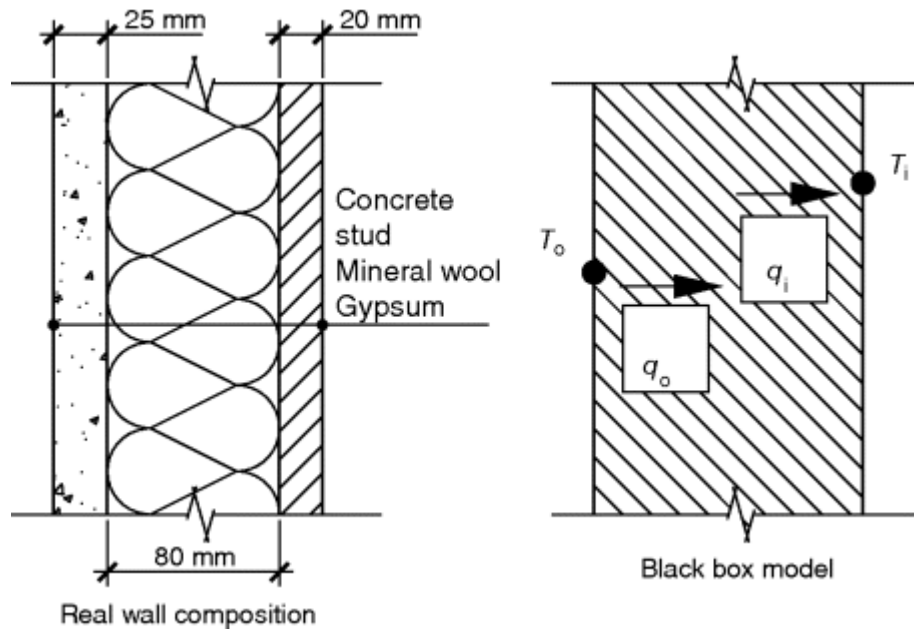
Fig. 2.5 TRNSYS wall simulation model example (boundary conditions)

The signals vary with the time t and can be the temperatures of the fluids adjacent to the wall or the heat fluxes through its surfaces.

If $U(z) = Z[u(t)]$ and $Y(z) = Z[y(t)]$ are the corresponding z-transformed signals, the transfer function of the system can be written in the form

$$G(z) = \frac{Z[y(t)]}{Z[u(t)]} = \frac{\text{num}(z)}{\text{den}(z)}$$

where $n(z)$ and $d(z)$ are polynomial expressions.

The roots of the denominator of $G(z)$ are called poles and they are mathematically infinite in number because of the hyperbolic, transcendental terms in the admittance equation (exact frequency domain solution).

A signal that is time sampled is said to be a discrete-time signal. The sampling period Δt_s is related to the time interval of data-collection (usually Δt_s is 1 h).

Excluding approximations linked to physical assumptions, the weakest point of this method is due to the truncation of the infinite coefficients that constitute the Transfer Functions (TFs). The absolute value of the coefficients n and d of the expression

$$\frac{\text{num}(z)}{\text{den}(z)} = \frac{n_0 + n_1 z^{-1} + n_2 z^{-2} + \ldots + n_R z^{-R}}{d_0 + d_1 z^{-1} + d_2 z^{-2} + \ldots + d_P z^{-M}} \tag{2.2}$$

very quickly decreases when the order of the addendum increases and, for this reason, it is possible to truncate the terms of $n(z)$ and $d(z)$.[5] In order to accomplish a correct truncation procedure, which is affected by the choice of the selected number of poles, it is necessary to evaluate the effect in the numerical response linked to either the insertion or to the elimination of the coefficient of order R + 1 or M + 1. Such evaluation can be correctly performed only if a large number of coefficients is available.

The non–steady-state heat transmission through a multilayered wall can be described using the following equations (see [Eqs. (2.1b)](#) and [(2.1c)](#)):

$$q_i(z) = \frac{1}{B(z)} T_0(z) - \frac{A(z)}{B(z)} T_i(z) \tag{2.3}$$

and the quantities

$$\begin{cases} H_1(z) = \dfrac{1}{B(z)} = \dfrac{\text{num}_1(z)}{\text{den}(z)} = \dfrac{b_0 + b_1 z^{-1} + b_2 z^{-2} + \ldots}{d_0 + d_1 z^{-1} + d_2 z^{-2} + \ldots} \\[3mm] H_2(z) = \dfrac{A(z)}{B(z)} = \dfrac{\text{num}_2(z)}{\text{den}(z)} = \dfrac{c_0 + c_1 z^{-1} + c_2 z^{-2} + \ldots}{d_0 + d_1 z^{-1} + d_2 z^{-2} + \ldots} \end{cases} \tag{2.4}$$

are the transfer functions necessary to solve the problem. If each expression is truncated to the first N terms, it is possible to write that

$$q_i(z) = q_{i,0} + q_{i,1} z^{-1} + \ldots + q_{i,N} z^{-N}$$

$$T_i(z) = T_{i,0} + T_{i,1} z^{-1} + \ldots + T_{i,N} z^{-N}$$

$$T_o(z) = T_{o,0} + T_{o,1} z^{-1} + \ldots + T_{o,N} z^{-N}$$

$$\frac{1}{B(z)} = \frac{b_0 + b_1 z^{-1} + \ldots + b_N z^{-N}}{d_0 + d_1 z^{-1} + \ldots + d_N z^{-N}}$$

$$\frac{A(z)}{B(z)} = \frac{c_0 + c_1 z^{-1} + \ldots + c_N z^{-N}}{d_0 + d_1 z^{-1} + \ldots + d_N z^{-N}}$$

where $d_0 = 1$.

Equation (2.3) can be rewritten in the following form:

$$\left(q_{i,0} + q_{i,1} z^{-1} + \ldots + q_{i,N} z^{-N}\right)\left(d_0 + d_1 z^{-1} + \ldots + d_N z^{-N}\right) \tag{2.5}$$
$$= \left(T_{o,0} + T_{o,1} z^{-1} + \ldots + T_{o,N} z^{-N}\right)\left(b_0 + b_1 z^{-1} + \ldots + b_N z^{-N}\right)$$
$$- \left(T_{i,0} + T_{i,1} z^{-1} + \ldots + T_{i,N} z^{-N}\right)\left(c_0 + c_1 z^{-1} + \ldots + c_N z^{-N}\right)$$

Performing the products and ordering with respect to the variable z, the last equation becomes:

$$\tag{2.6}$$
$$\left[(q_{i,0} + D_0) + \ldots + (q_{i,N} + D_N)z^{-N}\right] = \left(B_0 + \ldots + B_N z^{-N}\right) - \left(C_0 + \ldots + C_N Z^{-N}\right)$$

where:

$$D_n = \sum_{j=1}^{n} d_j q_{i,n-j}$$

$$B_n = \sum_{j=1}^{n} b_j T_{o,n-j}$$

$$C_n = \sum_{j=1}^{n} c_j T_{i,n-j}$$

In conclusion, it is possible to state that:

$$\left(q_{i0} + q_{i1} z^{-1} + \ldots + q_{iN} z^{-N}\right) \tag{2.7}$$
$$= (B_0 - D_0 - C_0) + (B_1 - D_1 - C_1)z^{-1} + \ldots + (B_N - D_N - C_N)z^{-N}$$

Thus, at a specific time t, the heat gain per unit area through a wall or a roof can be calculated using a simple, recursive equation with constant coefficients; the sol-air temperature $T_{\text{sol-air}}$ can be used to represent the outdoor conditions. Assuming that the internal temperature $T_i = T_{\text{indoor}}$ is constant, the indoor heat flux through a

multilayered wall at the current time is calculated by means of the following (ASHRAE, 2009a):

$$q(t) = A \left\{ \sum_{n=0}^{N_{MAX}} b_n [T_{\text{sol-air}}(t - n \cdot \Delta t)] - \sum_{n=1}^{N_{MAX}} d_n \left[\frac{q(t - n \cdot \Delta t)}{A} \right] - T_{\text{indoor}} \sum_{n=1}^{N_{MAX}} C_n \right\} \quad (2.8)$$

where $q(t)$ is the indoor heat flux at the current time; A is the indoor surface area of a wall; n is the summation index; N_{MAX} is the number of coefficients used; Δt is the time step; $T_{\text{sol-air}}$ is the sol-air temperature representing outdoor conditions; T_{indoor} is the constant indoor temperature.

The maximum number of coefficients that can be obtained from the polynomial transfer function depends on the number of poles P.

$$N_{MAX} = P - 1$$

Therefore the calculation of CTFs has two degrees of freedom. One is due to the choice of the number of poles P while the other is due to the choice of the number N of coefficients, which cannot be greater than $P - 1$.

2.1.4 Detailed Zone Model and Building Transfer Functions

We have seen various techniques for representing heat transfer through multilayered walls. Now we consider thermal zone models using thermal network techniques, followed by solutions in the frequency and time domains.

The thermal network model for a typical zone over a basement (Figure 2.6), with one window and convective auxiliary heating can vary in level of detail according to how convection and radiation heat transfer are modeled in the room interior. Two common choices are followed:

1. Combined radiative-convective coefficients (so-called film coefficients) are often assumed, leading to a *star-network* as shown in Figure 2.6. This type of model is acceptable if the temperature differences between the room air and the surfaces

are low (generally 1–3 °C). In rooms with high passive solar gains and radiant heating this can result in significant simulation errors.
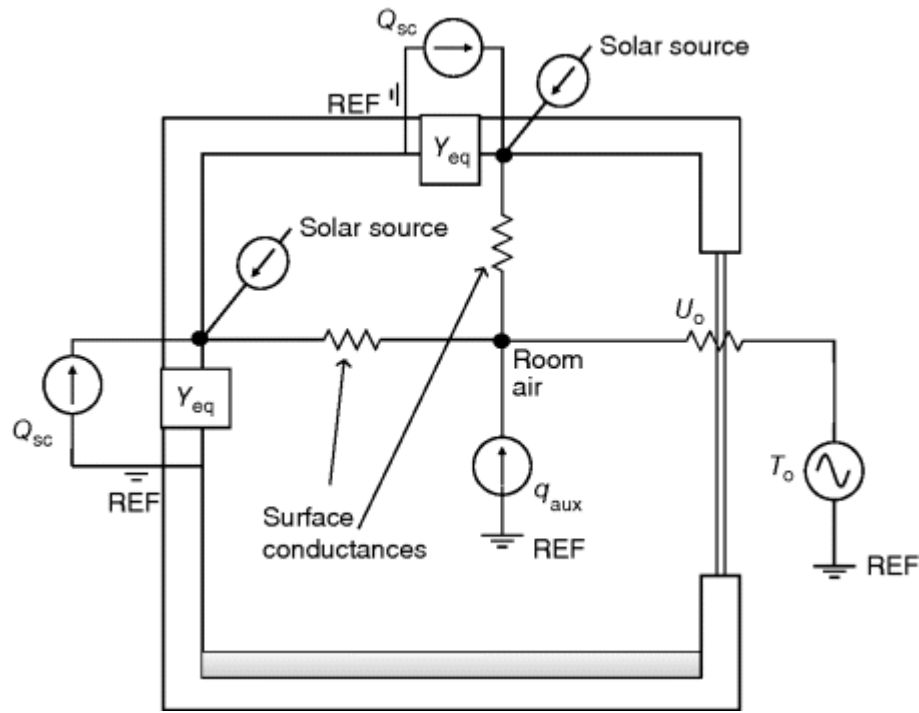
Fig. 2.6 Schematic of one-zone (heated by convective heating) with a star thermal network and equivalent networks for the walls without discretization (Norton equivalents) (Figure courtesy of Ali Saberi Derakhtenjani)

2. Separate modeling of convective and radiative exchanges in room interiors as depicted in Figure 2.7 (see also Athienitis, Stylianou, and Shou (1990)). The thermally massive walls are modelled by a two-port distributed element (as in the previous case), while the room air and light-weight room contents can be modeled by a lumped thermal capacitance. Although this capacitance has no effect on load calculations because of the relatively low frequencies involved, it is important to include it for short-term (high-frequency) control studies. Each two-port element represents the equivalent two-port for each wall, obtained after multiplying the cascade matrices for each massive and nonmassive layer as described previously.
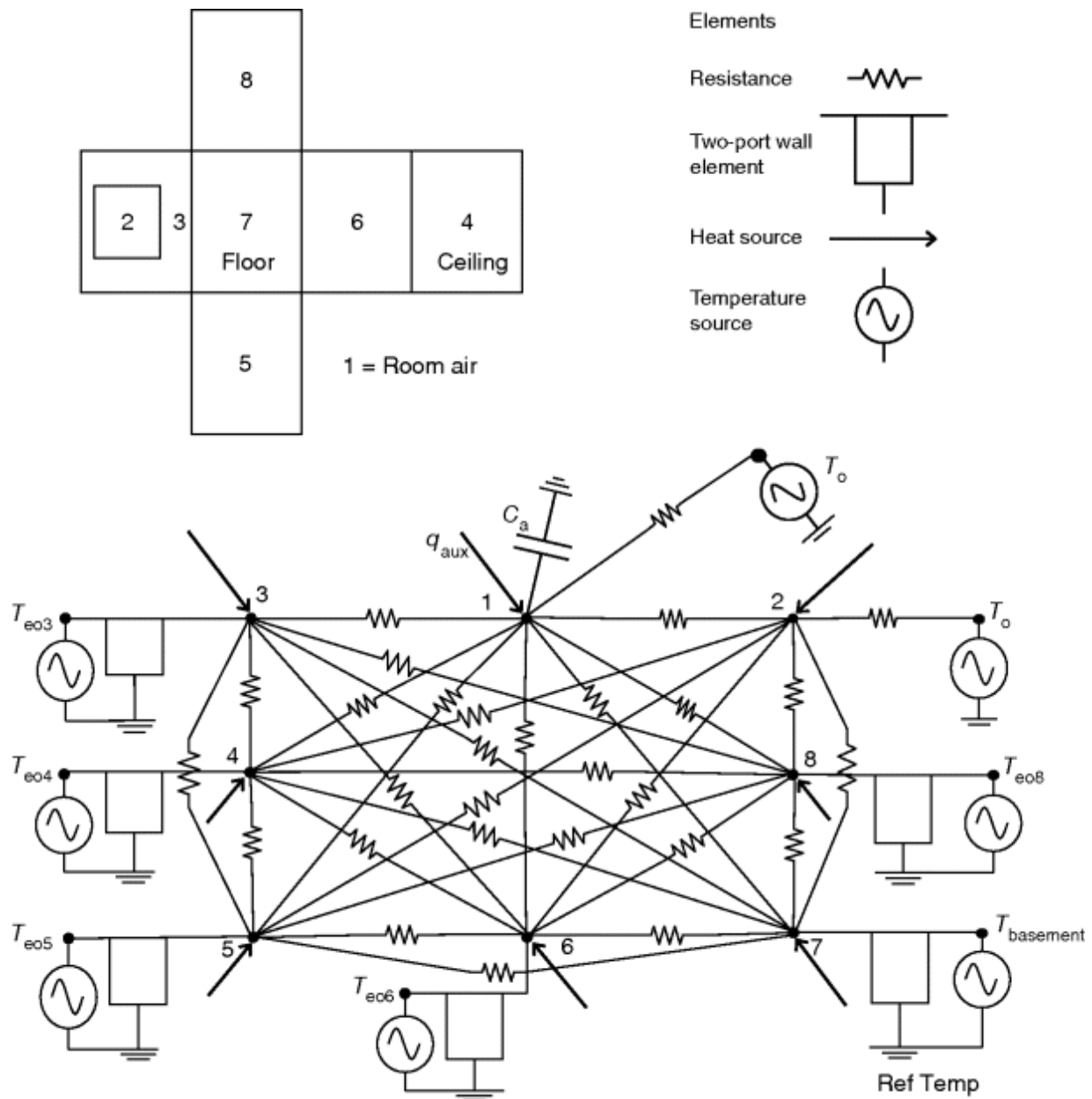
Fig. 2.7 Detailed thermal network model of zone in Figure 2.6 (node 1 is room air and nodes 2–8 are room interior surfaces) (Figure courtesy of Ali Saberi Derakhtenjani)

Convection and radiation in zones: The resistances connecting node 1 (room air) to the interior surfaces (nodes *j*) represent convective conductances (h_{c_j}) given by:

$$U_{ij} = A_j \cdot h_{c_j} \tag{2.9a}$$

The radiation conductances interconnecting room interior surface nodes 2–8 are given by:

$$U_{ij} = A_i \sigma 4 T_m^3 F_{ij}^*$$ (2.9b)

where σ is the Stefan-Boltzmann constant and $4T_m^3$ is a linearization factor which is based on an estimated mean temperature, T_m. The radiation exchange factors F_{ij}^* between pairs of surfaces under consideration (i and j) are determined from the radiation view factors F_{ij}, and the radiative properties of the room surfaces as follows:

$$F_{ij}^* = m_{ij}\, \varepsilon_i \varepsilon_j / \rho_i$$

where $\mathbf{m} = \mathbf{M}^{-1}$; the elements of matrix $\mathbf{M}$ are given by: $M_{ij} = I_{ij} - \rho_i F_{ij}$, with $I_{ij} = 1$ if $i = j$; otherwise, $I_{ij} = 0$ ($\mathbf{I}$ is the identity matrix).

Energy balances at the room interior nodes are readily obtained after replacing each wall by its Norton equivalent subnetwork consisting of an equivalent heat source Q_{sc} (sc: short circuit) and a self-admittance Y_{eq}, thereby eliminating all exterior nodes without discretizing the massive elements. The equivalent source Q_{sc} is equal to the wall transfer admittance times an external specified temperature. For the floor with self-admittance Y_{fs} and transfer admittance Y_{ft} we have $Q_{sc} = -T_{basement} Y_{ft}$ (the negative sign follows the sign convention used).

Inclusion of a lumped thermal capacitance at the room air node is represented by the constitutive equation $q = C_a\, dT/dt$ where q represents heat flow into the air capacitance C_a; the Laplace domain equation for this is $q(s) = s \cdot C_a$.

The energy balance for the model (with summations ΣU_{ij} over j = 1… 8) is as follows:

$$\begin{bmatrix} s\cdot C_\alpha + \Sigma U_{1j} + U_{inf} & -U_{12} & -U_{13} & -U_{14} & -U_{15} & -U_{16} & -U_{17} & -U_{18} \\ -U_{12} & Y_{2s}+\Sigma U_{2j} & -U_{23} & -U_{24} & -U_{25} & -U_{26} & -U_{27} & -U_{28} \\ -U_{13} & -U_{23} & Y_{3s}+\Sigma U_{3j} & -U_{34} & -U_{35} & -U_{36} & -U_{37} & -U_{38} \\ -U_{14} & -U_{24} & -U_{34} & Y_{4s}+\Sigma U_{4j} & -U_{45} & -U_{46} & -U_{47} & -U_{48} \\ -U_{15} & -U_{25} & -U_{35} & -U_{45} & Y_{5s}+\Sigma U_{5j} & -U_{56} & -U_{57} & -U_{58} \\ -U_{16} & -U_{26} & -U_{36} & -U_{46} & -U_{56} & Y_{6s}+\Sigma U_{6j} & -U_{67} & -U_{68} \\ -U_{17} & -U_{27} & -U_{37} & -U_{47} & -U_{57} & -U_{67} & Y_{7s}+\Sigma U_{7j} & -U_{78} \\ -U_{18} & -U_{28} & -U_{38} & -U_{48} & -U_{58} & -U_{68} & -U_{78} & Y_{8s}+\Sigma U_{8j} \end{bmatrix} \begin{bmatrix} T_1 \\ T_2 \\ T_3 \\ T_4 \\ T_5 \\ T_6 \\ T_7 \\ T_8 \end{bmatrix} = \begin{bmatrix} Q_1 \\ Q_2 \\ Q_3 \\ Q_4 \\ Q_5 \\ Q_6 \\ Q_7 \\ Q_8 \end{bmatrix}$$

(2.10)

or

$$Y_{NxN}T_N = Q_N$$

where **Y** is the admittance matrix, **T** is the temperatures vector and **Q** is the source vector. Note that the thermal storage terms occupy the diagonal of the admittance matric since thermal storage is relative to a common reference temperature. The element Y_{11} includes the air capacitance and sometimes interior furnishings that react quickly to heat inputs. The solution for **T** in the frequency domain is obtained by:

$$ZQ = T \tag{2.11}$$

where $Z = Y^{-1}$

Note that the star thermal network (Figure 2.6) can be considered a particular case of the network shown in Figure 2.7 with the radiation conductances between nodes 2–8 eliminated. A zone admittance can be defined based on the effect of heat input at node 1 on room air temperature (T_1). Also, all surface heat sources can be transferred to node 1, facilitating an analytical solution.

The elements of the admittance matrix may be obtained by inspection from the topology of the network as follows: (1) The diagonal entry Y_{ii} is equal to the sum of the component admittances connected to node i; (2) Off-diagonal entry Y_{ij} is the sum of component admittances/conductances connected between nodes i and j, multiplied by −1; (3) The heat source vector element Q_i is the sum of the heat sources (actual and equivalent) connected to node j (positive if directed to the node). As can be seen, for *linear* thermal

networks the admittance matrix has certain important characteristics: (1) it is symmetric, with all off-diagonal elements Y_{ij} being real, and equal to $-U_{ij}$ (conductance); (2) all capacitances and all self-admittances appear in the diagonal entries which are consequently complex, this being due to the fact that all energy storage elements are "connected" to the reference node. The transfer functions of interest are the elements of the inverse of **Y**, that is, the impedance transfer functions Z_{ij}. The temperature of node i for each frequency is given by:

$$T_i = \sum_{j=1}^{N} Z_{ij}Q_j \tag{2.12}$$

The room air temperature is determined for each frequency (harmonic) of interest by setting i to 1 in the equation. The functions Z_{ij} are determined at specific frequencies ($s = j\omega_n$) by inverting the admittance matrix **Y**. The room operative temperature, T_e is a scalar function of nodal temperatures ($T_1...T_8$).

Building transfer functions generally provide the response of interest - heat flow or temperature for unit heat input or unit temperature change at a node in the thermal network. The most important transfer function required in the present method is the impedance transfer function:

$$Z_{ij} = T_i/Q_j \tag{2.13a}$$

which represents the temperature change for node i due to unit heat input at node j for a given frequency. Thus for heat input Q_j, the room temperature change ΔT_1 (1 is the room air node number) is equal to:

$$\Delta T_1 = Z_{1j}Q_j \tag{2.13b}$$

It is often useful to not only determine a transfer function for individual room temperatures, but also a transfer function for an effective room temperature, such as the operative temperature (ASHRAE, 2009a). The operative temperature is defined as the uniform temperature of an enclosure in which an occupant would

exchange the same amount of heat by radiation plus convection as in the actual nonuniform environment; it is given by:

$$T_e = (h_r T_{mr} + h_c T_{ai})/(h_r + h_c)$$
(2.14)

where T_{ai} is the air temperature, T_{mr} is the mean radiant temperature, and h_r and h_c are radiative and convective coefficients for a person or object (sensor) respectively. The operative temperature transfer functions X_i are given by:

$$X_i = T_e/Q_i$$
(2.15)

and represent the effect of a source Q_i acting at node i on the operative temperature.

2.1.4.1 Analysis of Building Transfer Functions

Substantial insight into building thermal behavior *without simulation* may be obtained by studying the magnitude and phase angle of the important transfer functions. For example, consider the transfer functions Z_{11} and Z_{17} in the detailed model (Z_{11} and Z_{12} respectively in the simple model) which represent, respectively, the effects of heat sources at node 1 (room air) and node 7 (floor), on the temperature of node 1 (in both cases all other sources set to zero):

$$Z_{11}(s) = T_1(s)/Q_1(s)$$
(2.16)

$$Z_{17}(s) = T_1(s)/Q_7(s)$$
(2.17)

The magnitude of $Z_{17}(j\omega)$ may be used to determine the approximate room temperature swings due to solar radiation absorbed at the floor surface as follows:

If S_7 represents the solar radiation absorbed at the floor interior surface and $|S_7(j\omega_1)|$ represents the magnitude of its fundamental harmonic (for a period of one day), the approximate temperature swing amplitude is given by $|Z_{17}(j\omega_1)| \cdot |S_7(j\omega_1)|$. Another significant result is the time delay between the peak of $S(t)$ (noon for south-facing windows) and the resulting peak of the room temperature;

this is approximately equal to: φ_{17}/ω_1 (seconds) where φ_{17} is the phase angle of Z_{17} ($\varphi_{17} = \tan^{-1} \mathrm{Im}(Z_{17})/\mathrm{Re}(Z_{17})$).

Results

The room considered in the example has dimensions 7.3 m wide by 2.4 m high and the north-south depth is 6.7 m. The south-facing double-glazed window area is 11.1 m². The thermal mass is 4 cm thick concrete on the floor with thermal conductivity equal to 1.8 W/(m²·K), density 2242 kg/m³, and specific heat capacity 840 J/(kg·K). The interior lining on vertical walls and on the ceiling is a 13 mm thick gypsum board. The insulation is 3.5 RSI on vertical walls, 7.4 RSI on the ceiling and 1 RSI on the floor (connecting to a basement).

Figures 2.8 and 2.9 show the magnitude and phase variation (Bode plots) for the two cases of Z_{11}/carpeted floor and Z_{17}/concrete floor, including actual discrete frequency responses and fitted fourth-order transfer functions. Figures 2.8 and 2.9 show that the room response can be approximately separated into a short-term dynamics high-frequency range and a low-frequency range; in the high-frequency short-term dynamics region the room air thermal capacitance is significant and the difference between Z_{11} for the concrete floor and the carpeted one is small in both phase and magnitude. That is, the effect of thermal mass is minimal in this region. The separation between short-term and long-term building thermal dynamics begins at frequencies of approximately 35 cycles per day (cpd) or periods of about 40 minutes. More extensive studies (Athienitis, Stylianou, and Shou, 1990) for different constructions have produced similar results for Z_{11}, which represents the effects of convective heat gains or losses. Short-term dynamics are particularly important for feedback control studies. For lower frequencies such as one cycle per day the magnitude and phase of Z_{11} and Z_{17} is a strong function of room construction and there is a significant difference between the response of the massive (concrete) construction and the nonmassive one (carpet).
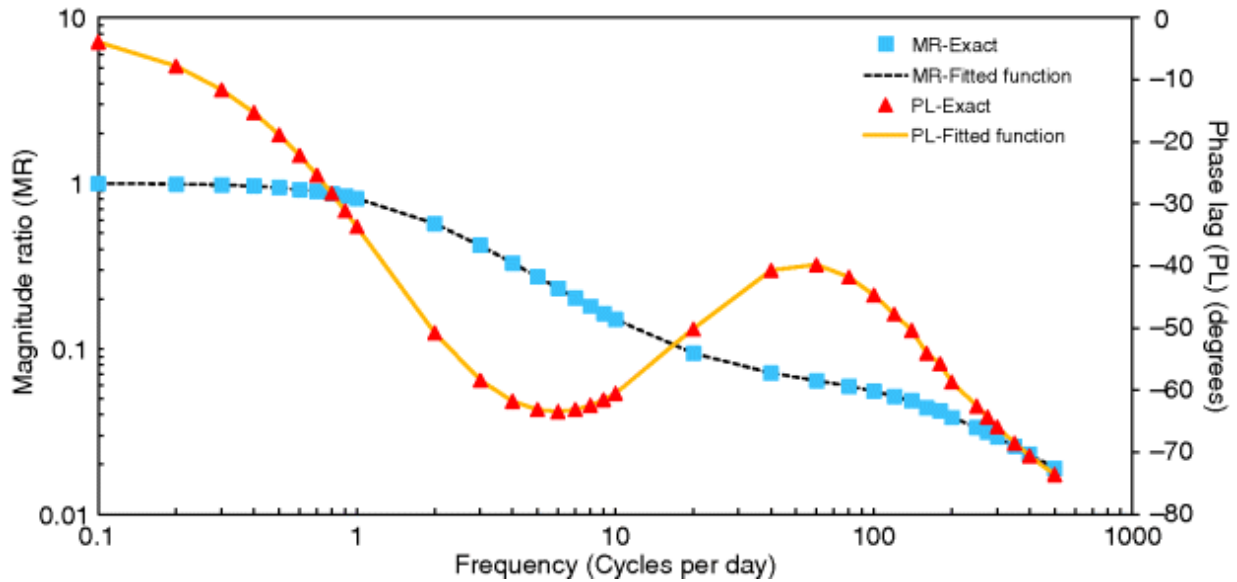
Fig. 2.8 Transfer function plots (magnitude and phase) for Z_{11}, carpeted floor (fitted fourth order transfer functions also shown) (Figure courtesy of Ali Saberi Derakhtenjani)
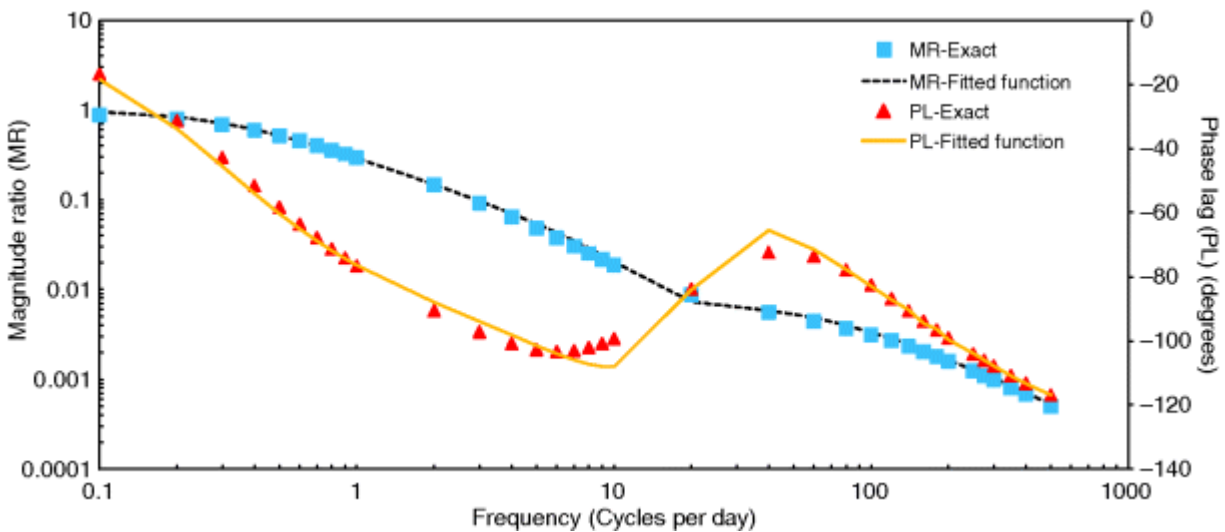
Fig. 2.9 Transfer function plots (magnitude and phase) for Z_{17}, concrete floor (fitted fourth order transfer functions also shown) (Figure courtesy of Ali Saberi Derakhtenjani)

An example of a fourth order fitted function for Z_{17} obtained with the above technique is given in Figure 2.9. As can be seen, this fit is good in both magnitude and phase, the error being less than 2% in the frequency range of interest. The fitted Laplace transfer function for Z_{17} is:

$$Z_{17} = \frac{-2.953 \times 10^{-7} s^4 + 6.858 \times 10^{-8} s^3 + 5.927 \times 10^{-9} s^2 + 8.545 \times 10^{-12} s + 1.154 \times 10^{-14}}{s^4 + 0.03168 s^3 + 0.0001071 s^2 + 7.077 \times 10^{-8} s + 1.516 \times 10^{-12}}$$

2.1.4.2 Heating/cooling Load and Room Temperature Calculation

Heating/cooling loads and associated room temperature calculations can be performed with the same building transfer functions employed in dynamic thermal control studies. These computations are performed by means of discrete Fourier series. The building transfer functions are calculated at discrete frequencies ($s = j\omega_n$) and a discrete Fourier transform (DFT) of the weather data and other inputs (e.g. internal gains) is performed. For example, for convective auxiliary heating we have:

$$Q_1 = q_{aux} + q_{int} + q_{eq} \tag{2.18}$$

where q_{int} represents the convective portion of internal gains and q_{eq} is an equivalent source representing heat flow due to infiltration and is given by $U_{inf} T_o$. Therefore, by substituting Eq. (2.12) into Eq. (2.18) and assuming that the room air temperature T_1 is specified, we may rearrange and determine the auxiliary heating/cooling power q_{aux} at each frequency of interest as:

$$q_{aux}(j\omega) = \frac{\left\{ T_1 - Z_{11} \left[q_{int} + U_{inf} T_o \right] - \sum_{j=2}^{N} Z_{1j} Q_j \right\}}{Z_{11}} \tag{2.19}$$

where all quantities are evaluated as complex numbers for $s = j\omega$ (N: number of nodes). Each source or specified temperature is represented by a discrete Fourier series and the time domain solution $q_{aux}(t)$ is obtained through an inverse discrete Fourier transform (IDFT). For design day analysis, 5–12 harmonics are usually adequate. These are the harmonics necessary for adequate representation of the inputs such as absorbed solar radiation, internal gains and ambient temperature T_o. One advantage of this approach over other methods is that the superposition principle is applied directly. Therefore, effects of various inputs may be studied separately, or a passive analysis ($q_{aux} = 0$) can be easily performed.

Note that the air temperature T_1 in Eq. (2.19) can be a profile, that is, it may vary with time. Thus, optimum setpoint profile variations may be determined to optimize solar gain utilization, such as in predictive control. The discrete Fourier series approach is described in more detail by Athienitis and Santamouris (2002), including a model for a proportional control source in the thermal network and a technique for modeling time-varying parameters, such as a conductance representing infiltration based on the substitution network theorem.

2.1.4.3 Discrete Fourier Series (DFS) Method for Simulation

Steady-periodic conditions are usually assumed in this method; for example, if the simulation is to be performed for a week, it is assumed that all previous weeks have been identical to the week considered. The steps needed for a periodic steady-state solution are as follows:

1. Select the number N of harmonics to perform the analysis. If n represents a harmonic number and P is the time length of the simulation or analysis (e.g., a day or a week), then a harmonic frequency ω_n is equal to $2\pi n/P$.

2. Obtain the appropriate discrete Fourier series representations for the sources. An arbitrary source $M(t)$ is represented by a complex Fourier series (inverse discrete Fourier transform) of the form:

$$M(t) = \sum_{n=-N}^{N} m_n(j\omega_n)\exp(j\omega_n t) \tag{2.20}$$

where the complex coefficients $m_n(j\omega_n)$ are determined numerically by a discrete Fourier transform as follows:

$$m_n = \frac{1}{P}\sum_{k=1}^{K} [M(t_k)\exp(-j\omega_n t_k)] \tag{2.21}$$

where $M(t_k)$ is the value of M at time t_k corresponding to point k (for a total of K values over the time period P). The number of harmonics N cannot exceed $K/2$.

3. Determine the discrete frequency response $Z(j\omega_n)$ of the output of interest to unit input at each node. The periodic response to each source is obtained by superposition of the output harmonics using complex (phasor) multiplication. The total response to more than one input is determined by a double summation for all inputs Q_i and all frequencies of interest ω_n. For example, for the room air temperature $T_1(t)$, we have:

$$T_1(t) = \sum_{n=-N}^{N} \left\{ \sum_{i=1}^{8} Z_{1i}(j\omega_n)Q_i(j\omega_n)\exp(j\omega_n t) \right\}$$

2.1.5 Building Transient Response Analysis

Transient thermal analysis of walls or zones may be performed with the following objectives:

1. Peak heating/cooling load calculations to size heating and cooling systems.

2. Calculation of dynamic temperature variation within walls, including solar effects, room temperature swings and condensation on wall interior surfaces; two-dimensional steady-state temperature profiles in walls (e.g., for investigation of thermal bridge effects).

For a multilayered assembly (wall or slab), an energy balance is applied at each node at regular time intervals to obtain the temperature of the nodes as a function of time. These equations may be solved with the implicit method as a set of simultaneous equations or with the explicit method in which we march forward in time from a set of initial conditions. Mixed differencing schemes are also often used in building simulation.

Here we consider the *finite-difference thermal network approach*. In this approach, each assembly layer is discretized (divided) into a number of sublayers (control volumes). Each control volume is represented by a *node* and is assumed to be isothermal. Each node (i) has a thermal capacitance (C_i) associated with it and resistances connecting it to adjacent nodes.

Transient thermal response analysis with finite difference techniques may generally provide a more accurate estimation of temperatures and heat flows due to the capability to model nonlinear effects such as convection and radiation. However, the initial conditions are usually unknown. Thus the simulation is repeated until a steady periodic response is obtained.

In the transient one-dimensional finite difference case we represent each assembly layer by one or more sub-layers (control volumes). Each control volume is represented by a central node with a thermal capacitance C connected to two thermal resistances, each equal to half the R-value of the layer. The energy balance for the thermal network is given by

$$T_{i,p+1} = \frac{\Delta t}{C_i} \left(q_i + \sum \frac{T_{j,p} - T_{i,p}}{R_{i,j}} \right) + T_{i,p} \tag{2.22}$$

Subscript i indicates the node for which the energy balance is written and j all nodes connected to node i, while p is the time interval; q_i represents a heat source at node i such as solar radiation or possible heat release in PCMs.

The time step (Δt) is selected based on the following condition for numerical stability:

$$\Delta t \leq \min_{i} \left(\frac{C_i}{\sum_j (1/R_{i,j})} \right) \tag{2.23}$$

for all nodes i; the summation is performed for all nodes j connected to the node i.

The explicit finite difference method is particularly suitable for modeling of nonlinear heat diffusion problems such as the heat transfer through phase change materials. It can easily accommodate nonlinear heat transfer coefficients and control actions.

2.1.5.1 Nomenclature

Symbols

$u(t)$	input signal
$y(t)$	output signal
$U(z)$	Z-transform of $u(t)$
$Y(z)$	Z-transform of $y(t)$
T_i, T_o	temperatures of the inside and outside air surrounding the wall
$T_i(z)$ and $T_o(z)$	z-transform of the temperatures T_i and T_o
A, B, C, D	coefficients of the wall conduction matrix
$q'(t)$	indoor heat flux at the current time
A	indoor surface area of a wall
N_{MAX}	number of used coefficients
Δt	time step
$T_{\text{sol-air}}$	sol-air temperature representing outdoor conditions
T_{indoor}	indoor temperature (assumed constant)
P	number of poles

2.2 Renewable Energy Generation Systems/Technologies Integrated in Net ZEBs

Renewable energy generation systems and technologies commonly integrated in Net ZEBs, including the following, are reviewed here.

- Building-integated photovoltaics and their integration
- Solar thermal systems
- Active building-integrated thermal storage
- Heat pump systems
- Combined heat and power systems.

2.2.1 Building-Integrated Photovoltaics as an Enabling Technology for Net ZEBs

Building-integrated photovoltaics (BIPV) are photovoltaic modules that are architecturally and functionally integrated into the building envelope,[6] replacing conventional and/or premium building materials, such as roof shingles, wall cladding, windows, and overhangs (Montoro, Vanbuggenhout, and Ciesielska, 2011). Unlike rack-mounted PV systems, BIPV is a multifunctional technology. Thus, in addition to generating electricity, BIPV can also act as a weather and noise barrier, may be used to generate useful heat (BIPV/thermal – BIPV/T), and possibly allow daylight transmission (semitransparent PV – STPV), ultimately capable of "converting" up to about 80% of the incident solar radiation into useful energy (electricity, heat, and transmitted daylight) (Figure 2.10). BIPV is expected to be the main technology for generating on-site electricity in net-zero energy buildings since it can be utilized to cover large roof and façade surfaces. For this to be done effectively, the orientation and shape of the main equatorial-facing surfaces must be optimized.
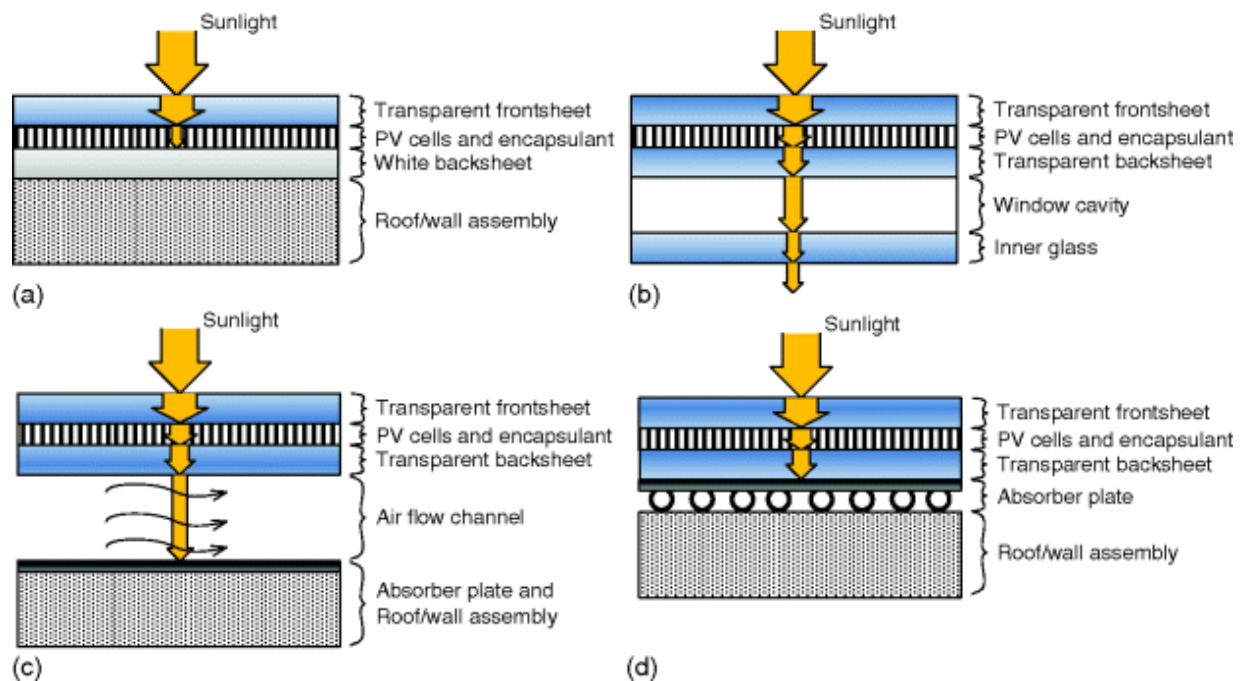
Fig. 2.10 Example schematics for (a) BIPV, (b) STPV, (c) BIPV/T air-based, and (d) BIPV/T water-based systems (not to scale)

BIPV does not need extra land for its installation, avoiding the use of valuable land and green space. On a community scale, BIPV provides distributed electricity generation that can contribute toward grid "peak demand shaving," which can help reduce power generation during peak periods, particularly when space cooling is required. During periods when excess electricity is produced that cannot be absorbed by the grid, it can be used to power water heaters, chillers or heat pumps to store heat or cold (such as chilled water or ice). In commercial building BIPV applications, on-site electricity generation can meet a portion of the daily electricity demand, while eliminating grid distribution losses associated with transporting the same quantity of electricity over long distances from power plants.

2.2.1.1 Technologies

BIPV Components

PV modules used for commercial, industrial or residential BIPV applications consist of three main layers: a highly transparent frontsheet, the PV cell layer and the backsheet. The PV cell layer is sandwiched between the frontsheet and the backsheet. Solar radiation incident on the module's surface is transmitted through the transparent frontsheet, captured and converted into electricity by the PV cell layer. Typical frontsheets are clear low-iron (low-Fe) glass with antireflective coating or polymer sheet, such as ethylene tetrafluoroethylene (ETFE). Polymer frontsheets are significantly lighter and thinner than glass frontsheets, while still maintaining high mechanical and impact strength.

The PV cell layer consists of PV cells connected in series and/or parallel and encapsulated for structural stabilization and protection against weathering and humidity. Typical encapsulation resins used are ethylene vinyl acetate (EVA) and polyvinyl butyral (PVB). Currently commercially available PV modules can convert between 5 and 21% of the incident solar radiation into electricity. The rest of the absorbed solar energy is converted into heat and contributes to increase the temperature of the cells. As the cell temperature increases, the diffusion current on the cells increases, leading to a reduction of the charges at the edges of the cells. As a result, the open-circuit voltage significantly decreases, while the short-circuit

current slightly increases, causing an overall reduction of the module power output. Since PV cell efficiency generally decreases as their temperature increase, this overheating is usually undesirable. Depending on the technology, the efficiency of PV modules can be affected at a rate of as much as −0.53%/°C; a rise in temperature of about 20 °C can result in about 10% reduction of electricity production.

Depending on the application, the backsheet can be either highly reflective to reduce excessive heat gains and PV cell temperature or highly absorptive and possibly transparent when heat gains are beneficial for heat recovery (e.g., BIPV with heat recovery). Typical backsheets found in the market are made from polyvinyl fluoride (PVF) and polyvinylidene fluoride (PVDF).

PV modules used for BIPV applications are commonly frameless because they form the outermost layer of a multi-layer assembly (e.g., window, wall cladding, curtain wall assembly). However, framed PV modules can be used in other building-integrated products such as exterior shading devices and canopies. A junction box located either on the back or the edge of the module allows interconnection of modules and the balance-of-system (Norton *et al.*, 2011).

BIPV with Heat Recovery (BIPV/T)

In building-integrated photovoltaics with heat recovery (BIPV/T), the absorbed solar energy that is converted into heat is recovered either actively, using a fan or pump, or passively by a heat removal fluid (HRF) flowing on the rear side of the PV layer. As the fluid circulates behind the PV module, it cools down the cells through convection, reducing the PV cell temperature and increasing the electrical efficiency. The main advantage of BIPV/T compared to side-by-side BIPV and solar thermal technologies is that generally, they require less surface area to produce the same amount of thermal and electrical energy. In the context of designing net-zero energy buildings where a limited amount of building surface area with solar potential is available, this benefit can be substantial.

BIPV/T systems can be separated into two main categories: air-based or water-based (Figure 2.11) depending on the heat removal fluid

used. BIPV/T-air systems have typically lower thermal efficiencies than water-based systems due to the poor thermo-physical properties of air compared to water (Tripanagnostopoulos, 2012) and need heat transfer enhancement measures (fins or roughness elements added at the back of the PV module). Air-based systems, however, do not require any significant maintenance because air leakage is not as critical as in liquid systems (where the liquid needs to be also periodically replaced or drained). In BIPV/T systems, the thermal energy recovered can be used for water and space heating either directly or indirectly (for example, indirectly using a heap pump). Depending on the HRF temperature, BIPV/T can be categorized as low-temperature (<60 °C) or high-temperature (>60 °C) systems. In commercial, multiresidential or industrial buildings, low-temperature, open-loop BIPV/T-air systems can be used to reduce space heating energy consumption by preheating the fresh air entering the HVAC system. Closed-loop BIPV/T-air or BIPV/T-water high-temperature systems can be used for domestic hot water heating, where higher outlet temperatures are required. Nevertheless, the PV cell temperatures are generally higher than in an open-loop system resulting in a lower electrical performance and accelerated PV module deterioration.
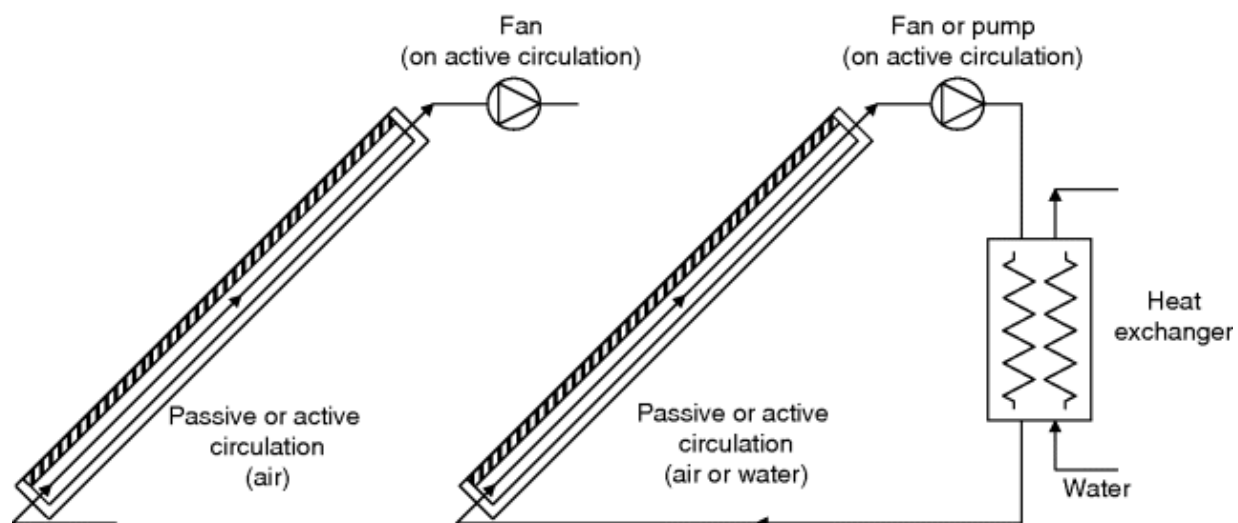
Fig. 2.11 Open-loop and closed-loop BIPV/T configurations

The economics of building integrated solar systems, such as BIPV/T, are complex. The upstream value chain of BIPV/T follows the sequence silicon-ingot-wafer-cell-module-PV system-building

envelope integration–HVAC system integration. The last two steps distinguish BIPV/T from BIPV systems and the value of the system is strongly linked with and affects the value of the building and its HVAC system. For example, the John Molson School of Business (JMSB) building at Concordia University in Montreal (latitude 45°N) has a BIPV/T system with peak electrical and thermal production of 25 kW and 75 kW, respectively (Figure 2.12a and b) covering a façade area of about 288 m²; it integrates unglazed transpired air collector with specially designed PV panels with black framing (to enhance fresh air preheating in winter) and covers about 70% of the area.
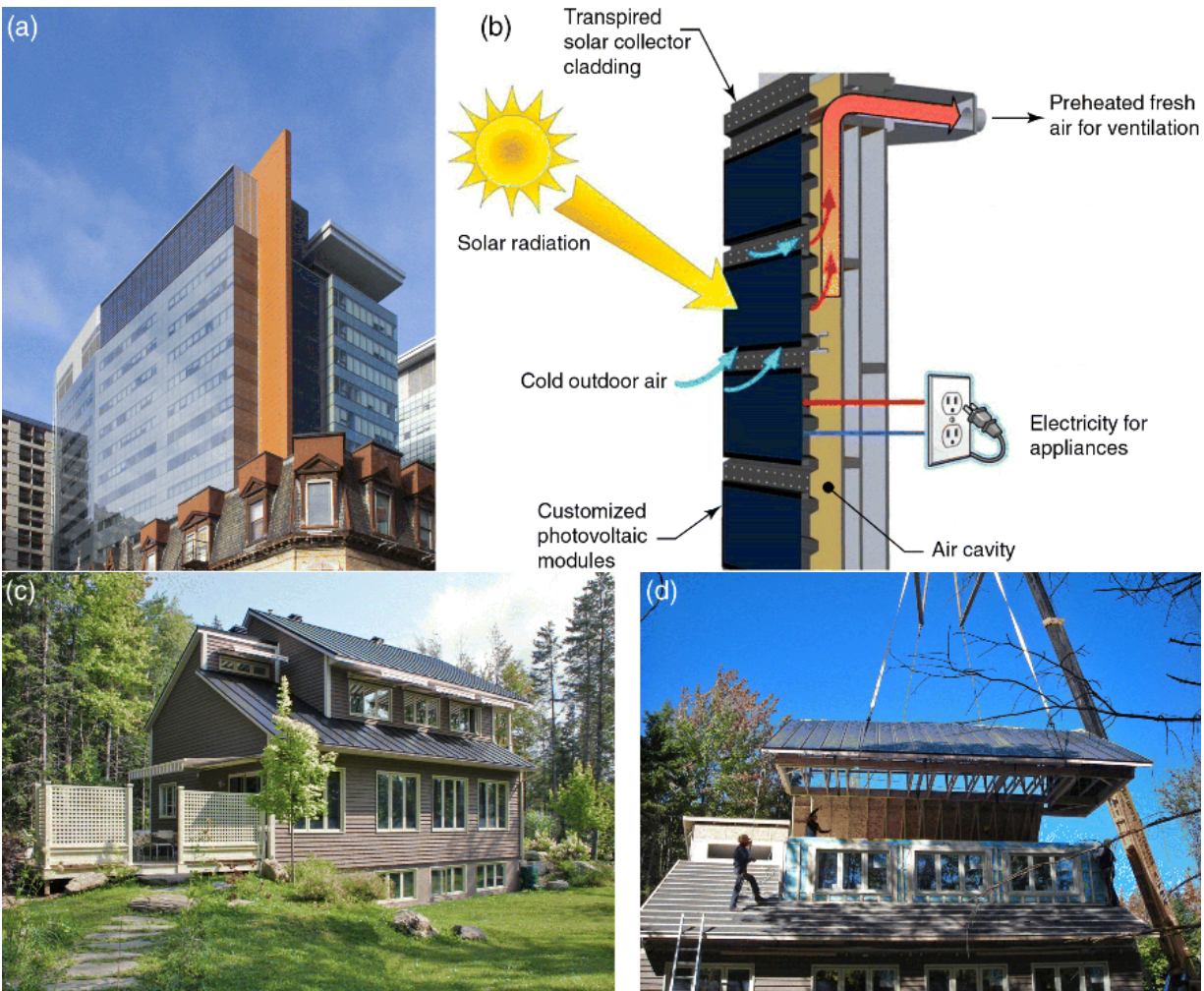
Fig. 2.12 (a) JMSB building BIPV/T façade (top, blue rectangular area) (Photo: Samson Yip) and (b) its schematic (Athienitis *et al.*, 2011), (c) ÉcoTerra Home (Photo courtesy of Agnieszka Koziol) and (d) its BIPV/T modular roof (Chen, Athienitis, and Galal, 2010a)

In such systems, major reductions in installation and system costs may be achieved by adopting curtain wall technology where 2 to 3 storey-high PV panel sections are mounted and prewired in a factory environment. This strategy was used to build the ÉcoTerra Home BIPV/T roof module (Figure 2.12c and d).

Special heating and cooling systems need to be designed to effectively use the heat recovered from BIPV/T systems and make them more affordable. Depending on the climate, operating conditions and design, BIPV/T systems can produce 2 to 4 times more heat than electricity. Thus, in addition to electricity pricing schemes and incentive measures, the relative values of thermal and electrical energy strongly affects the economics of BIPV/T systems. The design of BIPV/T systems usually requires the participation of the building designers to ensure that the systems are properly integrated with the building envelope design and with the HVAC system. Special considerations are also needed for retrofit applications.

Semitransparent PV (STPV)

Semitransparent PV is another type of BIPV system that can replace conventional windows and skylights in both commercial and residential buildings. In most commercial buildings, where reduction of cooling energy costs is important, double glazing with low-emissivity coatings is generally adopted to reduce heat transfer by longwave radiation. The outer glass layer often includes a tint to reduce transmission of solar radiation. Rather than having a tint or using ceramic frit on the outer glass to reduce solar transmittance, a STPV glazing may be used to reduce solar heat gains and generate solar electricity, while providing adequate daylighting and views to the outdoors. In residential buildings, STPV modules can be used in skylights or adjacent solaria and greenhouses. Commercially available STPV products use different PV cell technologies, from spaced opaque crystalline silicon cells to thin-film transparent PV cells (Figure 2.13), with the latter creating a uniform coverage on the window surface.
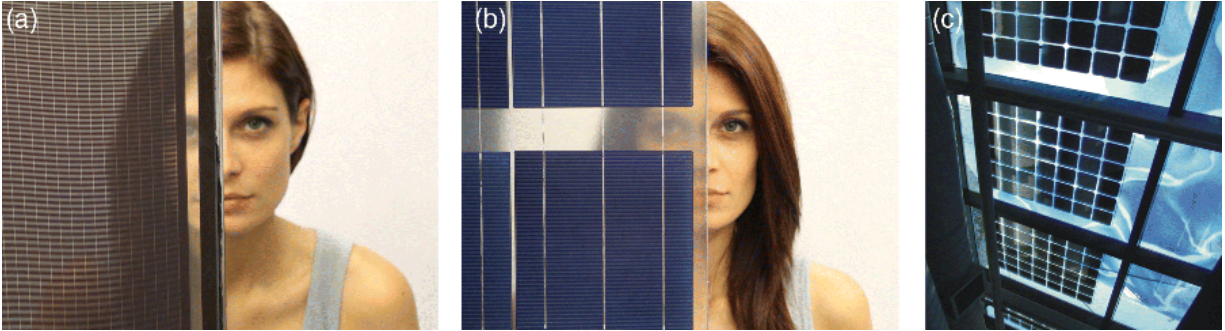
Fig. 2.13 (a) Micromorph (thin film transparent) STPV module; (b) poly-Si (spaced opaque cells) STPV module; (c) retrofit STPV installation at the Enwave theater (Toronto, Canada) (Image courtesy of Internat Energy Solutions Canada)

2.2.1.2 Modeling

In addition to electricity generation, BIPV systems can produce useful heat (BIPV/T) and/or possibly provide natural daylight (STPV). Various models have been developed to predict the electrical, thermal, and daylight potential of BIPV systems, with various degrees of accuracy and modeling approaches: analytical, numerical, and empirical.

Modeling the Electrical Performance

Several models can be used to estimate the electrical performance of PV systems (Skoplaki and Palyvos, 2009). One of the simplest models assumes that the efficiency of a PV module operating at the maximum power point is linearly dependent on the PV cell temperature:

$$\eta_{mp} = \eta_{mp,ref}\left[1 + \mu_{P,mp}(T_{PV} - T_{ref})\right] \text{ and } P_{PV} = \eta_{mp} \cdot G \quad (2.24)$$

where T_{PV} is PV cell temperature (K), T_{ref} is PV cell temperature under reference conditions (K), $\eta_{mp,ref}$ is PV module efficiency under reference conditions[7], η_{mp} is photovoltaic module efficiency, $\mu_{P,mp}$ is maximum power point efficiency temperature coefficient (%/K), P_{PV} is photovoltaic module power output at maximum power point (W) and G is total incident solar radiation (Wm^{-2}).

The maximum power point efficiency temperature coefficient ($\mu_{P,mp}$) is specific to every module, is empirically determined, and is provided by the manufacturer (Table 2.1). Such models are generally used in prefeasibility tools like RETScreen (NRCan, 2010).

Table 2.1 Typical module efficiencies (η_{mp}) and maximum power point efficiency temperature coefficients ($\mu_{P,mp}$) for various BIPV technologies

Crystalline silicon cells	$\mu_{P,mp}$ (%/K)[8]	η_{mp} (%)
mono-Si	−0.24 to −0.48	13.5 (PikeResearch, 2012)
poly-Si	−0.41 to −0.50	12 (PikeResearch, 2012)
Silicon Heterostructures (HIT)	−0.3	18.3
Thin film		
a-Si	−0.21 to −0.28	7 (PikeResearch, 2012)
Micromorph	−0.20 to −0.36	9
$Cu(In,Ga)Se_2$ (CIGS)	−0.31 to −0.53	16.6 (PikeResearch, 2012)
CdTe	−0.25	11.7 (PikeResearch, 2012)
Organic (OPV)	+0.05	5 (PikeResearch, 2012)

Other electrical models include the equivalent one-diode model (Duffie and Beckman, 2006) and King's model (King, Boyson, and Kratochvil, 2004). As the model becomes more complex, its accuracy tends to be better, but the number of required parameters increases. In addition to incident solar radiation, models typically require the PV cell temperature and a number of empirically determined parameters available in databases or provided by manufacturers.

A widely used model that is implemented in several simulation tools, such as PVsyst (2012) and EnergyPlus, is the equivalent one-diode

model.

This model requires as inputs the open circuit voltage (V_{oc}), short-circuit current (I_{sc}), current (I_{mp}), and voltage (V_{mp}) at maximum power point as well as the temperature coefficients for short-circuit current ($\alpha_{I,sc}$) and open-circuit voltage ($\beta_{V,oc}$), under reference conditions. These parameters can be found in manufacturer technical specification sheets.

The module current (I) is the resultant of the photo current (I_{ph}), the equivalent diode current representing the voltage-dependent current lost to recombination (I_D), and the parasitic shunt current (I_{sh}). In order to determine the PV performance under operating conditions, the diode reverse saturation current (I_o), the series resistance (R_s), the shunt resistance (R_{sh}), and the curve fitting parameter (a) should be obtained. These parameters depend on solar radiation and PV cell temperature. At a specific temperature and solar radiation level, the current–voltage (I–V) characteristics of a PV module, approximated by the one-diode model (Figure 2.14), is given by

$$I = I_{ph} - I_D - I_{sh} = I_{ph} - I_o\left(e^{\frac{V+IR_s}{a}} - 1\right) - \frac{V + IR_s}{R_{sh}} \tag{2.25}$$
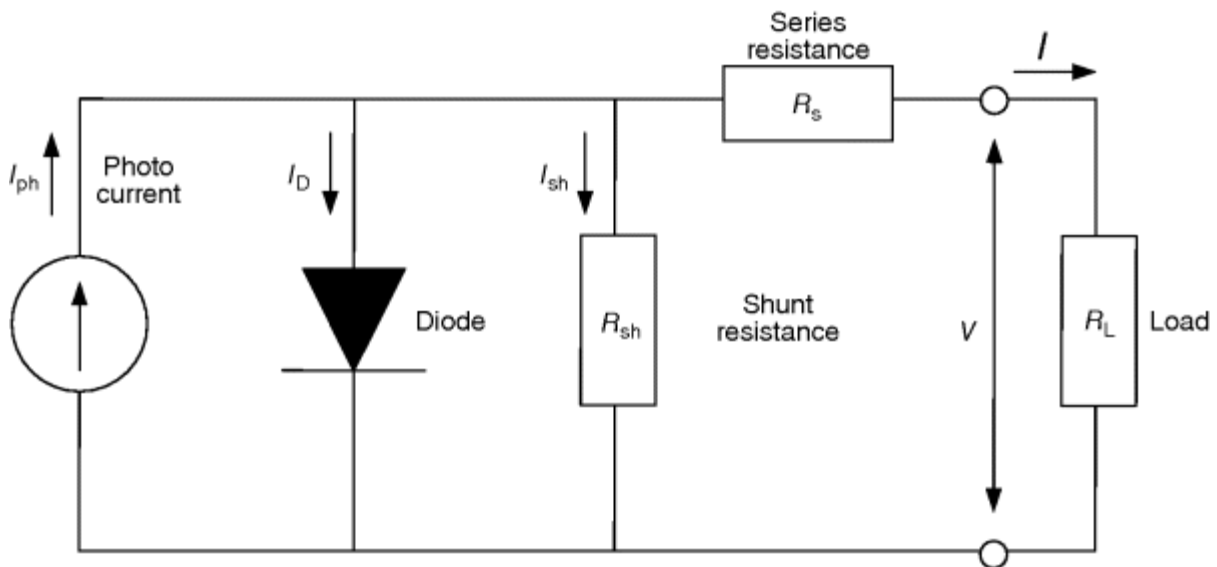
Fig. 2.14 Equivalent circuit for the one-diode model

The power is calculated as the product of the current, I and voltage, V:

$$P = IV \qquad (2.26)$$

To obtain the PV module maximum power point, the following equations must be solved:

$$\frac{I_{mp}}{V_{mp}} = \left[\frac{(I_o/a)\exp[(V_{mp} + I_{mp}R_s)/a] + (1/R_{sh})}{1 + (R_s/R_{sh}) + (I_oR_s/a)\exp[(V_{mp} + I_{mp}R_s)/a]} \right] \qquad (2.27)$$

$$I_{mp} = I_{ph} - I_o \left(e^{[(V_{mp} + I_{mp}R_s)/a]} - 1 \right) - \frac{V_{mp} + I_{mp}R_s}{R_{sh}} \qquad (2.28)$$

Equation (2.27) is obtained by differentiating Eq. (2.26) with respect to V and setting the result equal to zero, and Eq. (2.28) is obtained by substituting I and V by their respective value at maximum point (I_{mp} and V_{mp}) in Eq. (2.25). The detailed equations necessary to obtain the five unknown parameters (I_{ph}, I_o, R_s, R_{sh}, and a) can be found in books such as "Solar Engineering of Thermal Processes" (Duffie and Beckman, 2006).

Modeling the Thermal Performance

Predicting the PV cell temperature is essential as it affects the module electrical efficiency. The European Union project PVSAT-2 (2006), aiming at establishing the performance of PV system operation based on satellite data, used the following relation to estimate the PV cell operating temperature:

$$T_{PV} = T_a + C \cdot G \qquad (2.29)$$

where C is an empirically determined coefficient (0.058 for a roof-integrated installation) (m² KW^{-1}) (Drews $et\ al.$, 2007), G is total incident solar radiation (Wm^{-2}), and T_a is ambient temperature (K).

King, Boyson, and Kratochvil (2004) developed a more accurate (less than 3% effect on module power output) empirically based thermal model to predict PV cell temperature that takes into account the

effect of wind speed and the temperature gradient between the backsheet of the module and the actual PV cells:

$$T_{\mathrm{PV}} = T_{\mathrm{a}} + Ge^{(C_1 + C_2 \cdot V)} + (G/G_0)\Delta T \qquad (2.30)$$

where G_0 is the reference total incident solar radiation (1000 $\mathrm{Wm^{-2}}$), V is the wind speed measured at standard height of 10 m ($\mathrm{ms^{-1}}$), C_1 is the empirically determined coefficient expressing the upper limit for module temperature at low wind speeds and high solar irradiance (−2.98 for a glass/cell/glass, close roof mount module and −2.81 for a glass/cell/polymer, insulated-back module), C_2 is the empirically determined coefficient expressing the rate at which module temperature drops as wind speed increases (−0.0471 for a glass/cell/glass, close roof mount module and −0.0455 for a glass/cell/polymer, insulated-back module), and ΔT is the temperature difference between the cells and the module backsheet, under 1000 $\mathrm{Wm^{-2}}$ (1 K for a glass/cell/glass, close roof mount module and 0 K for a glass/cell/polymer, insulated-back module).

The temperature of PV cells can be estimated using finite difference models. This approach is useful when empirical coefficients for the specific module configuration cannot be obtained. It is also essential when additional information other than the cell temperature is required, such as the thermal output of a BIPV/T system or energy flow through an STPV system to the adjacent space. This method requires that the properties of each layer are known (or estimated); the method is applicable to any BIPV configuration. An energy balance is applied for each layer, taking into account radiative, convective, and conductive heat exchanges between layers and the environment. The models can be steady-state or dynamic and can be one, two or three dimensional. For BIPV systems without any heat recovery, a one-dimensional model in the direction normal to the collector surface is generally sufficient.

In BIPV/T systems, a significant temperature gradient exists in the direction of the heat removal fluid flow. For most purposes a one-dimensional model is still sufficient, but the collector is usually divided into a number of control volumes in the direction of the flow in order to obtain a better approximation of the temperature of the

fluid and PV cells. The choice of a steady-state or dynamic model is based on the level of resolution required. For daily or annual yield, a steady-state model is comparable to a dynamic model for a sheet-and-tube PV/T (Zondag *et al.*, 2002).

Figure 2.15 represents a simple one-dimensional finite difference model for a BIPV/T system (air system) with a possible STPV layer. In this system, it is assumed that (i) the various layers of the PV module are thin enough so their heat capacity can be neglected, and (ii) the PV module has uniform properties. The energy and mass balance (per unit area), for the n-th control volume, are given by
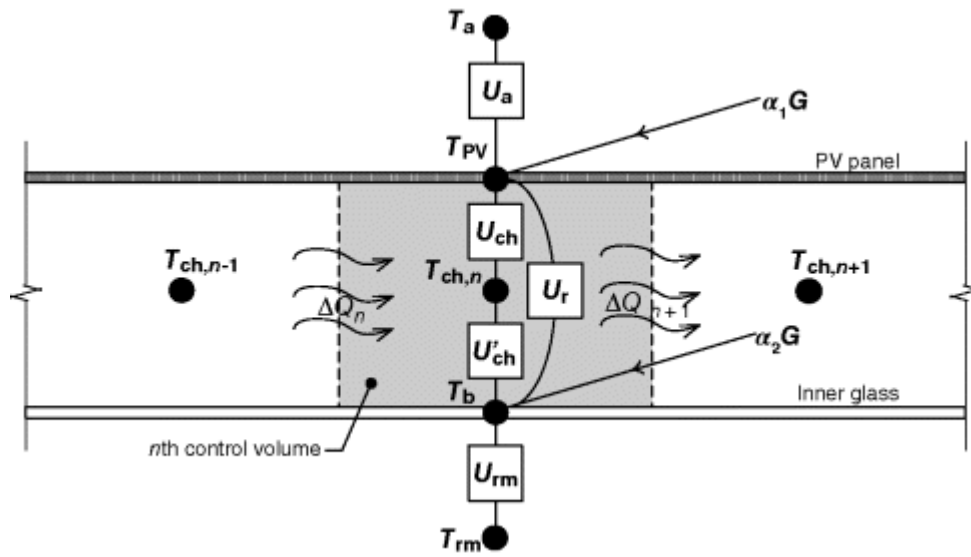
Fig. 2.15 Simplified, steady-state, finite difference model for an air BIPV/T system with possible STPV

PV module

$$U_a(T_a - T_{PV}) + \alpha_1 G - \eta_{mp} G = U_{ch}(T_{PV} - T_{ch,n}) + U_r(T_{PV} - T_b) \qquad (2.31)$$

Heat removal fluid channel (assumed to be air)

$$U_{ch}(T_{PV} - T_{ch,n}) + U'_{ch}(T_{ch,n} - T_b) = mc_p(T_{ch,n-1} - T_{ch,n}) \qquad (2.32)$$

Inner glass

$$U'_{ch}(T_{ch,n} - T_b) + U_r(T_{PV} - T_b) + \alpha_2 G = U_{rm}(T_b - T_{rm}) \qquad (2.33)$$

The optical properties of an *N*-layer STPV/T can be approximated by (International Organization for Standardization (ISO, 2003))

$$\tau_{i,j} = \tau_{i,j-1}\tau_{j,j}/(1 - \rho^f_{j,j}\rho^b_{j-1,i})$$

$$\rho^f_{i,j} = \rho^f_{i,j-1} + \tau^2_{i,j-1}\rho^f_{j,j}/(1 - \rho^f_{j,j}\rho^b_{j-1,i})$$

$$\rho^b_{j,i} = \rho^b_{j,j} + \tau^2_{j,j}\rho^b_{j-1,i}/(1 - \rho^f_{j,j}\rho^b_{j-1,i})$$

$$\alpha_j = \tau_{1,j-1}(1 - \tau_{j,j} - \rho^f_{j,j})/(1 - \rho^f_{j,N}\rho^b_{j-1,1}) + \tau_{1,j}\rho^f_{j+1,N}(1 - \tau_{j,j} - \rho^b_{j,j})/(1 - \rho^f_{j,N}\rho^b_{j-1,1})$$

where $\tau_{i,j} = 1$ and $\rho_{i,j} = 0$ if $i < 0$ or $j > N$

In the previous equations, i is the outermost layer (e.g., PV module) and j is the innermost layer (e.g., inner glass) of the *N*-layer assembly (for this example, $N = 2$), $i,j = 1,2...N$; A_{PV} photovoltaic module area (m²); m mass flow rate (kgs⁻¹); c_p specific heat capacity (Jkg⁻¹K⁻¹); α_j solar absorbance of layer j; $\tau_{i,j}$ solar transmittance through layers i to j; $\rho^f_{i,j}$ front (toward outside) solar reflectance from layers i to j; $\rho^b_{i,j}$ back (toward inside) solar reflectance from layers i to j; T_b, T_{rm} surface temperature of the inner glass and room air temperature, respectively (K); $T_{ch,n-1}$, $T_{ch,n}$ average heat removal fluid temperature of the $(n - 1)$-th control volume and the n-th control volume, respectively (K); U_{ch}, U'_{ch} convective conductances due to heat removal fluid (Wm⁻² K⁻¹); U_r radiative conductance between PV panel and inner glass (Wm⁻² K⁻¹); and U_a, U_{rm} combined (radiative and convective) conductance between, PV and ambient environment and, inner glass and room, respectively (Wm⁻² K⁻¹).

Alternatively, an *approximate analytical solution may be obtained for a control volume in a BIPV/T or PV/T open loop air system* as follows, assuming the average convective heat transfer coefficient h_{ch} corresponds to conductances U_{ch} and U'_{ch}. Note that the convective coefficient h_{ch} is an average for both cavity surfaces (in reality it will generally be higher on the upper surface).

The average channel air temperature T_{ch} is determined from a differential analysis, which finds the air temperature as a function of distance x along the flow path. It is assumed that the air speed is constant, and the, air is drawn by a fan (as fresh air or connected to a heat exchanger or an air-to-water heat pump). The actual air temperature $T_{ch}(x)$ is then used to determine T_{ch}. This is then employed to find the correct values of T_{PV} and T_b, which are utilized to fine-tune the calculations. Considering an element dx in the flow direction, we have

$$M \cdot c_p \cdot \rho \cdot \Delta T_{ch} = W \cdot h_{ch} \cdot dx \cdot [T_{PV} - T_{ch}] + W \cdot h_{ch} \cdot dx \cdot [T_b - T_{ch}]$$

where the air flow rate is equal to $M = V_{ch} \cdot A_{ch}$.

The following ordinary differential equation is obtained:

$$C \frac{d}{dx} T_{ch} + 2T_{ch} = T_{PV} + T_{in}$$

where $C = \frac{M \cdot c_p \cdot \rho}{W \cdot h_{ch}}$; A_{ch} is the average cross-section channel area (m²); V_{ch} is the average air velocity in the channel (ms⁻¹); W is the width of the air channel (m); x is the coordinate in the fluid flow direction (m); and ρ is the air density (kg m⁻³).

The air temperature variation inside a control volume can be calculated using Eq. (2.34) once the inlet air temperature T_{in} is known.

$$T_{ch}(x) = \frac{T_{PV} + T_{in}}{2} + \left[T_a - \frac{T_{PV} + T_b}{2} \right] e^{-\frac{2x}{C}} \qquad (2.34)$$

The PV and glazing or back side temperatures are obtained as

$$T_b = \frac{U_{ch}T_{ch} + U_{rm}T_{rm} + U_r T_{PV}}{U_b + U_{rm} + U_r}$$

$$T_{PV} = \frac{U_a T_a + U_{ch}T_{ch} + U_r T_b + S_{PV}}{U_a + U_{ch} + U_r}$$

where $S_{\mathrm{PV}} = (A_{\mathrm{PV}}\alpha_1 G - P_{\mathrm{PV}})$. A roof or façade section may be split into a number of control volumes in which the solution is applied to each individual one where the outlet temperature of one control volume is the inlet temperature for the next one.

2.2.2 Solar Thermal Systems

Solar thermal systems consist primarily of collectors, thermal storage tanks, heat exchangers, and distribution systems. See Figure 2.11 for example.

2.2.2.1 Solar Thermal Collectors

Solar thermal collectors convert absorbed solar radiation to useful thermal energy for domestic hot water, space heating, or industrial processes. A collector mainly consists of an absorber that absorbs solar radiation and transfers it to a working fluid that can be used directly or indirectly in the thermal process. Different types of solar thermal collectors are available on the market: unglazed transpired collectors (UTCs), flat plate collectors, vacuum collectors, and concentrating solar collectors.

Unglazed Transpired Collectors

Unglazed transpired collectors are mainly used for solar air preheating in ventilation systems, as well as in applications such as drying. The JMSB BIPV/T system described in the previous section uses an UTC system with specially designed PV panels and attachment brackets to preheat fresh air for the building in winter, while generating electricity.

Flat Plate Collectors

These are the most commonly used in building energy applications. For the same overall configuration, flat plate collectors can have water or air as a working fluid. Air collectors can be open loop or closed loop.

A flat plate collector (Figure 2.16) consists of a transparent cover system, an absorber, insulation, and a frame. Almost all solar radiation passing through the cover is captured by the absorber

plate. A working fluid circulating in tubes integrated to the absorber collects the heat.
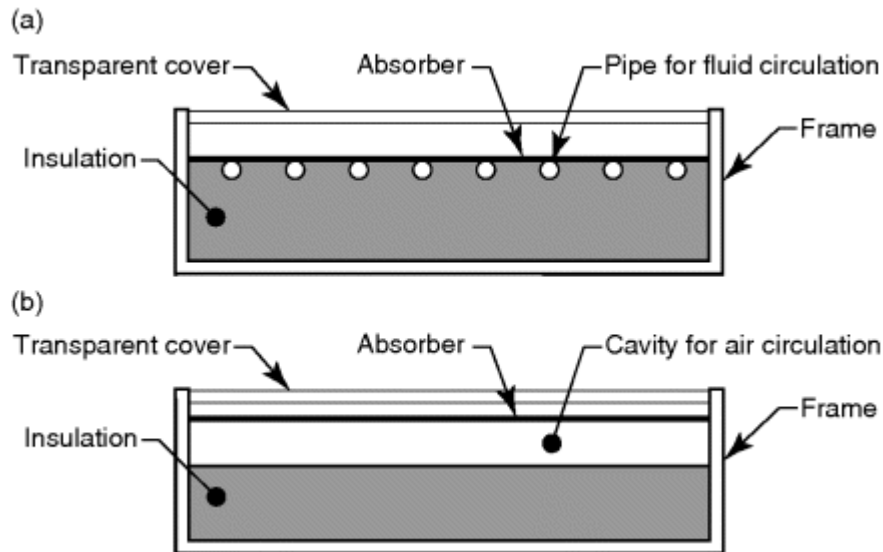
Fig. 2.16 Schematic of a flat plate collector: (a) liquid-based; (b) air-based

The cover should be as transparent as possible to short wavelength solar radiation (e.g., low-iron glass with antireflective coating) and possibly have a low-emissivity coating to reduce energy losses. The absorber has a high solar absorptance and a low emissivity; it generally undergoes a chemical treatment and is covered with a special coating, which enhances the solar absorption and reduces the longwave radiation emission. At the back of the absorber, a layer of insulation reduces back heat losses.

The collector heat losses also depend on outside temperature and wind conditions. To limit losses by convection, double glazing may be used to replace the simple transparent cover to improve performance; the cost of this change is the reduced overall transmittance–absorptance product of the collector.

In flat plate collectors using water as a working fluid, a pump is used to circulate the fluid through tubes integrated at the back of the absorber. The fluid collects the energy from the absorber and carries it to the desired application (DHW or space heating). In collectors using air as a working fluid, air circulates in the space between the absorber and the insulation and collects the energy of the absorber. A fan is used to circulate the air.

Vacuum Solar Collectors

To reduce convective and conductive heat losses through the transparent cover and insulation, vacuum tube collectors have been developed. A thin absorber is placed in a transparent vacuum cylinder. Its surface is covered with a coating to reduce its emissivity and significantly increase its absorptance. Incident solar radiation through the transparent glass cylinder reaches the absorber and heats it up. Generally, two methods are used to extract energy:

1. By a heat pipe welded to the absorber (heat pipe vacuum tube collectors)
2. By a fluid flowing in a tube welded to the absorber (direct flow vacuum tube collector).

In a heat pipe vacuum tube collector (Figure 2.17), a tube containing a vaporizable fluid is welded to the bottom of the absorber. The upper end of the tube is connected to a condenser. As the sun shines on the absorber, the fluid inside the heat pipe vaporizes and rises along the tube to the condenser. Through the condenser, the working fluid recovers the energy from the liquefied fluid of the heat pipe, which in turn descends by gravity to evaporate again and repeats its cycle.
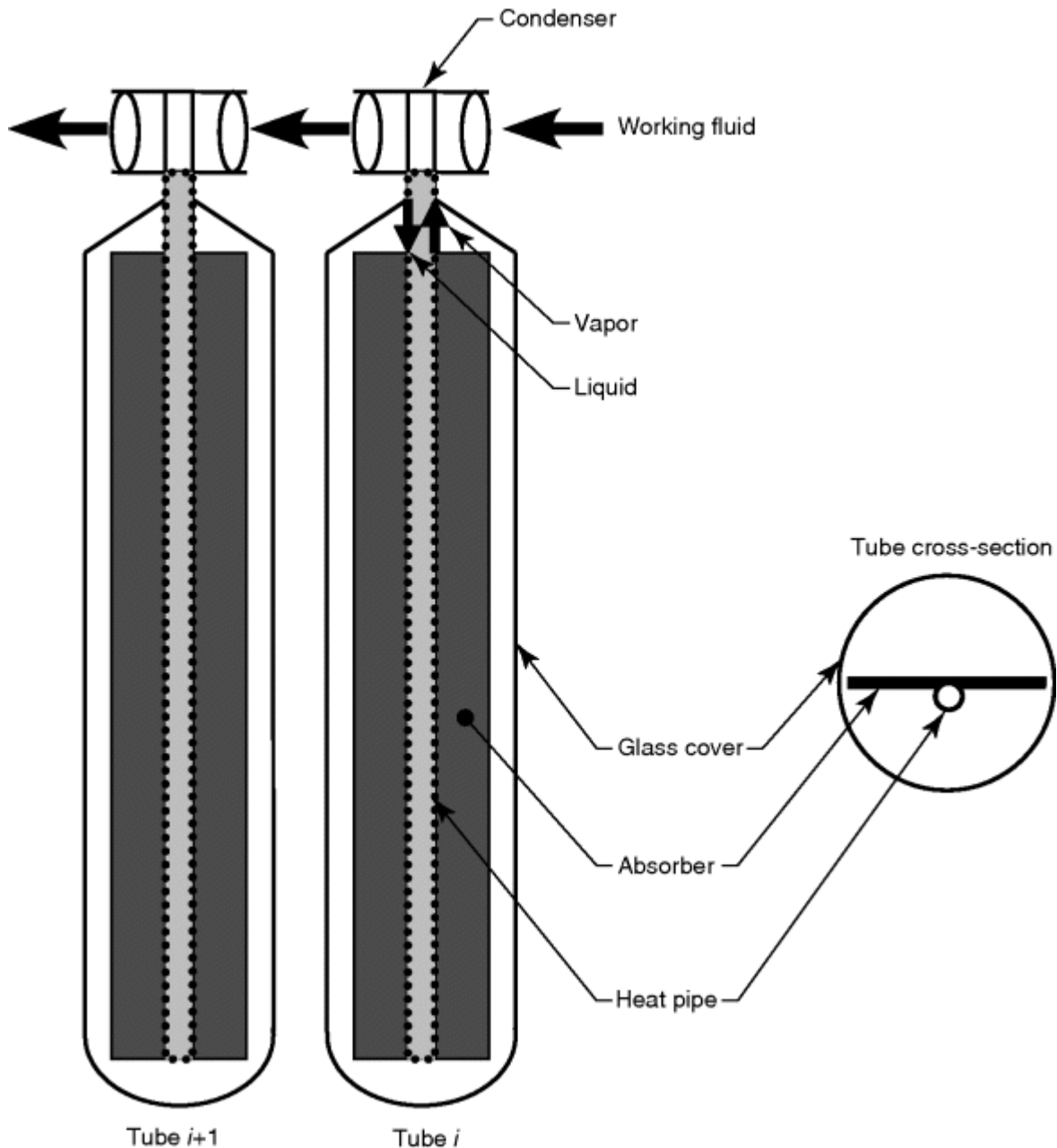
Fig. 2.17 Schematic of a vacuum tube collector (with a heat-pipe)

In a direct flow vacuum collector (Figure 2.18), the working fluid circulates through a tube welded to the absorber and can have one of the three following configurations:

1. Two coaxial tubes; the fluid is supplied through the inner tube then heats up and exits through the outer tube.

2. A single tube divided by a plane that separates the fluid entering and exiting the tube.

3. A U-shaped tube.
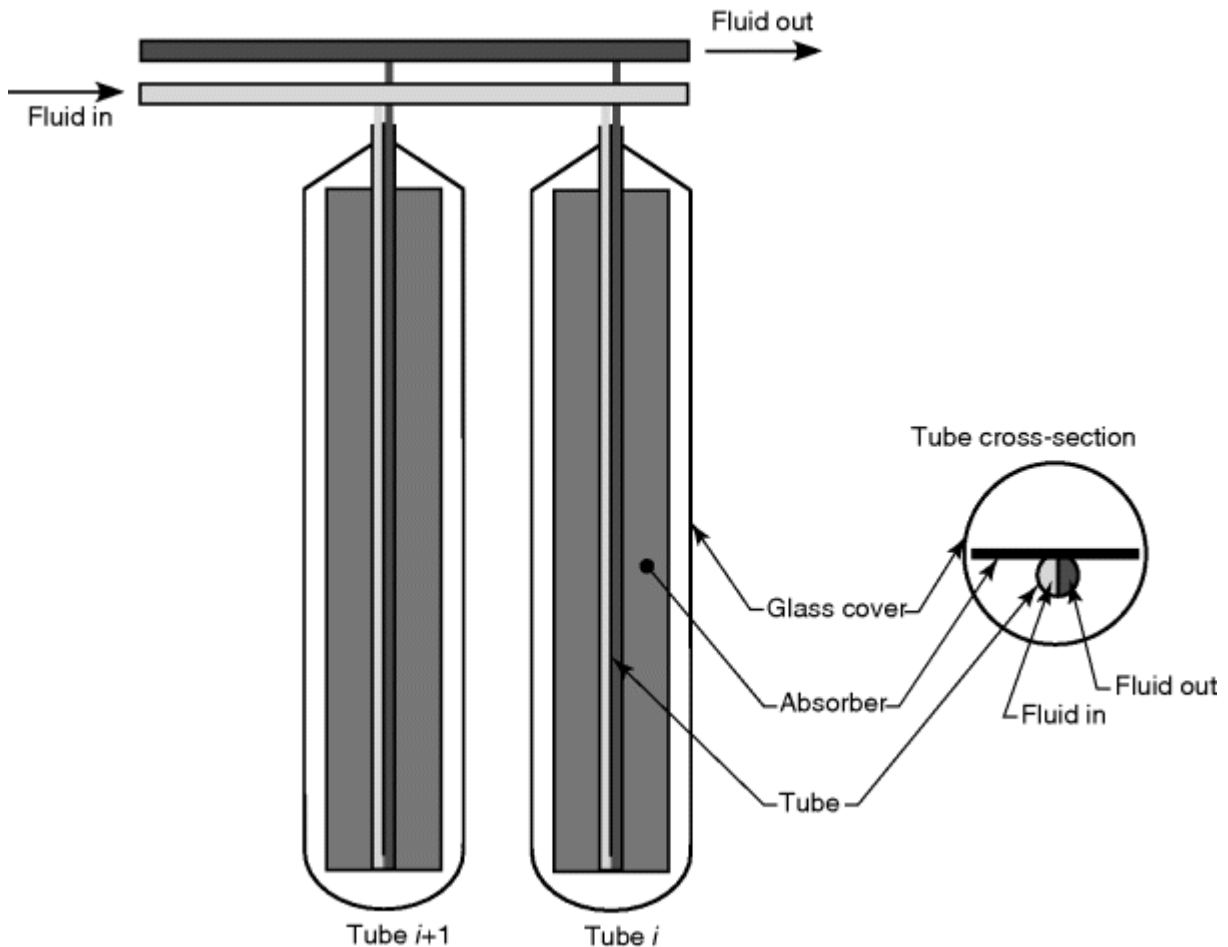
Fig. 2.18 Schematic of a vacuum tube collector (direct-flow)

In the case of vacuum collectors, losses are theoretically limited to the radiation exchange between the absorber and the glass and between the glass, the sky, and the ambient air.

Figure 2.19 illustrates a comparison of the efficiency of a typical flat plate collector and an evacuated vacuum tube collector under the same conditions.
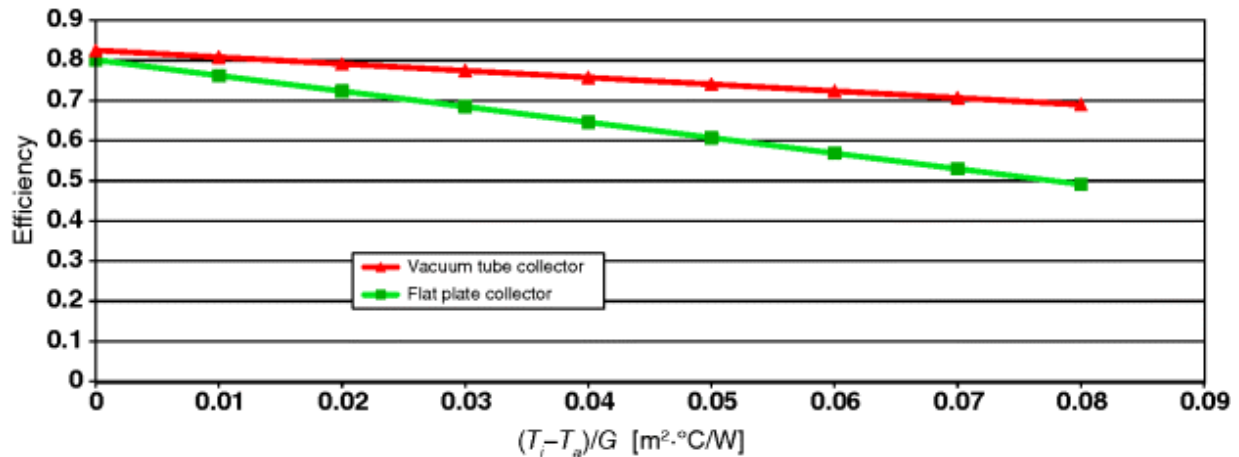
Fig. 2.19 Performance comparison between a flat plate collector and a vacuum tube collector (T_i is inlet temperature, T_a is ambient temperature and G incident solar radiation)

Concentrating Collectors

Concentrating collectors are used to supply heat to processes requiring high temperatures. They focus solar radiation by using reflecting mirrors that concentrate the flux on the tube containing the circulating working fluid. These mirrors are often made out of aluminum for its high reflectivity and reasonable price. Two types are available: the first is stationary while the second follows the path of the sun to maximize the energy captured.

For stationary systems, a parabolic shaped bowl is used to circumvent the apparent movement of the sun. This allows the concentration of solar radiation in a wide band of incident angles. Two methods are used for collectors with a displacement system following the path of the sun: the first follows the path exactly according to the height and azimuth of the sun (dual-axis tracking), while the second will follow the path along a single direction (single-axis tracking).

2.2.2.2 Modeling of Solar Thermal Collectors

The interest in solar collector modeling began with the industrialization of the first collectors in the late 1940s. Models were developed to predict the potential of solar energy in building applications. There are several models in the literature that can be

divided into three categories: stationary models, quasi-dynamic models, and dynamic models.

Steady-state Models

Simple steady-state models (Duffie and Beckman, 2006) calculate the efficiency of the solar collector as a function of the inlet fluid temperature, the total incident radiation, and the ambient temperature. The second-order efficiency curve for a glazed solar thermal collector is

$$\eta = \frac{Q_u}{GA_c} = \eta_0 - C_1 \frac{T_i - T_a}{G} - C_2 \frac{(T_i - T_a)^2}{G} \tag{2.35}$$

where A_c is the collector area (m²); C_1 is the first-order loss coefficient, dependent of fluid temperature (Wm^{-2} K^{-1}); C_2 is the second-order loss coefficient, dependent of fluid temperature (Wm^{-2} K^{-2}); Q_u is the useful power output of the collector (W); T_i is the inlet temperature of the fluid in the collector (K); η is the efficiency of the solar collector; and η_0 is the intercept of the collector efficiency curve.

Quasi-dynamic Models

Quasi-dynamic models account for the losses due to the wind speed, sky temperature, as well as the equivalent thermal capacity of the collector when determining the useful energy output of the collectors (Fischer *et al.*, 2004).

$$Q_u = F(\tau\alpha)K_b(\theta)G_b + F(\tau\alpha)K_dG_d - C_1(T_{ch} - T_a) - C_2(T_{ch} - T_a)^2 \tag{2.36}$$

$$-C_3V(T_{ch} - T_a) - C_4(E_L - \sigma T_a^4) - C_5\frac{dT_{ch}}{dt} - C_6VG$$

where C_3 is the wind speed loss coefficient (Jm^{-3} K^{-1}); C_4 is the longwave radiation loss coefficient; C_5 is the equivalent thermal capacity of the collector (Jm^{-2} K^{-1}); C_6 is the wind dependence of zero loss coefficient (sm^{-1}); E_L is the longwave radiation (Wm^{-2}); $F(\tau\alpha)$ is the zero loss coefficient; G_b is the beam incident solar

radiation (Wm^{-2}); G_d is the diffuse incident solar radiation (Wm^{-2}); $K_b(\theta)$ is the incident angle modifier for beam solar radiation; K_d is the incident angle modifier for diffuse solar radiation; and θ is the angle of incidence.

These models have two advantages: easy coupling with other component models of the solar system and short computation times. They also have the disadvantage of overestimating the potential of solar collectors during fluctuating periods of solar radiation (Schnieders, 1997). Another drawback is that the coefficients C_1 to C_6 are not usually provided by manufacturers and can only be determined experimentally, while coefficients for stationary models are usually provided with manufacturers' certification test results.

Dynamic Models

Dynamic models require a more complex implementation than steady-state models, but are generally more accurate if the appropriate inputs are used. For these models, the dynamic thermal behavior of each component of the collector (i.e., the cover, absorber, fluid) and the energy exchanges between them are modeled to predict the temperature output of the solar collector. These dynamic models have shown good performance and low error. One of the first dynamic models for solar collectors was presented by Kamminga (1985); it takes into account all the elements of the collector. The transparent cover, absorber, and fluid flow are considered separately. Each equation reflects the energy balance on every element. From this model, Schnieders (1997) proposed a model for a vacuum flat plate (using a lumped transfer coefficient for radiation transfer between the glass cover and the absorber).

– Glass cover

$$c'_{Pg}\frac{dT_g}{dt} = h_{g-p}(T_p - T_g) + h_{g\_a}(T_a - T_g) \qquad (2.37)$$

– Absorber

$$c'_{pp}\frac{dT_p}{dt} = h_{g-p}(T_g - T_p) + S + h_{p\_f}(T_f - T_p) \qquad (2.38)$$

– Fluid

$$c'_{pf} \left(\frac{\partial T_f}{\partial t} + v_f \frac{\partial T_f}{\partial x} \right) = h_{p\_f}(T_p - T_f) \qquad (2.39)$$

where c'_{pf} is the fluid heat capacity per unit area (Jm^{-2} K^{-1}); c'_{pg} is the glass cover heat capacity per unit area (Jm^{-2} K^{-1}); c'_{pp} is the absorber heat capacity per unit area (Jm^{-2} K^{-1}); h_{g_a} is the heat transfer coefficient glass-exterior (Wm^{-2} K^{-1}); h_{g_p} is the heat transfer coefficient glass-absorber (Wm^{-2} K^{-1}); h_{p_f} is the heat transfer coefficient absorber-fluid (Wm^{-2} K^{-1}); S is the solar radiation absorbed per unit area of the absorber (Wm^{-2}); T_f is the temperature of the fluid (K); T_g is the temperature of the glass cover (K); T_p is the temperature of the absorber (K); t is time (s); and v_f is the fluid velocity (ms^{-1}).

Praene, Garde, and Lucas (2005) proposed a version of this model for direct flow vacuum tubes detailing the energy exchanges between the absorber and the glass envelope and then performed a sensitivity analysis of the collector parameters, such as the exchange coefficients and thermal capacity. Bourdoukan *et al.* (2008) presented a model for vacuum tube collectors with heat pipes.

2.2.2.3 Thermal Storage Tanks

Both short-term thermal storage and long-term (seasonal) storage concepts are in development for use in solar systems. In the case of "short-term" thermal storage (i.e., hours to days), the use of water as a storage medium has been shown to be a readily available, cost-effective solution. It is important however, to ensure that the storage system is designed to maximize available energy and exergy by avoiding mixing and promoting stratification. The development and characterization of a new multitank, sequentially stratified thermal storage for use in medium-sized solar domestic hot water heating systems is described by Cruickshank and Harrison (2008, 2010). This work demonstrated modular, scalable, low-cost thermal storage for water heating systems, but still requires further development for use in combi-systems in low-energy buildings.

Producing domestic hot water (DHW) using solar energy is the most common application for solar thermal collectors. A typical solar domestic hot water system consists of a solar thermal collector, a circulating pump, and a hot water storage tank as shown in Figure 2.20.
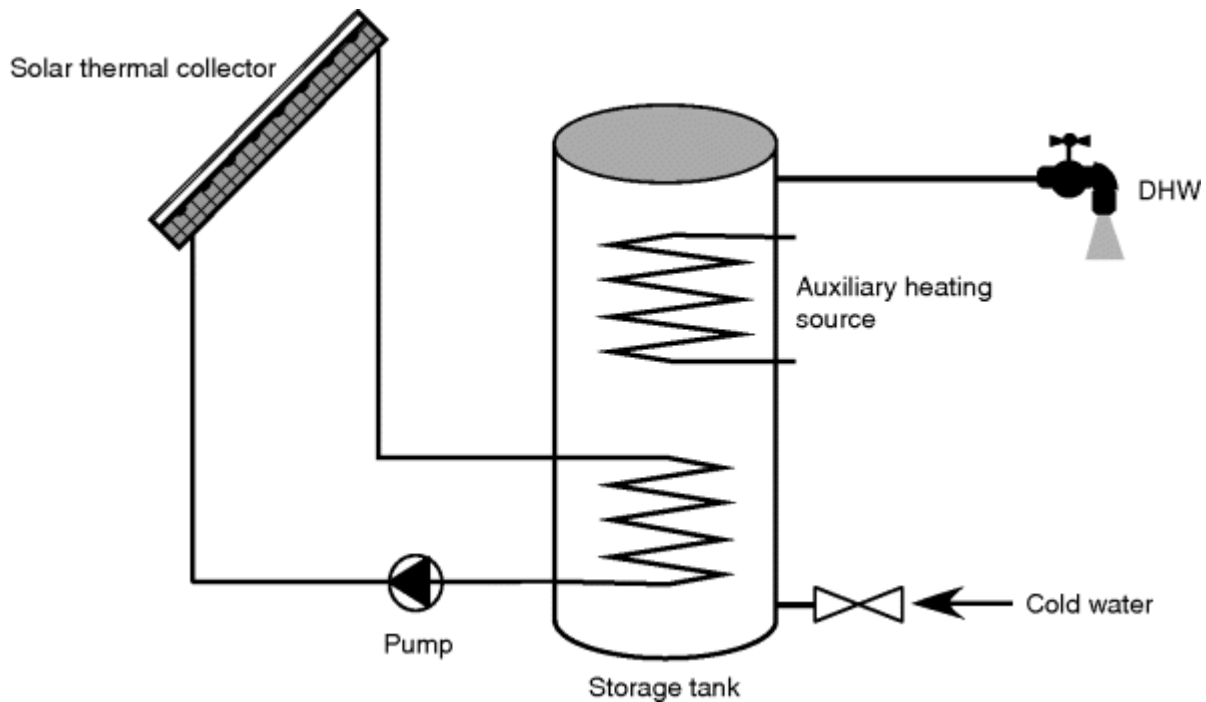
Fig. 2.20 Schematic of storage tank for DHW application

A storage tank is used to store a hot or cold medium for use in a process. The most common application is storage for domestic hot water (Figure 2.20). It consists of a fluid that circulates into the storage tank and delivers/recuperates energy to/from the storage medium and exits the tank. Heat exchanges between the fluid and the storage medium can be done through a heat exchanger or by direct contact; thus, different types of heat exchangers exist as follows:

– Storage tank without heat exchanger: heating or cooling fluid is the same as the storage medium. The fluid entering the storage tank mixes with the storage medium, delivers/recuperates energy, and exits the storage tank.

– Storage tank with one heat exchanger: a heat exchanger inside the storage tank ensures the heat exchange between the

heating/cooling fluid and the fluid in the storage tank.

– Storage tank with two heat exchangers: two heat exchangers inside the storage tank permit a heat exchange of the storage mass with two sources at different temperatures.

Depending on the volume of the storage tank, its level of insulation, the ambient temperature, and the level of fluid movement inside the tank, temperature stratification can be observed.

2.2.2.4 Modeling of Thermal Storage Tanks

Several models of storage tank have been developed with different levels of detail to account for thermal stratification.

The simplest approach considers the storage tank as a single node (). Performing an energy and mass balance (with or without heat exchanger) for that node allows the calculation of the node temperature evolution over time. This approach can be acceptable for small storage tanks. The following are the equations for a single node storage tank with one heat exchanger:

$$\rho V_T c_{pT} \frac{dT_T}{dt} = Q + m_2 c_{pT}(T_{i2} - T_T) + kA_T(T_a - T_T)$$

$$Q = m_f c_{pf}(T_{if} - T_{of})$$

$$Q = h(T_{mf} - T_T)$$

$$T_{mf} = \frac{T_{if} + T_{of}}{2}$$
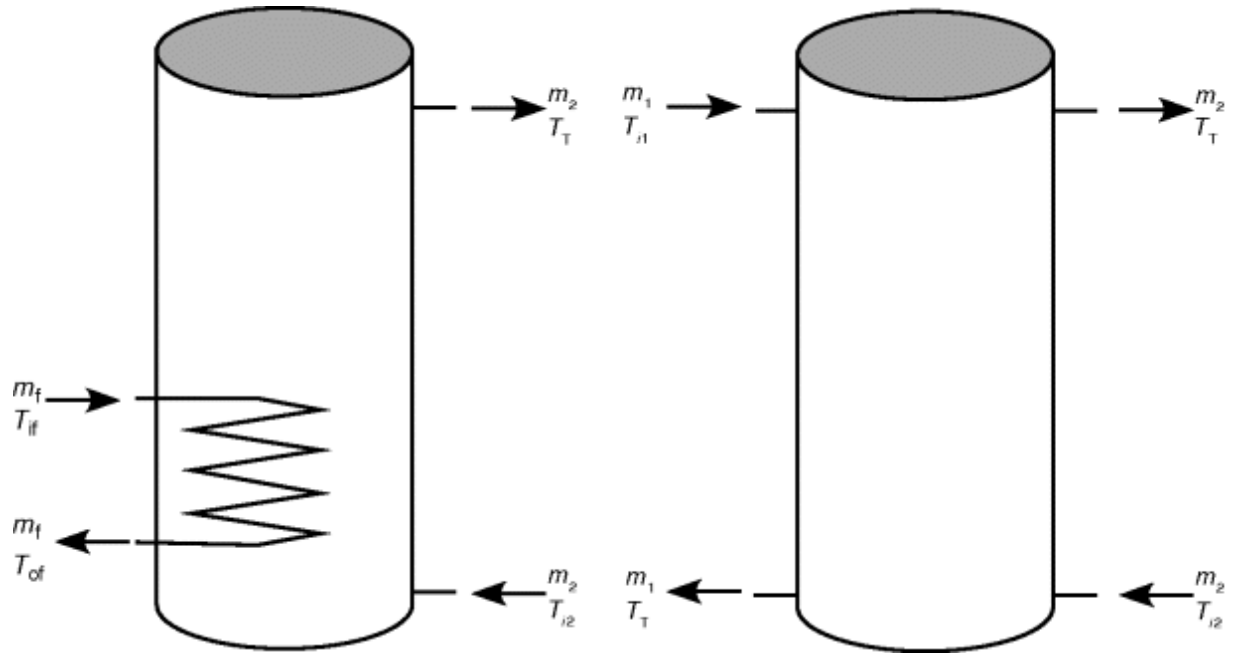
Fig. 2.21 Schematic of a single-node storage tank model (a) with internal heat exchanger; (b) without heat exchanger

For a one node storage tank without heat exchanger, the equations can be written as

$$\rho V_T c_{pT} \frac{dT_T}{dt} = m_1 c_{pT}(T_{i1} - T_T) + m_2 c_{pT}(T_{i2} - T_T) + kA_T(T_a - T_T)$$

A_T	is the exterior surface area of the storage tank (m²)
c_{pT}, c_{pf}	are the heat capacities of the storage fluid and heat exchange fluid, respectively (J · kg⁻¹ K⁻¹)
h	is the global heat exchange coefficient of the heat exchanger (W · K⁻¹)
k	is the global heat exchange coefficient between storage fluid and ambient air (W · m⁻² K⁻¹)
m_1, m_2	are the mass flow rates on the source side and demand side, respectively (kg · s⁻¹)
m_f	is the mass flow rate through the heat exchanger (kg · s⁻¹)
Q	is the heat flux exchanged between the storage fluid and the heat exchanger fluid (W)
T_{i1}, T_{i2}	are the inlet temperatures of the fluid on the source side and demand side, respectively (K)
T_{if}, T_{of}	are the temperatures of the fluid at the inlet and outlet of the heat exchanger, respectively (K)
T_T	is the temperature of the storage fluid (K)
T_{mf}	is the mean temperature of the heat exchanger fluid (K)
V_T	is the volume of the storage tank (m³)
ρ	is the density of the storage fluid (kg · m⁻³)

When thermal stratification needs to be considered in more detail, the tank can be divided into several control volumes (Klein, Beckman, and Duffie, 1976) ([Figure 2.22](#)). An energy and mass balance can be performed for each control volume. This method has shown satisfactory results.

— First volume

$$(2.40)$$

$$\rho_1 V_1 c_{pf} \frac{dT_1}{dt} = m_1 c_{pf}(T_{i1} - T_1) + \frac{\lambda A_i}{x_{1,2}}(T_2 - T_1) + m_2 c_{pf}(T_2 - T_1) + A_1 k_1 (T_a - T_1)$$

– *i*th control volume

$$\rho_i V_i c_{pf} \frac{dT_i}{dt} = m_1 c_{pf}(T_{i-1} - T_i) + \frac{\lambda A_i}{x_{i-1,i}}(T_{i-1} - T_i) + m_2 c_{pf}(T_{i+1} - T_i) \qquad (2.41)$$
$$+ A_i k_i(T_a - T_i) + \frac{\lambda A_i}{x_{i,i+1}}(T_{i+1} - T_i)$$

– Last volume

$$\rho_n V_n c_{pf} \frac{dT_n}{dt} = m_1 c_{pf}(T_{n-1} - T_n) + \frac{\lambda A_i}{x_{n-1,n}}(T_{n-1} - T_n) \qquad (2.42)$$
$$+ m_2 c_{pf}(T_{i2} - T_n) + A_n k_n(T_a - T_n)$$
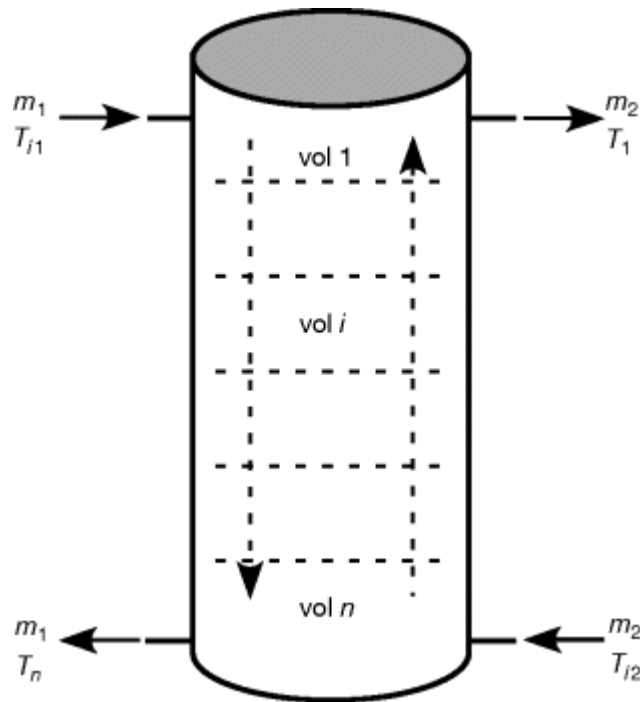
Fig. 2.22 Schematic of a multinode storage tank model

A_i	is the outside area of the storage tank ith control volume (m²)
$i = 1,2...n$	is the index for the control volumes of the storage fluid
k_i	is the global heat exchange coefficient between storage fluid and ambient air at the ith control volume (W · m⁻² K⁻¹)
T_i	is the temperature of the ith control volume of the storage fluid (K)
V_i	is the volume of the ith control volume of the storage tank (m³)
$x_{i-1,j}$	is the distance (m) between the centres of the ith and $(i-1)$th control volumes for $i = 2...n$
λ	is the thermal conductivity of the storage fluid (W · m⁻¹ K⁻¹)

Other approaches have been developed for specific cases. For example, the zonal method was developed by Inard, Kenjo, and Caccavelli (2007) to take into account the thermal stratification of a specific type of storage tank. Shah and Furbo (1998) found correlations from experimental results taking into account the stratification. Other correlations based on computational fluid dynamics (CFD) (Jivan Shah, 2000) can be used for tanks with internal heat exchangers.

2.2.2.5 Solar Combi-Systems

The feasibility of individual solar heating or cooling systems is strongly influenced by the fact that the heating or cooling system is not operational during a large part of the year. The combination of solar heating and cooling capability into an integrated system presents an opportunity to increase the viability and cost performance of the overall system. Various combi-system configurations have been previously investigated under the auspices of the IEA SHC Task 26 and Task 32 (Hadorn, 2008; Weiss, 2002). Within these tasks, various system configurations were cataloged and modeled, and test procedures were developed to allow standard performance evaluations to be conducted. As well, the later work of Task 32 addressed the integration of combi-systems into high solar

fraction, low-energy homes. Control schemes, heat exchange and distribution options, and advanced storage concepts were investigated.

The appropriate sizing and integration of these systems with conventional HVAC equipment is an area requiring study, as most combi-systems are engineered on site and do not benefit from pre-engineered and certified designs. Early experience with prototype combi-systems has shown that many of the difficulties previously associated with early compact solar domestic hot water heating systems (SDHW) were evident. The optimum system design is also strongly dependent on the ratio of cooling to heating loads, and there is a need to establish improved design tools, guidelines, and commissioning procedures to ensure that these systems perform to their potential under the climatic conditions being considered.

Combined systems improve cost performance but increase system and control complexity. The optimization of these systems requires the development of full system numerical simulations (Weiss, 2003) that accurately model the system operation and the time variation of solar energy and loads.

2.2.3 Active Building-Integrated Thermal Energy Storage and Panel/Radiant Heating/Cooling Systems

Active building-integrated thermal energy storage (BITES) systems are exposed to the indoor environment and typically use air or water as the heat transfer fluid to heat or cool the storage mass. Concrete and masonry are commonly used BITES materials (ACI committee 122, 2002). BITES systems can be categorized into passive and active types (passive/direct gain – so-called building thermal mass has been covered in Section 2.1.1). The system is considered active when it embodies an internal controllable charge and/or discharge system, such as a hydronic, ventilated (or air-core), electric, and capillary system (ASHRAE, 2008; Braham, 2000; Feustel and Stetiu, 1995; Lehmann *et al.*, 2011; Winwood, Benstead, and Edwards, 1997). It can be actively charged and passively discharged or actively charged and discharged. BITES systems can be wall, ceiling, or floor located (Figure 2.23).
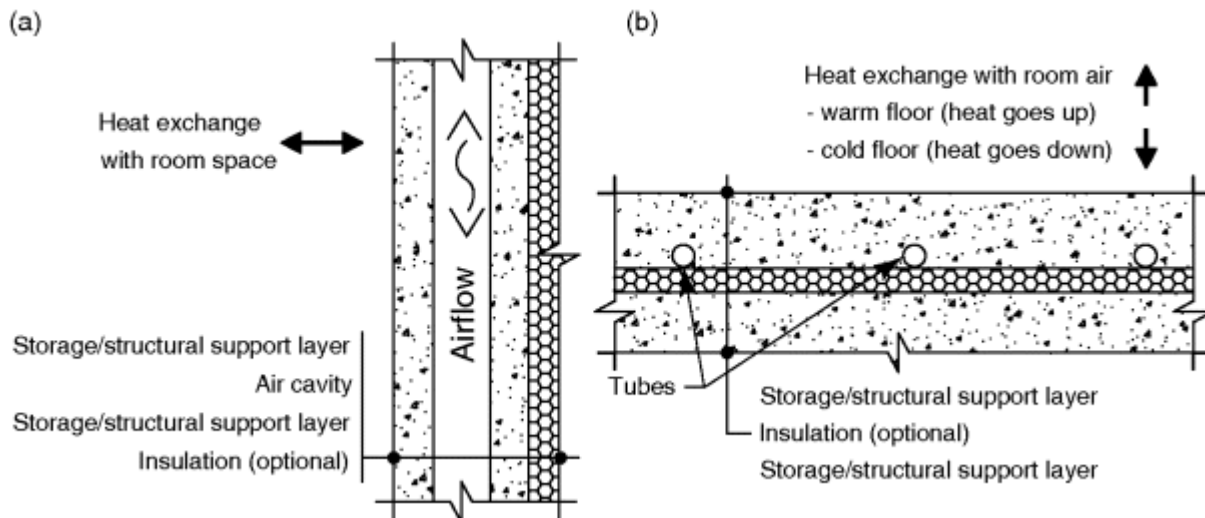
Fig. 2.23 Schematic of the typical cross- sections of (a) ventilated and (b) hydronic systems (either system can be a floor, wall, or roof; insulation is optional and can be placed on the other side of the tube to orient heat flow in the opposite direction) (Chen, Athienitis, and Galal, 2013)

Hydronic slab systems are often designated as thermo-active (or thermally active) building systems (TABS) when significant thermal storage is integrated (generally thicker than 5 cm of concrete). These systems provide energy-saving potential and improved thermal comfort as compared to traditional forced-air space conditioning systems (Henze *et al.*, 2008; Lehmann, Dorer, and Koschenz, 2007; Xu *et al.*, 2010). Examples for ventilated systems include ventilated concrete slabs (VCS) (Chen, Galal, and Athienitis, 2010b) and ventilated masonry block walls (Howard, 1986). Research on the efficient utilization of VCS in cooling applications for commercial buildings has been conducted by several groups (Ren and Wright, 1998; Winwood, Benstead, and Edwards, 1997). The air channels in these systems are often used as ventilation ducts. In this case, they integrate TES, space conditioning, ventilation, and structural systems into one. The air flow can be open-loop (inlet and/or outlet air mix with room air) or closed-loop (no mixing), and it is possible to switch based on applications (e.g., open-loop in slab cooling and closed-loop in slab heating). Open-loop ventilated systems have been shown to provide stronger thermal coupling between high-mass slabs and room air (e.g., higher total convective heat transfer rate, and direct mix of room and channel flowing air) and hence to

significantly reduce space conditioning load (Braham, 2000). Oswald and Sedlbauer (1995) suggested hygienic maintenance on open-loop systems.

Active charge and discharge BITES systems (e.g., hydronic or ventilated systems) with proper design and control have the following additional advantages compared to isolated thermal storage systems:

– They exploit the large space conditioning potential of the building fabric in a space-efficient and cost-effective way. Active charge/discharge enhances the TES function and adds TES to the original functions of the building component (e.g. structural and architectural) with reduced material cost.

– Active charge and discharge design can be used to reduce peak demand.

– Active BITES can be utilized to improve thermal comfort by reducing room temperature fluctuations and drafts. Ceiling/floor located active BITES systems may evenly discharge thermal energy directly into occupied space by radiation and convection. This reduces surface temperature differences and radiant temperature asymmetry. Thermal comfort is also improved with enhanced direct radiative heat exchange between occupants and active BITES systems (ASHRAE, 2009c; Feustel and Stetiu, 1995; Inard, Meslem, and Depecker, 1998).

2.2.3.1 Radiant Heating/Cooling Systems Integrated with Thermal Mass

Unlike air-conditioning systems that condition spaces primarily through convection, radiant systems (ASHRAE, 2007) condition the floor, ceiling, or walls, which in turn either radiate heat directly or absorb heat from occupants or objects, while also having a significant convective component when the heat flow is upward (cooling ceiling or heating floor). Heated floors have been used since the first millennium B.C. (Bean, Olesen, and Kwang Woo, 2010); for example, around 300 B.C. the Romans started to use them extensively. The system called "Hypocaustum" was defined by the furnace (hypocausis) and a series of flue passages realized under the floor by

means of pillars carrying a slab (i.e., like a ventilated concrete slab). In modern times, starting from the 1950s and the 1960s, radiant heating installations started to increasingly appear in Europe in the residential sector, but taking into consideration that buildings were not well insulated, the resulting operating temperature of the working fluid was higher than today's standards. Then, at the end of the 1970s, the introduction of plastic pipe for floor heating facilitated more widespread use of floor heating, especially in Germany, Switzerland, Austria, and the Nordic countries.

Three types of radiant floor heating exist: radiant air floors (air is the heat-carrier), electric radiant floors, and hot water radiant floors. All three types can be further subdivided by the type of installation: those that profit from the large thermal mass of a concrete slab floor (these are called "wet installations"); and those in which the radiant floor tubing is located between two layers of plywood or under the finished floor or subfloor ("dry installations"). Air-heated floors (like VCS) are often characterized by slow response; however, they can be coupled with air heating systems.

Hydronic (liquid) systems are the most popular radiant heating systems. In these systems heated water is pumped from a heating source through tubing laid out in a pattern in the floor massive layer (usually at its bottom). In some systems, the temperature in each room is controlled by regulating the flow of hot water through each tubing loop, through the use of motorized zoning valves. For hydronic floors it is recommended to use water at about 35 °C, while for cooling using water at a temperature lower than 15 °C should be avoided (ASHRAE, 2007; Olesen, 2002) to avoid condensation problems. These temperatures make the use of solar assisted heat pumps or solar combi-systems a good option for producing hot water in Net ZEBs. Geothermal systems may be used to provide both heat and cool using air-to-water heat pumps.

In "Wet" installations, the oldest form of modern radiant floor systems, the tubing is located within a solid floor. The tubing or cable can be inserted in a thick concrete foundation slab or in a thin layer of concrete, gypsum, or other material installed on top of a subfloor.

In "Dry" floors, the cables or tubing run in an air space beneath the floor. Usually a dry floor is faster and less expensive to build; it is

characterized by lower thermal inertia but requires higher operating temperatures. These installations are usually easier when planning retrofit actions and can often integrate acoustic solutions.

One of the main features of radiant floor heating (mostly in wet installations) is the uniform temperature conditions from floor to ceiling and the reduced thermal stratification (Olesen, 2002). Floor heating systems usually provide superior comfort conditions for occupants as air movement in the environment and vertical temperature gradient are very low and the thermal mass limits the temperature fluctuations; moreover, the working fluid average temperature is low, which allows for a wide set of solutions for the heating source (also district heating or geothermal heat pump systems can be used). On the other hand, the thermal mass causes the system to react slowly to temperature changes. Overheating can be an issue in poorly controlled zones; these systems usually have difficulties dealing with frequent setpoint temperature adjustments. Radiant cooling fluid temperatures must also never be lower than 13–15 °C to ensure comfort and avoid the formation of interstitial moisture. Predictive control is one efficient strategy to optimally control radiant heating in TABS (thermal massive systems). Ventilation and humidity control may be done separately.

Practical applications of active BITES systems with radiant heating/cooling are presented in this book. They include a hydronic BITES system installed in an institutional Net ZEB, Research Support Facility (RSF) building (Section 7.3), in the National Renewable Energy Laboratory (NREL) of the Department of Energy of the United States, a hydronic BITES system in the residential Net ZEB, Leaf House (Section 7.2), and a ventilated BITES system adopted in a residential near Net ZEB, ÉcoTerra (Section 7.1).

Two closely related thermal characteristic of BITES systems are their storage capacity and thermal inertia (i.e., response time). These two characteristics together with other parameters (e.g., thermal comfort, location) create challenges in the design and control optimization of BITES systems. Appropriate numerical models play an important role in these two aspects. In Section 2.2.3.2, different modeling approaches will be described. Control methodologies are introduced in Chapter 6.

2.2.3.2 Modeling Active BITES

Two mainstream modeling methods, finite difference discretization and transfer functions, are applied in this section to BITES.

Finite Difference Discretization Methods

Among common transient models for active BITES systems, discretization methods, such as finite difference models (Incropera and DeWitt, 2002; Kreith and Bohn, 2001), have been widely used. The main advantage of the finite difference approach is accurate treatment of nonlinearities (e.g., convective heat transfer and time-dependent variables). Equation (2.43) is in explicit finite difference form for the calculation of the temperature of a control volume node T_{node} located at coordinate (x, y, z) in a three-dimensional model. By assuming that the current values of the variables prevail throughout the next time step,

$$T_{node}(t + \Delta t)_{x,y,z} = T_{node}(t)_{x,y,z} + \frac{\Delta t}{C_{x,y,z}} \sum_j \left(\Delta T(t)^j_{x,y,z} \cdot U^j_{x,y,z} \right) \qquad (2.43)$$

where Δt is the time step and $C_{x,y,z}$ is the capacitance of the node. $\Delta T(t)^j_{x,y,z}$ is the temperature difference between the current node and the adjacent node at time t in direction j (i.e., in negative or positive x, y, or z directions). $U^j_{x,y,z}$ is the conductance between the current node and the adjacent node in direction j (j is between 1 and 6 for the three-dimensional model). The last term in Eq. (2.43) includes conductive heat transfer from adjacent nodes, as well as convective and radiative heat transfer in the cases where exterior nodes are involved.

In the explicit approach, in order to generate physically realistic results and stabilize forward marching in time, the discretization places a maximum value on the time step. The Fourier number (the ratio of the heat conduction rate to the rate of thermal energy storage) has to be less than 0.5. For uniform conductivity and uniform one-dimensional grids

$$\Delta t < \frac{\rho \cdot c \cdot \Delta x^2}{2k} \qquad (2.44)$$

where Δx is the grid spacing, k is the conductivity, ρ is the density, and c is the specific heat of the material.

See Section 2.1.5 for a one-dimensional example. For multidimensional discretization, Eq. (2.44) can be rewritten as Eq. (2.45), where $C_{x,y,z}$ is the capacitance of the node, and $U^j_{x,y,z}$ is the conductance between the current node and the adjacent node in direction j. If the node receives heat flux (e.g., solar radiation), the $U^j_{x,y,z}$ in the corresponding heat flux direction can be increased to a larger equivalent conductance to account for this heat flux.

$$\Delta t < \frac{C_{x,y,z}}{\sum_j U^j_{x,y,z}} \tag{2.45}$$

Implicit differencing approach is commonly used. The implicit formulation assumes that the future values prevail throughout the current time step. Generally, a system of equations can be solved simultaneously to obtain the variable values at the next time step. Alternatively, their values can also be initially guessed and then fine-tuned through iterations until overall energy balance is achieved (Incropera and DeWitt, 2002). The advantage of the implicit approach is that the limitation on the time step no longer exists. However, long time steps are not appropriate for cases when the values of the variables are changing rapidly. Furthermore, when controlled heat sources are used, time steps cannot be longer than the control time interval. The Crank–Nicolson approach lies between the explicit and implicit approaches – it assumes linear variations of the values over a time step.

For the fluid flowing inside the BITES systems, Eq. (2.46) (Chen, Athienitis and Galal, 2013) gives the analytical solution for the local temperature of the fluid with the assumptions of constant boundary and large Peclet number (Incropera and DeWitt, 2002; Patankar, 1980).

$$T_f(x) = T_{eqv\_bnd} + \left(T_{inlet} - T_{eqv\_bnd} \right) \cdot \exp(-a_{hx} \cdot x) \tag{2.46}$$

$$T_{eqv\_bnd} = \frac{\sum_{j=1}^{J} \left(T^j_{srf} \cdot ul^j_{srf} \right)}{\sum_{j=1}^{J} \left(ul^j_{srf} \right)} \tag{2.47}$$

$$a_{\text{hx}} = \sum_{j=1}^{J} ul_{\text{srf}}^j / (\dot{m}_{\text{f}} \cdot c_{\text{f}})$$

<div align="right">(2.48)</div>

where T_{srf}^j is the temperature of the jth boundary surface, and ul_{srf}^j is the conductance per meter length (stream-wise) between the surface and the fluid in W/(m · K), x is the distance from the inlet, $\dot{m}_{\text{f}}$ is the mass flow rate of the fluid, and c_{f} is the specific heat of the fluid.

In the context of the transport of heat, Peclet number $\text{No}_{\text{Peclet}}$ is the ratio of the strengths of convection and conduction, equivalent to the product of the Reynolds number and the Prandtl number (ASHRAE, 2009a) (Eq. (2.49)). If $\text{No}_{\text{Peclet}}$ is much larger than 1 (e.g., 100), the downstream fluid temperature has negligible influence on the upstream fluid temperature. In the applications of active BITES systems, $\text{No}_{\text{Peclet}}$ is usually much larger than 1.

$$\text{No}_{\text{Peclet}} = \text{Re} \cdot \text{Pr} = \frac{\rho \cdot v \cdot L_{\text{c}}}{\mu} \cdot \frac{c \cdot \mu}{k} = \frac{c \cdot \rho \cdot v \cdot L_{\text{c}}}{k}$$

<div align="right">(2.49)</div>

where L_c is the characteristic length, equal to the diameter of the pipe/channel in the cases of active BITES systems. v is the fluid velocity.

The mean temperature of the fluid in a control volume (Figure 2.24) can be calculated with Eq. (2.50)

$$T_{\text{mean}} = T_{\text{eqv\_bnd}} + \frac{(T_{\text{inlet}} - T_{\text{eqv\_bnd}}) \cdot (1 - \exp(-a_{\text{hx}} \cdot L_{\text{CV}}))}{a_{\text{hx}} \cdot L_{\text{CV}}}$$

<div align="right">(2.50)</div>

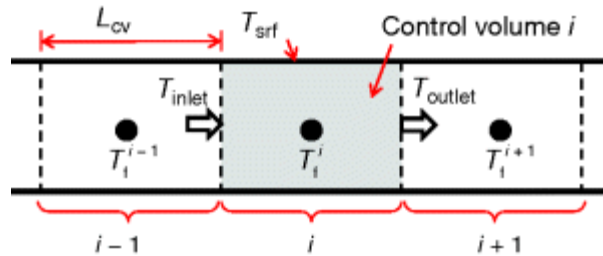where L_{CV} is the length of the control volume.

Fig. 2.24 Schematic of the fluid control volume

For discretization with fine mesh (i.e., small grid spacing), the mean fluid temperature inside one control volume can also be

approximated using upwind differencing scheme ([Eq. (2.51)](#)) (Chen, Athienitis, and Galal, 2012; Patankar, 1980).

$$T_f^i = \frac{\dot{m}_f \cdot c_f \cdot T_f^{i-1} + \sum_j \left(T_{srf}^j \cdot U_{srf}^j \right)}{\dot{m}_f \cdot c_f + \sum_j U_{srf}^j} \tag{2.51}$$

where T_f^{i-1} is the temperature of the fluid in the previous control volume. U_{srf}^j is conductance between the surface and the fluid.

Detailed models reflecting the actual heat transfer process, such as two- or three-dimensional spatial discretization, can provide more accurate results; however, they require more computational effort. Simple lumped-parameter finite difference models with acceptable accuracy are needed for long-period simulations, especially for implementation into whole building simulations and model-based control. Studies presented in literature have shown that a one-dimensional (normal to the room-side surface of the BITES) thermal model can approximate the thermal behavior of active BITES systems well in cases of practical interest (Barton, Beggs, and Sleigh, 2002; Chen, Galal, and Athienitis, 2010b; Ren and Wright, 1998; Strand, 1995).

Transfer Function Methods

Since active BITES systems usually involve large thermal capacitance (e.g., concrete slab), transient thermal behavior needs to be modeled. Transfer function methods are computationally efficient for the calculation of the transient thermal response of a thermal system. The *z*-transfer function method has been discussed in Section 2.1.3, and more general applications are discussed in [Chapter 6](#).

Generally, in time domain analysis, time-series coefficients are generated to relate the current outputs to its current and past inputs. Discrete-time transfer functions are used in this kind of approaches. Continuous-time transfer functions can also be used. Since discrete-time sampled values (e.g., hourly weather data) are commonly used in building simulations, time-series coefficient approaches are more popular. The transfer function method is also used in frequency domain analysis as described in Section 2.1.2.

To derive transfer functions, either in time or frequency domain, the Laplace transform method has been traditionally used. In time domain modeling, after taking a Laplace transform, time-series (discrete) response coefficients, such as thermal response factors (Stephenson and Mitalas, 1967), CTFs (Stephenson and Mitalas, 1971), and radiant time series (Spitler and Fisher, 1999; Spitler, Fisher, and Pedersen, 1997) are derived with different methods. CTF can also be obtained with state space formulation (Ceylan and Myers, 1979; Seem *et al.*, 1989).

When using transfer functions of thermal systems, the system under consideration can be a whole building or a component. In building thermal modeling software using *z*-transfer functions (see Section 2.1.3), such as EnergyPlus and TRNSYS, the outputs from each building component are calculated with their associated transfer functions (see Section 2.1.4). The inputs or response of these components for the next time step, such as the interior radiative heat transfer and room air temperature, are then calculated based on heat balance equations following the energy conservation principle (ASHRAE, 2009b). For a solid bounded by two parallel planes, such as wall and slab assemblies, the Laplace transform method is used in deriving transfer functions for transient heat conduction within them (Carslaw and Jaeger, 1959; Kimura, 1977) as described previously in Section 2.1.2.1. For assemblies with internal heat sources, such as the case of active BITES systems, Strand (1995) incorporated "source transfer functions" into CTF using Laplace transform and state space formulations. Considerations in substituting two-dimensional models with one-dimensional ones were further discussed by Strand (1995).

The frequency response (FR) approach facilitates the integration of design and model-based control. It can provide additional information, particularly for design optimization and comparison of design alternatives on relative bases and, without tedious simulation (Athienitis, Stylianou, and Shou, 1990). For example, the magnitude and phase angle of admittance or impedance obtained from the FR approach of an assembly provides substantial insight into its thermal behavior (Athienitis, 1994; Athienitis, Stylianou, and Shou, 1990; Balcomb and Jones, 1983). These variables can be readily used for parametric analysis and design optimization. Furthermore, the FR

approach provides an analytical solution and does not require spatial discretization. Another important application of the FR approach is in the development of model-based control strategies for building HVAC systems (Athienitis, Stylianou, and Shou, 1990; Candanedo and Athienitis, 2011). Athienitis (1994), Davies (1982, 1994), Athienitis, Sullivan, and Hollands (1986), and Hittle (1981) conducted studies on the thermal behavior of building components and thermal zones using this approach.

The advantage of using transfer function methods is their high computational efficiency for transient thermal simulations. In the analysis of multilayer assemblies (e.g., wall/floor/ceiling), the temperatures and heat flux at nodes of no interest do not need to be calculated. There is no need for spatial discretization. A disadvantage is that transfer functions cannot directly model nonlinear components. Instead, these methods assume linear or linearized systems. For example, the thermal characteristics of all material are assumed to be linear and time-invariant (e.g., conductivity and specific heat capacity do not depend on temperature or time). Radiant time series method in time domain and transfer functions in frequency domain can only be used under steady periodic excitations (e.g., temperature and heat flux). Besides transfer functions, a quasi-analytical algorithm was also developed to approximate the heat transfer among the assemblies, the heat transfer fluid, and room air (TRNSYS, 2012).

2.2.3.3 Methods used in Two Mainstream Building Simulation Software

EnergyPlus currently includes models for hydronic/ventilated floor/wall heating/cooling systems that are one-dimensional. Conduction transfer functions with heat source transfer functions (CTF/QTF) are used in calculating the system surface temperature and element internal temperature. The time series coefficients are calculated with state space formulation (Laplace transform formulation is also provided for comparison purpose) (Strand, 1995). Strand (1995) also stated that a two-dimensional model (on the transverse cross-section) is more desirable because it provides a more accurate internal (source location) temperature than a one-dimensional model.

To calculate the heat flow from the fluid to the system, the active BITES system is treated as a heat exchanger (EERE, 2013). The source location temperature is obtained using CTF/QTF time-series coefficients. One important assumption is made for the heat exchanger treatment: the system temperature along the length of the tubing/air channel is constant during one time step. The NTU method is chosen for heat exchange calculation between fluid and solid.

In TRNSYS, there are currently two models for hydronic systems: quasi-analytical formulation and a two-dimensional finite difference model (see Leaf House case study, [Chapter 7](#)). The quasi-analytical formulation is developed to calculate the internal and surface temperatures of the radiant systems based on room air and inlet water temperature and flow rate. Three-dimensional heat transfer is taken into account.

2.2.3.4 Nomenclature

Variables

c	Specific heat $(J/(kg \times K))$
C	Thermal capacitance (J/K)
j	Index of adjacent node or boundary surface
$\dot{m}$	Mass flow rate (kg/s)
t	Time
T	Temperature (K)
u	Thermal conductance per unit area $(W/(m^2 \times K))$
ul	Conductance per meter length $(W/(m \times K))$
U	Conductance (W/K)

Acronyms

ACD	Active charge and discharge
BITES	Building-integrated thermal energy storage
CTF	Conduction transfer functions
FR	Frequency response

2.2.4 Heat Pump Systems – A Promising Technology for Net ZEBs

Heat pumps are a particularly important technology for Net ZEBs to reach net-zero energy status in an efficient way. The heat source/sink can be the air or the ground (ground source heat pumps). For cold climates with high heating loads, a geothermal system can provide a reliable heat source/sink at temperatures of around 6–9 °C year-round compared to outdoor air that can be as low as −25 °C or as high as 30–35 °C in summer (in Montreal). However, a geothermal system has an additional cost for drilling boreholes needed to reach adequate depths for efficient heat exchange with the ground (normally about 50–70 m deep U-tube heat exchanger boreholes per ton of cooling/heating). Another alternative is to use thermal energy from a solar system (e.g., BIPV/T) as a heat source. Two of the case studies in Chapter 7 use geothermal systems with vertical boreholes for heating and cooling (the ÉcoTerra™ house in Canada and the Leaf multiapartment building in Italy). Generally, heat pumps will operate with higher coefficients of performance year-round (both heating and cooling) when the source/sink temperature approaches room temperature.

2.2.4.1 Solar Air-Conditioning

Solar cooling is an attractive technique since air-conditioning loads are usually coincident with periods of available solar energy. For example, in temperate regions of Canada, the heating load is typically significantly higher than the cooling load. As such, the most promising approaches are to utilize combined solar heating and cooling systems that maximize the use of solar energy. A number of concepts have been investigated for supplying space cooling and dehumidification in buildings, including vapor compression (VC), ejector cooling (EC), open cycle vapor absorption (OVA), adsorption,

solid desiccant (SD), liquid desiccant (LD), and hybrid cycles (see overviews by Henning (2007)).

Most thermally driven cooling technologies are geared toward producing chilled water, with the exception of the desiccant systems. The performance of EC, CVA, OVA, and adsorption systems is strongly dependent on the generator (hot side) operating temperature. This poses a significant disadvantage for solar thermal systems compared to fossil fuel powered systems. The performance of desiccant systems, however, is not strongly dependent on regeneration temperatures and allows for the independent control of the latent and sensible loads; an increasingly important feature with present higher ventilation standards and indoor air quality concerns. Another advantage of liquid-desiccant systems is the potential of using the desiccant solution for energy storage.

2.2.4.2 Solar Assisted/Source Heat Pump Systems

Heat pumps may be used either in parallel with a solar system to act as a source of auxiliary heating/cooling or in series with the solar system. Parallel application of heat pumps is usually straightforward since usually each system operates independently. The feasibility of using a parallel source heat pump then largely becomes a matter of the economics of competing auxiliary energy systems and may be influenced by local climatic conditions. Small heat pump systems are required to operate efficiently with the reduced loads experienced in Net ZEBs. The use of a heat pump to enhance the heat transfer from a solar collector to the thermal storage can improve overall performance over a wider range of seasons and weather conditions. Combining heat pumps with conventional solar systems also has the potential to produce high energy output from low-cost unglazed solar panels (Bridgeman and Harrison, 2008).

The example in Figure 2.25 (Candanedo and Athienitis, 2011) shows the possible utilization of a BIPV/T air system connected to an air-to-water heat pump in order to heat water in a thermal energy storage tank that can be used to heat room air or a floor (e.g., floor heating). The heat pump can also cool the water during the cooling season, but in this case it would make more sense to directly draw air from outside as opposed to the BIPV/T system. Also. if the air from

the BIPV/T is too hot, it might be preferable to use it first through an air–water heat exchanger and then through a heat pump. The addition of storage can serve to displace heating and cooling needs by converting solar electricity that the grid may not be able to take (due to high penetration of PV; for example in neighborhoods) into about four times as much useful stored heat or cool. The addition of storage will of course add extra cost, which may be comparable to that of boreholes in a geothermal system, but if combined with passive solar heating/cooling and heating/cooling system downsizing in conjunction with predictive control, it can result in reduce overall energy generating-HVAC system costs.
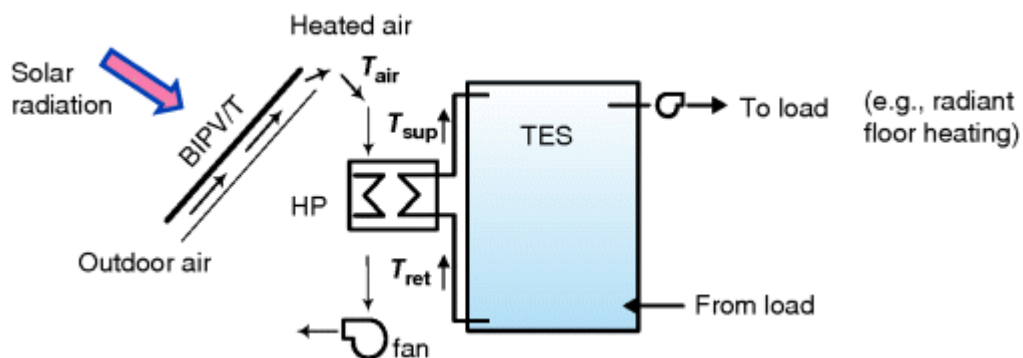
Fig. 2.25 Example of use of BIPV/T system as heat source for an air source heat pump connected to a thermal storage tank. Figure used with permission from Taylor & Francis (Candanedo and Athienitis, 2011), © 2011 Taylor & Francis

2.2.4.3 Ground Source Heat Pumps

Ground source heat pump systems can be sized (e.g., size and number of boreholes) based either on heating load or cooling load or both (but the highest one usually dominates). In the ÉcoTerra and Leaf House case studies in Chapter 7, the systems were primarily sized to meet peak heating demand. Sizing of boreholes can be done using (see Philippe, Bernier, and Marchio (2010)) the following equation, which is derived assuming that heat transfer in the ground occurs only by conduction and that moisture evaporation or underground water movement are not significant:

$$L = \frac{q_h R_b + q_y R_{10y} + q_m R_{1m} + q_h R_{6h}}{T_m - (T_g + T_p)} \tag{2.52}$$

where L is the total borehole length (in metres when SI units are used throughout the equation), T_m is the mean fluid temperature in the borehole, T_g is the undisturbed ground temperature, T_p, the temperature penalty, represents a correction to the undisturbed ground temperature due to thermal interferences between boreholes (in the case of a single borehole, $T_p = 0$), q_y, q_m, and q_h represent, respectively, the yearly average ground heat load (thermal annual imbalance), the highest monthly ground load, and the peak hourly ground load, R_{10y}, R_{1m}, and R_{6h} are effective ground thermal resistances corresponding to 10 years, one month, and 6 h ground loads, and R_b is the effective borehole thermal resistance.

The three ground thermal resistances are calculated assuming a cylindrical heat source solution in conjunction with temporal superposition (see Philippe, Bernier, and Marchio (2010) for more details).

2.2.5 Combined Heat and Power (CHP) for Net ZEBs

Another important technology for Net ZEBs are combined heat and power (CHP) systems, also known as cogeneration systems, or even trigeneration systems (Figure 2.26) (Dinçer and Rosen, 2002) when both useful heat and cooling are produced in addition to electricity using renewable fuels, such as biomass/biogas. Cooling is usually done using absorption chillers.
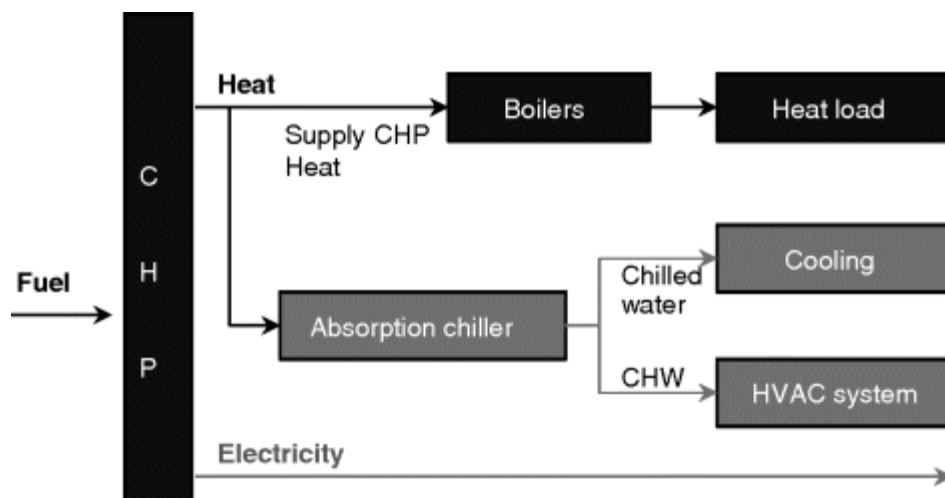
Fig. 2.26 Schematic of trigeneration system

Usually, it is difficult to achieve Net ZEB status based on a site energy balance for a house/building since the biomass usually has to be brought from another site. However, cogeneration is a thermodynamically efficient use of a renewable fuel and is *dispatchable* – that is, a CHP system can be run when electricity is needed. Standard electricity production systems discard some energy as waste heat whereas cogeneration systems use this thermal energy.

CHP systems using biofuels can be combined with solar systems (such as solar absorption cooling), thereby taking advantage of both options to reach net-zero energy consumption while reducing peak demand for electricity from the grid.

Thermal Efficiency

Heat engines are subject to the theoretical efficiency limits of the Carnot cycle. When the fuel is natural gas/biogas, a gas turbine based on the Rankine cycle is often used. Mechanical energy from the turbine drives an electric generator. The low-grade (i.e., low-temperature) waste heat rejected by the turbine can be used for space heating or cooling (using the heat to drive an absorption chiller).

Total efficiency in a trigeneration system is given by

$$\eta_T = (\text{electricity produced} + \text{useful heat} + \text{cooling})/(\text{total heat input})$$

Typical trigeneration models have losses as in any system. The energy distribution given next is represented as a percent of total input energy

$$\text{Electricity} = 45\%, \text{Heat} + \text{Cooling} = 40\%, \text{Heat Losses} = 13\%, \text{Line Losses} = 2\%$$

Microcogeneration devices producing electrical outputs less than 15 kW have a high potential to deliver energy efficiency and environmental benefits in a Net ZEB. The concurrent production of electrical and thermal energy from a single fuel source using fuel cells, Stirling engines, and internal-combustion engines can reduce energy consumption and associated greenhouse gas emissions, as described by the work of IEA/ECBCS Annex 42 (Beausoleil-Morrison, 2008). Numerous manufacturers are actively developing

microcogeneration devices (Onovwiona and Ugursal, 2006). The effective design of HVAC systems that can exploit and effectively utilize the thermal output of microcogeneration devices is critical if the benefits of microcogeneration are to be realized in a Net ZEB. Furthermore, research is required to develop effective control strategies to dispatch microcogeneration devices and associated HVAC components to match their performance with the low thermal and electrical demands of a Net ZEB. Small-scale CHP systems could possibly be combined with BIPV systems and biofuels to reach net-zero energy while reducing peak electricity demand from the grid since CHP is dispatchable. Studies showed that a PV+CHP hybrid system can enable the share of solar PV to be expanded by about a factor of five (Nosrat and Pearce, 2011; Pearce, 2009).

Notes

1. *Passive solar building:* a building that uses solar gains to reduce heating and possibly cooling energy consumption based on natural energy flows – radiation, conduction, and natural convection. The term "passive building" is often used instead of passive solar, particularly for cooling-dominated climates where natural ventilation is essential.

2. A linear lumped parameter system can be represented by a set of ordinary differential equations and thermal networks. A number of formulation approaches can be followed, including state-space (see Chapter 6). An important subset of linear systems are those with time-varying coefficients – also common in building energy analysis, where we can often represent some thermal conductances, such as a known but variable level of natural ventilation (or time-varying infiltration).

3. http://www.esru.strath.ac.uk/Reference/concepts/cibse_sum_temp/cibse_sum_temp.htm.

4. The TFM terminology used by ASHRAE and others refers usually to time domain coefficients and weighting factors based on *z*-

transforms and not Laplace or frequency domain transfer functions.

5. The number of poles is related to the number of wall layers (thermal capacitances) in a multilayered wall model. With no discretization, we have essentially infinite layers, infinite number of capacitances, and an infinite number of poles.

6. Building-added photovoltaics (BAPV) are also often referred to by many authors as BIPV – such as roof-mounted (ballasted) PV systems on racking structures. In this article, BIPV refers to PV modules integrated into the building envelope (roofs, walls) as an exterior layer.

7. Typical reference conditions are: (i) standard testing conditions (STC) of irradiance of 1000 Wm^{-2}, spectrum AM 1.5 and cell temperature of 25 °C, (ii) Nominal Operating Cell Temperature (NOCT) of irradiance of 800 Wm^{-2}, spectrum of air mass 1.5, ambient temperature of 20 °C and wind speed of 1 ms^{-1}.

8. Data generated based on specification datasheets of (up to) 50 PV module manufacturers.

References

ACI committee 122 (2002) 122R-02: Guide to thermal properties of concrete and masonry systems, in *Manual of Concrete Practice, American Concrete Institute (ACI)*, American Concrete Institute, Detroit, MI, USA.

American Society of Heating, Refrigerating and Air-Conditioning Engineers (ASHRAE) (2007) Radiant Heating and Cooling, in *ASHRAE Handbook – HVAC Applications*, American Society of Heating, Refrigerating, and Air-Conditioning Engineers (ASHRAE), Atlanta, GA, USA.

American Society of Heating, Refrigerating and Air-Conditioning Engineers (ASHRAE) (2008) Panel heating and cooling, in *ASHRAE Handbook – HVAC Systems and Equipment*, American Society of Heating Refrigerating and Air-Conditioning Engineers (ASHRAE), Atlanta, GA, USA.

American Society of Heating, Refrigerating and Air-Conditioning Engineers (ASHRAE) (2009a) *ASHRAE Handbook – Fundamentals*, SI edn, American Society of Heating, Refrigerating, and Air-Conditioning Engineers (ASHRAE), Atlanta, GA, USA.

American Society of Heating, Refrigerating and Air-Conditioning Engineers (ASHRAE) (2009b) Non-residential cooling and heating load calculations, in *ASHRAE Handbook – Fundamentals*, American Society of Heating, Refrigerating, and Air-Conditioning Engineers (ASHRAE), Atlanta, GA, USA.

American Society of Heating, Refrigerating and Air-Conditioning Engineers (ASHRAE) (2009c) Thermal comfort, In *ASHRAE Handbook – Fundamentals*, American Society of Heating, Refrigerating, and Air-Conditioning Engineers (ASHRAE), Atlanta, GA, USA.

Athienitis, A.K. (1994) *Building Thermal Analysis*, MathSoft Inc., Boston, MA, USA.

Athienitis, A.K., Bambara, J., O'Neill, B., and Faille, J. (2011) A prototype photovoltaic/thermal system integrated with transpired collector. *Solar Energy*, **85**, 139–153.

Athienitis, A.K. and Santamouris, M. (2002) *Thermal Analysis and Design of Passive Solar Buildings*, James & James, London.

Athienitis, A.K., Stylianou, M., and Shou, J. (1990) A methodology for building thermal dynamics studies and control applications. *ASHRAE Transactions*, **96**, 839–848.

Athienitis, A.K., Sullivan, H.F., and Hollands, K.G.T. (1986) Analytical model, sensitivity analysis, and algorithm for temperature swings in direct gain rooms. *Solar Energy*, **36**, 303–312.

Balcomb, J.D. and Jones, R.W. (1983) Passive solar design analysis, in *Passive Solar Design Handbook, Los Alamos National Laboratory*, American Solar Energy Society, Boulder, CO, USA, p. vii, 668 p.

Barton, P., Beggs, C.B., and Sleigh, P.A. (2002) A theoretical study of the thermal performance of the TermoDeck hollow core slab system. *Applied Thermal Engineering*, **22**, 1485–1499.

Bean, R., Olesen, B.W., and Kwang Woo, K. (2010) History of radiant heating & cooling systems. *Ashrae Journal*, **52**, 50–55.

Beausoleil-Morrison, I. (ed.) (2008) *An Experimental and Simulation-Based Investigation of the Performance of Small-Scale Fuel Cell and Combustion-Based Cogeneration Devices Serving*

Residential Buildings (Report of International Energy Agency (IEA) Annex42: Energy Conservation in Buildings and Community Systems Programme).

Beccali, G., Cellura, M., Brano, V.L., and Orioli, A. (2005a) Is the transfer function method reliable in a European building context? A theoretical analysis and a case study in the south of Italy. *Applied Thermal Engineering*, **25**, 341–357.

Beccali, G., Cellura, M., Brano, V.L., and Orioli, A. (2005b) Single thermal zone balance solved by transfer function method. *Energy and Buildings*, **37**, 1268–1277.

Beccali, G., Cellura, M., Lo Brano, V., and Orioli, A. (2003) An improved algorithm for thermal dynamic simulation of walls using Z-transform coefficients. Proceedings of 11th International Conference on Computational Methods and Experimental Measurements, Halkidiki, Greece, pp. 691–700.

Bourdoukan, P., Wurtz, E., Joubert, P., and Sperandio, M. (2008) Potential of solar heat pipe vacuum collectors in the desiccant cooling process: Modelling and experimental results. *Solar Energy*, **82**, 1209–1219.

Braham, G.D. (2000) Mechanical ventilation and fabric thermal storage. *Indoor and Built Environment*, **9**, 102–110.

Bridgeman, A. and Harrison, S. (2008) Experimental Evaluation of Solar Assisted Heat Pump Systems. *Eurosun 2008 Conference (Lisbon, Portugal).*

Candanedo, J.A. and Athienitis, A.K. (2011) Predictive control of radiant floor heating and solar-source heat pump operation in a solar house. *HVAC&R Research*, **17**, 235–256.

Carslaw, H.S. and Jaeger, J.C. (1959) *Conduction of Heat in Solids*, 2d edn, Clarendon Press, Oxford.

Cellura, M., Lo Brano, V., Mistretta, M., and Orioli, A. (2010) To assess the validity of the transfer function method: A neural model for the optimal choice of conduction transfer functions. Paper presented at: *ASHRAE Transactions (Albuquerque, NM).*

Ceylan, H.T. and Myers, G.E. (1979) *Long-time solutions to heat-conduction transients with tie-dependent inputs. American Society of Mechanical Engineers (Paper).*

Chen, Y., Athienitis, A., and Galal, K. (2013) Frequency domain and finite difference modeling of ventilated concrete slabs and

comparison with field measurements: Part 1, modeling methodology. *International Journal of Heat and Mass Transfer*, **66**, 948–956.

Chen, Y., Athienitis, A.K., and Galal, K. (2010a) Modeling, design and thermal performance of a BIPV/T system thermally coupled with a ventilated concrete slab in a low energy solar house: Part 1, BIPV/T system and house energy concept. *Solar Energy*, **84**, 1892–1907.

Chen, Y., Athienitis, A.K., and Galal, K. (2012) Thermal performance and charge control strategy of a ventilated concrete slab (VCS) with active cooling using outdoor air. *ASHRAE Transactions*, **118**, 556–568.

Chen, Y., Galal, K., and Athienitis, A.K. (2010b) Modeling, design and thermal performance of a BIPV/T system thermally coupled with a ventilated concrete slab in a low energy solar house: Part 2, ventilated concrete slab. *Solar Energy*, **84**, 1908–1919.

Cruickshank, C. and Harrison, S. (2008) Thermal Response of a Series-Connected Energy Storage to Multi-day Charge Sequences. *EuroSun 2008 Conference (Lisbon, Portugal)*.

Cruickshank, C. and Harrison, S. (2010) Heat loss characteristics for a typical solar domestic hot water storage. *Energy and Buildings*, **42**, 1703–1710.

Davies, M.G. (1982) Transmission and storage characteristics of walls experiencing sinusoidal excitation. *Applied Energy*, **12**, 269–316.

Davies, M.G. (1994) Thermal response of an enclosure to periodic excitation: the CIBSE approach. *Industrial and Engineering Chemistry Research*, **33**, 217–235.

Dinçer, I. and Rosen, M. (2002) *Thermal Energy Storage: Systems and Applications*, Wiley.

Drews, A., de Keizer, A.C., Beyer, H.G., Lorenz, E., Betcke, J., van Sark, W.G.J.H.M., Heydenreich, W., Wiemken, E., Stettler, S., Toggweiler, P. *et al.* (2007) Monitoring and remote failure detection of grid-connected PV systems based on satellite observations. *Solar Energy*, **81**, 548–564.

Duffie, J.A. and Beckman, W.A. (2006) *Solar Engineering of Thermal Processes*, 3rd edn, John Wiley & Sons, New York.

EERE (2013) EnergyPlus (Energy Efficiency & Renewable Energy (EERE), U.S. Department of Energy).

ESRU (2013) *ESP-r (Energy Systems Research Unit at the University of Strathclyde (ESRU))*.

Feustel, H.E. and Stetiu, C. (1995) Hydronic radiant cooling – preliminary assessment. *Energy and Buildings*, **22**, 193–205.

Fischer, S., Heidemann, W., Muller-Steinhagen, H., Perers, B., Bergquist, P., and Hellstrom, B. (2004) Collector test method under quasidynamic conditions according to the European Standard EN 12975-2. Paper presented at: *ISES 2001 Solar World Congress, 25 Nov-3 Dec 2001 (UK: Elsevier)*.

Hadorn, J.C. (2008) Advanced storage concepts for active solar energy, IEA-SHC Task 32 2003–2007. *EUROSUN 2008, 1st International Congress on Heating, Cooling, and Buildings (Lisbon, Portugal)*.

Henning, H.M. (2007) Solar assisted air conditioning of buildings – an overview. *Applied Thermal Engineering*, **27**, 1734–1749.

Henze, G.P., Felsmann, C., Kalz, D.E., and Herkel, S. (2008) Primary energy and comfort performance of ventilation assisted thermo-active building systems in continental climates. *Energy and Buildings*, **40**, 99–111.

Hittle, D.C. (1981) *Calculating Building Heating and Cooling Loads Using the Frequency Response of Multilayered Slabs*, University of Illinois at Urbana-Champaign, Illinois, United States, pp. 221.

Howard, B.D. (1986) Air core systems for passive and hybrid energy-conserving buildings. *ASHRAE Transactions*, **92**, 815–830.

Inard, C., Kenjo, L., and Caccavelli, D. (2007) Experimental and numerical study of thermal stratification in a mantle tank of a solar domestic hot water system. *Applied Thermal Engineering*, **27**, 1986–1995.

Inard, C., Meslem, A., and Depecker, P. (1998) Energy consumption and thermal comfort in dwelling-cells: A zonal-model approach. *Building and Environment*, **33**, 279–291.

Incropera, F.P. and DeWitt, D.P. (2002) *Fundamentals of Heat and Mass Transfer*, 5th edn, J. Wiley, New York.

International Organization for Standardization (ISO) (2003) *15099: Thermal performance of windows, doors and shading devices–detailed calculations (International Organization for Standardization)*.

iPHA (2013) *PHPP (The International Passive House Association (iPHA))*.

Jivan Shah, L. (2000) Heat transfer correlations for vertical mantle heat exchangers [for solar water heaters]. Paper presented at:

EuroSun 2000 ISES-Europe Solar Congress, June 2000 (UK: Elsevier).

Jury, E.I. (1964) *Theory and Application of the z-Transform Method*, vol. 3, Wiley, New York.

Kamminga, W. (1985) The approximate temperature within a flat plate solar collector under transient conditions. *International Journal of Heat and Mass Transfer*, **28**, 433–440.

Kimura, K.-I. (1977) Unsteady state heat conduction through walls and slabs, in *Scientific Basis for Air-Conditioning* (ed. K.-I. Kimura), Applied Science Publishers Ltd, London, UK.

King, D.L., Boyson, W.E., and Kratochvil, J.A. (2004) *Photovoltaic Array Performance Model*, Sandia National Laboratories, Livermore, CA.

Klein, S.A., Beckman, W.A., and Duffie, J.A. (1976) Design procedure for solar heating systems. *Solar Energy*, **18**, 113–127.

Kreith, F. and Bohn, M. (2001) *Principles of Heat Transfer*, 6th edn, Brooks/Cole Pub., Australia; Pacific Grove, Calif.

Lehmann, B., Dorer, V., Gwerder, M., Renggli, F., and Todtli, J. (2011) Thermally activated building systems (TABS): Energy efficiency as a function of control strategy, hydronic circuit topology and (cold) generation system. *Applied Energy*, **88**, 180–191.

Lehmann, B., Dorer, V., and Koschenz, M. (2007) Application range of thermally activated building systems tabs. *Energy and Buildings*, **39**, 593–598.

McQuiston, F.C., Parker, J.D., and Spitler, J.D. (2005) *Heating, Ventilating, and Air Conditioning: Analysis and Design*, 6th edn, John Wiley & Sons, Hoboken, N.J.

Montoro, D.F., Vanbuggenhout, P., and Ciesielska, J. (2011) *Building Integrated Photovoltaics: An overview of the existing products and their fields of application (6th Framework programme for Research and Technological development of the European Commission)*.

Norton, B., Eames, P.C., Mallick, T.K., Huang, M.J., McCormack, S.J., Mondol, J.D., and Yohanis, Y.G. (2011) Enhancing the performance of building integrated photovoltaics. *Solar Energy*, **85**, 1629–1664.

Nosrat, A. and Pearce, J.M. (2011) Dispatch strategy and model for hybrid photovoltaic and trigeneration power systems. *Applied Energy*, **88**, 3270–3276.

NRCan (2010) RETScreen (Version 4.0) (www.retscreen.net/: Natural Resources Canada (NRCan)).

Olesen, B.W. (2002) Radiant floor heating in theory and practice. *Ashrae Journal*, **44**, 19.

Onovwiona, H.I. and Ugursal, V.I. (2006) Residential cogeneration systems: review of the current technology. *Renewable & Sustainable Energy Reviews*, **10**, 389–431.

Oswald, D. and Sedlbauer, K.K.N. (1995) *Analyse und Prognose der hygienischen Zustände und Wartungsnotwendigkeiten in Außenwänden mit offenen Luftkreisläufen bei hybriden Heizsystemen (Report GB 128/1995) (Stuttgart, Germany: Fraunhofer Institut für Bauphysik).*

Patankar, S.V. (1980) *Numerical Heat Transfer and Fluid Flow*, Hemisphere Pub. Corp., New York, USA.

Pearce, J.M. (2009) Expanding photovoltaic penetration with residential distributed generation from hybrid solar photovoltaic and combined heat and power systems. *Energy*, **34**, 1947–1954.

Philippe, M., Bernier, M., and Marchio, D. (2010) Vertical geothermal borefields. *ASHRAE Journal*, **52**, 20–28.

PikeResearch (2012) *Building Integrated Photovoltaics - BIPV and BAPV: Market Drivers and Challenges, Technology Issues, Competitive Landscape, and Global Market Forecasts (Boulder: Navigant).*

Praene, J.P., Garde, F., and Lucas, F. (2005) Steady state model of a solar evacuated tube collector on sensitivity analysis. Paper presented at: *2005 ASME International Mechanical Engineering Congress and Exposition, IMECE 2005, November 5, 2005 - November 11, 2005 (Orlando, FL, United states: American Society of Mechanical Engineers).*

PVSAT-2 (2006) Intelligent Performance Check of PV System Operation Based on Satellite Data (European Commission thematic programme Energy, Environment, and Sustainable Development).

PVsyst (2012) PVSyst (Version 5.66) (http://www.pvsyst.com/en/).

Ren, M.J. and Wright, J.A. (1998) A ventilated slab thermal storage system model. *Building and Environment*, **33**, 43–52.

Schnieders, J. (1997) Comparison of the energy yield predictions of stationary and dynamic solar collector models and the models' accuracy in the description of a vacuum tube collector. *Solar Energy*, **61**, 179–190.

Seem, J.E., Klein, S.A., Beckman, W.A., and Mitchell, J.W. (1989) Comprehensive room transfer functions for efficient calculation of the transient heat transfer processes in buildings. *Transactions of ASME*, **111**, 264–273.

Shah, L.J. and Furbo, S. (1998) Correlation of experimental and theoretical heat transfer in mantle tanks used in low flow SDHW systems. *Solar Energy*, **64**, 245–256.

Skoplaki, E. and Palyvos, J.A. (2009) On the temperature dependence of photovoltaic module electrical performance: a review of efficiency/power correlations. *Solar Energy*, **83**, 614–624.

Spitler, J.D. and Fisher, D.E. (1999) On the relationship between the radiant time series and transfer function methods for design cooling load calculations. *HVAC&R Research*, **5**, 123–136.

Spitler, J.D., Fisher, D.E., and Pedersen, C.O. (1997) The radiant time series cooling load calculation procedure. *ASHRAE Transactions*, **103**, 503–518.

Stephenson, D.G. and Mitalas, G.P. (1967) Cooling load calculations by thermal response factor method. *ASHRAE Transactions*, **73**, 1–7.

Stephenson, D.G. and Mitalas, G.P. (1971) Calculation of heat conduction transfer functions for multi-layer slabs. *ASHRAE Transactions*, **77**, 117–126.

Strand, R.K. (1995) *Heat Source Transfer Functions and their Application to Low Temperature Radiant Heating Systems*, University of Illinois at Urbana-Champaign, IL, USA, pp. 185–185.

Torcellini, P., Deru, M., Griffith, B., Long, N., Pless, S., and Judkoff, R. (2006) Lessons learned from field evaluation of six high-performance buildings, in *ACEEE Summer Study*, National Renewable Energy Laboratory, Pacific Grove, California.

Tripanagnostopoulos, Y. (2012) Photovoltaic/thermal solar collectors, in *Comprehensive Renewable Energy* (ed. A. Sayigh), Elsevier, Oxford, pp. 255–300.

TRNSYS (2012) *Multizone Building (Type 56 – TRNBuild). In TRNSYS 17 Documention (Transient Energy System Simulation Tool (TRNSYS)).*

TRNSYS (2013) *Transient Energy System Simulation Tool (TRNSYS).*

Weiss, W. (2002) Solar combi-systems, in *IEA-SHC, Task 26 Report*, International Energy Agency (IEA).

Weiss, W.W. (2003) *Solar heating systems for houses: a design handbook for solar combisystems (Earthscan)*.

Winwood, R., Benstead, R., and Edwards, R. (1997) Advanced fabric energy storage I: review. *Building Services Engineering Research and Technology*, **18**, 1–6.

Xu, X., Wang, S., Wang, J., and Xiao, F. (2010) Active pipe-embedded structures in buildings for utilizing low-grade energy sources: A review. *Energy and Buildings*, **42**, 1567–1581.

Zondag, H.A., de Vries, D.W., van Helden, W.G.J., van Zolingen, R.J.C., and van Steenhoven, A.A. (2002) The thermal and electrical yield of a PV-thermal collector. *Solar Energy*, **72**, 113–128.

3
Comfort Considerations in Net ZEBs: Theory and Design

Salvatore Carlucci, Lorenzo Pagliano, William O'Brien and Konstantinos Kapsis

3.1 Introduction

A primary goal of buildings is to provide shelter, a space to live and engage in activities, and to facilitate provision of a comfortable environment. In the context of net-zero energy buildings (Net ZEBs), this means they should efficiently provide a comfortable environment while meeting the net-zero energy target. While comfort was once considered something that occupants passively tolerate, more recent research has recognized that occupants adapt themselves and their environment in order to improve comfort (de Dear and Brager, 1998). For this reason, comfort is tightly linked to energy performance; if occupants are not provided with comfortable conditions, they often adapt in the most convenient and responsive way rather than in energy conserving ways (Cole and Brown, 2009). Therefore, comfort should be critically assessed throughout the design and operation of Net ZEBs.

This chapter focuses on the three main categories of occupant comfort in buildings (thermal, visual, and acoustic) and indoor air quality (IAQ). These domains are all linked to each other and energy performance and must be incorporated into design as such, as shown in Figure 3.1. For instance, in naturally ventilated buildings, occupants are often faced with making compromises between acoustic comfort (noise from outside), thermal comfort (a cooling sensation from moving air or by introducing cooler outdoor air), and indoor air quality (fresh outdoor air).
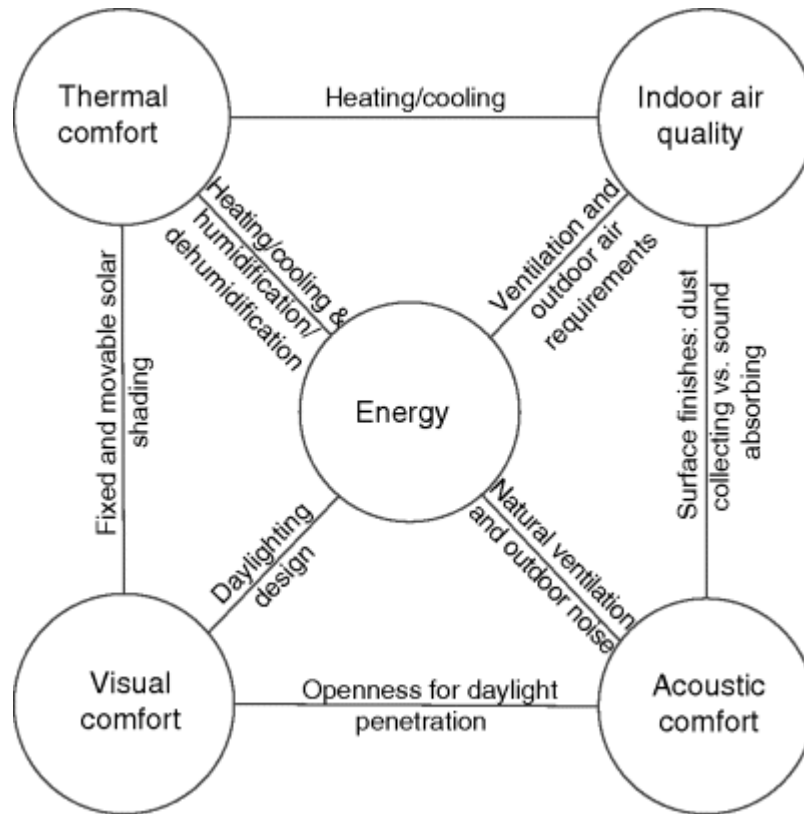
Fig. 3.1 Interactions between forms of comfort and building energy use with examples

Conventionally, thermal comfort has been considered a function of four environmental variables (air temperature, mean radiant temperature, relative humidity, and air speed) and two personal variables (metabolic activity and clothing level). Using an energy balance of the human body, comfort levels are predicted based on laboratory-based experiments and occupant ratings of comfort. A newer approach, known as adaptive thermal comfort, acknowledges that occupants tend to attempt to control the indoor environmental variables to restore comfort. Designing buildings according to comfort ranges suggested by adaptive comfort models generally predicts lower energy use as long as convenient, responsive, and effective means for occupants to improve their environment are available (e.g., operable windows).

Perspectives on visual comfort have also evolved recently due to renewed emphasis on daylighting as an important approach to reducing energy use for Net ZEBs, daylight's importance to health and well-being (Veitch, 2011), and the predominant use of vertically

oriented computer monitors (as opposed to deskwork). Visual comfort is affected by window size, position, and type, and interior geometry and finishes. Daylight glare can be controlled using fixed shading (e.g., overhangs and fixed louvers) and dynamic shading devices (e.g., blinds).

Acoustic comfort is often neglected during the design of standard and Net ZEBs because it can conflict with good daylighting and natural ventilation design. Recent reports of post-occupancy evaluation of low-energy buildings have revealed that they generally score high for all categories of occupant satisfaction except for acoustic quality and privacy (Abbaszadeh *et al.*, 2006; Newsham *et al.*, 2013). Acoustic comfort is directly linked to health and productivity (Crook and Langdon, 1974; Leaman and Bordass, 2000; Veitch, 1990). Furthermore, poor acoustic quality can compromise energy-conserving strategies like natural ventilation because occupants are faced with choosing between thermal comfort and having a quiet indoor environment.

Indoor air quality refers to the health and comfort-related properties of building air. Modern buildings tend to have high concentrations of occupants and materials that can compromise healthy IAQ unless sufficient solutions are implemented. While IAQ is typically good in new Net ZEBs and other high-performance buildings due to the emphasis on IAQ in many green building standards, the high concentration of synthetic materials presents a challenge.

As described in detail in this chapter, occupant comfort is complex and subtle; seemingly minor localized discomfort can adversely affect the perceived indoor environment. The objective of this chapter is to identify and quantify major sources of comfort.

3.2 Thermal Comfort

In order to assess the operational performance of a building and to quantify thermal discomfort, reliable methods to evaluate the long-term general thermal comfort conditions in a building are required. Net ZEBs are characterized by a notable reduction of energy required for space conditioning. But, such energy reduction should not compromise the quality of their indoor thermal environment.

In this section, a brief description of the two internationally-recognized thermal comfort approaches is reported, and a method to rate long-term thermal discomfort in a building is presented. Finally, two examples of the application of a thermal comfort assessment are introduced.

3.2.1 Explicit Thermal Comfort Objectives in Net ZEBs

Traditionally, the end-uses related to indoor environment control (heating, cooling, and ventilation) were dominant in the annual energy balance of a building (both residential and commercial) and constituted more than 50% of the total required primary energy (Pérez-Lombard *et al.*, 2008). Therefore, a strategy to reach the zero energy target consists of reducing the energy required for space heating and cooling as much as possible. However, in the words of the European standard EN 15251: "An energy declaration without a declaration related to the indoor environment makes no sense. Therefore, there is a need for specifying criteria for the indoor environment for design, energy calculations, performance and operation of buildings" (CEN, 2007). Thus, the specification of thermal comfort objectives that a building must achieve is a prerequisite for its design. Such objectives shall be explicitly included as an integral part of the definition of a Net ZEB and need to be quantitatively defined through reliable and explicit methods.

3.2.2 Principles of Thermal Comfort

Thermal comfort is usually used to indicate that an occupant of a building does not feel too hot or too cold in a given thermal environment. The concept has drawn the attention of a number of scientists and doctors and it has been defined according to three approaches: a physiological, a psychological, and an approach based on the heat-balance of the human body (also called the rational approach).

   – In the physiological approach, the thermal perception of an individual is due to the action of nervous impulses that start from thermal receptors in the skin and reach the hypothalamus. "Comfort, in this sense, is defined as the minimum rate of nervous signals from these receptors" (Höppe, 2002); therefore,

it is a state in which no pulses occur in an individual to correct the environment by his/her behavior (Hensen, 1991).

– In the psychological approach, thermal comfort is "that condition of mind which expresses satisfaction with the thermal environment" (ISO, 2005). This definition is reported in the international standard ISO 7730. A similar definition is reported in the ASHRAE Standard 55; although the ASHRAE definition highlights the subjective character of such a concept by adding to the previous definition the sentence "[...] and is assessed by subjective evaluation" (ANSI/ASHRAE, 2010).

– In the heat-balance approach, thermal sensation is related to the heat balance of the human body with its surroundings. Thermal comfort is the condition in which heat fluxes leaving the human body balance those incoming and the skin temperature and the sweat rate are within specified ranges depending on metabolic activity (Höppe, 2002).

In summary, the term thermal comfort is used to provide information about the thermal state of an individual within a given thermal environment. However, thermal comfort is not a single quantity that can be directly measured; its assessment is complex. Over time, a number of models and metrics have been proposed in the literature to quantify what thermal comfort is by predicting optimal environmental conditions or by assessing the predictable thermal stress caused to an individual given certain environmental conditions. Among all the proposed models, two main families have been used to describe the human thermal response in moderate environments: (i) the rational (or heat-balance) and (ii) the adaptive comfort models. These models have been used to develop standards that will be introduced in Section 3.2.2.3.

3.2.2.1 A comfort Model Based on the Heat-Balance of the Human Body

The heat-balance comfort model was mainly developed by Fanger and was derived by analyzing surveys carried out on Danish students exposed to steady-state conditions in controlled climate chambers for a 3 h period in winter at sea level, and by modeling the heat balance of the human body using a steady-state heat transfer model

(Fanger, 1970). Fanger's experiments showed that (i) skin wetness mainly indicates warm discomfort and mean skin temperature is strongly related to cold discomfort, (ii) skin wetness and mean skin temperature are both functions of activity level, and (iii) thermal dissatisfaction may be due to discomfort of the human body as a whole (general discomfort) or to the involuntary heating or cooling of one particular part of the body (local discomfort) (Djongyang, Tchinda, and Njomo, 2010). Specifically, the steady-state heat transfer model proposed by Fanger to describe thermal comfort requires that no local discomfort exist and that the human body be in heat balance with the environment. This last condition is necessary, but not sufficient because the human thermoregulatory system acts to restore "heat balance within wide limits of the environmental variables, even if comfort does not exist" (Fanger, 1970). It also assumes that mean skin temperature and skin wetness may fluctuate as a consequence of the action of the thermoregulatory system of the human body. But such fluctuations should remain within specified limits depending on the activity level, in order for a person to feel within the condition of thermal comfort. Fanger derived the relationships between the activity level (metabolic rate per body surface area) and both skin temperature and sweat secretion (evaporative heat loss per body surface area) using a linear regression model – Eqs. ((3.4), (3.5)). However, the source data are very scattered and correlation coefficients are not reported for either of the regression models.

Heat Balance of the Human Body

Summarizing the work of Fanger (1970) and Olesen (1982), the heat balance between an individual and his/her environment can be expressed, per unit of body surface area, by the equation

$$S = M \pm W \pm L_{cond} \pm L_{conv} \pm L_{rad} - E_{evap} - E_{res} \quad [\text{W m}^{-2}] \qquad (3.1)$$

where S is the rate of change of internal energy stored in the body, M is its metabolic rate, W is its external work, L_{cond} is the sensible heat loss by conduction due to contact of skin with solid objects, L_{conv} is the sensible heat loss by convection from the outer surfaces of the clothed body to air, L_{rad} is the sensible heat loss by radiation from

the outer surfaces of the clothed body to all surfaces of the environment viewed by the body, E_{evap} is the latent heat loss by evaporation (sweating and moisture diffusion) from the skin, and E_{res} is the total (sensible plus latent) heat loss by respiration. E_{evap} and E_{res}, if present, act to reduce the internal energy of the human body and both take negative values; the remaining heat fluxes on the right-hand side of Eq. (3.1) can be added or removed from a person (where addition is positive).

Assuming that the thermoregulatory system acts to prevent an increase of internal energy of the human body (so that $S = 0$) and that the heat loss for conduction with solids is negligible ($L_{cond} = 0$) and since L_{conv} and L_{rad} depend both on clothing, Eq. (3.1) can be rewritten as

$$M \pm W - E_{evap} - E_{res} = \pm L_{cloth} = \pm L_{conv} \pm L_{rad} \quad \left[\text{W m}^{-2}\right] \tag{3.2}$$

where

– Values of M for typical activities are reported in Table B.1 of ISO 7730;

– W is defined as the amount of energy that a human body absorbs or dissipated as a consequence of external loads. The human body is not an efficient thermal engine and its external mechanical efficiency, μ, defined as the ratio between the external work and the metabolic activity, $\mu = W/M$, is lower than 20% (Butera, 1998);

– E_{evap} is comprised of both heat loss by water vapor diffusion through the skin, (E_{diff}) – which is a function of skin temperature (t_{skin}) and the water vapor pressure in the ambient air ($p_{v,a}$) – and heat loss due to the evaporation of sweat on the skin (E_{sweat})

$$E_{diff} = 3.05 \cdot 10^{-3} \left(256 \cdot t_{skin} - 3373 - p_{v,a}\right) \quad \left[\text{W m}^{-2}\right] \tag{3.3}$$

$$t_{skin} = 35.7 - 0.0275(M - W) \quad [°C] \tag{3.4}$$

$$E_{\text{sweat}} = 0.42(M - W - 58.15) \quad [W\,m^{-2}]$$
(3.5)

– E_{res} is given by

$$E_{\text{res}} = 1.72 \cdot 10^{-5} M(5867 - p_{v,a})$$
(3.6)

– L_{cloth} is sensible heat loss by conduction due to skin contact with clothing. In Eq. (3.7) t_{cloth} is the clothing surface temperature and t_a is the ambient air temperature. The values of thermal insulation for typical clothing ensembles (I_{cloth}) are reported in Table C.1 of ISO 7730 and the values of thermal insulation for garments and chairs (I_{clu}) in Table C.2 and Table C.3 of the same standard.

$$L_{\text{cloth}} = \frac{t_{\text{skin}} - t_{\text{cloth}}}{0.155 \cdot I_{\text{cloth}}}$$
(3.7)

$$
\begin{aligned}
t_{\text{cloth}} = {}& 35.7 - 0.028(M - W) - 0.155\, I_{\text{cloth}} \cdot \\
& \cdot \{(M - W) - 3.05 \cdot 10^{-3}\,[5733 - 6.99(M - W) - p_{v,a}] \\
& -0.42[(M - W) - 58.15] - 1.7 \cdot 10^{-5} M(5867 - p_{v,a}) \\
& -0.0014\,M(34 - t_a)\}
\end{aligned}
$$
(3.8)

$$I_{\text{cloth}} = 0.161 + 0.835 \sum_i I_{\text{clu},i}$$
(3.9)

– L_{conv} is a function of the convective heat transfer coefficient (h_{conv}), which depends on the regime of convection around the body, the clothing area factor (f_{cloth}) and the difference between the temperature of the external surface of the clothing (T_{cloth}) and the ambient air temperature (T_a)

$$L_{\text{conv}} = f_{\text{cloth}} h_{\text{conv}}(T_{\text{cloth}} - T_a)$$
$$h_{\text{conv}} = \max\left\{2.38(T_{\text{cloth}} - T_a)^{0.25}; 12.1\sqrt{v_{\text{air}}}\right\}$$
(3.10)

where v_{air} is the relative air velocity.

– L_{rad} depends on the effective radiation area of the human body, which depends on its shape, and on clothing insulation. For

general purposes, it is used to approximate the effective radiation area of the human body. The term T_{mrt} is the mean radiant temperature, which is the "uniform surface temperature of an imaginary black enclosure in which an occupant would exchange the same amount of radiant heat as in the actual nonuniform space" (ANSI/ASHRAE, 2010).

$$L_{\text{rad}} = 3.95 \cdot 10^{-8} f_{\text{cloth}} \left[(T_{\text{cloth}} + 273.15)^4 - (T_{\text{mrt}} + 273.15)^4 \right] \qquad (3.11)$$

$$f_{\text{cloth}} = \begin{cases} 1.00 + 0.2\, I_{\text{cloth}} \text{ for } I_{\text{cloth}} < 0.5\ clo \\ 1.05 + 0.1\, I_{\text{cloth}} \text{ for } I_{\text{cloth}} > 0.5\ clo \end{cases}$$

In order to estimate the body area of an individual upon which these equations are based, the DuBois area (A_{DB}) can be calculated. It is a function of body weight (w_{b}) and height (h_{b}) (Du Bois and Du Bois, 1989):

$$A_{\text{DB}} = 0.20247\, w_{\text{b}}^{0.425}\, h_{\text{b}}^{0.725} \quad [\text{m}^2] \qquad (3.12)$$

The Thermal Comfort Equation

Inserting Eqs. ((3.3), (3.6), (3.10), (3.11)) in the energy balance Eq. (3.2) yields the so-called *thermal comfort equation*

$$\begin{aligned}
&(M - W) - 3.05 \cdot 10^{-3} \left[5733 - 6.99(M - W) - p_{\text{v,a}} \right] - 0.42[(M - W) - 58.15] \qquad (3.13) \\
&\quad - 1.72 \cdot 10^{-5} M \left(5867 - p_{\text{v,a}} \right) - 1.4 \cdot 10^{-3} M(34 - T_{\text{a}}) \\
&= 3.95 \cdot 10^{-8} f_{\text{cloth}} \left[(T_{\text{cloth}} + 273.15)^4 - (T_{\text{mrt}} + 273.15)^4 \right] - f_{\text{cloth}} h_{\text{conv}} (T_{\text{cloth}} -
\end{aligned}$$

This equation describes the heat balance of the human body, with the added constraints of Eqs. ((3.4), (3.5)), and depends on four environmental variables (air temperature, mean radiant temperature, velocity and humidity of ambient air) and on two personal variables (metabolic activity and clothing insulation). This equation permits, under the stated hypothesis, the calculation of the operative temperature, which will provide thermal comfort. Fanger (1970) assumes that "the thermal sensation at a given activity level is a function of the thermal load L of the body, defined as the difference between the internal heat production and the heat loss to the actual environment for an occupant hypothetically kept at the comfort

values of the mean skin temperature and the sweat secretion…". He further assumes that "in the comfort conditions the thermal load will be equal to zero" (Fanger, 1970). Operative temperature is defined as "the uniform temperature of an imaginary black enclosure in which an occupant would exchange the same amount of heat by radiation plus convection as in the actual nonuniform environment" (ANSI/ASHRAE, 2010). From the above definition, it can be shown that:

$$T_{op} = \frac{h_{rad} T_{mrt} + h_{conv} T_a}{h_{rad} + h_{conv}} \tag{3.14}$$

where T_{op} is the operative temperature, h_{rad} is the radiative heat transfer coefficient, and T_{mrt} is the mean radiant temperature of the surroundings of the occupant(s). These heat transfer coefficients are often assumed to be equal in magnitude, which may be a reasonable assumption for typical conditions and slow-moving air. Eq. (3.13) allows calculating the value of operative temperature for which the energy balance Eq. (3.2) is fulfilled. According to the rational approach, this value is the theoretical comfort temperature given a specific metabolic activity, clothing, air humidity and velocity. Being the value at which heat flows entering and leaving the body are balanced, or "neutralized", it is also called neutrality temperature and the thermal sensation corresponding is called neutral sensation or neutrality.

Fanger's Predicted Mean Vote and Predicted Percentage Dissatisfied

The thermal comfort equation allows us to calculate the sets of the values of the aforementioned variables for which the thermal load L of the body will be equal to zero. For conditions in which the thermal load L of the body is different from zero, Fanger proposes two indices to assess the degree of departure from the comfort situation: the *Predicted mean vote* (PMV) and the *Predicted percentage of dissatisfied* (PPD). PMV is an analytical index derived from the thermal comfort equation and tuned using approximately 1300 surveys:

$$\begin{aligned} \text{PMV} = {} & \left(0.303 e^{-0.036M} + 0.028\right)\left\{(M-W) - 3.05 \cdot 10^{-3}\left[5733 - 6.99(M-W) - p_{v,a}\right]\right. \\ & -0.42[(M-W) - 58.15] - 1.72 \cdot 10^{-5} M\left[5867 - p_{v,a}\right] - 1.4 \cdot 10^{-3} M(34 - T_a) \\ & \left. -3.95 \cdot 10^{-8} f_{\text{cloth}}\left[(T_{\text{cloth}} + 273.15)^4 - (T_{\text{mrt}} + 273.15)^4\right] - f_{\text{cloth}} h_{\text{conv}}(T_{\text{cloth}} - T_a)\right\} \end{aligned}$$

which allows us to estimate the mean value of the thermal sensation votes of a large group of people expressed according to the ASHRAE seven-point scale of thermal sensation (Table 3.1).

Table 3.1 ASHRAE seven-point scale of thermal sensation

Question	How do you feel at this time?						
Descriptor	Cold	Cool	Slightly cool	Neutral	Slightly warm	Warm	Hot
Value	−3	−2	−1	0	+1	+2	+3

Although PMV is derived for steady-state conditions, it can also be applied with an acceptable approximation if PMV is within the range [−2, +2] and the aforementioned variables describe small fluctuations within the following intervals (ISO, 2005):

– Metabolic activity: M ∈ [0.8, 4.0] met

– Clothing insulation: I_{cloth} ∈ [0.0, 2.0] clo

– Ambient air temperature: T_a ∈ [10.0, 30.0] °C

– Mean radiant temperature: T_{mrt} ∈ [10.0, 40.0] °C

– Relative air velocity: v_a ∈ [0.0, 1.0] m s^{-1}

– Partial pressure of water vapor in ambient air: $p_{v,a}$ ∈ [0, 2700] Pa

PPD is an index that predicts the percentage of people who are expected to feel uncomfortable (i.e., express a vote different from 0, +1, −1) if exposed to given environmental conditions and according to given metabolic rate and clothing. It is a function of PMV, and the so-called *PMV/PPD equation* is

$$PPD = 100 - 95\exp\left[-\left(0.03353\,PMV^4 + 0.2179\,PMV^2\right)\right] \in [5, 77) \qquad (3.16)$$
$$\text{subject to } PMV \in [-2, +2]$$

PPD can be plotted as a function of PMV (Figure 3.2). The rational model is often called the *PMV/PPD model.*
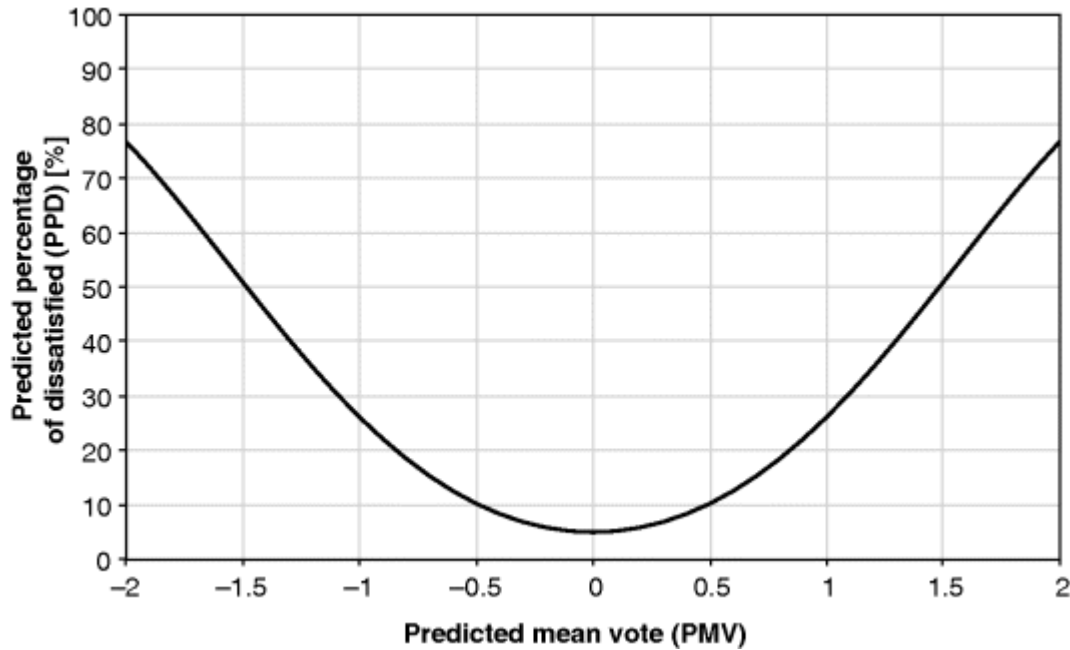

Fig. 3.2 PPD as a function of PMV

Local Thermal Discomfort

The thermal comfort equation can only be applied to the whole human body. However, a heat or cold stress acting only on one particular part of the body may also cause thermal discomfort. Local thermal discomfort is caused by excessive draughts, vertical air temperature gradients, radiant temperature asymmetry, and by physical contact with objects at high or low floor temperatures, among others.

In order to predict the likelihood of local thermal discomfort, a number of equations have been proposed and relate parameters describing the local discomfort phenomena with PPD. Threshold values are also suggested together with the equations and can be found in a number of existing standards and guidelines, such as ISO 7730 (ISO, 2005), CR 1752 (CEN, 1998), and ASHRAE 55 (ANSI/ASHRAE, 2010).

Limitations of the Heat-Balance Model

After the introduction of the rational model by Fanger, numerous studies supported it, (e.g., Parsons (2002)) or validated it (e.g., Humphreys and Nicol (2002)), or proposed modified formulations (e.g., Araújo and Araújo (1999); Mayer (1997); Xavier and Lamberts (2000); Yoon, Sohn, and Cho (1999)), or extensions (e.g., Lin and Deng (2007); Ole Fanger and Toftum (2002)), or highlighted its limitations (e.g., Croome, Gan, and Awbi (1993); Howell and Kennedy (1979); Humphreys and Hancock (2007)) and discrepancies (e.g., Benton, Bauman, and Fountain, (1990); Doherty and Arens (1988)). The main shortcomings of the Fanger model are: (i) people are considered *passive sensors* of the thermal environment, instead of active individuals who adapt their activity, clothing ensemble, and the customization opportunities of the building (operability of the windows, doors and solar shadings, or modification of set-points, etc.); (ii) it does not identify adaptation opportunities other than the modification of clothing ensemble; therefore, the model does not account for climatic differences and types of buildings, and is the same throughout the world; (iii) thermal neutrality may not necessarily represent the optimal conditions for a significant number of individuals since it does not account for psychological and cultural aspects; specifically (iv) thermal preferences are very asymmetrical around neutrality and, in some cases, people prefer non-neutral conditions; and consequently (v) the assumption that the interval [−1, +1] of the ASHRAE thermal sensation scale represents comfortable conditions may not universally reflect the preference for a large sample of people.

3.2.2.2 The Adaptive Comfort Models

Since the rational model was developed from studies in controlled climate chambers and it assumes steady-state conditions, the rational model is not reliable if applied to free-running (i.e., naturally ventilated) buildings according to some researchers. This is because it only partly takes into account human thermal adaptation to the indoor environment and other nonthermal factors, such as *personal factors* (age, sex, culture, economic status, etc.), *psychological factors* (thermal preference, thermal expectation, personal attitude, etc.), and *interaction with the environment* (visual and acoustic

perception, air quality level) (de Dear and Brager, 1998; La Gennusa *et al.*, 2010; Nicol and Humphreys, 2002). Also Fanger acknowledges that: "In non-air-conditioned buildings in warm climates, occupants may sense the warmth as being less severe than the PMV predicts" (Fanger, 2002). Instead, "if a change occurs such as to produce discomfort, people react in ways which tend to restore their comfort" (Nicol and Humphreys, 2002), since "[...] people [...] are not inert recipients of the environment, but interact with it to optimize their conditions" (Humphreys, 1994).

From the aforementioned research, the theoretical basis of adaptive comfort models is the concept of adaptation, which "might be interpreted broadly as the gradual diminution of the organism's response to repeated environmental stimulation" (de Dear and Brager, 1998). Adaptation manifests itself in three ways: physiological, psychological, and behavioral (Figures 3.3 and 3.4).
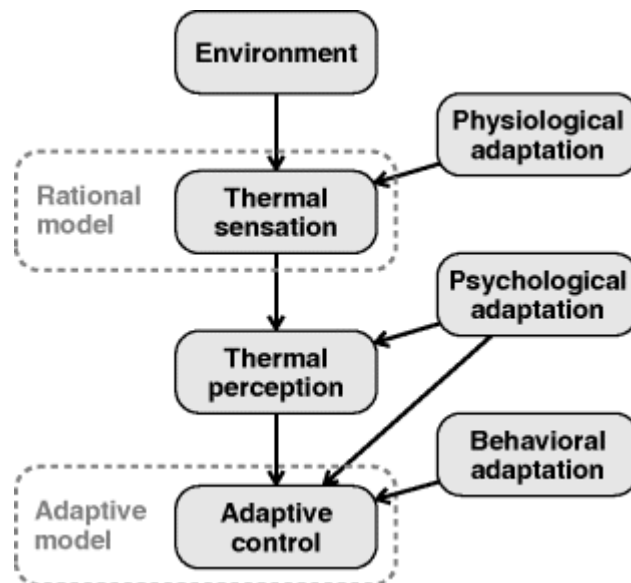
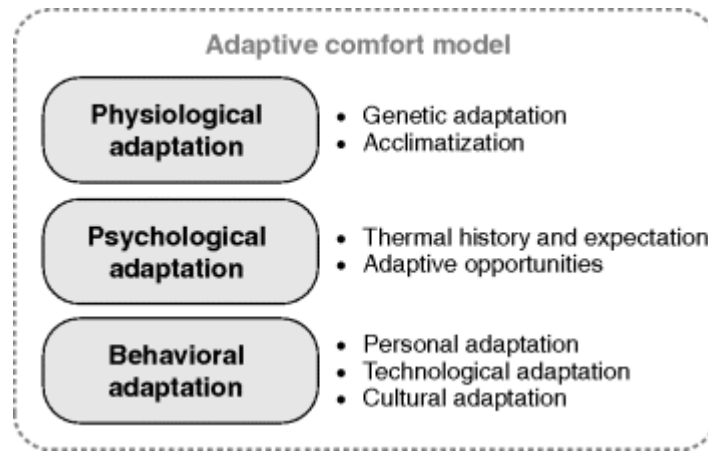**Fig. 3.3** Adaptive mechanisms and thermal comfort models

Fig. 3.4 Adaptive opportunities organized by typology of adaptation

Physiological Adaptation

Physiological adaptation can be considered as the set of all the changes used by the human thermoregulatory system to maintain constant the body internal temperature around a value of 37 ± 0.5 °C, in order to prevent damage to organs. Physiological adaptation is usually separated into two items: *genetic adaptation*, which involves an adaptive opportunity being passed from a generation to the next, and *acclimatization*, which manifests itself within one generation; the former could be considered as a result of a long-term adaptation to one given thermal environment, and the latter as a short-term adaptation that happens within hours to months.

Psychological Adaptation

Psychological adaptation can be considered as an altered perception of a given thermal environment, caused by an individual's thermal history and expectation. It is related to the habituation of an individual to a given thermal condition, since if an individual is repeatedly exposed to a certain thermal stimulus, his/her perception of the thermal stress, such as his/her expectation, diminishes. According to this, psychological adaptation is difficult to evaluate. It also depends on the adaptive opportunities that an individual can use to customize the indoor environment, since an individual attempts to tolerate, up to a certain degree, uncomfortable conditions if they can control them (Paciuk, 1989).

Behavioral Adaptation

Behavioral adaptation can be considered as the set of all those activities that are, voluntarily or involuntarily, implemented by an individual in order to modify the amount of energy and mass exchanges between his/her body and the surrounding thermal environment. Behavioral adaptation is usually classified into three types of action: *personal*, for example, removing one garment; *technological*, for example, modifying the set-point temperature of a building system, opening a window, or operating a shading device; and *cultural*, for example, a socially shared practice of resting during the hottest hours of summer days.

Bases and Formulations of the Adaptive Comfort Models

The models based on the heat balance of the human body were developed using climate chambers. The adaptive models, however, were derived from the statistical analysis of data from field studies of people in real buildings, for example, de Dear, Brager, and Cooper (1997) and Nicol and McCartney (2001). Humphreys (1978) and Auliciems (1981) demonstrated that, specifically in buildings in free-floating mode, the neutral temperatures are mostly linked to the outdoor temperatures, rather than to the indoor conditions as assumed by the rational model. The rational models are deterministic models; instead the adaptive models are derived from a black-box approach and relate indoor neutral temperatures to outdoor temperatures, by linear regression analysis. For this reason, the canonical equation of adaptive models is

$$T_{\text{comfort}} = a \cdot f(T_{\text{ext}}) + b \qquad (3.17)$$

Many adaptive approaches have been presented in the literature over the years and a number of them are summarized in Table 3.2.

Table 3.2 Terms of the canonical equation of adaptive models according to several studies

Author and year	a	$f(T_{ext})$	b	Range of applicability
(CEN, 2007)	0.33[a]	Exponentially weighted running mean outdoor air temperature	18.8[a]	$f(T_{ext}) \in [10, 30]$ °C
(ANSI/ASHRAE, 2004)	0.31[a]	Monthly mean outdoor air temperature	17.8[a]	$f(T_{ext}) \in [10, 33.5]$ °C
(Fato, Martellotta, and Chiancarella, 2004)	0.315[c] 0.34[a]	Exponentially weighted running mean outdoor air temperature	17.82[c] 17.63[a]	$f(T_{ext}) \in [5, 30]$ °C
(Nicol and McCartney, 2001)[1]	0.302[a]	Exponentially weighted running mean outdoor air temperature	19.39[a]	$f(T_{ext}) > 10$ °C
(Humphreys and Nicol, 2000)	0.54[a]	Monthly mean outdoor air temperature	13.5[a]	$f(T_{ext}) \in [10, 30]$ °C
(Nicol *et al.*, 1999)	0.36[c]	Historical monthly mean outdoor temperature	18.5[c]	$f(T_{ext}) \in [5, 35]$ °C
(de Dear and Brager, 1998)	0.255[a] 0.04[b]	Monthly mean outdoor effective temperature (ET^{*})	18.9[a] 22.6[b]	$f(T_{ext}) \in [5, 32]$ °C
(Nicol and Roaf, 1996)	0.38[b]	Monthly mean outdoor air temperature of the previous month	17.0[b]	$f(T_{ext}) \in (5, 35)$ °C

Author and year	a	$f(T_{\mathrm{ext}})$	b	Range of applicability
(Nicol and Humphreys, 1995)	0.534[b]	Exponentially weighted running mean outdoor air temperature	12.9[b]	N.d.
(Auliciems and de Dear, 1986)	0.31[a]	Running mean of the preceding fortnight	17.6[a]	N.d.
(Humphreys, 1978)	0.534[a]	Monthly mean outdoor air temperature	11.9[a]	N.d.

[a] Model exclusively developed for free-floating and naturally ventilated buildings.

[b] Model exclusively developed for air-conditioned buildings.

[c] Model developed for all types of buildings (naturally ventilated, mixed mode, conditioned).

[1] During the SCATs project, specific values of a and b were derived for the participating countries (France, Greece, Portugal, Sweden and UK).

Limitations of the Adaptive Models

One of the main limitations of adaptive models is that since they focus only on (operative) temperature, they neglect the effect of the other indoor environmental variables, such as air velocity and humidity. In particular, the increase of the average air velocity around the body increases convective heat exchange (ANSI/ASHRAE, 1982; Nicol, 2004). A correction for the effect of air velocity is presented in both EN 15251 and ASHRAE 55.

In the rational model, the effect of humidity on human thermal perception is "modest", since "typically a 10% higher relative humidity is felt to be as warm as a 0.3 °C rise in the operative temperature" (ISO 7730, annex F), but it is not negligible in the case of high air temperatures. According to Nicol (2004), high levels of relative humidity reduce the acceptability range around the

theoretical comfort temperature. However, this revision is not yet implemented in the current adaptive comfort models.

3.2.2.3 Standards Regarding Thermal Comfort

The ANSI/ASHRAE introduced the Fanger model in the ASHRAE Standard 55 for the first time in 1982 (ANSI/ASHRAE, 1982) and it was revised in 1992 (ANSI/ASHRAE, 1992), in 2004 (ANSI/ASHRAE, 2004), and in 2010 (ANSI/ASHRAE, 2010). The main modifications dealt with the upper limit for humidity in the comfort zone (based on the 10% dissatisfaction criterion). And the 1992 version introduced the diagram to estimate the temperature rise for comfort purposes as a function of air velocity produced by devices under direct control of occupants.

The adaptive comfort model, as proposed in ASHRAE Standard 55 (ANSI/ASHRAE, 2004, 2010), presents two acceptability classes: the 80% acceptability class, which is normative, and the 90% acceptability class, which is informative. Their ranges are reported in Table 3.3.

Table 3.3 Acceptability classes in ASHRAE 55

ASHRAE 55 class	Scope	PPD (%)	Fanger PMV	Adaptive ΔT_{op} (K)
90%	To be used when a higher standard of thermal comfort is desired	≤10	−0.5 ≤ PMV ≤ +0.5	±2.5
80%	To be used for typical applications and when other information is not available	≤20	−0.85 ≤ PMV ≤ +0.85	±3.5

The target comfort class has to be chosen on the basis of the level of thermal acceptability required in a building and whether very low variations of indoor environmental variables are required (e.g., in the case of sensitive or unhealthy occupants).

The model developed by Nicol and Humphreys (2002) has been more recently included in the European standards EN 15251 (CEN, 2007); hence, it is sometimes referred to as the European adaptive comfort model. EN 15251 proposes four comfort categories, which

are called I, II, III, IV, and are defined according to the ranges of PMV proposed by ISO 7730, but, in this case, the standard provides a description of the scope for every category (Table 3.4).

Table 3.4 Thermal comfort categories and acceptability ranges according to EN 15251

EN 15251 category	Description	Fanger	Adaptive	
		PPD (%)	PMV	ΔT_{op} (K)
I	High level of expectation and is recommended for spaces occupied by very sensitive and fragile people with special requirements like handicapped, sick, very young children and elderly persons	≤6	$-0.2 \leq$ PMV $\leq$ $+0.2$	±2
II	Normal level of expectation and should be used for new buildings and renovations	≤10	$-0.5 \leq$ PMV $\leq$ $+0.5$	±3
III	An acceptable, moderate level of expectation and may be used for existing buildings	≤15	$-0.7 \leq$ PMV $\leq$ $+0.7$	±4
IV	Values outside the criteria for the above categories. This category should only be accepted for a limited part of the year	>15	PMV<-0.7 and PMV > 0.7	

Again, the target comfort category has to be chosen on the basis of the application – new building or refurbishment – and whether very low variations of indoor environmental conditions are required.

3.2.3 Long-Term Evaluation of Thermal Discomfort in Buildings

In order to assess the thermal comfort performance of a building, a concise relationship between simulated or actual indoor hygrothermal conditions provided by a building, and occupants' expectation needs to be formulated. The thermal comfort models offer methodologies to calculate optimal predicted indoor conditions and provide ranges of the physical parameters of the indoor environment, which should be perceived as comfortable by a larger group of people. However, such optimal predicted indoor conditions are in the form of time series values; hence, they allow for visualizing the dynamic performance of a building with respect to set-point comfort conditions, but they do not provide an overall picture of its comfort performance.

A number of metrics for assessing human thermal response to climatic conditions or thermal stress have been proposed in the literature over the past decades. Several researchers have used terms such as *discomfort index*, *stress index*, or *heat index* to identify the (expected or actual) human thermal perception of the thermal environment to which an individual or a group of individuals is exposed. More recently, a new type of *discomfort index* has been proposed in scientific literature, standards, and guidelines. The new type allows for describing the long-term thermal discomfort in a building and for predicting uncomfortable phenomena in a concise way; in particular summer overheating. Most of these new indices summarize the thermal performance of a building in a single value. They are called *long-term thermal discomfort indices* and their ranking capability was evaluated by Carlucci (2013).

3.2.3.1 Background

The Chartered Institution of Building Services Engineers (CIBSE) introduced some overheating criteria based on the dry-resultant temperature (CIBSE, 2002) that, for low air velocity, can be approximated with the arithmetic mean of air and mean radiant temperatures of a given thermal zone. In 2005, ISO 7730 proposed five methods developed upon the Fanger comfort model. More recently, in 2007, EN 15251 reproposed three of the ISO 7730 indices and extended their use also to the adaptive comfort model, if compatible. Nicol *et al.* (2009) introduced an *Overheating risk* index, which is derived from the statistical analysis of the measured

data collected in free-running buildings during the SCATs Project (Nicol and McCartney, 2001). Robinson and Haldi (2008) also proposed an *Overheating risk* index based on the analogy between human thermal comfort perception and an electric capacitor. Often *degree-hours* are also used to estimate heating or cooling loads, but with different base temperatures. More recently, Borgeson and Brager (2011) used a particular weighted degree-hour index, called Exceedance$_M$, which weighs discomfort hours by hourly average occupancy in a specified zone of a building. Carlucci and Pagliano (2012) reviewed 16 long-term discomfort indices. Carlucci (2013) deemed that none of these fully satisfied the needs for assessing long-term thermal comfort in a building; hence, they developed a new index called Long-term Percentage of Dissatisfied (LPD). It improves upon previous work by establishing an index for evaluating the general comfort conditions in a building over the long term. According to the nomenclature introduced in Carlucci and Pagliano (2012), it is a symmetric and comfort-model-based index, not depending on comfort categories, and it is applicable to both summer and winter assessments. Its analytical expression accounts for hourly predicted Likelihood of Dissatisfied, which is calculated for each zone of a building. The hourly predicted Likelihood of Dissatisfied is weighted, at each time step, with the number of people inside the zone during the current time step, and is normalized over the total number of people inside the building, and over the total occupied period during the seasonal calculation period. The equation for calculating LPD is

$$\text{LPD}(p, \text{LD}) = \frac{\sum_{t=1}^{t_f} \sum_{z=1}^{Z} \left(p_{z,t} \cdot \text{LD}_{z,t} \cdot h_t \right)}{\sum_{t=1}^{t_f} \sum_{z=1}^{Z} \left(p_{z,t} \cdot h_t \right)} \tag{3.18}$$

where t is the index for the time step of the calculation period, t_f is the last progressive time step of the calculation period, z is the index number for the zones of a building, Z is the number of the zones, $p_{z,t}$ is the zone occupancy at a certain time step, $\text{LD}_{z,t}$ is the Likelihood of Dissatisfied inside a certain zone at a certain time step, and h_t is the duration of a calculation time step (by default 1 h). This index can be used to quantify thermal discomfort during cold periods, warm periods, or the whole year. Its formulation depends on (i) the chosen

thermal comfort model, (ii) the calculation period, and (iii) the type of discomfort.

3.2.3.2 The Likelihood of Dissatisfied

A Likelihood of Dissatisfied is a mathematical relationship that estimates the severity of the deviations from a theoretical thermal comfort objective, given certain outdoor and indoor conditions at a specified time and space location. The LDs are, therefore, short-term and local thermal discomfort indices. Since the theoretical thermal comfort objective depends on the reference comfort model, three different Likelihoods of Dissatisfied shall be identified; each of them based on one of the comfort models. Carlucci (2013) shows that the *Average PPD* (<PPD>) and the *Nicol et al.'s Overheating Risk* (NaOR) are useful indices for the following reasons: (i) they aim to predict the percentage of dissatisfied occupants in an environment by accounting for the nonlinear relationship between indoor conditions and human thermal sensation, and (ii) they provide a similar long-term ranking assessment, although they are based on the Fanger and on the European adaptive models, respectively.

Regarding the ASHRAE adaptive model, Carlucci (2013) proposes the new *ASHRAE Likelihood of Dissatisfied*, which has been developed only for naturally ventilated buildings by analyzing the data recorded in the ASHRAE RP-884. This short-term index is comparable with the previous two indices.

Average PPD

Average PPD (<PPD>) consists of calculating the mean PPD over the occupied hours within a given calculation period. It is an index based on the rational comfort model, but it does not depend on comfort categories. As currently defined, it could be used for assessing discomfort caused by overheating and overcooling. Its most important feature is that it accounts for the actual discomfort stress assessed through the PPD, according to the Fanger comfort model, without introducing a discontinuity as the indices based on comfort categories. It can be used for comfort optimization procedures and for comparing the thermal comfort performance of different buildings. However, since it relies only on the Fanger model, it is less suitable for the design of naturally ventilated buildings.

Nicol *et al.*'s Overheating Risk

Nicol *et al.* (2009) introduced an index (called here NaOR) to assess the summer overheating risk and proposes that thermal discomfort is not related to a specified temperature threshold, but to the difference between the actual operative temperature and the EN adaptive comfort temperature. It was derived from the analysis of comfort questionnaires collected in European naturally ventilated office buildings during the SCATs Project and takes into account that some people may feel uncomfortable even at the theoretical comfort temperature. In order to calculate NaOR, when the theoretical comfort temperature is exceeded, for each hour in a specified period, the offset from theoretical comfort temperature is recorded and a weighting factor is calculated. The weighting factor shows the nonlinear relationship between thermal discomfort and the deviation from the theoretical comfort temperature ([Eq. (3.19)](#)) (Nicol *et al.*, 2009). The authors derived the likelihood of overheating from a logistic regression analysis. The index predicts the percentage of individuals, $P(\Delta\theta_{op})$, voting +2 or +3, respectively warm or hot, on the ASHRAE seven-point scale of thermal sensation ([Table 3.1](#)):

$$P(\Delta\theta_{op}) \equiv \frac{\exp(0.4734 \cdot \Delta\theta_{op} - 2.607)}{1 + \exp(0.4734 \cdot \Delta\theta_{op} - 2.607)} \in [0.069, 1) \qquad (3.19)$$

where $\Delta\theta_{op}$ is the absolute value of the difference between the indoor operative temperature and the optimal comfort temperature calculated according to the European adaptive model. NaOR was derived from the EN 15251 adaptive comfort model and it is not related to comfort categories. It is an asymmetric index, which aims at predicting overheating phenomena and it is not suitable for mechanically cooled buildings.

ASHRAE Likelihood of Dissatisfied

An index for estimating the likelihood of thermal discomfort with respect to the ASHRAE adaptive model is missing in the literature; thus, it was necessary to build a new analytical function, called *ASHRAE Likelihood of Dissatisfied* (ALD), which has been determined via a logistic regression analysis performed on the data collected in the ASHRAE RP-884 database. Its final expression is

$$\text{ALD}\left(\Delta\theta_{op}\right) = \frac{\exp\left(0.008\,\Delta\theta_{op}^2 + 0.406\,\Delta\theta_{op} - 3.050\right)}{1 + \exp\left(0.008\,\Delta\theta_{op}^2 + 0.406\,\Delta\theta_{op} - 3.050\right)} \in [0.05,\ 1.00) \tag{3.20}$$

where $\Delta\theta_{op}$ is the absolute value of the difference between the indoor operative temperature and the optimal comfort temperature calculated according to the ASHRAE adaptive comfort model.

Comparison of the Selected Likelihood of Dissatisfied

In order to provide a graphical comparison among the three selected likelihood distributions, it is necessary to present them in a form where they have the same input variable, for example, the operative temperature. Hence, for the distribution based on the Fanger model, a selection of PMV values has to be translated in operative temperatures by making some assumptions. In this case, we assume that the dry-bulb air temperature is equal to the mean radiant temperature (hence equal to the operative temperature), indoor relative humidity is equal to 50%, air velocity amounts to 0.1 m s^{-1}, metabolic activity is 1.2 met, the external work is zero met, and clothing resistance is 0.5 clo in summer, and 1.0 clo in winter. According to these assumptions, there are two likelihood distributions derivable for the Fanger model: one for summer and one for winter. The four likelihood distributions show quite similar trends (Carlucci, 2013), although there are a number of differences among them:

   – Their scopes: the Fanger ones apply to mechanically conditioned buildings, while the Adaptive ones apply to free-floating buildings.

   – The datasets where they were derived from: data recorded in thermal chamber (Fanger, 1970), data from field measurements and surveys as in the SCATs Project (Nicol and McCartney, 2001) and ASHRAE RP-884 (de Dear, 1998).

   – The methods used for deriving them: Griffiths's method (Griffiths, 1990) and binning of sample data method (de Dear, Brager, and Cooper, 1997).

– The values of their theoretical comfort temperatures are different.

3.2.3.3 Applications of the Long-Term (Thermal) Discomfort Indices

Two possible uses of the long-term discomfort indices are introduced here and are applied in the following sections.

Thermal Assessment of Buildings

The basis of a long-term thermal discomfort index is that it is a single value, which aims to estimate the overall predicted percentage of dissatisfied people inside the whole building over a given period. Therefore, LPD can be used to assess the quality of a building (envelope and mechanical systems) in providing thermal comfort and to identify if there are differences in its winter or summer performance during the optimization of a new building or during the operational ranking of an existing building. The long-term discomfort index based on an adaptive comfort model (NaOR for the European adaptive model and ALD for the ASHRAE adaptive comfort model) is suggested for free-floating buildings and one based on the Fanger comfort model (Average PPD) is suggested for conditioned buildings.

Although the statement of discomfort thresholds or comfort categories is a challenging issue and it is also a subject of debates (Alfano, d'Ambrosio, and Riccio, 2001; Arens *et al.*, 2010), there are two assumed thermal discomfort levels: a standard level corresponding to 80% of acceptability (or equally, to 20% of dissatisfaction) and a level corresponding to a 90% of acceptability (or equally, to a 10% of dissatisfaction). Under this assumption, some acceptability thresholds could be suggested for the long-term discomfort indices in the adaptive and Fanger versions (Table 3.5).

Table 3.5 Proposal for thresholds to be used with the Long-term Percentage of Dissatisfied

Type of building	Version of LPD	Threshold for LPD	
		80% acceptability	90% acceptability
Conditioned	Fanger	LPD ≤ 30%	LPD ≤ 17%
Free-floating	Adaptive (both European and American)	LPD ≤ 20%	LPD ≤ 10%

Building Optimization as Minimization of Thermal Discomfort

Since long-term discomfort indices allow comfort to be assessed from building simulation, they can be used within multiobjective optimization problems. Thus, the optimization problem results in a bi-objective optimization.

$$\min_{x \in X} F = \begin{cases} \text{LPD}_{\text{summer}}(x^+) \\ \text{LPD}_{\text{winter}}(x^+) \end{cases} \quad \text{for} \quad x^* \in X \tag{3.21}$$

An example of this optimization approach is presented in Section 5.4.

This section on thermal comfort has discussed traditional thermal comfort models, adaptive thermal comfort, and finally long-term thermal comfort indices and their application. Thermal comfort is also discussed in Chapters 5 and 7 through examples and case studies.

3.3 Daylight and Visual Comfort

3.3.1 Introduction

Occupants clearly prefer having windows in their working environment as a means of illumination and view to the outdoors (Boyce, Hunter, and Howlett, 2003). Moreover, daylight and views may have a positive effect on occupants' health, well-being, and productivity (Farley and Veitch, 2001; Veitch and Galasiu, 2012). In

addition, the presence of windows or skylights on buildings may have a positive effect on retailing (Heschong, Wright, and Okura, 2002). Finally, windows can provide useful passive solar gains and offer a means, if operable, for occupants to introduce fresh outdoor air into the space and increase local air speeds. All case studies in Chapter 7, and particularly ENERPOS and NREL RSF, demonstrate the driving role that daylighting should play in buildings and their design process.

Despite the architectural, comfort, energy, and functional benefits of glazing, it often adds to construction costs and may increase space conditioning energy if not designed carefully. Glazing typically has lower thermal resistance than opaque wall or roof constructions and can cause unwanted solar gains – particularly in cooling-dominated climates and/or buildings that have high internal gains.

Modestly sized windows with fixed shading devices are the preferred configuration to simultaneously optimize energy performance and occupant comfort. Façades with more than a 60% window-to-wall ratio should be avoided, as they tend to cause thermal and visual discomfort due to excess daylight and solar gains. Fixed shading devices function best for equator facing façades and do not perform well for non-equator-facing façades; nor do they offer privacy or the ability to darken a space (e.g., for presentations or sleeping). Because of this lack of flexibility, dynamic shading systems have gained popularity as a means to complement fixed shading. The three-section façade concept (Tzempelikos and Athienitis, 2003) allows fenestration system properties to be tailored to the particular function of the façade at different heights above the floor. A three-section façade (Figure 3.5) consists of: (i) a bottom (spandrel) section, which is opaque (e.g., insulated wall) as it would contribute little to daylighting (LBNL, 1997), (ii) a middle (viewing) section, which normally extends from the workplane (0.8 m above the floor) to about 1.5–2.0 m above the floor and allows views to the outdoors, and (iii) a top (daylight) section, which has the primary function of admitting daylight deep into the space while protecting occupants from glare and direct solar radiation. When applied to shallow buildings, three-section façades can be optimized to reduce electric lighting and maximize natural ventilation (e.g., see the ENERPOS and NREL RSF case studies in Chapter 7). In addition, it has been

shown that occupants prefer shallow (no more than 15 or 20 m wall to wall) over deep buildings, due to daylight availability, views to the outdoors, and natural ventilation potential (Leaman and Bordass, 2005). However, in order to fully realize the energy savings from daylighting, manual or automated lighting controls must allow for it to be properly integrated as a complement to electric lighting.
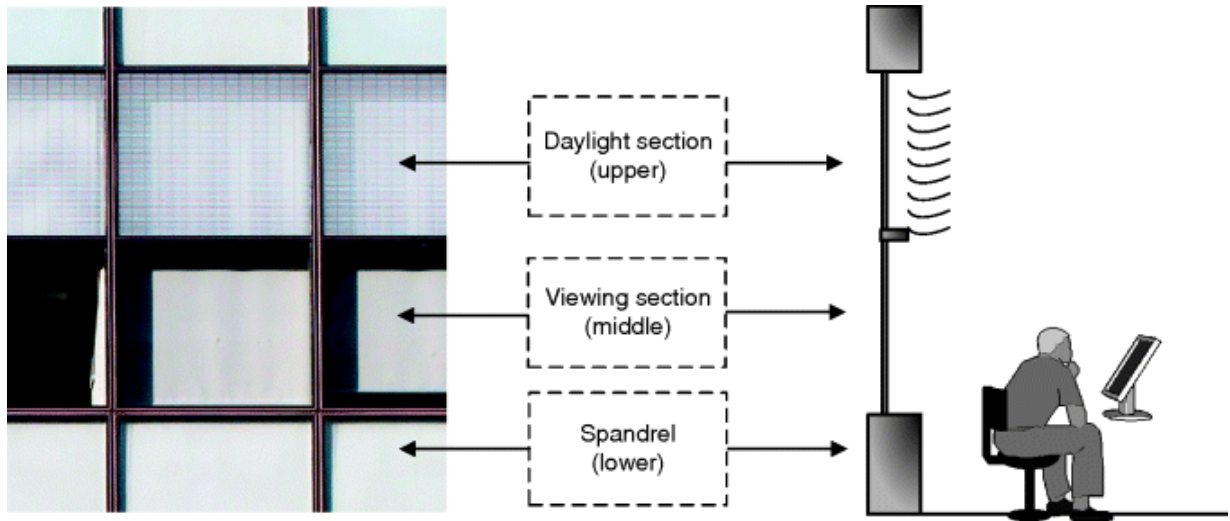

Fig. 3.5 Three-section façade concept and three-section façade of the Engineering, Computer Science and Visual Arts Integrated Complex (EV) at Concordia University, Montreal, Canada

This section provides an overview of visual comfort issues with emphasis on their quantification, including illuminance- and luminance-based metrics.

3.3.2 Adaptation Luminance

For the eye to be able to function well, it has to adapt to the prevailing luminance conditions (adaptation luminance) by constricting and dilating the iris, neurologically, and photochemically (Rea, 2002). Adaptation to varying transient luminance takes some time (seconds to minutes, depending on the magnitude of the luminance shift) and varies through the period of a task, either because of the eye movement from one point to another or due to daylight variation (Osterhaus, 2009). If high contrast conditions are present, the eye stresses to adapt, which translates to feelings of annoyance (discomfort glare). Hence, the luminance ratio

between the visual task, its adjacent surroundings, and more distant surfaces is recognized as a major, if not the most important, determinant for a glare-free environment (ISO, 2006). Depending on the environment, the luminance levels might significantly vary from one viewpoint to another. However, recommendations (Table 3.6) can be followed to ensure that in the case of nonuniform luminance surfaces, visual comfort can be maintained.

Table 3.6 Luminance ratio recommendations (Rea, 2002)

Maximum luminance ratios	Description
3 : 1 or 1 : 3	Between visual task and immediate surroundings
10 : 1 or 1 : 10	Between visual task and near surroundings
20 : 1 or 1 : 20	Between visual task and remote surroundings
40 : 1 or 1 : 40	Between visual task and any surface in the field of view

In addition, it is more difficult for the eye to adapt when a high luminance source is located at the center of the visual field than on the periphery. Considering that most tasks require the occupant to look straight ahead (e.g., at a computer screen), the preferred orientation of the occupant relative to the window is 90° (Osterhaus, 2005) or an orientation close to this angle. In all cases, having the window, shaded or unshaded, located in front or behind the occupant should be avoided, as it increases the probability of glare (*discomfort glare*, when the occupant faces the window, or *veiling glare* due to the window reflection on the computer screen) occurring.

3.3.3 Illuminance-Based Performance Metrics

Most lighting design standards and metrics rely primarily on illuminance-based levels and provide guidelines mainly for horizontal (workplane) illuminance levels. However, the human eye responds to luminance levels and variations. Moreover, most visual

tasks take place on nonhorizontal planes (e.g., a computer screen). Existing daylight metrics based on workplane illuminance and conventional daylight glare metrics have not yielded consistent predictions of daylight glare (Wienold and Christoffersen, 2006). However, useful metrics exist that can be used to influence design decisions toward a luminance-balanced environment.

3.3.3.1 Daylight Autonomy and Continuous Daylight Autonomy

Daylight autonomy (DA) indicates the fraction of time when the workplane illuminance meets or exceeds a set threshold (e.g., 500 lux for typical office environments), by daylight alone (Reinhart, Mardaljevic, and Rogers, 2006). The metric can be expressed as a fraction of occupied hours, daylit hours or occupied hours that are daylit, over a given period of time (e.g., a year). For nondimmable (i.e., on/off) electric lighting that is automatically controlled by occupancy and/or a daylight sensor, DA can be directly translated into potential energy savings.

An extension to DA is continuous Daylight Autonomy (DA_{cont}), which indicates the fraction of time when the minimum workplane illuminance requirements are partly or fully met by daylight alone. This is suitable for quantifying the energy savings from automatically dimmable lighting.

$$DA_{cont} = \frac{\sum_{t=1}^{n} \min\left\{\frac{E_{daylight}}{E_{min}}, 1\right\}}{n} \tag{3.22}$$

where n is the total number of time steps (e.g., hours), E_{min} is the minimum workplane illuminance requirement, and $E_{daylight}$ is the workplane illuminance provided by daylight only, at a given time step t.

3.3.3.2 Useful Daylight Illuminance

Useful daylight illuminance (UDI) categorizes workplane illuminance levels for typical office spaces, due to daylight only, into three bins as shown in Table 3.7 (Nabil and Mardaljevic, 2006). UDI offers the advantage over DA and DA_{cont} that it quantifies the

duration of high illuminance and thus, may indicate cause for concern from chronic visual discomfort. However, there is some discussion in the research community about whether the thresholds for the bins are appropriate (Mardaljevic, Heschong, and Lee, 2009). All metrics are relatively straightforward to obtain from BPS tools or measurements (e.g., on scale models and full-size mock-ups) and provide an indication of year-round daylight quality for the building design and climate of interest.

Table 3.7 Useful daylight illuminance (UDI) (Nabil and Mardaljevic, 2006).

Workplane illuminance range	Symbol	Implications
<100 lux	$UDI_{<100lux}$	Fraction of time when daylight is insufficient as the only source of illumination
100 to 2000 lux	$UDI_{100-2000lux}$	Fraction of time when daylight is sufficient to completely or partially (in the lower part of the range) offset electric lighting
>2000 lux	$UDI_{>2000lux}$	Fraction of time when daylight is likely associated with visual discomfort

3.3.4 Luminance-Based Performance Metrics

Several luminance-based metrics have been developed through the years to try to predict and quantify glare. However, further research and validation studies are still needed to produce robust luminance metrics that will be able to assess the impact of potential glare sources. Daylight glare probability (DGP) proposed by Wienold and Christoffersen (2006) has shown promising results. DGP is a directional view-dependent metric; thus, the designer should be aware of the possible locations and orientations of the occupants relative to the window as well as the tasks to be performed. Furthermore, DGP allows the impact of interior design and surface finishes to be evaluated.

3.3.4.1 Daylight Glare Probability

Daylight glare probability, which is based on vertical eye illuminance and glare source luminance, detects glare sources by contrast ratios. DGP uses luminance mapping of a scene generated either by daylighting BPS tools or using high dynamic range (HDR) images (e.g., Figure 3.6). Thus, it can be used for new building designs or retrofits. DGP uses a scale to evaluate glare risk, such that if $DGP < 0.30$ then the glare source is "barely perceptible," if $0.3 \leq DGP \leq 0.45$ the glare source is "disturbing," while if $DGP > 0.45$ then glare source is "intolerable." The DGP is calculated as follows:

$$DGP = 5.87 \cdot 10^{-5}\, E_v + 9.18 \cdot 10^{-2} \log\left(1 + \sum_i \frac{L_{s,i}^2\, \omega_{s,i}}{E_v^{1.87}\, P_i^2}\right) + 0.16 \qquad (3.23)$$
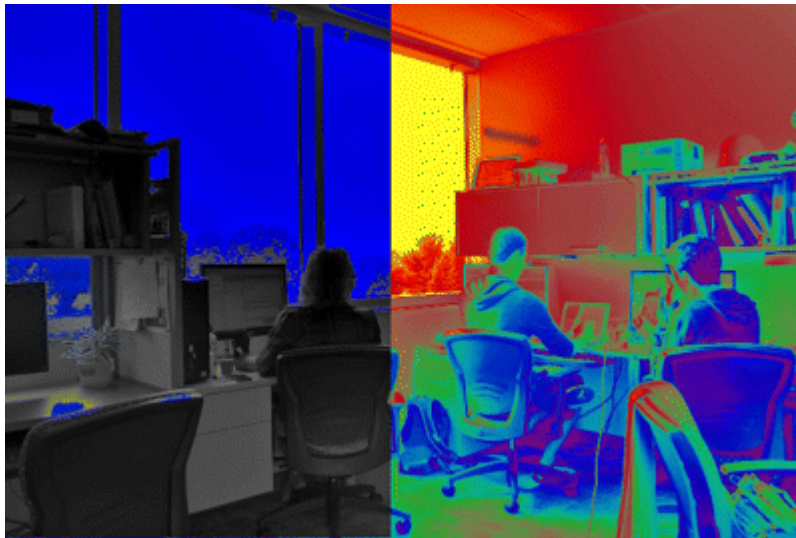
Fig. 3.6 Daylight glare analysis for a shared office space: False color image of high dynamic range (HDR) photograph (right) and glare analysis performed with Evalglare software, where the colored regions indicate sources of daylight glare (left). (Photo courtesy of Brent Huchuk)

The position index (P) located above the line of vision is expressed as

$$\ln P = \left[35.2 - 0.31889\tau - 1.22e^{-2\tau/9}\right] \cdot 10^{-3}\sigma + \left[21 + 0.26667\tau - 0.002963\tau^2\right] \cdot \qquad (3.24)$$

while P located below the line of vision is expressed as

$$P = 1 + 0.8\frac{R}{D} \quad \text{if} \quad R < 0.6D \tag{3.25}$$

$$P = 1 + 1.2\frac{R}{D} \quad \text{if} \quad R \geq 0.6D \tag{3.26}$$

$$R = \sqrt{H^2 + Y^2} \tag{3.27}$$

where E_v is the vertical eye illuminance (lux), L_s is the source luminance (cd/m²), ω_s is the solid angle of the source (°), P is the position index, τ is the angle from the vertical of plane containing source and line of sight (°), σ is the angle between line of sight and line from eye to source (°), D is the distance between eye and plane of source, in the view direction, H is the vertical distance between source and view direction, and Y is the horizontal distance between source and view direction.

3.3.5 Daylight and Occupant Behavior

The last aspect described in this section is about the interaction between occupants and the daylighting/lighting domain. Dynamic window shading devices are normally installed with the design intent to be temporarily closed to provide privacy and protection from glare, while remaining partly or fully open to exploit daylight and passive solar gains, when possible. However, observations have revealed that occupants tend to be inactive users of shading systems (e.g., blinds and roller shades). The mean rate of shade movement is well below once per day for most office buildings with some shades being never moved (Van Den Wymelenberg, 2012). Instead of being highly responsive to daylight conditions, occupants tend to leave their shades in a position that "causes the least trouble" (Bordass *et al.*, 2001) or minimizes conflict between occupants in shared offices (Cohen *et al.*, 1999), namely, partly or fully closed. This leads to reduced views and unnecessary electric lighting use that ultimately increases energy use relative to what designers predicted. An effective daylight design should create a pleasant, glare-free environment, so as to minimize actions that will reduce daylight admission (Boyce, Hunter, and Howlett, 2003), while exploiting daylight. Good passive and indoor design, such as window geometry, window type, fixed exterior shading, interior design surface

reflectances, and strategic furniture layout, can reduce the frequency of closed shades and increase the daylight utilization and view to the outdoors. Moreover, field surveys reveal that occupants value some degree of individual control over the shading devices and windows (Leaman and Bordass, 2005). This aspect cannot be ignored as occupants are significantly less active and energy-conserving than designers might expect.

3.4 Acoustic Comfort

Acoustic comfort describes the indoor acoustic conditions of a building with regard to providing a healthy and productive environment for occupants. It is critical to properly functioning buildings, yet often neglected during design and in green building standards (Hodgson, 2008). Acoustic comfort has become even more critical because strategies to reduce energy use and improve indoor air quality often directly contradict good acoustic comfort design practices:

– Natural ventilation improves both real and perceived thermal comfort, provides fresh air to supplement or temporarily eliminate the need for mechanical ventilation, and in many climates can completely eliminate the need for mechanical cooling. However, open windows often introduce outdoor noise into the workplace, which is a particular concern in urban areas or beside busy streets (Ghiaus *et al.*, 2006). Furthermore, good cross-ventilation requires an open concept design. However, a lack of partitions between spaces (e.g., cubicles instead of floor-to-ceiling walls) results in higher levels of sound transmission. Thus, distracting conversations and other noises can cause poor occupant concentration and comprehension.

– Deep daylight penetration in a space requires an open concept design, similarly to natural ventilation. Closed offices and other small perimeter spaces, if enclosed, prevent daylight from being able to penetrate to its full potential (about 1.5 to 2.5 times window height for standard windows (Reinhart, 2005) and five to six times window height if advanced reflective systems are in place (Guglielmetti, Pless, and Torcellini, 2010)).

– Exposed thermal mass (e.g., concrete structures) facilitates greater ability to absorb solar gains and regular air temperatures – an important element of low-energy passive buildings. However, hard smooth surfaces are also poor sound absorbers and can lead to poor acoustic comfort if such surfaces dominate a space.

The strategies to mitigate poor acoustic quality (the so-called ABCs of acoustic design) include absorbing, blocking, and covering noise. Absorbing means the use of strategically placed surfaces (e.g., acoustic ceiling tiles, wall panels, carpeting, furniture, and/or sound-absorbing artwork) to reduce sound reflectance in a space. Blocking requires that the source of sound be isolated (e.g., servers or photocopiers in a separate room). Covering means masking sounds with white noise generators such that individual sounds (e.g., occupant chatter) are indistinguishable. For instance, the NREL RSF (see Chapter 7 for details) uses white noise generators to cover conversations and other sounds. While mechanical ventilation often plays this role, RSF does not use forced-air for heating and cooling, so ventilation rates and the corresponding noise levels are relatively low. Regardless, HVAC systems (e.g., fans and ducts) can be a source of unwanted noise and careful design is important.

As for other forms of occupant comfort, metrics for quantifying acoustic comfort are diverse and complex. Metrics for interior surfaces include sound transmission class (STC), which quantifies a surface's ability to block sound from being transmitted, and noise reduction coefficient (NRC), which defines the fraction of sound that is absorbed upon hitting it. Speech intelligibility index is a measure of how clearly one occupant can hear others and has been used in numerous postoccupancy evaluations of buildings (Hodgson, 2008; Newsham *et al*., 2013). Ambient noise level, measured in decibels (dB), indicates the magnitude of background noise in a space. A noise criterion (NC) level of between 30 and 40 is acceptable (Hodgson, 2008). Normally, noise levels are based on an A-weighting, which defines the human ear's hearing ability at different frequencies.

3.5 Indoor Air Quality

Indoor air quality is a measure of the healthiness and comfort of air in buildings. IAQ gained considerable attention during the oil embargos of the 1970s when building operators significantly reduced ventilation rates in an effort to reduce energy use. While this strategy achieved its original objective, it resulted in very poor air quality and many health effects that became known as sick building syndrome (SBS) (Redlich, Sparer, and Cullen, 1997).

Contaminants in the air are normally categorized as gaseous, particulates, or microbial. These vary in harmfulness and at least a dozen official standards impose limits on safe levels, depending on exposure duration (Charles *et al.*, 2005). This brief section provides an overview of IAQ, including some common contaminants and design and operational strategies to mitigate high levels of indoor air contaminants.

The main contaminants of concern or interest include: tobacco smoke, radon, molds, legionella, carbon monoxide, bioeffluents, volatile organic compounds (VOCs), asbestos fibers, ozone, and carbon dioxide. Details on these contaminants and recommended maximum exposure levels can be found in ASHRAE Standard 62.1 (ASHRAE, 2010) and reports by the US EPA (2013). Their origin can be materials and substances that are indoors, occupants, equipment and HVAC distribution, or the outdoors (e.g., a point source of pollution or from polluted urban environments).

Carbon dioxide is frequently cited as a major source of IAQ problems. However, this is because carbon dioxide is a good indicator of IAQ in occupied buildings and it is considered a *surrogate*. It correlates well with occupancy since occupants are the primary source of CO_2 in most buildings and can be used to approximate the outdoor air supply rate if the occupancy and outdoor CO_2 concentration are known, as follows:

$$C_{CO_2}(\infty) = \frac{PQC_{CO_{2}o} + S/V}{Q} \tag{3.28}$$

where $C_{CO_2}(\infty)$ is the steady state indoor carbon dioxide concentration, *P* is the fraction of outdoor air in the air supply, *Q* is the air supply rate, $C_{CO_{2}o}$ is the outdoor carbon dioxide concentration,

S is the generation rate of carbon dioxide, and *V* is the volume of the space. Many ventilation standards (e.g., ASHRAE Standard 62.1 (ASHRAE, 2010)) use a certain allowable carbon dioxide concentration (e.g., 1000 ppm) to provide minimum ventilation rates for different space types (e.g., classroom, office, kitchen).

The three main methods to ensure good IAQ are: (1) removal or reduction of source of contaminants, (2) ventilation, or (3) filtration of contaminants. The first approach, to attempt to eliminate the source of contaminants, is the preferred option because it requires no maintenance or operating energy use. Use of low-VOC paints, furniture, and other finishes are also good approaches to achieve this. Careful design of walls and HVAC systems to minimize chronic moisture or sitting water is essential to minimize mold growth and other bioaerosols. Ventilation and filtration cost energy: electrical energy (fans and pumps) and thermal energy (for conditioning supply air) for ventilation and electrical energy to run fans to overcome pressure drops in filters. The thermal energy demands of ventilation can be partly reduced using heat or energy recovery ventilation.

3.6 Conclusion

This chapter examined thermal, visual, and acoustic comfort, and indoor air quality. These elements of indoor environmental quality are critical to the success of Net ZEBs. While indoor conditions were traditionally viewed as being passively endured by occupants, it is now widely accepted that occupants actively adapt their environment and themselves to improve comfort. They normally do so in the most convenient and effective ways and only once a "crisis of discomfort" has occurred (Haigh, 1981). Because these adaptations may have a significant effect on energy use (e.g., window opening on heating or cooling and blind-closing on electric lighting), comfort and energy are tightly linked. As such, maintaining comfort through careful building design and operation should be considered throughout the building life cycle. Readers are encouraged to refer to the case studies of this book (Chapter 7) for examples of occupant comfort and design for comfort; particularly the ENERPOS case study, which

owes much of its success to achieving comfortable conditions with very low energy use.

References

Abbaszadeh, S., Zagreus, L., Lehrer, D., and Huizenga, C. (2006) *Occupant Satisfaction with Indoor Environmental Quality in Green Buildings*, Center for Environmental Design Research, UC Berkeley.

Alfano, G., d'Ambrosio, F.R., and Riccio, G. (2001) Sensibility of the PMV index to variations of its independent variables, in *Thermal Comfort Standards into the 21st Century*, Windsor, UK.

American Society of Heating, Refrigerating and Air-Conditioning Engineers (ASHRAE) (2010) 62.1-2010, Ventilation for acceptable indoor air quality. In American Society of Heating, Refrigerating and Air-Conditioning Engineers, Atlanta.

ANSI/ASHRAE (1982) *Thermal Environmental Conditions for Human Occupancy*, American Society of Heating, Refrigerating and Air,-Conditioning Engineers, Atlanta, USA.

ANSI/ASHRAE (1992) *Thermal Environmental Conditions for Human Occupancy*, American Society of Heating, Refrigerating and Air,-Conditioning Engineers, Atlanta, USA.

ANSI/ASHRAE (2004) *Thermal Environmental Conditions for Human Occupancy*, American Society of Heating, Refrigerating and Air,-Conditioning Engineers, Atlanta, USA.

ANSI/ASHRAE (2010) *Thermal Environmental Conditions for Human Occupancy*, American Society of Heatingrrcrr, Refrigerating and Air,-Conditioning Engineers, Atlantarrcrr, USA.

Araújo, V.M.D. and Araújo, E.H.S. (1999) The applicability of ISO 7730 for the assessment of the thermal conditions of users of the buildings in Natal-Brazil, in *Indoor Air 1999* (eds G. Raw, C. Aizlewood, and P. Warren), Edinburgh, UK, pp. 148–153.

Arens, E., Humphreys, M.A., de Dear, R., and Zhang, H. (2010) Are 'class A' temperature requirements realistic or desirable? *Building and Environment*, **45**, 4–10.

Auliciems, A. (1981) Towards a psycho-physiological model of thermal perception. *International Journal of Biometeorology*, **25**, 109–122.

Auliciems, A. and de Dear, R.J. (1986) Airconditioning in Australia I – Human thermal factors. *Architectural Science Review*, **29**, 67–75.

Benton, C.C., Bauman, F.S., and Fountain, M.E. (1990) A field measurement system for the study of thermal comfort. *ASHRAE Transactions*, **96**, 623–633.

Bordass, B., Cohen, R., Standeven, M., and Leaman, A. (2001) Assessing building performance in use. 2: Technical performance of the Probe buildings. *Building Research & Information*, **9**, 103–113.

Borgeson, S. and Brager, G. (2011) Comfort standards and variations in exceedance for mixed-mode buildings. *Building Research and Information*, **39**, 118–133.

Boyce, P., Hunter, C., and Howlett, O. (2003) *The Benefits of Daylight through Windows*, U.S. Department of Energy, Troy, NY.

Butera, F.M. (1998) Chapter 3 - Principles of thermal comfort. *Renewable and Sustainable Energy Reviews*, **2**, 39–66.

Carlucci, S. (2013) *Thermal Comfort Assessment of Buildings*, vol. **1**, Springer, London.

Carlucci, S. and Pagliano, L. (2012) A review of indices for the long-term evaluation of the general thermal comfort conditions in buildings. *Energy and Buildings*, **53**, 194–205.

CEN (1998) *Design for Indoor Environments. In Ventilation For Buildings*, European Committee for Standardization, Brussels, Belgium.

CEN (2007) *Indoor Environmental Input Parameters for Design and Assessment of Energy Performance of Buildings Addressing Indoor Air Quality, Thermal Environment, Lighting and Acoustics*, European Committee for Standardization, Brussels, Belgium.

Charles, K., Magee, R., Won, D., and Lusztyk, E. (2005) Indoor Air Quality Guidelines and Standards. In Final Report 51 – CMEIAQ-II: Consortium for Material Emission and IAQ Modelling II (National Research Council Canada).

CIBSE (2002) *Guide J- Weather, Solar and Illuminance Data*, Chartered Institution of Building Services Engineers, London.

Cohen, R., Ruyssevelt, P., Standeven, M., Bordass, W., and Leaman, A. (1999) *Building Intelligence in Use: Lessons from the Probe Project*, Usable Buildings, UK.

Cole, R.J. and Brown, Z. (2009) Reconciling human and automated intelligence in the provision of occupant comfort. *Intelligent Buildings International*, **1**, 39–55.

Crook, M.A. and Langdon, F.J. (1974) The effects of aircraft noise in schools around London airport. *Journal of Sound and Vibration*, **34**, 221–232.

Croome, D.J., Gan, G., and Awbi, H.B. (1993) Thermal comfort and air quality in offices, in *Indoor Air 1993* (eds J.J.K. Jaakkola, R. Ilmarinen, and O. Seppänen), Helsinki, pp. 37–42.

de Dear, R.J. (1998) Global database of thermal comfort field experiments. *Paper presented at: Proceedings of the 1998 ASHRAE Winter Meeting (San Francisco, CA, USA: ASHRAE).*

de Dear, R.J. and Brager, G.S. (1998) Developing an adaptive model of thermal comfort and preference. *Paper presented at: 1998 ASHRAE Winter Meeting (San Francisco, CA, USA: ASHRAE).*

de Dear, R.J., Brager, G.S., and Cooper, D. (1997) Developing an Adaptive Model of Thermal Comfort and Preference — Final report ASHRAE RP-884 (Macquarie Research Ltd. (Macquarie University) and Center for Environmental Design Research (University of California)).

Djongyang, N., Tchinda, R., and Njomo, D. (2010) Thermal comfort: A review paper. *Renewable and Sustainable Energy Reviews*, **14**, 2626–2640.

Doherty, T.J. and Arens, E. (1988) Evaluation of the physiological bases of thermal comfort models. *ASHRAE Transactions*, **94**, 1371–1385.

Du Bois, D. and Du Bois, E.F. (1989) A formula to estimate the approximate surface area if height and weight be known. 1916. Nutrition (Burbank, Los Angeles County, Calif) 5, 303–311; discussion 312.

Fanger, P.O. (1970) *Thermal Comfort: Analysis and Applications in Environmental Engineering*, Danish Technical Press, Copenhagen.

Fanger, P.O. and Toftum, J. (2002) Extension of the PMV model to non-air-conditioned buildings in warm climates, Energy and Buildings, **34**, 533–536.

Farley, K.M.J. and Veitch, J.A. (2001) *A Room with a View: A Review of the Effects of Windows on Work and Well-Being*, Institute for Research in Construction., Ottawa, ON.

Fato, I., Martellotta, F., and Chiancarella, C. (2004) Thermal comfort in the climatic conditions of southern Italy. *Paper presented at: Technical and Symposium Papers - 2004 Annual Meeting of the*

American Society of Heating, Refrigerating and Air-Conditioning Engineers (Nashville, TX).

Ghiaus, C., Allard, F., Santamouris, M., Georgakis, C., and Nicol, F. (2006) Urban environment influence on natural ventilation potential. *Building and Environment*, **41**, 395–406.

Griffiths, I. (1990) *Thermal Comfort Studies in Buildings with Passive Solar Features: Field Studies*, Commission of the European Community., UK.

Guglielmetti, R., Pless, S., and Torcellini, P. (2010) On the Use of Integrated Daylighting and Energy Simulations to Drive the Design of a Large Net-Zero Energy Office Building. In SimBuild 2010 (New York, New York), pp. 301–309.

Haigh, D. (1981) User response to environmental control, in *The Architecture of Energy* (eds D. Hawkes and J. Owers), The Pitmen Press, Bath, UK, pp. 45–63.

Hensen, J.L.M. (1991) *On the Thermal Interaction of Building Structure and Heating and Ventilating System*, Technische Universiteit Eindhoven.

Heschong, L., Wright, R., and Okura, S. (2002) Daylight impact on retail sales performance. *Journal of the Illuminating Engineering Society*, **31**, 21–25.

Hodgson, M. (2008) Acoustical evaluation of six 'green' office buildings. *Journal of Green Building*, **3**, 108–118.

Höppe, P. (2002) Different aspects of assessing indoor and outdoor thermal comfort. *Energy and Buildings*, **34**, 661–665.

Howell, W.C. and Kennedy, P.A. (1979) Field validation of the Fanger thermal comfort model. *Human Factors*, **21**, 229–239.

Humphreys, M. (1978) Outdoor temperatures and comfort indoors. *Batiment International, Building Research and Practice*, **6**, 92–105.

Humphreys, M.A. (1994) An adaptive approach to the thermal comfort of office workers in North West Pakistan. *Renewable Energy*, **5**, 985–992.

Humphreys, M.A. and Hancock, M. (2007) Do people like to feel 'neutral'?: Exploring the variation of the desired thermal sensation on the ASHRAE scale. *Energy and Buildings*, **39**, 867–874.

Humphreys, M.A. and Nicol, F.J. (2002) The validity of ISO-PMV for predicting comfort votes in every-day thermal environments. *Energy and Buildings*, **34**, 667–684.

Humphreys, M.A. and Nicol, J.F. (2000) Outdoor temperature and indoor thermal comfort: raising the precision of the relationship for the 1998 ASHRAE database of field studies. *ASHRAE Transactions*, **106**, 485–492.

ISO (2005) Analytical determination and interpretation of thermal comfort using calculation of the PMV and PPD indices and local thermal comfort criteria, in *Ergonomics of the Thermal Environment*, International Organization for Standardization, Geneva, pp. 52.

ISO (2006) ISO 9241-110:2006 Ergonomics of human-system interaction – Part 110: Dialogue principles (Geneva, CH).

La Gennusa, M., Marino, C., Nucara, A., Pietrafesa, M., Pudano, A., and Scaccianoce, G. (2010) Multi-agent systems as effective tools for the user-based thermal comfort: an introduction. *World Applied Sciences Journal*, **10**, 179–195.

Lawrence Berkeley National Laboratory (LBNL) (1997) *Tips for Daylighting with Windows*, The University of California, Berkeley, CA.

Leaman, A. and Bordass, B. (2000) Productivity in buildings: the 'killer' variables. *Building Research & Information*, **27**, 4–19.

Leaman, A. and Bordass, B. (2005) *Creating the Productive Workplace*, 2nd edn, Taylor and Francis, New York, NY.

Lin, Z. and Deng, S. (2007) A study on the thermal comfort in sleeping environments in the subtropics – Developing a thermal comfort model for sleeping environments. *Building and Environment*, **43**, 70–81.

Mardaljevic, J., Heschong, L., and Lee, E. (2009) Daylight metrics and energy savings. *Lighting Research and Technology*, **41**, 261–283.

Mayer, E. (1997) A new correlation between predicted mean votes (PMV) and predicted percentages of dissatisfied (PPD), in *Healthy Buildings-IAQ '97* (eds J.E. Woods, D.T. Grimsrud, and N. Boschi), Washington, USA, pp. 189–194.

Nabil, A. and Mardaljevic, J. (2006) Useful daylight illuminances: a replacement for daylight factors. *Energy and Buildings*, **38**, 905–913.

Newsham, G.R., Birt, B.J., Arsenault, C., Thompson, A.J.L., Veitch, J.A., Mancini, S., Galasiu, A.D., Gover, B.N., Macdonald, I.A., and Burns, G.J. (2013) Do 'green' buildings have better indoor

environments? New evidence. *Building Research & Information*, **41**, 415–434.

Nicol, F. (2004) Adaptive thermal comfort standards in the hot-humid tropics. *Energy and Buildings*, **36**, 628–637.

Nicol, F. and Humphreys, M. (1995) *Standards for Thermal Comfort: Indoor Air Temperature Standards for the 21st Century*, Chapman & Hall.

Nicol, F. and Roaf, S. (1996) Pioneering new indoor temperature standards: The Pakistan project. *Energy and Buildings*, **23**, 169–174.

Nicol, J.F., Hacker, J., Spires, B., and Davies, H. (2009) Suggestion for new approach to overheating diagnostics. *Building Research and Information*, **37**, 348–357.

Nicol, J.F. and Humphreys, M.A. (2002) Adaptive thermal comfort and sustainable thermal standards for buildings. *Energy and Buildings*, **34**, 563–572.

Nicol, J.F. and McCartney, K.J. (2001) *Final Report of Smart Controls and Thermal Comfort (SCATs) Project. Report to the European Commission of the Smart Controls and Thermal Comfort Project*, Oxford Brookes University, Oxford, UK.

Nicol, J.F., Raja, I.A., Allaudin, A., and Jamy, G.N. (1999) Climatic variations in comfortable temperatures: The Pakistan projects. *Energy and Buildings*, **30**, 261–279.

Ole Fanger, P. and Toftum, J. (2002) Extension of the PMV model to non-air-conditioned buildings in warm climates. *Energy and Buildings*, **34**, 533–536.

Olesen, B.W. (1982) Thermal Comfort. Technical review - Bruel & Kjaer English ed, 3–41.

Osterhaus, W.K.E. (2005) Discomfort glare assessment and prevention for daylight applications in office environments. *Solar Energy*, **79**, 140–158.

Osterhaus, W.K.E. (2009) *Design Guidelines for Glare-free Daylit Work Environments*, Aarhus School of Engineering, Aarhus.

Paciuk, M. (1989) *The role of Personal Control of the Environment in Thermal Comfort and Satisfaction at the Workplace*, University of Wisconsin, Milwaukee, USA, pp. 436.

Parsons, K.C. (2002) The effects of gender, acclimation state, the opportunity to adjust clothing and physical disability on

requirements for thermal comfort. *Energy and Buildings*, **34**, 593–599.

Pérez-Lombard, L., Ortiz, J., and Pout, C. (2008) A review on buildings energy consumption information. *Energy and Buildings*, **40**, 394–398.

Rea, M. (2002) *IESNA Handbook*, The Illuminating Engineering Society of North America, U.S.A.

Redlich, C.A., Sparer, J., and Cullen, M.R. (1997) Sick-building syndrome. *The Lancet*, **349**, 1013–1016.

Reinhart, C.F. (2005) A simulation-based review of the ubiquitous window-head-height to daylit zone depth rule-of-thumb. *Paper presented at: Building Simulation 2005 (Montreal, Canada. August 15–18)*.

Reinhart, C.F., Mardaljevic, J., and Rogers, Z. (2006) Dynamic daylight performance metrics for sustainable building design. *Leukos*, **3**, 7–31.

Robinson, D. and Haldi, F. (2008) Model to predict overheating risk based on an electrical capacitor analogy. *Energy and Buildings*, **40**, 1240–1245.

Tzempelikos, A. and Athienitis, A.K. (2003) Simulation for façade options and impact on HVAC system design. *Paper presented at: Build Simul (Eindhoven, NL)*.

United States Environmental Protection Agency (US EPA) (2013) The Inside Story: A Guide to Indoor Air Quality.

Van Den Wymelenberg, K. (2012) Patterns of occupant interaction with window blinds: A literature review. *Energy and Buildings*, **51**, 165–176.

Veitch, J. (2011) The physiological and psychological effects of windows, daylight, and view at home. In *4th VELUX Daylight Symposium (Lausanne, Switzerland)*.

Veitch, J.A. (1990) Office noise and illumination effects on reading comprehension. *Journal of Environmental Psychology*, **10**, 209–217.

Veitch, J.A. and Galasiu, A.D. (2012) The physiological and psychological effects of windows, daylight, and view at home: Review and research agenda (Ottawa, ON: Institute for research in construction).

Wienold, J. and Christoffersen, J. (2006) Evaluation methods and development of a new glare prediction model for daylight

environments with the use of CCD cameras. *Energy and Buildings*, **38**, 743–757.

Xavier, A.A.d.P. and Lamberts, R. (2000) Indices of thermal comfort developed from field survey in Brazil. Paper presented at: *2000 ASHRAE Winter Meeting (Dallas, TX, USA: ASHRAE)*.

Yoon, D.W., Sohn, J.Y., and Cho, K.H. (1999) The comparison on the thermal comfort sensation between the results of questionnaire survey and the calculation of the PMV values, in *Indoor Air 1999* (eds G. Raw, C. Aizlewood, and P. Warren), Edinburgh, UK, pp. 137–141.

4
Net ZEB Design Processes and Tools

William O'Brien, Paul Bourdoukan, Véronique Delisle, and Samson Yip

4.1 Introduction

This chapter discusses strategies and issues associated with designing Net ZEBs using building performance simulation (BPS) and other tools and strategies. It targets both beginner and advanced designers with suggested approaches for designing Net ZEBs. The first major section examines how the design process of Net ZEBs differs from that of conventional buildings. It also looks at the different stages of design and at how BPS can be integrated at various stages. This section suggests that Net ZEBs be designed following the three iterative stages:

1. Concept (or early) design: This stage focuses on the building form and architectural concept to facilitate the integration of renewable energy technologies (RETs) and passive features. These features include: daylight harvesting, solar shading, thermal mass, natural ventilation, building envelope assemblies, solar energy exposure, and control concepts.

2. Design development: This stage complements the concept design stage by refining building features, such as the envelope material choices and thermal mass, daylighting, lighting, RETs and heating, ventilation, and air conditioning (HVAC) system. This stage is also used to finalize the architectural concept.

3. Technical design: This stage refines the work from design development by completing the whole building design, including all construction details and specifications. In particular, this stage addresses specific design details, such as interior finishing, control algorithms development (e.g., for HVAC and lighting), and HVAC/RET system refinement. Computational fluid

dynamics (CFD) can be used during this stage; for example, to study airflow in critical zones or atria.

The second major section approaches the Net ZEB design problem from a more technical/research-oriented point of view. The issues that are examined include a general discussion of appropriate model resolution in BPS tools, approaches to modeling different Net ZEB features and systems, and suggestions on how to use BPS tools to influence design and visualize the design space.

While the two sections each approach the Net ZEB design problem from a different perspective – practice and research – they yield very similar conclusions. One of the main conclusions is that the design of Net ZEBs requires that energy-related design considerations occur significantly earlier in the design process than for conventional buildings. Also, the most permanent design decisions should be made early in the design process. Many of these specifications – building form, thermal mass strategies, opening area, envelope design, structural systems, and potential for integration of renewable energy systems – greatly affect energy use. Finally, one of the key needs in simulation tools development is to enable escalating model resolution in simplified tools as the design progresses. Certain phenomena should be assessed early in design because they could be very influential over building form and other major decisions, but require detailed analysis, namely, natural ventilation, daylighting, and control strategies are nontrivial aspects. This chapter provides theory and examples for possible simplified methods.

4.2 Integrating Modeling Tools in the Net ZEB Design Process

4.2.1 Introduction

The design process of conventional buildings without specific objectives related to energy or environmental aspects is generally linear. The building owner establishes his priorities and requirements; the architect is responsible for building siting, orientation, form, and building envelope; the structural and electrical engineers are responsible for their respective systems; and

the mechanical engineer selects and sizes the appropriate HVAC system. The issue with this type of design process is that major irreversible decisions about the building design, such as form and orientation, are sometimes made with little regard for energy performance.

When the design target is to build a Net ZEB, energy consumption, environmental impact, and comfort are major concerns. Relevant decisions have to be made carefully during early design stages because they have an enormous impact on building energy consumption and potential for RET integration. As a result, it becomes necessary to get feedback at the early stages of the design not only on the building energy consumption, but also on the economic, environmental, and comfort aspects of the building. This feedback can be obtained by introducing building performance simulation tools (Athienitis *et al.*, 2010) and by involving stakeholders[1] with diverse expertise at the beginning of the design process to help with decision-making. This process is known as an integrated design process (IDP) (AIA, 2008; Löhnert, Dalkowski, and Sutter, 2003) or integrative process (ANSI, 2012). In this approach, all team members are required to collaborate at every stage of design to achieve the comprehensive project objectives as opposed to working in *silos* like in a conventional process. This section provides an overview of the different stages that can be followed to design a Net ZEB. It also discusses the design decisions that are likely to be made during these stages and the tools that can be used to help designers in this process. It concludes with an overview of project delivery methods and their influence on achieving the net-zero energy goal.

4.2.2 Overview of Phases in Net ZEB Realization

The process map from project conception to building completion varies from one project to another, but can be generalized in a conventional building design process with the following phases (AIA, 2008; RIBA, 2007):

1. Preparation, or programming
2. Concept design, or schematic design

3. Design development

4. Technical design, or construction documentation

5. Construction

6. Commissioning, operation and monitoring.

In other modes of project delivery, such as construction management at risk and design-build, there can be an overlap between the phases, or shortening and lengthening of the phases for the purpose of optimizing the design by strategically allocating the design team's resources where required (AIA, 2008).

In the preparation phase, the building owner provides important information, such as the budget available for the construction, the building site details, the functionality and occupancy level, as well as the economic, energy, and environmental goals or requirements.

At the beginning of the concept design phase, some specific energy-saving strategies should already be considered while ensuring thermal and visual comfort and considering environmental impact. These strategies include integrating passive solar design, a high-performance building envelope, load management, daylighting, and natural ventilation. Considering the integration of these specific elements as well as their control strategies in the early design stage along with strategies for RETs increases the chances that the net-zero energy objective remains attainable. The decisions made at this stage are critical. For example, an insufficient window opening to wall ratio could limit the potential for daylighting and natural ventilation, increase the space cooling load and have important unrecoverable consequences on the size and cost of the cooling equipment and RETs. At the end of the concept design phase, the building designer provides a global sketch of the building. In this phase, the overall heat transfer coefficients (U-values) for the envelope components are used because the details of the composition of the opaque and glazing elements are usually unknown. Control strategies and system concepts for HVAC are retained, but the specific details and components remain undefined.

In the third phase, design development, decisions are made regarding the integration of efficient HVAC systems and the

refinement of RETs for heating, cooling, and power. During this stage, the major elements of the architectural concept including the composition of the building envelope and the details of the HVAC system are developed.

In the fourth phase, the building details are finalized. At the fifth stage, the building is constructed. Lastly, during the commissioning, operation, and monitoring phase, the building operation and performance are assessed to ensure that the building economic, energy, and environmental goals are achieved and that the occupants are confirmed to be comfortable.

This section focuses on the building design stages: the concept design, the design development, and the technical design stages. Table 4.1 shows generally how the building design is refined as it advances from one stage to the next. Even though these stages are shown in this table as linear and well-defined, it is important to mention that the building design process involves several iterations within each stage. Similarly, while the different systems are shown as being separate, they are intertwined and must be treated as such. Depending on regional differences or particular project conditions, such as delivery method or contractual requirements, tasks may overlap or shift from one stage to another, and the stage names themselves can be different. What follows is one possible approach to the design of a Net ZEB.

Table 4.1 Design stages flow of information

	Concept Design	Design Development	Technical Design
DAYLIGHTING	Window-to-wall ratio Window visible transmittance Daylight factor Daylight autonomy Useful daylight illuminance	Window location and detailed composition Electric lighting design to complement daylighting Daylight factor Daylight autonomy Useful daylight illuminance	Detailed evaluation of daylighting level with interior finishing details and shading devices
PASSIVE SOLAR	Window-to-wall ratio and glazing properties Type of solar shading devices and their controls Thermal mass level	Shading devices location, size and control strategies Thermal mass composition type and location	Window specifications Interior finishing details (ceiling, floor, HVAC terminals and acoustics)
NATURAL VENTILATION	Opening dimensions, positions, and controls for each zone	Opening dimensions and position for each zone coordinated with control strategies and thermal mass (passive design)	Thermal mass accessibility
BUILDING ENVELOPE	U-values for opaque and glazing elements	Building envelope detailed composition	

	Concept Design	**Design Development**	**Technical Design**
ELECTRIC LIGHTING and PLUG LOADS	Typical power densities	Plug loads and electric lighting requirements Equipment type and control (dimming) strategies Associated internal gains	Integration with daylighting design and possible shading controls Occupant comfort studies
HVAC	System concept for heating and cooling generation and distribution	System sizing in accordance with building envelope, plug loads and coupling with RET Control strategies	Optimal HVAC control HVAC network dimensioning
RET	System concept for RET and building integration	RET sizing in accordance with HVAC system and economical and environmental concerns	RET dimensioning Optimal RET control

4.2.3 Tools

As the envelope and mechanical aspects of the building become better defined, more information is required on the effect of the design decisions made on the building energy performance. Thus, the criteria for the tools required to evaluate the building's performance evolve as the design progresses. This performance is typically assessed based on economic, energy, environmental, or comfort criteria. The importance given to each criterion will depend on which Net ZEB definition is used (Marszal *et al.*, 2011).

As part of the International Energy Agency Solar Heating and Cooling Program (IEA SHC) Task 40 – Energy in Buildings and Communities EBC Annex 52 Towards Net Zero Energy Solar Buildings, a survey was conducted among building experts (architects, researchers, and engineers) on low-energy and net-zero energy building design tools and design processes (Athienitis *et al.*, 2010). The results of this survey show that Net ZEB designers use as many as 10 different tools in the design process of a single building. One reason for using different software programs is that, while simple models with a limited number of inputs and outputs are sufficient during the concept design phase, more complex tools with a larger number of outputs at a finer time step are necessary during the design development phase. Consider, for example, the design of thermal energy storage. In the concept design phase, monthly annual energy balances may be sufficient because only the general effect of the thermal mass on the overall building monthly or annual energy performance is required, in order to estimate the order of magnitude for renewable energy system capacity. In the design development phase, however, the designer may want to understand the effect of the thermal mass on comfort and indoor temperature during typical days of the year. This type of study requires building simulations that can be performed at a sub-hourly time step. Appropriate model resolution is discussed at length in Section 4.3.

Another reason that multiple tools are required during the different design stages is that since each tool was developed for a specific purpose and in a certain context (e.g., for code compliance or a specific type of building or climate), each has its own assumptions, capabilities, strengths, and constraints that limit its range of applications and make it appropriate to obtain only certain information. These limitations are a concern when modeling conventional buildings, but they present an even greater challenge for low- or net-zero energy buildings because of the particular features of these buildings. Net ZEBs will typically include some passive design features, energy efficiency, and conservation measures, as well as on-site RETs generating thermal and electrical energy. As shown during a benchmarking exercise (Athienitis *et al.*, 2010) produced by the IEA SHC Task 40 – EBC Annex 52, these particularities are not necessarily part of conventional buildings and

as a result, are not always fully implemented or supported in all commercial design tools. Thus, it is common that multiple tools are required to encapsulate the interactions between different building components and obtain necessary feedback to complete a design.

A review of building performance simulation tools shows that up to now, most developed tools are not design tools but rather tools to evaluate performance of a design. Even complex and very advanced tools can rarely be used at all stages of design simply because they require a set of inputs often unavailable at the early design phases of the building. Complex tools can be used to judge a design, but most of them cannot provide guidelines to achieve a high-performance building. Conversely, simple tools that require a limited set of inputs are not suited for a precise evaluation when dealing with complex integrated systems. However, their simplicity allows them to offer more design guidance than advanced tools. Designers alternate the use of different tools in an iterative way during each design phase to obtain the desired energy performance. This section takes a closer look at how different tools can be integrated to the concept design, design development, and technical design stages of Net ZEBs. The suggested tools are commonly used by building designers. They only represent a small fraction of all building energy simulation software available on the market. A comprehensive database of BPS programs can be found in the tools directory developed by the US Department of Energy (DOE) (2013a).

4.2.4 Concept Design

When designing Net ZEBs, the intent is to reduce building energy consumption first. In the concept design stage, the aim is to approach this goal by prioritizing the following building aspects:

1. Daylight
2. Solar protection
3. Building thermal inertia (thermal mass)
4. Natural ventilation
5. Building envelope insulation
6. Building-integrated solar energy technologies.

These aspects all need to be considered because they help define essential parts of the architectural concept – including building form, orientation of surfaces, and fenestration – and are difficult to modify at a later stage of the design. If these aspects are addressed carefully during the early design phase and the operation of the building is considered, achieving net-zero energy can be a realistic goal. These aspects influence each other and are essential to optimize a building for solar energy collection. For example, compact buildings that have a small envelope area to volume ratio have the advantage of low thermal energy losses, but conversely, have less daylight and natural ventilation potential. To reach net-zero energy, the concept design phase should be developed in an iterative procedure to get the most rational design satisfying the points raised earlier. For example, if the window-to-wall ratio is very low, it is difficult to achieve significant daylighting or natural ventilation, and if this detail is not considered early on, it will be translated into additional lighting and cooling energy costs – or additional design and time costs to redesign – at the later design stages.

Internal gains generated by plug loads and electric lighting have an important impact on space heating and cooling energy requirements. In the concept design phase, typical power densities for electrical equipment and lighting should be introduced in the model according to the building type.

The concept for the building-integrated solar energy technologies should be an integral part of the early stage Net ZEB design. Aside from solar energy systems' impact on the building's net energy balance, they have inherent effects on many of the building's other aspects, such as form, program, envelope composition, and structure. For instance, the ÉcoTerra house's roof shape was largely dictated by the dimensions of the preferred photovoltaic modules (more details in [Chapter 7](#)).

Even though no detailed work is done regarding HVAC at this stage, the future integration of HVAC must still be considered in the design process. The general concepts for this aspect might have already been discussed in the preparation phase.

Operating strategies and some comfort parameters need to be considered at this stage. If radiant floor heating is to be used, then

the thermal mass integrated in the floor should be considered both for storage of passive gains and auxiliary heat as well as an appropriate control strategy should be established. Operating strategies also need to account for the expected occupancy profile of the building. For example, night cooling using cool outdoor air is a better strategy in office buildings, where occupants normally leave the building at night, than in homes where it could cause discomfort. Thus, the zone temperature setpoints and their allowable fluctuation need to be decided.

4.2.4.1 Daylight

A building with a well-insulated envelope may have high energy consumption if the architectural concept does not allow for natural light to penetrate into the building, especially for office buildings. Natural light is more a geometrical problem than a technical problem and typically, the potential for natural lighting is better in a long and narrow building than in one that is deep and compact. An atrium is an example of a strategy that can be used to provide natural lighting in a compact building. Figure 4.1 presents an example of a commercial building with an atrium at the center of the space. This atrium is surrounded by rooms that do not have any windows or walls in contact with the outdoors. Thus, the atrium contributes to reducing the amount of electric lighting required in these spaces.

Fig. 4.1 Atrium providing natural lighting to internal zones (BC-EPFL Lausanne Switzerland, Architect: R. Luscher Lausanne, Energy Concept: Sorane S.A, Ecublens)

In the concept design phase, the architect should ensure that the building has sufficient daylight and should evaluate the design for the whole building or for particular zones using simulation tools or rules of thumb. This evaluation is useful for estimating the level of daylight or inversely, to evaluate the required glazing area to achieve a particular daylight factor (defined as the ratio of internal light level to external light level). Rules of thumb, such as equations providing the daylight factor for a given glazing area, or other simplified methods for atrium calculations, can be used for such design or assessment. These rules of thumb can be found in O'Connor *et al.* (1997) or in the literature produced by the IEA Task 21 (Johnsen and Watkins, 2010). Other simple tools include daylight autonomy diagrams and sun path charts. Metrics suitable for quantifying daylighting design effectiveness include daylight autonomy and useful daylight illuminance and are defined in Section 3.3 on visual comfort.

Detailed simulation tools for daylight usually require accurate geometry information of the zone, the visible transmittance of

glazing, as well as the reflectance of internal surfaces. Fixed shading devices details are also required. During the concept design phase, optical properties of internal surfaces are often unknown, so assumptions have to be made regarding these optical properties in order to evaluate the daylighting potential. Typical reflectances for floors, walls, and ceilings are 10–30%, 40–60%, and 70–80%, respectively. If fixed shading devices are to be implemented, it is preferable to have a simple dimensioning of the overhangs and fins in order to integrate them in daylight evaluation. For windows with moveable shading devices (e.g., roller blinds or venetian blinds), at a minimum daylight should be assessed both for open and closed positions. Ideally, an occupant behavior model would be used, as described in Section 4.3.3.7. There are several simulation tools on the market for assessing the natural light potential in buildings, such as DIAL-Europe (Estia SA, 2009), DAYSIM (Reinhart, 2013), RADIANCE (Ward, 2013), Relux (Relux Informatik AG, 2012), and IDA ICE (Equa Simulation AB, 2009).

4.2.4.2 Solar Protection

In order to achieve the net-zero energy goal, a building should manage solar gains effectively. Load management using solar shading devices and thermal mass can help reduce overheating from solar gains.

In nontropical climates, well-designed solar shading devices should allow solar radiation transmission to the space during winter, but protect it from the sun during summer and shoulder seasons. In addition, they should ensure a good level of daylight in the space, while minimizing glare. When climatic and economic conditions permit, solar shading devices are preferred to be external because solar radiation is reflected before being transmitted by the glazing. Moveable shading devices are an interesting option because these products are intended to simultaneously protect the space from solar gains and provide a good level of daylight by varying the inclination of the slats or the height of the blinds. On the other hand, moveable shading devices require some control (manual or automatic) and as a result, a failure or slow response to the sun's position can defeat the purpose of these devices. One option is to have the shading devices automatically controlled and coupled with electric lighting, and

heating and cooling control strategies to form a feedback loop. Particular attention needs to be placed in incorporating control strategies into the early design process.

The design of fixed shading devices (e.g., overhangs, wingwalls or fins) is challenging because they have to provide good management of both solar gains and daylight. The design of solar shading devices is especially difficult for east and west façades because of low solar altitude angles. Furthermore, the lag between solar altitude and annual temperature variations can lead to overheating in shoulder seasons when the solar altitude allows deep solar penetration but temperatures are still mild. The advantage of fixed shading devices, however, is that they do not rely on occupant controls to manage solar gains or reduce daylight glare. The design of fixed solar protection can be done using sun path diagrams for the location of the building or commonly used formulas that allow dimensioning of the overhang depth and fin width as a function of the starting day when solar protection becomes necessary (Gronbeck, 2012; Milne, 2013; O'Connor *et al.*, 1997). Considering that solar shading devices also influence the amount of daylighting that can penetrate into the building, the dimensioning of fixed solar protection devices should be done in parallel with the control and dimensioning of electric lighting. In Chapter 7, the National Renewable Energy Laboratory (NREL) Research Support Facility (RSF) building case study includes an extensive analysis and discussion of daylighting considerations, control of solar gains, night cooling, and the option of using controlled motorized louvers for daylighting rather than fixed louvers.

4.2.4.3 Building Thermal Inertia

Thermal mass influences the dynamic thermal behavior of a building because it reduces the indoor temperature fluctuation. By storing or releasing heat, thermal mass elements delay and moderate the response of indoor air temperature to load variation. For example, internal loads and solar gains during summer can be, up to a certain point, absorbed by the building thermal mass and contribute to delaying the cooling needs - possibly to later, unoccupied periods of the day when there is less demand. As discussed in Chapter 2, different types of thermal mass elements can be embedded in the

building, such as heavy floors, heavy ceilings, heavy façades, actively charged mass (e.g., ventilated concrete slabs (VCS)), floor heating, or phase change materials (PCMs). Thermal mass is a very important design element that should be considered during the early design phase – not in detail, but at least, with an estimated order of magnitude depending on the expected internal loads. A well-designed building would ideally store the solar and internal gains during the day and release it at night. For moderate climates in summer conditions, one method to determine the appropriate thickness of thermal mass is to ensure that the thermal mass temperature increases by no more than 5 °C during the day, assuming that this mass is regenerated during a night shift where operation between 21 and 26 °C is allowed. The admittance approach described in Chapter 2 may be used in the early stage of the design to decide mass thickness. The amount of mass has important implications on structural design since the structure must safely support the thermal mass.

In complex simulation tools, the design of exposed thermal mass requires coupling of the thermal and air flow networks. This kind of simulation is not possible in the early design phase due to the lack of available inputs (e.g., optical properties and thermal capacitance of building material and furniture, and specific location of windows). As a result, in the concept design, building designers should keep in mind that thermal mass (e.g., exposed concrete, phase change materials or other) may need to be incorporated in the design. Figure 4.2 presents an example of thermal mass integration in a commercial building where the concrete columns and slabs are exposed. Structural considerations need to be taken into account when implementing thermal mass.
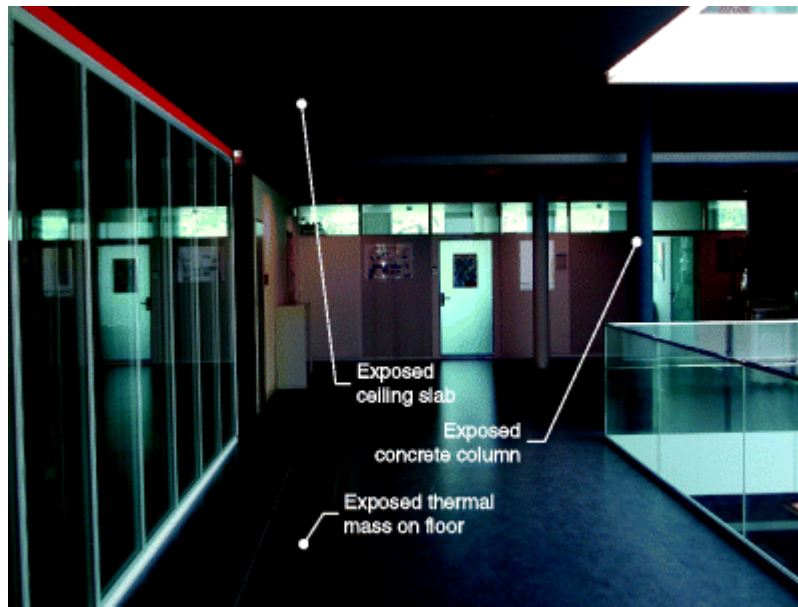
Fig. 4.2 Example of thermal mass integration in a commercial building (BC-EPFL Lausanne Switzerland, Architect: R. Luscher Lausanne, Energy Concept: Sorane S.A, Ecublens)

4.2.4.4 Natural and Hybrid Ventilation

When the climate permits, natural ventilation is an important part of the design of low- or net-zero energy buildings because it provides free air exchange as well as free cooling, reducing the mechanical ventilation and air-conditioning requirements. It also provides a means for occupants to control their environment and is one of the main contributors to adaptive comfort models. In such models, the occupants' comfort temperature range is considered to depend on outdoor temperature. Operable windows provide a level of individualized control that can improve both real and perceived control – both important to overall occupant satisfaction (de Dear and Brager, 1998; Paciuk, 1989).

The capability to perform natural ventilation in a building depends on various factors. For most applications, however, natural ventilation can be used when outdoor conditions combine a favorable wind regime to an outdoor temperature fluctuation of at least 16 to 28 °C from daytime to nighttime. Natural ventilation is promoted by creating openings in the building envelope and designing a building geometry that facilitates the air flow by better exploiting the stack effect and wind pressure. Furthermore, there is

potential for low night temperatures to precool the building for the next day (night cooling). A natural ventilation system that operates at night can increase its cooling potential and displace the need for cooling during the day–especially for buildings with high thermal mass. To be efficient, natural ventilation requires good solar protection and significant thermal inertia. Otherwise, the natural ventilation may not be sufficient alone to dump the internal and solar gains and reduce the amount of active cooling required. In Montreal, Canada, for example, summers tend to be humid so the main months suitable for natural ventilation are shoulder months (April, May, September and October), which represent 30 to 40% of the year. More information on natural ventilation design guidelines can be found in Allard and Santamouris (1998) and COMIS (LBNL, 1999). Additionally, natural ventilation can be fan-assisted in a form of hybrid ventilation. One example is a study by Karava *et al.* (2012) that shows the beneficial effects of integrating motorized solar shading devices with high levels of thermal mass in an atrium space with hybrid ventilation.

Figure 4.3 presents an example of how natural ventilation can be achieved in a commercial building with an atrium. In this building, the atrium and most of the office spaces are naturally ventilated with operable openings located at the top and bottom of the atrium and on the office façades. These openings have rain protection barriers that allow night ventilation to occur, even when it rains. The building has natural and mechanical ventilation because some laboratories require mechanical ventilation for health reasons. As this building design shows, the fact that some spaces require mechanical ventilation does not prevent the rest of the building from being naturally ventilated.
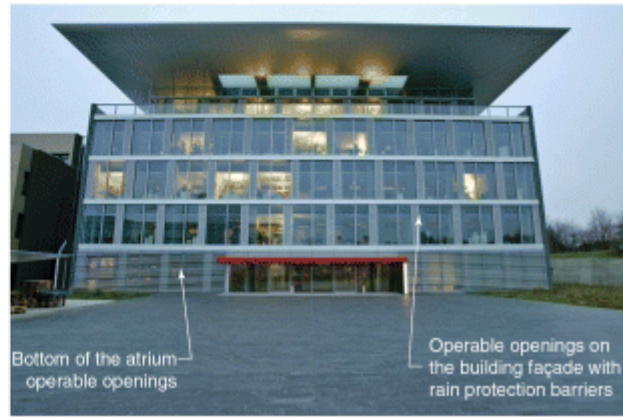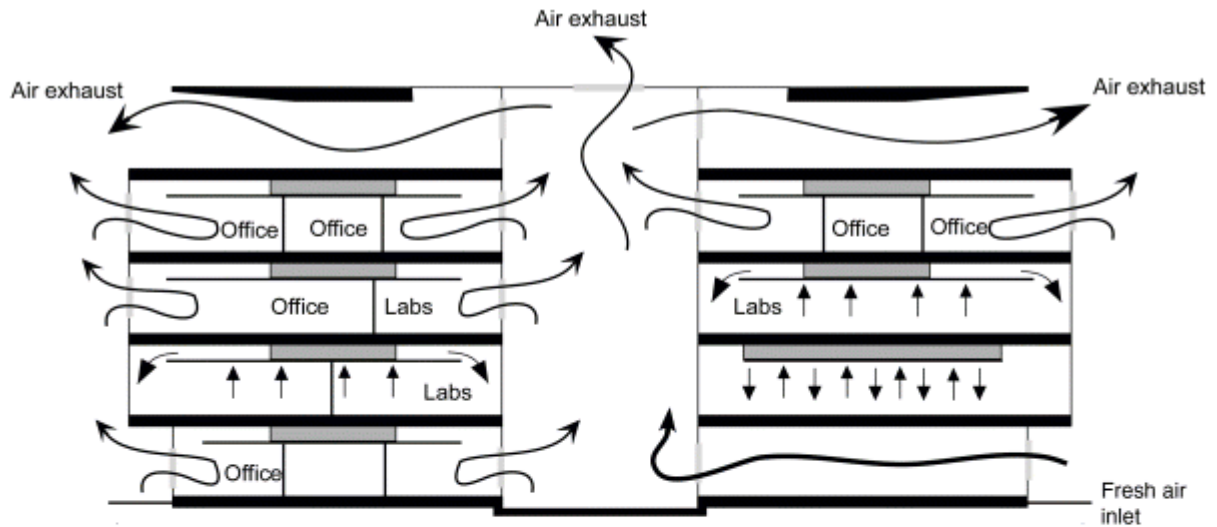
Fig. 4.3 Natural ventilation in an atrium (BC-EPFL Lausanne Switzerland, Architect: R. Luscher Lausanne, Energy Concept: Sorane S.A, Ecublens)

Similar to the case of thermal inertia, evaluating the effectiveness of natural ventilation requires coupling the thermal and the airflow networks. Such coupling is provided in advanced building simulation tools (e.g., TRNSYS and TRNFLOW (University of Wisconsin, 2012), EnergyPlus (DOE, 2012)). During the concept design phase, however, the implementation of a detailed model is difficult because it would be very time consuming and it would require many assumptions, such as details of the building envelope, internal gains, fenestration, and shading devices. At this stage of the design, simple tools like COMIS are better adapted for early-stage natural ventilation modeling. These simple tools can evaluate the air exchange rate and the effectiveness of the natural ventilation with a limited number of inputs like the wind pressure coefficients, the

height of the openings and their discharge coefficient (a characteristic of openings that takes both the contraction and the friction losses into account), or equivalent. This parameter is required in the calculation of the air flow going through an opening. Assumptions have to be formulated with regards to zone temperature, but nonetheless, this procedure provides a good estimate of the required opening area. This aspect of the building will be refined later during the design development stage.

The concepts of solar protection, thermal mass, and daylight use, even though treated separately in this section, are all interrelated concepts. For example, design decisions regarding shading devices will simultaneously affect the solar gains, the effectiveness of the thermal mass and the amount of daylight available in the space. Thus, it is important to analyze the effect of every design decision on the building solar protection, daylight, natural ventilation, and thermal mass activation.

4.2.4.5 Building Envelope Thermal Resistance

Building geometry (orientation, aspect ratio, etc.) and envelope thermal resistance influence the space heating and cooling energy consumption. The building form is normally known during the concept design stage but the composition of the walls is not yet fully defined. The detailed characteristics of walls and windows are difficult to predict at this stage, since the decisions regarding the building envelope composition will be based on energy calculations and functionality.

Considering that the details of the building envelope components are unknown, their insulation thickness and type are sufficient to estimate their overall heat transfer coefficient (*U*-value). If respecting the level of insulation previously determined, the U-value should not be affected significantly by the detailing of the wall composition that will occur later in the design process. For a given shape, when assuming heat transfer coefficients for the walls, roofs, floors, and windows in conjunction with other inputs like weather data, the building energy consumption can be calculated and the shape and aspect ratio can be adjusted until the targeted energy consumption is reached. The evaluation of the building energy

consumption for heating can be performed using simple tools that require a limited number of inputs such as the *U*-value of the walls, floors, and roof as well as the *U*-value and solar heat gain coefficient (SHGC) of the glazing elements. At this point, the requirements of the opaque surfaces' insulation and the windows' *U*-values and SHGC are selected. This will not guarantee the performance of the building. It is simply a performance figure required but not essential to meet the net-zero goal. It has to be complemented by the other aspects considered during the design phase as discussed earlier. Simple tools that can be used at the concept design phase for calculating the space heating energy consumption should have a limited number of inputs, such as the *U*-values, SHGC, thermostat setpoints, building orientation, and occupancy schedule. Simple tools like PHPP (Passive House Institute, 2010) and RETScreen (Natural Resources Canada, 2013) can be used at this stage.

4.2.4.6 Solar Energy Technologies Integration

Solar energy technologies integration is a key element to Net ZEB design. For this reason, solar energy resource availability should be studied as early as possible in the concept design stage. Preliminary studies on solar energy availability and accordingly, on solar technologies' expected energy production will help guide decisions not only on the selection of these technologies, but also on building form, envelope, and architectural concept. In addition, it will provide valuable information on the actual amount of energy that can be provided by solar and therefore, on the energy consumption level that the designers should target for a particular building. At this stage, simple tools like RETScreen and rules-of-thumb can be used.

4.2.5 Design Development

The design development of a Net ZEB has two main objectives: (i) to refine the solutions for the architectural concept and RETs, and (ii) to design the HVAC systems. Thus, during the design development phase, the solutions that have been considered in the concept design phase regarding daylighting, solar protection, load management, building thermal mass, natural ventilation, envelope thermal performance, and RETs are further developed and the HVAC systems are proposed. The following aspects are considered:

– Envelope and thermal mass

– Daylight

– Plug loads and electric lighting

– RETs and HVAC.

Similar to the concept design phase, the design development phase is an iterative process. This means that each building element is considered one at a time, and revisited as the solutions are refined. In addition, as in all other design stages, back-and-forth communication between the engineers and architects should exist. Typically, the engineer formulates recommendations to the architect to allow the most efficient design and the architect may integrate these recommendations into the design. This iterative process will continue until the building is optimized. From the energy calculations, the engineer will then propose – while taking into account the RETs – the HVAC systems to match the calculated load. In an efficient Net ZEB the design of the RETs and the HVAC systems should be fully integrated.

4.2.5.1 Envelope and Thermal Inertia

In the design development phase, the building envelope composition is further developed and the design and calculation of thermal mass elements (thermal inertia) is refined. For example, if raised floors or false ceilings are integrated in the design, other solutions have to be considered to integrate thermal mass elements, such as incorporating thermal mass into the walls. The refinement of these particular aspects of the building will allow a better evaluation of the space heating and cooling energy consumption.

At this stage, some details should be specified to limit thermal bridges and prevent the resulting condensation risk. In addition, thermal mass elements should be designed in conjunction with wall compositions and natural ventilation. In the concept design phase, thermal mass elements were estimated using rules of thumb. In the design development phase, rules of thumb can also be used at the beginning, but eventually, the evaluation will require the use of complex energy simulation tools that can handle detailed wall compositions, occupancy schedules, internal gains, solar gains, as

well as forced and natural ventilation. The simulation tools that can be used in this case ideally permit a coupling between thermal and airflow networks so that the thermal envelope, thermal inertia, and natural ventilation can be efficiently studied.

It is not necessary to perform calculations for the whole building. Calculations using detailed simulation tools can be limited to specific zones to save time and focus efforts. Results from these critical zones are usually sufficient to study the efficiency of the solution sets and to assess the impact on the cooling and heating loads. Such calculations allow refining the building design with regard to building envelope and thermal inertia until the desired heating and cooling load profiles are obtained.

In order to assess thermal bridges and condensation, simple tools like catalogs and handbooks from the American Society of Heating, Refrigerating and Air-Conditioning Engineers (ASHRAE) can be used (ASHRAE, 2009). For innovative or one-of-a kind solutions, more complex tools like 2D and 3D conduction software can be useful, such as THERM (LBNL, 2012), HEAT 2D, and HEAT 3D (Blomberg, 1996). These tools can be used first to obtain the internal surface temperature for extreme conditions and second to evaluate the heat flow across the bridge for a certain temperature difference. Effective U-values including framing and thermal bridging can then be calculated. These effective U-values can then be used in simulation tools like EnergyPlus, TRNSYS, IDA ICE or ESP-r (ESRU, 2010) to estimate the heating and cooling energy consumption.

4.2.5.2 Daylight

In the design development phase, details regarding window types and sizes as well as fixed shading devices are finalized. Calculations integrate more elements than in the concept design phase because information such as the coefficient of reflection of the internal walls and the window visible transmittance and frame fraction are now known. At this point, detailed simulation tools can be more appropriate than simple tools because they can integrate frame details and shading devices. They can also take into account interactions between zones, especially between atria and adjacent zones. Figure 4.4 presents a comparison of the daylighting

evaluation in zones adjacent to an atrium obtained with both detailed and intermediate simulation tools. This figure shows that while both tools provide similar results for the first floor, there are significant discrepancies for the second and third floors. In addition, the atrium mean daylight factor predicted by the intermediate software is much greater than that predicted by the detailed software. This shows the importance of revising calculations with more appropriate tools as the design is refined. A comparison between the results obtained with a Radiance simulation and a photograph of the constructed atrium is shown in Figure 4.5.

Daylight Factor (DF) and Mean Daylight Factor (MDF) on a workplane (Desk 0.8 m above floor)

Detailed software calculation

Intermediate software calculation

DF [%]

Facade — Back

5 m

Floor 3   MDF = 2.7

Floor 2   MDF = 1.7

Floor 1   MDF = 1.2

Floor 0   MDF = 11 : MDF = 39

Floor 3   MDF = 5.2

Floor 2   MDF = 3.2

Floor 1   MDF = 1.5

Floor 0
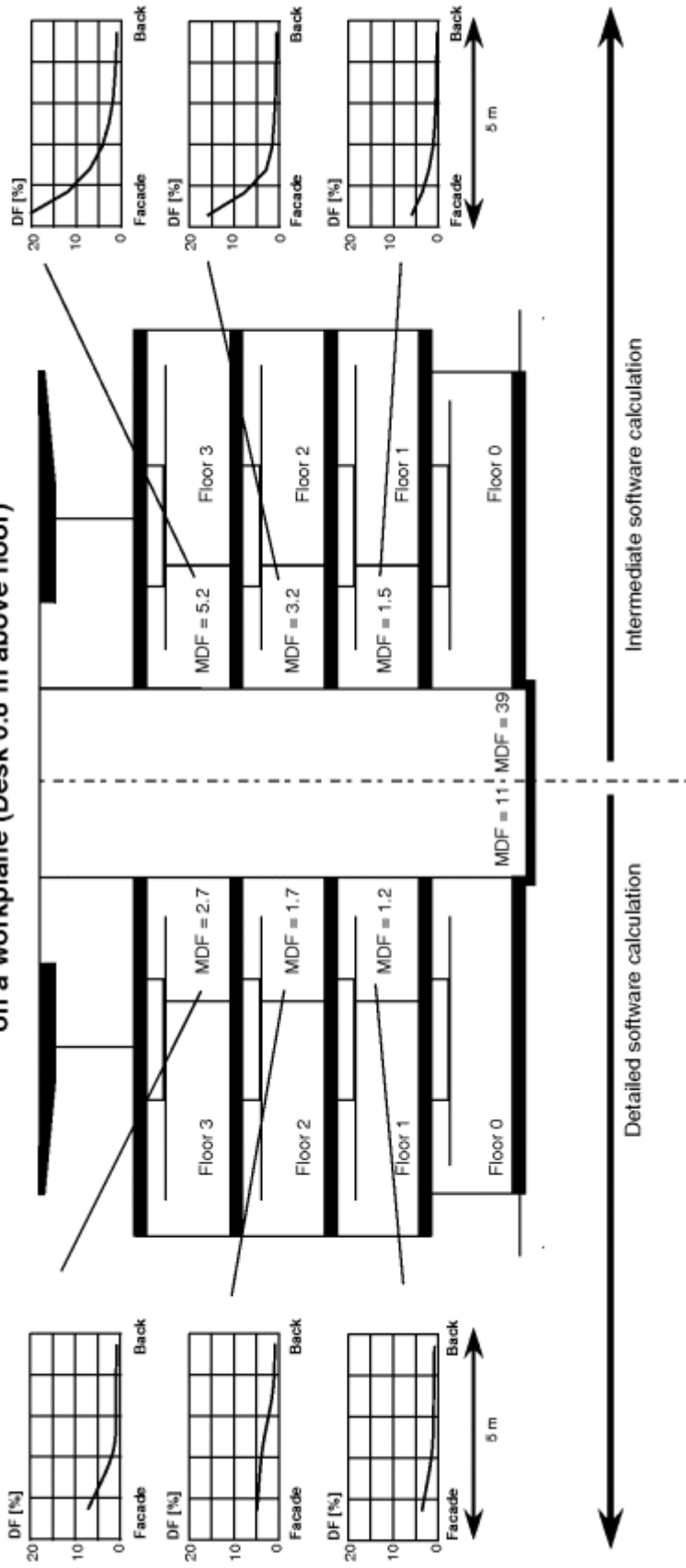
Fig. 4.4 A comparison between a detailed and intermediate tool for daylighting calculations

Fig. 4.5 A comparison between Radiance simulation (left) and photograph (right) of atrium

4.2.5.3 Plug Loads and Electric Lighting

In the concept design stage, generic plug loads and electric lighting requirements were used in the model. In the design development phase, plug loads and electric lighting are estimated more carefully.

The lighting requirements should be determined from the daylighting factors or other outputs obtained from daylighting studies, such as daylight autonomy and useful daylight illuminance. Strategies for dimming based on daylighting factors, daylight autonomy, or useful daylight illuminance can also be elaborated. Simple control systems that use readings from vacancy and illuminance sensors can help ensure that electric lighting is reduced when sufficient daylight is available. When choosing the equipment, energy-efficient lighting fixtures and electrical equipment should be prioritized. Once the type of equipment and lighting fixtures are determined, the internal gains due to lighting and plug loads can be estimated.

Internal heat gains from plug loads and electric lighting can have a significant impact on a building's energy consumption. They can reduce the heating load in the winter, but increase the space cooling energy requirements in the summer. Energy-efficient lighting or appliances will typically produce less heat gains than standard

equipment. The net benefit of using energy-efficient equipment on an annual basis depends on the climate, building type, and HVAC system, but is generally positive (Parekh *et al.*, 2005).

4.2.5.4 RET and HVAC

Once all the measures discussed in the previous paragraphs are considered in the architectural concept to limit the energy consumption, heating, cooling, and electrical load, energy consumption profiles can be determined, the HVAC system can be proposed, and the RETs can be refined. Analyzing the heating and cooling load profiles helps determine the most suitable HVAC systems and the required RETs to suit the demand. These systems should account for the type of terminals and distribution network used to heat and/or cool the building (e.g., radiators, floor heating, and cold ceiling).

Generally, Net ZEBs have high-efficiency heating and cooling systems, such as hydronic radiant floors, evaporative coolers, energy-efficient air-conditioning units, and heat pumps. Low-temperature (32 to 35 °C) heating systems generally provide more effective coupling with renewable energy systems, such as solar thermal collectors or geothermal heat pumps. Similarly, high-temperature cooling systems (15 to 20 °C) can typically be directly coupled with renewable energy cooling systems like geothermal heat pumps and can ensure better performance of the active cooling system. Often, these technologies will be coupled with heat and energy recovery ventilation systems (HRV and ERVS) with variable-speed fans.

RETs typically integrated in Net ZEBs include earth tubes, air and liquid solar thermal collectors, building-integrated photovoltaics (BIPV), and BIPV/thermal systems (BIPV/T) that produce both electricity and useful heat from the same surface (see Chapter 2).

Net ZEBs' HVAC systems generally combine multiple pieces of equipment, passive or active heat recovery and storage systems, as well as RETs that are more than often unique and innovative solutions. Sometimes, certain pieces of equipment can also be utilized in more than one system. For example, a solar thermal collector and a geothermal heat pump will both be used for water and space heating. Implementing such advanced systems requires

that complex simulation tools be used not only to model the systems, but also to couple these systems with the building. EnergyPlus, ESP-r, and TRNSYS are well suited for these requirements even though, sometimes, they cannot support the full model implementation and some assumptions are required. Simulations assist in achieving net-zero energy by refining the whole system and its components through numerous design iterations.

Coupling the HVAC system(s) and the RETs in the building model is ideal, but often difficult because some models are not available or the coupling is not easy to achieve (especially for controls). In lieu of an integrated model, the contribution from the renewable energy system can be estimated by modeling the HVAC systems without it (assuming adequate supply from the RET). Then, the RETs can be simulated separately (e.g., solar photovoltaics, geothermal heat pump, solar thermal, etc.) to obtain the resource availability and the energy demand, and production can be compared to demand to further optimize the coupling. This is, of course, a nonideal procedure, but it allows dimensioning the production unit and estimating how far the building is from reaching the net-zero goal. As described in Section 4.3, this approach can lead to significant errors when RET performance is dependent on demand or has tight thermal coupling with the HVAC system(s). Thus designers and modelers should have a deep understanding of the physics and operation of the system(s) before using such simplified modeling approaches.

4.2.6 Technical Design

During the technical design stage, refinement of the solutions can occur but it should not significantly modify the design development. In this phase, the following details of the solution set are evaluated:

- Interior finishing details regarding walls, ceilings, floors, HVAC terminals, and acoustics

- Technical details and location of lighting fixtures

- CFD simulation for critical zones (atrium ventilation, optimum opening geometry)

– Control algorithms development and refinement (HVAC, lighting, etc.)

– HVAC/RET: refinement of the calculations of the energy performance

– Dimensioning of the HVAC distribution network and terminal units.

Interior finishing for the walls, ceilings, and floors should be done in accordance with the thermal inertia calculated previously. For example, if a false ceiling is integrated and the thermal inertia of that ceiling was taken into consideration previously, the false ceiling should be designed so that this thermal inertia is still accessible. Determining the interior finishing provides detailed geometry and reflectances and allows evaluation of the daylighting potential with more precision. It will also help assess its impact on acoustics. Figure 4.6 presents an example of an effective solution to expose thermal mass while admitting daylight and absorbing sound. In this figure, a gap was left between the false ceiling and the wall to allow for air to reach the concrete deck above.

Fig. 4.6 Example of false ceiling that permits air circulation for thermal activation of concrete ceilings (BC-EPFL Lausanne Switzerland, Architect: R. Luscher Lausanne, Energy Concept: Sorane S.A, Ecublens)

Electric lighting optimization requires complex simulation tools, such as Radiance or Relux, that take into account detailed geometry, internal surface finishes, as well as internal partitions or objects. In the technical design phase, results obtained with these types of tools will allow optimizing the location of the lighting fixtures and refining the dimming and other control strategies.

Some zones cannot be simulated accurately using standard simulation tools, especially large glazed spaces like atria. CFD simulations can be used to study the ventilation of atria and optimize the openings and the control algorithm. CFD can also be used to optimize the location of terminals because the draft caused by HVAC terminals can affect occupant comfort. If considered critical, CFD can also be a useful tool for in-depth studies of temperature stratification. Figure 4.7 shows the results of a CFD analysis performed to study temperature stratification in a naturally ventilated atrium during peak summer load. It shows the building areas where the highest temperatures occur.
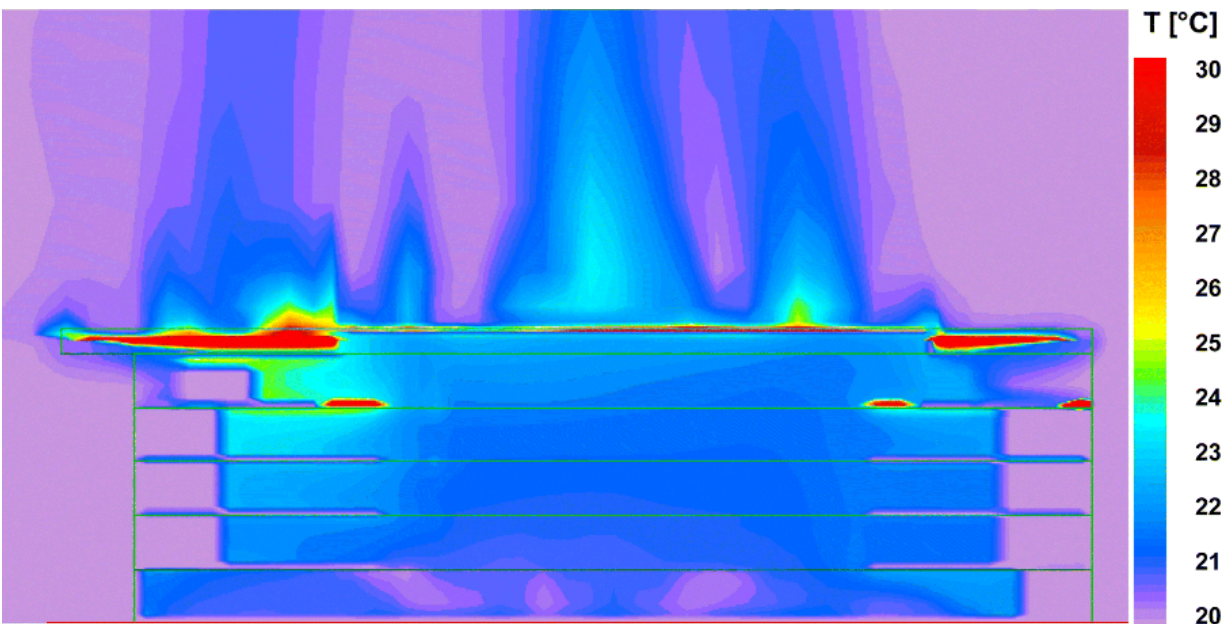
Fig. 4.7 Results of CFD analysis showing typical temperature distribution with natural ventilation in a building

Figure 4.8 presents results obtained from a CFD analysis conducted to evaluate the thermal comfort of two occupants in an office space in the summer following the implementation of a radiant ceiling (cold

ceiling). In this case, the air temperature around the occupants and the associated predicted mean vote (PMV) index were used as thermal comfort indicators.
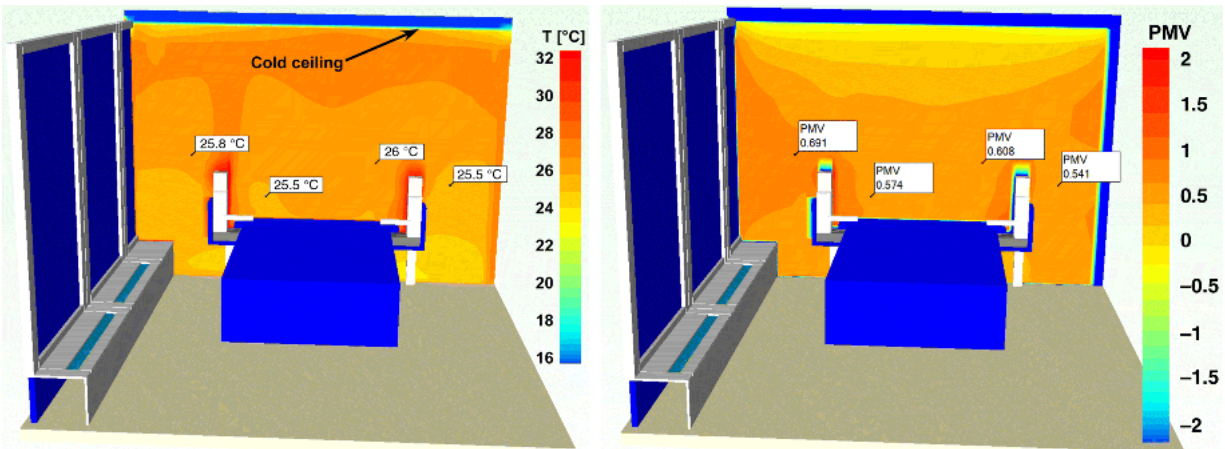
Fig. 4.8 Results of CFD analysis showing temperature stratification (left) in an office space and the associated occupants' predicted mean vote (right)

The technical design phase allows finalizing the whole concept of the building with its systems. Simulating the building coupled with its systems with advanced tools will provide energy consumption and production performance indicators and help finalize the integration of the active and passive design features. These results will allow evaluating the target values concerning energy, comfort, and environment. The evaluation of the Net ZEB goal during this phase will allow optimizing the control strategies for the openings for natural ventilation, the building interactions with the RETs, the solar shading devices, and the electric lighting. Further evaluation can be achieved for economic target values using a combination of the building energy performance, construction, and operating costs.

The design process map presenting the inputs, outputs, and tools at the different design stages is shown in Table 4.2.

Table 4.2 Design process map

		Concept Design	Design Development	Technical Design
DAYLIGHTING	Windows	Propose window-to-wall ratio (coordinate with envelope thermal performance)	Determine exact window locations	
	Visible transmittance	Propose visible transmittance of windows	Select windows and obtain detailed optical properties	
	Interior finishes	Estimate reflectances	Refine reflectance estimates	Determine interior finishes and obtain reflectances
	Controls[a]	Concept for automatically controlled shading devices	Coordinate controls with passive solar and thermal mass	Optimize controls
	Example of tools[c]	Rules of thumb, pattern guides, daylight autonomy diagrams, sun path charts	DAYSIM, DIAL–Europe, OpenStudio with Radiance, Radiance, Relux	DAYSIM, DIAL–Europe, DIALUX, OpenStudio with Radiance, Radiance, Relux
	Outcomes and conclusions	Approximate evaluation of daylight factor, daylight autonomy, useful daylight illuminance	Detailed evaluation of daylight factor, daylight autonomy, useful daylight illuminance	Refined calculations of daylight factor, daylight autonomy, useful daylight illuminance, and glare metrics
PASSIVE SOLAR	Windows	Choose suitable window-to-wall ratio and window thermal and optical properties considering effects on daylight as well	Select specific window types and sizes	Refine window sizes and framing to minimize thermal bridging

PASSIVE DESIGN SOLUTIONS

DEMAND ABATEMENT and IMPROVED ENERGY EFFICIENCY

		Concept Design	Design Development	Technical Design
	Solar shading devices	Determine solar shading device types and estimate dimensions	Design overhangs and other fixed shading devices (coordinate with daylighting)	
	Thermal mass	Include thermal mass in the design (e.g., admittance), if appropriate	Design thermal mass in detail by coordinating with windows and natural ventilation	Ensure that thermal mass remains exposed to facilitate effective heat transfer to indoor air
	Controls[a]	Concept for automatically controlled shading devices	Coordinate controls with daylighting and thermal mass	Optimize controls
	Example of tools	Rules of thumb, sun path charts, admittance technique	EnergyPlus, ESP-r, TRNSYS	EnergyPlus, ESP-r, TRNSYS
	Outcomes and conclusions	Rough evaluation of heating energy requirements provided by passive solar	Detailed evaluation of heating energy requirements provided by passive solar	Refined evaluation of heating energy requirements provided by passive solar
NATURAL (and HYBRID) VENTILATION	Opening sizes	Estimate opening dimensions (coordinate with daylighting and passive solar)	Determine exact opening sizes coordinating with thermal mass	
	Opening positions	Propose rough opening positions for cross ventilation or stack effect (coordinate with daylighting and passive solar)	Determine exact opening positions	

PASSIVE DESIGN SOLUTIONS

DEMAND ABATEMENT and IMPROVED ENERGY EFFICIENCY

	Propose opening controls depending on thermal mass	Detailed design of opening controls	Optimize opening controls
Opening controls[a]			
Example of tools	COMIS	EnergyPlus, ESP-r, TRNSYS	EnergyPlus, ESP-r, TRNSYS
Outcomes and conclusions	Rough evaluation of the cooling effect provided by natural ventilation (air change rates)	Detailed evaluation of the amount of cooling provided by natural ventilation	Refined evaluation of the amount of cooling provided by natural ventilation
BUILDING ENVELOPE — Opaque elements	Estimate U-values for all opaque elements based on insulation level (coordinate with building-integrated renewable energy system options)	Determine detailed wall composition considering thermal mass and insulation level; study thermal bridges	
Glazing	Estimate U-values and SHGC for glazing elements	Obtain all glazing element U-values, SHGC and visible transmittance	
Example of tools	RETScreen, PHPP	Transient simulation tools like EnergyPlus, ESP-r, TRNSYS	
Outcomes and conclusions	Evaluation of building heating and cooling energy requirements	Evaluation of heating and cooling energy requirements integrating internal gains	

		Concept Design	Design Development	Technical Design
ELECTRIC LIGHTING and PLUG LOADS	Equipment	Estimate based on typical values for similar buildings	Evaluate plug loads and electric lighting requirements; specify equipment type; estimate internal gains	
	Controls	Relate to daylighting concept and operation	Determine dimming strategies in conjunction with daylighting controls	Refine controls
	Example of tools	Precedents, experience, and rules of thumb from similar existing buildings		ASHRAE Standard 90.1
	Outcomes and conclusions	Typical power densities and occupancy scenarios	Evaluation of the energy requirements of plug loads and electric lighting and associated internal gains	Refined evaluation of the energy requirements of plug loads and electric lighting and associated internal gains
HVAC	Equipment	Evaluate advantages of different concepts with on–site available renewable energy	Propose production and distribution unit for heating and cooling coordinating with RET and heating/cooling load	Dimension HVAC devices and piping/ducting
	Controls	Basic control concept related to passive design solutions (passive solar and natural ventilation) and RETs	Further development of control strategies	Optimize HVAC control in conjunction with passive design solutions (passive solar and natural ventilation) and RETs

EFFICIENCY/CONSERVATION

DEMAND ABATEMENT and IMPROVED ENERGY EFFICIENCY

	Precedents, experience, and rules of thumb from similar existing buildings	EnergyPlus, ESP-r, TRNSYS	EnergyPlus, ESP-r, TRNSYS
Example of tools	Precedents, experience, and rules of thumb from similar existing buildings	EnergyPlus, ESP-r, TRNSYS	EnergyPlus, ESP-r, TRNSYS
Outcomes and conclusions	HVAC concept options	Evaluation of the building fuel and electricity consumption; integration with RET to achieve Net ZEB target	Refined evaluation of the building fuel and electricity consumption
Equipment	Evaluate on-site renewable energy (solar, wind, geothermal)	Refine RET after analyzing the heating, cooling and electrical load profile	Dimension RET
Controls	Concept for operation including interaction with HVAC and passive design solutions	Development of control strategies	Optimize RET control
Example of tools	Rules of thumb; RETScreen	Specific RET tools (for PV, wind turbines, etc.); RETScreen	EnergyPlus, ESP-r, TRNSYS
Outcomes and conclusions	From RET options, propose suitable RET and coordinate with building envelope	Evaluation of the building energy requirements met by RET; integration with HVAC to achieve Net ZEB target	Evaluation of the Net ZEB goal and calculation of performance figures

Row group label: **RENEWABLE ENERGY TECHNOLOGIES**

Bottom bars: **RENEWABLE ENERGY GENERATION** / **DISPLACE FOSSILS WITH RENEWABLES**

a) Although controls are not properly considered a part of passive design, they are included here due to their significance to the design process.

4.2.7 Integrated Design Process and Project Delivery Methods

As previously mentioned in Section 4.1, the growing importance of building energy performance has put pressure on the building design process to allow for increased feedback at the early design stage. Concerns such as these have led to the IDP (AIA, 2008; Löhnert, Dalkowski, and Sutter, 2003) or integrative process (ANSI, 2012). This approach specifically addresses the limitations of the traditional process with flexibility and adaptability. IDP recognizes that all projects are unique and that there is not necessarily a rigid, predefined series of steps to building realization and that the process itself needs to be able to respond to evolving needs due to industry, technology, or other social, ecological, and economic change.

The defining characteristics of the IDP are as follows:

– *An iterative, nonlinear process:* In sharp contrast to the conventional linear design process where team members often work in silos, the IDP promotes increased feedback loops between all project stakeholders.

– *Collaboration and innovation:* It is essential that all parties share the same project vision and be present from the beginning of the project to provide input and feedback to the rest of the team. Team members may be required to take on tasks outside of their usual scope. The IDP encourages all parties to share in learning from, and improving, the process as a whole.

– *A multidisciplinary team:* Ideally, the IDP includes all stakeholders in a project, from the building owner, to the design professionals, the builder, the building users, and the building operators. They are all present from the early design stages and each provides valuable expertise to the design process. There may be additional consultants required based on specific project needs.

Additionally, there are two contributing factors to ensuring the success of an IDP: well-defined goals, and a facilitator, who sets the tone for collaboration and effective communications throughout the design process.

The implementation of any design process such as IDP will involve a project delivery method. In this area, there has also been much

movement toward new project delivery models that optimize the timely expertise of all stakeholders in a project. This movement originated from building owner dissatisfaction with quality, cost overruns, delays, and the adversarial nature of the enterprise, as well as the acknowledgment that building projects have become increasingly complex – with part of that complexity being the integration of new technologies such as renewables into a building.

The design phases that have been described in Section 4.2.2 form the "traditional" design-bid-build project delivery method, which will serve as a reference point for the innovative new project delivery models that follow.

> – *Construction management at-risk (CM@R):* This method adds a construction manager to the traditional design process. The construction manager's role is to provide to the design team construction expertise, such as budgeting, scheduling, cost control, sequencing, and technology integration, site and subtrade coordination early on in the design process. The term at-risk refers to the fact that it is the construction manager who holds the trade contracts and the performance risk for the construction. Some overlapping of phases usually occurs, aiding in the Net ZEB design process. Although the design and construction teams work together, they hold separate contracts with the building owner.

> – *Design-build (DB):* This method integrates the design and construction teams into one legal entity stemming from building owners' desire for one single point of responsibility for design and construction. Projects benefit fully from the expertise of both designers and construction experts working together from the early design stages. This permits more feedback loops and collaboration since design phases are more fluid with simple tasks being shortened and more complex ones lengthened or continued after the start of construction. Since designers and contractors are now part of the same team, their goals are closely aligned and innovation is encouraged. The NREL used this model in conjunction with the integrated design process in the realization of their RSF. See the relevant case study in Chapter 7.

– Integrated Project Delivery (IPD): This method proposes a multiparty arrangement between, at a minimum, the building owner, the building professionals, and the contractor. Unlike the other delivery methods, in IPD each party is an equal stakeholder in the project, and share both the risk and the reward in the project. Their relationships must be based on mutual respect and trust for what each member brings to the project. Collaboration in innovation and decision making are emphasized since all members are involved from the beginning of the project. Each party contributes their unique expertise to the project in a timely fashion. This breaks down the barriers between the design and construction phases of a project, which are required in traditional models. Focus is placed on optimizing the project for long-term benefit – including operating costs – and not based on initial costs.

As a final note, while IDP is adaptive and flexible, and can be used with any project delivery method, there are limitations. It is ultimately the building owner's level of comfort and risk that determines the choice of project delivery method and the level of integration of the IDP. For example, if using the traditional design-bid-build method, the contractor is not selected until the construction phase and therefore cannot be present at the early design stage to take part in the IDP.

4.2.8 Conclusion

This section presented the different stages that can be followed to design Net ZEBs. At the preliminary stages of the design, a detailed model of the building with all its systems is difficult to develop because only a few pieces of information are known such as the building location, size, and form.

Ideally, a Net ZEB should focus on demand abatement through a design that responds to its climatic conditions – instead of resisting them – by appropriately managing daylighting, natural ventilation, thermal envelope, and solar gains. The remaining energy demand is fulfilled by efficient HVAC systems coupled with RETs. At every design stage, building designers are invited to evaluate the design with the adapted calculation method or software depending on the

amount of information available. At the early design stages, simple calculation tools can be sufficient. The use of various tools at different stages of the design process is inevitable because as the building design is refined, the target values evolve and specific studies become necessary.

4.3 Net ZEB Design Tools, Model Resolution, and Design Methods

4.3.1 Introduction

Building performance simulation (BPS), a method for predicting a building's performance prior to construction, has been available since the 1960s (Clarke, 2001). With the additional objective of aiming to achieve absolute performance targets (e.g., net-zero energy), demands placed on the usability and accuracy of BPS tools increase substantially. The prevalent contemporary use of BPS in practice is to substantiate that the proposed building performs well relative to a reference case (e.g., ASHRAE Standard 90.1 (ASHRAE, 2010a)) and for equipment sizing. One of the major objectives of this chapter, in contrast, is to demonstrate the value of BPS in design, from conception to detailed design, and to provide more absolute performance data. Extensive use of BPS in this way is also presented in the four detailed case studies in [Chapter 7](#).

By the most common Net ZEB definitions (Marszal *et al.*, 2011), a detailed model must predict both annual energy demand and on-site generation. Corollary requirements include (a) a high temporal resolution of electrical power demand and supply from and to the grid in order to assess grid-interaction considerations and (b) data about occupant comfort to ensure that meeting energy objectives does not jeopardize comfort. Thus, the three following requirements are imposed on Net ZEB modeling tools:

1. Ideally, at least one of the BPS tools used during the design process must be capable of modeling all systems in an integrated manner. Depending on the proposed building systems, an unintegrated model (e.g., assessing a house and its solar thermal system separately) could lead to poor modeling accuracy. Nearly

all building systems have some degree of interaction and should be treated as such.

2. Absolute performance of the building and all subsystems should be estimated by using accurate inputs and circumscribing the uncertainty of weather, occupant behavior, and construction quality. This is a significant development from most modeling methodologies and building energy codes, which emphasize typical building conditions (e.g., occupancy patterns) and accept relative predicted performance.

3. BPS tools used for Net ZEB design require detailed outputs. This includes flexibility on the output reporting frequency (e.g., sub-hourly) and the detail of outputs (e.g., zonal air and surface temperatures).

Despite these constraints, the value of simpler, lower-resolution tools has never been greater because the design of affordable Net ZEBs necessitates integrated design from the beginning of the design process. It is only with simpler tools that a sufficient number of design variations can be properly examined in the early design stage when the building design is least defined and when there is the greatest opportunity to influence it (Reed and Gordon, 2000).

While BPS can be applied systematically and based on sound engineering practice, it is undeniable that it is an art form and that good judgment is critical. Augenbroe (2012) stated that "the art of modeling and simulation is leaving things out that don't affect the answer." Designers must focus on the phenomena of interest and exclude the unrelated phenomena.

A number of specific tools are discussed throughout this chapter. A comprehensive and up-to-date database of BPS tools is maintained by the US Department of Energy (2013a). Crawley *et al.* (2008) thoroughly compared and contrasted 20 of these tools. Furthermore, many of the tools are discussed throughout this section for illustrative purposes. All mentioned tools can be found on the aforementioned US DOE BPS tool database website.

This section examines some fundamental Net ZEB design and modeling issues, including choice of appropriate model resolution, methods for simulation-supported design, several examples of how

BPS can be used for Net ZEB design, and finally, recommendations for future BPS tools.

4.3.2 Model Resolution

A conscious effort should be made by designers of Net ZEBs (and any advanced buildings) to select the appropriate level of model resolution. As shown in Figure 4.9, the opportunity for quantitative analysis (i.e., use of BPS) to influence design rapidly decreases as the design process progresses. Simultaneously, the cost to change a design increases, as decisions have become finalized and documented in architectural drawings and specifications. The challenge of incorporating BPS into early design is not restricted to the usability and accuracy of the tools themselves, but also the adoption of BPS in the design process.
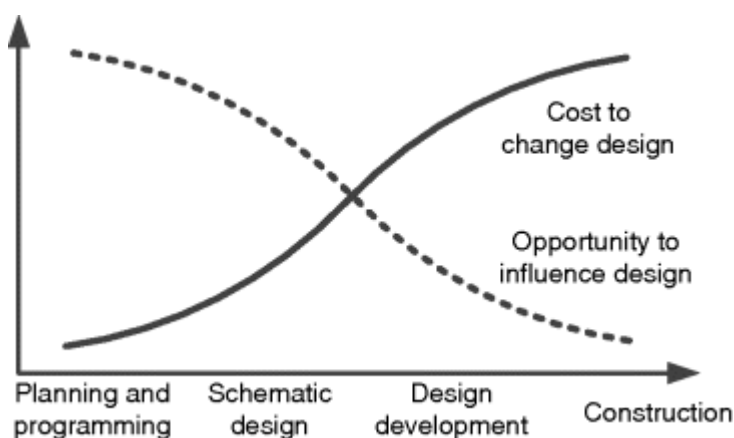
Fig. 4.9 The opportunity to influence building design rapidly decreases beyond schematic design

Since the design timeline is generally very short in early planning stages, it is impractical to develop a highly detailed model for standard building design strategies. A single detailed BPS model may take longer to construct (weeks or months) than the architects allow for all consultants' feedback! Thus, at best, the use of a detailed BPS model would confirm initial performance estimates without providing any opportunity for design feedback. Therefore, the use of simple tools in which a model can be developed quickly enough that results can influence design and also for which the results can be easily interpreted is essential. The simplest of these tools should provide results fast enough that they can be used during or

immediately prior to design charrettes.[2] These tools are intended to answer order of magnitude-type questions, such as

– What passive strategies are best for this particular climate?

– How much solar energy can be collected and stored on the building site?

– Approximately how much can space heating energy be reduced by upgrading windows or walls?

While the answers to these questions do not provide an absolute sense of performance (or at least they should not be taken at face value), they do provide information on the relative effectiveness of design techniques and technologies to approach net-zero energy.

The use of simplified tools in early design is further justified by the fact that (a) there are diminishing returns on model accuracy as model resolution increases, and so, simple models can still provide significant accuracy (see Figure 4.10), and (b) simple tools are typically easier to understand and thus, confidence through understanding tends to be higher. However, transparency of the underlying mathematical model of BPS tools should be high so that users are aware of their assumptions and limitations. One of the reasons why designers may avoid simplified tools in favor of detailed ones is that they feel detailed models are risk-free since all building aspects are supposedly modeled in an integrated way. However, evidence suggests that the use of complex tools, beyond a certain point, can decrease model accuracy (Chwif, Barretto, and Paul, 2000). This is primarily because complex models have many more inputs (e.g., building details) that may be obscure to nonexperts who enter or set them inappropriately. Furthermore, errors in complex models are more difficult to identify and may go unnoticed.
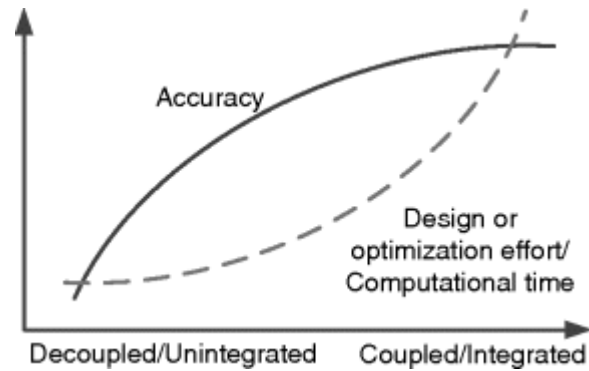
Fig. 4.10 The conceptual relationship between model integration and accuracy and computational time

Recommended simplified tools and approaches for early-stage Net ZEB design are as follows:

– *Databases and case studies* represent a starting point for exploring other high-performance buildings of a similar type and climate. These can identify successful and poor design features. Example Net ZEB databases include Net-zero energy buildings map of international projects (Musall, 2013), The Zero Energy Buildings Database (DOE EERE, 2013a), and Chapter 7 of this book.

– *Assessing typical local climate* for conditions can identify the most promising passive strategies. Prior to specific building design knowledge, a portfolio of suitable design strategies can be established that specifically exploits or has superior tolerance to steady state or dynamic sequences of weather conditions (e.g., solar, wind, temperature, relative humidity). Example tools to visualize climate data include Climate Consultant and Ecotect. Use of such tools in the design process is discussed at length later in the chapter.

– *Tools based on look-up tables, design charts, or rules of thumb* can provide an efficient means for applying preconceived or simplified situations to the design at hand. Such methods are typically based on experimental or numerical results that would be time consuming or expensive to obtain for early stage design. Their limitation is that they are based on assumptions of the software developer and may not be suitable for application to other design circumstances. Examples include: Advanced

Buildings' Daylighting Pattern Guide (Advanced Buildings Institute, 2013), Tap the Sun (CMHC, 1998), and passive solar design charts from Sander and Barakat (1985).

– *Single-component or single-aspect tools* allow designers to focus on one building aspect at a time. As explained in Section 4.3.2, this can lead to the risks of neglecting interactions between systems. However, where coupling is weak, using single-feature tools can be a helpful approach to design because they allow the designer to focus on a single system (e.g., windows, wall constructions, PV systems). Examples of single-component tools include: LBNL Window for window thermal and optical property analysis, RETScreen for RETs, DAYSIM for daylighting analysis, and MOIST for combined heat and moisture transfer through wall constructions. An example of the use of a single-aspect tool is Radiance for the NREL RSF building. Later, the results from Radiance were used in other tools for assessing total energy use.

– *Simplified tools based on dynamic sub-hourly-timestep simulations but with a limited number of inputs*. While these programs may have underlying complex models or simulation engines, the inputs are normally restricted to reasonable values by the tool developer; thus, the aforementioned risks of complex models is partially avoided. The primary limitation to this category of tool is the available range of preconceived designs and building systems. Examples of simplified tools (and their underlying simulation engine) include: HOT3000 (ESP-r), DAYSIM (RADIANCE), Example File Generator (EnergyPlus), eQUEST (DOE2.2), COMFEN (RADIANCE and EnergyPlus), and SPOT (RADIANCE).

The aforementioned categories of tools are mostly well-tested and have minimal inputs, rapid output of results, and are mostly fast to learn and deploy. In many cases, these tools have underlying assumptions that are reasonable and prevent inexperienced building designers from venturing into unrealistic parameter values. This is very convenient for designers and other tool users who may not have detailed information at the beginning of design. These advantages come at the cost of reduced flexibility (e.g., limited number of technologies, design features, and geometries).

Only when the design advances to a detailed level should a model of higher resolution be used. Two proven strategies for incorporating escalating model resolution into the design process are the following:

1. *Use of multiple models or interfaces of increasing complexity for a single simulation engine* is one promising approach for escalating model resolution through the design process. Certain tools have multiple component models with different levels of detail. For instance, EnergyPlus has three photovoltaic models of increasing detail: simple, equivalent one-diode, and Sandia (Department of Energy, 2013b). A simulationist could conceivably start a building model with the simplest PV model, thus providing faster results with reasonable accuracy and then progress to more complex models as data become available (e.g., exact product specifications) and the demand for accuracy increases (e.g., when the energy balance is being performed). Similarly, other building features, such as daylighting, HVAC, and envelopes, lend themselves well to escalating model resolution.

   Another way that a single tool can facilitate evolving model complexity is to use one of the simulation front ends (the last category of simplified tools, presented earlier) to build an initial model as a take-off point and then proceed using the simulation engine directly to add details. For example, numerous front ends for EnergyPlus (e.g., Example File Generator (DOE EERE, 2013b)) enable simulationists to create a simple model (e.g., rectangular building with a certain window-to-wall ratio and a standard code-compliant HVAC system) and then export this model for direct use and detailed modeling in EnergyPlus. This approach normally provides inputs for many typical building characteristics (e.g., standard occupancy and plug loads schedules for schools) – a task that is otherwise time-consuming. A limitation of this approach is that it restricts the modeler to use the simulation engine that is behind the front end. Furthermore, this workflow is normally unidirectional, meaning that once the model is modified in the detailed tool, the user cannot return it to the front-end interface.

2. *Interoperability between tools* allows the same model to be saved and opened by multiple design tools – ideally of different model

resolution. Recent advances in industry standards (e.g., Industry Foundation Classes (IFC), and Green Building Extensible Markup Language (gbXML)) have attempted to remove barriers between tools. However, this remains a challenge rooted largely in the conflicting demands of different tools and their intended audiences. For instance, building information modeling (BIM) tools have a high degree of detail in geometry, and to a lesser extent in building materials. Building energy modeling tools, in contrast, require a high degree of detail in building materials (e.g., thermo-optical properties), but do not require as high a resolution for geometry (e.g., trim and other intricate detailing). In fact, inclusion of such details results in excessively complex models that do not yield significantly better accuracy (see Figure 4.10), and may take unacceptably long to detect bugs and simulate. BIM is recognized as a process that has reinvented the building design industry, though widespread adoption has not yet occurred for energy modeling.

Another method to simplify models is to decouple certain model aspects (e.g., modeling renewable energy systems independently of the rest of the building systems vs. a single integrated model). In order to avoid overlooking any interactions, simulationists often try to integrate every possible building element into a single model. However, efficiency at the early design stage can be expedited if opportunities for decoupling are exploited.

If two or more systems have minimal physical interactions, it may be possible to decouple the models and even use two different tools to model a single building. For instance, Figure 4.11 shows a Venn diagram to represent the major subsystems of a net-zero energy house. It indicates that the PV and the house have no major thermal coupling; and therefore, the house can be modeled as a separate entity from the PV. For this case, the performance of the house does not significantly affect the performance of the PV system and vice versa. It should be noted that this is only valid for grid-tied PV and BIPV systems that are essentially thermally isolated from the house's interior with insulation. For off-grid applications, the issue of electrical storage becomes important, at which point there is value in modeling an integrated system (e.g., to attempt to shift and reduce

the peak electrical load to ensure that the PV system can meet it and that the battery charge is maintained within limits).
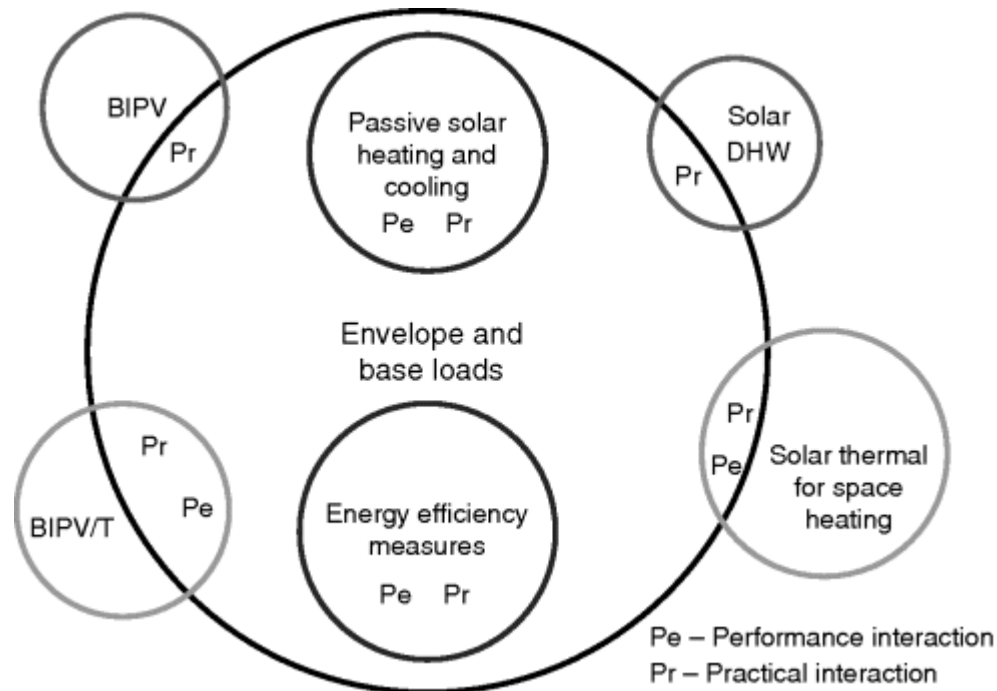
Fig. 4.11 Example Venn diagram showing the level of interactions between systems in a net-zero energy house

For solar thermal systems that solely provide energy for domestic hot water, decoupling is normally reasonable because the thermal interactions between the system and the building are minimal. For instance, the storage tanks and the building envelope upon which the collectors are mounted are both well-insulated. Critical inputs to the solar domestic hot water systems (draw profile, component efficiency, and controls) are not dependent on the building performance, though may be related to occupancy and water fixtures.

For solar thermal systems that provide space heating, integrated models are far more important because of the interdependency between the solar thermal system and the building. The performance of the building depends on the energy delivered by the solar thermal system, but the performance of the solar thermal system depends on the heating demand and on the temperature of the fluid that is returned to the solar collector. For instance, in the ÉcoTerra house case study (Chapter 7), the ability for the BIPV/T collector to deliver

useful energy to the ventilated slab is quite sensitive to the temperature of the slab, which in turn depends on the passive solar gains and thermal dynamics of the house.

Even if thermal interactions are minimal, practical interactions should be considered. For instance, BIPV must be carefully sized and oriented so that it can be directly integrated into the building.

The ability to decouple certain component models from each other not only has modeling implications but also has design process implications. For instance, decoupled models allow fractional factorial design. To explain this, consider a building concept that requires selection of three distinct systems, each with two options (see Figure 4.12). If these systems have strong interactions, it would be inappropriate to decouple the models because each one impacts the other two. Therefore, full factorial design should be used, whereby there are 8 (2^3) possible designs and corresponding model permutations (or more generally, x^n possible designs, where x is the number of options for each of the n decisions). However, if these models can be decoupled such that there are three independent decisions with two options each, then as few as four distinct models are required.

Full factorial design: Eight permutations

Fractional factorial design: four permutations
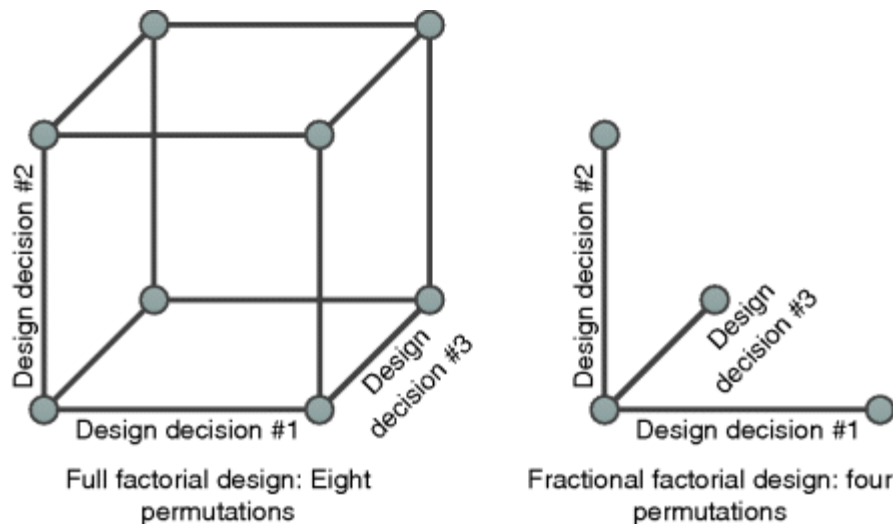
Fig. 4.12 Full factorial and fractional factorial design

A further advantage to decoupling models, where it is technically sound, is a reduction in simulation time. If the simulation is based on simultaneously solving equations by inverting a matrix, then the

computational time to invert the matrix is proportional to X^3, where X is the number of rows in the matrix.

In certain situations, it may be appropriate to simulate different building phenomena in two or more different tools sequentially. This is permissible if multiple phenomena do not interact dynamically yet one may affect other(s). This allows the most suitable tool to be chosen for modeling each phenomenon. For example, it is usually assumed for indoor air quality (IAQ) modeling that contaminants are trace elements, meaning that their mass is very small compared to the total mass of the air in a building. Therefore, the airflow rates and pressures may be resolved first and then this information, after the entire simulation has run, can be provided to the contaminant model. The caveats to this are the following: (a) the tools must be able to read from and write to a file that is recognized by both (e.g., a simple text file), and (b) the assumption of unidirectional data flow must be acceptable. In the IAQ and airflow example, sequential simulation does not allow demand controlled ventilation (DCV) to be modeled because for such buildings the ventilation rate depends on the carbon dioxide concentrations and vice versa.

Another method for combining multiple building analysis tools is to use tools that statically assess the properties of a particular system and then import the performance results into a dynamic simulation tool. For instance, most simulation engines assume one-dimensional conductive heat transfer through opaque walls and do not necessarily enable a user to provide information for each window pane and window frame. However, through the use of tools such as Lawrence Berkeley National Laboratory (LBNL) THERM and WINDOW, detailed wall and window system performance data can be exported so that the equivalent properties (e.g., one-dimensional conductance and angle-dependent optical properties) can be used by dynamic simulation engines. Many simulation engines (e.g., ESP-r and EnergyPlus) further support this method by importing data files from WINDOW software. Similarly, HVAC performance curves are normally preferred over complex HVAC models that are based on first principles.

In recent years, time-step coupling between tools has gained significant research attention (e.g., Wetter and Haves (2008)). These

approaches enable the features of multiple tools to be combined into a single model, as if it were a single tool. This has the advantage of using existing component models rather than recreating them. Building Control Virtual Test Bed (BCVTB) and the ESP-r-TRNSYS Harmonizer (Beausoleil-Morrison, 2011) are among the most promising co-simulation efforts. In the case of the latter effort, the motivation of the harmonizer is to use the building load modeling strength of ESP-r and the detailed HVAC and renewable energy system strengths of TRNSYS. The necessity of this approach depends on the interdependency of systems, as illustrated in [Figure 4.11](#).

4.3.3 Model Resolution for Specific Building Systems and Aspects

The following sections elaborate on specific aspects of Net ZEB modeling. The intent is to discuss some of the major challenges and issues with respect to selecting appropriate model resolution.

4.3.3.1 Geometry and Thermal Zoning

Building geometry, or at least a simplified representation of building geometry, is fundamental to BPS. Building models are typically comprised of one or more thermal zones that are completely bounded by surfaces (windows, walls, and doors), though some tools (e.g., ESP-r) allow the use of artificial or "fictitious" surfaces to represent openings. Most BPS tools assume that the air within the zones is perfectly mixed, though more complex models consider several vertically stacked air masses for vertical stratification or use multidimensional CFD.

A building should be discretized into thermal zones such that any space with significantly different heat gains, solar exposure, operating conditions (e.g., temperature), and occupancy patterns are unique. Furthermore, the zonal configuration should reflect the HVAC control zones (primarily for detailed design) (Department of Energy, 2013c). O'Brien, Athienitis, and Kesik (2011b) showed that the tendency to model buildings with few zones in early design stages can under-predict energy use and overpredict thermal comfort. They modeled a two-story house with one, two, three, and five zones and plotted the heating and cooling energy use for the different south-

facing window sizes (see Figure 4.13). The results in Figure 4.14 clearly show that modeling the house as a single zone not only reduces the predicted energy use but also increases the optimal window-to-wall ratio. This is because the single zone configuration assumes that all solar gains in the southern part of the house are instantaneously distributed to the entire house (perfectly mixed air assumption). In reality, the solar gains would likely only heat up the southern part of the house and could cause the need for simultaneous heating (northern part of the house) and cooling (direct gain zone).
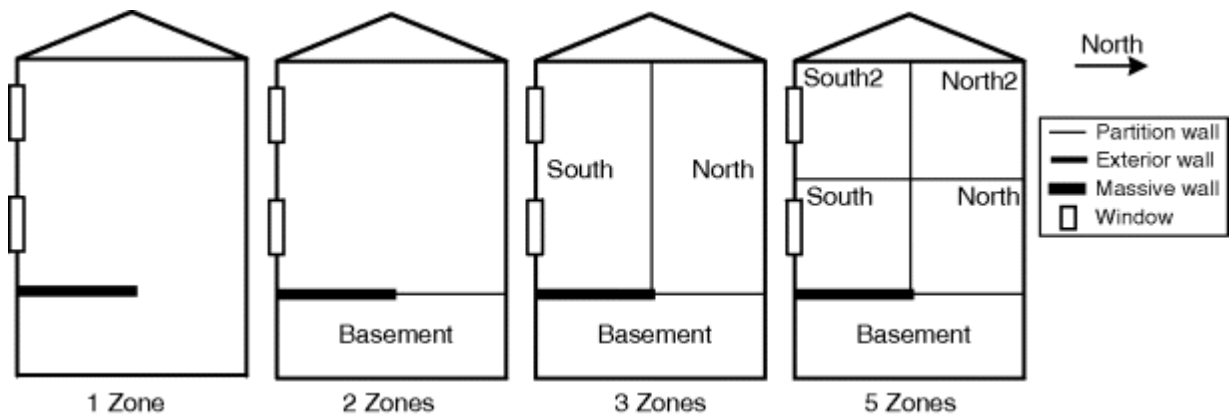
Fig. 4.13 Four different thermal zone configurations for a passive solar house (O'Brien, Athienitis, and Kesik, 2011b)
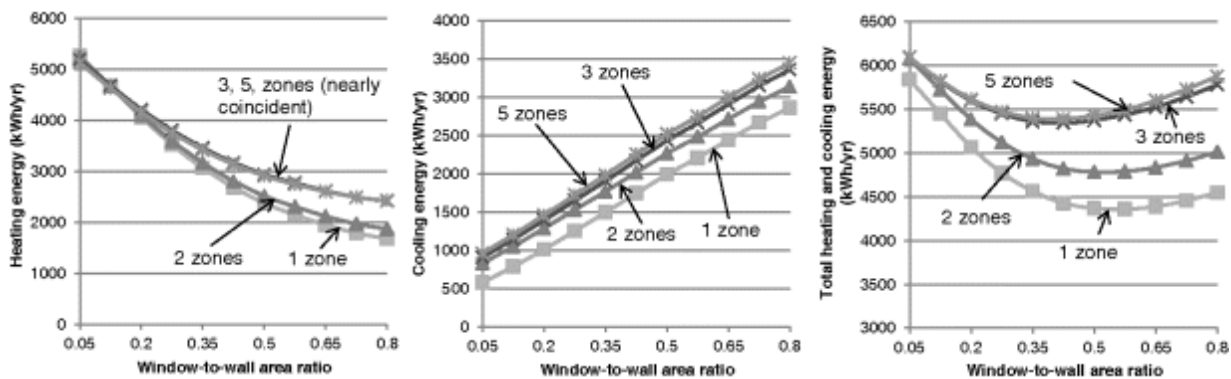
Fig. 4.14 Total heating and cooling energy for four thermal zoning configurations of the same house model

One of the most time-consuming building modeling tasks is geometry input (Bazjanac, 2001). Bazjanac estimated that geometry-related tasks account for about 80% of simulation input time resources (Figure 4.15). However, this will depend greatly on

geometry complexity and whether or not the HVAC systems, another time consuming category of inputs, are modeled in detail.
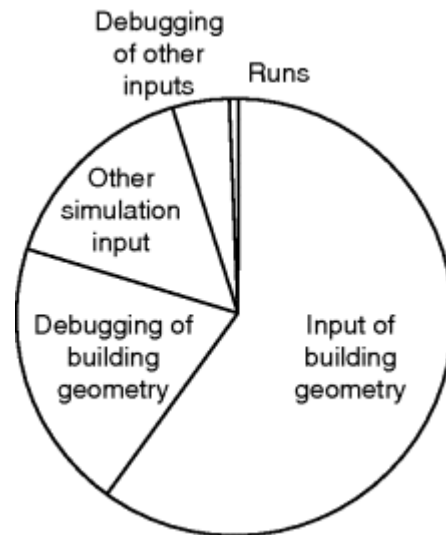
Fig. 4.15 Proportion of time devoted to different tasks for building energy modeling (reproduced from data from (Bazjanac, 2001))

Several approaches that can shorten the process of geometry input include

– *Import from 3D modeling software*. Many BPS tools allow direct import from 2D or 3D architectural drawing and modeling tools, or at least allow a drawing to be imported and traced (e.g., in ESP-r and eQUEST). A straightforward transition from 3D models to energy models is not yet possible. The challenge is not limited to the translation of geometry but also the logic of combining rooms into thermal/HVAC zones and other geometric simplifications that are recommended for energy modeling.

– *Simplify geometry of whole building*. Another approach is to create simplified geometry, which excludes minor details (e.g., bay windows and dormers) and combines zones. Grouping rooms into zones saves on effort to create models, but also on debugging and simulating models.

– *Analyze one zone at a time*. For buildings with a high degree of repetitiveness (e.g., multiple identical offices, dwelling units, or stories), much can be learned by focusing on one part of the building at a time. In fact, this can help designers reduce the

overwhelming amount of data that are produced from BPS tools. Several tools (e.g., EnergyPlus) facilitate simplifying the geometry if zones or floors are repetitive by allowing zones to be multiplied by some integer such that only a single zone or group of zones needs to be modeled.

The required resolution of the model geometry is dependent on the phenomenon being studied, as summarized in Figure 4.16. For determining thermal loads resulting from heat transfer through the building envelope, a simple model may suffice. Detailed HVAC simulation models should have zones sized according to the HVAC control zones for the actual building. This ensures different space loads – sensible and latent – can be met by the proposed HVAC system under the expected thermal loads (e.g., solar, occupants, equipment, and heat loss). Detailed daylight and acoustic analysis are among the most demanding on zonal configuration because most BPS tools typically require zone boundaries to represent interior surfaces. In fact, grouping rooms into a single zone is likely to overpredict daylight illuminance because fewer partitions between spaces causes better daylight penetration. This is in contrast to thermal domain modeling where it is normally acceptable to merge several rooms of similar air temperature into a single zone.
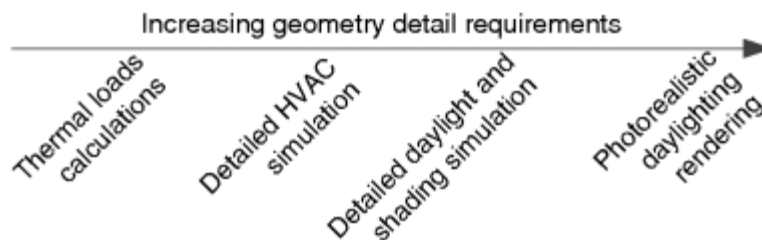
Fig. 4.16 Model geometry resolution by building aspect

Ultimately, the limiting factor for zonal configuration may be dictated by the most advanced aspect required (as per Figure 4.16). For energy analysis, modeling every room as a zone should be avoided if possible (especially for large buildings) because it is not only computationally expensive, but also very time consuming to model and can create excessive volumes of output data and difficulty for debugging models.

4.3.3.2 HVAC and Active Renewable Energy Systems

Heating, ventilation, and air conditioning equipment is usually responsible for the majority of energy use in buildings – especially those that are in cold or hot humid climates, actively conditioned, and sealed (i.e., not reliant on natural ventilation).

For early-stage design, when passive strategies (e.g., building form, insulation level, window size, type, and placement, and thermal mass) are being evaluated, idealized HVAC systems are normally adequate. Such systems are modeled to deliver heating and cooling as needed to maintain simplified comfort conditions (e.g., based on air temperature and humidity). Idealized methods become less accurate when issues such as HVAC capacity, distribution energy (fans, pumps), and controls are established in the design. For Net ZEBs, these details can be significant because distribution (fan or pump) energy can be relatively high and controls are often advanced.

The sheer number of available HVAC configurations and components means that HVAC systems are among the most difficult to model. This has been resolved in many BPS tools and interfaces (e.g., eQUEST, EnergyPlus, and Example File Generator) using templates in which several common HVAC configurations are provided to the user. For the frequent occurrence in which the designed HVAC configuration is not represented by one of the built-in templates, a common workflow strategy is to use the template as a starting point and then modify it, as needed, to represent the configuration of interest. In the context of Net ZEBs, the vast number of HVAC configurations is further complicated by the fact that renewable energy systems are often integrated into the building, systems, and/or plant, as shown in Figure 4.17. Thus, in order to accurately model these integrated systems, a detailed coupled model is necessary.
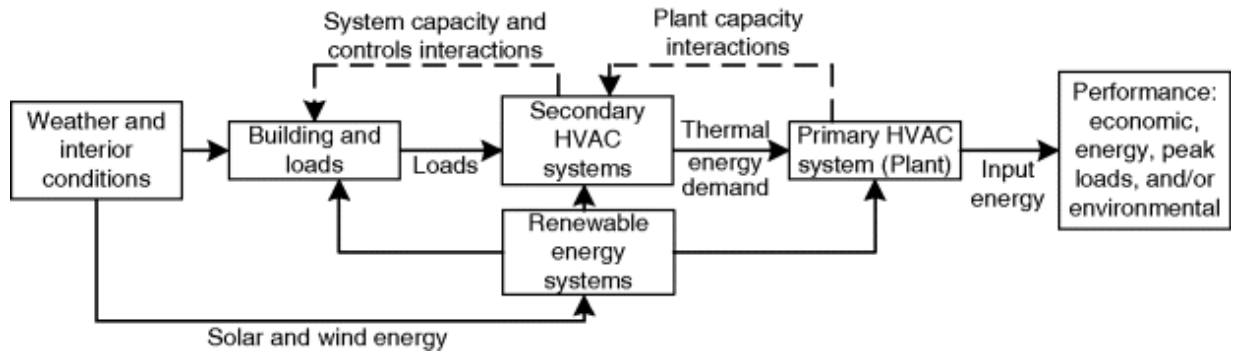
Fig. 4.17 Data flow in decoupled (——————) and coupled (– – – – –) building-HVAC modeling approaches for Net ZEBs

The ÉcoTerra house, which has a novel BIPV/T collector that is integrated to an actively charged ventilated concrete slab, faced the challenge of having no readily available models for such a system during design (Chen, Athienitis, and Galal, 2010a; Chen, Galal, and Athienitis, 2010b). The requirement for a coupled model in this case was undeniable; the usefulness of the thermal energy output of the collector is highly dependent on the demand for heating within about 12 h (the approximate storage capacity of the ventilated slab). Furthermore, the ability of the collector to offset purchased heating energy is highly dependent on the collector outlet air temperature and the slab temperature. The collector outlet temperature must be at least as warm as the ventilated slab; ideally at least 5 °C warmer to justify the fan energy use and compensate for losses in the duct that runs to the slab. In general, it is essential for renewable energy systems that are integrated into the HVAC system to be modeled as a coupled system because usability of the collected energy must be quantified. Arguably the most powerful and flexible tool for modeling custom mechanical systems is TRNSYS.

Most modern detailed BPS engines have evolved from using separate building and HVAC models to combining them such that their performance is solved simultaneously at each time step. Figure 4.17 depicts the flow of data between buildings and HVAC equipment in conventional and modern tools. For each timestep, decoupled models (i.e., the "loads–systems–plant sequence" (McQuiston, Parker, and Spitler, 2005)) proceed from left to right in this figure with no feedback loops. This means, for example, that the heat load data required to maintain a space at the setpoint temperature is sent

to the secondary or terminal HVAC equipment (e.g., a hydronic radiant heating panel). This, in-turn is used to calculate how much thermal energy is required from the plant. Finally, the plant model determines the amount of fuel or electricity required to supply that amount of thermal energy. Each step is essentially a transfer function that quantifies the energy conversion efficiency. However, the underlying assumption is that each system to the right of the previous one is capable of supplying exactly the requested amount of energy and at that exact moment or timestep. Thus, complex interactions between a plant, the distribution system, and spaces may not be accurately represented. This may be a major limitation for Net ZEBs, which generally seek passive solutions in order to reduce both energy use and plant capacity. Furthermore, decoupled HVAC models also have limited accuracy if the HVAC system has substantial thermal mass (e.g., a concrete radiant heating floor) (McQuiston, Parker, and Spitler, 2005).
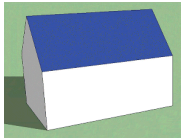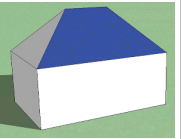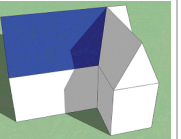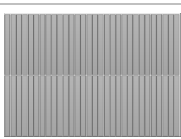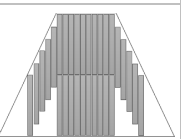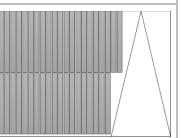
Program such as BLAST and DOE-2 use decoupled models, while EnergyPlus and ESP-r use coupled models (McQuiston, Parker, and Spitler, 2005). Since the burden of coupling the building and HVAC models is primarily the computational time rather than increased user input, there is little practical reason to use decoupled HVAC models to support Net ZEB design.

4.3.3.3 Photovoltaics and Building-Integrated Photovoltaics

Photovoltaic systems are among the most common renewable energy systems in Net ZEBs because they consistently generate electricity during daylight hours, require relatively little maintenance, have considerable flexibility in capacity and surface area, are not highly angularly dependent, and can be installed on the near-south-facing façades and flat or near-south facing roofs. While numerous tools are available for the prediction of stand-alone PV system performance, there is significant value in explicitly modeling PV modules within the main building model. Self-shading of PV (i.e., when BIPV modules are shaded by the building structure) is avoidable and should be minimized wherever possible. Beyond the much lower performance for shaded modules (which can be proportionally worse than the fraction of shaded area), PV modules can be damaged if they are not properly wired with a bypass diode (GSES, 2004).

Microinverters can partially alleviate this problem because each module is operated independently and does not affect the others' performance. As shown in Table 4.3, complex roof geometries (e.g., a cross-gable) can significantly reduce PV performance. Many BPS tools neglect individual module geometry, and instead, treat BIPV as continuous surfaces. Thus, care during design must be taken to avoid self-shading and other geometrical compatibility issues.

Table 4.3 Three different BIPV roof configurations showing geometrical implications of complex roof geometries. The modules illustrated are amorphous silicon and available in lengths of 2.8 and 5.6 meters

	Gable	Hip	Cross-gable
Example			
Average annual solar radiation on largest section of south-facing roof (indicated by blue) in Toronto, Canada (kWh/m²/year)	1481	1481	1214
Effective annual shaded fraction	0%	0%	18%
Typical array layout based on modules similar to those on the ÉcoTerra house			
Effective fraction of roof (in reference to gable roof) covered in PV cells	80%	40%	57%

4.3.3.4 Lighting and Daylighting

With electric lighting energy use representing an average of about 15–25% of energy use in commercial buildings (DOE EERE, 2010; NRCan, 2008; Pérez-Lombard, Ortiz, and Pout, 2008) and a greater proportion in mild climates, it is a major target for energy reductions

in the design of Net ZEBs. Furthermore, numerous building standards mandate daylighting as one of the primary objectives for new buildings; not just for energy savings, but also for the psychological benefits of view and variable illuminance (Veitch, 2001). Barriers to daylight modeling include a lack of detailed information about geometry and interior finishes and limitations of accurate modeling capabilities in many common BPS tools. The ENERPOS and NREL RSF case studies of Chapter 7 demonstrate the importance of considering daylighting early in design; daylight requirements can have a profound influence on building form.

Rules of thumb and pattern guides for daylighting design remain among the most efficient methods to support major daylight-related decisions including window type, size, and position, room depth, room surface optical properties, and static and dynamic shading devices (O'Connor *et al.*, 1997). However, in order to accurately quantify energy savings, especially for new daylight strategies, technologies, or unusual geometries, use of dynamic daylight simulation is valuable. There are three predominant algorithms used in daylight simulation in order of increasing model resolution: (i) split flux method, (ii) radiosity, and (iii) raytracing (Hensen and Lamberts, 2012). The split flux method calculates illuminance on the workplane based on direct views of interior points to exterior light sources (e.g., the sky) and surface-reflected light, but neglects multiple light reflections and thus it can underestimate daylight availability. It generally leads to inaccurate results for rooms with a high aspect ratio, specular (mirror-like) surfaces, or interior obstructions (Department of Energy, 2013b). Radiosity was originally developed to calculate nonvisible radiative heat transfer between surfaces, but has been adapted for daylighting applications. It uses surface reflectances and luminance exitance to simultaneously solve the illuminance on all interior surfaces. Its major limitation is that it treats all surfaces as perfectly diffuse reflectors, and thus may be inaccurate for specular surfaces, such as metals, glasses, and highly polished surfaces. This could be a limitation for specular solar shading devices such as light louvers and spaces that are prone to glare.

Raytracing is a daylighting analysis method that – as its name suggests – traces light from the source to interior surfaces (forward

raytracing) or vice versa (backward raytracing). Unlike the previously discussed methods, raytracing can accurately treat specular surfaces with complex geometries. Raytracing can yield photorealistic images, but such a detailed method may not be necessary for Net ZEB design. Forward raytracing follows rays of light from all light sources to a surface (Hensen and Lamberts, 2012). The number of bounces that the ray of light is followed for is normally specified by the tool user depending on the desired accuracy and complexity of the geometry. Backward raytracing starts with a final surface and then traces light back until (if ever) it reaches a source. Raytracing is generally considered superior for complex geometries with small and/or specular surfaces (e.g., see Figure 4.18). Numerous comparative studies of daylight simulation methods and tools are available (Carrol, 1999; Ramos and Ghisi, 2010; Reinhart and Fitz, 2006; Reinhart and Herkel, 2000; Yun and Kim, 2013).

Fig. 4.18 Reflected sunlight from Venetian blinds that are designed to protect occupants from direct solar radiation while reflecting it onto the ceiling to provide diffuse daylight

As for the modeling of most building phenomena, the choice of daylight simulation algorithm depends on the design objectives and

details of the building. Simpler daylight models are faster to construct and simulate, but may be prone to error for complex geometries and may fail to diagnose glare and other sources of visual discomfort (Hensen and Lamberts, 2012). The majority of the burden for detailed daylighting models is on the computer; thus, the choice should be based on available processing power and time rather than modeling time. However, the power of advanced daylighting analysis algorithms cannot be fully realized unless geometrical details and optical properties are provided by the tool user. To a much greater extent than thermal analyses, accuracy of daylight simulation can be significantly improved with details about interior furnishings and surface finishes.

Electric lighting simulation is considerably simpler than daylight analysis because of the static nature of electric lights (Hensen and Lamberts, 2012). Unlike the uncertainty of sky conditions, luminance output from luminaires can be obtained from manufacturers in the Illuminating Engineering Society (IES) format. Normally, if a software tool is used for luminaire selection and layout, a light loss factor (LLF) is used to account for all factors that depreciate the lumen output of luminaires from their rated values.

For coupling of lighting and daylighting models, a one-way data flow path is generally acceptable. The following steps are performed manually or automatically, depending on the BPS tool:

1. A daylighting simulation is performed and the necessary level of supplementary electric lighting is calculated and passed to Step 2.

2. The electric lighting schedule profile is used to activate electric lights, as needed to supplement daylighting, in the main building model. The resulting heat gains and power consumption are incorporated into the simulation.

This sequence is acceptable because the illuminance levels from daylight and electric lights are additive and can be superimposed on any surface. The advantage to this sequential approach is that detailed daylight analysis tools can be integrated into the design process. However, the major shortcoming of the sequential approach is that it is less suitable for dynamic shading devices (e.g., roller

shades or electrochromic windows) that are controlled for both visual and thermal comfort (e.g., for stochastic occupant modeling).

Moveable window shading systems offer control of solar gains and visual discomfort so that a building can adapt to varying climatic conditions. These systems are ideally positioned on the exterior and light colored to maximize the ability to prevent solar gains. However, interior movable shades in colder climates, especially in North America, are much more common; likely because of concerns of ice and snow build-up and cost. Published results of combined optical and thermal properties of complex fenestration systems (i.e., windows and movable shading systems) are still quite sparse, despite their significant effect on building performance (Newsham, 1994; Tzempelikos and Athienitis, 2007). Lawrence Berkeley National Laboratory's WINDOW software can provide the effective thermal and optical properties of complex fenestration systems.

Several mainstream tools, including eQUEST (based on DOE-2.2) and EnergyPlus have integrated daylight calculation modules based on simplified methods like split-flux. Many BPS tools that specialize in daylighting and electric lighting analysis, including DAYSIM, SPOT, and ESP-r, use RADIANCE as their daylight simulation engine (Guglielmetti, Pless, and Torcellini, 2010). The key light and daylighting metrics, including for visual comfort, are discussed at length in [Chapter 3](#).

4.3.3.5 Airflow

Airflow within and through building envelopes is often critical to the success of Net ZEBs. Whether it is naturally or mechanically driven, it has three main functions: (i) delivering outdoor and filtered air to maintain contaminants below an acceptable threshold, (ii) thermally conditioning a space (applicable primarily to forced-air HVAC systems), and (iii) providing a cooling sensation by increasing the rate of sensible and latent heat transfer from occupants to the air.

Modeling airflow is one of the most complex aspects of building physics and deserves significant attention. The three dominant modeling methods, in order of ascending resolution and theoretical accuracy, are (i) scheduled airflow, (ii) airflow networks (a.k.a. zonal methods), and (iii) CFD. Scheduled airflow simply imposes a certain

mass or volume flow rate between zones, outdoors, and HVAC equipment, such as ducts and air handling units. It is most suitable for mechanical ventilation because the airflow rates are approximately known. It can also be used for sensitivity analysis to determine the effect of airflow rates (e.g., to estimate the size of window that would be required to achieve a certain level of natural ventilation). For instance, the NREL RSF case study in [Chapter 7](#) explores the effect of different nighttime ventilation rates on cooling loads.

Airflow network methods are composed of a collection of nodes that represent zones, ducts, and outdoor conditions and a network of connections that represent airflow paths such as windows, cracks, and other openings. The limitations of airflow networks are that they assume perfectly mixed zone air within zones, they neglect momentum effects, and flow-through openings are normally based on empirical pressure-driven models (Costola, Blocken, and Hensen, 2009). Since the set of conservation of mass equations for each node are normally nonlinear, the solution for the system is usually solved numerically. Airflow networks are significantly more common in dynamic BPS than other methods (Hensen, 1999) and normally adequate for performing energy simulations. The lack of information provided about localized conditions and velocity means that the airflow's effects on indoor air quality, thermal comfort, and convective heat transfer are simplified. The significance of this is highly dependent on the size of the room, airflow rates, and the type of ventilation.

Computational fluid dynamics (CFD) in buildings uses a numerical solution to the Navier–Stokes equations and discretizes zones into thousands of control volumes (Bartak *et al.*, 2002). CFD can be used to determine localized air velocity and temperature within a zone. This is particularly useful for assessing heat transfer between surfaces and the air and analyzing the localized impact of natural and mechanical ventilation. However, CFD is very computationally expensive, which has reduced its use in most practical applications to steady-state or very short periods. Furthermore, use of CFD requires considerably more model detail than the simpler models and a deep understanding of the underlying algorithms.

Newer air distribution technologies that rely on more effective delivery of outdoor air to the breathing zone, such as displacement ventilation, for which there is vertical stratification in a zone – both for air temperature and contaminant concentrations – cannot be properly modeled using the perfectly mixed zone assumption (Mora, Gadgil, and Wurtz, 2003). EnergyPlus uses several variations on the airflow network model to incorporate temperature stratification including a one-node model with an air temperature profile that varies with height and a three-node model that discretizes zones into three vertically stacked zones.

Infiltration, the unwanted air exchange between indoors and out, can significantly increase heating and cooling loads and have implications on indoor air quality because of its uncontrollable nature. It can be assessed and quantified using a top–down approach (e.g., prescribed air change rate in air changes per hour) or a bottom–up approach (e.g., specified crack geometry or equivalent leakage area (ELA) (Sherman, 1987)). Since infiltration is as much a function of construction quality as it is design in modern buildings, it contributes significant uncertainty to energy use and is a major challenge for Net ZEBs. Designers should study the typical range of infiltration rates measured from similar buildings. Ultimately, quality construction is essential to mitigate the effects of infiltration.

The appropriate choice of airflow analysis model is dependent on the design stage, the geometry and technologies of the building, and the type of questions being asked. Airflow network methods are normally suitable for energy simulations, but heavy reliance on natural ventilation and assessment of localized thermal comfort could benefit from CFD. Examples of tools for airflow analysis include CONTAM (for analysis of contaminant flow using airflow networks and 2D CFD), ESP-r (airflow network and 3D CFD), DesignBuilder, and IES VE (both 2D and 3D CFD).

4.3.3.6 Occupant Comfort

Occupant comfort – thermal, visual, and acoustic – cannot be neglected during building design. Traditionally, comfort and energy have been viewed as opposing each other and that a high level of occupant comfort requires more energy (for HVAC and lighting) to

maintain. However, in recent years, it has been recognized that providing comfort is essential to high-performance building design. If a building fails to provide comfortable conditions, as designed, then occupants will adapt themselves and/or their environment to achieve comfort. In some cases these actions have adverse effects on energy performance. For instance, the owners of the ÉcoTerra house installed an electric resistance heater in the garage – a space that was not intended to be heated because it was nominally designed to shelter a car. The 5 kW electric resistance heater was installed to maintain comfort conditions required for a workshop. The result was that the garage, in its first year, used 29% as much electricity for space heating as the rest of the house (Doiron, O'Brien, and Athienitis, 2011)! Clearly occupant behavior cannot be perfectly predicted during design; however, attention to occupant comfort is important for achieving net-zero energy.

Theoretical aspects of comfort are discussed in detail in Chapter 3; this section focuses on the modeling aspects of comfort.

Thermal Comfort

Traditionally, air temperatures, and sometimes operative temperatures, were used to determine whether a space was comfortable or not. The operative temperature is normally estimated as the average of the mean radiant temperature of a space and the air temperature, for spaces with low air movement (<0.15 m/s). However, the steady-state heat exchange between occupants and the indoor environment is complex and is summarized in Section 3.2. All occupant-building heat exchange terms are highly influenced by the occupant properties (e.g., activity level and clothing level) and the indoor environmental conditions (air temperature, relative humidity, surface temperatures, and air speed). Most detailed BPS tools calculate the environmental conditions (e.g., air and surface temperatures) and allow them to be readily used to predict comfort levels, based on assumed occupant properties. Several tools, including EnergyPlus, provide higher-level thermal comfort metrics, such as PMV and predicted percentage of people dissatisfied (PPD) (Fanger, 1970). In environments where occupants have a greater ability to adapt (e.g., operable windows and change clothing level and activity level), static assumptions neglect occupants' ability to

improve their comfort level (de Dear and Brager, 1998). Instead, an adaptive comfort model should be considered (e.g., ASHRAE Standard 55 (ASHRAE, 2010c)). Adaptive comfort models, which are valid for naturally ventilated buildings, suggest that occupants are tolerant to wider operative temperature ranges.

There are a number of additional thermal comfort conditions that must be considered during design. These include drafts (localized elevated airspeeds from cold windows, cracks, or diffusers), which may require CFD to accurately determine; asymmetrical radiant temperatures (e.g., a particularly hot or cold surface in one direction); warm or cold floor surfaces (which can affect occupants via conduction); rapid changes in temperature over time; and high vertical temperature gradients (ASHRAE, 2004). Though many of these cannot be quantified with BPS without using CFD, building material and geometry and HVAC system (e.g., radiant floor heating) selection can be guided by these considerations. For instance, ASHRAE Standard 55 (ASHRAE, 2010c) provides limitations on the comfortable floor temperature range. Floor temperature output is available from many BPS tools (e.g., EnergyPlus and ESP-r).

Modeling thermal comfort accurately should be a major priority in Net ZEB design as soon as sufficient detail is available to apply the aforementioned models. Knowledge of typical occupant activities, clothing level (e.g., dress codes), personalized controls, and corporate culture (in commercial buildings) are all important inputs to modeling efforts. The ASHRAE Thermal Comfort Tool (ASHRAE, 2010b) can be used to predict comfort based on several different comfort models if the main environmental and occupant conditions are known.

Visual Comfort

The objectives of electric lighting and daylighting are to ensure adequate light levels to achieve the task at hand, ensure that conditions are not too bright and avoid glare, and minimize total energy use (electric lighting energy and the resulting HVAC energy required to remove unwanted heat gains). Visual comfort metrics based on workplane illuminance, while being the conventional method for controlling electric lighting, has not yielded consistent

predictions of daylight glare (Wienold and Christoffersen, 2006). Daylight glare probability (DGP) (Wienold and Christoffersen, 2006), which is based on vertical eye illuminance, glare source luminance, and occupant orientation and position, has demonstrated – through experiments – good predictions of visual discomfort. Daylighting and DGP can be quantified in several BPS tools, including OpenStudio/Radiance, DAYSIM, Evalglare, and DIVA for Rhino. Effort should be made to minimize the occurrence of glare through careful sizing and positioning of glazing, exterior fixed shading, appropriate selection of surface reflectances, providing furniture and floor layouts with flexible occupant positioning, and installing effective window shades/blinds. Aside from causing visual discomfort and reducing productivity in workplaces, frequent glare can motivate occupants to semipermanently close window blinds and prevent useful daylight from entering the space (O'Brien, Kapsis, and Athienitis, 2013). Hourly or sub-hourly analyses should be performed because even momentary diurnal glare can prompt occupants to leave blinds closed (Bordass, Leaman, and Willis, 1994; Reinhart, 2004). All of these strategies can be tested using the aforementioned tools.

Acoustic Comfort

Several common strategies in Net ZEBs (openness of interiors, hard surfaces, exposed thermal mass, and operable windows) are generally contradictory to good acoustic performance, as explained in [Chapter 3](). For that reason, coupling an acoustic model into a building performance model with detailed occupant model could yield some insightful results.

During the design and modeling of Net ZEBs, detailed knowledge of interior surfaces (including furnishings) including scattering coefficient and impedance is very useful. However, as with daylighting simulation, detailed acoustical information is typically not known until the later stages of design. Thus, reasonable estimates of these properties must be made earlier in design, when the architect or interior designer has the best opportunity to select good acoustic strategies. Using the daylighting analogy again, it is possible to use acoustic simulation approaches to "auralize" a room such that the simulationist can produce the predicted acoustic

environment of a building before it is built. Several tools for acoustic assessment in BPS are available, including CATT-Acoustic and the ESP-r acoustic module. Mahdavi (2012) stated several future needs of building acoustics simulation including more detailed algorithms and an extensive and accurate database of material acoustical properties.

4.3.3.7 Occupant Behavior

The role of occupant behavior in a Net ZEB cannot be overlooked because such buildings can be particularly sensitive to occupants (Hoes *et al.*, 2009). Occupant behavior has been shown to affect energy use by a factor of two or more (Gram-Hanssen, 2010; Haldi and Robinson, 2011). Many studies (O'Brien, Kapsis, and Athienitis, 2013; Rubin, Collins, and Tibbott, 1978; Saldanha and Beausoleil-Morrison, 2012) have demonstrated that predicting the energy use associated with occupant behavior is quite difficult; especially if occupants are not motivated by cost savings (e.g., in their workplace) (Rea, 2000). Buildings with passive features (e.g., natural ventilation) often give more control to occupants to maintain comfort, which can also lead to significant uncertainty (Hoes *et al.*, 2009). Also, as building envelopes become better-insulated, HVAC systems become more efficient, and the number of electricity-consuming devices (e.g., computers and appliances) increases, the so-called plug loads contribute an increasing share of total energy use. The challenge associated with designing for plug loads is that they are often based on small appliances and other equipment that occupants install themselves after the design is realized. While plug loads are often considered beyond the control of building designers and in the past, merely quantified to estimate peak cooling loads for HVAC sizing, the Net ZEB definition normally positions them within the energy balance. Therefore, Net ZEB designers must estimate them with better accuracy and even try to influence them through good design. This is especially true in small buildings and houses, where the energy use is largely at the mercy of the habits of the occupants and not formally managed. In larger buildings, the diversity of occupants normally reduces energy use uncertainty.

The value of comfort (thermal, visual, and acoustic) and productivity (in the workplace) is paramount. If a building does not provide

comfortable conditions, occupants may react in unexpected ways that increase energy use uncertainty. Contrary to what conventional BPS tools imply – that occupants are simply powerless as they are imposed with a rigid indoor environment – occupants often adapt their conditions to improve comfort; normally in ways that result in the most immediate improvement with the least amount of effort (Bordass, Bromley, and Leaman, 1993; Cole and Brown, 2009). New models need to reflect the numerous adaptive measures that are taken. The ways in which occupants affect building energy use include the following:

– Use of lights, computers, appliances, and other electricity-consuming devices. In the NREL RSF building, the building owners actually modified the phones such that the backlight was disabled. This was done after the owners calculated that every continuous Watt of electricity saved reduces the value of the necessary PV capacity by about US$30! Other than lights, building designers have minimal influence over the type of electricity-consuming devices occupants use, and how they are used. However, reasonable estimates should be made for BPS to assess the impact on heating and cooling loads. Further field studies (e.g., Saldanha and Beausoleil-Morrison, 2012) are necessary to obtain more realistic plug load profiles. The matter is complicated by the fact that occupants of residential Net ZEBs are usually faced with small energy costs, and thus have less incentive to act in energy-conserving ways (Sunikka-Blank and Galvin, 2012).

– Adjustment of thermostats can have a profound effect on energy use because the balance point of buildings with high-performance envelopes and ventilation systems tends to be higher than for conventional buildings.

– Adjustment of window blinds or operable windows can have a profound effect on energy performance; normally 10 to 30% (Newsham, 1994; Reinhart and Voss, 2003; Rijal *et al.*, 2007; Tzempelikos and Athienitis, 2007). Window blinds, which are primarily intended to protect against daylight glare, are often used suboptimally and left closed for long periods after conditions causing visual discomfort have been relieved.

– Occupants' mere presence increases heat gains and can influence the behavior of building systems through sensors (e.g., for demand-controlled ventilation) (Mahdavi *et al.*, 2008).

Stochastic Occupant Modeling

A newer approach to incorporating the effects of occupants on energy use is to use stochastic (random) models within BPS (Bourgeois, Reinhart, and Macdonald, 2006; Bradley, 2003; Gunay, O'Brien, and Beausoleil-Morrison, 2013; Hoes *et al.*, 2009; Nicol, 2001; Rijal *et al.*, 2007). Numerous stochastic occupant models have been developed based on field studies and experiments to predict the probability of adaptive occupant actions (e.g., window opening, light switching, blind control) based on one or more environmental variables (e.g., indoor air temperature). The majority of these models are represented as single-variable logistic functions (e.g., Figure 4.19). However, some stochastic models are intended for specific times of day (e.g., arrival in the office) when behavior has been observed to be significantly different.
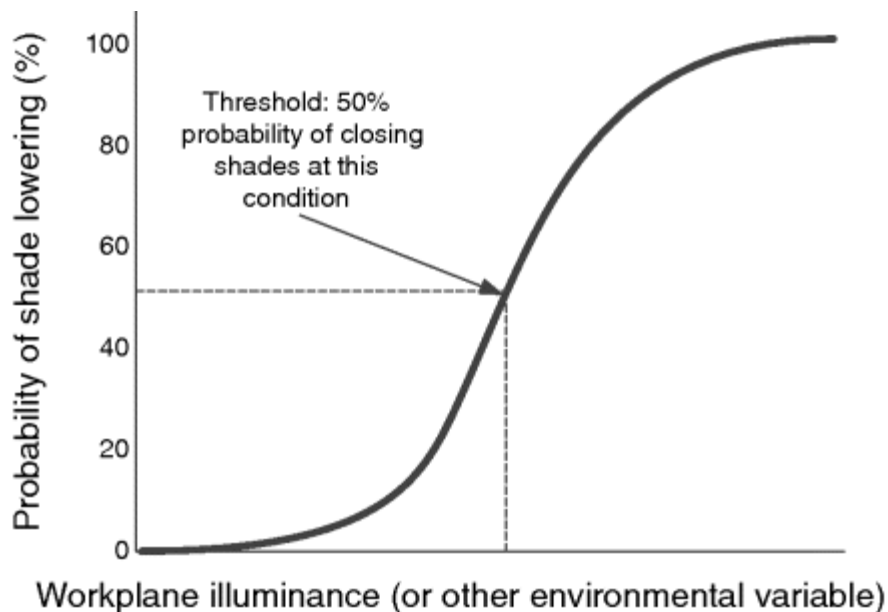
Fig. 4.19 Graphical representation of an example of a stochastic occupant model for manual window shade control

Stochastic occupant models provide some randomness with regard to occupant behavior and yield two major benefits: (1) identify peak loads and (2) prevent designers from optimizing a building to

perform around a rigid set of unlikely occupant-related patterns. More work is required to expand the field of knowledge and generalize these models to a greater number of building types, technologies, and climates. A comprehensive review of window shade use patterns revealed that most researchers have attempted to correlate occupant actions with weather conditions; but without detailed knowledge of the building envelope, these conditions do not necessarily translate into indoor conditions (the likely motivator of occupants) (O'Brien, Kapsis, and Athienitis, 2013).

Figure 4.20 shows the data flow in BPS with more advanced occupant modeling. Instead of assuming that occupants should tolerate discomfort, BPS models should incorporate the effect of adaptive actions on energy use.
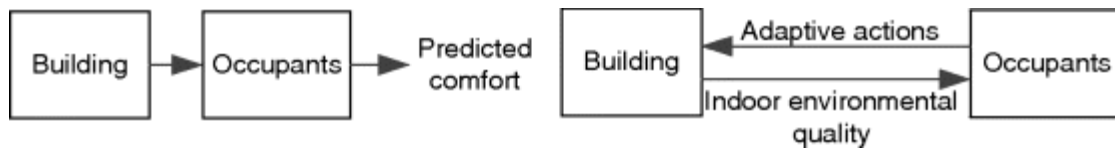
Fig. 4.20 Conventional and future occupant-building interaction models

Robust Design

An emerging area in the field of BPS-supported design is robust design (Hoes *et al.*, 2009; O'Brien, 2013). The concept is that buildings should not simply aim to achieve high targets (e.g., net-zero energy), but should also do so with higher certainty. In practical terms, that means the building design should be resilient to a variety of occupant behaviors, weather conditions, climate change, and other operating conditions. For example, manual window shade control is notoriously uncertain and difficult to predict using BPS. NREL RSF avoided this uncertainty by implementing fixed louvers and overhangs that do not require occupant interference to function properly (i.e., admit daylight while minimizing glare) (Figure 4.21). Mitigating uncertainty played a significant role in this Net ZEB design, since one of the major objectives was to achieve an absolute performance target.

Fig. 4.21 National Renewable Energy Laboratory (NREL) Research Support Facility (RSF): window with fixed louvers on top half (left) and the resulting upward-reflected daylight on the ceiling of the office space (right)

In an example by O'Brien (2013), a small 9 m² single-occupancy south-facing office was modeled with a stochastic occupant behavior model. The occupant was assumed to have randomly varying solar thresholds that triggered them to close the shade and then reopen it after a varying number of days (a normal distribution with a mean of 3 days and standard deviation of 3 days). After 100 simulation runs in EnergyPlus (i.e., Monte Carlo analysis), a normal probability distribution was fit to the simulated lighting energy results (right side of Figure 4.22). The simulations were repeated for a case with a 2 m deep overhang above the window. The results indicate that the presence of the overhang greatly reduces mean simulated energy use and uncertainty (standard deviation) because the direct solar radiation on the workplane is reduced. Thus, the glare conditions that trigger the occupant to close their shade are much rarer and as a result, the occupant leaves the shade open for longer and admits more diffuse daylight.
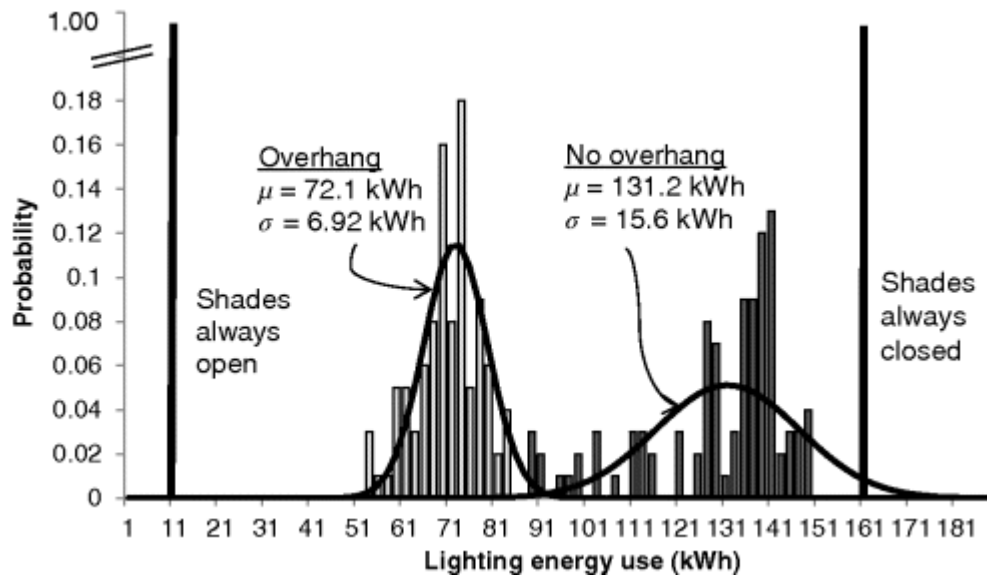
Fig. 4.22 Example robustness assessment of lighting energy in an office with manually controlled window shades (O'Brien, 2013)

4.3.4 Use of Tools in Design

The current use of tools is predominantly focused on verifying performance after design has largely been completed. However, this, arguably, does not achieve our objectives of reducing the environmental and economic impact of buildings. This section focuses on strategies for employing BPS tools to support the design of Net ZEBs; particularly in the early stages of design.

4.3.4.1 Climate Analysis

A first step in design programming is to establish the local climatic forces (daily and annual profiles of temperature, solar radiation, wind, and relative humidity) that must either be opposed, or better, harnessed, to achieve a net-zero energy design. One promising tool to support this is Climate Consultant. This tool can be used to synthesize and visualize whole-year typical weather data (based on the EPW weather file format). Among its many features, the average hourly data can be superimposed on a psychrometric chart (example shown in Figure 4.23). The addition of numerous comfort models, including the ASHRAE Standard 55 comfort models (ASHRAE, 2004), can further be superimposed to quantify the number of hours in which building occupants would be comfortable with no passive or

active conditioning measures. Another useful feature in Climate Consultant is that it lists the effectiveness of 16 different building design strategies (e.g., passive solar heating and natural ventilation). As the user selects these strategies, the red points in the psychrometric chart, representing an hour of discomfort, turn green to indicate that the strategy has addressed some of the uncomfortable hours. In particularly extreme climates, the user may find that no passive strategies exist to achieve comfort; at which point mechanical heating, cooling, or humidification/dehumidification would be required.
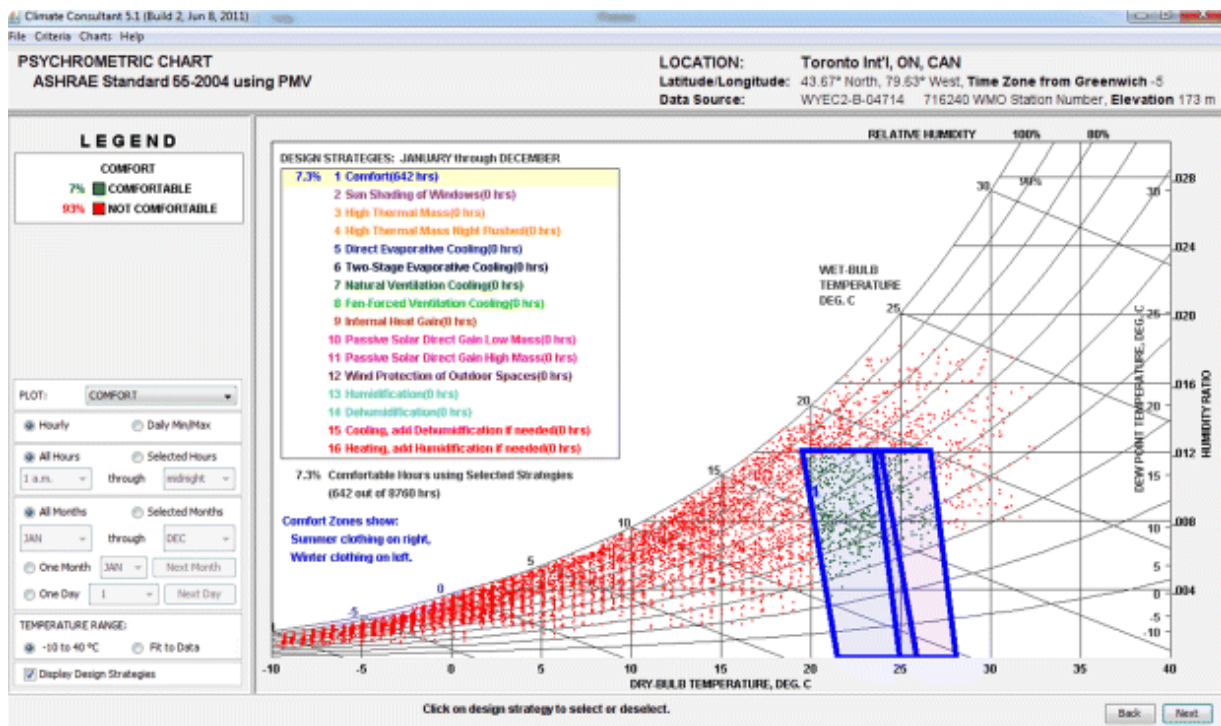
Fig. 4.23 Screenshot of Climate Consultant V5.1 (Milne, 2013), showing the psychrometric chart for Toronto

A limitation to using climatic data to guide building design is that it largely assumes a steady-state building. However, Climate Consultant does provide visualization of diurnal monthly averages, which can be an excellent indicator of the success of numerous passive strategies, including those shown in Table 4.4.

Table 4.4 Examples of clues about climate phenomena that can be translated into effective passive building strategies

Climate Phenomenon	Possible Passive Strategies
Cool or cold (<10 °C) and sunny	Passive solar heating using large south-facing windows and thermal mass
Cold and cloudy days	An envelope with a low *U*-value (which may include sparsely distributed windows)
Hot conditions (>25 °C) during the day but cool nights (<15 °C)	If the building is mechanically cooled, nighttime ventilation coupled with thermal mass should be used, whereby the building is flushed with cool air at night such that it discharges thermal energy stored in the mass. If the building is not mechanically cooled, natural ventilation strategies should be implemented to increase airflow. Regardless, solar shading (ideally fixed) should be used to minimize solar gains during the warm season.
Hot conditions throughout the day	Same as above, but nighttime ventilation is ineffective. Solar shading, strategies to enhance air movement, and possibly a low *U*-value envelope if mechanical cooling is used, is necessary.

The nature of the major building loads should also be considered in early-stage design decisions, whereas Climate Consultant and other climate visualization tools do not necessarily account for the specific building. For example, the user of Climate Consultant must input the *balance point temperature*; that is, the outdoor temperature at which no mechanical heating or cooling is required to maintain comfort conditions (because of internal heat gains). However, this will be highly dependent on the nature of the building (e.g., occupant density, equipment, and lighting, and level of solar gains). Therefore, early in design, the designer should determine whether the building will be *envelope load dominated* or *internal load dominated*.

Envelope load dominated buildings are those for which the majority of energy is used to maintain indoor thermal comfort conditions and

combat heat loss/gain and humidity heat/gain from or to the outdoors. They are usually located in climates where outdoor temperatures often deviate relatively far from balance point temperatures (10–15 °C) and have low occupancy and equipment densities (e.g., detached houses). For such buildings, design should focus on achieving a high-quality envelope (well-insulated, high-quality windows with strategically selected thermo-optical properties and orientation) and an efficient HVAC system. These thermal loads can be offset by renewable energy systems that produce thermal energy (e.g., solar thermal or biomass) or the efficient use of renewably generated electricity (e.g., a PV system coupled with a heat pump).

Internal load dominated buildings are those for which the majority of energy is used to power internal equipment and lighting. These are typically commercial buildings in temperate and mild climates in which the space-conditioning loads are low compared to that from office equipment, lighting, elevators, kitchen equipment, and so on. With the exception of lighting, which can be partially offset by daylight, these loads can be best met by on-site renewably generated electricity (e.g., PV, wind turbines). The ENERPOS building, presented in [Chapter 7](#), is an internal load dominated building.

4.3.4.2 Solar Design Days

A strategy for a slightly more advanced design using climate data is the use of *solar design days (SDDs)*, as described by O'Brien, Athienitis, and Kesik (2008). The technique addresses the issue that a year's worth of performance data is overwhelming and cannot be easily synthesized by designers to influence design decisions. The analysis period of 24 h is selected because it represents the approximate period during which a full charge and discharge cycle of passive thermal mass occurs. Specific to passive solar buildings, though they could be used for any dynamic passive strategies, SDDs are intended to highlight the performance of a building through several key metrics during a few typical diurnal weather patterns. For example, the effect of glazing area, glazing type, major geometry, thermal mass, solar shading, and control strategies, can quickly be identified and addressed. SDDs act as a diagnostic tool, allowing

issues such as overheating and high peak heating loads to be avoided through sound design.

O'Brien, Athienitis, and Kesik (2008) chose a cold sunny, cold cloudy, warm sunny, and mild sunny day to illustrate passive solar phenomena. In the following example, a typical solar neutral (Hayter *et al.*, 2001) house is first simulated. Noting the modest solar gains, the second iteration includes larger windows and substantial thermal mass. As seen in [Figure 4.24](#), these actions reduce daily heating energy substantially – and by about 45% annually.
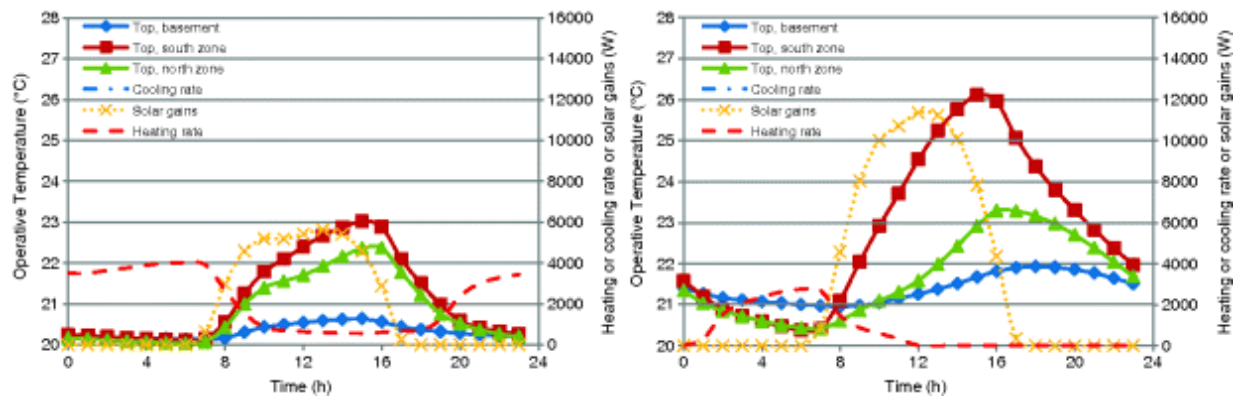
[Fig. 4.24](#) Example of use of solar design days. Both graphs show house performance on a cold sunny day (clear with an overage outdoor temperature of –15 °C). The graph on the left is for a house with small windows that are distributed in all orientations, while the graph on the right is for one with large south-facing windows and added thermal mass

A drawback to SDDs is that they require a model to be created in a simulation tool that calculates (and reports) in an hourly or finer resolution. This excludes some tools, such as HOT2000, which reports monthly energy demand.

4.3.4.3 Parametric Analysis

Parametric analysis – the varying of a building parameter and performing a simulation to quantify that parameter's impact – is a widely used design strategy and application for BPS. The concept of Lines of Influence (LoI) was described by Kesik and Stern (2008) to assess the plotted performance metric (e.g., heating energy) as a

parameter is changed. Parametric analyses provide at least three valuable pieces of information:

1. *The optimal or near-optimal value of a parameter.* If the LoI for a particular parameter indicates that an optimum value for it exists, the designer may wish to use this value in the design, assuming it is practical, economical, and compatible with other design aspects.

2. *The relative sensitivity of a parameter.* This is particularly useful when multiple parameters are compared. For instance, if there are multiple methods for obtaining the same desired result, the parameter with the steepest LoI may be the one for which the desired outcome is easiest to achieve. Furthermore, if a costly upgrade has little bearing on energy performance, there would be little benefit to making that investment.

3. *The relative importance of accurately modeling a building system.* Generally, the most care in accurate modeling should be given to the aspects that are most sensitive. For instance, if the model indicates that the optical properties of windows are important, then care should be given to obtain specifications for the window that are based on detailed measurements. Sensitivity analysis is a very important confidence-building exercise for modelers.

The implementation of parametric analyses in Ecos (O'Brien, Athienitis, and Kesik, 2009) is shown in Figure 4.25, where the effect of window size for four different orientations is explored. Parametric analysis was used extensively in the design process of ÉcoTerra, as described in Chapter 7.
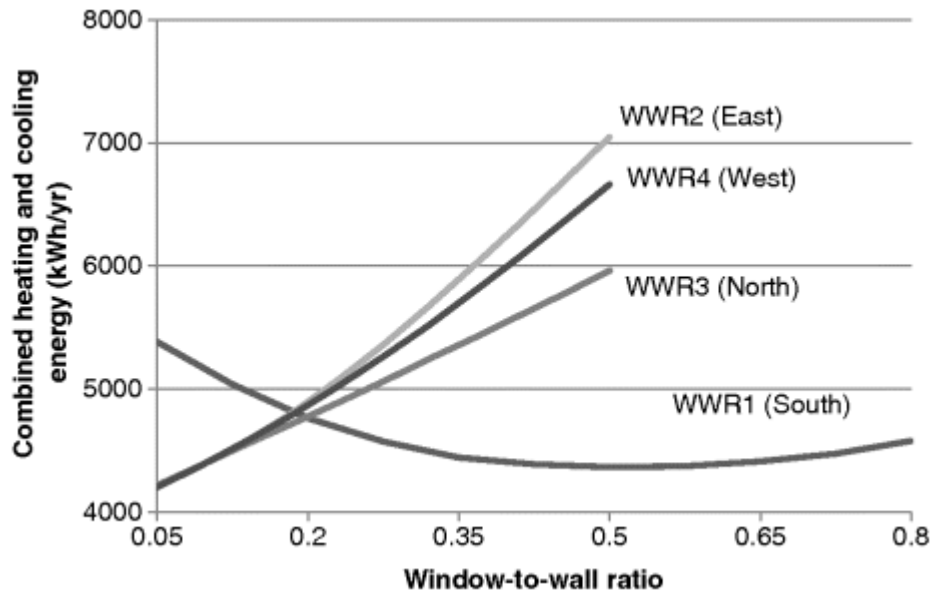
Fig. 4.25 Parametric analysis in Ecos (O'Brien, Athienitis, and Kesik, 2009), where lower points on the curves indicate lower annual heating and cooling energy

4.3.4.4 Interactions

In many cases, it would be unwise to merely optimize each parameter independently since they usually interact to some level. For instance, O'Brien, Athienitis, and Kesik (2008) showed that the optimal south-facing glazing area for a house with high internal gains was a third of the size of the optimal size with low internal gains. Therefore, one can conclude that certain parameters should be manipulated in subsets, rather than individually. Manipulating more than several parameters simultaneously is tedious and yields an exponentially expanding design space, as previously illustrated in Figure 4.12.

For the population of 30 parameters used in Ecos (O'Brien, Athienitis, and Kesik, 2009), there are 435 (30 choose 2) two-way interactions to consider. The current focus is on two-way interactions since higher-order interactions are unusual (Shah, Kulkarni, and Vargas-Hernandez, 2000). One common method to understand interactions is to create interactions plots, as is commonly performed in the field of design of experiments (DOE) (Mason, Gunst, and Hess, 2003). If the main effects plots are approximately linear, interactions can be quantified using (Eqs. 4.1) through (4.3)

$$E_{A,B(-1)} = R_{A(-1)B(-1)} - R_{A(+1)B(-1)} \tag{4.1}$$

$$E_{A,B(+1)} = R_{A(-1)B(+1)} - R_{A(+1)B(+1)} \tag{4.2}$$

$$I_{A,B} = 0.5(E_{A,B(+1)} - E_{A,B(-1)}) \tag{4.3}$$

where *A* and *B* are the two parameters being examined for interactions, $I_{A,B}$ is the magnitude of the interaction, $E_{A,B(+1)}$ is the effect of parameter *A* at the high level of parameter *B*, and $E_{A,B(-1)}$ is the effect of parameter *A* at the low level of parameter *B*, and the R_{AB} terms are the response (sum of heating and cooling energy for this application) depending on the values of *A* and *B*. The responses (R_{AB}) are shown in Figure 4.26.
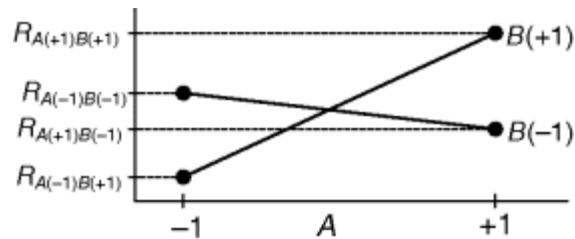
Fig. 4.26 Generic representation of responses and interactions, © 2011 ASHRAE (www.ashrae.org). Used with permission from ASHRAE (ASHRAE Transactions, Vol. 117, Issue 1, 2011, O'Brien, Athienitis, Kesik, Parametric Analysis to Support the Integrated Design and Performance Modeling of Net Zero Energy Houses, pp. 945–960)

4.3.4.5 Multidimensional Parametric Analysis

If building parameters or systems are expected to strongly interact, multidimensional parametric analyses should be performed. This involves simultaneously varying two or more parameters (while keeping the others constant). Figure 4.27 shows two 2-dimensional sensitivity analyses.
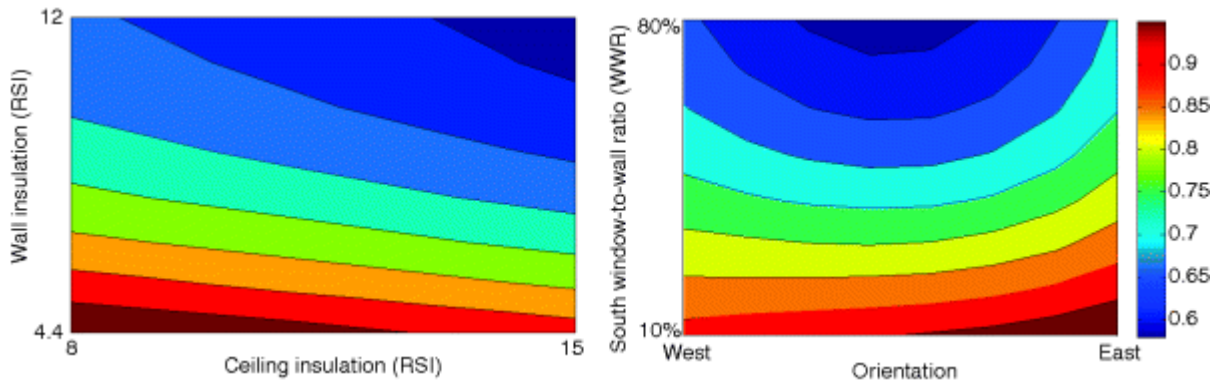
Fig. 4.27 Two-dimensional sensitivity analysis for two parameters that weakly interact: wall and ceiling insulation (left), and strongly interact: window-to-wall area ratio and house orientation (right) (O'Brien, Athienitis, and Kesik, 2011a)

4.3.4.6 Visualization

Providing a means to synthesize and visualize performance data is a key role of building modelers – given that the intended audience is primarily designers and other stakeholders. Care must be taken to provide enough information to make meaningful decisions without overwhelming the audience.

One strategy for representing energy flows in a building and ultimately identifying the best strategies for achieving net-zero energy is through the use of Sankey diagrams (Schmidt, 2008). As illustrated in Figure 4.28, Sankey diagrams help identify the major energy sources and sinks within a building. For instance, it shows the solar heat gains through and heat losses from windows in each orientation. Thus, the net heat gain can be determined. Furthermore, the Sankey diagram identifies any major weaknesses (i.e., major sources of heat loss) in the envelope. Finally, energy conversion processes (e.g., use of electricity for a heat pump to extract heat from the environment) and feedback loops (e.g., use of a heat recovery ventilator – not shown) can be visualized. The creation of Sankey diagrams forces designers to ask the right questions about Net ZEB design, including

1. What are the major energy sinks in the design and how can they be reduced?

2. If energy sinks cannot be reduced through conservation measures, how can renewable energy sources be used to offset these sinks?

3. What is the appropriate balance between energy conservation measures and renewable energy generating capacity?
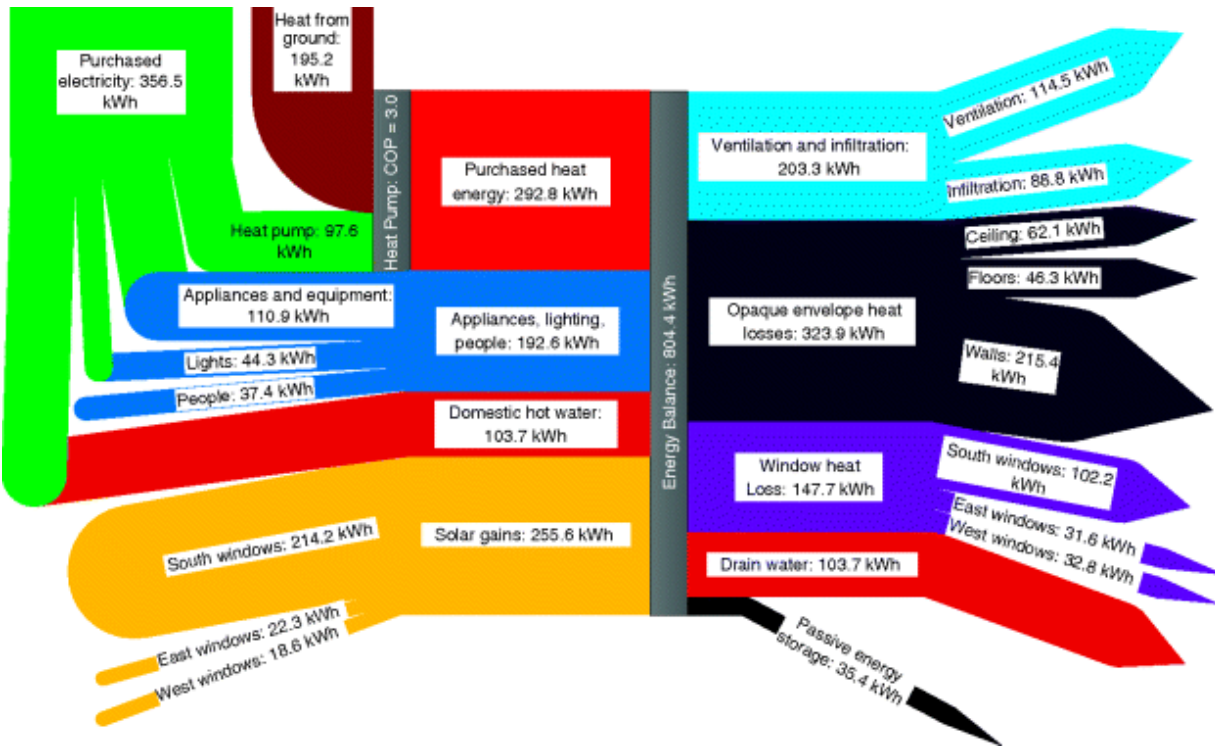
Fig. 4.28 Example Sankey diagram for a passive solar house during a winter week

4.3.5 Future Needs and Conclusion

This section examined different Net ZEB building design and simulation methodologies and demonstrated the importance of choosing the appropriate model resolution at different design stages. There is generally a trade-off between accuracy and modeling effort. The time required to create high-resolution models normally prevents them from being useful at the beginning of the design process – when designers require rapid performance feedback. Therefore, the use of one or more simple tools is encouraged as long as the limitations are understood. Escalation to more detailed models can be achieved in numerous ways, as previously described.

The qualities needed from Net ZEB tools differ from tools required for conventional buildings in two major ways:

1. *Need for tools with higher levels of accuracy and certainty.* The Net ZEB definition demands an absolute level of certainty in energy performance, unlike most types of buildings. This means that tools must be able to predict whether a building can achieve net-zero energy both in accurate and certain terms. This requires more accurate and realistic mathematical models for virtually all aspects of buildings (materials, construction quality), occupant-building interactions, and current and future climate scenarios.

2. *Need for models for advanced technologies.* The ambitious objective of net-zero energy often requires a combination of established technologies and design concepts with state-of-the-art technologies and controls. Currently, there is a lag time between building system development and the corresponding BPS models. This presents a barrier to building designers who want to confidently demonstrate that a building with advanced technologies will achieve predicted performance.

Several extensive reviews for the needs of future tools and features can be found in the literature (Attia *et al.*, 2009; Augenbroe, 2002; Ellis and Mathews, 2002). Furthermore, a survey was conducted about the strengths and shortcomings of existing simulation tools in the context of Net ZEBs among the experts of IEA SHC Task 40/EBC Annex 52. Key results of the aforementioned studies are provided here:

– Ease of use: Net ZEB tools must be easy to use so that they appeal to a wider range of designers. This means intuitive user interfaces, transparency (e.g., no hidden features or assumptions), standard user interface features (e.g., undo and auto-save), minimal redundant inputs, efficient input methods, and comprehensible outputs.

– Accuracy: Net ZEB design tools need to be accurate in order to help designers predict net-zero energy with a high level of certainty. While early stage design tools can afford some inaccuracy since they provide rapid feedback and focus on

relative performance, tools used for detailed design must be accurate. Accuracy extends beyond the numerical methods representing heat transfer and other physical phenomena to having reasonable built-in assumptions and default values (e.g., for occupants, weather conditions, and plug loads).

– Availability of building features and technologies: Net ZEBs tend to involve technologically advanced building features in order to achieve this aggressive energy target. As discussed in [Chapter 7](#), many of the case studies utilize customized tools to model certain aspects of the buildings. It is important to have some tools that are capable of modeling these technologies. At least as important is a tool's ability to provide flexibility to integrate models for new technologies (e.g., TRNSYS allows custom models to be built, and EnergyPlus has the Energy Management System, which is a facility to add custom code).

– Interoperability: It would be unreasonable to expect a single tool to provide all features required for architectural design. However, many current tools are stand-alone and use proprietary or uncommon file formats, meaning that porting a model between programs may require partial or complete reentry of data. Future tools should allow more seamless portability between them.

– Rapid feedback: Rapid feedback of simulation results is important, where possible, to enable a greater number of design alternatives to be explored. It also builds confidence in the modeler that simulation will work before they invest too much modeling time. Rapid feedback can be realized in two ways: (1) faster input and (2) faster simulation. As computer processing power increases, the importance of the former will increase. This can be achieved through design templates, interoperability between tools, "smart" defaults, and efficient input methods.

– Detailed documentation: BPS tools should provide thorough documentation not only on how to use the tools, but also on the modeling methodologies and assumptions used. Limitations of different tool features (e.g., simplifications) should be documented so that users understand the potential risks of using the tool. It is widely understood that two tool users can get

significantly different results from the same tool. Thus, all underlying assumptions and modeling methodologies must be fully disclosed.

– Built-in design guidance and rules of thumb: Most current BPS tools do not provide guidance toward better designs; they merely provide predicted performance indicators based on user inputs. Future tools should have a built-in feature to provide rules of thumb as a starting point.

– Parametric analysis and optimization: Very few tools currently provide a feature for parametric analysis, despite the fact that it is commonly used in design practice. Performing parametric analysis manually can be a time consuming process because multiple simulations, input files, and results must be maintained. Similarly, few tools provide built-in optimization features. Currently, most optimization studies are performed using an external optimization engine (e.g., GenOpt (Wetter, 2001)) to drive the BPS engine. This requires knowledge of optimization, programming, and file management and structures. Ideally, future Net ZEB tools will provide greater support for optimization and interpretation of results.

– Knowledgebase and database: Building modelers must usually adhere to at least one building code or standard (e.g., LEED (CaGBC, 2011), ASHRAE Standard 90.1 (ASHRAE, 2010a), and local building energy codes). Ideally, tools should have the compliance details for these standards and facilitate entry of code-minimum building specifications.

– Useful graphical feedback: BPS tools tend to provide vast amounts of data (e.g., extensive spreadsheets or automated reports) that can overwhelm designers. Continued development in this area to provide useful visual feedback about design performance would help facilitate the Net ZEB design process. Several methods for graphical feedback, including multidimensional parametric analysis and Sankey diagrams, were suggested earlier.

4.4 Conclusion

This chapter has provided detailed discussions of two aspects of incorporating building performance simulation and other tools into the design process. The first focused on Net ZEB design practice and the appropriate design stages for introducing different design features and tools. The main conclusions drawn from that section are that emphasis should be placed on establishing major decisions that affect energy performance early in design; even if simple tools are used. These include major geometry (for daylighting, passive solar heating, natural ventilation, renewable energy collection), thermal mass (for passive solar design and night cooling), effective envelope properties (e.g., insulation value and window-to-wall area ratio), and basic control strategies. The later design stages are mainly reserved for minor refinements and detailing. However, because of the ambitious nature of Net ZEBs, the design stages are not rigidly defined and many iterations may be required to achieve all objectives. Finally, the IDP in conjunction with three innovative project delivery methods, including construction management at-risk (CM@R), design-build (DB), and IPD, were described.

The second major section of this chapter focused on modeling specific building phenomena and went into more depth on appropriate model resolution for different building systems and different design stages. The advantages and disadvantages of coupling different building system models were discussed at length. While an integrated model that includes all major energy-related systems is highly recommended to verify that net-zero energy (and/or other energy and comfort-related targets) is met, this section advocated cautiously using simpler, standalone tools during early-design stages. Though designers may be tempted to jump to complex models using powerful and detailed simulation tools, such an approach is often so time-consuming that very few design options can be explored and much of the output of the tools comes too late to effectively influence design. Finally, numerous techniques for using BPS tools and interpreting results are suggested, including multidimensional parametric analysis and solar design days.

The next chapter discusses formal optimization of Net ZEBs. Optimization should not be seen as a competing approach to traditional design methods covered in the current chapter, but rather

as a technique that can be introduced at any stage to support the overall design process.

Notes

1. Stakeholders are comprised of three primary groups: the client, which includes the owner and end users; the design team, which includes the architect, the engineers, and their consultants; and the builder, which includes all the trades. On large or public projects, community members can also be considered stakeholders.

2. A design charrette is a meeting that facilitates collaborative design and idea-sharing involving expert designers from multiple disciplines (architects, mechanical engineers, electrical engineers, renewable energy professionals, landscape architects). They usually range between one and five days in length and are sometimes spaced out to allow designers to return to work individually to further develop ideas before convening again. The ÉcoTerra case study in Chapter 7 describes a two-day charrette.

References

Advanced Buildings Institute (2013) Daylighting Pattern Guide.
Allard, F. and Santamouris, M. (1998) *Natural Ventilation in Buildings - A Design Handbook*, James & James Ltd., London, UK.
American Institute of Architects (AIA) (2008) *The Architect's Handbook of Professional Practice*, 14 edn, Wiley, Hoboken.
American National Standards Institute (ANSI) and Institute for Market Transformation to Sustainability (MTS) (2012) *Integrative Process (IP): ANSI Consensus National Standard Guide, Design and Construction of Sustainable Buildings and Communities*, American National Standards Institute, Institute for Market Transformation to Sustainability, Washington, DC.
American Society of Heating, Refrigerating and Air-Conditioning Engineers (ASHRAE) (2004) Standard 55 - Thermal environmental conditions for human occupancy (Atlanta, GA).

American Society of Heating, Refrigerating and Air-Conditioning Engineers (ASHRAE) (2009) *ASHRAE Handbook - Fundamentals*, SI edn, American Society of Heating, Refrigerating, and Air,-Conditioning Engineers (ASHRAE), Atlanta, GA, USA.

American Society of Heating, Refrigerating and Air-Conditioning Engineers (ASHRAE) (2010a) ANSI/ASHRAE/IESNA Standard 90.1–2010: Energy standard for buildings except for low-rise residential buildings.

American Society of Heating, Refrigerating and Air-Conditioning Engineers (ASHRAE) (2010b) ASHRAE Thermal Comfort Tool.

American Society of Heating, Refrigerating and Air-Conditioning Engineers (ASHRAE) (2010c) Standard 55 - Thermal environmental conditions for human occupancy (Atlanta, GA).

Athienitis, A.K., Torcellini, P., Hirsch, A., O'Brien, W., Cellura, M., Klein, R., Delisle, V., Attia, S., Bourdoukan, P., and Carlucci, S. (2010) Design, Optimization and Modelling Issues of Net-Zero Energy Solar Buildings. In EuroSun (Graz, Austria).

Attia, S., Beltrán, L., De Herde, A., and Hensen, J. (2009) Architect Friendly: A comparison of ten different building performance simulation tools. Paper presented at: *11th International IPBSA Conference (Glasgow, Scotland)*.

Augenbroe, G. (2002) Trends in building simulation. *Building and Environment*, **37**, 891–902.

Augenbroe, G. (2012) The role of simulation performance based design, in *Building Performance Simulation for Design and Operation* (eds J. Hensen and R. Lamberts), Spon Press, an imprint of Taylor & Francis, London.

Bartak, M., Beausoleil-Morrison, I., Clarke, J., Denev, J., Drkal, F., Lain, M., Macdonald, I., Melikov, A., Popiolek, Z., and Stankov, P. (2002) Integrating CFD and building simulation. *Building and Environment*, **37**, 865–871.

Bazjanac, V. (2001) Acquisition of building geometry in the simulation of energy performance. Paper presented at: *Building Simulation 2001 (Rio de Janeiro)*.

Beausoleil-Morrison, I. (2011) The design of an ESP-r and TRNSYS co-simulator. *In 12th Conference of International Building Performance Simulation Association (Sydney, Australia)*, pp. 2333–2340.

Blomberg, T. (1996) *Heat Conduction in Two or Three Dimensions - Computer Modelling of Building Physics Applications*, Lund University, Sweden, p. 188.

Bordass, B., Bromley, K., and Leaman, A. (1993) User and occupant controls in office buildings. Paper presented at: *International conference on building design, technology and occupant well-being in temperate climates, Brussels, Belgium.*

Bordass, W., Leaman, A., and Willis, S. (1994) Control strategies for building services: the role of the user. Paper presented at: *Chartered Institute of Building Conference on Buildings and the Environment, Building Research Establishment, UK.*

Bourgeois, D., Reinhart, C., and Macdonald, I. (2006) Adding advanced behavioural models in whole building energy simulation: A study on the total energy impact of manual and automated lighting control. *Energy and Buildings*, **38**, 814–823.

Bradley, J. (2003) The acoustical design of conventional open plan offices. *Canadian Acoustics*, **31**, 23–34.

Canada Green Building Council (CaGBC) (2011) Introduction to LEED.

Canada Mortgage and Housing Corporation (CMHC) (1998) Tap the Sun passive solar techniques and home designs (CHMC).

Carrol, W.L. (1999) Daylighting simulation: methods, algorithms, and resources (Lawrence Berkeley National Laboratory: A report of IEA SHC Task 21/ECBCS Annex 29).

Chen, Y., Athienitis, A.K., and Galal, K. (2010a) Modeling, design and thermal performance of a BIPV/T system thermally coupled with a ventilated concrete slab in a low energy solar house: Part 1, BIPV/T system and house energy concept. *Solar Energy*, **84**, 1892–1907.

Chen, Y., Galal, K., and Athienitis, A.K. (2010b) Modeling, design and thermal performance of a BIPV/T system thermally coupled with a ventilated concrete slab in a low energy solar house: Part 2, ventilated concrete slab. *Solar Energy*, **84**, 1908–1919.

Chwif, L., Barretto, M.R.P., and Paul, R.J. (2000) On simulation model complexity. Paper presented at: *Simulation Conference, 2000 Proceedings Winter (IEEE).*

Clarke, J. (2001) *Energy Simulation in Building Design*, 2nd edn, Butterworth-Heinemann, Oxford.

Cole, R.J. and Brown, Z. (2009) Reconciling human and automated intelligence in the provision of occupant comfort. *Intelligent*

Buildings International, **1**, 39–55.

Costola, D., Blocken, B., and Hensen, J. (2009) Overview of pressure coefficient data in building energy simulation and airflow network programs. *Building and Environment*, **44**, 2027–2036.

Crawley, D.B., Hand, J.W., Kummert, M., and Griffith, B.T. (2008) Contrasting the capabilities of building energy performance simulation programs. *Building and Environment*, **43**, 661–673.

de Dear, R.J. and Brager, G.S. (1998) Developing an adaptive model of thermal comfort and preference. Paper presented at: *1998 ASHRAE Winter Meeting (San Francisco, CA, USA: ASHRAE)*.

Department of Energy (DOE) (2012) EnergyPlus V7.2.

Department of Energy (DOE) (2013a) Building Energy Software Tools Directory.

Department of Energy (DOE) (2013b) EnergyPlus Engineering Reference.

Department of Energy (DOE) (2013c) EnergyPlus Input/Output Reference.

Department of Energy (DOE): Energy Efficiency and Renewable Energy (EERE) (2010) Building Energy Data Book.

Department of Energy (DOE): Energy Efficiency and Renewable Energy (EERE) (2013) EnergyPlus Example File Generator.

Department of Energy (DOE): Energy Efficiency and Renewable Energy, E (2013) Zero Energy buildings Database.

Doiron, M., O'Brien, W., and Athienitis, A.K. (2011) Energy performance, comfort and lessons learned from a near net-zero energy solar house. *ASHRAE Transactions*, **117**, 1–13.

Ellis, M.W. and Mathews, E.H. (2002) Needs and trends in building and HVAC system design tools. *Building and Environment*, **37**, 461–470.

Energy Systems Research Unit (ESRU) (2010) ESP-r (University of Strathclyde).

Equa Simulation AB (2009) IDA ICE (Sweden).

Estia SA (2009) DIAL-Europe.

Fanger, P.O. (1970) *Thermal Comfort: Analysis and Applications in Environmental Engineering*, Danish Technical Press, Copenhagen.

Gram-Hanssen, K. (2010) Residential heat comfort practices: understanding users. *Building Research & Information*, **38**, 175–186.

Gronbeck, C. (2012) Overhang Design, (Seattle, Washington, USA).

GSES (2004) *Planning and Installing Photovoltaic Systems*, 2nd edn, James & James\Earthscan Publications Ltd., London.

Guglielmetti, R., Pless, S., and Torcellini, P. (2010) On the Use of Integrated Daylighting and Energy Simulations to Drive the Design of a Large Net-Zero Energy Office Building. In SimBuild 2010 (New York, New York), pp. 301–309.

Gunay, H.B., O'Brien, W., and Beausoleil-Morrison, I. (2013) A critical review of state-of-the-art energy and comfort related occupant behavior in office buildings. *Building and Environment*, **70**, 31–47.

Haldi, F. and Robinson, D. (2011) The impact of occupants' behaviour on building energy demand. *Journal of Building Performance Simulation*, **4**, 323–338.

Hayter, S.J., Torcellini, P.A., Hayter, R.B., and Judkoff, R. (2001) The energy design process for designing and constructing high-performance buildings. In CLIMA 2000 (Naples, Italy).

Hensen, J. and Lamberts, R. (2012) Introduction to building performance simulation, in *Building Performance Simulation for Design and Operation* (eds J. Hensen and R. Lamberts), Spon Press, an imprint of Taylor & Francis, London.

Hensen, J.L.M. (1999) A comparison of coupled and de-coupled solutions for temperature and air flow in a building. *ASHRAE Transactions*, **105**, 962–969.

Hoes, P., Hensen, J.L.M., Loomans, M.G.L.C., de Vries, B., and Bourgeois, D. (2009) User behavior in whole building simulation. *Energy and Buildings*, **41**, 295–302.

Johnsen, K. and Watkins, R. (2010) Daylight in Buildings - ECBCS Annex 29/SHC Task 21 Project Summary Report (United Kingdom).

Karava, P., Athienitis, A.K., Stathopoulos, T., and Mouriki, E. (2012) Experimental study of the thermal performance of a large institutional building with mixed-mode cooling and hybrid ventilation. *Building and Environment*, **57**, 313–326.

Kesik, T. and Stern, L. (2008) Representation of Performance Indicators for the Conceptual Design of Passive Solar Houses. Paper presented at: *eSim 2008, The 5th IBPSA-Canada Conference (Quebec City, QC, May 23–25, 2008)*.

Lawrence Berkeley National Laboratory (LBNL) (1999) COMIS.

Lawrence Berkeley National Laboratory (LBNL) (2012) THERM.

Löhnert, G., Dalkowski, A., and Sutter, W. (2003) *Integrated Design Process: A Guideline for Sustainable and Solar-Optimised Building Design*, IEA International Energy Agency, Berlin.

Mahdavi, A. (2012) Room acoustics performance prediction, in *Building Performance Simulation for Design and Operation* (eds J. Hensen and R. Lamberts), Spon Press.

Mahdavi, A., Mohammadi, A., Kabir, E., and Lambeva, L. (2008) Occupants' operation of lighting and shading systems in office buildings. *Journal of Building Performance Simulation*, **1**, 57–65.

Marszal, A.J., Heiselberg, P., Bourrelle, J.S., Musall, E., Voss, K., Sartori, I., and Napolitano, A. (2011) Zero Energy Building – A review of definitions and calculation methodologies. *Energy and Buildings*, **43**, 971–979.

Mason, R., Gunst, R., and Hess, J. (2003) *Statistical Design and Analysis of Experiments: With Applications To Engineering And Science*, Wiley-Interscience, Hoboken, NJ.

McQuiston, F.C., Parker, J.D., and Spitler, J.D. (2005) *Heating, Ventilating, and Air Conditioning: Analysis and Design, 6th edn*, John Wiley & Sons, Hoboken, N.J.

Milne, M. (2013) Climate Consultant V5.4 (University of California Los Angeles).

Minister of Natural Resources Canada (2013) RETScreen International: Clean Energy Project Analysis (Natural Resources Canada).

Mora, L., Gadgil, A., and Wurtz, E. (2003) Comparing zonal and CFD model predictions of isothermal indoor airflows to experimental data. *Indoor Air*, **13**, 77–85.

Musall, E. (2013) Net zero-energy buildings – Map of international projects.

Natural Resources Canada (NRCan) (2008) Energy use data handbook tables (Canada), Office of Energy Efficiency (OEE), ed.

Newsham, G.R. (1994) Manual control of window blinds and electric lighting: Implications for comfort and energy consumption. *Indoor and Built Environment*, **3**, 135.

Nicol, J.F. (2001) Characterising occupant behaviour in buildings: towards a stochastic model of occupant use of windows, lights, blinds, heaters and fans. Paper presented at: *Building Simulation (Rio de Janeiro, August 13–15)*.

O'Brien, W. (2013) Evaluating the performance robustness of fixed and movable shading devices against diverse occupant behaviors In SimAUD, April 8–10 (San Diego, CA).

O'Brien, W., Athienitis, A., and Kesik, T. (2008) Sensitivity Analysis for a Passive Solar House Energy Model. Paper presented at: *International Solar Energy Society - Asia Pacific (ISES-AP) Conference (Sydney, Australia, Nov. 25–27, 2008).*

O'Brien, W., Athienitis, A.K., and Kesik, T. (2009) The development of solar house design tool. Paper presented at: *11th International Building Performance Simulation Association (IBPSA) Conference (Glasgow, Scotland, July 27–30, 2009).*

O'Brien, W., Athienitis, A.K., and Kesik, T. (2011a) Parametric analysis to support the integrated design and performance modeling of net-zero energy houses. *ASHRAE Transactions*, **117** (Part 1), 1–13.

O'Brien, W., Athienitis, A.K., and Kesik, T. (2011b) Thermal zoning and interzonal airflow in design of solar houses: a sensitivity analysis. *Journal of Building Performance Simulation*, **4**, 239–256.

O'Brien, W., Kapsis, K., and Athienitis, A.K. (2013) Manually-operated window shade patterns in office buildings: a critical review. *Building and Environment*, **60**, 319–338.

O'Connor, J., Lee, E., Rubinstein, F., and Selkowitz, S. (1997) Tips for Daylighting with Windows - The Integrated Approach (Lawrence Berkeley National Laboratory).

Paciuk, M. (1989) The role of Personal Control of the Environment in Thermal Comfort and Satisfaction at the Workplace (Milwaukee, USA: University of Wisconsin), pp. 436.

Parekh, A., Swinton, M.C., Szadkowski, F., and Manning, M.M. (2005) *Benchmarking of Energy Savings Associated with Energy Efficient Lighting in Houses*, Natural Resources Canada - Canadian Center for Housing, Technology, Ottawa, p. 40.

Passive House Institute (2010) PHPP: Passive House Planning Package.

Pérez-Lombard, L., Ortiz, J., and Pout, C. (2008) A review on buildings energy consumption information. *Energy and Buildings*, **40**, 394–398.

Ramos, G. and Ghisi, E. (2010) Analysis of daylight calculated using the EnergyPlus programme. *Renewable and Sustainable Energy Reviews*, **14**, 1948–1958.

Rea, M.S. (2000) *The IESNA Lighting Handbook: Reference & Application*, Illuminating Engineering Society of North America, New York, NY.

Reed, W.G. and Gordon, E.B. (2000) Integrated design and building process: What research and methodologies are needed? *Building Research and Information*, **28**, 325–337.

Reinhart, C. (2013) DAYSIM V3.1.

Reinhart, C. and Fitz, A. (2006) Findings from a survey on the current use of daylight simulations in building design. *Energy and Buildings*, **38**, 824–835.

Reinhart, C.F. (2004) Lightswitch-2002: A model for manual and automated control of electric lighting and blinds. *Solar Energy*, **77**, 15–28.

Reinhart, C.F. and Herkel, S. (2000) An Evaluation of Radiance Based Simulations of Annual Indoor Illuminance Distributions due to Daylight. In Building Simulation 1999 (Kyoto, Japan).

Reinhart, C.F. and Voss, K. (2003) Monitoring manual control of electric lighting and blinds. *Lighting Research & Technology*, **35**, 243–260.

Relux Informatik AG (2012) Relux.

Rijal, H., Tuohy, P., Humphreys, M., Nicol, J., Samuel, A., and Clarke, J. (2007) Using results from field surveys to predict the effect of open windows on thermal comfort and energy use in buildings. *Energy and Buildings*, **39**, 823–836.

Royal Institute of British Architects (RIBA) (2007) Outline Plan of Work 2007 (London, UK: Royal Institute of British Architects).

Rubin, A.I., Collins, B.L., and Tibbott, R.L. (1978) *Window Blinds as a Potential Energy Saver – A Case Study*, NBS Building Science Series 112, National Institute for Standards and Technology, Gaithersburg, MD.

Saldanha, N. and Beausoleil-Morrison, I. (2012) Measured end-use electric load profiles for 12 Canadian houses at high temporal resolution. *Energy and Buildings*, **49**, 519–530.

Sander, D.M., Barakat, S.A. and National Research Council, Canada, and Division of Building Research (1985) Mass & Glass: How Much? How Little? (National Research Council Canada, Division of Building Research).

Schmidt, M. (2008) The Sankey diagram in energy and material flow management. *Journal of Industrial Ecology*, **12**, 82–94.

Shah, J.J., Kulkarni, S.V., and Vargas-Hernandez, N. (2000) Evaluation of idea generation methods for conceptual design: Effectiveness metrics and design of experiments. *Journal of Mechanical Design*, **122**, 377–384.

Sherman, M.H. (1987) Estimation of infiltration from leakage and climate indicators. *Energy and Buildings*, **10**, 81–86.

Sunikka-Blank, M. and Galvin, R. (2012) Introducing the prebound effect: The gap between performance and actual energy consumption. *Building Research & Information*, **40**, 260–273.

Tzempelikos, A. and Athienitis, A.K. (2007) The impact of shading design and control on building cooling and lighting demand. *Solar Energy*, **81**, 369–382.

University of Wisconsin (2012) TRNSYS.

Veitch, J.A. (2001) Psychological processes influencing lighting quality. *Journal of the Illuminating Engineering Society*, **30**, 124–140.

Ward, G. (2013) RADIANCE.

Wetter, M. (2001) GenOpt® - A Generic Optimization Program. Paper presented at: *Building Simulation 2001 Conference (Rio de Janeiro)*.

Wetter, M. and Haves, P. (2008) A modular building controls virtual test bed for the integration of heterogeneous systems. Paper presented at: *SimBuild 2008 (Berkeley, California)*.

Wienold, J. and Christoffersen, J. (2006) Evaluation methods and development of a new glare prediction model for daylight environments with the use of CCD cameras. *Energy and Buildings*, **38**, 743–757.

Yun, G. and Kim, K.-S. (2013) An empirical validation of lighting energy consumption using the integrated simulation method. *Energy and Buildings*, **57**, 144–154.

5
Building Performance Optimization of Net Zero-Energy Buildings

Shady Attia, Mohamed Hamdy, Salvatore Carlucci, Lorenzo Pagliano, Scott Bucking and Ala Hasan

5.1 Introduction

Building performance optimization (BPO) paired with building performance simulation (BPS) is a promising solution for evaluating many different design options and obtaining the optimal or near-optimal solution for a given objective or combination of objectives (e.g., lowest life-cycle cost, lowest capital cost, highest thermal comfort) while complying with constraints (e.g., net zero-energy) (Brown, Glicksman, and Lehar, 2010; Bucking *et al.*, 2010; Charron and Athienitis, 2006; Christensen and Anderson, 2006; Wetter, 2001). Traditionally, buildings have been designed based on heuristic rules separating the design process into several major design stages with multiple disciplines (architects, mechanical engineers, structural engineers, electrical engineers, etc.). Optimization can facilitate greater continuity between disciplines and design stages by identifying and evaluating major building design parameters (see Figure 5.1), in a holistic way. Based on this perspective, the previously, often ill-defined, design problem would be defined as a problem with explicit multiobjective criteria. This will promote fully integrated net zero-energy building (Net ZEB) designs where the building designers can act to influence the direction of the optimization. Despite the fact that optimization's potential for Net ZEBs is relevant, it remains largely a research tool and has yet to enter common industry practice.
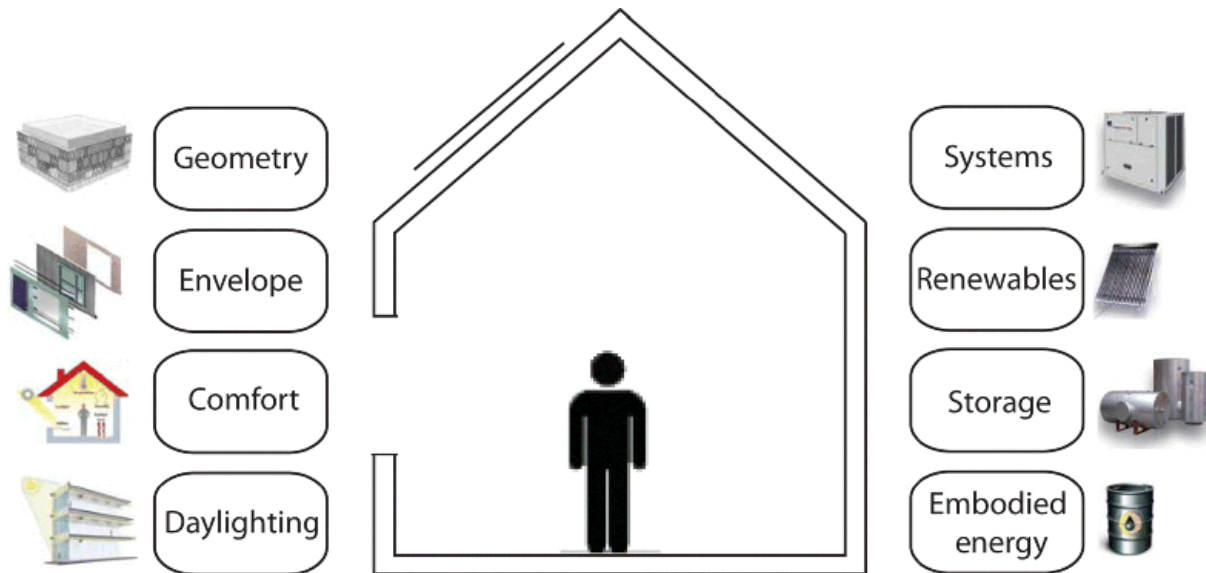
Fig. 5.1 Optimization as a holistic approach for multiobjective approach for Net ZEB design

This chapter discusses major obstacles to BPO in the building design and construction industry including lack of appropriate tools, lack of resources (time, expertise), and the

requirement that the problem be very well defined (e.g., constraints, objective function, finite list of design options). The objective of this chapter is to document the current state-of-the-art and future research and development needs for Net ZEB optimization tools in practice and its use for design and operation of buildings for energy, comfort, and cost optimization. The content is intended to aid the reader in better understanding areas of active research in building optimization as well as tools and methods commonly used by researchers and designers.

5.1.1 What is BPO?

Automated building performance optimization is a process that aims to select the optimal solutions from a set of available alternatives for a given design or control problem, according to a set of performance criteria and constraints. Such criteria can be expressed as mathematical functions, called objective functions. Automated optimization is a combination of different types of optimization algorithms, setting each algorithm to optimize one or more design functions. The optimization objectives for Net ZEBs are to identify impacts on cost, energy, environmental impact (embodied energy, materials life cycle), comfort, and indoor air quality.

An objective function is defined as a mathematical function subjected to optimization. Optimization searches for the optimal solution with respect to the objective functions to be maximized or minimized, subjected to some constraints (e.g., of the dependent variables and objective functions). If no constraints are specified, the problem is denoted an unconstrained optimization problem. A constraint limits the problem space to a subset of elements (Snyman, 2005). If the optimization problem aims at minimizing a single objective function, it is called a single-objective optimization problem; otherwise, if the objective functions are more than one, it is called a multi-objective optimization problem.

Visualization techniques are helpful to facilitate the extraction of relevant information regarding performance trade-offs, propagation of uncertainties, and sensitivity analysis. By providing visualization during the optimization process, it is possible for the designer to interact with the optimization process (Flager *et al.*, 2009). This facilitates a hybrid approach between traditional design ([Chapter 4](#)) and optimization (current chapter).

5.1.2 Importance of BPO in Net ZEB Design

Since building performance optimization of Net ZEBs is aimed at an absolute goal, the number and complexity of energy efficiency measures forming the energy concept may be high (Athienitis *et al.*, 2010). The Net ZEB performance objective has raised the bar of building performance, and will change the way buildings are designed and operated. This means that evaluating different design options is becoming more arduous than ever before. The building geometry, envelope, and many building systems interact with each other, thus requiring optimizing the building and systems together rather than sub-system optimization which lacks integration (Hayter *et al.*, 2001).

One promising solution is to use BPO paired with BPS as a means to evaluating many different design options and obtain the optimal or near-optimal solutions. A number of energy simulation engines exist and are often used in different stages of the design process of a building. However, out of the 406 BPS tools listed on the U.S. Department of Energy (DOE) Web site in 2012, less than 19 tools are allowing BPO as shown in [Figure 5.2](#).

Automated optimization tools

	1997	1998	1999	2000	2001	2002	2003	2004	2005	2006	2007	2008	2009	2010	2011	2012
	107	116	156	168	198	210	235	285	296	317	324	345	378	389	404	395
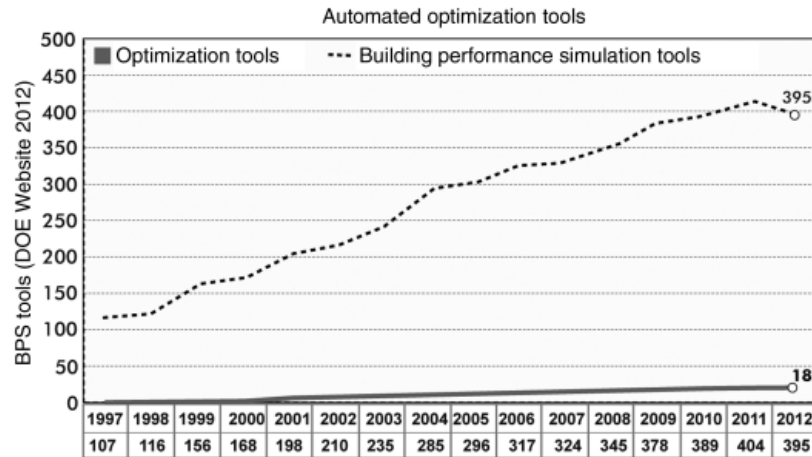
Fig. 5.2 Evolution of building performance simulation and optimization tools (Attia *et al.*, 2013)

Based on a literature review, Figure 5.3 reports the number of times a given BPS and BPO tool has been used to optimize a building design. Progressions in building simulation tool development and in coupling or combining complementary BPS tools at run-time expand the domains where BPS optimization studies can occur.
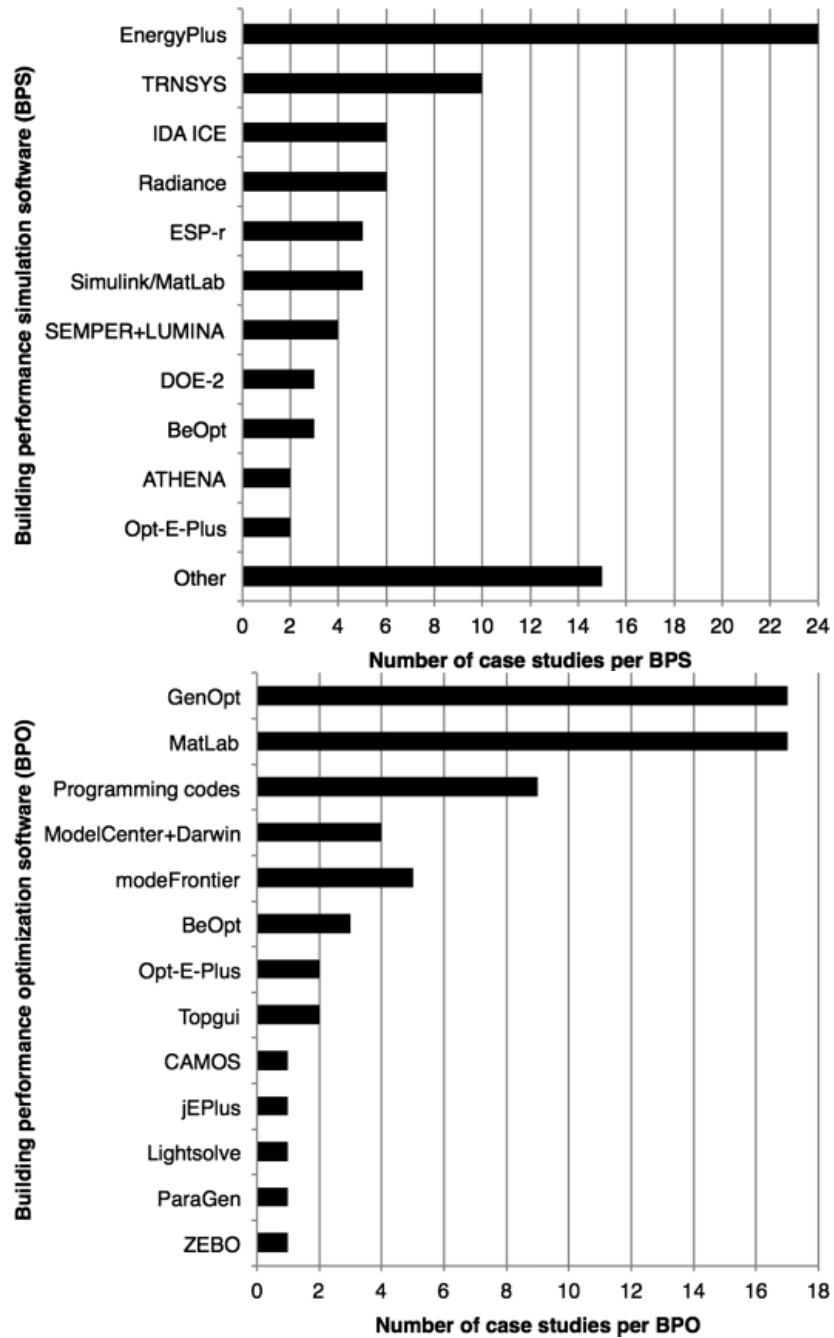
Fig. 5.3 Distribution of BPS tools used in literature

In the architecture, engineering, and construction (AEC) industry, there is a growing research trend for automated optimization approaches to be used to map out and find pathways to building designs with desirable qualities, such as aesthetics, geometry, structure, comfort, energy conservation, or economic features, rather than focusing on one particular outcome. Although optimization studies are most commonly performed in the early design stage, where the majority of design decisions are made, optimization approaches can be equally useful in the late design and operation stages. For example, optimization can be used for selecting and fine-tuning heating, ventilation, and air-conditioning (HVAC) control strategies, including model predictive control.

The use of optimization as a means of providing input to energy policy (e.g., for setting levels for minimum performance standards or incentive measures) is one of its most important applications in recent years. For example, using optimization to evaluate the energy and cost-savings potential from constructing more efficient new homes and net-zero energy homes in the United States (Christensen, 2005). Also, this includes the call of the European Commission for implementing a methodology to calculate cost-optimal levels in the Energy Performance of Buildings Directive (EPBD) framework. European Member States are required to define cost-optimal levels of minimum energy performance according to their specificities (Constantinescu, 2010).

5.2 Optimization Fundamentals

Applications of optimization are rapidly evolving for both building design and operation. The most appropriate search algorithms and modeling approaches vary depending on the application area including optimization objectives.

5.2.1 BPO Objectives (Single-Objective and Multi-Objective Functions)

In mathematics, optimization is the discipline concerned with finding inputs of a function that minimize or maximize its value, which may be subjected to constraints (Pardalos and Resende, 2012). In the AEC community, most BPO methods have focused on solving single-objective or multi-objective functions (Caldas, 2001; Choudhary, 2004; Hamdy, 2012; Hopfe, 2009; Nielsen, 2002; Pedersen, 2007; Verbeeck, 2007; Wang, 2005; Wetter, 2004).

In the case of single-objective functions, an optimum solution of the problem is either its global maximum or minimum, depending on the purpose. On the other hand, in multi-objective optimization problems, a specific building variant is often not able to simultaneously minimize or maximize each objective function. Instead, when searching for solutions, one comes to limit variants such that a further improvement toward the minimum value of one of the objective function causes the others to deviate from the minima. Therefore, the aim of a multi-objective optimization problem consists in finding such variants and possibly in quantifying the trade-off in satisfying the individual objective functions. The role of the optimization algorithm is to identify the solutions that lie on the trade-off curve, known as the Pareto frontier (a set of optimal solutions plotted in the form of a curve; named after the Italian–French economist, Vilfredo Pareto). These solutions all have the characteristic that none of the objectives can be improved without prejudicing another.

In the past two decades, researchers have solved design problems for real buildings using single-objective or multi-objective functions. Figure 5.4 shows the distribution by objective of 92 papers that use optimization algorithms, applied to buildings. It is observed that most researchers consider energy as the main objective for BPO.
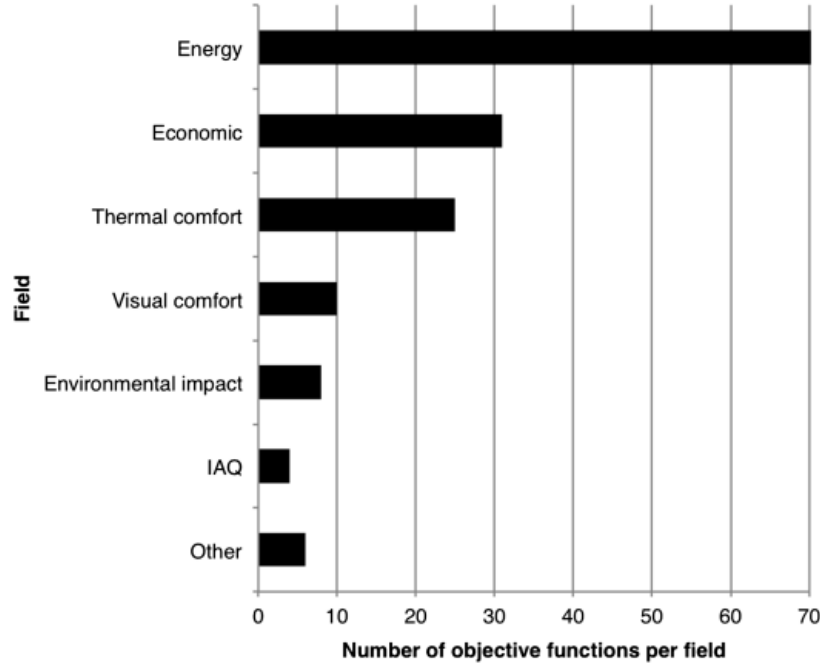
Fig. 5.4 The distribution of objective functions using BPO in literature

5.2.2 Optimization Problem Definition

The formal goal of a minimization study is to find the value x^* of a design variable vector, **x**, such that $f(x^*)$ is the minimum value of $f(\mathbf{x})$, with x varying within a certain feasible design space. More formally

$$\min_{x \in \mathbf{X}} f(\mathbf{x}) = f(x^*)$$ (5.1)

where **x** is the design variable vector $\mathbf{x} = (x_1, x_2,..., x_N)^\mathrm{T}$ in design space $\mathbf{X} \subset \mathbb{R}^N$; the objective or fitness function, $f()$, maps the set of design variables onto an objective vector **y** $= (y_1, y_2,..., y_M)^\mathrm{T}$ where $f_i \in \mathbb{R}^M$, $y_i = f_i(\mathrm{x})$, $f_i: \mathbb{R}^N \to \mathbb{R}^1$ for i = 1, 2,..., M, describes the objective solution space $\mathbf{Y} \subset \mathbb{R}^M$; the search for $\min\{f(\mathbf{x})\}$ is subject to L constraints $g_i(\mathbf{x}) \leq 0$ where i = 1, 2,..., L; feasible design vectors set $\mathbf{x}|g_i(\mathbf{x}) \leq 0$ form the feasible design space $\mathbf{X}^*$, and corresponding objective vectors set $\mathbf{y}|\mathbf{x} \in \mathbf{X}^*$ form feasible objective space $\mathbf{Y}^*$; for a minimization problem, a design vector $\mathbf{a} \in \mathbf{X}^*$ is Pareto optimum if no design vector $\mathbf{b} \in \mathbf{X}^*$ exists such that $y_i(\mathbf{b}) \leq y_i(\mathbf{a})$, i = 1, 2,..., M.

5.2.3 Review of Optimization Algorithms Applicable to BPS

In this section, suitable optimization approaches for building simulation studies are reviewed. A general overview of several methods and algorithms, which have proven to be versatile in BPS applications, are presented. The following approaches are discussed: (i) deterministic searches, (ii) population-based searches, and (iii) hybrid search approaches.

A deterministic search attempts to operate on individual building representations to identify optimal regions by changing the value of variables using small increments or decrements. Although the goal of a deterministic search is to identify global optimums, there is a risk of preconverging to local optimums in multimodal problems. Two

deterministic searches are discussed: (i) hill-climbing search and (ii) Hooke–Jeeves search. These searches are called deterministic, as a search operation on a given individual will always result in the same outcome.

Hill-climbing searches are a simple deterministic search strategy. Building design variables are incrementally changed to improve an objective function. Typically, the order in which variables are searched and the particular building design representation being searched will greatly affect the search outcome. Renders (1994) recommended integrating a hill-climbing search into the mutation operator of a genetic algorithm or as a forked process interwoven into the search algorithm. Bucking *et al.* (2010) compared the search performance of using hill-climbing searches at the beginning and end of an Evolutionary Algorithm (EA). This research demonstrated that performing a hill-climbing search on weakly interacting variables at the start of the hybrid algorithm and locking them inside an EA improves algorithm performance and search resolution. Performing a hill-climbing search after an EA was found to only marginally improve search outcomes.

The Hooke–Jeeves (HJ) search (Hooke and Jeeves, 1961), a member of the general pattern search family (Audet and Dennis, 2002), is a deterministic search algorithm that explores defined step-sizes in each continuous design variable coordinate. The algorithm selects the design variable, for a given step-size, that best improves fitness. If fitness is not improved, then the process is repeated to find the best step-size improvement in the other design variable coordinates. When no further improvements are made, the step-size is decreased, as previous step-sizes are assumed to be too large to resolve local optimums. Decreasing step-sizes requires the algorithm to be constantly converging. This feature can be overcome by combining the HJ algorithm with other global searches, as demonstrated by Wetter and Polak (2004).

Figure 5.5 illustrates a Hooke–Jeeves pattern search using a two-dimensional test function. The cross with round circles represents the search grid. The search grid has the same number of dimensions, as there are optimization variables. Dots represent the selected direction of the next search iteration. Note in the third iteration (3) that the fitness is not improved so the algorithm halves the search grid size and continues from the last known improvement. Step-sizes are decreased again in iterations 4, 5, and 6 until the global optimum is found and the search terminated.
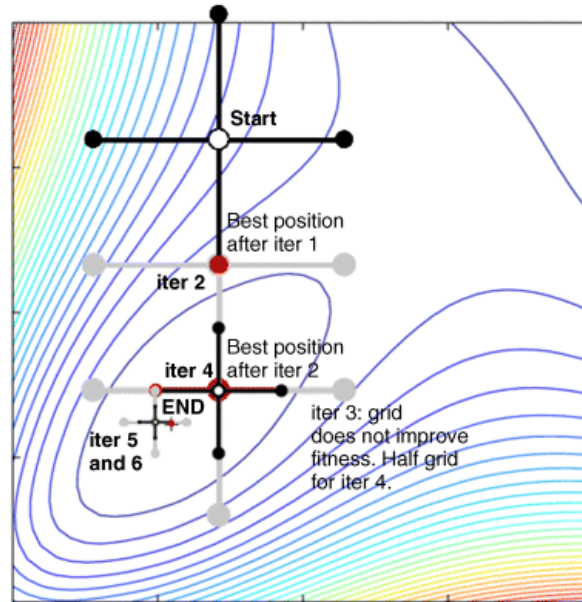
Fig. 5.5 Example of Hooke–Jeeves pattern search on the Broyden function

Population-based algorithms perform operations on populations of representative building designs. Often, they are called metaheuristics due to their nature of finding near-optimal solutions to a wide range of problems. Two common population-based search algorithms used with BPS are genetic, a type of evolutionary algorithm, and the particle swarm algorithm.

The first algorithm selected for discussion from the group of population-based algorithms is the Genetic Algorithm (GA), from the EA family. GAs have become popular due to their ease of implementation and proven ability to solve multimodal and multi-objective problems. Computational pseudo-evolution was first demonstrated by Goldberg (1989) using biological inspirations. Performing genetic operations, such as mutations and crossovers, on representations in combination with selection operators emulate the "survival of the fittest" found in biological evolution. Eiben and Rudolph (1999) described members of the EA family as "adaptive systems having a "basic instinct" to increase the average and maximum fitness of a population." In typical implementations, design variables are represented using binary or discrete formats. Genetic algorithms are a well-studied group within the broader metaheuristic family. Wang, Rivard, and Zmeureanu (2006) used a GA to perform a multi-objective optimization using lifecycle cost and exergy on a green building with a polygonal-shaped floor plan. Caldas (2008) used a GA to simultaneously optimize building geometry, energy efficiency, and visual comfort. Many modifications exist combining the best elements of other search strategies from the evolutionary algorithm family, such as Differential Evolution (DE) (Price, Storn, and Lampinen, 2005), Evolutionary Strategies (ES) (Eiben and Smith, 2003), and Genetic Programming (GP) (Poli, Langdon, and McPhee, 2008). Literature commonly refers to a modified GA by their more general family name, EA, to avoid confusion. EAs have been scaled to building optimization problems with many design variables. For example, Kampf and Robinson (2010) optimized the layout of a buildings cluster to maximize available solar radiation, while considering design parameters, such as insulation in ceilings and walls, window types and areas, infiltration, and thermal mass. A benefit of EAs is the flexibility to include subspecialized search strategies. For example, multi-island EAs allow for the population in one generation to be divided into subpopulations, or islands, where

specialized subpopulation searches can be performed. This approach is useful to deconstruct large optimization problems into smaller, more solvable problems. Ooka and Komamura (2009) utilized a multi-island EA to design, schedule, and control an HVAC system for a hospital in Japan.

A particle swarm optimization (PSO) is fundamentally different from evolutionary cycles found in EAs (Eberhart and Kennedy, 1995). Instead of forming a new population of individuals at each iteration, the existing population is allowed to gravitate toward other more fit individuals, or particles, in the population. Particles are updated using the best local and global particles in the swarm. Representations are vectors of continuous design variables, although binary and discrete representations can also be used (Kennedy and Eberhart, 1997). PSO competes favorably with other optimization algorithms. For example, Elbeltagi, Hegazy, and Grierson (2005) compared five evolutionary-based algorithms and found that PSO outperforms the other algorithms for a discrete design problem, with regard to reproducibility of optimal solutions and ability to scale with increasing problem sizes. PSOs are the primary population-based search approach used in the Generic Optimization Program (GenOpt) (Wetter, 2001). Hasan, Vuolle, and Siren (2008) utilized GenOpt's PSO algorithm to optimize envelope and HVAC systems with respect to life cycle cost of a single detached home in Finland using IDA-ICE as a simulation tool. Wetter and Wright compared a GA, with HJ search using GenOpt (Wetter and Wright, 2004). They found that stochastic methods are effective at finding near-global optimums; however, deterministic searches may be required to further resolve searches.

More recently, researchers have combined the strengths of population-based and deterministic algorithms into a hybrid approach. Population-based algorithms identify near optimal regions; deterministic searches intensify the search process around near optimal landscapes. Although hybridization can occur at different levels, the most common approach is to augment a population-based search with a local deterministic search (Feoktistov, 2006). The GenOpt tool performs an HJ search on the optimal individual resulting from a PSO (LBNL and Wetter, 2011). This algorithm was found to have better convergence properties for nonmultimodal problems compared to a hybrid DE algorithm (Kampf, Wetter, and Robinson, 2010).

5.2.4 Integration of Optimization Algorithms with BPS

Several steps are required to use an optimization algorithm with BPS, see Figure 5.6. First, the upper and lower limits of design variables are defined within the optimization algorithm. These limits define the entire possible set of designs available to the optimization algorithm. Design representations of the algorithm are converted into simulation files. Simulation files are evaluated using a building simulation tool to evaluate the performance of each design under analysis. The optimization algorithm uses databases, such as text file or SQL interactions, to store relevant simulation information. Building representations are improved upon in the optimization iteration loop until a termination criterion is satisfied. Figure 5.7 presents an overview of the evolutionary cycle common to an EA.
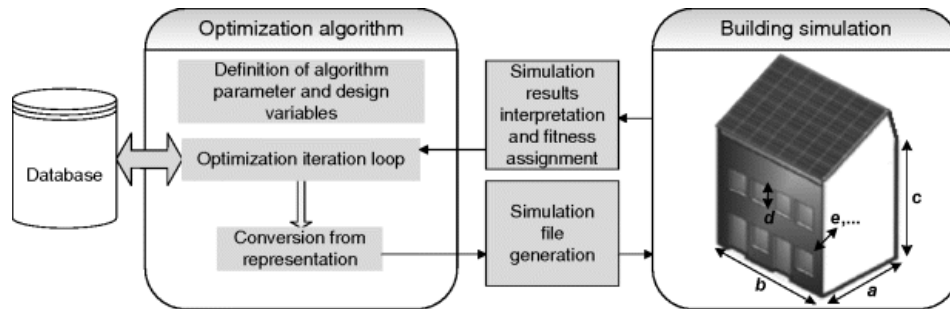
Fig. 5.6 Integration of an optimization algorithm with BPS (Bucking *et al.*, 2013)
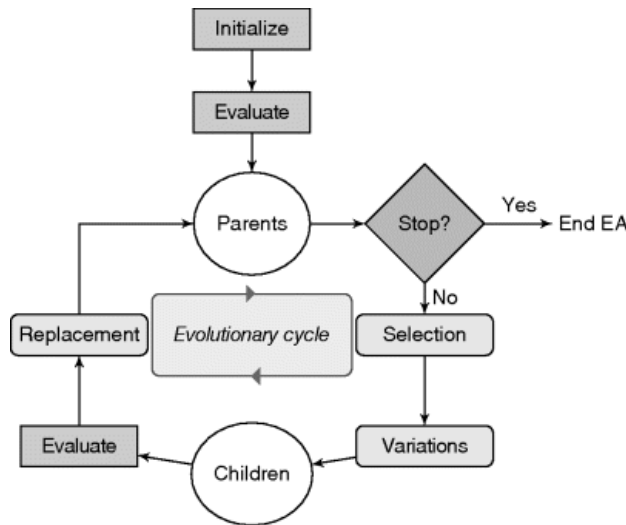
Fig. 5.7 Overview of evolutionary algorithm (Bucking, 2013)

A set of genomes, or simplified representations of building designs, forms the population. In Figure 5.7, the population is initialized by randomly creating a population of a specified size. The fitness of each individual is evaluated using a building simulation tool. This population becomes the parent population as it enters the evolutionary cycle. Parent selection is used to select genomes for variation operators, such as recombination and mutations. The fitness of new individuals, called children, is evaluated. Survivor selection, or replacement, selects which genomes from the old and new population will survive in the next generation. The process is repeated until a termination criterion is reached, typically a set number of evolutionary cycles sometimes called iterations or generations. Individuals are elite if there exists no other individual in the present population with a better fitness. Elitism is an algorithm feature where a specified number of elite individuals pass to the next generation.

5.2.5 BPO Experts Interview

This section presents a sample of results from an interview of 28 optimization experts that took place in 2011. Each interview included 25 questions. The complete study report results can be found in Attia (2012) and Attia *et al.* (2013). The most important findings of this report are listed here; namely, the major obstacles and opportunities of integrating optimization techniques in Net ZEB design.

The major obstacles of integrating optimization techniques in Net ZEB design can be classified under two main categories: (1) soft obstacles and (2) hard obstacles. The main

four soft obstacles – those based on attitudes, processes, and skills – and their frequency are listed as follows:

– Low return and the lack of appreciation among the AEC industry (19).

– Lack of standard systematic approach to perform optimization; in most cases researcher follow many different methods and *ad hoc* approaches without a structure and categorization in use (16).

– Requirement of high expertise (11).

– Low trust in the results (5).

The interviewees indicated that in practice, there is a lack of awareness and confidence on the use of optimization. Also, it is very important that users understand the optimization process. There is a large educational need before BPO gets applied routinely in the design process. Regarding the hard or technical obstacles, the interviewees' comments and their frequency is listed as follows:

– Uncertainty of simulation model input (27)

– Long computation time (24)

– Missing and uncertain information on costs (19)

– Difficulty of problem definition (objectives arrangement, constraint violation) (12)

– Lack of software environments integrating and linking simulation and optimization seamlessly (16)

– Low interoperability and flexibility of models for exchange between different design, construction, simulation, cost estimation, and optimization tools (11)

– Lack of environment with friendly GUI allowing postprocessing and visualization techniques (7).

The interviewees agreed that computation time is very long and this may inhibit the initial take-up of optimization in practice. The optimization process also magnifies the idea of "rubbish-in-rubbish-out" since rather than simulate a single design solution, the errors or inaccuracies in a simulation are exposed across a wide range of the design space. This may lead to a need for better education and improved user interfaces for simulation, as well as more work on the uncertainty associated with simulation models.

According to the interviewees, BPO has been applied successfully in numerous Net ZEB projects. However, the building simulation community still rarely uses optimization and little investment has been made to advance BPO. Interviewees indicated that many opportunities exist in integrating simulation-based BPO in Net ZEB design and operation. The most mentioned opportunities include the following:

– *Supporting the decision making for Net ZEB design*. Many elements, including government policy that pushes the design of low-energy buildings, have driven the rise of building performance simulation. At present, any increase in the use of optimization will be driven by the extent to which it aids design decision making. In this respect, one of the most powerful forms is multi-objective optimization, since it gives a set of solutions that lie on the trade-off between two or more conflicting design objectives. The trade-off can be used to explore the impact of less capital investment on the

increase in carbon emissions. This kind of information is useful in decision making of Net ZEB, requires little effort, and generates different ideas and alternatives.

– *Designing innovative integrated Net ZEBs with smart and efficient thermal (and visual) comfort control systems* is difficult to achieve because it involves complex dynamic interactions. Optimization algorithms can help in finding the optimal and near-optimal solutions regarding the design and sizing of passive and active energy systems and finding the balance between demand and production.

– *Achieving cost-effective Net ZEBs* by analyzing and synthesizing multi-physics systems that may include passive and active facades, lighting controls, natural ventilation, HVAC, and storage of heat in the building structure combining advanced technologies, such as micro-CHP, BIPV, BIPV/T, solar thermal collectors, and microwind turbines. The complexity of such systems poses a serious challenge to designers. The use of BPO is an opportunity to inform designers of optimal and cost-effective design decisions during building design and operation.

– *Allowing optimal systems scheduling through Model Predictive Control (MPC)* taking into account the dynamics of Net ZEB systems and anticipated future energy load. When solving the optimal control problem using the MPC algorithm, it determines near-optimal control settings during design and operation are determined and the load-matching problem is addressed.

5.3 Application of Optimization: Cost-Optimal and Nearly Zero-Energy Building

5.3.1 Introduction

According to the recast of the European Energy Performance of Buildings Directive (EPBD-r) (European Parliament and Council, 2010), the minimum energy performance requirements of buildings should be set with the aim of achieving cost-optimal levels for buildings, building units, and building elements (Constantinescu, 2010). Higher-energy performance levels, like net-zero energy, should also be economically feasible. The EPBD indicates that all new buildings should be "nearly zero-energy buildings" (Nearly ZEB) by the end of 2020, and two years prior to that for public buildings. According to the Recital 15 of the EPBD-r

> As the application of alternative energy supply systems is not generally explored to its full potential, alternative energy supply systems should be considered for new buildings, regardless of their size, pursuant to the principle of first ensuring that energy needs for heating and cooling are reduced to cost-optimal levels
>
> (European Parliament and Council, 2010).

These alternatives should range from those in compliance with the current regulations to solutions that realize Nearly ZEBs. Those should also include various options for renewable energy generation.

Finding optimal solutions requires exploring the environmental and economic viabilities of all compatible designs (Constantinescu, 2010). Figure 5.8 shows the cost-optimal curve that would be found from the exploration where the environmental and economic viabilities are presented in terms of PEC (Primary Energy Consumption) and dLCC (Difference in Life Cycle Cost) per square meter of a building, respectively. The dLCC is the difference between the LCC for any design and that for the reference one. The lowest

part of the curve (the economic optimum) is the cost-optimal range of solutions. The part of the curve to the right of the economic optimum represents solutions that underperform in both aspects (environmental and economic). The left part of the curve, starting from the economic optimum point, represents the optimal solutions toward Nearly ZEB, where the extreme left of the curve is the Net ZEB optimal solution.
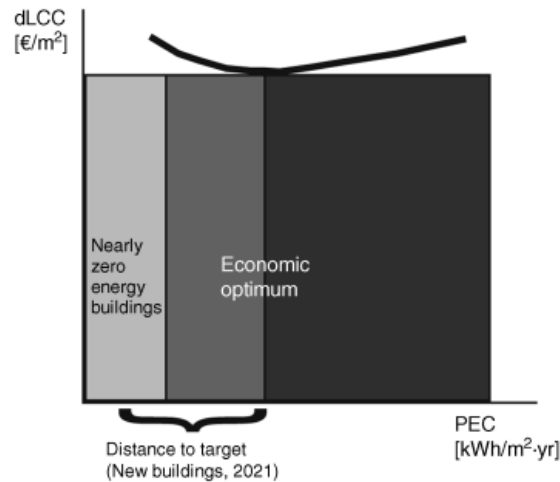
Fig. 5.8 Cost-optimal curve

Here, we summarize a multi-stage optimization method for cost-optimal and Nearly ZEB solutions in line with the EPBD-recast 2010. The method (Hamdy, Hasan, and Siren, 2013) provides efficient, transparent, and time-saving explorations:

– *Efficient exploration* is performed by combining a two-step optimization approach (PR_GA) (Hamdy *et al.*, 2009, Hamdy, Hasan, and Siren, 2009) and a detailed building performance simulation program (IDA-ICE 4.0). In the first optimization phase, a single-objective deterministic algorithm is used to minimize the two-objective functions (PEC and dLCC) one by one, sequentially, then to minimize the first objective considering maximum value of the second as a constraint. From the evaluations' history of the first optimization step, optimal solutions are found by sorting code and fed as a seed (a good initial population sample) to the second optimization step, continuing the optimization process by multi-objective genetic algorithm, which is a variant of the Non-dominated Sorting Genetic Algorithm-II (NSGA-II) by Deb *et al.* (2002). This two-step optimization approach improves the quality and the repeatability of the optimization results,

– *Transparent exploration* is presented via multistage optimization showing the effect of the design-variable combinations on the objective and constraint functions,

– *Time-saving exploration* is achieved by speeding up the exploration by avoiding the unrealistic/unfeasible design-variable combinations and using presimulated results instead of running time-consuming simulations (when possible).

5.3.2 Case Study: Single-Family House in Finland

In order to find optimal trade-off relations between PEC and dLCC for a single-family house in the cold climate of Finland, a multi-stage optimization method is proposed to explore more than 3×10^9 ($16 \times 8 \times 13 \times 3 \times 3 \times 4 \times 3 \times 2 \times 4 \times 31 \times 71$) combinations of the design-variable options (Table 5.1). The dLCC is calculated for 30 years. The design

variables are selected to cover packages of measures ranging from compliance with the requirements of the current Finnish building code (C3-2010) to combinations that realize Nearly ZEBs (e.g., *U*-values typical of a Passivhaus, photovoltaic, and solar thermal collectors). The variables include a number of external wall, roof, and floor insulation thicknesses, three building tightness levels, three window types, four shading methods, three heat recovery units, two cooling options, four heating systems, and different sizes of on-site solar systems. The detailed description of the design variable option can be found in Hamdy, Hasan, and Siren (2013). A reference case is calculated according to the National Building Code of Finland C3-2010. The life cycle costs of the candidate solutions are calculated relative to the reference case one. Considering the impact of the design variables on the objective functions (PEC and dLCC), the exploration is performed in three stages:

- *Stage*-1 aims to find the optimal combinations of the design variables that influence the building thermal performance (heating, cooling, and thermal comfort) of the house, that is, building envelope parameters and a heat recovery ventilation system;

- *Stage*-2 assesses the economic and environmental viability of the studied primary heating/cooling systems to the optimal building combinations (packages) found in *Stage*-1; and,

- *Stage*-3 investigates improving the economic and/or environmental viability of the optimal combinations of building envelope parameters and HVAC systems assessed in *Stage*-2. *Stage*-3 addresses the renewable energy systems as supplementary systems.

Table 5.1 Design variables

	Design Variable	Description	Options
1	U-value of the external wall [W m^{-2} K^{-1}]	From 0.17 to 0.07	16
2	U-value of the ceiling [W m^{-2} K^{-1}]	From 0.09 to 0.07	8
3	U-value of the floor [W m^{-2} K^{-1}]	From 0.17 to 0.08	13
4	Building air tightness levels (at 50 Pa) [1/h]	2, 1, 0.5	3
5	Window type (all with Wood–aluminum frames)	Triple-Laminated glass (Air filled), Triple-Laminated glass (Argon filled), or Quadruple Laminated (Argon filled)	3
6	Shading type	External blinds, horizontal laths, Blinds between the outer panes, horizontal laths, Blinds between the inner panes, horizontal laths, or Internal blinds, horizontal laths	4
7	Heat recovery type	Cross-flow heat exchanger, Counter-flow heat exchanger, or Regenerative heat exchanger	3
8	Cooling options	No cooling or small cooling unit	2
9	Heating system	Direct electricity with electrical radiators (EH), oil boiler with water radiators (OB), district heating with water radiators (DH), GSHP with radiant floor heating (GSHP)	4
10	Solar thermal collector area	From 0 to 30 m²	31
11	PV collector area	From 0 to 70 m²	71

The aim of *Stage*-1 is to find representative energy-efficient building designs, irrespective of the type of heating, cooling, and energy supply systems. In order to achieve this, the space heating energy demand of the house and the present worth (PW, defined later) of the influencing measures (insulation level, building tightness, window type, shading method, and heat recovery type) are minimized, while a penalty function is applied when the summer comfort criterion ($DH_{27} \geq 150$ °Ch) is violated.

According to the Finnish building code D3, degree-hours (DH_{27}) are used to measure the summer overheating risk

$$DH_{27} = \sum_{i=1}^{8760} dT_{27}\Delta t \qquad (5.2)$$

$$\begin{cases} (T_i - 27) > 0 \Rightarrow dT_{27} = (T_i - 27) \\ (T_i - 27) \le 0 \Rightarrow dT_{27} = 0 \end{cases}$$

where T_i is the mean air temperature [°C] at the warmest zone and Δt is a 1 h time period [h].

The minimization work is performed by the two-step optimization approach (PR_GA) mentioned earlier. The first objective (space heating energy demand), to be minimized in *Stage*-1, presents the major energy demand in the residential building in the cold climate. The second objective (PW) presents the initial and replacement costs (IC and RC) of the key influencing ESMs (external wall, ceiling, and floor insulation levels, building tightness, window type, shading method, and heat recovery type). PW is calculated as follows:

$$PW = \sum_{i=1}^{7} IC_i + \sum_{i=1}^{7} RC_i \qquad (5.3)$$

5.3.3 Results

Figure 5.9 presents the optimization results of *Stage* 1. The results are two optimal trade-offs (Group 1 and 2) between the space heating energy and the present worth (PW) of the influencing ESMs. Group 1 presents the optimal building designs, which satisfy the summer overheating criterion (Eq. (5.2)), while Group 2 presents the designs that do not fulfill the criterion. Groups 1 and 2 consist of 19 and 13 solutions, respectively. Group 2 packages are not eliminated as noncomfort solutions, because they could be addressed with mechanical cooling. In terms of LCC, implementing RES (e.g., photovoltaic) might improve the economic feasibility of the mechanical cooling solutions by covering a portion of their electricity demands. The feasibility of using the cooling and RES systems will be investigated in forthcoming optimization stages 2 and 3, respectively.
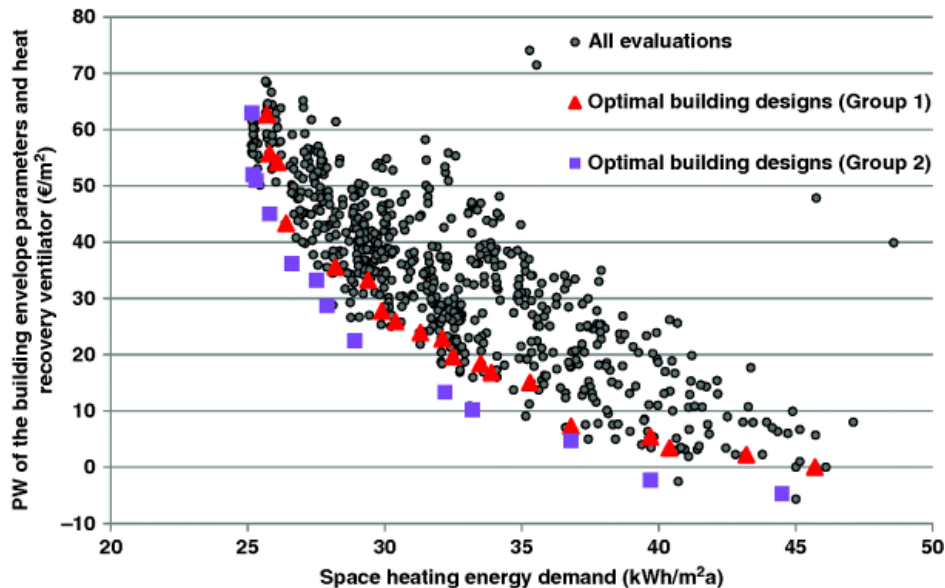
Fig. 5.9 Stage-1 optimization results (Hamdy, Hasan, and Siren, 2013)

[Figure 5.10](#) presents the results of *Stage*-2. The results are the dLCC and PEC of *Stage*-1 optimal solutions (Group 1 and 2; [Figure 5.9](#)) when the offered primary heating systems (direct electrical, district heating, oil fire boiler, and GSHP) are installed. In line with the EPBD-recast 2010, 3% real interest rate (r) and 2% energy price escalation rate (e) are used as recommended values. Primary energy factors, efficiencies, capital and service costs, subscription fees, and energy prices ([Table 5.2](#)) are used to calculate *Stage*-2 s results (dLCC vs PEC). Since the current investigation aims to compare different designs in the specified solution space, the absolute value of the LCC is not calculated, but the difference ($dLCC_i$) between the LCC for any design (LCC_i) and that for the reference one (LCC_r) is calculated

$$dLCC_i = LCC_i - LCC_r, \tag{5.4}$$

$$LCC = \sum_{j=1}^{11} IC_j + \sum_{j=5}^{11} RC_j + MC + OC + C$$

where IC is the investment costs of the 11 investigated design variables ([Table 5.1](#)), *RC* is the replacement cost of the replaced building elements and systems (e.g., window, shading, heat recovery unit, etc.), and MC is the maintenance costs of the heating systems ([Table 5.2](#)). OC is the operating cost of energy and *C* is a constant for other costs, such as construction and design cost, *i* denotes indexes for the design solution, and *j* is an index for the design parameter ([Table 5.1](#)).
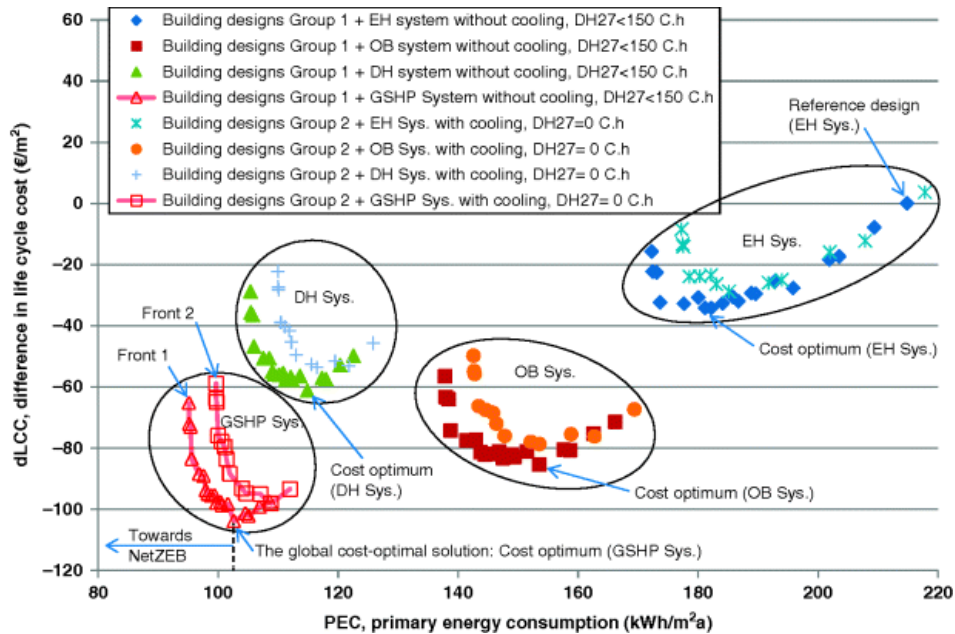
[Fig. 5.10](#) Stage-2 postprocessing results (Hamdy, Hasan, and Siren, 2013)

Table 5.2 Primary heating systems (Hamdy, Hasan, and Siren, 2013)

System	Capital Cost Formula [€]	Service Cost [€/a]	Subscription Fee [€/a]	Energy Price [€ cent/kWh]	η_{SHS} [%]	η_{DHWS} [%]	η_{dist} [%]	Primary Energy Factor (F)
Direct electricity with electrical radiators (EH)	50 kW$_p$ + 2700	30	83	13.5 10.9[a]	100	88	94	1.7
Oil boiler with water radiators (OB)	286 kW$_p$ + 7143	135	83	6.12	81	81	87	1
District heating with water radiators (DH)	50.5 kW$_p$ + 9050	40	404[b]	6.5	94	94	87	0.7
GSHP with floor heating (GSHP)	592.5 kW$_p$ + 12155	145	83	13.5 10.9[a]	300	250	84	1.7

[a] The price of day electricity (13.5 € cent/kWh) on weekdays, from Monday to Friday, 7 A.M. to 8 P.M. The price of night-time electricity (10.9 € cent/kWh) at other times.

[b] Besides the 83 € annual fee for the electrical connection, 321 € is added for district heating connection.

The PEC considers the total energy use of the building including heating, cooling, ventilation, lighting, pumps, and fans, as well as the energy-saving from RES. The PEC is calculated by using nonrenewable primary energy factors F according to the energy source (Table 5.2)

$$\text{PEC} = F\,\text{SH}_{\text{delivered}} + F\,\text{DHW}_{\text{delivered}} + F\,\text{Ele}_{\text{delivered}}$$ (5.5)

$$\text{SH}_{\text{delivered}} = (Q_h/\eta_{\text{dist}})/\eta_{\text{SHS}}$$

$$\text{DHW}_{\text{delivered}} = (Q_{DHW} - \text{d}Q_{DHW})/\eta_{\text{DHWS}}$$

$$\text{dEle}(t) = Q_c(t)/\text{COP}_{\text{Cu}} + \text{SH}_{\text{ele}}(t) + \text{DHW}_{\text{ele}}(t) + E_{\text{hv}}(t) + E_{\text{la}}(t) - \text{PV}_e(t)/\eta_{\text{inven}}$$

$$\text{Ele}_{\text{delivered}} = \sum_{t=1}^{t=8761} \max\{\text{dEle}(t),\,0\}$$

where

DHW	Domestic hot water
DHW_{ele}	The electrical portion of domestic hot water,
Ele	The electricity consumption,
E_{vh}	The electrical consumption of the HVAC system
E_{la}	The electrical consumption of the appliances and lighting
PV	Photovoltaic
PV_{e}	The useful electricity produced by photovoltaic system.
Q_{c}	Space cooling energy demands,
Q_{h}	Space-heating energy demands
SH	Space heating
SHele	The electrical portion of space heating,
η_{SHS}	Efficiency of the space heating system
η_{DHWS}	Efficiency of the domestic hot water system
η_{dist}	Distribution efficiency of the heating system
η_{inverter}	Efficiency of the photovoltaic inverter

Equation (5.5) divides the energy demands (Q_{h}, Q_{DHW}-dQ_{DHW}, Q_{c}) by the annual efficiencies to calculate the delivered ones (SH$_{\text{delivered}}$, DHW$_{\text{delivered}}$, dEle$_{\text{delivered}}$). According to the heating application (SH or DHW), two efficiencies (η_{SHS} and η_{DHWS}) are considered as being consistent with the Finnish regulation. Based on the installed space heating system (electrical radiator, water radiator, or floor heating), the distribution efficiency (η_{dist}) is assumed to be 94, 84, or 87%, respectively (Table 5.2). The implementation of a flat-plate solar thermal collector reduces the domestic hot water demand Q_{DHW} by dQ_{DHW}. When mechanical cooling (Q_{c}) is needed, it will take place for a short period. Therefore, the coefficient of performance for the cooling system for nominal operating conditions (25 °C outdoor air temperature) is used. Only 13 simulations are carried out to calculate the cooling energy required for the Group 2 solutions. Implementing the mechanical cooling options, with a 25 °C indoor temperature setpoint, reduced the DH$_{27}$ (Eq. (5.2)) of the Group 2 solutions to zero.

Figure 5.11 presents improvements to the environmental viability of *Stage*-2 building envelope and HVAC-system optimal solutions (Figure 5.10, front 1 and 2) by implementing optimal sizes of RES systems (solar-thermal and photovoltaic collector areas). A simulation-based optimization model is developed, using MATLAB 2008b and IDA ESBO (a building performance simulation program that includes the possibility of implementing RES systems), to find the optimal combinations of the front 1 and 2 solutions and the RES options (from 0 to 31 m² solar thermal collector areas and from 0 to 71 m² photovoltaic array area). The optimization is performed by PR_GA approach (Hamdy, Hasan, and Siren, 2009).
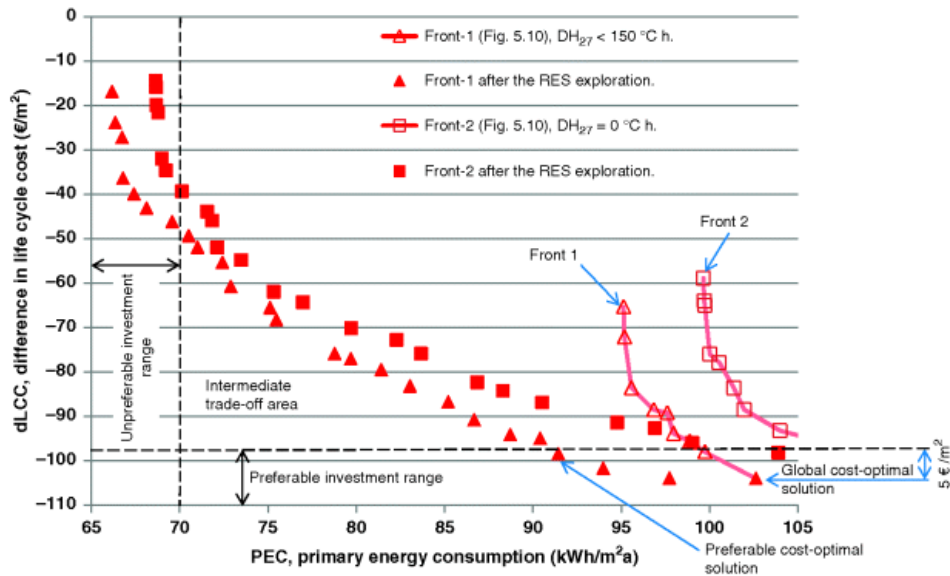
Fig. 5.11 Stage-3 optimization results (Hamdy, Hasan, and Siren, 2013). Note that the fronts labeled "Front 1" and "Front 2" are the same as those in Figure 5.10

5.3.4 Final Considerations About the Case Study

According to the Directive 2010/31/EU, the minimum LCC solution (global cost-optimal solution) should be used by Member States when setting the minimum energy performance requirements. However, a slightly higher LCC solution could be preferable if it reduces the PEC significantly. Figure 5.11 shows the global and preferable cost-optimal designs. The difference between the LCC of the cost-optimal solutions is 5 €/m². Based on the resulted global and preferable cost-optimal solutions, the calculated minimum energy performance level of the single-family house in Finland is 103 or 92 kWh/m² a of primary energy, depending on the decision maker's preferences. These cost-optimal energy performance levels are 40 and 47% lower, respectively, than that for the reference case defined by the current Finnish regulation.

5.4 Application of Optimization: A Comfortable Net-Zero Energy House

Optimization is a versatile technique that in this case study is used to identify the most suitable technical solutions to guarantee a comfortable environment inside a building and, hence, to minimize its energy needs for space conditioning. This design strategy is a rational and promising path toward Net ZEBs (Carlucci, Zangheri, and Pagliano, 2013; Pagliano, Zangheri, and Carlucci, 2010). The European standard EN 15251 (CEN, 2007) also suggests a path, which starts with optimizing the building envelope and its passive strategies by analyzing the building in free-floating mode; the indoor thermal comfort is assessed with respect to an adaptive comfort model (de Dear and Brager, 1998; Nicol and Humphreys, 2002). However, in case thermal comfort requirements cannot be met only with the building envelope and its passive strategies, efficient HVAC systems are then introduced, and thermal comfort requirements have to be verified against the Fanger comfort model (Fanger, 1970). In other words, this means designing the building envelope for achieving thermal comfort by using primarily passive strategies, so that, at the next

step (if required), efficient HVAC systems need only a limited amount of energy to provide the required thermal comfort conditions. At the same time, efficient lighting and electrical appliances have to be selected to reduce the electricity demand of the building. Then, the overall energy required by the building has to be covered by renewable energy preferably produced on-site (Marszal *et al.*, 2011).

An automated computer-based workflow is applied to optimize a single family net zero-energy house in the Mediterranean climate. It uses EnergyPlus (Crawley *et al.*, 2001) as the building performance simulation engine, guided by GenOpt (Wetter, 2001) as the optimization engine. The identified optimal building variant reduces both the seasonal long-term discomfort indices to values lower than 10% in free-floating mode. A monocrystalline PV field with an area of 21.0 m² can provide all the needed energy required by the house (on a yearly basis and via exchange with the electric grid). In case the identified optimal building variant is equipped with a reversible electric heat pump, the thermal comfort requirements expressed with respect to the Fanger comfort model are met with a delivered energy for heating of 7.3 $kWh_{el}/(m^2 a)$ and for cooling (sensible plus latent) of 9.5 $kWh_{el}/(m^2 a)$. Therefore, the area of the monocrystalline PV field shall rise to 32.6 m² to meet the overall primary energy consumption of the home. It should be noted that the proposed optimization approach can be applied to any residential or commercial building prototype.

5.4.1 Description of the Building Model

The case study is a detached single-family house, located in Mascalucia (CT) in Southern Italy (Figure 5.12). The single-family home is composed of one occupied story and one unoccupied basement used as a technical room. Its net floor area is 148 m² and its net conditioned volume is 445 m³.
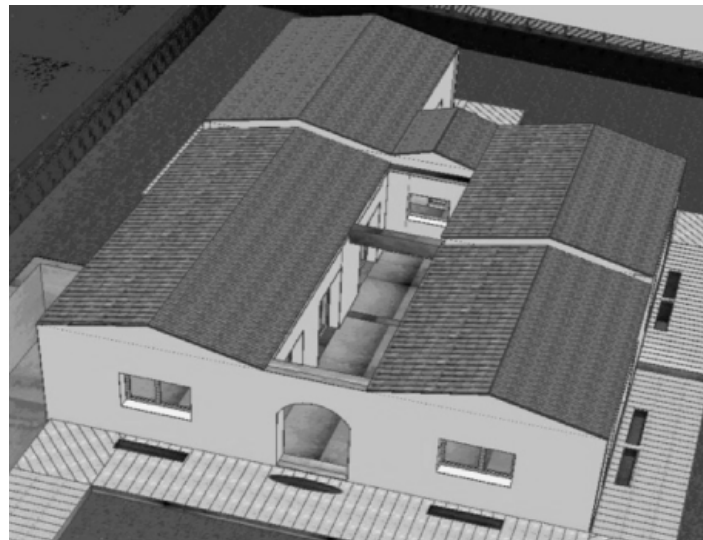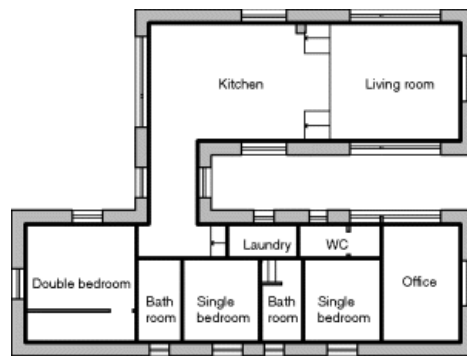
Fig. 5.12 (a) Three-dimensional model. (b) Plan and indication of the thermal zones of the house

Mascalucia is in the zone "Csa" (Köppen, 1930), characterized by a temperate climate with dry summer, also called Mediterranean climate. To simulate the most representative local weather conditions, a typical weather year was constructed using the measured hourly weather data recorded from 2003 to 2009 in Pedara (CT), located 1 km far from the construction site.

The daily typical occupancy schedule and the daily typical lighting and electrical appliances usage rates were defined according to owner information about intended use. In order to provide a comfortable indoor air quality, the minimum air change rate of 0.6 h^{-1} was estimated according to EN 15251 and a mechanical ventilation system, equipped with a high-efficiency (92%) heat recovery unit, was provided.

The energy simulations of the building were run with EnergyPlus release 6.0.0.23 and the default physical models for calculating heat exchanges were selected to take into account the trade-off between accuracy and computation time: (i) the update frequency for calculating sun paths was set to 20 days, (ii) the heat conduction through the opaque envelope was calculated via the conduction transfer function method with four time steps per hour, and (iii) the natural convection heat exchange near external and internal surfaces was calculated via the adaptive convection algorithm (Department of Energy (DOE), 2013).

5.4.2 The Adopted Methodology and the Statement of the Optimization Problem

The energy design of a building is a multi-variable problem, which can accept different sets of solutions. The number of design alternatives can be very large and not all of them can be simulated in a time span compatible with the design phase of a building. In order to explore a very large number of building variants compatible with the design phase in a relatively short time, the adopted methodology consists of (i) identifying the design parameters of the building to be optimized, (ii) identifying the options for every design parameter, (iii) running the dynamic energy simulations of the building in free-floating mode via EnergyPlus, and (iv) driving the selection of the design parameters via an optimization engine.

The design parameters and the options for each of them are reported in Table 5.3. The number of all available building variants is larger than 17 million. The single values have been introduced in the optimization as discrete variables.

Table 5.3 Design parameters and their values used in the optimization run

Design Parameters	Physical Quantities	Possible Alternatives
External wall construction	U-value (W m^{-2} K^{-1}) | Time shift (h)	0.149|14.0; 0.147|9.9; 0.152|4.6; 0.261|12.9; 0.254|9.2; 0.246|2.9; 0.387|12.6; 0.387|8.9; 0.410|2.2.
Roof construction	U-value (W m^{-2} K^{-1}) | Time shift (h)	0.154|12.3; 0.148|8.2; 0.147|4.9; 0.252|13.1; 0.251|9.4; 0.248|5.0; 0.398|12.3; 0.404|9.3; 0.381|5.8.
Floor construction	U-value (W m^{-2} K^{-1}) | Time shift (h)	0.143|12.8; 0.150|9.6; 0.152|5.7; 0.250|13.1; 0.240|9.0; 0.246|5.4; 0.397|12.9; 0.401|9.3; 0.401|4.8.
Construction of glazing units on south-east façade	U-value (W m^{-2} K^{-1}) | SHGC (%)	0.586|36; 0.582|49; 1.099|38; 1.065|53; 2.667|34; 2.667|75.
Construction of glazing units on south-west façade	U-value (W m^{-2} K^{-1}) | SHGC (%)	0.586|36; 0.582|49; 1.099|38; 1.065|53; 2.667|34; 2.667|75.
Construction of glazing units on north-east/north-west facades	U-value (W m^{-2} K^{-1}) | SHGC (%)	0.586|36; 0.582|49; 1.099|38; 1.065|53; 2.667|34; 2.667|75.
Construction of glazing units on the central court facade	U-value (W m^{-2} K^{-1}) | SHGC (%)	0.586|36; 0.582|49; 1.099|38; 1.065|53; 2.667|34; 2.667|75.
Control strategies for shading devices	Set-point	Indoor air temperature >25 °C; Outdoor air temperature >25 °C; Global irradiance on window >100 W/m².
Opening pivoted windows	Percentage of the window area open (%)	0; 100.
Opening double-leaf windows	Percentage of the window area open (%)	0; 50; 100.

The optimization engine GenOpt release 3.1.0 was used to minimize specified seasonal thermal discomfort objectives. The *Long-term Percentage of Dissatisfied* (LPD) in the ASHRAE adaptive version (Carlucci, 2013) is used to quantify predicted long-term thermal discomfort by a weighted average of discomfort over the thermal zones and over time.

$$\text{LPD} = \frac{\sum_{t=1}^{T} \sum_{z=1}^{Z} \left(p_{z,t} \cdot \text{ALD}_{z,t} \cdot h_t \right)}{\sum_{t=1}^{T} \sum_{z=1}^{Z} \left(p_{z,t} \cdot h_t \right)} \tag{5.6}$$

where t is the counter for the time step of the calculation period, T is the last progressive time step of the calculation period, z is the counter for the zones of a building, Z is the total number of the zones, $p_{z,t}$ is the zone occupation rate at a certain time step, h_t is the

duration of a calculation time step (e.g., 1 h) and $\text{ALD}_{z,t}$ is the ASHRAE Likelihood of Dissatisfied calculated inside a certain zone at a certain time step, given by the equation

$$\text{ALD} = \frac{\exp\left(0.008 \cdot \Delta T_{op}^2 + 0.406 \cdot \Delta T_{op} - 3.050\right)}{1 + \exp\left(0.008 \cdot \Delta T_{op}^2 + 0.406 \cdot \Delta T_{op} - 3.050\right)} \tag{5.7}$$

where ΔT_{op} is the absolute value of the difference between the indoor operative temperature and the optimal comfort temperature calculated according to the ASHRAE adaptive model. This index, calculated for summer and winter, constitutes the two objective functions of the optimization problem.

Assuming a preference for building variants that minimize their distance from the *optimum*, *scalarization* is used to solve the bi-objective optimization problem, by adopting the weighted exponential sum method with the *utility function*, *U*,

$$U = \sum_{i=1}^{n} w_i [F_i(\mathbf{k})]^p \quad : \quad F_i(\mathbf{k}) > 0 \quad \forall i \tag{5.8}$$

where w_i are the weighting factors of each objective function, such that $w_i > 0$, and $\mathbf{k}$ is the vector of the values of each design parameter. For this optimization problem, there is not an apparent reason to weigh the two objective functions differently, thus the weighting factors were set to 1. The exponent *p* was set to 2. Hence, the utility function is a distance function that measures the squared distance between a certain solution point and the utopia point, so that the shorter the distance, the better the building variant. This optimization approach does not provide a set of optimal solution belonging to the Pareto frontier, but only one optimal solution; this simplifies the activity of the final user, but the use of the utility function forces the result of optimization.

The *PSO algorithm* was selected due to its robustness and efficiency to converge toward the global minimum (Hopfe, 2009). The setting parameters of the algorithm are: the type of algorithm was the PSO with inertia weight, neighborhood topology was von Neumann, neighborhood size was 5, 20 particles, 30 generations, cognitive acceleration was 2.8, social acceleration was 1.3, initial inertia weight was 1.2, and final inertia weight was zero. The number of simulation runs for the optimization was 600.

5.4.3 Discussion of Results

The optimization procedure identified an optimal solution that provides both winter and summer aforementioned Long-term Percentage of Dissatisfied lower than 10% when the building is in free-running mode during the whole year ().
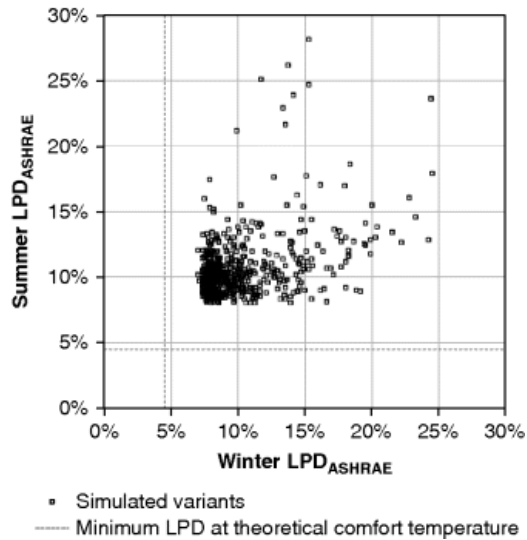
Fig. 5.13 Result of optimization run

The main features of such optimal building variant are: (i) external walls and the roof with very low steady-state thermal transmittance, $U = 0.15$ W/(m² K), to reduce heat exchange with outdoor in both the seasons; (ii) the floor with relatively high steady-state transmittance, $U = 0.40$ W/(m² K), to use the basement as a heat sink during summer without compromising excessively winter performance; (iii) the roof and the floor with high time shift ($S > 12$ h) and external walls with a lower time shift (8 h $< S <$ 10 h); (iv) for every orientation, glazing units should have very low values of transmittance, $U_g = 0.59$ W/(m² K), and solar factor, $g = 0.36$, to reduce uncontrolled heat exchange through glazing; (v) only on the southeast orientation (such orientation is characterized by large glazed surfaces in this building), glazing units have a slightly higher solar factor, $g = 0.49$, to enhance solar gain during winter; (vi) the opening of windows (only in the living rooms) should be maximized during summer nights to provide maximum night natural ventilation cooling; (vi) the control parameter of solar shading (e.g., the beam solar radiation incident on a window) has to be selected and set considering the trade-off with other nonthermal performance aspects, such as daylighting and glare risk for occupants. The optimal building variant, in free-floating mode, offers indoor operative temperatures compatible with the 80% acceptability class of the Standard ASHRAE 55 (ASHRAE, 2010); only few deviations occur outside the adaptive comfort zone defined in such standard (Figure 5.14).
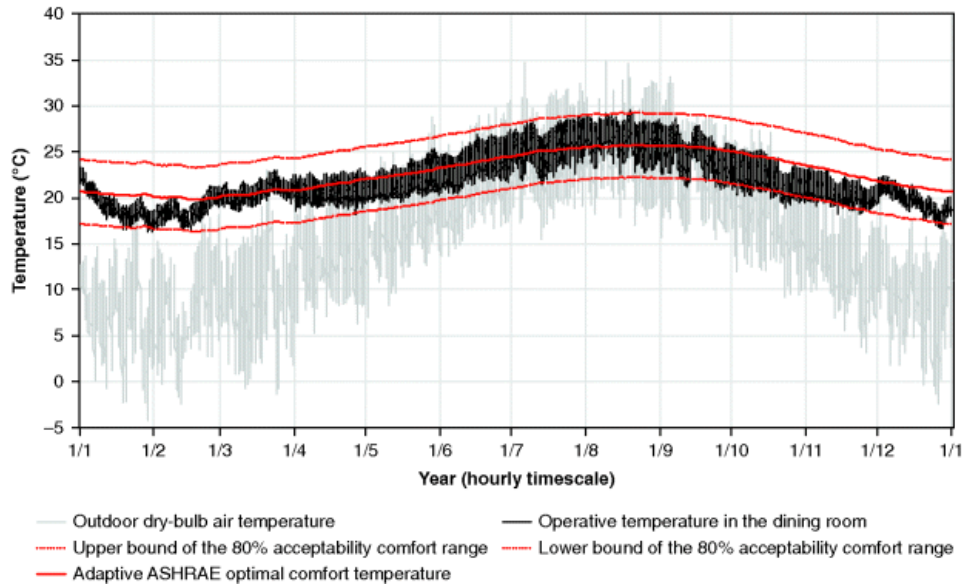
Fig. 5.14 Operative temperature profiles inside the living room in free-floating mode compared with the 80% acceptability range of the ASHRAE adaptive model

Regarding its energy performance, the delivered energy breakdown in energy uses is (i) 3.1 $kWh_{el}/(m^2\,a)$ for ventilation; (ii) 6.5 $kWh_{el}/(m^2\,a)$ for lighting; (iii) 15.3 $kWh_{el}/(m^2\,a)$ for electric equipment; (iv) 2.6 $kWh_{el}/(m^2\,a)$ for the production of domestic hot water (DHW). The annual required electricity is 4087 kWh_{el}. The slope of the roof is 22° and it was assumed that a southwest-facing PV array was installed with monocrystalline modules. The single module has a nominal efficiency of 18.4% and a nominal power generation of 300 W. It is also assumed that its overall DC to AC derate factor is 0.77. Under these conditions, 13 PV panels, with a covered roof area of 21.2 m², cumulate an overall nominal peak power of 3.9 kW_p, and should theoretically generate 4911 kWh_{el} per year. Thus, the expected electricity production should be slightly higher than the whole electrical demand ([Figure 5.15](#)).
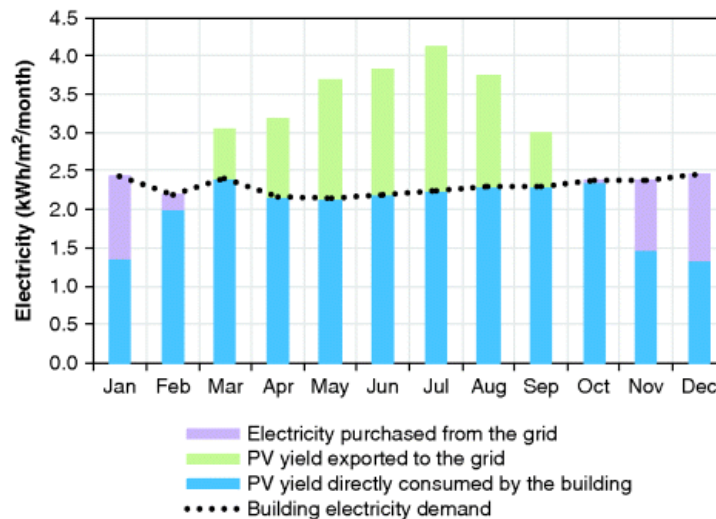
Fig. 5.15 Electricity balance of the home including PV yield

If these indoor conditions are not considered satisfactory for the occupants, a mechanical heating and cooling system (e.g., a reversible heat pump) may be added to the optimal variant in order to control the indoor environment in a stricter manner. In this new scenario, indoor thermal comfort requirements shall be referred to the Fanger comfort model. The seasonal optimal comfort temperatures (used as setpoint operative temperatures in the model) were calculated assuming a metabolic activity of 1.2 met, a summer clothing resistance of 0.5 clo, a winter clothing resistance of 1.0 clo, an air velocity of 0.1 m/s, a relative humidity of 50% and an external work set at zero met. The boundary temperatures of the comfort range were calculated in compliance with the Category II of EN 15251 suitable for new buildings mechanically conditioned (Figure 5.16).

Legend:
- Outdoor dry-bulb air temperature
- Fanger upper boundary of the winter comfort range
- Optimal comfort temperature for winter
- Fanger lower boundary of the winter comfort range
- Operative temperature in the dining room
- Fanger upper boundary of the summer comfort range
- Optimal comfort temperature for summer
- Fanger lower boundary of the summer comfort range

Fig. 5.16 Operative temperature profiles inside the living room in conditioned mode compared with the Category II range of the Fanger model

According to this scenario, the building is all-electric and delivered energy is alternative to primary energy to express the breakdown of energy uses. Annual delivered electric energy for space heating amounts to 7.3 kWh/(m² a) and annual delivered electric energy for space cooling (sensible plus latent) is 9.5 kWh/(m² a). Thus, the overall electricity demand is 7253 kWh per year, that is, 48.8 kWh/(m² a). Therefore, using the previous assumptions about the PV array, 20 PV panels are sufficient to cover the whole electricity demand of this scenario. The PV array is characterized by a nominal peak power of 6.0 kW_p and covering an area of 32.6 m². The expected annual PV yield is 7580 kWh per year, hence the building, also in this scenario, is expected to produce (over a year) more electricity than it requires.

5.4.4 Final Considerations

A novel optimization procedure aiming at minimizing two seasonal long-term discomfort indices in a free-floating building is presented and it was used to support the design of a real building. This procedure identified an optimal building variant, which, in free-floating mode, offers indoor operative temperatures compatible with the 80% acceptability class of the Standard ASHRAE 55 with only few deviations outside such comfort zone.

If this optimal building variant is equipped with a heating and cooling system, its primary energy for space conditioning is much lower than primary energy for lighting, electrical appliances, DHW production, and ventilation. Finally, since annual primary energy required by the house amounts to 108 kWh/(m² a), the optimized building fulfills also the *Passivhaus* certification criteria of having a primary energy requirement lower than 120 kWh/(m² a). It should be noted that the modeling and the optimization approach outlined here can be applied to any residential or commercial building prototype.

5.5 Conclusion

Building simulation is becoming a major tool in the building design process. At present, any increase in the use of optimization will be driven by the extent to which it aids design decision-making, particularly for large projects. In this respect, one of the most powerful approaches is multi-objective optimization, since it provides a set of solutions and presents a trade-off between two or more possibly conflicting objectives. For instance, the trade-off can be used to explore the impact of lower capital investment on the increase in carbon emissions. Optimization can support a multidisciplinary design process by addressing all building design aspects in a holistic approach. This will enhance fully integrated Net ZEB designs where building designers can act to influence the direction of the optimization.

Despite the potential for building performance optimization, decision support, time, knowledge, lack of tools, and uncertainty are the themes that need to be addressed for its enhanced market penetration in the AEC industry. The factors that inhibit the uptake of BPO are not only related to the optimization techniques or the tools themselves, but also to the simulation models inputs, causing significant restraint in AEC industry take-up. From the evidence available and the presented case studies, the optimization process has generally been shown to be applicable to real design practice. For policymakers, it can facilitate development of incentive measures and policies that integrate many objectives, such as integration of renewables with energy efficiency measures, as well as optimized operation that reduces and shifts peak electricity demand while enhancing comfort.

References

American Society of Heating, Refrigerating and Air-Conditioning Engineers (ASHRAE) (2010) Standard 55 - Thermal environmental conditions for human occupancy (Atlanta, GA).
Athienitis, A.K., Torcellini, P., Hirsch, A., O'Brien, W., Cellura, M., Klein, R., Delisle, V., Attia, S., Bourdoukan, P., and Carlucci, S. (2010) Design, Optimization and Modelling Issues of Net-Zero Energy Solar Buildings. In EuroSun (Graz, Austria).
Attia, S. (2012) *Computational Optimisation for Zero Energy Building Design: Interviews with Twenty Eight International Experts*, Architecture et Climat, Louvain-la-Neuve: Université, catholique de Louvain, Louvain-la-Neuve, Belgium.
Attia, S., Hamdy, M., O'Brien, W., and Carlucci, S. (2013) Assessing gaps and needs for integrating building performance optimization tools in net zero energy buildings design. *Energy and Buildings*, **60**, 110–124.
Audet, C. and Dennis, J.E. (2002) Analysis of generalised pattern searches. *SIAM Journal of Optimization*, **13**, 889–903.
Brown, C., Glicksman, L., and Lehar, M. (2010) Toward zero energy buildings: optimized for energy use and cost. Paper presented at: SIMBuild fourth National Conference of

IBPSA-USA (New York City).

Bucking, S. (2013) Pathways to net-zero energy buildings: an optimization methodology. PhD thesis, Concordia University. Available at http://spectrum.library.concordia.ca/978083/1/Bucking_PhD_S2014.pdf.

Bucking, S., Athienitis, A., Zmeureanu, R., O'Brien, W., and Doiron, M. (2010) Design Optimisation Methodology for a Near Net Zero Energy Demonstration Home Paper presented at: EuroSun (Graz, Austria).

Bucking, S., Zmeureanu, R., and Athienitis, A. (2013) An information driven hybrid evolutionary algorithm for optimal design of a Net Zero Energy House. *Solar Energy*, **96**, 128–139.

Caldas, L. (2001) *An Evaluation Based Generative Design System: Using Adaptation to Shape Architectural Form*, MIT Press.

Caldas, L. (2008) Generation of energy-efficient architecture solutions applying GENE ARCH: An evolution-based generative design system. *Advanced Engineering Informatics*, **22**, 59–70.

Carlucci, S. (2013) *Thermal Comfort Assessment of Buildings*, vol. **1**, Springer, London.

Carlucci, S., Zangheri, P., and Pagliano, L. (2013) Achieving the Net zero-energy target in Northern Italy: lessons learned from an existing Passivhaus with earth-to-air heat exchanger. *Advanced Materials Research*, **689**, 184–187.

CEN (2007) EN 15251: Indoor Environmental Input Parameters for Design and Assessment of Energy Performance of Buildings Addressing Indoor Air Quality, Thermal Environment, Lighting and Acoustics, (Brussels, Belgium: European Committee for Standardization).

Charron, R. and Athienitis, A.K. (2006) The Use of Genetic Algorithms for a Net-Zero Energy Solar Home Design Optimisation Tool. Paper presented at: PLEA (Geneva, Switzerland.).

Choudhary, R. (2004) *A Hierarchical Design Optimisation Framework for Simulation based Architectural Design*, University of Michigan, USA.

Christensen, C. (2005) BEopt: Software for identifying optimal building designs on the path to zero net energy. Paper presented at: ISES Solar World Congress, (Orlando, FL, USA.).

Christensen, C. and Anderson, R. (2006) BEopt software for building energy optimisation: features and capabilities (National Renewable Energy Laboratory).

Constantinescu, T. (2010) *Cost Optimality Discussing Methodology and Challenges with the Recast Energy Performance of building Directive*, The Buildings Performance Institute Europe (BPIE), Brussels.

Crawley, D.B., Lawrie, L.K., Winkelmann, F.C., Buhl, W.F., Huang, Y.J., Pedersen, C.O., Strand, R.K., Liesen, R.J., Fisher, D.E., Witte, M.J. *et al.* (2001) EnergyPlus: Creating a new-generation building energy simulation program. *Energy and Buildings*, **33**, 319–331.

de Dear, R.J. and Brager, G.S. (1998) Developing an adaptive model of thermal comfort and preference. Paper presented at: 1998 ASHRAE Winter Meeting (San Francisco, CA, USA: ASHRAE).

Deb, K., Pratap, A., Agarwal, S., and Meyarivan, T. (2002) A fast and elitist multiobjective genetic algorithm: NSGA-II. *IEEE Transactions on Evolutionary Computation*, **6**, 182–197.

Department of Energy (DOE) (2013) EnergyPlus Input/Output Reference.

Eberhart, R. and Kennedy, J. (1995) Particle swarm optimisation. Paper presented at: IEEE International Conference on Neural Networks (Perth, Australia).

Eiben, A.E. and Rudolph, G. (1999) Theory of evolutionary algorithms: a bird's eye view. *Theoretical Computer Science*, **229**, 3–9.

Eiben, A.E. and Smith, J.E. (2003) *Introduction to Evolutionary Computing*, Springer, London, UK.

Elbeltagi, E., Hegazy, T., and Grierson, D. (2005) Comparison among five evolutionary-based optimization algorithms. *Advanced Engineering Informatics*, **19**, 43–53.

European Parliament and Council (2010) Energy performance of buildings, Vol L. 153/13, (recast) edn (Luxembourg: Official Journal of the European Union).

Fanger, P.O. (1970) *Thermal Comfort: Analysis and Applications in Environmental Engineering*, Danish Technical Press, Copenhagen.

Feoktistov, V. (2006) *Differential Evolution: In Search of Solutions*, Springer, New York, USA.

Flager, F., Welle, B., Bansal, P., Soremekun, G., and Haymaker, J. (2009) Multidisciplinary process integration and design optimization of a classroom building. *Journal of Information Technology in Construction*, **1**, 595–612.

Goldberg, D. (1989) *Genetic Algorithms in Search, Optimization and Machine Learning*, Addison-Wesley, New York.

Hamdy, M. (2012) *Combining Simulation and Optimisation for Dimensioning Optimal Building Envelopes and HVAC Systems*, Aalto University, Finland.

Hamdy, M., Hasan, A., and Siren, K. (2009) Combination of optimization algorithms for a multi-objective building design problem. Paper presented at: IBPSA: 11th International Building Performance Simulation Association Conference (Glasgow, Scotland).

Hamdy, M., Hasan, A., and Siren, K. (2013) A multi-stage optimization method for cost-optimal nearly-zero-energy building solutions in line with the EPBD-recast 2010. *Energy and Buildings*, **56**, 189–203.

Hasan, A., Vuolle, M., and Siren, K. (2008) Minimisation of life cycle cost of a detached house using combined simulation and optimisation. *Building and Environment*, **43**, 2022–2034.

Hayter, S.J., Torcellini, P.A., Hayter, R.B., and Judkoff, R. (2001) The energy design process for designing and constructing high-performance buildings. In CLIMA 2000 (Naples, Italy).

Hooke, R. and Jeeves, T.A. (1961) " Direct search" solution of numerical and statistical problems. *Journal of the Association for Computing Machinery*, **8**, 212–229.

Hopfe, C. (2009) Uncertainty and sensitivity analysis in building performance simulation for decision support and design optimisation (Eindhoven University).

Kampf, J. and Robinson, D. (2010) Optimisation of building form for solar energy utilisation using constrained evolutionary algorithms. *Energy and Buildings*, **42**, 807–814.

Kampf, J., Wetter, M., and Robinson, D. (2010) A comparison of global optimization algorithms with standard benchmark functions and real-world applications using EnergyPlus. *Journal of Building Performance Simulation*, **3**, 103–120.

Kennedy, J. and Eberhart, R. (1997) A discrete binary version of the particle swarm algorithm. Paper presented at: IEEE, International Conference on Neural Networks (Indianapolis, USA).

Köppen, W.P. and Geiger, R. (1930) *Handbuch der Klimatologie*, Gebrüder Borntraeger, Berlin.

LBNL and Wetter, M. (2011) *GenOpt, Generic Optimisation Program*, Lawrence Berkeley National Laboratory, University of, California, California.

Marszal, A.J., Heiselberg, P., Bourrelle, J.S., Musall, E., Voss, K., Sartori, I., and Napolitano, A. (2011) Zero Energy Building – A review of definitions and calculation methodologies. *Energy and Buildings*, **43**, 971–979.

Nicol, J.F. and Humphreys, M.A. (2002) Adaptive thermal comfort and sustainable thermal standards for buildings. *Energy and Buildings*, **34**, 563–572.

Nielsen, T. (2002) *Optimisation of Buildings with Respect to Energy and Indoor Environment*, Technical University of Denmark.

Ooka, R. and Komamura, K. (2009) Optimal design method for building energy systems using genetic algorithms. *Building and Environment*, **44**, 1538–1544.

Pagliano, L., Zangheri, P., and Carlucci, S. (2010) A Way To Net Zero Energy Buildings For Italy: How The Earth-To-Air Heat Exchanger Could Contribute To Reach The Target In Warm Climates. In EuroSun 2010 – International Conference on Solar Heating, Cooling and Buildings (Graz).

Pardalos, P. and Resende, M. (2012) *Handbook of Applied Optimisation*, Oxford University Press, Oxford, UK.

Pedersen, F. (2007) *A Method for Optimizing the Performance of Buildings*, Technical University of Denmark.

Poli, R., Langdon, W., and McPhee, N. (2008) A field guide to genetic programming.

Price, K., Storn, R., and Lampinen, J. (2005) *Differential Evolution: A Practical Approach to Global Optimization*, Springer-Verlag, Heidelberg, Germany.

Renders, J. (1994) Hybridizing genetic algorithms with hill-climbing methods for global optimization: two possible ways. Paper presented at: IEEE World Congress on Computational Intelligence (Orlando, FL).

Snyman, J. (2005) *Practical mathematical optimisation – An Introduction to Basic Optimisation Theory and Classical and New Gradient-Based Algorithms*, Springer Science+Business Media, New York, USA.

Verbeeck, G. (2007) Optimisation of extremely low energy residential buildings. In Department of Civil Engineering (Leuven, Belgium: Catholic University of Leuven).

Wang, W. (2005) *A Simulation-Based Optimisation System for Green Building Design*, Concordia University, Montreal Quebec.

Wang, W., Rivard, H., and Zmeureanu, R. (2006) Floor shape optimization for green building design. *Advanced Engineering Informatics*, **20**, 363–378.

Wetter, M. (2001) GenOpt® - A Generic Optimization Program. Paper presented at: Building Simulation 2001 Conference (Rio de Janeiro).

Wetter, M. (2004) *Simulation-Based Building Energy Optimization*, University of California at Berkeley.

Wetter, M. and Polak, E. (2004) Building design optimization using a convergent pattern search algorithm with adaptive precision simulations. *Energy and Buildings*, **37**, 603–612.

Wetter, M. and Wright, J. (2004) A comparison of deterministic and probabilistic optimisation algorithms for nonsmooth simulation-based optimisation. *Building and Environment*, **39**, 989–999.

6
Load Matching, Grid Interaction, and Advanced Control

JoséCandanedo, Jaume Salom, Joakim Widén, and Andreas Athienitis

6.1 Introduction

Load matching[1] refers to the degree of agreement or disagreement between the on-site generation and building load profiles. *Grid interaction*, a closely related topic, refers to the pattern of energy exchange between a building and the utility grid, and its impact on the overall load of the grid ([Figure 6.1](#)). Both issues are collectively designated by the acronym LMGI (Salom *et al.*, 2011). This chapter provides an overview of these topics in the context of Net ZEBs. Quantitative indices used to describe LMGI are presented. This chapter also discusses design and control approaches that may be used to achieve LMGI objectives, with particular emphasis on model-based predictive control (MPC) in buildings.
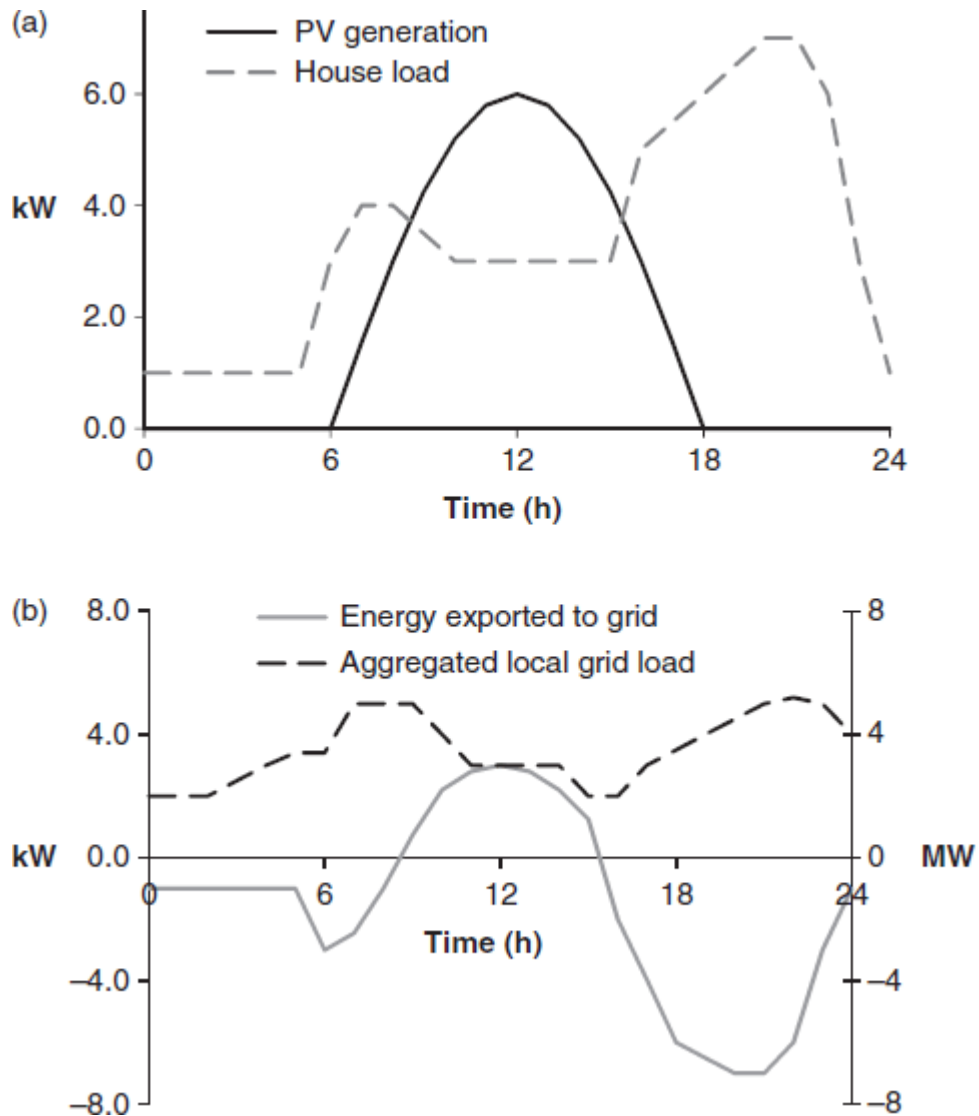
Fig. 6.1 Load matching (a) refers to the relationship between a building's own generation and load. Grid interaction (b) alludes to the relationship between the energy exported/imported to the grid and the load conditions of the grid itself

6.1.1 Beyond Annual Energy Balance

Achieving net-zero energy performance over a yearly period is a worthwhile goal in itself. However, keeping in mind that the final objective is the reduction of the energy use and environmental impact associated with buildings, designers and policymakers must consider energy balances evaluated at shorter time scales, such as monthly, weekly, daily, or hourly periods. It is not enough to simply

look at the measurements recorded at the metering point, and then weigh the energy delivered to the grid against the energy taken from it at the end of the year. Such a "bookkeeping" practice would leave aside the effects of local demand fluctuations, the impact of the variability of building-integrated photovoltaics, and the seasonal and daily variations in the cost of energy. A serious approach to Net ZEB design or to the development of adequate policies for the promotion of Net ZEBs must include a discussion of LMGI.

A perfect balance at all times between load and generation – which would result in a nearly autonomous building, quasi-independent from the grid (Marszal *et al.*, 2011) – is not necessary. It is often convenient to deliver power to the grid at times of high demand and thus reduce the need of utilities to start "peaking" power plants. In contrast, a utility grid with high penetration rates of renewable energies might encounter difficulties when dealing with surplus generation. In this case, increasing the power use by the building can actually be beneficial.

6.1.2 Relevance of LMGI Issues

6.1.2.1 Peak Demand and Peak Power Generation

Control of peak demand is one of the most widely known issues related to LMGI. In any energy system, the key limiting factor is the maximum power (i.e., maximum energy transfer rate) required to accomplish a given task. For example, the maximum heating power required to keep a comfortable temperature in a space determines the size of the equipment installed.

Peak demand is often identified with peak *electric* demand. The case of electricity is special, since unlike other energy carriers (e.g., fuels) electric energy cannot be readily stored. The concept of the net-zero energy building was introduced to account for this fact: in a Net ZEB, the grid is used as a virtual electric energy storage system. Supplying the entire electric load of a building at all times by using only on-site resources would be technically challenging and cost-prohibitive. District heating networks share to some extent the peak load problems of electric grids (Dotzauer, 2002; Heller, 2002) although

large-scale energy storage is more readily available for the case of thermal distribution networks (McClenahan *et al.*, 2006).

Distributed peak power *generation* is another issue that will become progressively important (maybe even more so) than peak demand. With increasingly higher penetration rates of building-integrated photovoltaics and other distributed energy generation resources, utility grids will have to accommodate power flows in the "opposite" direction with an infrastructure (transformers, breakers, etc.) that has not been designed for this mode of operation.

The electric grid was built in a hierarchical way, in which energy flows from power plants through transmission lines, and then to the distribution networks that deliver the power to the customers. Along this way, transformers change voltage levels. Distribution system operators (DSOs) must deliver electric power to the customers at the distribution level with performance indices within certain limits (e.g., voltage). The layout of distribution grids and the sizing of cables and transformers are carefully planned in order to comply with these parameters.

At low penetration rates, the effect of distributed generation might be beneficial, for example by helping to maintain voltage levels. However, some problems are likely to appear in distribution grids with high penetration rates, including power quality issues (overvoltage, harmonic distortion), overloading of components, and increased local losses (Katiraei, Mauch, and Dignard-Bailey, 2007). The concept of *hosting capacity* (loosely defined as the amount of distributed generation that can be safely handled by the grid) has been introduced (Bollen and Hassan, 2011). Grid-interaction indicators will be critical to adequately characterize and manage bidirectional energy flows.

6.1.2.2 Load Management in the Grid and Buildings

Load management has traditionally been an important issue for the utility grid. Higher peak loads imply starting "peaking" power plants, which are often more expensive, inefficient and polluting. In the electricity spot market, the cost of electricity is higher during peak hours. A utility may be forced to buy electricity from neighboring jurisdictions at very high cost. In the long run, increasing peak loads

will lead to the construction of additional power plants as well as transmission and distribution infrastructures, with the associated economic and environmental cost. At shorter time scales, highly fluctuating loads complicate the already challenging problem of matching the customers' needs with the power supplied from power plants while maintaining voltage and frequency requirements. Load management is a problem that is present at different scales (e.g., national grids, regional grids, and distribution networks).

In contrast with the utility grid, load management and peak load reduction have received somewhat less attention in buildings. Buildings have been largely considered as passive consumers that take energy from the grid or other energy carriers to supply their own needs as they appear. When peak load reductions are achieved, it is often not the result of a deliberate effort, but the by-product of energy efficiency measures (e.g., adding insulation results both in less energy use and smaller peaks). Regardless of the metering point or energy carrier considered, *annual* energy use has been the yardstick traditionally used when describing the performance of a building. Peak load prevention adds an additional element of complexity to the task of maintaining a comfortable temperature while fulfilling all the other functions required in a building, such as communications, lighting and waste disposal.

A building designer or operator has at least two important reasons for aiming to reduce peak loads:

- *Utility savings*. Depending on the tariff structure in place, reducing peak loads can offer significant savings in utility bills. In the case of commercial buildings, utilities and DSOs apply rate structures that heavily penalize energy use during peak hours, via demand charges or time-of-use (TOU) rates. In these buildings, a combination of technologies and heuristic operational strategies are used to reduce peak loads. Traditionally, flat rates have often been applied to residential customers, and as a result, home owners tend to be less concerned about peak-shedding measures. However, this situation is rapidly changing, and time-of-use rates may soon become more widespread even in residential buildings.

- *Equipment size reductions*. Lower cooling and heating peak loads allows for the use of smaller (i.e., lower rating) installed

equipment. The customary practice today, recommended by professional organizations (ASHRAE, 2005), is the installation of mechanical equipment sized to match peak cooling or heating loads. These loads can effectively be reduced by incorporating more thermal mass in the building itself (Braun, 1990) or by adding thermal inertia as part of the building technical systems. The use of thermal energy storage (TES) devices allows a "time decoupling" of the building loads from the cooling or heating power provided by the equipment ([Figure 6.2](#)).

$$Q_{direct} + Q_{TES} = Q_{bldg}$$

Direct action
Q_{direct}

| Heating or cooling source | | Building |

Charge
Q_{charge}

Discharge
Q_{TES}

Thermal energy storage (TES)
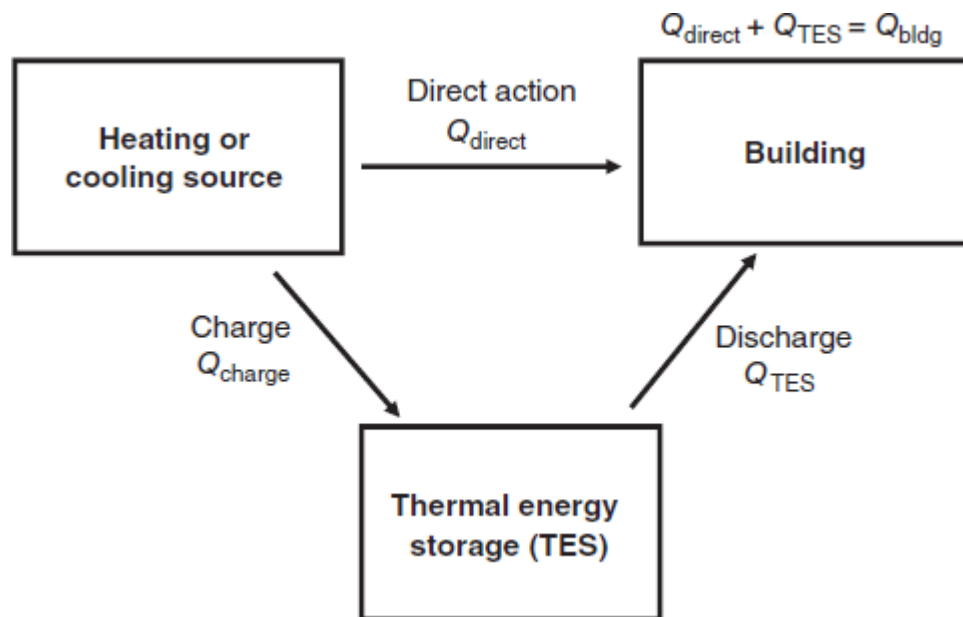
Fig. 6.2 Use of a thermal energy storage device to decouple the main equipment from the building load. Adapted from (ASHRAE, 2007)

Although not necessarily a primary motivation, reducing peak loads also increases the degree of autonomy of the building, which is a desirable feature in the case of remote locations or when security requirements are essential. Other incentives may include qualification for a specific energy label or compliance with legal, environmental, or safety regulations.

Customarily, and unfortunately, building operation and control have been relegated to the last stages of the building design process. As load management in buildings becomes an increasingly important issue, the development of appropriate control strategies during the design stage should play an increasingly relevant role.

6.1.2.3 Smart Grid and Other Technology Drivers

The problem of load matching and grid interaction lies at the interface between "smart buildings" and "smart grid" (Figure 6.3). Although the concept of smart grid is still evolving, it commonly refers to technologies that enable an intensive, automated use of bidirectional data flow among utility grid components (generators, substations, customers) to improve the performance of the entire system in terms of cost, resource utilization, and reliability, and to favor the development of distributed energy generation.
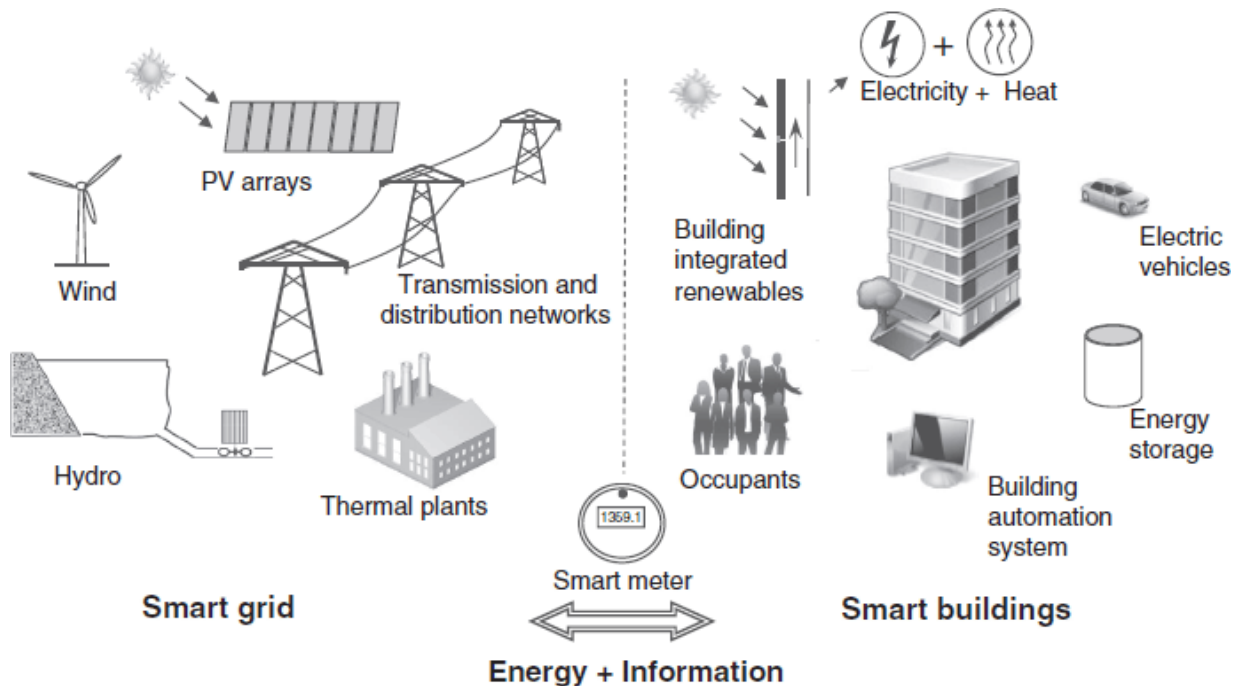
Fig. 6.3 Links between the smart grid and smart buildings

According to the European Energy Regulators Group for Electricity and Gas (ERGEG), a smart grid can be defined as

> An electricity network that can cost-efficiently integrate the behavior and actions of all users connected to it – generators, consumers and those that do both – in order to ensure economically efficient, sustainable power system with low losses and high levels of quality and security of supply and safety.
>
> (ERGEG, 2010)

Large-scale deployment of smart grids is still years ahead; it will take significant technology development and a daunting amount of

financial resources. However, the prospects are very promising. A smart grid would enable, for example, the transmission of pricing signals in real time to large customers so that the local demand can be adjusted accordingly.

A predictive control system designed for a utility grid with smart grid capabilities must consider the aggregated loads and total generation foreseen for a community or a group of buildings. The energy used or generated by a group of buildings will be a function of the expected weather. In a grid with renewable energy, the expected output of wind or photovoltaic generators can also be taken into account.

The building automation system (BAS) of a smart building can also make use of energy price information from the smart grid, along with weather and occupant forecasts, to determine the best strategy for its own energy management problem, concerning decisions about the charge or discharge of energy storage devices, temperature set-points, schedules for charging or discharging electric vehicles, appliance usage, and so on. The BAS will also decide whether it is convenient to sell the power generated by building-integrated renewables or to use it internally.

It is still a matter of debate whether the smart grid should be able to directly intervene in the operation of the building systems (as in demand response schemes[2]), provide pricing signals or power constraints to the BAS to enable it to make its own decisions, or apply a combination of both approaches. The answer will likely depend on the particularities of each jurisdiction.

Smart meters – which permit two-way, near real-time communication between a building and the grid – are one of the technologies enabling the migration toward advanced load management strategies in commercial and residential buildings. In contrast with conventional meters, which record only cumulative values, smart meters permit obtaining real time pricing signals for the BAS, thus providing clear information about incentives.

Energy storage technologies, either electric or thermal, are a major technology driver for load management. Energy storage allows planning the use of energy resources over time. Increasing the

capacity for energy storage significantly adds to the potential of advanced control strategies to improve the system performance.

Building-integrated or on-site renewable energies (always required in Net ZEBs) are another technology factor driving the evolution toward advanced load management strategies.

6.2 LMGI Indicators

6.2.1 Introduction

Given the complexity of the issue, many different quantitative indicators have been developed to describe LMGI (Salom *et al.*, 2011; Verbruggen, 2011). These indicators permit evaluating the impact of adopting advanced control or incorporating energy storage devices, and allow making comparisons between buildings, between operation strategies, or performance changes at different days, months or years. The indicators described here refer to buildings using electricity as their only energy carrier.

Figure 6.4 illustrates the relevant on-site energy flows used to calculate LMGI indicators, as well as the symbols used to represent them in this document (Table 6.1).
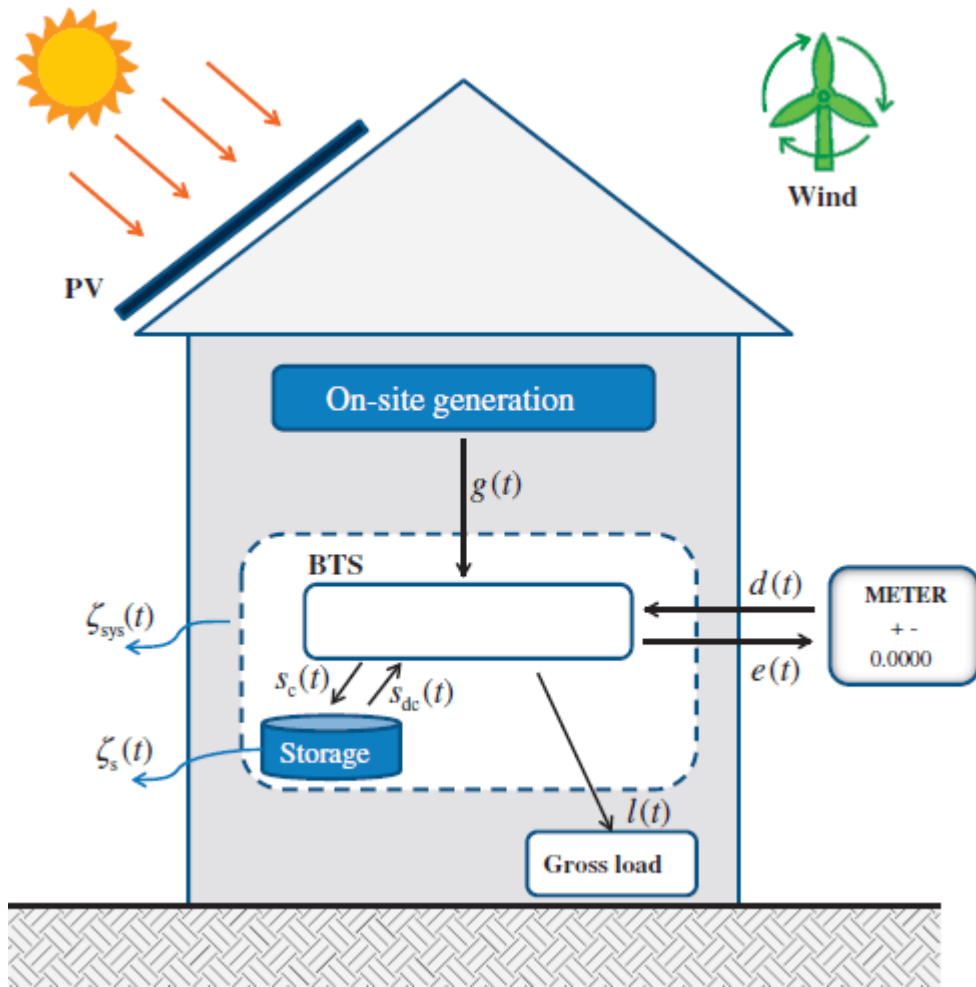
Fig. 6.4 Energy flows at a Net ZEB

Table 6.1 Nomenclature

Variables	Description
t	time
e, E	exported energy
d, D	delivered energy (by the grid)
ne	net exported energy
g	on-site generation
g_{net}	net on-site generation
g_{gross}	gross on-site generation
s_c	charging storage energy
s_{dc}	discharging storage energy
S	storage energy balance
U_s	internal storage energy
T	evaluation period
τ_1	start of the evaluation period
τ_2	end of the evaluation period
w	weighting factor
l	load
l_{net}	net load
l_{gross}	gross load
ζ	energy losses
ζ_g	generation energy losses
ζ_s	storage energy losses
ζ_{sys}	building technical systems energy losses (excluding storage)
ζ_l	load energy losses (e.g., distribution losses)
BTS	building technical systems
E_{des}	design/required connection capacity

Subindices	
d	delivered
e	exported
b	building

Equation (6.1) represents the energy balance in the building, considering that the difference between the energy used for charging and discharging the storage system is due to the variation of internal energy in the storage and the losses in the storage system itself (Eq. (6.2))

$$g(t) + d(t) = l(t) + \zeta_S(t) + \zeta_{\text{sys}}(t) + e(t) + \frac{dU_S}{dt} \tag{6.1}$$

$$s_c(t) = s_{dc}(t) + \zeta_S(t) + \frac{dU_S}{dt} \tag{6.2}$$

The difference between exported energy from the building to the grid, $e(t)$, and delivered energy, $d(t)$, is also known as the net exported energy represented by $ne(t)$:

$$ne(t) = e(t) - d(t) \tag{6.3}$$

The quantities shown in Figure 6.4 refer to instantaneous values. The integrated value of these quantities over time is used to evaluate the energy balance in a known period of time, between τ_1 and τ_2. In case that the difference between internal energy of the storage system at the beginning and the end of the time period, for example, one complete year, can be considered negligible, the balance equation is

$$\int_{\tau_1}^{\tau_2} g(t)\, dt + \int_{\tau_1}^{\tau_2} d(t)\, dt = \int_{\tau_1}^{\tau_2} l(t)\, dt + \int_{\tau_1}^{\tau_2} \zeta(t)\, dt + \int_{\tau_1}^{\tau_2} e(t)\, dt \tag{6.4}$$

6.2.2 Categories of Indicators

The choice of LMGI indicator depends on the objective (assessment, control, description, certification, etc.) and on the information at hand. Salom *et al.* (2011) have identified four different kinds of indicators depending on (a) whether they refer to load matching or grid interaction and (b) whether they can be obtained with on-site data only or need additional information (e.g., grid conditions). The four resulting categories of indicators, as shown in Table 6.2, are briefly discussed next. Some examples are presented for the case of all-electric buildings.

Table 6.2 Categorization of LMGI indicators (Salom *et al.*, 2011)

		Type of Indicator	
		Load matching	**Grid interaction**
Data Requirements	On-site load and generation	**I** Load match index (Voss *et al.*, 2010) Solar fraction (Widén, Wäckelgård, and Lund, 2009c) Cover factor (Verbruggen *et al.*, 2011) Self-consumption factor (Castillo-Cagigal *et al.*, 2010) Loss-of-load probability (Verbruggen *et al.*, 2011)	**II** Grid interaction index (Voss *et al.*, 2010) Capacity factor (Verbruggen *et al.*, 2011) Peak power indicators (Verbruggen *et al.*, 2011) Dimensioning rate (Verbruggen *et al.*, 2011) Grid citizenship tool (Colson and Nehrir, 2009)
	Additional data	**III** Mismatch compensation factor (Lund, Marszal, and Heiselberg, 2011) Market matching (Widén and Wäckelgård, 2010b)	**IV** Profile addition indicators (Widén and Wäckelgård, 2010b) Coincidence factor (Willis and Scott, 2000)

Category I. This category includes load matching indicators that do not need any additional information besides the load and generation profiles. The first four, namely the *load match index*, the *solar fraction*, the *cover factor*, and the *self-consumption factor*, contain essentially the same information (the fraction of the load covered by on-site generation), but they differ slightly on the mathematical

formulation or simply in the name. For example, the load cover factor (example shown in Figure 6.5) is defined as

$$\gamma_{\text{load}} = \frac{\int_{\tau_1}^{\tau_2} \min[g(t) - S(t) - \zeta(t), l(t)]\, dt}{\int_{\tau_1}^{\tau_2} l(t)\, dt} \tag{6.5}$$
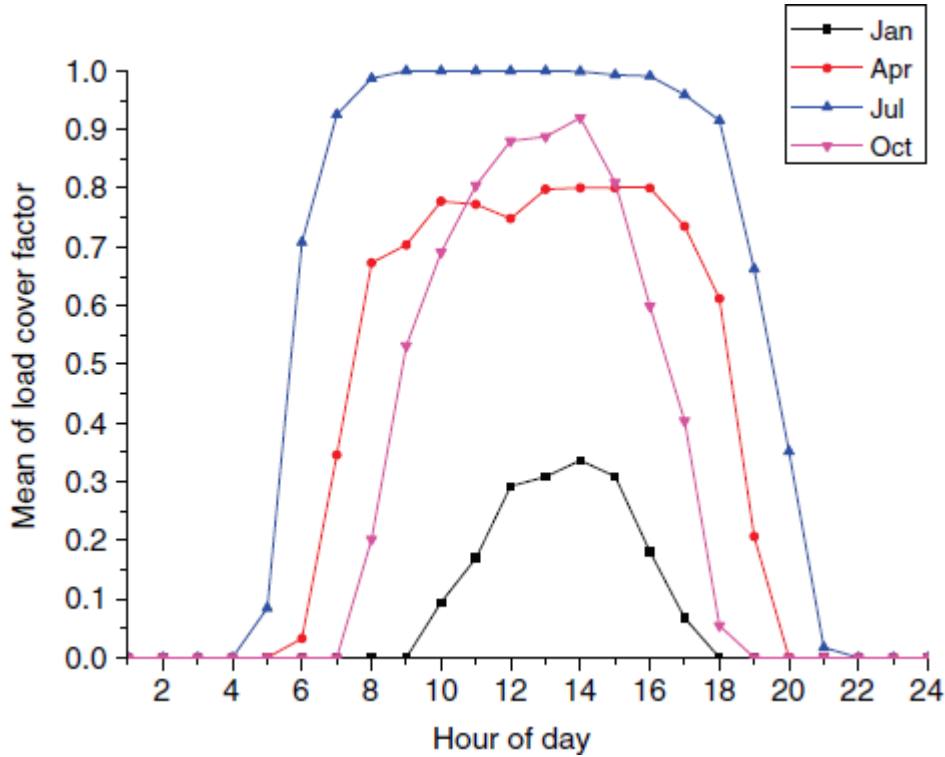
Fig. 6.5 Mean hourly values of load cover factor for different months in the year in an all-electric Net ZEB

Category II. This category collects indicators used to describe the grid interaction of a building using only *on-site* load and generation profiles. The *grid interaction index* shows the variability of the amount of purchased or delivered energy for a given time resolution (*i*), normalized by the highest absolute value in a given period.

$$f_{\text{grid},i} = \frac{ne(t_i)}{\max(|ne(t_i)|)}, \text{ over a period of interest} \tag{6.6}$$

Figure 6.6 shows the load match and grid interaction indices, for a near-Net ZEB in Portugal (Voss *et al.*, 2010). The different evaluation periods have respectively 12, 365, and 8760 data points, which correspond to monthly, daily, and hourly values. It is clear

from the figure that this building matches nearly all its *monthly* load in August ($f_{\text{load,month}}$ = 100%), but the *daily* match is not as good. As expected, as resolution increases (i.e., shorter time steps), more "gaps" are observable between generation and load.
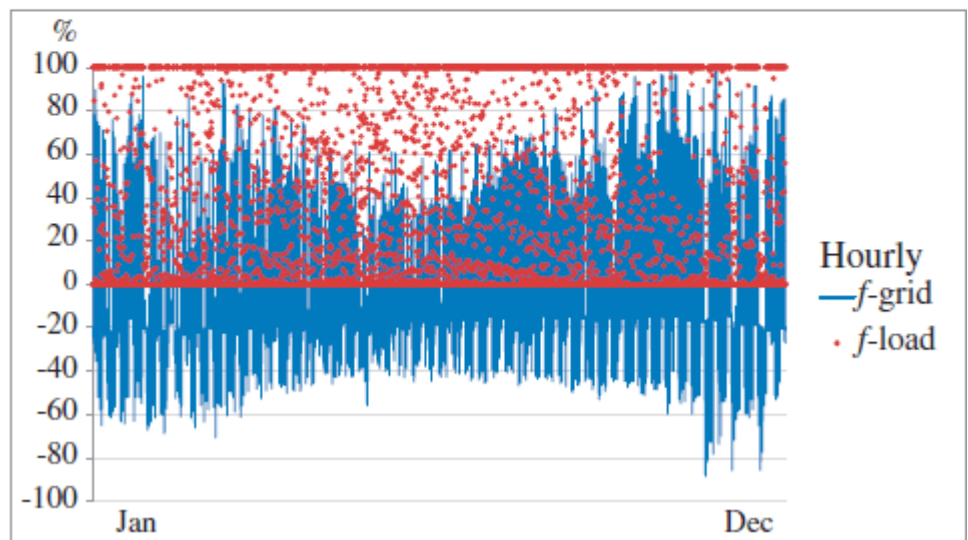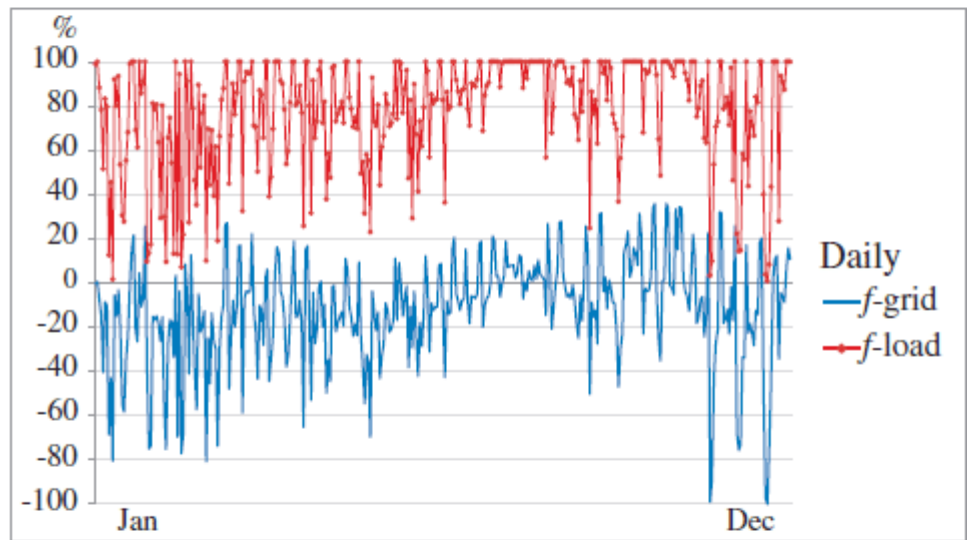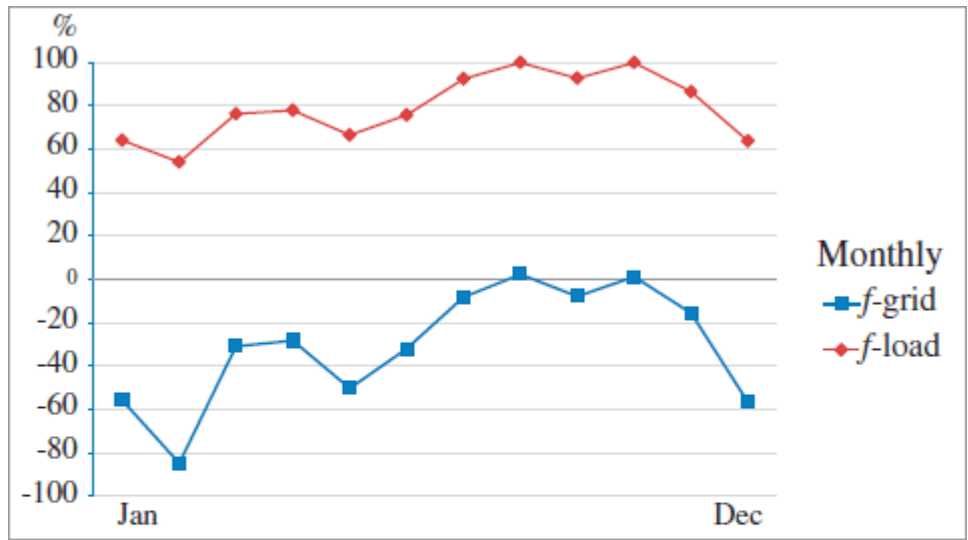
Fig. 6.6 Load match ($f_{\text{load},T}$) and grid interaction ($f_{\text{grid},T}$) indices for the Solar XXI Building in Portugal (Voss *et al.*, 2010). The load match index, similar to the load cover factor, is defined as

$$f_{\text{load},T} = \min\left(1, \frac{\text{on-site generation}}{\text{load}}\right) \times 100\,(\%) \text{ over a period of interest}$$

The *capacity factor*, as formulated in Verbruggen *et al.* (2011) shows the total energy exchange with the grid divided by the exchange that would have occurred at nominal connection capacity. It provides a measure of the utilization of the grid connection. The capacity factor is defined as

$$CF_b = \frac{\int_{\tau_1}^{\tau_1} |ne(t)|\, dt}{E_{\text{des}} T} \tag{6.7}$$

where E_{des} is the nominal (or design) capacity of the "energy exporting" system (e.g., the nominal installed capacity between the building and the grid) and T is the time period between τ_1 and τ_2.

Category III. This category contains load matching indicators that require information beyond on-site load and generation. For example, the *mismatch compensation factor* (MMCF) is the quotient between the on-site generation capacity providing annual energy balance and the capacity that compensates economically for the mismatch (i.e., the capacity that makes total generated electricity worth as much as demanded electricity on an annual basis). As defined in Lund, Marszal, and Heiselberg (2011)

$$MMCF = \frac{C_{\text{COST BALANCE}}}{C_{\text{ENERGY BALANCE}}} \tag{6.8}$$

The MMCF requires information about electricity pricing. An MMCF<1 means that the system that compensates for the mismatch is smaller than the system giving a net-zero energy balance because generated electricity is, on average, worth more than demanded electricity (Lund, Marszal, and Heiselberg, 2011).

A similar index is the *market matching* indicator, proposed in Widén and Wäckelgård (2010b). The market matching indicator shows the

difference between the market values of delivered and bought energy, respectively $\tilde{P}(k)$ and $\tilde{L}(k)$, with a cost $C(k)$:

$$\Delta V = \sum_k \tilde{P}(k)C(k) - \sum_k \tilde{L}(k)C(k) \qquad (6.9)$$

Category IV. This category refers to grid interaction indicators requiring additional information beyond on-site data.

The *profile addition indicators* are evaluated for the aggregate load of a local distribution grid to show the marginal effect of adding a Net ZEB profile of a building. In this case, information of the aggregate load is required.

The *coincidence factor* is the fraction between the observed peak of a customer group and the sum of the individual peaks of each customer. It illustrates to what extent individual peaks coincide, and how much "smoothing" is observed when aggregating a large number of buildings. For a grid company, information on typical coincidence factors for different types of Net ZEBs would probably be interesting, since this information could be useful to size grid components (Willis and Scott, 2000). This indicator needs a set of Net ZEB grid interaction profiles to be evaluated.

6.3 Strategies for Predictive Control and Load Management

Several design and operational strategies can affect LMGI. These issues are related to the management of energy resources over time. Addressing LMGI implies looking at a building and its systems from a dynamic viewpoint, rather than a static one. Consequently, the introduction of additional *energy storage* capacity in the building and the implementation of *predictive control* are two complementary measures that can have a significant impact on LMGI. Some methods for energy storage and predictive control for buildings are presented in this section.

6.3.1 Energy Storage Devices

The role of an energy storage device is not to eliminate the need for the utility grid. Instead, an energy storage system must be conceived as a way of helping the building fill up the troughs of low energy generation over short time periods, providing a buffer.

6.3.1.1 Electric Energy Storage

In general, current battery technology does not allow storing an amount of electric energy that would be significant for a building at a reasonable cost, although efforts are being made in that direction (Lamonica, 2012). In off-grid buildings, such as those located in very remote or inaccessible locations, batteries can provide an economically attractive solution, but this is more the exception rather than the rule. A possible alternative for electricity storage is the use of fuel cells, but several practical shortcomings (cost, efficiency, size) prevent its widespread adoption for the time being.

Batteries in electric vehicles (EVs) or plug-in hybrid electric vehicles (PHEVs) provide an interesting potential for peak load shedding in buildings. Car batteries can store an amount of energy in the order of tens of kWh. With the electric installation commonly available in a household, charging an electric car might take many hours (at a charging power of about 3 kW). To charge an EV battery within a reasonable timeframe, special electrical installations are required to supply significant charging power (up to 50 kW). While such power requirements pose their own challenges for load management, the car battery can also be used to supply power to the building at a similar rate. For instance, in a "vehicle-to-home" scheme (V2 H) car batteries could supply some or all the power needed by appliances when operated during peak hours. The charge/discharge cycles of the EV battery will be scheduled considering factors such as the hours when the vehicle is parked, the tariff structure of the utility, and occupant habits, among others.

6.3.1.2 Thermal Energy Storage

The building thermal mass provides some energy storage capacity by allowing moderate temperature fluctuations – the so-called *passive* energy storage. This principle is used, for example, in night precooling strategies (i.e., the building is cooled before occupancy hours). Likewise, the indoor temperature of a passive solar house can

be allowed to increase because of solar gains, so that the building can "coast" for several hours without heating. In practice, however, passive energy storage is limited by thermal comfort constraints – for example, occupants might complain if the temperature is too low in the morning – and other limitations (esthetic, economical, functional, etc.), which limit the thermal inertia of the building. As the increase of thermal inertia has mostly positive benefits, research and pilot projects exist, which treat to adapt materials with high energy density to the walls (e.g., PCM – phase change materials).

Thermal energy storage is also a key element in building mechanical systems. It allows covering heating and cooling needs in an efficient and economical way, particularly domestic hot water (DHW). TES storage is present in HVAC and CHP systems worldwide both for cold storage (in the form of ice or chilled water) and heat storage. Heat storage technologies can be found at different degrees of technical development, from basic research to market-ready. These technologies include sensible heat storage (water tanks, aquifers, ground/soil), latent heat storage (ice banks, PCMs), and thermochemical heat storage. A TES device allows decoupling the generation of energy from its use in the buildings to cover the user's needs, both in conventional HVAC and DHW systems and in renewable solar thermal energy systems. Use of surplus renewable electrical power could be also one option to produce heat or cold and store it to be used when it is needed.

6.3.2 Predictive Control for Buildings

The large majority of control algorithms in buildings are based on simple feedback loops: a corrective action is taken when an error signal is observed, that is, when the measured output (feedback) deviates from a reference value. Typically, the corrective action consists of turning an actuator on or off (bang-bang control) or adjusting the position of the actuator depending on the magnitude of the error (P, proportional control), its evolution in time (I, integral control), or its speed of variation (D, derivative control). A PID controller combines the three indicators so that the control system aims to minimize the deviation (either or positive) from the set-point value.

Knowledge of the expected weather and occupancy patterns may be used to take preventative actions according to a predetermined set of rules. For example, if the maximum temperature is expected to exceed a threshold, cooling should start a couple of hours before to avoid high peaks near the beginning of the daytime period. Such an approach, rule-based predictive control (RBPC), provides a simple way to use projections.

Model-based predictive control (MPC) is the name given to a control approach consisting of using a mathematical model of a system together with information about expected disturbances to decide on the best course of action for the near future. In the case of a building, the disturbances are typically weather variables (temperature, solar radiation, humidity, wind speed, etc.) and the internal loads due to the occupants. Figure 6.7 compares MPC with a conventional control approach. Note that a TES device is included in the MPC approach, which allows better planning of the use of energy resources. In general, some kind of feedback action is still required in an MPC scheme to add robustness to the control strategy.
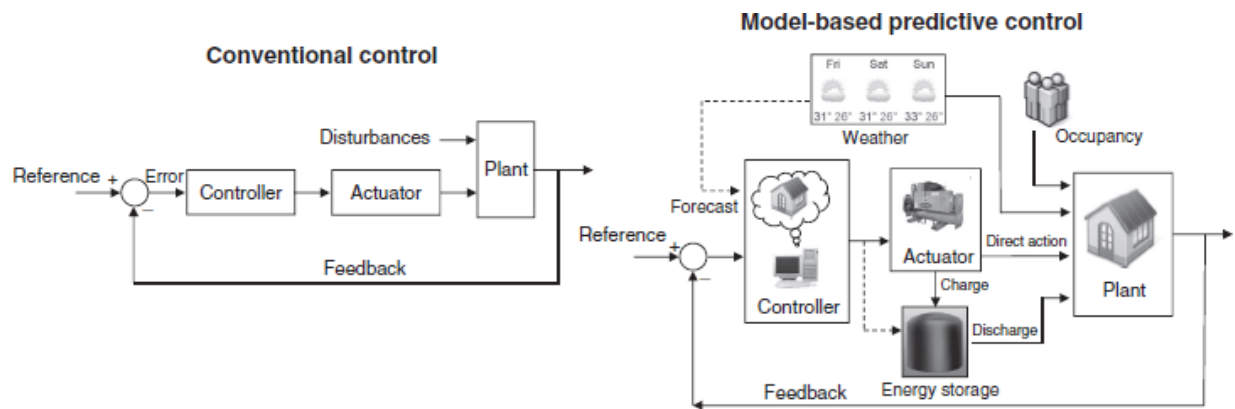
Fig. 6.7 Model-based predictive control compared to conventional control

Numerous studies have been made on MPC for buildings (Gyalistras and OptiControl Team, 2010; Henze and Krarti, 2005; Oldewurtel *et al.*, 2010a; Oldewurtel *et al.*, 2010b). Most of these studies have focused on the control of cooling systems. This is no coincidence; cooling equipment is electricity-driven, and therefore it can have an impact on peak loads. Since in most jurisdictions heating is delivered

by burning a fuel, such as natural gas, planning over a time horizon is less of an issue.[3.]

In a wider sense, any strategy making use of forecast information and a model of the building might be called an MPC strategy. With this understanding, a simple rule-based strategy, such as "if sunny weather is expected tomorrow, then delay the start of the heating system," would qualify as MPC. However, the term MPC is usually reserved for strategies involving some kind of formal mathematical optimization.

In MPC, an *objective function, J,* (typically total cost over a control horizon *H*) is defined.

$$J = \int_0^H C(t)\mathrm{d}t \qquad (6.10)$$

The cost, $C(t)$, may include the power associated with electric HVAC equipment (P_{HVAC}), hot water (P_{DHW}), appliances (P_{appl}), and auxiliary equipment (P_{aux}) multiplied by a time-of-use rate. For example

$$C(t) = \left[P_{\mathrm{HVAC}}(t) + P_{\mathrm{DHW}}(t) + P_{\mathrm{aux}}(t) + P_{\mathrm{appl}}(t)\right] \cdot \mathrm{TOU}(t) \qquad (6.11)$$

The problem consists in deciding a set of *control actions* that will minimize *J* given a set of *constraints*. These constraints can be, for example

$21\,^\circ\mathrm{C} \le T_{\mathrm{air}} \le 26\,^\circ\mathrm{C},$	required indoor air temperature	(6.12)
$55\,^\circ\mathrm{C} \le T_{\mathrm{DHW}} \le 65\,^\circ\mathrm{C},$	domestic hot water temp. limits	
$0 \le Q_{\mathrm{heat,space}} \le 15\,\mathrm{kW},$	minimum and maximum heating capacity	
$0 \le Q_{\mathrm{heat,hot\ water}} \le 15\,\mathrm{kW},$	minimum and maximum heating power at DHW	
$0 \le Q_{\mathrm{cool}} \le 10\,\mathrm{kW},$ etc.	minimum and maximum cooling power	

The objective function may be modified to account for other factors. For instance, a term may be introduced to penalize suboptimal thermal comfort or peak demand charges.

$$J = \alpha \int_{t}^{t+H} C(t)dt + \beta \int_{t}^{t+H} \sqrt{(T_{sp} - T_{air}(t))^2} dt \qquad (6.13)$$

where T_{sp} is the set-point temperature.

In Eq. (6.13), the factors α and β are weighting factors that may be adjusted depending on the needs of the user.

As in the case of the objective function, the set of constraints may encompass a large number of operational limits of the equipment involved. Among many others, constraints may include duty cycles, minimum temperature for the operation of an air-source heat pump, and even maintenance breaks.

It is clear that the optimization problem can become quite complex given the number of parameters and constraints that come into play. Different algorithms have been used in the literature to find solutions for the optimization problem. However, appropriate simplifications facilitate the formulation of the control problem and its solution.

What follows is an introductory discussion on the development of MPC strategies for buildings. An exhaustive presentation of this topic, currently an active research area, is beyond the scope of this chapter. The interested reader is referred to Gyalistras and OptiControl Team (2010), Henze *et al.* (2010), May-Ostendorp *et al.* (2011), and Oldewurtel *et al.* (2010a). This text is intended as an introduction to MPC for buildings, and discusses appropriate modeling, challenges encountered in its implementation, and some guidelines to address these issues.

6.3.2.1 Preliminary Steps

The formulation of the control problem (objective function, constraints, control variables, disturbances, and models) is unique for each building. The first step should be the detection of opportunities in which knowledge of future weather and occupancy inputs might be helpful. In some buildings – for example, those with little or no energy storage – MPC may not be very beneficial. The following questions can help in identifying the potential for MPC:

- What energy carriers are used (electricity, fuels) and what kind of tariff structure is in place? What are the main energy systems in the building (cooling and heating equipment, main appliances, auxiliary systems, CHP systems)? Do renewables (photovoltaics, solar thermal systems, solar-assisted heat pumps) play an important role, as is the case in Net ZEBs? This question should be addressed in a holistic manner.

- What are the energy storage capabilities available in the building? This inventory should include passive and active thermal energy storage, as well as any potential for electric energy storage (e.g., electric vehicles).

- Which are the *control variables* (i.e., the ones that can be manipulated in order to improve the building performance)? These variables include control signals to turn main domestic appliances on or off, cooling or heating rates for the building, ventilation rates, position of blinds and other active fenestration devices, fan and pump speed, and chiller stages.

- Are weather and occupancy forecasts readily available and reliable? Can they be easily incorporated into the control strategy? Which information is relevant?

6.3.2.2 Requirements of Building Models for Control Applications

In any engineering endeavor, choosing the right kind of model and the right level of modeling resolution – for the building, energy storage devices, and other equipment – is critical. Unfortunately, finding an adequate level of resolution for each application is a difficult task.

In building engineering, it has become customary to identify a "building model" with one created by using a building performance simulation (BPS) tool, such as EnergyPlus, ESP-r, or TRNSYS. These software tools are based on detailed models of physical phenomena for the building and its systems. Building performance simulation software tools represent the "next best thing" to actually having a building. As such, they are a valuable tool for design and research. Models created in a building simulation tool can be used in the development of control strategies. In recent years, the general

building performance optimization (BPO) tool GenOpt has been used for this purpose (Coffey *et al.*, 2010). The tool BCVTB has been developed to link building simulation programs with programming tools, such as MATLAB, more traditionally used in controls (Wetter and Haves, 2008). A wider description of BPS and BPO tools is presented in Chapter 4.

Although it is certainly possible to use a building simulation tool with an optimization package in an MPC strategy, the high number of parameters complicates the formulation of the optimal control problem. Moreover, having more parameters implies longer computation times. It also makes it more difficult to develop user-friendly interfaces and tools.

Low-order RC thermal networks – thermal networks of resistances and capacitances – have been used to model buildings for decades. Building simulation tools are based on the same principle (i.e., thermal networks), the most significant difference being the number of parameters employed. Figure 6.8 compares a building simulation model with a low-order RC circuit.
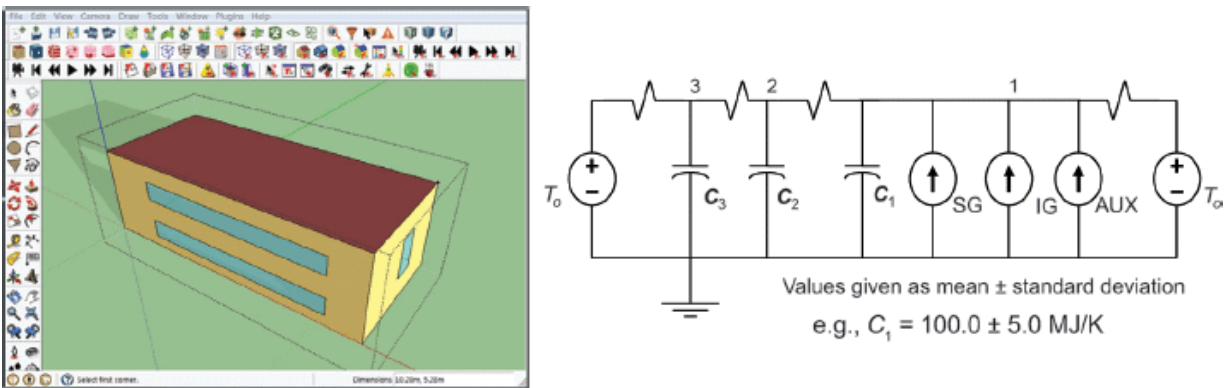
Fig. 6.8 Building simulation model (EnergyPlus) compared to a low-order RC circuit

One should not see models as purely "white-box" or "black-box." In any "white-box" model there are many simplifying assumptions. The only "perfect" model is the building itself. For example, heat transfer in a wall is usually modeled as a one-dimensional phenomenon; a wall is divided into a discrete number of control volumes; the layout of the furniture, which affects radiative heat transfer, is not known, and so on. Modeling resolution should be regarded as a "continuum,"

in which it is always possible to add or remove details ([Figure 6.9](#)). The term "gray-box model" is usually applied to a model in which a "structure" with a limited number of parameters is proposed and then found by using diverse mathematical techniques.

| Artificial intelligence (neural networks, fuzzy logic, expert systems, etc.) | "Black-box" models (time-series, statistical inference) | Gray-box models (dimensional analysis, RC lumped parameters) | White-box or transparent (First-principles) |

Increasing level of modeling resolution
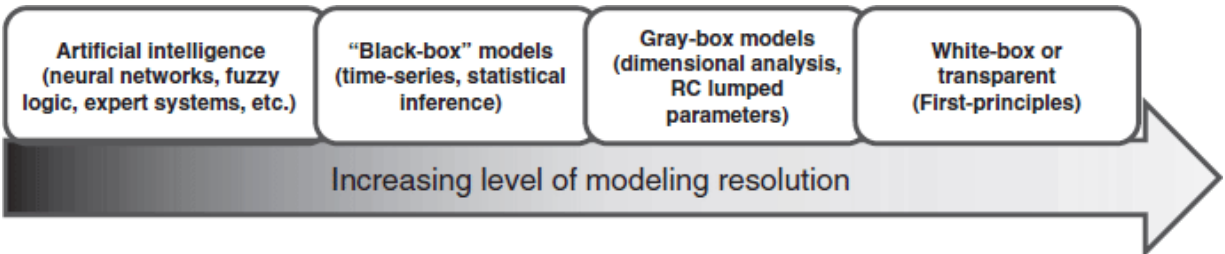
Fig. 6.9 Continuum from white-box to black-box models. Adapted from Wang and Ma (2008)

Fundamentally, it should be remembered that a model is a tool used to solve a problem. As the mathematician G.E.P. Box said, "all models are wrong, but some are useful" (Box, 1979). Given that a model should fit the task, it is entirely valid to use different models for different purposes.

Apart from the models just discussed, other models used in building studies include artificial neural networks, fuzzy logic, performance maps, and so on. Although models having some physical basis offer clear advantages – notably generality and physical insight – different kinds of models are useful for different kinds of applications. Different approaches commonly used in advanced controls are presented in Section 6.4.

6.3.2.3 Modeling of Noncontrollable Inputs

In conventional feedback-based building control systems, modeling the inputs (internal gains, solar gains, outdoor temperature, etc.) is not critical. Heating or cooling is provided "as required" by comparing the current temperature with the desired value, as in the case of a PID loop. Forecast information is rarely used in conventional control systems.

In contrast, in predictive control, it is important to have a reasonably good idea of the relevant input profiles to anticipate the building needs. The quality of the forecasts deserves as much attention as the quality of the model. The effort spent in the development of a model

might be wasted if the forecasts are neglected. Furthermore, while low-resolution data might be sufficient for design purposes, in the development of a control strategy, higher-resolution data are required.

The two main sets of inputs that influence the performance of a building are: (a) weather variables (exterior temperature, solar radiation, humidity) and (b) occupancy and related energy use and heat gains.

Forecasts released by weather service organizations are becoming increasingly accurate and detailed, and tend to contain information with higher spatial and time resolution (Poulin, 2006). They are often available online, free of charge. This has not always been the case: the earliest studies on predictive control in buildings relied on "home-made" predictors based on qualitative forecasts or historical records (Chen and Athienitis, 1996), or the likelihood of weather conditions for the following day based on the current conditions (Nygård-Ferguson and Scartezzini, 1989). In the case of large commercial buildings, which are less dependent on weather conditions, optimal control studies were based on typical hourly variations from average measurements for a given day of the year (Braun, 1990).

The information available in weather forecasts may not be set in a format that could facilitate its immediate incorporation in building simulation. For example, solar radiation on a horizontal surface is usually available, but some kind of solar radiation modeling must be used to calculate solar gains into the building.

Weather forecast uncertainty is another important issue. Weather forecasts are never an exact prediction: however, it is possible to quantify their margin of uncertainty and incorporate this information into the control strategy.

Internal gains and occupancy patterns play a significant role, especially in low and net-zero energy buildings. Just as in the case of weather forecasts, a methodology to quantify uncertainty margins should be followed. In recent years, stochastic modeling of occupancy and internal gains has received considerable attention by the research community (Page, Robinson, and Scartezzini, 2007; Widén *et al.*, 2009a; Widén, Molin, and Ellegård, 2012; Widén,

Nilsson, and Wäckelgård, 2009b; Widén and Wäckelgård, 2010a). Stochastic approaches are particularly relevant for LMGI, since many decisions should be made in terms of probabilities of an outcome.

In residential applications, DHW loads provide a good case study for the application of stochastic modeling techniques (Dolan, Nehrir, and Gerez, 1996; Laurent and Malhamé, 1994; Wong and Pelland, 2012). Domestic water tank typically use heating elements with a nominal electric power rating of a few kW (roughly 3–5). This represents a significant portion of the electric load of the house. The aggregate load of the water heaters in a community of 10,000 homes can easily result in tens of MW of additional demand.[4)]

6.3.2.4 Development of a Control Strategy

Having appropriate models for the building and its systems, along with sufficiently accurate weather and occupancy forecasts, the next step is the development – and implementation – of the control strategy. General rules are difficult to state, but some guidelines might be mentioned. The selection of a control strategy depends on the quality of the model and the forecasts, operational constraints, and the satisfaction of the requirements of the building occupants. Simplicity is another relevant consideration: simpler strategies should be preferred to more complex ones, even if this results in minor detrimental effects on performance. Simpler strategies tend to be more robust, cheaper, and easily implemented. This does not mean that complexity must be avoided at all costs; it means that the addition of complexity must be justified by a significant advantage in terms of cost, performance, or practicality.

Implementing a strategy consisting of an MPC algorithm, or based on an MPC algorithm, is not necessarily a difficult task. Once the model is in place, a solver tool will be able to find the value of the "control variables," such as cooling/heating power, ventilation rates, or valve positions. An alternative path is to obtain appropriate rules based on the results of the MPC algorithm under numerous scenarios (May-Ostendorp *et al.*, 2011).

6.4 Development of Models for Controls

The control engineering community has carried out significant research efforts on MPC for buildings in recent years. In these studies, simple linear models have been the most common approach (Deng, Barooah, and Mehta, 2012; Goyal and Barooah, 2011; Gyalistras and OptiControl Team, 2010; Oldewurtel *et al.*, 2010a). Simple linear models are, of course, not new in the thermal modeling of building components or whole buildings. However, their usefulness for advanced control applications makes it relevant to revisit these models from a different, control-oriented perspective.

Simple models with a reduced number of parameters provide some advantages for the application of advanced control strategies: insight, flexibility, computational efficiency and, above all, ease of formulation and implementation.

This section presents a brief introduction for building engineering specialists to the use of linear models for advanced controls, as well as the different incarnations that linear models might take. This text is not aimed as an exhaustive discussion on building physics or control engineering. Instead, the objective is to provide a bridge for building engineers to the language and methodologies used in controls.

6.4.1 Building Components: Conduction Heat Transfer

Conduction transfer functions (CTFs), proposed decades ago (Stephenson and Mitalas, 1971), are *z*-transform transfer functions that significantly facilitate the calculation of conduction through opaque building envelope components. CTFs are presented in depth in [Chapter 2](#). CTFs play a very important role in ASHRAE's heat balance (HB) and the radiant time series (RTS) methods (ASHRAE, 2009). Different algorithms exist for the calculation of coefficients in CTFs (Spitler, Fisher, and Pedersen, 1997).

Once the parameters of a linear model – such as the coefficients of a transfer function – are determined, calculations are straightforward and computationally efficient. For this reason, CTFs are commonly used in building simulation tools for conduction heat transfer calculations. If fact, CTFs are still the default method in EnergyPlus and TRNSYS for the calculation of conduction heat transfer through walls, roofs, and floors.

6.4.2 Thermal Modeling of an Entire Building

Low-order RC circuits have been used since the middle of the twentieth century to calculate cooling loads in buildings (Rees *et al.*, 2000). Room response factors, developed in the late 1960s, also make use of *z*-transfer functions to calculate cooling loads (Stephenson and Mitalas, 1967). Methods for the determination of comprehensive room transfer functions for load calculation have also been investigated (Seem, 1987).

As computational power became more accessible and affordable, prompting the emergence of building simulation tools since the 1970s, the use of *low-order* linear models for the thermal modeling gradually fell out of favor for building design and load calculation, even if building simulation tools rely on large sets of interrelated linear models – effectively forming a *high-order* linear model or quasi-linear model.[5] The main difference between a building simulation thermal model and a simple linear model is the number of parameters employed.

The number of parameters can grow very rapidly in a building simulation model, as has been noted by control engineering researchers. For example, a recent control engineering paper (Deng *et al.*, 2010) shows that a four-room building can quickly generate a model of nearly fortieth order. Models with hundreds or thousands of capacitors emerge in relatively small buildings.

In spite of the rapidly growing order of the model, a few parameters suffice to capture most of the relevant dynamics. For example, a third- or fourth-order model is often enough to model a house satisfactorily (Athienitis, Stylianou, and Shou, 1990; Kämpf and Robinson, 2007), especially if we focus on a specific output – such as the average indoor temperature or the required cooling load. In other words, it is possible to approximate reasonably well a more complex model with a simpler one.

Linear models might take different mathematical shapes. The following pages present an overview of these alternative representations.

6.4.3 Linear Models

A linear model is one satisfying the properties of superposition and scalability (or homogeneity) (Ogata, 2002). These properties imply that (a) the resulting effect of different inputs is the sum of their individual effects, and (b) multiplying an input by a factor results in multiplying its corresponding effect by the same factor. This can be expressed mathematically with an operator H mapping inputs into outputs.

Superposition implies that

$$y_T = H\{u_1(t) + u_2(t)\} = H\{u_1(t)\} + H\{u_2(t)\}$$
$$= y_1(t) + y_2(t)$$

(6.14)

Scalability implies

$$kH\{u(t)\} = H\{ku(t)\}$$

(6.15)

These two properties significantly facilitate finding the response due to several complex inputs acting simultaneously. When the system parameters correspond to a mapping H that does not change over time, the system is called *linear-time invariant* (LTI).

Physical systems can often be approximated with one or more ordinary differential equations (ODEs) with constant coefficients (Ogata, 2002; Spiegel, 1980):

$$a_n y^{(n)} + a_{n-1} y^{(n-1)} + \ldots + a_1 y' + a_0 y = u$$

(6.16)

The solutions of such an equation satisfy the conditions of linearity (i.e., superposition and homogeneity). This type of differential equation is found, for example, in circuits with linear components (resistors, capacitors, and inductors).[6] In an RC circuit, the order of the differential equation(s) corresponds to the number of capacitors.

6.4.3.1 Continuous-Time Transfer Functions

In an LTI system, such as the one shown in Eq. (6.16), it is possible to describe the relationship between an input u and an output y in a simple manner. The transfer function between the input and the output is defined as the Laplace transform of the output divided by

the Laplace transform of the input, when all initial conditions are equal to zero.

$$G(s) = \frac{Y(s)}{U(s)} = \frac{L(y(t))}{L(u(t))}$$
(6.17)

where *s* is the complex frequency variable.

Equations (6.16) and (6.17) refer to a single-input, single-output (SISO). Transfer functions can also be found between any pair of input and output variables, either in multiple-input, single-output (MISO) systems, or in multiple-input, multiple-output (MIMO) systems. An output of interest can be found by using the transfer functions, relevant inputs, and the application of the superposition principle (Figure 6.10).
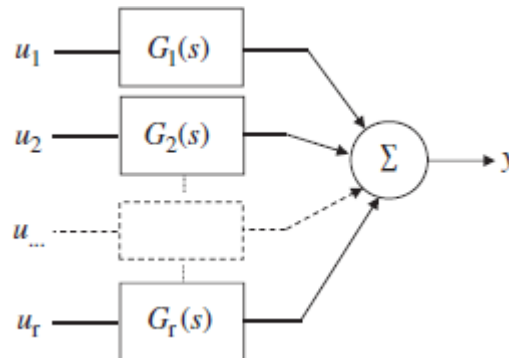
Fig. 6.10 Superposition principle in a MISO system with continuous-time transfer functions

6.4.3.2 Discrete-Time Transfer Functions (Z-transforms Transfer Functions)

Transfer functions in the Laplace domain provide insight on the dynamics of the building (for example, simple periodic functions can be used to represent weather variables). However, the input functions acting on a building system are never "well-behaved" periodic functions, such as those usually found in a Laplace transform table. In practice, modeling the response of a building to actual inputs requires the use of *z-transforms* transfer functions (Candanedo, 2011). These transforms are the discrete-time counterpart of the Laplace transforms. They are more suitable for

inputs sampled at discrete time intervals. The *z*-transform of a sequence $\{u(n)\}$ is given by

$$Z(\{u(n)\}) = U(z) = \sum_{n=0}^{\infty} u(n)z^{-n}$$

(6.18)

This effectively results in replacing the sequence with a polynomial in terms of z^{-1}. The definition presented in Eq. (6.18) implies that the z-transform of a sequence of values can simply be found by inspection. In a *z*-transform, the auxiliary variable *z* is defined as

$$z = e^{sT}$$

(6.19)

This substitution illustrates that the *z*-transform corresponds to a special case of the Laplace transform applied to a sequence of rectangular pulses with period T. By definition, the Laplace transform of a function $y(t)$ is

$$Y(s) = \int_{0}^{\infty} y(t)e^{-st}dt$$

(6.20)

Let the function $y(t)$ be a sequence of values at time intervals T.

$$y(t) = \{y(nT)\}$$

(6.21)

Equation (6.20) can be then written in terms of *z* as

$$Y(z) = \sum_{n=0}^{\infty} y(nT)z^{-n}$$

(6.22)

Transfer functions can also be defined in terms of *z*-transforms:

$$G(z) = \frac{Y(z)}{U(z)}$$

(6.23)

The advantage of a *z*-transfer function, such as the one in Eq. (6.23), is that it can be linked to a difference equation involving consecutive values of the input and output (Moudgalya, 2007). For example, consider the *z*-transfer function

$$G(z) = \frac{Y(z)}{U(z)} = \frac{0.10 + 0.03z^{-1} - 0.10z^{-2}}{1 - 0.6z^{-1} - 0.5z^{-2} + 0.06z^{-3}} \tag{6.24}$$

With some algebraic manipulation

$$Y(z)\left(1 - 0.6z^{-1} - 0.5z^{-2} + 0.06z^{-3}\right) = U(z)\left(0.10 + 0.03z^{-1} - 0.10z^{-2}\right) \tag{6.25}$$

$$Y(z) - 0.6Y(z)z^{-1} - 0.5Y(z)z^{-2} + 0.06Y(z)z^{-3} = 0.10U(z) + 0.03U(z)z^{-1} \tag{6.26}$$
$$- 0.10U(z)z^{-2}$$

Translation, a property of the *z*-transform, can be exploited at this point. The translation theorem implies that

$$Z(y(t - nT)) = z^{-n}Z(y(t)) \tag{6.27}$$

This means that multiplying a *z*-transform by the expression z^{-n} results in a backward displacement of *n* time steps. Equation (6.26) can be written as

$$Y(z) - 0.6Y(z - T) - 0.5Y(z - 2T) + 0.06Y(z - 3T) = 0.10U(z) + 0.03U(z - T) \tag{6.28}$$
$$- 0.10U(z - 2T)$$

Finally, applying the inverse *z*-transform (i.e., returning to the sequence in the time domain), one obtains

$$y(t) - 0.6y(t - T) - 0.5y(T - 2T) + 0.06y(t - 3T) = 0.10u(t) + 0.03u(t - T) \tag{6.29}$$
$$- 0.10u(t - 2T)$$

The current value of the output, $y(t)$, can then be expressed in terms of the current and previous values of the input and previous values of the output.

$$y(t) = 0.10u(t) + 0.03u(t - T) - 0.10u(t - 2T) + 0.6y(t - T) + 0.5y(T - 2T) \tag{6.30}$$
$$- 0.06y(t - 3T)$$

Using Eq. (6.30), it is quite easy to model the output $y(t)$ having data for the expected values of the input $u(t)$ at regular intervals. When more than one input comes into play, the effect of each of the inputs can be considered separately; the superposition principle can then be applied in a similar way to that shown in Figure 6.10.

6.4.3.3 Time Series Models

The difference equation shown in [Eq. (6.30)](#) describes a set of rules for a sequence of values over time. Essentially, this is a time series model. Time series analysis is a branch of mathematics concerned with the study of patterns in ordered trails of measurements or observations collected over time (Box, Jenkins, and Reinsel, 1994; Madsen, 2008). Evidently, the coefficients of [Eq. (6.30)](#) are related to the coefficients of the *z*-transfer function shown in [Eq. (6.24)](#). A time series model basically contains the same information as a set of transfer functions. An approach for obtaining the coefficients of z^{-n} in transfer functions is presented in [Chapter 2](#).

The field known as system identification investigates how to determine the values of the parameters in a model after a structure for the model is proposed. System identification (SI or "SysID") algorithms have often been applied to the determination of coefficients in time series models (Ljung, 1999).

A time series, such as the one in [Eq. (6.30)](#), is autoregressive (AR); the current output depends on previous values of the output. This model can also be described as having an *exogenous input*, since the output depends on the value of an independent input.

The *backward shift operator* (q^{-1}) is commonly used in system identification of time series models.[7] The effect of this operator, also known as time-shift operator, is similar to that of multiplying a *z*-transform by z^{-1}. The backward shift operator acts on an element of a sequence as follows (Ljung, 2010):

$$q^{-1}u(t) = u(t - T) \tag{6.31}$$

In general, for *i* time steps

$$q^{-i}u(t) = u(t - iT) \tag{6.32}$$

The backward shift operator allows writing time series in a more compact way. As illustrated in Ljung (2010), the expression

$$y(t) + a_1 y(t - T) + a_2 y(t - 2T)$$

may be written as

$$y(t) + a_1 q^{-1} y(t) + a_2 q^{-2} y(t) = \left(1 + a_1 q^{-1} + a_2 q^{-2}\right) y(t) = A(q) y(t)$$

where $A(q) = 1 + q^{-1} + q^{-2}$. Time series models are often written in terms of polynomials of the backward shift operator. For instance, two common models used in system identification are the autoregressive model with exogenous input (ARX), and the autoregressive moving-average model with exogenous input (ARMAX). These models have the following structures (Ljung, 2010) for multiple inputs:

$$A(q) y(t) = \sum_{i=1}^{nu} B_i(q) u_i(t - nk_i) + e(t) \, [\text{ARX}] \tag{6.33}$$

$$A(q) y(t) = \sum_{i=1}^{nu} B_i(q) u_i(t - nk_i) + C(q) e(t) \, [\text{ARMAX}] \tag{6.34}$$

In which "nu" is the number of inputs and nk_i is the number of time steps of delay associated with the ith input. The difference between both models is how they deal with noise. The ARMAX model applies a particular treatment to the noise $e(t)$.

The main problem in system identification is the determination of the coefficients of the polynomials so that they represent as accurately as possible the actual system. Input and output data, obtained from measurements or simulations, can be introduced in system identification software tools (Ljung, 2010; National Instruments, 2004) that significantly facilitate this task.

6.4.3.4 State-Space Representation

Yet another equivalent (but more compact) depiction of linear systems is given by the *state-space representation*. This type of model, commonly applied in MIMO systems, makes use of a set of variables containing all the relevant information that fully determines the *state* of the system. It is well known that a particular solution of a differential equation requires as many initial conditions as the order or the system (e.g., a first-order ODE requires one initial condition; a second-order ODE requires two). Similarly, in a state-

space model there are as many state variables as needed[8] to fully describe the system at time $t = 0$. Although the possibilities for selecting state variables are literally infinite, in reality some representations provide more insight or information on the system. For example, in RC circuits the temperature of the nodes with capacitances can be a convenient choice for state variables.

A state-space representation consists of a system of first-order differential equations in a matrix representation. The standard linear state-space representation is given by the following pair of equations:

$$\dot{\mathbf{x}} = \mathbf{A}\mathbf{x} + \mathbf{B}\mathbf{u} \tag{6.35}$$

$$\mathbf{y} = \mathbf{C}\mathbf{x} + \mathbf{D}\mathbf{u} \tag{6.36}$$

in which $\mathbf{x}$ is the state vector with n state variables:

$$\mathbf{x} = \begin{bmatrix} x_1 \\ x_2 \\ \vdots \\ x_n \end{bmatrix} \tag{6.37}$$

$\mathbf{u}$ is the vector of r inputs and

$$\mathbf{u} = \begin{bmatrix} u_1 \\ u_2 \\ \vdots \\ u_r \end{bmatrix} \tag{6.38}$$

and $\mathbf{y}$ is the vector of m outputs

$$\mathbf{y} = \begin{bmatrix} y_1 \\ y_2 \\ \vdots \\ y_m \end{bmatrix} \tag{6.39}$$

The matrix $\mathbf{A}$ ($n \times n$) is called the *dynamic* matrix or *state* matrix and represents how the state variables are related to their own

derivatives. The matrix **B** ($n \times r$) is called the *input* or *control* matrix and describes the effect of inputs on the rate of change of state variables. The matrix **C** ($m \times n$), the *output* or *sensor* matrix, describes how the state variables affect the outputs or measurements of interest. Finally, the matrix **D** ($m \times r$), the *direct transmission matrix*, describes the direct effect of inputs on the output variables.

To illustrate the application of state-space representations, consider the RC thermal circuit shown in [Figure 6.11](). C_1 is the equivalent thermal capacitance of the indoor air node and C_2 is the thermal capacitance of the building envelope. T_o and Q_{IG} represent the outdoor temperature and internal heat gains, respectively. The nodes are connected by thermal conductances.
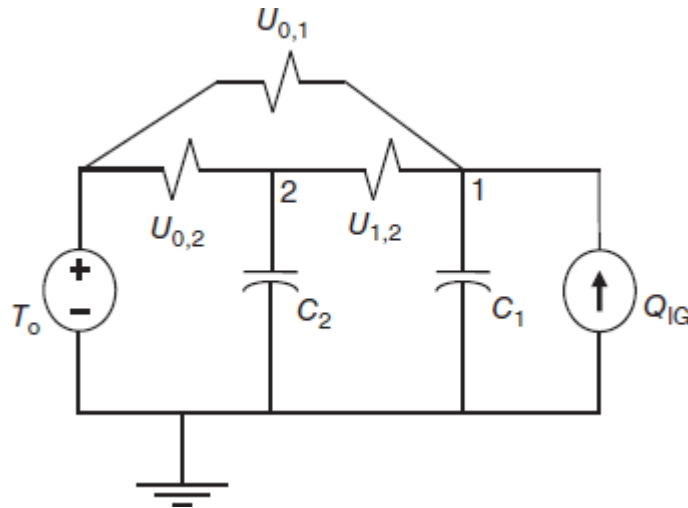
Fig. 6.11 Second-order RC thermal network for a house

This system can be described by two differential equations:

$$C_1 \frac{dT_1}{dt} = Q_{IG} + U_{o,1}(T_o - T_1) + U_{1,2}(T_2 - T_1) \tag{6.40}$$

$$C_2 \frac{dT_2}{dt} = U_{o,2}(T_o - T_2) + U_{1,2}(T_1 - T_2) \tag{6.41}$$

In this case, it is convenient to select the following state and input vectors:

$$\mathbf{x} = \begin{bmatrix} T_1 \\ T_2 \end{bmatrix} \quad \text{and} \quad \mathbf{u} = \begin{bmatrix} T_o \\ Q_{IG} \end{bmatrix} \tag{6.42}$$

Equations (6.40) and (6.41) can then be written as follows:

$$\begin{bmatrix} \dot{x}_1 \\ \dot{x}_2 \end{bmatrix} = \begin{bmatrix} -\dfrac{U_{0,1} + U_{1,2}}{C_1} & \dfrac{U_{1,2}}{C_1} \\[3mm] \dfrac{U_{1,2}}{C_2} & -\dfrac{U_{0,2} + U_{1,2}}{C_2} \end{bmatrix} \begin{bmatrix} x_1 \\ x_2 \end{bmatrix} + \begin{bmatrix} \dfrac{U_{o,1}}{C_1} & -\dfrac{1}{C_1} \\[3mm] \dfrac{U_{o,2}}{C_2} & 0 \end{bmatrix} \begin{bmatrix} T_o \\ Q_{IG} \end{bmatrix} \tag{6.43}$$

The output variables are selected depending on the needs of each case. For instance, in this case, the output variable can be the indoor temperature. Therefore

$$\mathbf{y} = [T_1] \tag{6.44}$$

Then, the four matrices for this state-space representation are

$$\mathbf{A} = \begin{bmatrix} -\dfrac{U_{0,1} + U_{1,2}}{C_1} & \dfrac{U_{1,2}}{C_1} \\[3mm] \dfrac{U_{1,2}}{C_2} & -\dfrac{U_{0,2} + U_{1,2}}{C_2} \end{bmatrix} \quad \mathbf{B} = \begin{bmatrix} \dfrac{U_{o,1}}{C_1} & \dfrac{1}{C_1} \\[3mm] \dfrac{U_{o,2}}{C_2} & 0 \end{bmatrix} \tag{6.45}$$

$$\mathbf{C} = \begin{bmatrix} 1 & 0 \end{bmatrix} \qquad\qquad\qquad \mathbf{D} = \begin{bmatrix} 0 & 0 \end{bmatrix}$$

With a state-space representation, the state of the system and the outputs of interest can be readily found. As presented in Åström and Murray (2009), the state at a time step k is given by

$$\mathbf{x}[k] = \mathbf{A}^k \mathbf{x}_0 + \sum_{j=0}^{k-1} \mathbf{A}^{(k-1)-j} \mathbf{B} \mathbf{u}[j] \tag{6.46}$$

and the system output is

$$\mathbf{y}[k] = \mathbf{C}\mathbf{A}^k \mathbf{x}_0 + \sum_{j=0}^{k-1} \mathbf{C}\mathbf{A}^{(k-1)-j} \mathbf{B} \mathbf{u}[j] + \mathbf{D}\mathbf{u}[k] \tag{6.47}$$

To recap, having the four matrices, the system output can be easily found. Likewise, after some algebraic manipulation, it is also possible to find the required input (e.g., heating or cooling power) to obtain a certain output.

Figure 6.12 shows some of the embodiments that linear systems can take. In spite of technical subtleties, these representations are largely equivalent. None of them is intrinsically better than the others, although some provide an advantage for a given purpose in a given context. An RC circuit may be more appropriate to provide physical insight; a thermal capacitance is more readily associated with the properties of building materials. A state-space scheme is particularly flexible for advanced control applications. With some caveats, it is also possible to transform from one representation into another while keeping in mind that diverse RC circuits structures or state-space models can yield similar transfer functions.

RC circuit

Set of continuous transfer functions

Set of discrete transfer functions

$$G_1(z) = \frac{b_{1,1}z^{-1}+b_{1,0}}{a_2 z^{-2}+a_1 z^{-1}+a_0}$$

$$G_2(z) = \frac{b_{2,1}z^{-1}+b_{2,0}}{a_2 z^{-2}+a_1 z^{-1}+a_0}$$

$$G_3(z) = \frac{b_{3,1}z^{-1}+b_{3,0}}{a_2 z^{-2}+a_1 z^{-1}+a_0}$$

State-space model

$$\dot{x} = Ax + Bu$$
$$y = Cx + Du$$

Time-series models

$$A(q)\,y(t) = \sum_{i=1}^{nu} B_i(q)u_i(t - nk_i) + C(q)e(t) \quad [\text{ARMAX}]$$
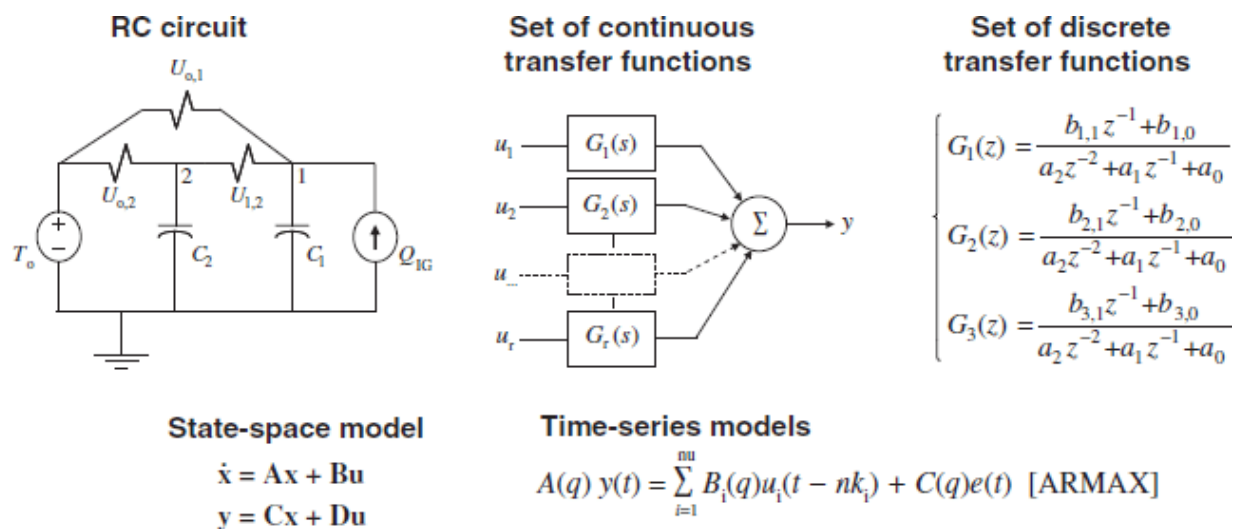
Fig. 6.12 Alternative representations of linear models

6.5 Conclusion

This chapter has presented a brief introduction to load matching and grid interaction in the context of net-zero energy buildings. Load matching and grid interaction are central issues that must be taken into consideration in the development of policies, design methodologies, and technologies for net-zero energy buildings. Ignoring load matching and grid interaction would promote inadequate solutions for net-zero energy buildings.

This chapter has presented a brief overview of some of the indicators used in the characterization of load matching and grid interaction. The reader interested in a deeper analysis of load matching and grid

interaction indicators is referred to Salom *et al.* (2014a) and Salom *et al.* (2014b).

Finally, this chapter has discussed control strategies aimed at managing building loads and facilitating the interaction of buildings with the grid. The possibility of making use of simplified building models for the development and implementation of predictive control strategies has been discussed.

Notes

1. The wording "load mismatch" is discouraged since it suggests that a difference between load and generation always has a negative connotation.

2. In demand response schemes, applied in residential and commercial buildings, the electric utility sends a request directly to the appliances or equipment of their customers during periods of high demand.

3. In some Canadian regions, where the price of electricity is very low, electric heating is common.

4. The case of DHW is so relevant for the main electric utility in Québec that it prompted the development of a water tank with three heating elements (Laperrière *et al.*, 2009). The heater at the bottom of the tank, sized at 800 W, provides heat nearly continuously. The top element, rated at 3.8 kW, supplies heat when hot water is needed as soon as possible.

5. Thermal modeling in building simulation tools includes non-linear phenomena (e.g., radiative or convective heat transfer). However, linear models are often a good approximation.

6. Inductors do not appear in thermal networks used for building modeling.

7. The notation B^k is sometimes used for the backward shift operator (Madsen, 2008). Time Series Analysis (Chapman & Hall/CRC):

$$B^k u(t) = u(t - kT) X$$

8. Another important reason to choose low-order systems is that initial conditions (i.e., the initial value of the state variables) must be provided. This can be quite difficult when hundreds or thousands of states are involved, as in a building simulation tool.

References

American Society of Heating, Refrigerating and Air-Conditioning Engineers (ASHRAE) (2005) *Handbook of Fundamentals*, American Society of Heating, Refrigerating and Air,-Conditioning Engineers, Atlanta, USA.

American Society of Heating, Refrigerating and Air-Conditioning Engineers (ASHRAE) (2007) *Handbook of HVAC Applications*, American Society of Heating, Refrigerating and Air-Conditioning Engineers, Atlanta, USA.

American Society of Heating, Refrigerating and Air-Conditioning Engineers (ASHRAE) (2009) *Handbook of Fundamentals. In Ventilation and Infiltration*, American Society of Heating, Refrigerating and Air,-Conditioning Engineers, Inc., pp. 36.

Åström, K.J. and Murray, R. (2009) *Feeback Systems: An Introduction for Scientists and Engineers*, Princeton University Press.

Athienitis, A.K., Stylianou, M., and Shou, J. (1990) A methodology for building thermal dynamics studies and control applications. *ASHRAE Transactions*, **96**, 839–848.

Bollen, M.H.J. and Hassan, F. (2011) *Integration of Distributed Generation in the Power System (IEEE Press Series on Power Engineering)*, John Wiley & Sons.

Box, G.E.P. (1979) *Robustness in the Strategy of Scientific Model Building* (eds R.L. Launer and G.N. Wilkinson), Academic Press. pp. 201–236.

Box, G.E.P., Jenkins, G.M., and Reinsel, G.C. (1994) *Time Series Analysis: Forecasting and Control*, 3rd edn, Prentice Hall, New Jersey.

Braun, J.E. (1990) Reducing energy costs and peak electrical demand through optimal control of building thermal storage. *ASHRAE Transactions*, **96**, 876–888.

Candanedo, J.A. (2011) A study of predictive control strategies for optimally designed solar homes, in *Building, Civil and Environmental Engineering*, Concordia University.

Castillo-Cagigal, M., Matallanas, E., Masa-Bote, D., Caamaño-Martín, E., Gutiérrez, A., Monasterio, F., and Jiménez-Leube, J. (2010) Self-consumption enhancement with storage system and demand side management: GeDELOS-PV system. In *5th International Renewable Energy Storage Conference (IRES 2010) (Berlin, Germany)*.

Chen, T.Y. and Athienitis, A.K. (1996) Ambient temperature and solar radiation prediction for predictive control of HVAC systems and a methodology for optimal building heating dynamic operation. *ASHRAE Transactions*, **102**, 26–35.

Coffey, B., Haghighat, F., Morofsky, E., and Kutrowski, E. (2010) A software framework for model predictive control with GenOpt. *Energy and Buildings*, **42**, 1084–1092.

Colson, C.M. and Nehrir, M.H. (2009) A review of challenges to real-time power management of microgrids. In *2009 IEEE Power & Energy Society General meeting (Calgary, Alberta)*.

Deng, K., Barooah, P., and Mehta, P.G. (2012) Mean-field control for energy efficient buildings. In *2012 American Control Conference (Montréal, Canada)*.

Deng, K., Barooah, P., Mehta, P.G., and Meyn, S.P. (2010) Building thermal model reduction via aggregation of states. Paper presented at: *2010 American Control Conference (Baltimore, Maryland: IEEE)*.

Dolan, P.S., Nehrir, M.H., and Gerez, V. (1996) Development of a Monte Carlo based aggregate model for residential electric water heater loads. *Electric Power Systems Research*, **36**, 29–35.

Dotzauer, E. (2002) Simple model for prediction of loads in district-heating systems. *Applied Energy*, **73**, 277–284.

ERGEG (2010) Position paper on Smart Grids - an ERGEG conclusions paper (European Regulators Group for Electricity & Gas).

Goyal, S. and Barooah, P. (2011) A method for model-reduction of nonlinear building thermal dynamics. In *American Control Conference (San Francisco, California: IEEE)*, pp. 2077–2082.

Gyalistras, D. and OptiControl Team (2010) Final Report: Use of Weather and Occupancy Forecasts for Optimal Building Climate

Control (OptiControl) (Zürich, Switzerland: ETH Zürich).

Heller, A.J. (2002) Heat-load modelling for large systems. *Applied Energy*, **72**, 371–387.

Henze, G. and Krarti, M. (2005) *Predictive Optimal Control of Active and Passive Building Thermal Storage Inventory*, University of Nebraska - Lincoln.

Henze, G.P., Florita, A.R., Brandemuehl, M.J., Felsmann, C., and Cheng, H. (2010) Advances in near-optimal control of passive building thermal storage. *Journal of Solar Energy Engineering*, **132**, 1–9.

Kämpf, J.H. and Robinson, D. (2007) A simplified thermal model to support analysis of urban resource flows. *Energy & Buildings*, **39**, 445–453.

Katiraei, F., Mauch, K., and Dignard-Bailey, L. (2007) Integration of photovoltaic power systems in high-penetration clusters for distribution networks and mini-grids. *International Journal of Distributed Energy Resources*, **3**, 207–224.

Lamonica, M. (2012) A startup's smart batteries reduce buildings' electric bills. In MIT Technology Review.

Laperrière, A., Brassard, R., and Nesreddine, H. (2009) Analyse d'un nouveau concept de chauffe-eau: Le chauffe-eau trois éléments. *ASHRAE Montréal Chapter*, Technical Mini-Session, Feb. 9.

Laurent, J.C. and Malhamé, R.P. (1994) A physically-based computer model of aggregate electric water heating loads. *IEEE Transactions on Power Systems*, **9**, 1209–1217.

Ljung, L. (1999) *System Identification: Theory for the User*, 2nd edn, Prentice Hall PTR.

Ljung, L. (2010) *System Identification Toolbox User's Guide*, The Mathworks, Inc.

Lund, H., Marszal, A., and Heiselberg, P. (2011) Zero energy buildings and mismatch compensation factors. *Energy and Buildings*, **43**, 1646–1654.

Madsen, H. (2008) *Time Series Analysis*, Chapman & Hall/CRC.

Marszal, A.J., Heiselberg, P., Bourrelle, J.S., Musall, E., Voss, K., Sartori, I., and Napolitano, A. (2011) Zero Energy Building – A review of definitions and calculation methodologies. *Energy and Buildings*, **43**, 971–979.

May-Ostendorp, P., Henze, G.P., Corbin, C.D., Rajagopalan, B., and Felsmann, C. (2011) Model-predictive control of mixed-mode

buildings with rule extraction. *Building and Environment*, **46**, 428–437.

McClenahan, D., Gusdorf, J., Kokko, J., Thornton, J., and Wong, B. (2006) Okotoks - seasonal storage of solar energy for space heat in a new community. In *ACEEE Summer Study on Energy Efficiency in Buildings - 2006*.

Moudgalya, K.M. (2007) *Digital Control*, John Wiley & Sons, Chichester, UK.

National Instruments (2004) *LabVIEW System Identification Toolkit User Manual*, National Instruments, Austin, Texas.

Nygård-Ferguson, M. and Scartezzini, J.-L. (1989) Experimental performance of a predictive controller designed for passive solar buildings. In *ISES Solar World Congress (Kobe, Japan)*.

Ogata, K. (2002) *Modern Control Engineering*, Prentice-Hall, Inc., Upper Saddle River, NJ, USA.

Oldewurtel, F., Parisio, A., Jones, C.N., Morari, M., Gyalistras, D., Gwerder, M., Stauch, V., Lehmann, B., and Wirth, K. (2010a) Energy Efficient Building Climate Control using Stochastic Model Predictive Control and Weather Predictions. In *American Control Conference (Baltimore, Maryland)*.

Oldewurtel, F., Ulbig, A., Parisio, A., Andersson, G., and Morari, M. (2010b) Reducing peak electricity demand in building climate control using real-time pricing and model predictive control. Paper presented at: *49th IEEE Conference on Decision and Control (Atlanta, Georgia, USA)*.

Page, J., Robinson, D., and Scartezzini, J.-L. (2007) Stochastic simulation of occupant presence and behaviour in buildings. In *Proceedings of the Tenth Building Simulation Conference (Beijing, China)*.

Poulin, L. (2006) Renewable energy forecasts for solar powered applications: an Environment Canada perspective. In *CanSIA (Canadian Solar Industries Association) Solar Conference, 2006 (Ottawa, Canada)*.

Rees, S., Spitler, J., Davies, M., and Haves, P. (2000) Qualitative comparison of North American and UK cooling load calculation methods. *International Journal of Heating, Ventilating, Air-Conditioning and Refrigeration Research*, **6**, 75–99.

Salom, J., Widén, J., Candanedo, J.A., Sartori, I., Voss, K., and Marszal, A. (2011) Understanding Net Zero Energy Buildings:

Evaluation of Load Matching and Grid Interaction Indicators. In *12th International Building Simulation Conference (IBPSA 2011) (Sydney, Australia)*.

Salom, J., Marszal, A.J., Candanedo, J.A., Widén, J., Lindberg, K.B., Sartori, I. (2014a) Analysis of load match and grid interaction indicators in Net ZEB with high resolution data. IEA SHC Task 40 and ECB Annex 52, Subtask A Report. http://task40.iea-shc.org/data/sites/1/publications/-T40A52–LMGI-in-Net-ZEBs–STA-Technical-Report.pdf

Salom, J., Marszal, A., Widén, J., Candanedo, J., and Lindberg, K.B. (2014b) Analysis of load match and grid interaction indicators in net zero energy buildings with simulated and monitored data. *Applied Energy*, **136**, 119–131.

Seem, J.E. (1987) *Modeling of Heat Transfer in Buildings. In Mechanical Engineering*, University of Wisconsin-Madison.

Spiegel, M.R. (1980) *Applied Differential Equations*, 3rd edn, Prentice Hall.

Spitler, J.D., Fisher, D.E., and Pedersen, C.O. (1997) The radiant time series cooling load calculation procedure. *ASHRAE Transactions*, **103**, 503–518.

Stephenson, D.G. and Mitalas, G.P. (1967) Cooling load calculations by thermal response factor method. *ASHRAE Transactions*, **73**, 1–7.

Stephenson, D.G. and Mitalas, G.P. (1971) Calculation of heat conduction transfer functions for multi-layer slabs. *ASHRAE Transactions*, **77**, 117–126.

Verbruggen, B., De Coninck, R., Baetens, R., Saelens, D., Helsen, L., and Driesen, J. (2011) Grid impact indicators for active building simulation. In *IEEE PES Conference on Innovative Smart Grid Technologies (Anaheim, California)*.

Voss, K., Sartori, I., Napolitano, A., Geier, S., Gonçalves, H., Hall, M., Heiselberg, P., Widén, J., Candanedo, J.A., Musall, E. *et al.* (2010) Load Matching and Grid Interaction of Net Zero Energy Buildings. Paper presented at: *EUROSUN 2010 (Graz, Austria)*.

Wang, S. and Ma, Z. (2008) Supervisory and optimal control of building HVAC Systems: A Review. *HVAC & R Research*, **14**, 3–32.

Wetter, M. and Haves, P. (2008) A modular building controls virtual test bed for the integration of heterogeneous systems. Paper presented at: *SimBuild 2008 (Berkeley, California)*.

Widén, J., Lundh, M., Vassileva, I., Dahlquist, E., Ellegård, K., and Wäckelgård, E. (2009a) Constructing load profiles for household electricity and hot water from time-use data – Modelling approach and validation. *Energy and Buildings*, **41**, 753–768.

Widén, J., Molin, A., and Ellegård, K. (2012) Models of domestic occupancy, activities and energy use based on time-use data: deterministic and stochastic approaches with application to various building-related simulations. *Journal of Building Performance Simulation*, **5**, 27–44.

Widén, J., Nilsson, A.M., and Wäckelgård, E. (2009b) A combined Markov-chain and bottom–up approach to modelling of domestic lighting demand. *Energy and Buildings*, **41**, 1001–1012.

Widén, J. and Wäckelgård, E. (2010a) A high-resolution stochastic model of domestic activity patterns and electricity demand. *Applied Energy*, **87**, 1880–1892.

Widén, J. and Wäckelgård, E. (2010b) Net zero energy solar buildings at high latitudes: the mismatch issue. In *EASST 2010 Conference: Practicing Science and Technology (Trento, Italy)*.

Widén, J., Wäckelgård, E., and Lund, P. (2009c) Options for improving the load matching capability of distributed photovoltaics: methodology and application to high latitude data. *Solar Energy*, **83**, 1953–1966.

Willis, H.L. and Scott, W.G. (2000) *Distributed Power Generation: Planning and Evaluation*, CRC Press, New York.

Wong, S. and Pelland, S. (2012) Internal Report (NRCan).

7
Net ZEB Case Studies

Andreas Athienitis and William O'Brien

7.1 Introduction

Four in-depth case studies of existing occupied net or near net-zero energy buildings (Net ZEBs) were performed and are described in this chapter. The purpose of the case studies is to illuminate realistic aspects of the design process (parties involved, stages, software, and other tools used), construction process, the final designs, and the operation of the buildings based on measured data. Following this, redesign studies are provided where the authors investigate alternative solutions to achieve net-zero energy or to achieve it more effectively. These alternative solutions consider ways of reaching the net-zero goal for near net-zero buildings, such as higher-efficiency PV systems, integration of different technologies, such as controlled motorized shading as opposed to fixed shading, change of operating strategies including zone setpoints, and night cooling.

The case study buildings are diverse in type, climate, and Net ZEB strategy, offering considerable insight into Net ZEBs from conception to occupancy. Rather than acting as models from which exact Net ZEB design replicas should be developed, the case studies are intended to inspire new design approaches and consideration of alternative pathways to the level of net-zero energy. They are also intended to provide examples of strengths and deficiencies in the design processes and tools used. The criteria for selecting the case studies were that they

    – Demonstrate low-energy design strategies and technologies,

    – Have high-resolution (spatial and temporal) monitored data for at least one year,

    – Are intimately understood by the authors and researchers from conception to occupancy, and

    – Are economical so that many of the design concepts can be reproduced or at least inspire other Net ZEBs.

The buildings are briefly summarized here and explained in depth in the following four sections. ÉcoTerra is a single detached near-Net ZEB house near Montreal, Quebec, Canada that demonstrates the viability of economical prefabricated houses with passive solar strategies and advanced renewable energy technologies. These technologies include a building-integrated photovoltaic with thermal recovery (BIPV/T) roof and a ventilated concrete slab (VCS) in the basement to reduce heating loads. The Leaf House is a six-unit, three-story residential Net ZEB located midway up the east coast of Italy, in Ancona. It uses similar strategies to ÉcoTerra to reduce heating loads (e.g., a high performance envelope), but de-emphasizes the passive solar heating to accommodate the climate's slightly milder and less sunny winters while reducing cooling loads. The Leaf House is equipped with a large roof-mounted PV array and solar domestic hot water system. Both of these residential buildings are equipped with ground source heat pumps (GSHPs) to supplement passive and renewable energy systems to provide heating and cooling. The National Renewable Energy Laboratory's (NREL) 20,400 m² Research Support Facility (RSF) is primarily comprised of office space and is located west of Denver, CO, USA. The sunny climate enables effective daylight harvesting and a relatively high output from the very large 1.6 MW photovoltaic (PV) array. Other notable features include the building's geometry with predominantly south- and north-facing façades, good cross-ventilation, heat recovery from a large data center, a woodchip boiler with hydronic distribution, and radiant heating and cooling panels. Finally, ENERPOS, which represents a tropical academic building, is located in St-Pierre, Reunion Island, France. Somewhat similar in shape to RSF, with its major axis in the east–west direction, ENERPOS aims to be predominantly daylit and has cross-ventilation. A unique feature of ENERPOS, due to its very warm, often humid climate is that it has large solar shading slats that protect not only the windows, but also the walls from solar radiation. Because of ENERPOS' relatively low lighting and equipment loads and its reliance on natural ventilation and ceiling fans to nearly eliminate the need for mechanical cooling, its measured energy generation (from PV) is about seven times higher than its consumption. The buildings are summarized in Table 7.1.

Table 7.1 Summary of four case study Net ZEBs

Name	Type	Climate	Featured Passive and Energy Efficiency Strategies	Renewable Energy Technologies	Tools Used in Original Design Process
ÉcoTerra, Eastman, Quebec, Canada	Single-family detached house	Temperate with cold sunny winters and warm humid summers	Well-insulated airtight envelope with emphasis on passive solar; natural ventilation; GSHP	BIPV/T roof with VCS for space and water heating	HOT2000, RETScreen, simple custom tools
Leaf House, Ancona, Italy	Six-unit residential building	Mediterranean with warm sunny summers and cool winter	High-performance envelope, GSHP, passive solar, solar tubes, natural ventilation	PV, Solar thermal collector for DHW	DesignBuilder, MC4 Suite
National Renewable Energy Laboratory (NREL) Research Support Facility (RSF), Golden, Colorado, USA	Large government-based office space and data center	Temperate and very sunny year-round	High-performance envelope, modest window area, fixed solar shading, daylighting and lighting controls, labyrinth thermal storage, radiant heating and cooling, natural ventilation, heat recovery from data center, demand-controlled displacement ventilation	PV, transpired solar collectors	eQUEST, RADIANCE, IES VE
ENERPOS, St. Pierre, Reunion Island, France	Academic building with classrooms and offices	Tropical and sunny with minimal daily temperature swings	Natural ventilation, solar shading and daylighting; ceiling fans to minimize air conditioning	PV	EnergyPlus, DAYSIM, CATT-Acoustic, PVsyst

7.2 ÉcoTerra

William O'Brien, Yuxiang Chen, and Andreas Athienitis

7.2.1 Description of ÉcoTerra

ÉcoTerra is a two-story, two-bedroom, near-net-zero energy house located near Montreal in the rural town of Eastman, Quebec, Canada (45.3°N, 72.3°W) (see Figure 7.1). The house has a heated floor area of 211.1 m² (including a 76.9 m² basement), and an unheated attached garage (26.6 m²). The typical climate conditions for nearby Sherbrooke, Quebec are summarized in Table 7.2. The local climate is characterized by cold sunny winters and warm humid summers with moderate daily temperature swings.

Fig. 7.1 The ÉcoTerra House from southwest (Image courtesy of Agnieszka Koziol)

Table 7.2 Typical climate for Sherbrooke, Québec

Month	Daily Solar Radiation (kWh/m²)			Average Monthly Temperature (ºC)
	Horizontal	Vertical	30° from horizontal (south-facing)	
January	1.61	3.47	2.81	−12.8
February	2.63	4.57	4.06	−11.0
March	3.91	4.72	5.05	−5.3
April	4.46	3.00	4.83	3.8
May	5.27	2.76	5.24	11.8
June	5.49	2.60	5.26	17.4
July	5.51	2.71	5.37	19.8
August	4.67	2.82	4.86	18.8
September	3.56	2.92	4.11	13.9
October	2.30	2.68	3.05	6.2
November	1.41	2.23	2.15	−0.8
December	1.27	2.9	2.26	−8.7

ÉcoTerra's design objective was to use significantly less energy (near-net-zero energy) than houses of a similar size in the region, while demonstrating several innovative technologies, including a building-integrated photovoltaic system with thermal energy recovery and a hollow-core slab in the basement for thermal storage. Demonstration of suitability for passive solar design principles and a ground source heat pump were also planned early in design. The selected builder specializes in modular homes; hence, ÉcoTerra also demonstrates modular construction of high-performance houses. This revealed several benefits including mass-producability, quality of construction, and facilitated integration of the PV modules (discussed later). Shipment and assembly of the seven modules of the ÉcoTerra house took approximately 8 h, though the basement concrete floor and walls were built prior to these steps. Figure 7.2 shows the timeline of the design, construction, and occupancy. Photographs of the construction process are shown in Figure 7.3.
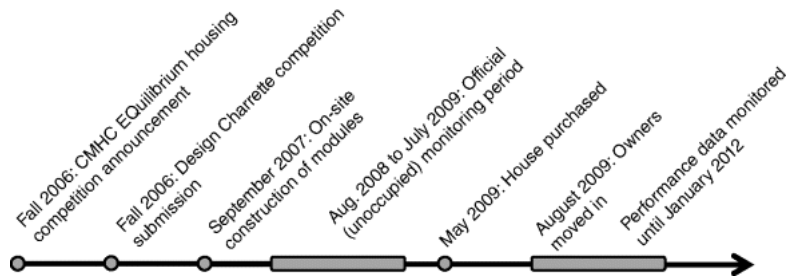
Fig. 7.2 Timeline of ÉcoTerra: from conception to occupancy

Fig. 7.3 Assembly of the ÉcoTerra house modules (a) main floor module; (b) lower roof section being lowered into place; (c) BIPV/T roof suspended above the second floor bedrooms; and, (d) all modules in place and connected

ÉcoTerra is the first of 15 demonstration houses that was selected to be built through a competition conducted under the Canada Mortgage and Housing Corporation (CMHC) EQuilibrium Healthy Housing Initiative (CMHC, 2010). The house was prefabricated in a factory in seven modules, including one module for the mechanical room. The modules were delivered and assembled on the chosen site in one workday in September, 2007.

Due to the prominence of cold sunny conditions in the region's winters, passive solar design is emphasized. To maximize solar exposure in the heating season, the house was oriented along the east–west axis with an aspect ratio of 1.38 – a level that was found to be approximately optimal for balancing solar gains potential with heat loss through the envelope. The south-facing window-to-wall area ratio is about 40%, with nearly 20 m² of triple-glazed low-emissivity argon-filled windows distributed between the basement and above-grade floors. The other façades have considerably fewer windows with areas of 6.5, 0.82, and 5.0 m² on the east, north, and west faces, respectively. The U-value of the main windows is 1.2 W/m² K and the solar heat gain coefficient (SHGC or g-value) is about 0.5. The thermal properties of the other ÉcoTerra surfaces are summarized in Table 7.3.

Table 7.3 Calculated effective thermal properties of main envelope components

Surface Type	Thermal Resistance (m² K/W)	Thermal Conductance (W/(m² K))
Walls	6.3	0.16
Roof	9.1	0.11
Under slab	1.5	0.67
Basement walls (above and below grade)	6.3 and 5	0.16 and 0.2

The southern part of the interior of ÉcoTerra has several thermally massive surfaces, including

– A 15 cm concrete floor on the main level, topped with dark-colored slate tiles.

– A knee wall on the main floor that extends 0.9 m above the floor and consists of 25 cm of concrete finished with the same slate tiles.

– A 12.5 cm concrete slab in the basement (the ventilated concrete slab that is discussed later).

– A 25 cm thick concrete wall that separates the north and south parts of the basement.

These surfaces help to regulate high levels of solar gains to prevent large temperature swings. This is critical for energy performance and comfort. A comfortable house is fundamental for good energy performance in passive solar houses because chronic overheating could prompt the owners to close blinds or open windows, even when it is very cold outside, thus reducing the benefits of solar gains. The floor plans and a photograph of the interior of ÉcoTerra are shown in Figure 7.4.
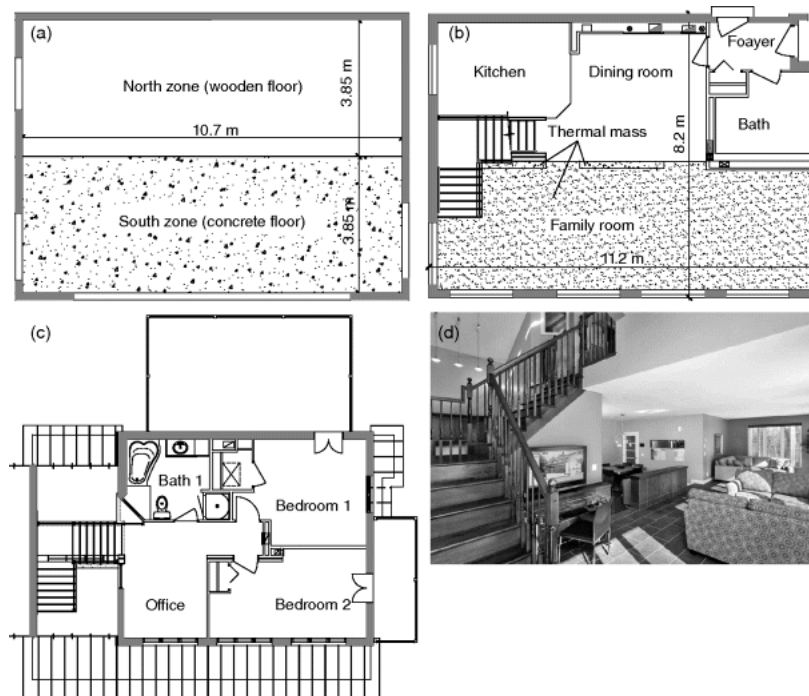
Fig. 7.4 Floor plans of (a) basement, (b) ground floor, and (c) second floor; (d) photograph of interior of ground floor living space

To help control unwanted solar gains – particularly in the summer and shoulder seasons – several fixed and movable shading devices were installed. A proportional-integral controller extends the exterior awnings to shade the bedroom windows when the temperature becomes uncomfortable. It is notoriously difficult to shade east- and west-facing windows with overhangs and other horizontally oriented shading surfaces; however, since construction, the owners installed a trellis system that shades the largest windows on the west façade. While 45 cm overhangs provide some shading for all south-facing windows,

the south-facing windows on the main floor are additionally equipped with manually controlled top–down dark-brown roller shades. These offer some solar gains rejection, though the dark color is not ideal for reflectivity. Approximately two-thirds of the windows are operable and casement type, which facilitates natural ventilation during the summer. The windows are not automatically controlled; thus, the occupants are relied upon to open the windows as needed in an attempt to improve comfort and reduce mechanical cooling needs.

Shortly after construction, a blower door test was performed. The test revealed an infiltration rate of 0.85 air changes per hour (ach) at 50 Pa differential pressure. The design goal was originally 0.5 ACH; nonetheless, the measured rate is considered very airtight.

To supplement passive solar gains, ÉcoTerra has a 55 m² building-integrated photovoltaic/thermal (BIPV/T) collector on the upper part of the roof. The BIPV/T collector is a hybrid in that it converts incident solar energy into both electrical and thermal energy. The outer layer of the roof consists of 21–136 W amorphous silicon photovoltaic modules with an area of 2.1 m² each and a nominal efficiency of 6.3%. The total PV array peak capacity is 2.8 kW (direct current). These modules extend from the soffit to the peak of the roof. This has the dual benefit of superior architectural integration and that the upper end of the modules is protected by the roof cap. The modules are epoxied onto the underlying black-colored steel roof.

There is a 4 cm thick air channel under the steel deck of the roof, as shown in Figure 7.5, that is used to heat air as it travels from the inlet of the roof (at the soffit) to the outlet (at the peak). The underside of the channel is composed of plywood sheathing and approximately 2.5 cm of spray foam insulation behind it. Once the air has reached the peak, it is sucked by a fan through round ducts that are evenly spaced across the roof, as shown in Figure 7.6. The variable speed fan sucks air from the roof at a nominal rate of about 200 l/s (and consumes about 400 W of power at this rate). The airflow rate was designed to be approximately double this; however, complex ducting significantly increased pressure drops between the roof and the sites of thermal energy use. In sunny conditions, the air temperature can increase by up to 40 °C from inlet to outlet of the collector.
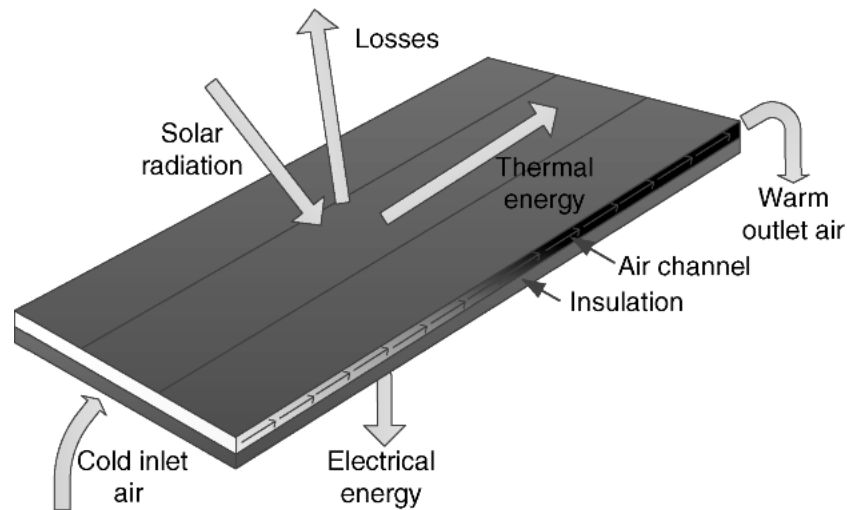
Fig. 7.5 Schematic of a BIPV/T roof showing the main energy flows

Fig. 7.6 BIPV/T roof: (a) finished roof module with PV modules attached; (b) underside of roof showing manifold (before insulation); and (c) underside of roof (insulated). Figures 7.6a and 7.6c reprinted with permission from Elsevier (Chen, Athienitis, and Galal, 2010a) © 2010, Elsevier

The benefit of combining electrical and thermal energy collection into a single surface is that more useful energy can be obtained from the limited roof area. Furthermore, hybrid solar collectors are designed to increase the overall solar energy collected (by collecting both electrical and thermal energy) and it is integrated into the building itself, forming the outer layer of the metal roof (on the south top side; see Figure 7.6). An added benefit to coupling PV and solar thermal is that the movement of air under the PV modules helps to cool them, which improves performance (the PV modules' performance decreases by about 0.21% per °C above the nominal temperature (25 °C)) and could help to extend their useful life since PV can deteriorate at high temperatures.

The energy balance of the roof is as follows.

$$IA = E_{PV} + E_{Thermal} + E_{Lost} + \rho IA \tag{7.1}$$

where I is the incident solar radiation, A is the roof area, E_{PV} is the rate of electrical energy generation, $E_{Thermal}$ is the rate of thermal energy collection, E_{Lost} is the rate that absorbed solar energy is lost to the surroundings, and ρ is the mean reflectance of the roof. For instance, for the ÉcoTerra roof under sunny conditions at about solar noon, it is possible to have about 1000 W/m² of incident solar radiation, of which nearly 6% (3 kW) can be converted to electrical energy and about 20% (12 kW) can be converted to thermal energy.

The PV array is connected to the central utility grid; though the utility does not currently pay a premium for its output. While the electricity generated from the PV can be used in the house or sold to the grid, the thermal energy output must be stored locally. The space heating demand is normally minimal during periods of high solar gains from the passive solar gains alone. Thus, thermal storage is essential for the thermal energy output of the BIPV/T roof to be useful for space heating.

The heated air from the BIPV/T roof has three possible uses to reduce total purchased energy of the house, as follows:

1. Space heating by charging the ventilated concrete slab (VCS) in the basement. The basement slab, pictured in Figure 7.7, is constructed of corrugated metal decking with about 12.5 cm of concrete above it. Air is injected into the channels at one end of the basement and it is exhausted outdoors at the other end. Measured results have shown that the system can store about 12 kWh (3.6 MJ) of thermal energy and charge at a rate of about 2 to 3 kW during peak conditions. It should be noted that the VCS can also be used for cooling, if it is discharged during cool summer nights.

2. Preheating domestic hot water using an air-to-water heat exchanger.

3. Drying clothes in a conventional clothes dryer that was modified to receive heated air in fan mode without electric heating.
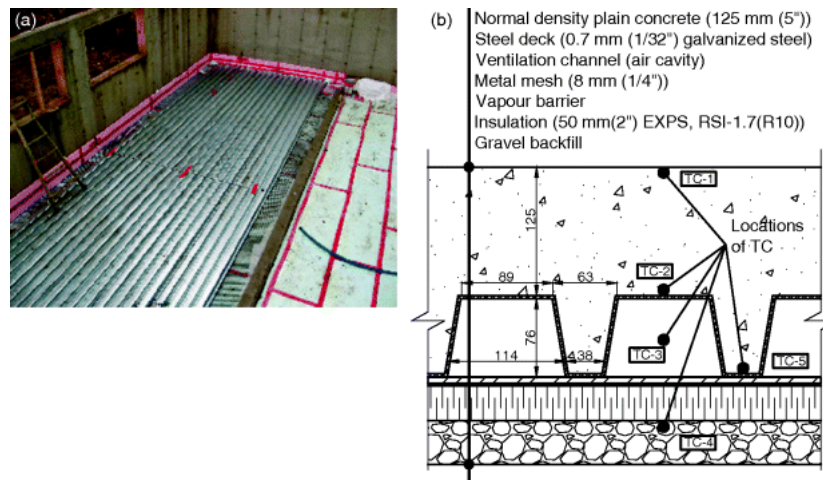
Fig. 7.7 Basement ventilated concrete slab: (a) prior to concrete being poured (left side) and under-steel-decking (right side of photo); (b) cross-section of VCS (right)

A series of fans and dampers are controlled by a central control system to optimally divert heated air in order to maximize its usefulness, as shown in Figure 7.8. If the outlet air is determined to be not useful (i.e., it is too cold or there is no demand for thermal energy), the main BIPV/T fan is turned off. Otherwise, it is powered to achieve between 40 and 80% of the rated airflow. A detailed explanation of the controls is described by Doiron (2011).
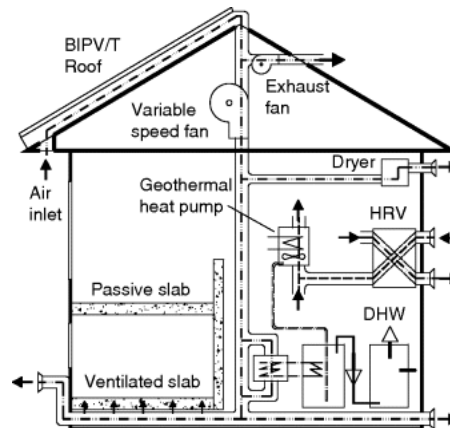
Fig. 7.8 ÉcoTerra system schematic (Chen, Athienitis, and Galal, 2010a)

To supplement the heating contribution from the passive solar heat gains and the BIPV/T system, the ÉcoTerra house includes a two-stage ground-source heat pump (GSHP) with an 11.1 kW thermal output capacity. The coefficient of performance (COP) of the GSHP was measured to be between 3.5 and 4.0 – slightly below the rated COP of 4.2 at full load.

The heat pump is controlled to operate in zero, one, or two stages depending on the outdoor temperature and the apparent heating load (as determined by the amount of time required to reach the heating setpoint once the indoor air temperature falls 1 °C below the setpoint). There is also an auxiliary heater (electric resistance) if the heat pump, alone, is deemed insufficient for achieving the heating setpoint. Operating in this mode is very undesirable because the COP effectively declines to 1.0 – an efficiency loss of about 75%.

Heating is distributed to all conditioned zones of the house via ducts using a forced-air system. The distribution fan has three rates: 355, 495, 590 l/s. The house is controlled as a single control zone for

heating and cooling, based on the temperature on the main level of the house. However, a motorized damper prevents heat from being delivered via ducts to the bedrooms if overheating is detected. This quasi-single zone configuration has the advantage of simplicity, but prevents some controllability – particularly if different temperatures are desired in different spaces or if heat gains (e.g., equipment or solar) are unbalanced.

Care of thermostat placement must be taken in passive solar houses. For instance, if it is placed in the direct solar gain zone, there is a risk that that space will overheat and the thermostat will send the control signal to turn off the heating supply – even if other parts of the house are too cold. The ÉcoTerra house has two means to mitigate this risk: (1) it is an open concept, so natural air circulation helps distribute solar gains and (2) the high-efficiency air distribution fan can be activated in circulation mode, such that air is circulated within the house even with no heating or cooling.

A heat recovery ventilator (HRV) was installed to recover sensible heat from the exhaust air. The selected model has a sensible effectiveness of 72%, consumes 95 W and exchanges air at 70 l/s at high speed mode. While it was initially configured to always operate in high speed mode, this was later modified such that it remains in low speed mode (34 W of power consumption) unless the bathroom or kitchen fans are activated. An air-cleaner is connected in series with the HRV; however, it is somewhat redundant to the HRV since the HRV also has an air filter.

The domestic hot water (DHW) heating is achieved in one of three ways: (i) preheating by the BIPV/T air, (ii) desuperheater from the GSHP, or (iii) by an auxiliary electric heater. The system has both a preheat and regular tank – both with a volumetric capacity of 240 l.

The installed major appliances are primarily low-energy and EnergyStar rated. They are all electric, including a refrigerator, oven/stove, and clothes washer and dryer. While the installed lamps were mainly compact fluorescent, the owners installed approximately 24 halogen lamps after they moved in (discussed later).

7.2.2 Design Process

This section provides a brief summary of the design process that was applied to ÉcoTerra in 2006. Its main purpose is to document the process so that it can be used as a model; meanwhile, the effectiveness of the process is discussed.

7.2.2.1 Design Objectives

The design objectives of the house were to achieve near-net-zero energy performance, low environmental impact (i.e., materials that are non-toxic and have low volatile organic compound emissions), and a comfortable and healthy indoor environment. The design team also sought to demonstrate innovative integrated and low-cost solar and energy storage technologies. Finally, a low overall house cost was important because ÉcoTerra is a demonstration and the designers wanted to ensure that mass production of the house (or similar houses) for the middle class would be feasible.

7.2.2.2 Design Team and Design Process

The design team consisted of about 10 experts and was led by an architect–engineer team. The design process is summarized in Figure 7.9. Initially, once the design objectives were established, the lead energy systems engineer and researcher, Dr. Andreas Athienitis from Concordia University, provided some basic guidelines for the major geometrical and construction properties of the house to the architect, Masa Noguchi. Because of the emphasis on passive solar heating, an aspect ratio of about 1.3, two stories, and a south-facing window-to-wall area ratio of about 40%.

Design Charrette

Members: Concordia University research team (energy systems design), architect, builder, municipality representative, and ground source heat pump (GSHP) distributor.

Background work prior to charrette:
- Proposed architectural drawings.
- Predicted plug loads (lighting, appliances, etc.).
- Fixed major geometry to reduce size of design space.

Tasks and decisions during the charrette:
- Performed parametric simulations using HOT2000 to determine effect of insulation, windows, and form.
- Performed design day calculations (using custom model in MathCAD) to assess passive solar performance and thermal comfort.
- Estimate BIPV/T output.
- Size PV to achieve desired EnerGuide for Houses (EGH) rating – a Canadian residential energy rating system. Priority was given to reaching target while maintaining affordability.
- Assumed a 45° slope for BIPV/T roof (near optimal for the local climate).
- Size GSHP (it was later downsized to account for passive solar contribution).

Left column flow:
- Rules of thumb for passive solar houses were applied to obtain starting point for main passive solar features and major dimensions.
- Using the rules of thumb, the architect created proposed architectural plans.
- A two-day design charrette was held (see right for details).
- A one-day follow-up charrette was held to discuss the ventilated slab system.
- Alouette Homes performed lighting, forced-air ducting, and other electrical detailed design.
- Detailed design by architect, based on charrette, was completed.
- The control system was designed by a commercial building controls company and the researchers.

Fig. 7.9 Outline of the design process of ÉcoTerra

Once the architect was provided with the approximate geometrical details, he provided some preliminary drawings to the engineers. Prior to the design charrette, the appliance, lighting, and plug loads were estimated using a bottom–up approach, whereby energy consumption of each appliance and other electricity-consuming item was predicted.

A two-day design charrette was held to start the detailed design of ÉcoTerra. It involved about 10 experts, including the lead engineer and architect, graduate students, the builder, a representative from the local municipality, and several technology experts. From the charrette, several key features of the design were identified, including

1. A direct gain passive solar design combined with a well-insulated, airtight envelope;
2. A BIPV/T roof solar collector coupled with a ventilated concrete slab for active charging and passive discharging; and
3. A ground-source heat pump with vertically drilled wells coupled with a forced-air heat distribution system.

One of the design modifications that occurred during the design charrette is that the main part of the roof that was to be the solar collector was reduced in slope from 45 to 30 degrees (and south facing). This is because the nature of the construction – prefabrication in a factory – posed constraints on the maximum allowable height of each module. The theoretical difference in annual electrical energy output from the PV, according to RETScreen (explained later), is merely 1.4%, not accounting for the difference in total surface area. However, as described later, the eventual consequence of this design change is that wintertime PV performance is significantly diminished because the shallow slope is not adequate to readily shed snow.

Following the two-day design charrette, a follow-up one-day charrette was held to focus on the design of the ventilated concrete slab storage system. The builder, Alouette Homes, completed the detailed standard electric and mechanical design and drawings. Following that, the architect finalized the drawings. The ÉcoTerra controls, which are considerably more complex than for a standard house because of the BIPV/T and VCS systems, was designed and implemented by a large commercial building controls company.

7.2.2.3 Use of Design and Analysis Tools

The EQuilibrium House design competition required the use of two tools – HOT2000 (NRCan, 2010) and RETScreen (RETScreen International, 2005) – for predicting performance, as a minimum.

HOT2000 is normally used as an energy auditing tool for existing Canadian houses, and is thus not aimed at aiding design. RETScreen is a prefeasibility tool for assessing the performance of renewable energy systems, including PV and solar domestic hot water systems. The spreadsheet-based tool uses simplified methods, but is very fast to use and efficiently quantifies the sensitivity of key parameters.

HOT2000 uses a bin method and is intended to assess the performance and possible retrofits of detached houses. Its features are aimed at Canadian homes and the associated construction practices (e.g., wood frame) and technologies (e.g., natural gas furnaces with forced-air distribution). HOT2000's calculation method makes it less suitable for assessing dynamic behavior – something that is fundamental for passive solar performance assessment. Also, its lowest reporting frequency for output is monthly, meaning that hourly comfort metrics, which are fundamental to informed passive solar design, are unavailable.

Regardless of HOT2000's limitations, it was useful in estimating annual performance – an essential element of predicting the net energy consumption (or production) of the house in a standardized way. One of the common methods used for deciding on key elements of ÉcoTerra design was parametric analysis. For example, Figure 7.10 shows results that were presented at the design charrette to support the decision to not "super-insulate" the house. It clearly indicates that increasing wall insulation from RSI-8 to 10 only has about half the impact of increasing it from RSI-6 to 8. The vertical scale of the graph shows fairly marginal gains, indicating that other approaches to reducing net energy consumption (e.g., higher efficiency PV) may become more economical.
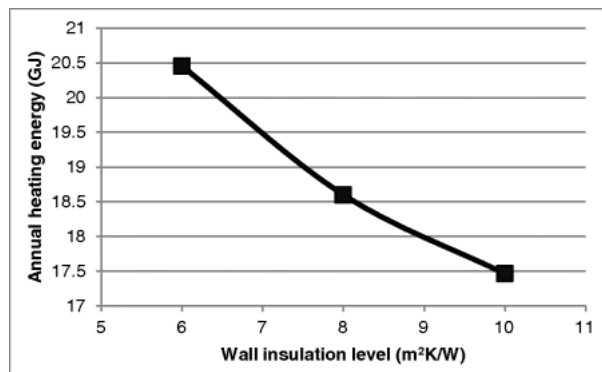
Fig. 7.10 Results of parametric analysis that was used to decide on the optimal insulation level in the walls

To supplement this, the design team used customized software programmed in MathCAD (Chen, Athienitis, and Galal, 2010a; Chen, Galal, and Athienitis, 2010b). The custom software uses an explicit finite difference method for spatial and temporal discretization, so that short timesteps could be used and the benefit of thermal mass could be accurately assessed (see Figure 7.11). This approach also provided greater flexibility, such as coupling the BIPV/T and VCS to the house model. Rather than performing whole-year simulations, the emphasis was on characterizing performance for a cold sunny day, which is typical of the region's winters.
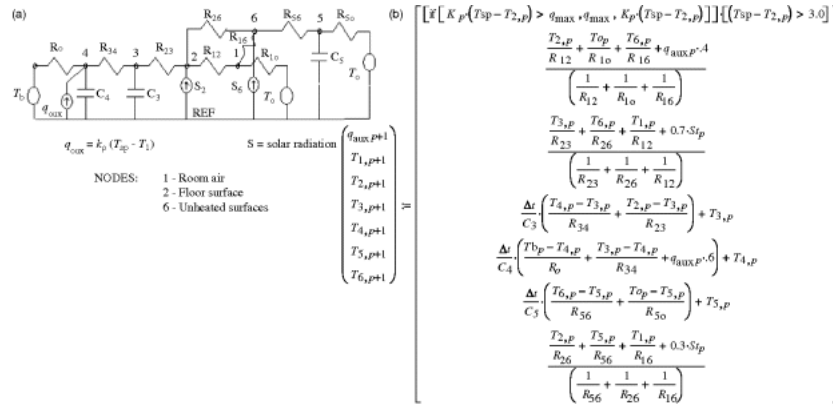
Fig. 7.11 (a) Diagram of simplified lumped capacitance model used to simulate ÉcoTerra during design and (b) the corresponding explicit finite difference equations

RETScreen's role in the design of ÉcoTerra was to predict the performance of the PV element of the proposed BIPV/T roof. The tool's simplicity allowed the effect of many design options (such as slope, orientation, and technology) to be explored very quickly. However, the model is steady-state and only intended for stand-alone (non-building-integrated) PV installations. This means that the effect of heat transfer to the roof is neglected. Furthermore, thermal coupling with the thermal energy collection aspect of the roof was not possible. Finally, the RETScreen model does not consider snow accumulation, a factor that proved to be significant in ÉcoTerra. Athienitis (2007) recommends roof slopes of at least 40° and smooth surfaces (e.g., no eaves troughs) to prevent snow accumulation.

To assess the combined performance of the thermal and electrical aspects of the BIPV/T roof, a custom program was built, similar to the one for assessing the house's passive solar performance. The results of this analysis were used to make design changes and ultimately to predict the net-energy consumption of the house (Chen, Galal, and Athienitis, 2010b).

7.2.2.4 Assessment of the Design Process

Upon interviewing several design team members, several notable conclusions were drawn. They stated that the main (two-day) design charrette was very effective, that the collaboration between the large group of experts exceeded expectations, and that the work that was completed in advance was essential to a productive group design session. However, improved communication between the designers and builder teams regarding some of the more innovative aspects of the house, such as the ductwork linking the BIPV/T roof to the sites of demand would have been desirable. Also, the use of design tools was somewhat fragmented, since at least four separate models were used. It would have been preferable to use a single tool, so that proper thermal couplings between house components could be assessed (O'Brien, Athienitis, and Kesik, 2009). However, such a tool for early design stage is currently unavailable. This is difficult when new technologies, such as the BIPV/T roof linked to a ventilated slab, are being modeled.

7.2.3 Measured Performance

ÉcoTerra's zone temperatures and energy consumption were monitored by over 150 sensors from construction to early 2012. The data were collected at regular intervals and stored in an on-site database. The database could be queried remotely for ongoing analyses that were being performed on the house for several years following occupancy. The major categories of electricity use that are measured are PV generation, the heat pump, DHW, and total electricity use. The data were disaggregated using knowledge of power draw and by using pattern recognition on the total power draw, as explained by Doiron, O'Brien, and Athienitis (2011). The heat pump electricity consumption for both heating and cooling are combined. For the purpose of the analysis that follows, it is assumed that only heating or cooling occur in any given month and that therefore, there is a modest amount of cooling in July and heating is used for the months other than June through August.

Key results are shown in Figures 7.12 and 7.13. Some notable lessons from the data for the period from December 2009 to November 2010 are explained next.

	Dec	Jan	Feb	Mar	Apr	May	Jun	Jul	Aug	Sep	Oct	Nov
Fan, misc. pump	97.27	104.48	106.08	139.79	146.17	155.42	144.78	153.53	154.86	151.34	137.15	119.78
Light, app, plug	567.52	443.73	365.70	412.60	313.46	314.97	361.86	398.73	392.28	358.00	451.81	334.16
Aux HP heater	35.61	68.42	0.00	0.00	0.00	0.00	0.00	0.00	0.00	0.00	0.00	0.00
Controls	25.00	25.00	22.58	25.00	24.19	25.00	24.19	25.00	25.00	24.19	25.00	24.19
Aux garage heater	331.98	216.90	132.34	62.99	2.36	0.00	0.00	0.00	0.00	0.00	11.68	4.52
BIPV/T fan and pump	0.00	0.00	8.47	22.09	19.96	22.02	16.52	22.68	10.96	9.72	4.47	5.47
HRV/air cleaner	83.81	83.08	73.74	80.65	77.19	79.85	84.65	92.20	96.59	108.53	83.61	78.39
DHW	105.37	92.17	93.79	133.72	138.49	137.29	151.18	171.34	200.69	162.52	96.15	95.51
Heat pump	686.93	609.04	388.55	182.72	116.50	26.98	51.28	14.56	0.00	31.09	202.07	348.38

Fig. 7.12 ÉcoTerra's monthly energy use in 2010 (Dec. 2009 to Nov. 2010)
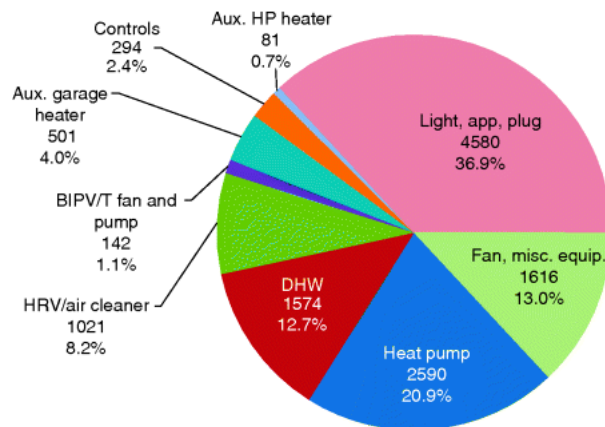
Fig. 7.13 Annual breakdown of electricity use in ÉcoTerra house

Total heating electricity (space heating and DHW) is only about one-third of the total. This is in contrast to the existing housing stock, for which this fraction is closer to 80% (NRCan, 2008). Three major reasons for this are the decreasingly important impact of heating as envelopes become higher in quality, the strong passive solar component, and the fact that a heat pump was used, reducing the space heating and cooling energy by a factor of about 3.7. It should be noted that because of the desuperheater's assistance in domestic hot water heating, the DHW load appears lower in the winter. This is simply because the DHW load is measured based on auxiliary electric water heating, not total DHW load.

The HRV and air cleaner account for about 8% of total annual electricity use. Future effort to optimize the controls to minimize ventilation when it is not needed or when natural ventilation is sufficient would be beneficial.

The lighting, appliances, and plug loads account for over one-third of the total energy use, yet this was given a disproportionately low level of attention relative to other aspects of the design. While new high-efficiency appliances were selected, the potential for real-time display of data in an effort to impact occupant behavior was not examined. This result emphasizes the importance that Net ZEB designers also examine energy-conserving approaches to lighting and appliances.

The monthly PV performance showed reasonably good comparison to modeled performance (based on RETScreen) during the summer months (see Figure 7.14). However, during the four coldest months – November through February – generated electricity was only 20–40% as much as expected. This is almost exclusively due to chronic snow accumulation. Figure 7.15 shows a typical winter day after snowfall.
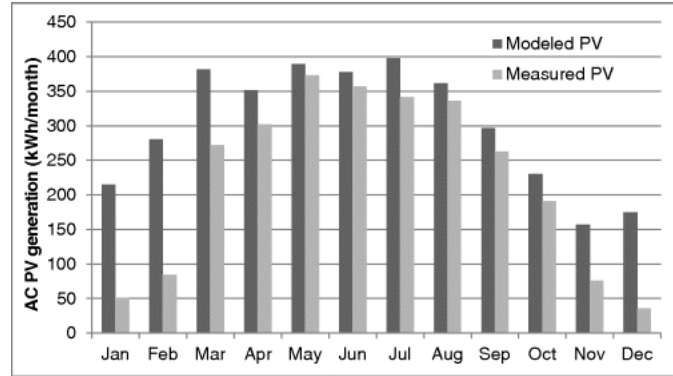
Fig. 7.14 Modeled and measured PV performance (for the current design with a 30° slope)

Fig. 7.15 ÉcoTerra on a typical winter day after a snowfall

Short-term high-resolution electricity use and supply profiles are valuable for providing information about ÉcoTerra's thermal characteristics and its controls. Figure 7.16 shows the house's performance on a typical sunny shoulder season day. Particularly notable is that there are several large spikes in electricity draw – particularly early in the morning when the heating setpoint increases, and then throughout the rest of the day for DHW and appliances. Other causes of high peaks are from cooking (e.g., from the electric oven).
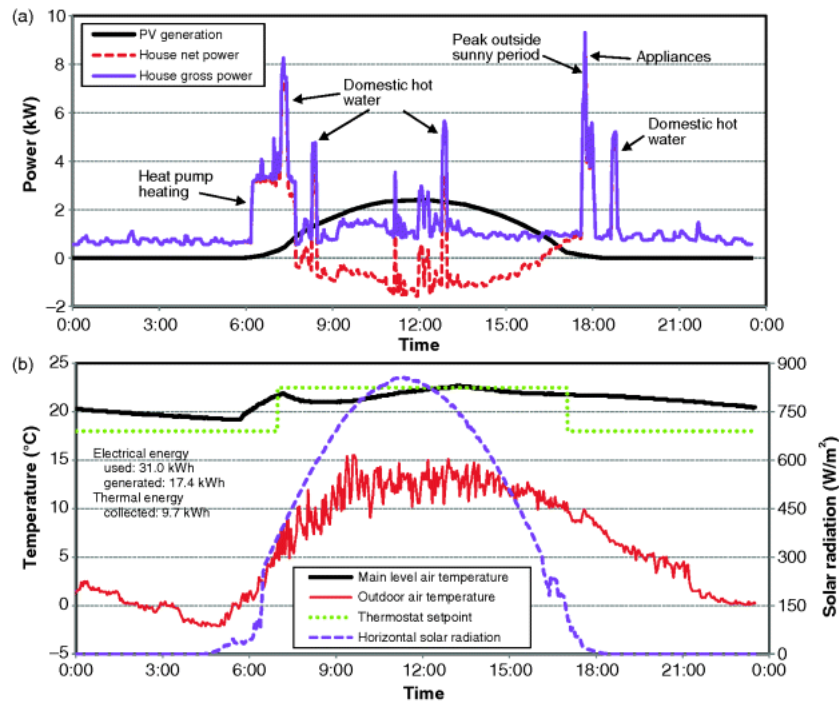
Fig. 7.16 Key performance metrics on April 13: (a) PV power generation and gross and net power consumption; (b) passive solar performance, including indoor temperature response from solar gains (from Doiron, O'Brien, and Athienitis (2011))

7.2.4 Redesign Study

In order to perform further analysis on ÉcoTerra, a detailed model was created. EnergyPlus (Department of Energy (DOE), 2009) was selected for its relative ease of use, extensive features, and interoperability with a variety of other tools. This section describes the modeling that was performed including boundary conditions, form and fabric, operations, renewable energy systems, and results.

7.2.4.1 Boundary Conditions

Since ÉcoTerra is near Sherbrooke, Quebec, the model was run using Sherbooke EPW weather files. A limitation of using an existing weather file is that it does not capture the year-to-year variation in weather. However, the effect is largely reduced by comparing monthly values, for which many of the variations are mostly canceled out.

7.2.4.2 Form and Fabric

The geometry was derived from the architectural drawings and manually input using SketchUp/OpenStudio (DOE, 2009). The house was modeled as four conditioned zones, in an attempt to properly characterize any discomfort resulting from stratification, as shown in Figure 7.17. In addition, a zone was assigned to the roof space and to the garage.
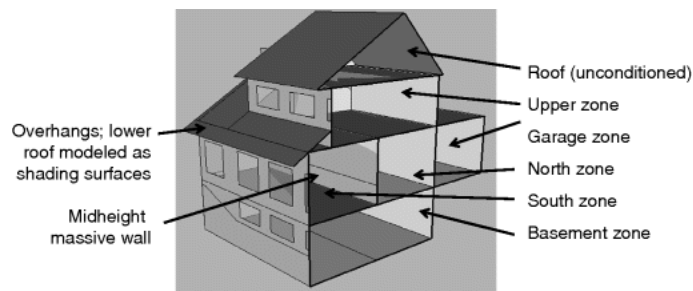
Fig. 7.17 Section view of thermal model with zoning scheme

The thermal resistances of the different envelope components are summarized in Table 7.3. Stud wall equivalent thermal resistance values were calculated using the "parallel path" method.

7.2.4.3 Operations

A survey of energy-consuming household objects was performed to determine an appropriate heat gains schedule. Appliance, lighting, and air distribution loads were assumed to be seasonally invariant. The total internal gains were distributed into an hourly schedule based on results from Armstrong *et al.* (2009). The occupant schedule assumed that three adults occupied the space according to a typical working family. The infiltration rate was input based on that measured for the house using a blower door test. The infiltration rate at 50 Pa was measured to be 0.85 ACH, which is approximately equivalent to 0.043 ACH under typical conditions with a pressure difference of 4 Pa. This was assigned at a fixed rate and evenly distributed to all zones. Similarly, the 0.3 ACH of ventilation was reduced to an effective ventilation rate of 0.12 ACH because of the HRV, which is approximately 60% effective. The HRV system was not explicitly modeled.

7.2.4.4 Renewable Energy Systems

In adherence with the rest of the model's level of detail, the BIPV was modeled as being thermally coupled to the roof. The 21 UniSolar PVL-136 amorphous silicon modules were modeled using EnergyPlus' one-diode model (DOE, 2013). The simple inverter model was used with an assumed operating efficiency of 92%.

Since EnergyPlus does not have a readily available air-based BIPV/T model, a custom model was created in MATLAB. The limitation to this approach is that the model is decoupled from the main EnergyPlus model (i.e., there is not two-way communication between the models during simulation). However, this approach can be used to assess the thermal energy availability relative to household thermal energy demand, in an effort to approximate its value.

7.2.4.5 Simulation Results

Figure 7.18 shows the measured and simulated heat pump energy consumption. Monthly heating and cooling energy were converted to electricity consumption using a COP of 3.7 (as measured to be the annual average for ÉcoTerra's heat pump). The annual modeled electrical energy consumption is 2519 kWh versus the 2524 kWh that was measured for the same period. The results indicate that the thermal model is an accurate representation of real performance and suitable for assessing the building upgrades that are described in the sections that follow.
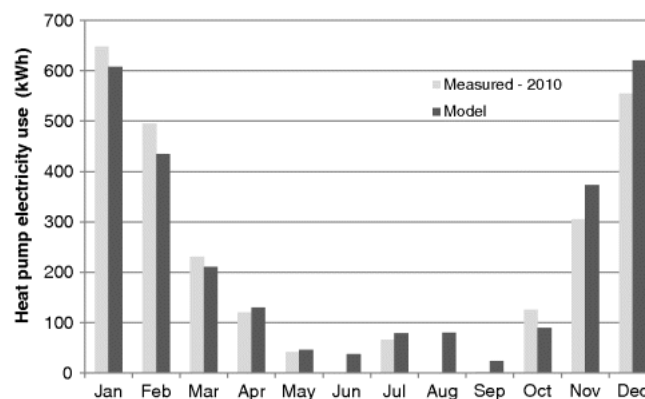
Fig. 7.18 Comparison between measured heat pump electricity and modeled values

Unlike for heating, which is tightly controlled, the occupants had the option of overriding mechanical cooling by merely switching it off. Consequently, the model overpredicted cooling energy. There was anecdotal evidence from the owners that natural ventilation was used as a means for cooling and increasing air movement. While this was coarsely modeled, other discrepancies could occur from a high tolerance for high temperatures or significant periods of absence during summer vacation.

Another interesting peculiarity is that the model consistently under-predicts heating energy from January to March and overpredicts heating energy in November and December. Possible explanations

are shading from trees, ground reflectance variability (from snow) or simply, a change in occupant behavior (e.g., greater internal gains or a changed heating setpoint).

7.2.4.6 Implementation of Redesign Strategies

This section outlines the redesign study that was performed. The fundamental question being asked is how could ÉcoTerra and other similar low-energy houses have been designed to achieve net-zero energy status? The EnergyPlus model was used to assess each upgrade for energy performance. There are three major categories of possible upgrades:

1. Operational changes: existing hardware with changes to control strategies, such as setpoints and logic for controls related to solar heat collection and usage/storage;

2. Building envelope changes: either passive or active envelope components to change how the house interacts with the environment; and

3. Generation: active systems to offset energy use.

For redesign, the operational changes will be considered first because they are noninvasive and have no material costs. The last two options – envelope upgrades and generation – will be considered simultaneously. A fourth category of upgrades could consider a modification to occupant behavior. Nearly 40% of the electrical loads are related to appliances, lighting, and plug loads. Furthermore, some of the heating and cooling can be attributed to the fact that the occupants have the set points at values other than anticipated during design. For instance, the daytime heating setpoint is 22.5 °C instead of 21 °C, resulting in a predicted 10% increase in heating loads, according to the model. However, these social aspects are considered beyond the scope of the current study. Making assumptions that could lead to sacrifices in comfort and convenience would undermine the occupants' values. While the designer cannot predict discretionary energy use to a high degree of certainty, they can inform the occupants about their habits; either informally or through the installation of an "energy dashboard" that provides useful feedback. For example, the authors visited the occupants at their home after several months of occupancy to show them a breakdown of energy use. Upon informing the occupants that the electric resistance heater in the garage was using nearly as much energy as the heat pump, they reduced its use to negligible levels. Chetty, Tran, and Grinter (2008) stated that real-time feedback of household energy consumption can lead to 10% savings with minimal change in behavior. Further grid-side benefits can be achieved through shifting non-time-sensitive loads, such as clothes drying and dish washing. Such habits can be encouraged using different time-of-use electricity rates.

The analysis of many of the upgrades described are made possible because EnergyPlus is a detailed tool that has a powerful output facility with which many low-level outputs (e.g., nodal temperatures and heat fluxes) are available on the timestep level. Many earlier stage design/simulation tools, such as HOT2000, use standard configurations. However, the creation of the EnergyPlus model took about five days, which is an order of magnitude longer than for the HOT2000 model.

Major savings that can be achieved through changing the controls of the house were explored first. The "equipment" category of energy use is mainly comprised of the distribution fan built into the heat pump. The fan is currently operated at a constant rate, even when fresh air and conditioning requirements are met. Simulations were run to determine the potential benefit from reducing the fan (when heating and cooling are unneeded) to only operate when the mean air temperature difference between zones exceeds 2 °C. The simulation indicates that the fan can be set to low speed for 8% of the year, yielding fan energy savings of about 130 kWh. Additional savings (460 kWh/yr) can be achieved by removing the air cleaner, which can be considered redundant to the air filter in the heat recovery ventilator (HRV), and unnecessary in the rural setting.

In order to assess the best opportunities for improvement to the envelope, the sources of heat loss were predicted for the house during the heating season (Figure 7.19). While the window losses account for 21% of total losses, the net energy balance for the windows including solar gains is positive – by about 1000 kWh. Since the house is relatively airtight, there is little benefit to further sealing the envelope. Similarly, the ventilation rate cannot be lowered and the house is already equipped with an HRV. A modest reduction in the effective ventilation rate would be possible with an HRV of a higher effectiveness (e.g., 80%). However, upgrades to the envelope represents the main practical potential to reduce total heat loss.
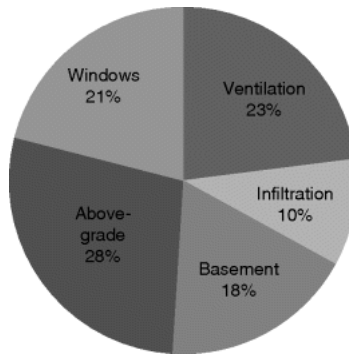
Fig. 7.19 Distribution of heat losses

The benefit of removing the dividers in the windows was examined. Currently, most of the large south-facing windows are operable and have two dividers in them. This not only increases the conductance of the envelope, it also reduces solar gains. The removal of two-thirds of these (leaving enough operable windows to enable natural ventilation) reduces predicted heating energy by about 12%. The upgrade to better-insulated window frames and doors only yields a modest reduction in heating loads and thus they were not changed.

The addition of intelligent shade control – either manual or automated – was considered. For the cooling season, shades were assumed to be closed during periods when the zone air temperature exceeds 22 °C. This is predicted to reduce cooling loads by about one-third, resulting in 90 kWh of electricity savings. Proper shade control also improves thermal comfort by mitigating overheating and direct beam solar radiation on occupants.

The addition of 1 m² K/W of insulation on the basement and above-grade walls of the house was found to yield an annual reduction in electricity use of about 150 kWh. This was not considered practical, and thus, the insulation levels were left as-is.

The energy implications of each upgrade are quantified in Figure 7.20. With these upgrades, there are few good remaining opportunities to reduce consumption without modifying occupant behavior. The total predicted energy use was reduced by 7%. This is a positive outcome, since it indicates that the designers of ÉcoTerra did not miss any major opportunities. In order to attempt to offset all energy use with renewable energy, the gap should be filled with the energy supply side.
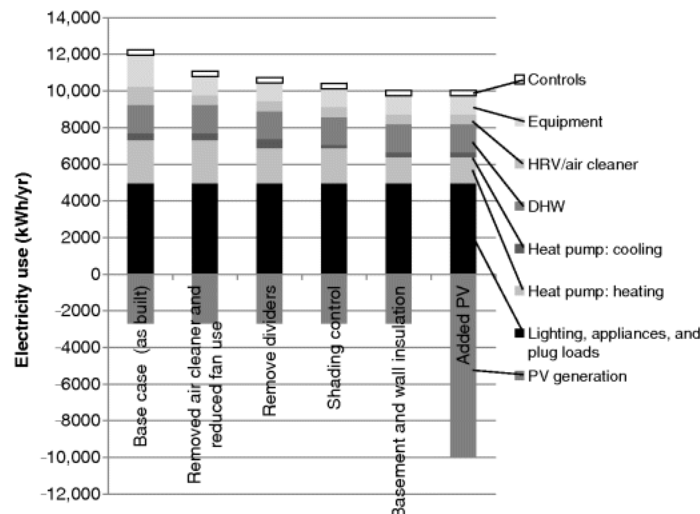
Fig. 7.20 Electricity use and generation for successive upgrades

For active solar energy collection, an existing issue that should be considered is snow accumulation on the roof and its negative impact on wintertime generation. For example, the performance in 2010 clearly indicates that the performance in the winter fell short of theoretical performance (Figure 7.14). Thus, the effect of increasing the BIPV/T roof slope to 45° (from 30°) was examined. From experience, this slope

has been found to effectively shed snow (Athienitis, 2007). RETScreen (RETScreen International, 2005) indicates that the difference in slope has a minor effect on annual incident solar radiation, since both slopes are in the near-optimal range for the site's latitude – 45°N. Assuming that the base of the south-facing roof remains the same, the additional pitch results in a 22% increase in area for a total surface area of 65.6 m².

Assuming annual electricity use of 10,000 kWh, an inverter efficiency of 92%, shading losses of 8% (as measured for the site), and 90% module coverage area (for spaces and edges), a minimum module efficiency of 12.9% is required to achieve net-zero energy. This level of efficiency is above the range (5–7%) of common amorphous silicon modules, thus poly-silicon or other higher-performance modules are needed. The total capacity of the array must be at least 8.0 kW (or 280% greater than the existing array). To put this in context of current technologies, newer PV modules can achieve 18–22% efficiency. Such efficiencies would facilitate substantially smaller array areas, if needed or desired.

As discussed earlier, timing is critical to BIPV/T performance; the energy is only useful if it is used immediately or stored for future use. Figure 7.21 compares the monthly combined space and DHW heating energy with BIPV/T thermal energy generation. The air is considered to be useful only if its temperature exceeds 20 °C. This is because most of the applications for the heat require this. For instance, in order for heat to be transferred to the ventilated concrete slab, the air temperature must exceed the slab temperature.
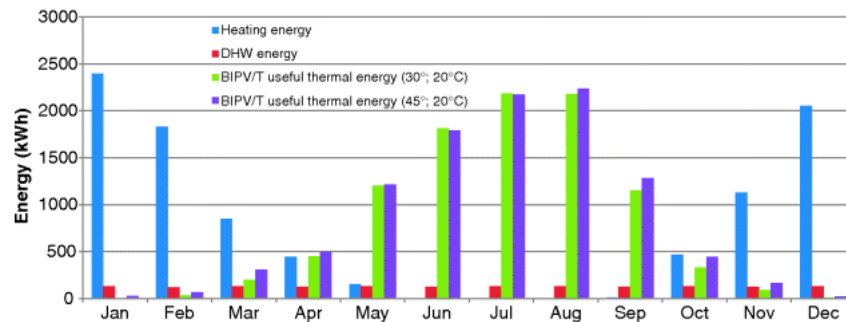
Fig. 7.21 Comparison of thermal loads and BIPV/T useful energy output

Predicted annual performance is similar for both 30° and 45° designs. However, in the winter, though performance is low, useful energy output is nearly double for the steeper roof. This is due to the slightly longer (soffit to peak distance) roof and the fact that the roof is oriented better to face the low winter sun.

While total energy output and demand are relatively similar in magnitude over the course of a year, they vary significantly by month and the peaks are about six months out of phase. The most reasonable method to solve this problem is to use seasonal storage, such that the gap is closed. The use of a heat pump to upgrade the thermal energy to higher temperatures would also be beneficial. For example, this was done for the Alstonvale House design (Pogharian *et al.*, 2008), since it significantly decreases the outlet temperature threshold above which the energy is in a useful form. Following the previous analysis on BIPV/T performance, the simulations were repeated for a case where this threshold is reduced to 10 °C (results shown in Figure 7.22). While there is still a seasonal mismatch between supply and demand, the supply increases significantly – especially in the shoulder seasons and the summer. These results indicate that without the use of a heat pump, effective BIPV/T performance is limited to the warmer months.
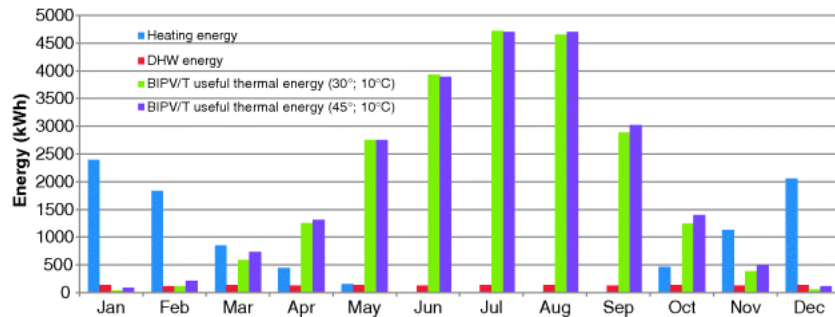
Fig. 7.22 Comparison of thermal loads and BIPV/T useful energy output

As mechanical systems and their controls become more complex, the capabilities of traditional building performance simulation tools is approached or exceeded. The ÉcoTerra house, as built, would be difficult to fully model in EnergyPlus because of the BIPV/T, VCS storage, and the associated controls. TRNSYS (TRNSYS, 2012) is more capable of modeling these systems, but is not as sophisticated in the building domain. An emerging option is to use two tools that are capable of time-step coupling (e.g., Harmonizer (Beausoleil-Morrison, 2011) allows co-simulation in ESP-r and TRNSYS).

7.2.5 Conclusions and Lessons Learned

This case study examined the design process of a near-net-zero energy house, presented measured performance results, and suggested how net-zero energy status could be achieved through some design changes. Simulations showed that only modest electricity savings are possible without taking any uneconomical measures. Beyond that, additional active building-integrated solar energy generation becomes the most practical upgrade to achieve net-zero energy. After the design upgrades, discretionary loads account for nearly half of electricity use. In houses for which the envelope heat transfer and passive solar performance have been optimized, one of the greatest remaining opportunities is to influence occupant behavior by means of advanced controls, display of resource consumption, and education. This represents a significant and necessary area for further research. For instance, Gram-Hanssen (2010) reported that occupant behavior can influence heating energy by as much as 350%. Two major trends are expected to aid the movement toward widespread implementation of low-energy houses: (1) the improvement of efficiency and intelligence of appliances and equipment, and (2) the improvement of active solar energy collectors. This means that even a house that is not net-zero energy today may become so as old equipment is replaced with higher-performance equipment over its life cycle.

ÉcoTerra's form and fabric were selected for optimal passive solar performance. It has a south-facing width-to-depth ratio of 1.38, an overall window-to-wall-area ratio of 15% (40% for the south façade), which is equivalent to a solar aperture (south-facing window area-to-total floor area ratio excluding the garage) of 9.1%. The windows are triple-glazed, low-e coated, and argon-filled. To supplement heating and cooling in southern Quebec's heating-dominated climate, a BIPV/T system was built. The upper south-facing roof section consists of 21 laminate amorphous silicon (a-Si) modules with an air space underneath, through which air is drawn and warmed by the absorbed solar radiation. The energy content of this air is used to warm (or cool during summer nights) a ventilated slab in the basement, preheat domestic hot water, or dry clothes, depending on the current demands. A ground-source heat pump with a COP of about 3.7 is used to supplement the passive and active solar heating. ÉcoTerra's building envelope was designed according to passive solar design principles.

There is significant thermal mass integrated into the basement and main level of the house. The basement floor is divided into northern and southern halves. The northern part has a standard concrete slab with a thickness of 75 mm, while the southern part has 125 mm of concrete cast over steel decking to form a ventilated slab. There is a 250 mm thick concrete dividing wall between the basement's main areas (in the east–west direction) and it extends 900 mm up into the first floor of the living space. There is a 150 mm concrete slab on the floor in the south zone.

Due to the heavy involvement of many experts during the design process and a formal integrated design process, many of the fundamental enclosure and equipment parameters were verified to be near-optimal and practical for the southern Québec site. However, useful lessons were obtained from the operations and occupant behavior aspects of the project.

There is an important trade-off between thermal performance and daylighting in any building. For ÉcoTerra, in the interest of minimizing north-facing glazing, which barely contributes any solar gains in the heating season, daylight availability was sacrificed. However, this unintentionally led to the owners installing about 24 additional light bulbs to illuminate the space. With increasingly high performance windows, perhaps future designs should provide a greater emphasis on daylighting even at the cost of thermal performance.

The ÉcoTerra owners placed large shag carpets over the slate floor, rendering the covered part of the thermal mass significantly less effective at storing solar energy. Their motivation could be esthetic, acoustical, or for thermal comfort. Thermal and acoustic comfort could both be quantified during design; yet it is rare to model buildings – especially residential – to such a high resolution. If the issue is acoustic, sound-absorbing panels or furniture could be strategically positioned. If the issue is cold feet from the highly conductive floor, two solutions can be used: (1) radiant floor heating could replace forced-air to increase the floor temperature, or (2) the other room surfaces (i.e., walls, ceiling) could be used for thermal mass while ensuring the floor is reflective but not highly conductive.

The electric auxiliary heater in the ground source heat pump, before intervention, was being triggered on a daily basis when the setpoint increased from 18 to 22.5 °C each morning. The controls caused this when immediate heating loads could not be met by the heat pump alone. However, this heat comes at a cost that is three to four times greater than from the heat pump. To resolve this, the controls were tweaked. As a result, the space does not reach the daytime setpoint as quickly. Another method for reducing energy use would be to delay the setpoint increase until after some solar gains have occurred (around 10 A.M.) such that the space is warmed for free. The suitability of this approach depends on the lifestyle of the occupants.

As can be expected, the rooms of the house are not being used exactly as planned. The most extreme instance of this is that the garage was converted into a workshop. To warm the space, the owners installed a 5 kW electric resistance heater. For the few months that this went undetected by the Concordia University research team, this heater was using one-third of the electricity that was used to heat the entire house! This is despite the fact that the garage represents a mere 10% of the floor area of the house and was never heated to the temperatures of the rest of the house. If the space must be heated, it would be favorable to either heat it with the central heat pump, or more interestingly, with the BIPV/T roof. Since the BIPV/T outlet air is often less than 15 °C, it would still be of use in the garage (due to adaptive comfort, elevated activity levels, and the fact that warm clothes may be warn) despite not being useful in the house.

The shallow ÉcoTerra roof slope resulted in poorer than expected BIPV/T performance. A solution to overcome this (for future houses) would be to build the roof on-site to remove the constraint from module transportation. Alternatively, a heater could be used to act as a catalyst in melting snow. More complex approaches could be to route exhaust ventilation air through the BIPV/T air space or to have a small steeper solar collector that is used to melt snow. While all of these solutions come at some cost (energy, equipment), it may be worthwhile considering that measured wintertime PV generation was only at a fraction of its potential.

Despite the high resolution of monitoring equipment for certain aspects of the house performance – particularly the innovative technologies – it would have been ideal to submeter many of the electricity consumers, including lights, appliances, the HRV and air cleaner, and the other fans. A total of two-thirds of the electricity use is measured only in aggregate form, leaving some uncertainty as to exact final use. As a result, detailed studies, such as understanding the electric lighting use and its relationship with occupancy and daylight availability, cannot be performed. Another aspect of monitoring that could be improved is to have a single data acquisition system recording all data. In the current configuration, the heat pump is being monitored separately at a different sampling frequency and at a significant delay with respect to the other measurements.

7.3 Leaf House

Maurizio Cellura, Francesco Guarino, and Davide Nardi Cesarini

7.3.1 Main Features of the Leaf House

The Leaf House (LH), shown in Figure 7.23, is located in Angeli di Rosora, Ancona, Italy; the building is south oriented (latitude 43°28′N, longitude 13°04′E) and the altitude is 130 m above sea level (Cellura *et al.*, 2010a). The site is characterized by a moderate climate, with

 – minimum annual temperature of –5 °C,
 – maximum annual temperature of 37 °C,
 – mean annual humidity of 67%, and
 – the average monthly climate parameters shown in Table 7.4.

Fig. 7.23 Leaf House (Image courtesy of Loccioni Group)

Table 7.4 Average monthly climate parameters for Ancona, Italy

Month	Daily Solar Radiation (kWh/m²)			Average Monthly Temperature (°C)
	Horizontal	**Vertical**	**21° from horizontal (south-facing)**	
January	1.20	1.71	1.60	7.6
February	2.06	2.49	2.61	7.9
March	3.33	3.02	3.87	10.8
April	4.63	3.01	4.96	13.9
May	5.90	2.93	5.96	19.0
June	6.27	2.78	6.17	23.3
July	6.51	2.97	6.48	26.0
August	5.46	3.16	5.72	26.2
September	4.31	3.52	4.91	22.3
October	2.77	3.26	3.51	17.6
November	1.52	2.23	2.06	12.5
December	1.09	1.67	1.49	9.0

The building is composed of three levels with each level containing two mirror image twin flats. The ground and the first floor flats measure 85.39 m² each while the second floor flats measure 70.1 m² each. The architectural plans for the three levels of the house are shown in Figures 7.24 and 7.25.
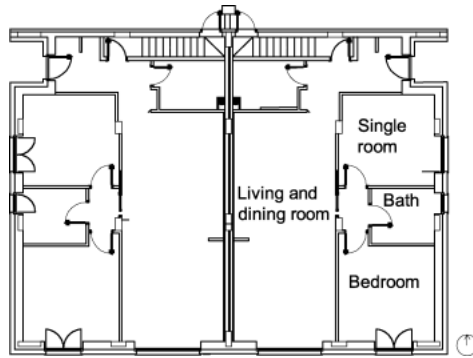
Fig. 7.24 Plan of the ground and of the first floor
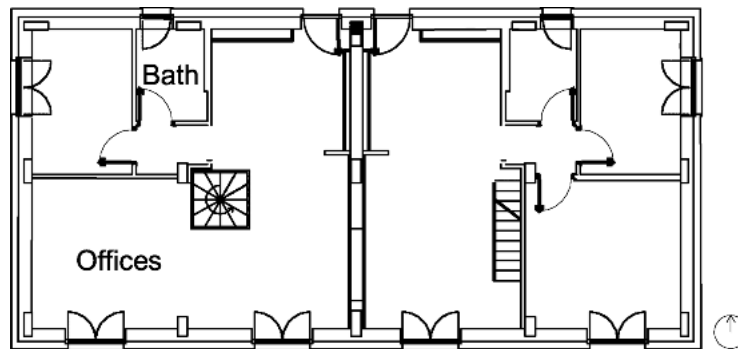
Fig. 7.25 Plan of the second floor

Two of the apartments are occasionally occupied; each of the remaining four flats is occupied by two people. To maximize the solar radiation gain, the ratio of the lengths of the south and east façades was set to 1.34. The southern façade presents external fixed overhangs used as shading elements (see Figure 7.23).

A photovoltaic (PV) system and a solar thermal system account for electricity and domestic hot water (DHW) needs, while a geothermal heat pump (GHP) is integrated with the DHW production and covers the heating and cooling needs.

The building envelope (Cellura *et al.*, 2011b) is comprised of

Walls: Plaster 0.02 m, light weight brick 0.30 m, polystyrene 0.18 m and plaster 0.02 m;

Roof: Plasterboard 0.03 m, vapor barrier 0.001 mm, wood fiber (170 kg/m^3) 0.10 m, rock wool 0.10 m, sheathing 0.001 m, air space, and pinewood 0.02 m;

Floor: Terracotta tiles 0.02 m, concrete subfloor 0.05 m, polyurethane foam 0.04 m, lightweight concrete 0.05 m, bitumen 0.005 m, concrete 0.20 m, air cavity 0.19 m, gravel 0.115 m. Table 7.5 lists the calculated *U*-values of the opaque structures.

Table 7.5 External structures *U*-values

External structures	*U*-value (W/(m²K))
Walls	0.15
Floor	0.30
Roof	0.25

The south-facing window area-to-wall ratio is about 24%, while the rest of the orientations are kept below 10%. The windows are made of a double panel insulated glazing (*U* = 1.1 W/(m² K)) with 0.006 m external glass, 0.14 m gap filled with argon and 0.004 m internal glass; the average global window *U*-value is 1.40 W/m² K. The solar heat gain coefficient (SHGC) is 0.6.

7.3.2 Description of the Design Process

The idea of creating a case study in the field of carbon neutral buildings was first developed in June 2004 by the Architetture Sostenibili s.r.l. and the Loccioni group. The first target was later modified and recalibrated toward the Nearly Net ZEB objective.

The preliminary design took place over 1 year (October 2004 – October 2005) and was prolonged in order to include in the design the feedback from the early design simulations. This latter phase (November 2005 – December 2006) included thermal plant and architectural software simulations using: DesignBuilder (based on EnergyPlus) and Mc4Suite.

DesignBuilder was adopted by the Architetture Sostenibili team in order to model the Leaf House from a thermo-physical point of view. It has a comprehensive user interface developed to work with the EnergyPlus engine; it allows the import of 3D CAD models, allowing for changes in the building or modifications to the description of the zones. DesignBuilder was used to calculate heating and cooling loads using the Heat Balance method, integrated in the EnergyPlus engine. Energy consumption breakdown, internal air, mean radiant and operative temperatures, comfort outputs, weather data, and heating and cooling loads were assessed with an early-design level of detail.

The Mc4Suite is a fully integrated, stand-alone software package powered by a CAD visual engine that allows detailed sizing and modeling of HVAC systems. The thermal system was simulated and the results in terms of systems sizing were used as feedback for the design.

At the end of the preliminary design optimization phase in 2006, the final project was presented in January 2007, by the Architetture Sostenibili s.r.l. and the Loccioni Group; the building phase lasted until June 2008, when the Leaf House was inaugurated. The whole process is described in Figure 7.26.
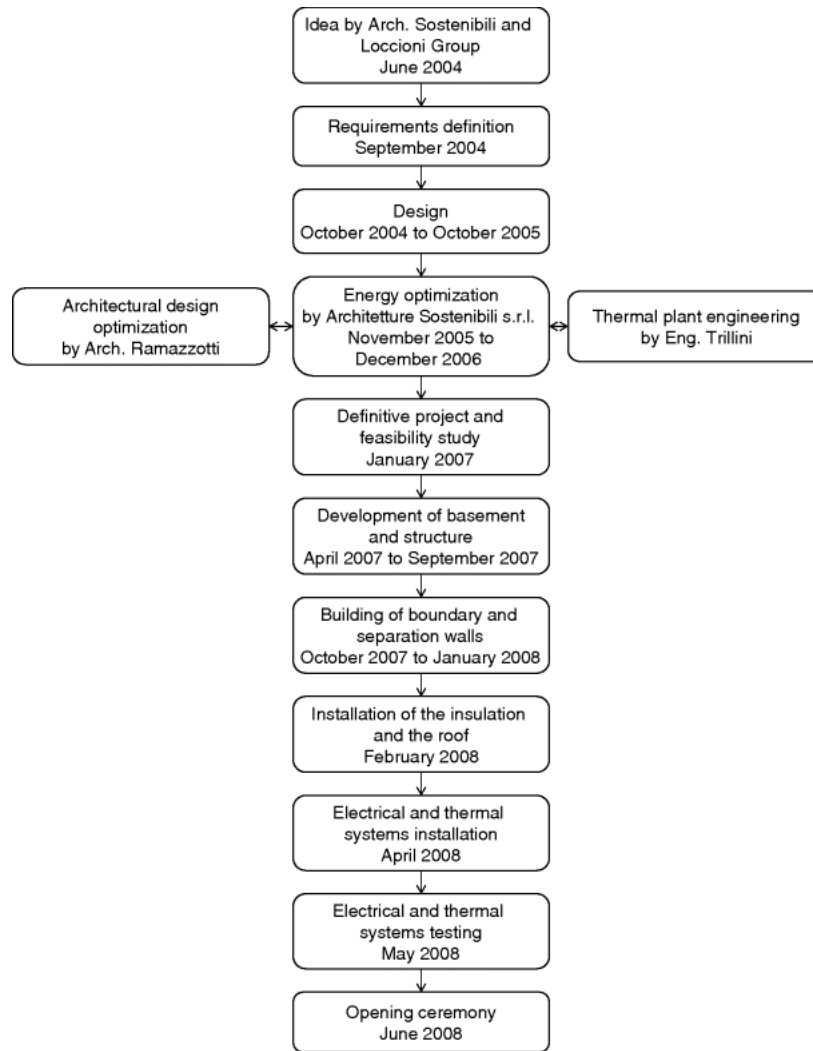
Fig. 7.26 Scheme of the design process

7.3.3 Purposes of the Building Design

The initial goal of the design was to develop a carbon neutral house; later, a Net ZEB (Voss and Riley, 2009) was conceived. A building can be defined as Net ZEB when the following equation is verified:

$$\text{Net ZEB Balance}: |\text{weighted supply}| - |\text{weighted demand}| = 0 \tag{7.2}$$

7.3.4 Description of the Thermal System Plant

The heat is generated by a ground source heat pump which exchanges heat with the ground through three vertical boreholes (100 m), solar thermal collectors and an auxiliary boiler. During the summer season, the solar system covers all DHW needs. During the winter the solar system is integrated with the heat pump in heating mode in order to reach around 40 °C in the upper part of the storage tank, thus allowing the production of DHW and of water to supply the radiant floors from the middle part of the tank. DHW is therefore heated and then collected in a smaller secondary tank, connected to an auxiliary gas burner that is employed when the system needs thermal integration according to a fixed setpoint temperature.

The LH is equipped with a mechanical ventilation system that uses a 10 m underground duct to precondition air prior to entering the air-handling unit (AHU). The ventilation rate is automatically provided according to a fixed range of CO_2 levels registered in the rooms. It is normally about 0.2 air

changes per hour when rooms are occupied, but equals to zero when windows are open. The efficiency of the heat recovery system is about 80%. Sensors activate the mechanical ventilation only when the CO_2 concentration is higher than the setpoint value; other sensors automatically stop the mechanical ventilation when the windows are open. The AHU supplies the air in rooms and there is a heat recovery system before the expulsion of exhausted air.

The main subsystems of the plant, described in Figure 7.27, are:

- the solar collector system (Seven solar thermal collectors, 2.15 m × 1.25 m, see Figure 7.28)
- the geothermal probes;
- the heat pump;
- the air handling unit;
- the auxiliary boiler;
- the photovoltaic system.
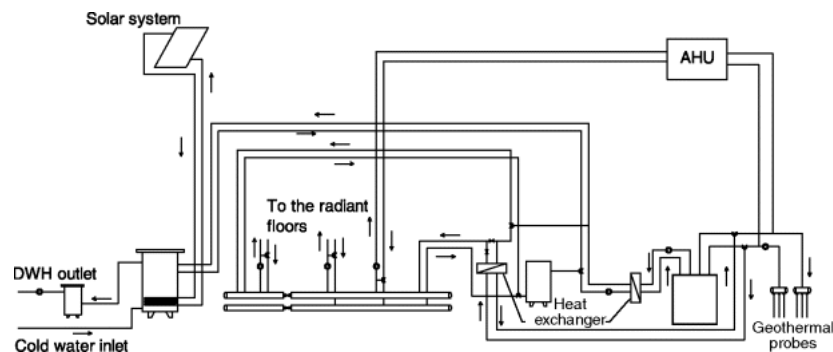
Fig. 7.27 Simplified schematic of the plant
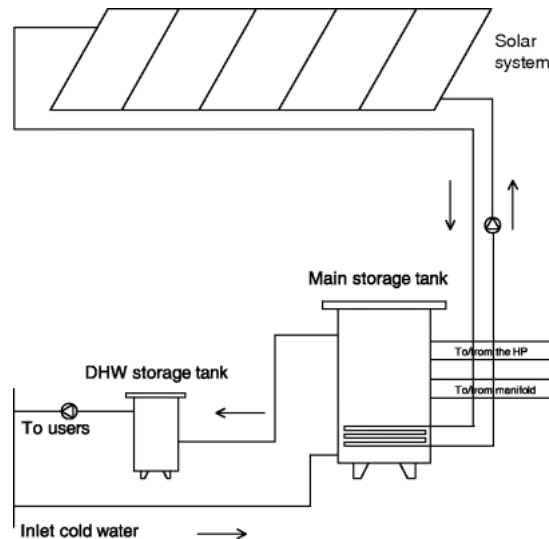
Fig. 7.28 Schematic of the solar collector system

A recirculation system provides hot water in order to reduce water waste. A glycol–water mixture transfers the heat from the solar collectors to the coil of the storage tank.

Figure 7.29 shows a simplified scheme of the geothermal probes and the heat pump. The manufacturer stated that the nominal GHP has a COP of 4.6, but the monitored value is lower. The efficiency reduction is due to

- the nonoptimal setup of the controllers;

– the anomalous electrical consumption of the compressor with respect to the declared data (7–8% higher);

– mismanagement of the ignition system characterized by short cycles.
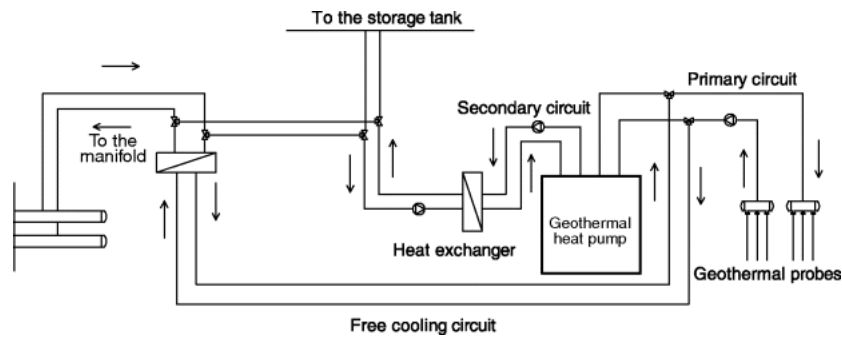
Fig. 7.29 Scheme of GHP system

The geothermal circuit is connected to the free-cooling heat exchanger during the summer season. A grid-connected PV system (20 kW peak power) generates electricity for the LH. The PV array, made of 115 panels, covers the entire roof surface (150 m²). It faces south with a 21° slope. The panels are arranged in nine strings and connected to three inverters. The nominal efficiency of the PV panels is 12%.

In each flat there is a radiant floor connected to the GHP. The room air temperature is controlled by the regulation of the water flow in each tubing loop. In the summer, cooling is mainly provided by the GHP and, to a small extent, rooms can be free cooled with the water provided by a ground coupled heat exchanger, during the start-end of the cooling season. Cold water is supplied in the range of 15–18 °C through the use of mixing valves. The supply water temperature for space heating is between 25 and 28 °C.

To admit daylight, the LH has large south-facing windows; the rear part of the house has solar tubes to increase daylight levels.

A building automation system (BAS) optimizes energy performance of the LH (e.g., HVAC system stops if windows are opened, the inlet temperature of the water in the radiant floors is regulated according to the external temperature, the air flow rate is regulated according to the CO_2 level in each apartment).

Regarding the monitoring of the building (see Figure 7.30), more than 1200 sensors and actuators have been integrated with drivers that allow communication between devices and systems.

Fig. 7.30 Leaf House user interface

The sensors are classified in three main groups: (i) room sensors (CO_2, air temperature and humidity sensors, electricity and thermal energy meters), (ii) mechanical plant sensors (temperature sensors,

thermal energy meters, water flow meters, etc.), and (iii) weather station sensors. All data are normalized and stored in a database.

7.3.5 Monitored Data

The energy balance of the LH was calculated based on the primary energy consumption. Therefore, the weighting factors for the electric energy (derived from the average efficiency of the Italian generation system, 0.35) and for the thermal energy production in the auxiliary boiler (derived from the Italian average efficiency, 0.9) have been chosen. For instance, about 3 (1/0.35) units of primary energy are required to supply a building with 1 unit of electrical energy.

The following equation summarizes the energy balance of the LH:

$$\text{LH energy balance} : |PV \times w_{ee}| - |EEn \times w_{ee} + TEn \times w_{te}| \tag{7.3}$$

where PV is the photovoltaic annual production, w_{ee} and w_{te} are the aforementioned weighting factors, EEn and TEn the electric energy and auxiliary thermal energy consumption of the LH. Table 7.6 reports the balance of monitored data in 2009, 2010, and 2011.

Table 7.6 Energy balance for the Leaf House

	2009	2010	2011
LH energy balance [MWh]	−37.09	−4.61	−5.11
LH energy balance [%]	−33.60	−6.14	−6.26
Consumption [MWh]	110.38	75.08	81.6
Production [MWh]	73.29	70.47	76.49

The substantial difference between the energy performance of 2009 and those of 2010 and 2011 is due to the initial inefficiencies in the thermal system. Improved GHP control has allowed a consistent reduction in consumption in 2010 and 2011. The net-zero energy target has still not been achieved by the LH, even though the deficit in 2010 and 2011 was only 6.63% and 12.68%, respectively. The breakdown of the Leaf House electricity consumption for 2011 is reported in Figure 7.31.
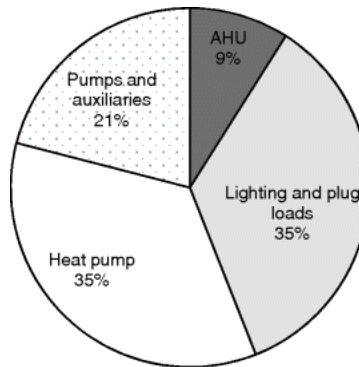
Fig. 7.31 Electricity consumption breakdown

Different indices are employed for describing the load matching. The following equation defines the load match index (f_{load}) (Salom *et al.*, 2011):

$$f_{load} = \frac{1}{N} \times \sum_{year} \min\left[1, \frac{g_i(t)}{l_i(t)}\right] \tag{7.4}$$

where g and l stand for generation and load, i stands for energy carrier, t is the time interval used (e.g., hourly, daily, weekly, monthly), and N is the number of events considered. The f_{load} index is very dependent on time resolution (Sartori, Napolitano, and Voss, 2012). The grid interaction index ($f_{grid,i}$) represents the variability (standard deviation) of the energy flow (net export) within a year, normalized by the highest absolute value (Voss *et al.*, 2010).

$$f_{\text{grid},i} = \text{STD}\left[\frac{e_i(t) - d_i(t)}{|\max[e_i(t) - d_i(t)]|}\right] \qquad (7.5)$$

where e and d stand for exported and delivered, respectively, i stands for energy carrier, and t is the time interval used. The LH does not completely fulfill the Net ZEB targets previously defined; in the following sections the magnitude of the deficit from the net zero target will be described through the use of the above indices.

Tables 7.7 and 7.8 show the values of load match index and grid interaction index of the LH, which were evaluated for different time bases.

Table 7.7 Effect of time base on the load match index

Load Match Index (Eq. (7.4))	2009 (%)	2010 (%)	2011 (%)
Hourly	36	37	39
Daily	65	72	76
Monthly	69	79	80

Table 7.8 Effect of time base on the grid interaction index

Grid Interaction Index (Eq. (7.5))	2009 (%)	2010 (%)	2011 (%)
Hourly	32	31	32
Daily	38	39	38
Monthly	40	50	51

7.3.6 Features and Limits of the Employed Model

The thermal building simulation in non-steady-state conditions (Beccali *et al.*, 2003, 2005a, 2005b; Cellura *et al.*, 2010b) of the LH was developed in TRNSYS 16.1 (Bradley and Kummert, 2005). The model deals with a large number of variables; it shows some limits and does not take into consideration the aspects summarized below:

1. The LH thermal plant is extremely complex. Therefore, many recirculating nodes have been omitted in order to have a clearer, simpler, and faster simulation;

2. TRNSYS offers limited tools to simulate the natural ventilation behaviors of the LH. Schedules to model natural ventilation have been assumed and used for the simulations;

3. Infiltration can be estimated with Type 571. It uses the following formula to determine infiltration in air changes per hour (ASHRAE, 2009):

$$\text{ACH} = k_1 + k_2 \cdot \Delta t + k_3 \cdot v_{\text{wind}} \qquad (7.6)$$

The values chosen for the three constants have been estimated for "tight fitting walls." Δt is the temperature difference between inside and out and v_{wind} is the windspeed. In type 571 there is no reference to the wind direction;

4. Heat exchanger types require a fixed efficiency or an estimation of the heat exchanged. An overall 0.75 efficiency was chosen for the simulation based on the equipment specification.

In the TRNBuild simulation each flat has been divided into

– two symmetrical zones for the ground and first floor apartments (Figure 7.32a): Zone 1, Zone 2;

– three zones for each of the second floor flats (Figure 7.32b): Zone 1, Zone 2, and Zone 3.
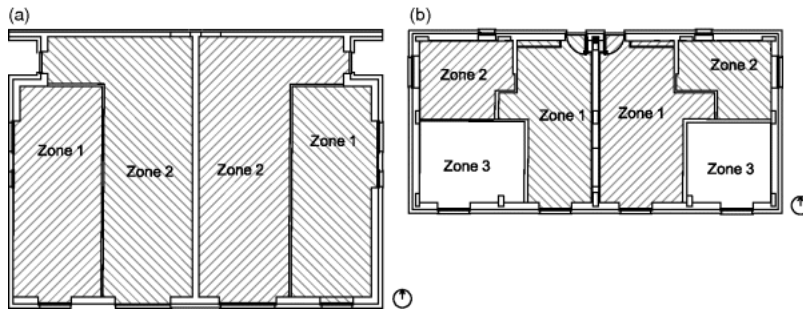
Fig. 7.32 (a) The thermal zones of the ground, first floor and (b) second floor

Proportional-integral-derivative (PID) controllers were used to set the fluid flow circulating inside the radiant floors. As the temperature in a thermal zone drops below the setpoint, water is drawn from the storage tank (using geothermal probes or from the heat pump in cooling mode), its temperature is regulated through the use of mixing valves, and the water is fed to the radiant floor of the zone. Fourteen PID controllers (one for each thermal zone) have been introduced in the model. The thermal exchanges due to the mechanical ventilation are evaluated using 0.1 or 0.2 volumes/h of ventilation, depending on the occupancy schedule. The ground-building interface has been simulated using Type 703 to calculate the outside surface temperature of the floor using the inside surface temperature of the floor as the input. To better calibrate the thermal model, real climatic data monitored by the weather station of the LH was used (TRNSYS Type 109).

7.3.7 Calibration of the Model

The process of calibration has been carried out with a detailed comparison between simulated data and monitored data; in Figures 7.33 and 7.34 the real PV production and GHP electrical consumption are compared.
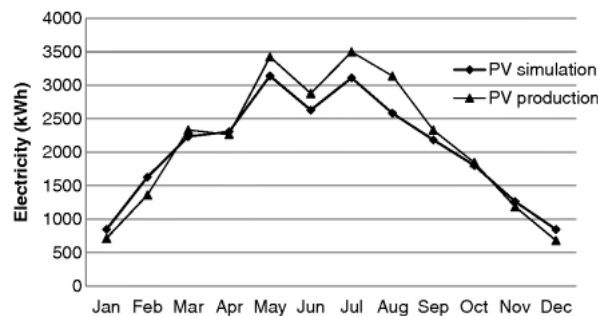
Fig. 7.33 Simulated and monitored PV production
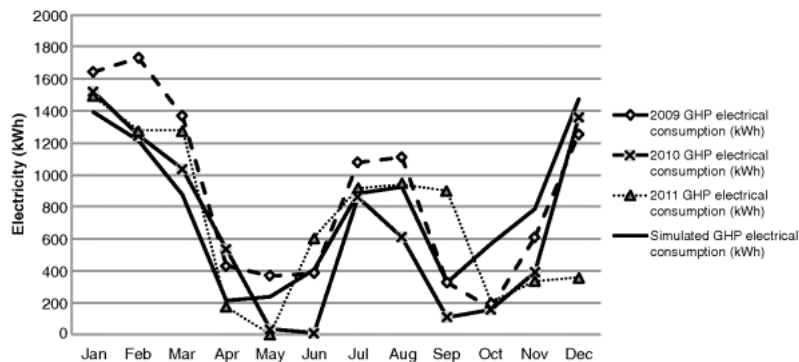
Fig. 7.34 GHP simulated and monitored electrical consumption

The simulated 2009 average air temperature values are compared to the monitored values in Figures 7.35 and 7.36, the difference is rarely greater than 1 °C. Flats 3 and 4 were chosen as examples.
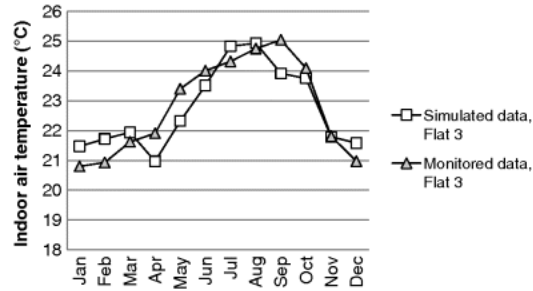
Fig. 7.35 Average monthly air temperatures – Flat 3

Fig. 7.36 Average monthly air temperatures – Flat 4

The thermal collectors provide approximately 4200 kWh of energy while the simulation predicted 4350 kWh. The measured performance indicates that the solar thermal collectors provide 63% of the domestic hot water heating. During the summer season the production is even higher than the consumption while during winter it is necessary to integrate with the GHP and the auxiliary boiler.

For the calibration of the model, real and monitored interior temperature and PV production of four particular days were compared. The chosen days are the following (Torcellini and Crawley, 2006):

- January 24th (cloudy, cold);
- March 6th (sunny, cold);
- July 24th (sunny, hot);
- August 4th (cloudy, hot).

Figures 7.37–7.39 show the results for the hot sunny day.
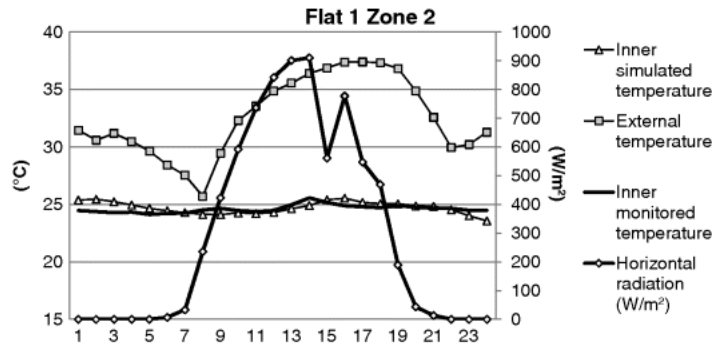
Fig. 7.37 Comparison between monitored and simulated air temperature data on July 24th
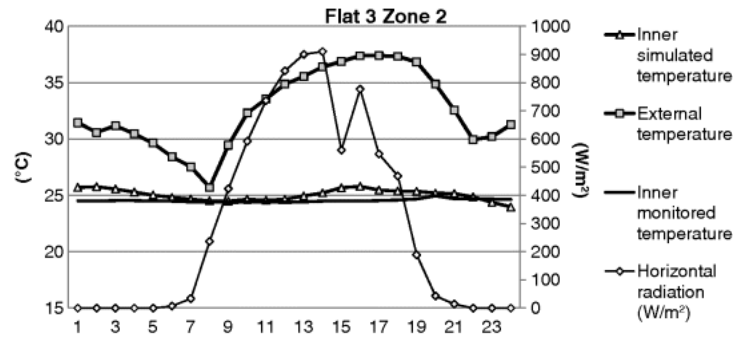
Fig. 7.38 Comparison between monitored and simulated air temperature data on July 24th
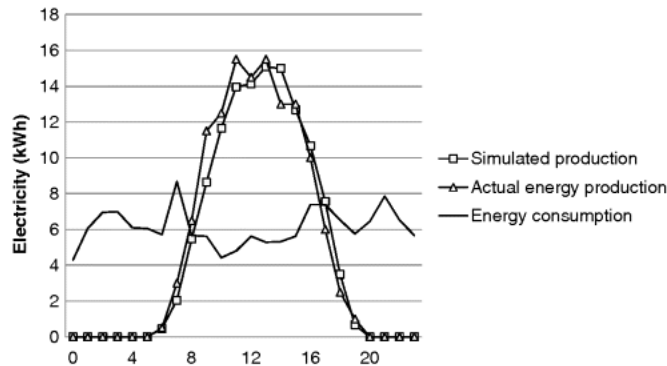
Fig. 7.39 Comparison between monitored and simulated energy production data on July 24th

The average difference between simulated and monitored interior temperature is about 0.5 °C. The maximum difference is about 1.4 °C. In Figure 7.39, simulated and monitored data of PV production are compared. Figures 7.40 and 7.41 show cooling and heating loads for the LH split for the different subsystems of the plant.
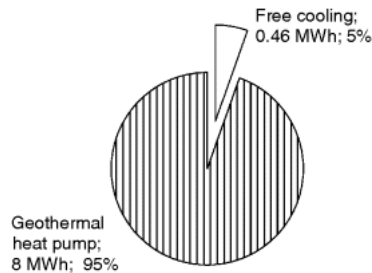
Fig. 7.40 Breakdown of how the cooling load was supplied
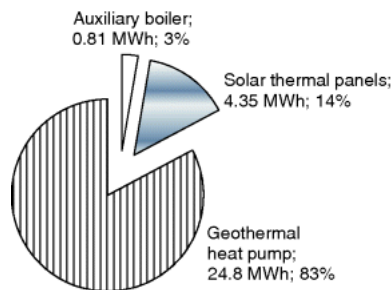
Fig. 7.41 Breakdown of how the heating load was supplied

Further analysis has been made on the radiant floor modeling. In TRNSYS, there are two models for hydronic systems – quasi-analytical formulation (Active Layer) and a two-dimensional finite difference model (Type 705). The quasi-analytical formulation was developed to calculate the internal and surface

temperatures of the radiant systems based on room air and inlet water temperature and flow rate. Three-dimensional heat transfer is taken into account. Radiant floors have been modeled as an active layer of the floor (Type 56). However, TRNSYS offers also other solutions – Type 705 and others. Type 705 has more inputs and a higher degree of customization of the geometry of the pipes, while the chosen active layer model of Type 56 calculates thermal parameters from the data introduced in the layer definition window. A comparison between the two options described was performed on a single thermal zone with an inlet temperature fixed at 28 °C. A simulation of the building was run for 100 h and the results are shown in the following graphs; they show the internal air temperature and the fluid flow into the zone (controller driven). Using the same controllers in the two simulations, equivalent results were obtained for the air temperatures and the fluid flow (see Figures 7.42 and 7.43).
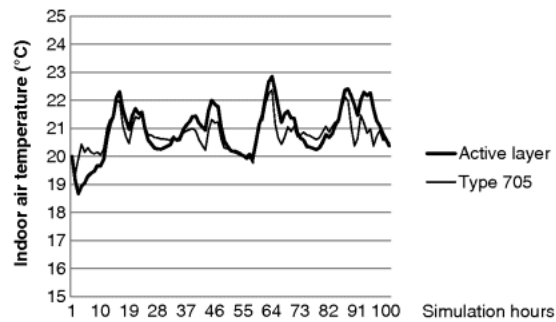
Fig. 7.42 Comparison between different solutions in modeling radiant floors – Air temperatures
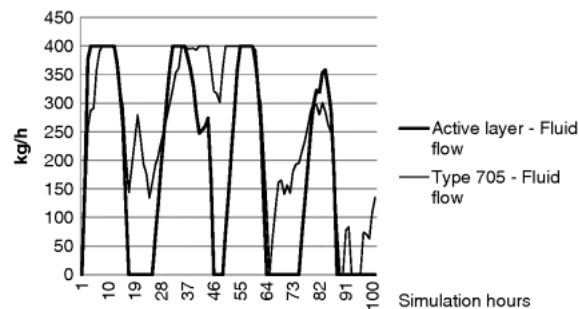
Fig. 7.43 Comparison between different solutions in modeling radiant floors – Fluid flow

7.3.8 Redesign

To achieve the net-zero energy target, the following redesign options have been considered (Cellura *et al.*, 2011a):

1. Replacement of the PV panels with more efficient ones (19% module efficiency, electrical properties are listed in Table 7.9);

2. Replacement of the GHP with a more efficient model;

3. Elimination of the GHP heat exchanger and direct connection with the main pipeline of the fluid heated/cooled;

4. Modification of the composition of the roof in order to get a smaller U value (0.15 W/m² K);

5. Different volume of the main storage tank to evaluate effects on GHP consumption;

6. Integration of a night setback on the PID temperature setup;

7. Addition of blinds, on the south-oriented windows, working in the hottest hours during summer season, if occupancy schedules are set to 0.

Table 7.9 PV modules electrical properties

	On-site	Redesign
P_{max} [W]	175	240
V_{mp} [V]	36.40	43.70
I_{mp} [A]	4.67	5.51
OPEN circuit V [V]	43.50	52.40
Short circuit I [A]	5.20	5.85

The simulations yielded the following results (also summarized in Table 7.10):

1. Substitution of PV panels with a 19% efficiency model, the forecasted energy yield (TRNSYS simulation) would be about 38MWh. This solution would allow the electrical loads to be completely met;

2. The design COP value of the GHP was 4.6, but the monitored data showed a smaller value. This is due to the inefficiency of the plant and we estimated the magnitude of these energy losses. According to the results of thermal simulations, if the real COP value for the GHP is 4.6, 1.4 MWh would be saved per year;

3. The elimination of the heat pump heat exchanger was examined to reduce the complexity of the thermal plant. The simplification of the plant could yield approximately 2300 kWh$_e$ of savings (around 25% of the overall GHP consumption);

4. While the envelope thermal resistance is above standard, a simulation was performed by adding 0.1 m of rock wool in the roof composition (global U-value for the roof = 0.15 W/m² °C). A smaller U-value of the roof would lead to overall electric energy savings of 200 kWh for the whole year;

5. A 1.2 m³ storage volume would allow a 1.1% energy savings. In this case, the storage tank was well designed because the operating point (real tank volume = 1 m³) is very close to the point of lowest consumption;

6. PID temperature setpoints have been set to 21.5 °C for the heating season and 25.5 °C for the cooling season. Moreover, around 600 kWh (9.1% of heating consumption) can be saved by selecting a night setback of 19 °C from 00:00 to 06:00;

7. The addition of blinds on south-facing windows is estimated to achieve approximately 15 kWh of further savings during the cooling season (less than 1% of the total electrical cooling consumption).

Table 7.10 Redesign scenario results

Production increase	
Scenario 1	13 MWh
Electric energy savings	
Scenario 2	1400 kWh
Scenario 3	2300 kWh
Scenario 4	200 kWh
Scenario 5	85 kWh
Scenario 6	600 kWh
Scenario 7	15 kWh

Although the first redesign strategy is estimated to achieve the net-zero energy target, some of the other options are also viable. Figure 7.44 shows the results of the redesign, considering a combination of different energy-saving scenarios. The total energy reduction is approximately 2.8 MWh (30% on the total GHP consumption).
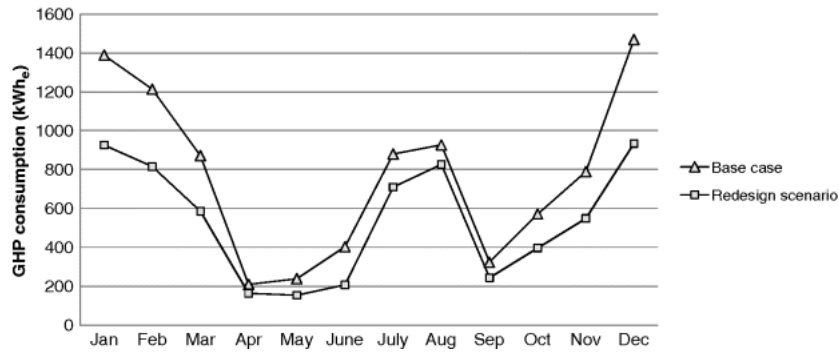
Fig. 7.44 Redesign 2–7 combined – GHP consumption

The following tables summarize energy results of the redesign options of the LH. Results show that the LH redesign would achieve the net-zero energy target (see Tables 7.11 and 7.12).

Table 7.11 LH energy balance (2009) – Redesign 2–7 combined

LH energy balance [MWh]	−29.09
LH energy balance [%]	−28.41
Consumption [MWh]	102.38
Production [MWh]	73.29

Table 7.12 LH energy balance (average values 2010–2011) Redesign 2–7 combined

LH energy balance [MWh]	5.45
LH energy balance [%]	7.86
Consumption [MWh]	69.30
Production [MWh]	74.75

If the first scenario is also considered, the balance would be far over the net-zero energy point, as summarized in Table 7.13.

Table 7.13 Redesign – all options combined

LH primary energy balance [MWh]	42.59
LH primary energy balance [%]	61.45
Consumption [MWh]	69.30
Production [MWh]	111.89

In order to strengthen the reliability of the model and evaluate variations in the GHP heating consumption, a sensitivity analysis on different parameters was carried out. The variation of PID setpoint temperatures, air infiltration, tank setpoint temperature, and occupancy level was taken into account. The PID setpoint temperatures were set between 20 and 23 °C, numerical values of infiltration were varied from 50 to 150% of the initial value, and the tank setpoint temperature was fixed in the range of 35–45 °C while the occupancy level was set up to 0–5 people. The highest variation of the GHP consumption is related to the PID setup temperature sensitivity (nearly +40%), the lowest is connected to the occupancy level variation (+/−10%). The sensitivity analysis has proven that the choice of values for user-defined parameters can have a major impact on the results of the simulations and on the reliability of the model. Other parameters evaluated are maximum/minimum fluid flow for every loop, lighting and electrical appliances gains, efficiencies of system components, deadbands and setpoints for heating/cooling systems, thermo-physical properties of the envelope, and so on. Figure 7.45 shows some examples of the sensitivity analysis results obtained.
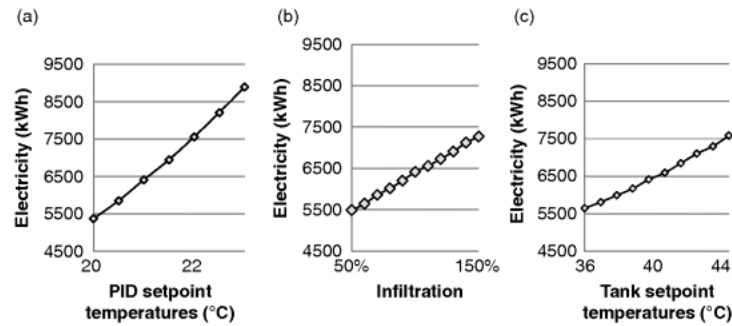
Fig. 7.45 Sensitivity analysis of GHP electricity consumption for heating on (a) PID setup temperatures, (b) infiltration, and (c) tank setpoint temperature

7.3.9 Conclusions and Lessons Learned

This section described an Italian case study of a net-zero energy house – the Leaf House. A thermo-physical model of the LH was created in the TRNSYS environment. Due to the fact that the active plant of the LH is particularly complex, some assumptions were made to simplify the description of the model (e.g., some recirculating nodes were not considered). During the implementation of the model some limits of the tool in the description of the real environment were observed. Nevertheless, the obtained calibrated model is very reliable considering the results of the comparison between monitored and simulated data. For strengthening the obtained results, an SA on the main important parameters of the model was carried out; it permitted observing parameters that play a major role in variations of outputs. According to this experience we believe that the development of a sensitivity analysis is an important step for obtaining a reliable model and calibrating it. Attention must be paid to the selection of gains (e.g., occupation levels, lighting, and appliances) and other user-defined parameters; they usually are a cause of great variability in the results and they must be chosen carefully. An analysis has been performed on the monitored data in order to achieve detailed information on the thermo-physical behavior of the building and on the load matching/electricity grid interaction.

With regards to the electricity load-matching analysis, it has been concluded that the Leaf House is quite dependent on the grid. The building suffers from a high level of mismatch between generation and load of energy at an hourly level and also at an aggregated monthly/seasonal level. The use of electricity storage devices might be appropriate to minimize stress on the electricity grid.

The LH energy consumption for pumps and auxiliaries on the total is very high. Therefore, as a general principle, it must be stated that it is important to reduce this term as much as possible, through a bioclimatic design approach and with simpler thermal plants. "Simple is better," as a general guideline: according to the size of the LH a simplified thermal plant might reach a Net ZEB target and a good level of indoor comfort with lower complexity and costs.

7.4 NREL RSF

Yuxiang Chen, Samson Yip, and Andreas Athienitis

The aim of this study is to draw lessons from the design and performance of the Research Support Facility of the National Renewable Energy Laboratory (Figure 7.46). As a final output of this case study, abstraction to an archetype cross-section of a high-performance office building will be proposed. The case study scopes are as follows:

– Present the current design, operation, and modeled/monitored thermal and energy performance.

– Investigate alternative designs (with the purpose of abstraction to general archetypes) focused on daylighting and solar heat gain control for different climates.

– Study the potential contribution from transpired solar thermal collectors, active building-integrated thermal energy systems (BITES), and building precooling with nighttime ventilation.

– Demonstrate, in the context of office buildings, how to model advanced high-efficiency buildings, and how to perform model-based integrated design and optimization.

Fig. 7.46 NREL RSF (Image: Dennis Schroeder, NREL)

7.4.1 Introduction to the RSF

The NREL RSF is located in Golden, CO, USA (39.7°N, 105.2°W) at an altitude of 1829 m above sea level. The local climate is heating dominated with large daily temperature fluctuations of about 8 °C in the winter and 12 °C in the summer. Most days of the year are sunny and the air is dry. The building being investigated in this study is Phase 1 of the RSF building, which comprises a north wing and a south wing (Figure 7.47). In Phase 2 of the RSF, a third wing was added to the north of the Phase 1 building shown.
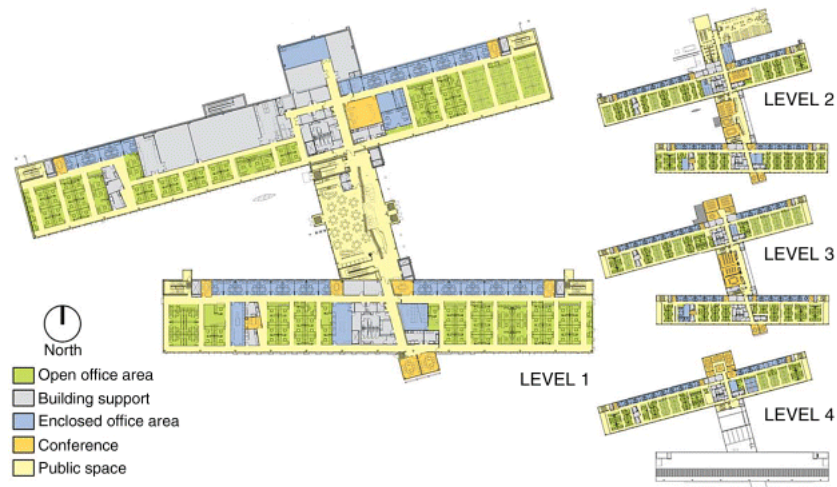
Fig. 7.47 Floor plan of the RSF, Phase 1 (Figure courtesy of RNL Design)
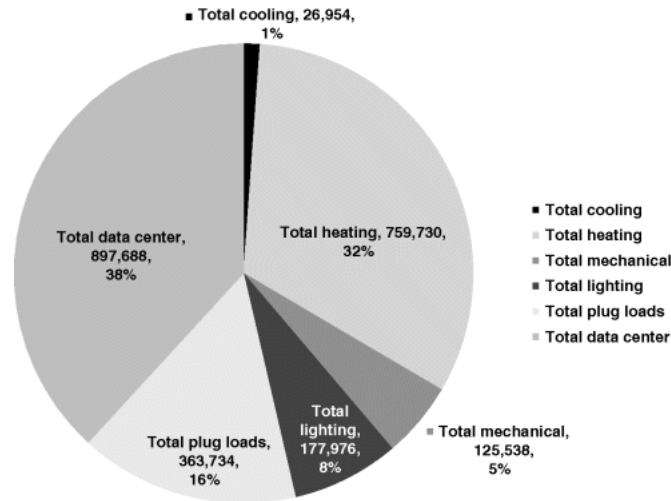
Fig. 7.48 Total annual measured energy consumption [kWh] (NREL, 2013)

The RSF building (herein referring to Phase 1) is a 20,440 m² (220,000 ft²) office building designed to accommodate 822 occupants. Construction cost was US $64.3 million. With its roof-mounted photovoltaic system, the RSF is designed to produce as much renewable energy as it consumes on an annual basis. The total energy consumption target, including data center energy consumption, is 110.7 kWh/m²/yr (35.1 kBTU/ft²/yr), which is half the energy of an equivalent, minimally code-compliant building. These energy goals and their substantiation through simulation were explicitly included in the project's firm fixed-price design-build contract. The monitored energy consumption for the first year of building occupation is 111.7 kWh/m²/yr (Hootman, 2012). Figure 7.48 shows the measured complete energy consumption for 2011.[1]

Computer modeling played an important role throughout the design process and in ensuring the energy goals would be met within the specified budget. eQuest, a whole building energy simulation program, was used as the main tool. Other programs were used to provide more detail or to complement the whole-building simulation tool. Hirsch *et al.* (2011) detailed the models used in the design process and how they informed important design decisions on the path from preliminary design to the completed building.

7.4.2 Key Project Design Features

A detailed description of the RSF building, its design concept and targets, energy efficient systems, the design-build process, monitored energy performance, and other relevant information are presented on the official RSF Web site.[2] Technical papers are available in the NREL publication database.[3] In this section, the design, operation strategy, and monitored performance for each key design feature are presented. Figure 7.49 is a conceptual building section illustrating some of these features.
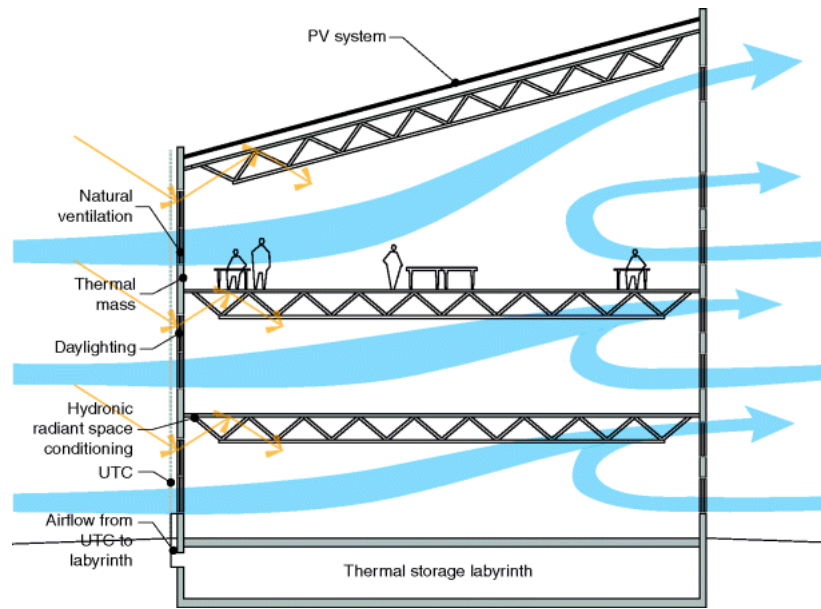
Fig. 7.49 Conceptual building section illustrating strategies for daylighting, thermal mass, and natural ventilation/night cooling

7.4.2.1 Design Process

A design-build project delivery method was selected for the design and construction of the RSF. In the request for proposals, the building owner listed, in terms of priority, a specific set of building performance and budget objectives that the design-build team were to fulfill. This method was chosen as an effective way to ensure an exemplary building energy performance and occupant comfort level. It also shifts the risk of the project from the building owner to the design-build team. Accordingly, the design-build team is motivated to work in an integrated design process to draw upon the strengths of each member to contribute to innovative solutions. This integration happens right from the initial schematic design. The traditional adversarial relationship of building designer (architect and engineer) to building constructor is eliminated and the two work together on the same team allowing such synergies as constructor input into the early stages of design. The closer collaboration also permits more communication between architect and engineer, which becomes essential when designing the intricate systems in high-performance buildings.

The following sections detail the elements that figured significantly in this integrated design process.

7.4.2.2 Envelope

The exterior façade is constructed with modular precast concrete panels: 76 mm (3 in.) exterior concrete, RSI 2.5 (R 14) rigid foam insulation, and 152 mm (6 in.) interior concrete. The interior concrete surface is painted white and left exposed. The roof is composed of a 76 mm (3 in.) concrete slab poured on steel decking, with a layer of RSI 5.8 (R 33) insulation on the exterior side of the concrete.

The window areas as a percentage of the façade areas are as follows: south, 30%; east, 32%; west, 31%; north, 21%. This is a very important design parameter in Net ZEBs as it determines passive solar gains and useful daylight throughout the year. The optimum window area as a percentage of façade area depends on climate, function, selected shading/daylighting device, control strategy, and importance of views to the exterior (Tzempelikos, Athienitis, and Karava, 2007). The RSF has no separate interior zone and has an open plan in order to maximize daylight penetration and natural ventilation. The floor plate depth was chosen to be 18 m (60 ft) as a balance between exposed exterior wall area to volume ratio and daylight availability.

The south-facing window aperture is divided into two portions. The lower *vision window* is triple-glazed. Its low-e glazing has an RSI-value of 1.04, an SHGC of 0.23, and a visible light transmittance of 43%. Insulated framing decreases the assembly RSI-value to 0.52 (m² K/W) – half of the glazing value. The upper *daylighting window* is double-glazed. Its low-e glazing has an RSI-value of 0.65, SHGC of

0.38, and a visible light transmittance of 70%. Insulated framing decreases the assembly RSI-value to 0.4. The vision window is used for all of the north-facing windows. Specialized highly reflective louvers are used on the top portion of the windows on the south façade, as further explained later. These enable daylight to penetrate much more deeply (at least double the depth) than would be possible without the louvers. On the south façade, overhangs shade the lower vision glass. The north glazing is not shaded and permits indirect natural light to enter (Torcellini *et al.*, 2010).

7.4.2.3 Daylighting and Electric Lighting

The daylighting window is equipped with a light-reflecting device, the "Lightlouver™." Incoming transmitted solar radiation is reflected toward the ceiling, and then diffusely reflected again deeper into the space, onto the workplane (as shown in Figure 7.50). This has the secondary benefit that the occupants adjacent to the window are protected from direct solar radiation for nearly the entire year. Thus, movable shading devices (e.g., blinds) were not installed. The view window portion is equipped with exterior shading, which is tailored to block low-altitude beam radiation from entering through the window. The window properties assumed for the redesign study are summarized in Table 7.14.
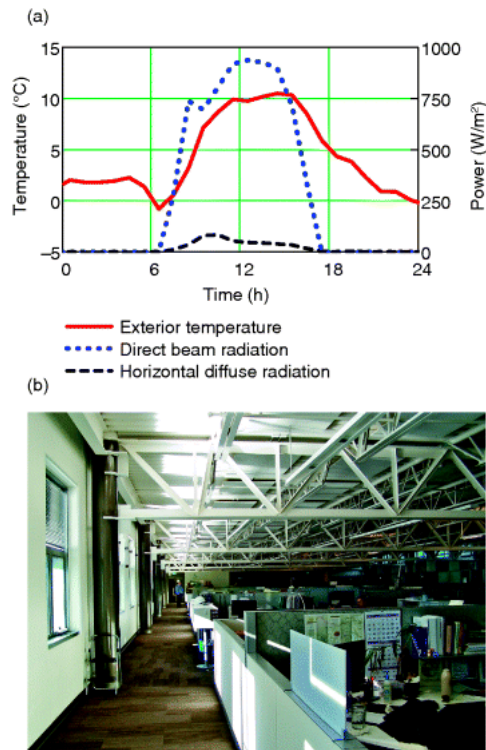
Fig. 7.50 (a) Weather conditions on Jan. 16, 2013, and (b) photo taken at 10 A.M

Table 7.14 Window optical characteristics (Diffuse values for the RSF are assumed. Windows types not used in the RSF are to be used later for thermal and daylighting modeling)

Glazing Type		SHGC		Daylight Transmittance		Suitable Application
		Normal incidence	Diffuse	Normal incidence	Diffuse	
Triple-glazed window	Low SHGC (RSF vision window)	0.23	0.15	0.43	0.28	Cooling-dominated climate
	High SHGC	0.62	0.52	0.68	0.57	Heating-dominated climate
Double-glazed window	Low SHGC (RSF daylighting window)	0.38	0.32	0.7	0.59	Cooling-dominated climate, daylighting window
	High SHGC	0.70	0.61	0.76	0.66	Heating-dominated climate, daylighting window

For the open office area, during the daytime when the electric lights are turned on, the light output is dimmed according to the sensed light level on the workplane. Starting at 6:00 P.M., timed lights-OFF sweeps will occur (with a blink-warn function allowing occupants to override to ON) every 2 h. If lights are manually turned on, they remain on for 2 h. Typical light levels, as measured on a sunny winter day, are shown in Table 7.15.

Table 7.15 Daylight measurement in the north wing open office area on a winter sunny day, Jan. 16, 2013

Time	Workstation Illuminance (lux) (Measured at 0.84 m Height from Ground)			
	South (3 m from south façade)	Center (9 m from south façade)	North (12 m from south façade)	Cubical office (1.8 m from north façade)
09:00	700	210	90	150
10:00 (shown in Figure 7.50)	810	230	100	170
11:00	950	260	110	200
12:00	980	330	130	150
13:00	790	310	130	150
14:00	590	220	90	120

Note: Desktop is 0.71 m in height; the partitions around desktops are 1.07 m high; and, partitions between workstations are 1.37 m high. The office walls have a height of 2.03 m.

7.4.2.4 Space Conditioning System

The space conditioning of the office area is provided through a hydronic ceiling slab radiant conditioning system (Figure 7.51) with significant thermal mass (a TABS system – see Section 2.2.3). The hot/chilled water is provided by the NREL campus district heating/cooling center, which has a central woodchip boiler and high-efficiency chillers. As shown in Figure 7.51, a displacement ventilation strategy was adopted, partially in order to fully expose the ceiling to the office space below. A raised floor creates 0.3 m height of space for under-floor air distribution. The 100% fresh air is supplied at a neutral temperature of about 19.5 °C. The upper surface of the concrete slab is covered with 25 mm of batt insulation with foil faces (RSI 0.5) to improve the effectiveness of delivering heating or cooling in the slab downward to the office space. Acoustic panels are hung just below the ceiling slab to improve the open space acoustic isolation. Normal weight concrete 76 mm (3 in.) thick was poured on 50 mm (2 in.) steel decking for roof and intermediate ceiling slabs. Pipes are spaced at 15 cm (6 in.), center-to-center, following the flute spacing of the deck.

Carpet (10 mm)
Raised floor panel
Partitioned space for air distribution
Batt insulation with foil faces
Concrete with pipes embedded
Steel deck
Suspended acoustic panel

Diffuser

Pipes

Support post

38
242 mm
25
76
50
150
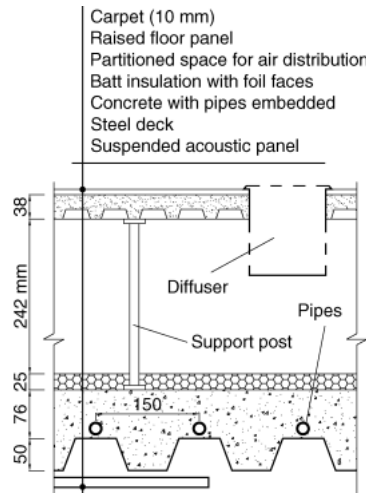
Fig. 7.51 Cross-section of the raised floor and the hydronic radiant slab

The ceiling slab temperature is controlled by regulating the valve open time based on the temperature difference between the room heating/cooling setpoint and the actual sensed room temperature using a pulse-width-modulation control (essentially proportional control). The open time is linearly related to the temperature difference – 20 min for 2 °C temperature difference, and zero minutes for zero temperature difference. Occupants are allowed to modify the programmed setpoint by ±0.5 °C – these are the only two values provided on the thermostat of each thermal zone (Figure 7.53).

In heating mode, the supply hot water temperature to the ceiling slab is regulated at about 40.5 °C (105°F) by mixing return hot water with hot water supplied from the boiler. The boiler supply temperature ranges between 42 and 58 °C.

7.4.2.5 Thermal Storage Labyrinth

A labyrinth of concrete walls was poured into the below-grade crawl spaces of two wings (see Figure 7.52). It is used as a thermal sink to preheat/precool the incoming fresh outdoor air. Insulation is placed around the labyrinth (e.g., between the labyrinth and the first floor). In the summer, the south labyrinth is precooled at night and then used to precool outdoor fresh air during daytime office hours. The north labyrinth is only used for data center hot air outlet in the summer. In the winter, data center warm exhaust air is drawn directly into the air-handling units (AHUs) and supplied to different areas. Any partially used or unused hot air is blown to the south labyrinth. The inlets of the labyrinth for cool outdoor air will be used as outlets of this data center warm air.

Fig. 7.52 Thermal mass "labyrinth" during construction (Image courtesy of Pat Corkery, NREL)

When the south labyrinth temperature is lower than the transpired thermal collector temperature by a preset amount, the fan of the transpired solar thermal collector is turned on. The hot air from the collector is passed to the AHU or to the south labyrinth. See details on the operation of the transpired thermal collector in Section 7.4.2.6. The air path differs from time to time depending on pressure variation caused by demands. For data center ventilation, when outdoor air is too cold (less than 7.2 °C (45°F)), the air is mixed with data center warm exhaust air before entering the data center.

7.4.2.6 Transpired Solar Thermal Collector

About 300 m² of collectors are installed on the south façade of the south wing. The flow rate is 4720 m³/s (10,000 CFM) at 100% fan speed and it varies approximately linearly with fan speed. The solar air heating system was sized based on ventilation and space heating needs.

When the average labyrinth temperature is lower than the setpoint temperature of 19.5 °C (67°F), and the transpired solar collector temperature is 8 °C higher than the setpoint temperature, the fan will start. The fan speed will ramp up slowly. A coefficient (0 to 100) for controlling the fan speed is calculated based on several variables, but the fan speed is limited between 10 and 80% of the maximum rate. If the fan speed coefficient is lower than 90, and if the outdoor temperature is higher than 18.3 °C (65°F) or the transpired collector temperature is not more than 3 °C higher than that of the average labyrinth temperature, the fan stops.

Some performance data for the transpired solar collector were measured during a visit to the building by the authors. On a clear sunny day at 10:30 A.M., with inlet at 10 °C (50°F) and 3.78 m³/s (8000 CFM), the outlet air reached 26.3 °C (79.4°F). The collector plate temperature was 29.4 °C (85°F). The collected heat rate was about 72.5 kW.

7.4.2.7 Natural Ventilation

For natural ventilation (Figure 7.49), the southern vision windows are manually operable or controlled with an automatic actuator, while on the north side, the lower windows are manually operable and upper windows are automatically controlled (because they are out of reach). The building occupants

manually operate the windows to suit their needs. A workstation-based task manager interface notifies occupants when conditions are optimal for natural ventilation and windows may be opened. The actuated windows are operated primarily to support nighttime precooling. Rules of thumb for optimizing natural ventilation could be summarized as follows:

– A short building depth, like the RSF's 18 m depth. A large building length to depth ratio (in plan) allows outdoor air to easily flow in and out of the building, particularly at night to cool building thermal mass;

– Open plan interior and low-height furniture to facilitate air circulation;

– Operable and automatic motorized windows that open at night.

One side effect is that the same advantageous conditions for increasing daylighting penetration and natural ventilation can reduce acoustic quality (see Section 3.4 on acoustic comfort). The RSF uses displacement ventilation, which necessarily uses a low airflow rate. White noise generators are used to add background noise – which would normally be present in buildings with entrainment ventilation.

7.4.2.8 Building Operation, Typical Monitored Data, and Thermal Performance

For each bay of the south wing, the floor space is divided into four types of thermal zones as shown in Figure 7.53: SE/SW for east/west end zone of the south wing, N for north, I for interior, and S for south zone. The room/ceiling slab temperatures and ventilation rate are controlled separately. The ventilation supply air is 100% fresh (i.e., no mixing with return air), and the setpoint is 19.4 °C (67°F) for the whole building for all seasons. The typical section identified in Figure 7.53 is used later for thermal modeling.
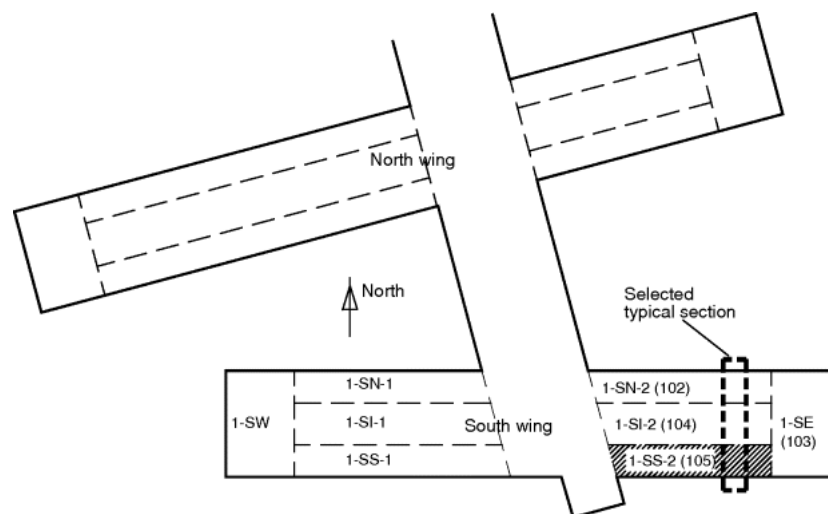
Fig. 7.53 Schematic floor plan showing thermal zones of the first floor ("1-SI-2" represents first floor, south wing, interior thermal zone, and east bay of the RSF building)

Monitored data from a few days in January 2013 was obtained for this case study. Figure 7.54 shows the monitored weather conditions and room temperature profiles during these days. A handheld infrared thermometer was used to validate the monitored data. The temperatures from the two measurement methods closely match.
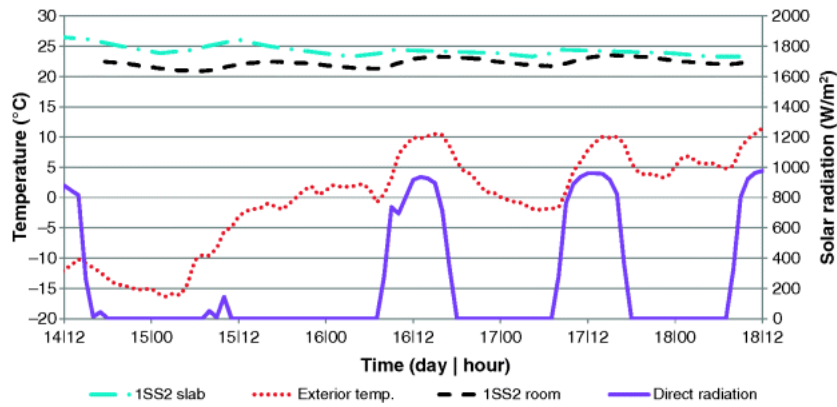
Fig. 7.54 Outdoor weather conditions with temperature profiles of thermal zone "1SS2"

Figure 7.55 shows the ventilation rate and supply air temperature of the 1SS2 zone. The ventilation rate is about 0.2 air changes per hour (ACH), but between 6 P.M. and 6 A.M., the ventilation is turned off. A CO_2 sensor can override the ventilation flow rate. The measured average supply air temperature is about 18.9 °C.
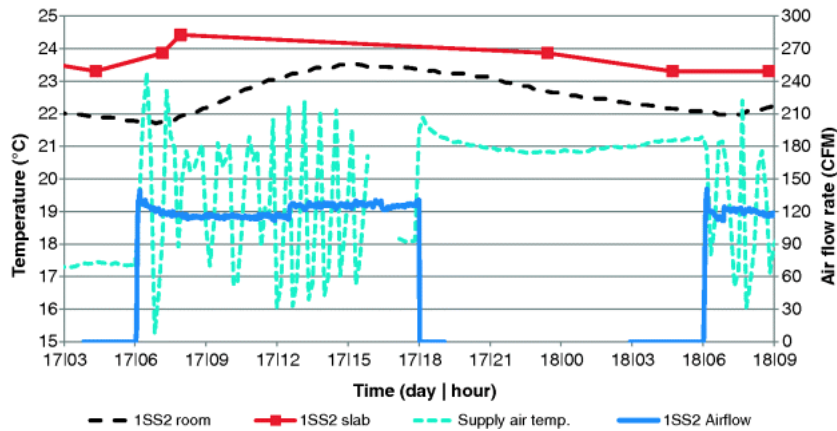
Fig. 7.55 Ventilation flow rate and temperature profiles of the 1SS2 thermal zone (100 CFM equals to 47 l/s; 1SS2 slab is the ceiling slab of thermal zone 1SS2)

As shown in Figure 7.56, the room temperatures were relatively stable regardless of the outdoor conditions. The room temperature is allowed to drop slightly after 6 P.M., and is regulated back to the normal room heating setpoint after 6 A.M. The other operation strategy for space conditioning using the hydronic radiant ceiling slab was described earlier in Section 7.4.2.4. A relatively higher slab temperature is required for the north thermal zone to bring the room temperature back up to its setpoint in the early morning (6 A.M.) after the nighttime set-back in winter.
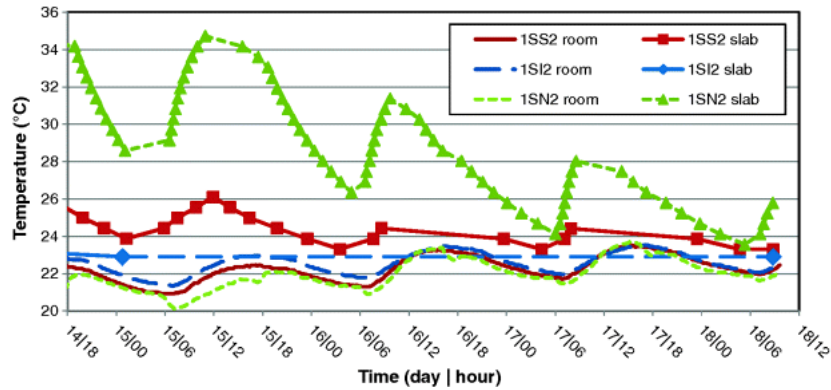
Fig. 7.56 Temperature profiles of rooms and their ceiling slabs

January 16 was a cool, sunny day (Figure 7.54). Cold water was needed to cool down the slab temperature for the interior and south zones (Figure 7.57; the monitored hot water flow rate was zero). This indicates a potential improvement in the control strategy. For example, a lower supply air temperature can be used during a sunny winter day.
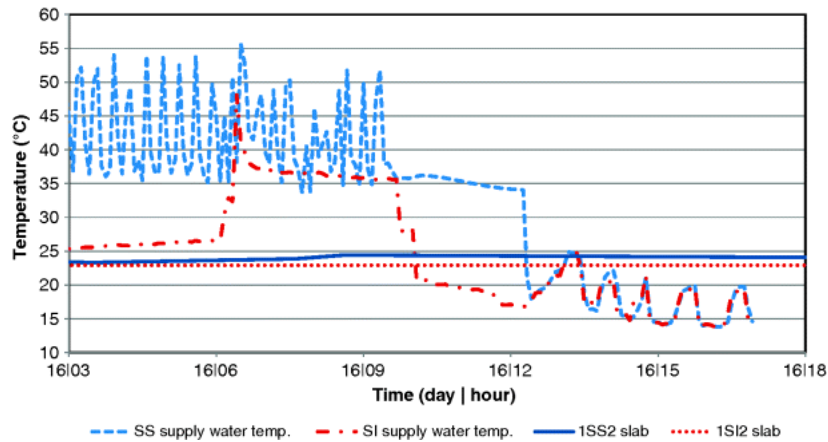
Fig. 7.57 Supply hot water temperature to the ceiling slabs

7.4.2.9 Photovoltaics

The RSF makes extensive use of photovoltaics as its choice of RET to reach net-zero energy. There are three systems totaling 1.7 MW. The first is a 449 kW system on the roof of the RSF (south-facing, slope 10°, attached to standing seam metal roof). The second is a 524 kW system that acts as a shade canopy over the visitors' parking lot. And the third is a 706 kW system, also a shade canopy, over the adjacent staff parking garage. Altogether, the Net ZEB boundary for the project is comprised of Phase I and Phase II of the RSF, the staff parking garage, and the visitors' parking lot.

The second and third PV systems' surface areas are approximately 40 and 100%, respectively, of the size of the RSF rooftop PV system. This is significant because it means approximately 140% of additional roof surface area is needed to generate enough electricity for the RSF to attain Net ZEB status if the Net ZEB boundary for the project was limited to the building only. This would be the case for buildings on dense urban sites where surface areas for possible PV integration are limited. In fact, from the beginning of the project, it was understood that the RSF roof alone could not provide enough surface area for PV generation and that the adjacent parking areas would be needed as well.

Based on 2011 data, the total annual energy consumption of the RSF is about 2.35 GWh, and the PV energy generation is about 0.92 GWh. During that year, energy consumption was matched by generation in July. This feat was achieved with only the first two of the PV systems operational. The complete PV system was not fully operational until April 2013. Figure 7.58 shows the monthly total energy consumption (which includes the energy consumption from the data center) and energy generation from 2011.
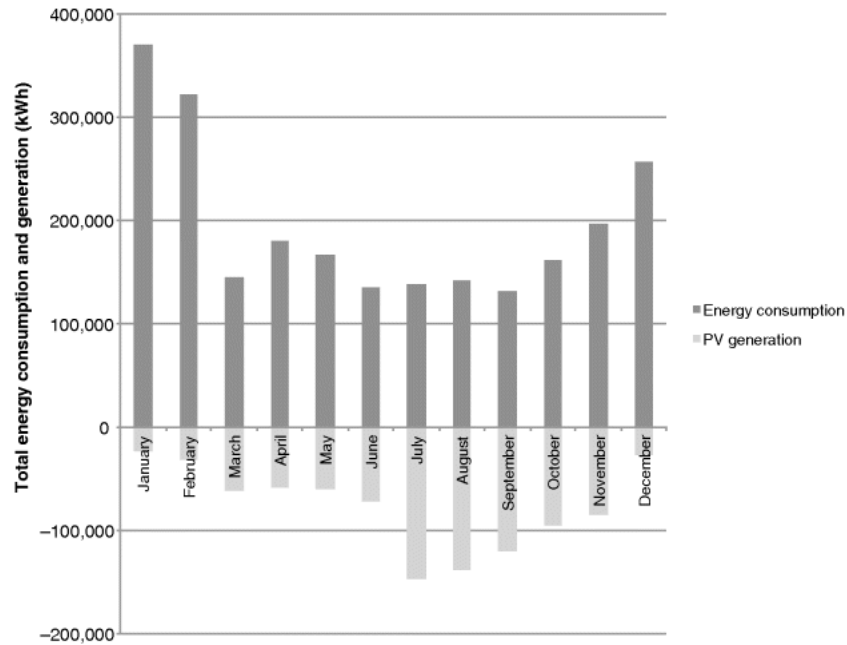
Fig. 7.58 Energy consumption and generation for 2011

7.4.2.10 Building Simulation Software Support

Because of the ambitious Net ZEB goals for the RSF, particular attention was paid to the simulation tools used in the project. Specialized simulation tools were used independently to design the major innovative components of the building and then integrated into a whole-building simulation program. A brief summary of the major tools and their associated building components follows (Hirsch *et al.*, 2011):

– RADIANCE was used for daylighting, including shading and daylight redirection, and the design of electric light controls.

– IES VE was used specifically to study the thermal effects of the natural ventilation strategies.

– The data center was modeled separately for its cooling and heat recovery design, including information technology (IT) electric consumption, cooling energy, fan energy, and heat recovery. This information was then input to eQuest and the thermal labyrinth model.

– The PV systems were dimensioned and their output sized to match the RSF's total energy consumption, including optimizing orientation and tilt angle.

– The transpired solar thermal collector was modeled using manufacturer and TMY weather data to calculate air temperature and flow rate, which were then transferred to the thermal labyrinth model.

– The thermal labyrinth model calculates the thermal exchanges between the concrete and the air, taking into account the temperature and flow rate of the source heat from the data center and the transpired solar thermal collector.

– eQuest was used as the whole-building energy modeling program to integrate the various components of the energy model.

7.4.2.11 Software Limitations

Due to the nature of the RSF design brief, situations occurred when the building simulation software could not easily handle the innovative design solutions. A key design element for the project was the daylighting. This element was also the hardest to model – partly due to the innovative LightLouver™ system – requiring clever workarounds to overcome current limitations in modeling software.

RADIANCE was used from the beginning of the conceptual design stage since NREL mandated daylighting in its request for proposals (RFP) through the targeting of the Leadership in Energy and

Environmental Design (LEED) 2.2 Interior Environmental Quality (IEQ) credit 8.1: Daylight and Views – Daylight.

Since daylighting influences many systems in a building, RADIANCE simulations helped to establish many design parameters very early on: the building depth at 60′–0″ (18 m), the fenestration, the glazing transmittance, and the ceiling heights.

RADIANCE use continued through design development to track the evolving design. As information became more precise, such as for room finishes and furniture dimensions, these simulations helped guide the design team to make changes to compensate, such as increasing the size and changing the mounting height of the LightLouvers™.

Up to this point, the RADIANCE simulations were calculated at a single point in time, noon on the equinox, for clear sky conditions. This was to fulfill the simulation requirements for the LEED 2.2 IEQ 8.1 credit. Once the daylighting design needed to be integrated with the electric lighting design and the energy model, daylight modeling became more complex, as described later.

Annual (hourly) illuminance distributions were required to aid in optimizing the electric lighting control zones. For this work, Radmap was used to prepare a "cumulative sky" for use in RADIANCE. However, no luminous output description (photometric) files were available for the LightLouver™ under such sky conditions. They were only available for a clear sky at noon. Instead, the actual complex geometry of the LightLouver™ was inserted into the 3D model for RADIANCE to use, making the simulations more time intensive.

Furthermore, complex fenestration devices usually require forward raytracing to properly characterize daylight transmission. Since RADIANCE uses backward raytracing, the design team had to compensate by setting very conservative simulation parameters to account for some solar flux that may not be calculated accurately with this method.

Once the electric light control strategy was designed, yet another piece of software, Sensor Placement and Optimization Tool (SPOT), was required to translate these requirements into a lighting schedule in a form useable by eQuest (Guglielmetti, Pless, and Torcellini, 2010).

7.4.2.12 Significance of the Early Design Stage

Generally speaking, the cost of design changes increases the later they occur in the design and construction process. This is due to the nature of the design and construction process that is normally linear. Design decisions are funneled in a cumulative manner toward key milestones that are used to evaluate a design's appropriateness in terms of performance and cost. As a project passes through these key milestones, the building design becomes fixed and complete.

Conversely, the degree of influence any building stakeholder has on the final project decreases with time. The inertia built-up through the chain of decision-making in the design process makes it more time and cost prohibitive to implement any significant change to the set direction of the project. (See Chapter 4 for more detailed discussion).

These design changes can come from any one of the building stakeholders. They can come from the designers due to incomplete or erroneous information or coordination; the building owner due to scope, program, budgeting, or timeline changes; the contractors due to design/constructability errors, construction errors, or other site-specific conditions.

In this respect, the early design stage is crucial for ensuring that the most important elements for any building design project are accounted for. Therefore, right from the early design stage of a project, construction costs and operations and maintenance costs must be considered (Paulson, 1976).

Otherwise, making major changes late in the design process usually causes downstream consequences, such as redesign, recoordination with all affected professional disciplines, and rebuilding of energy models, among other things. From a construction perspective, such late design changes may also have important effects on coordination of trades and sequencing of the work, thereby increasing construction costs and causing delays. Furthermore, such changes during construction can produce effects that extend even further to the normal operations and maintenance, and expected usage of the completed building.

Some important design parameters in solar Net ZEBs that must be addressed at the early design stage have already been discussed but are summarized here with comments on their impacts on the global

project of the RSF.

1. Building siting, orientation, and geometry (including roof pitch and area). Building siting and orientation are the first steps in determining solar accessibility on any particular building site. From there, building geometry further defines the quantity of solar energy that can be captured in a project.

   The RSF is sited on a predominantly east–west axis to maximize building insolation. The wings are spaced far enough apart to avoid self-shading and the roof slope is 10° to facilitate installation with a standing seam metal roof while making it easy to maintain or replace components of the PV system.

2. Building depth. Once the building has been sited in an optimal position, the maximum amount of solar energy to be used for daylighting is determined in part by the building depth. The building must be shallow enough to ensure that all normal work surfaces are sufficiently illuminated for productivity, yet not so shallow that the envelope area to volume significantly increases construction costs.

   The building depth for the RSF was determined very early in the design process. This permitted the design team to fix the building geometry, which is one of the most difficult parameters to change late in the design process due to the number of building systems it affects.

3. Window-to-wall ratio (WWR) on equator-facing façades and window height. This is sized, in conjunction with the building depth, principally for the purpose of daylighting. By extension, the WWR affects the electric lighting design that is complementary to daylighting. It also has an important effect on the structural systems of the façade. The solar heat gain from the fenestration will also affect the heating and cooling design.

   In the RSF, the WWR and window height was adjusted once the building depth was fixed. In terms of design process, it is easier to modify WWR and window height instead of building depth, which is intimately connected to space planning and utilization.

4. A design is required to integrate some form of solar control to prevent glare and excessive solar gain. This contributes to productivity and reduces cooling load. The solar control element can be fixed or moveable, placed on the exterior or interior of the building. It can also be placed between the glazing surfaces in windows. Exterior sun control is the most effective since it prevents solar radiation from penetrating into the interior. Interior sun control can be more practical because the elements are protected from environmental conditions. Fixed solar control elements are the simplest and require little maintenance, while movable elements (e.g., shades and blinds) allow adjustments at the expense of increased maintenance.

   The RSF uses exterior fixed metal sunshades, one covering each south-facing vision window.

5. Façade design. The façade design can be viewed from the interior as a system fulfilling three requirements: (i) protection from the outdoor environment, (ii) daylighting, and (iii) visual connection to the exterior. All incident solar radiation is maximized for interior use, such as daylighting and thermal gain, and exterior use for solar electricity generation and solar air heating. One proposed ordering of these requirements is in the form of the three-section façade (Tzempelikos, Athienitis, and Karava, 2007), of which the RSF is a variation. Three-section façades are described in detail in [Chapter 3](#).

   In the RSF, a portion of the south façade is used as a solar thermal collector. For increased solar utilization of the south façade, PV can be used to cover the opaque portions of the façade. However, because of the low latitude of Golden, a façade would generate considerably less energy than a sloped orientation (e.g., the roof).

6. Natural ventilation. The inclusion of operable windows permits nighttime ventilation to help cool down the building in the summer. It also aids in providing building occupants with the possibility of personalized control over their building environment. In conjunction with building controls and thermal mass, natural ventilation provides an energy-efficient cooling solution.

   Since the RSF is an office building, it is normally unoccupied at night allowing the nighttime ventilation to proceed without the restrictions necessary for occupied spaces.

7.4.3 Abstraction to Archetypes

From the design and operation of the RSF building, this section abstracts the essential elements in the design and operation of an *archetype cross-section for similar high-performance office buildings* (Figure 7.59), with a focus on optimizing the design and control for daylight and solar gain. The approach is as follows:

1. With available design and operation information, an integrated daylighting and thermal model is created for a typical cross-section of an intermediate floor. See Figure 7.53 for location.

2. Validate and calibrate the models with monitored data.

3. Investigate the application of the Vision Control® (VC) window, a window with integrated, between-glazing motorized shading louvers (venetian blinds), for daylighting and solar heat gain control. This is another possible approach as compared to the fixed louvers, which were effectively used in the RSF. A suitable approach will usually depend on climatic conditions and function of the space as well as cost.

4. Evaluate the thermal and daylighting performance of the cross-section after integrating active daylighting and solar heating control, natural ventilation, and building-integrated thermal energy storage.

5. Based on the temperature and load profiles resulting from existing and alternative designs, the design and operation will be studied in an integrated manner.

6. Abstract the key elements in design and operation, and suggest potential design options for better performance.
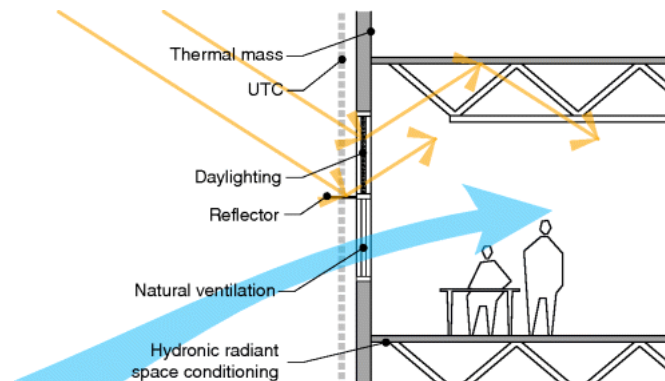
Fig. 7.59 Archetypal cross-section

7.4.3.1 Model Development

A *numerical thermal network model with explicit finite differencing approach (using Mathcad)* was created for a typical section of the office area (Figure 7.53) on the second floor. The width of the typical section in the numerical model is 3.05 m, equal to the building's modular width and windows' spacing (Figure 7.60). For heat flow between thermal zones (i.e., furniture, partition between work stations) and its surroundings, the convective and radiant heat transfer modeling are coupled, but modeled within two enclosures: physical and radiosity (Figures 7.60 and 7.62). Solar heat gain and daylighting due to transmitted solar radiation are calculated in the radiosity model with the radiosity method. All other thermal calculations are conducted in the physical enclosure model. The two enclosures have slightly different dimensions, due to different representations of the floor plan (Figure 7.62).
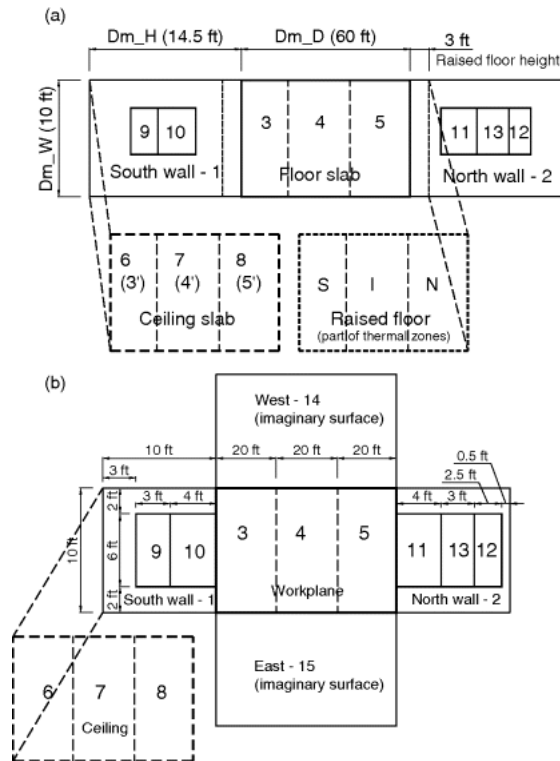
Fig. 7.60 (a) Physical enclosure: dimensions of the typical section for thermal modeling, its thermal zoning and surface indexing, and (b) radiosity enclosure and its dimensions

Figure 7.61 presents the internal heat gain schedules based on monitored data. Since the occupancy density is low, the internal heat gain intensity is low as well. The average intensity for the whole RSF building is about twice of the values indicated here.
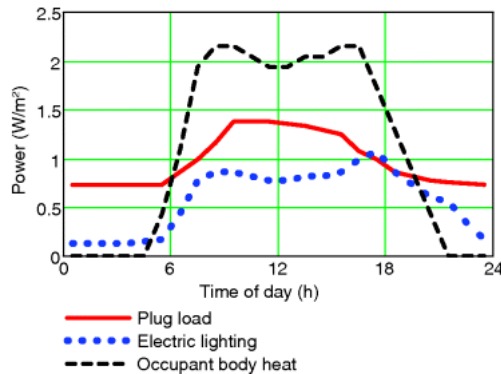
Fig. 7.61 Internal heat gain profiles based on published data[4]

Thermal Modeling in Physical Enclosure

The building section, along with its associated ceiling and floor slabs, is divided into three thermal zones. Two-dimensional heat conduction is considered in the concrete slabs; one-dimensional heat transfer for the wall assemblies. As shown in Figure 7.62, the raised floor is treated as part of the control volume of the occupied space. The temperatures of surface 6, 7, and 8 are equal to the corresponding bottom surface temperatures of floor slab 3, 4, and 5, as shown in Figures 7.60 and 7.62.
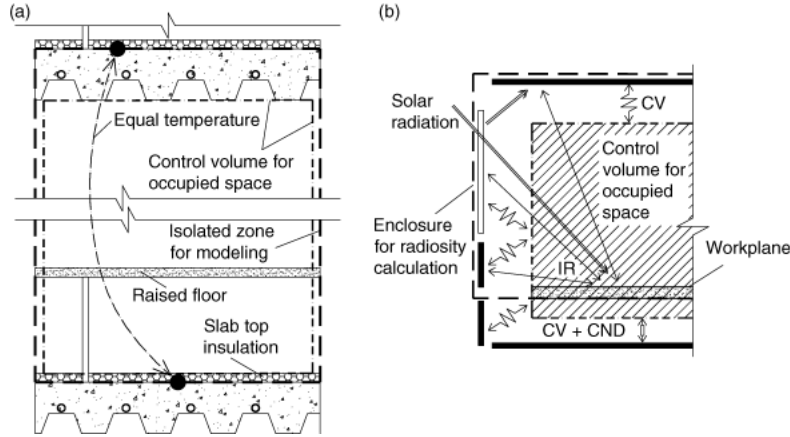
Fig. 7.62 (a) Physical enclosure: control volume of the occupied space (surrounded with dashed-dotted line) and the typical cross-section of the modeled section (thick dashed line), and (b) radiosity enclosure: boundary for radiosity calculation (CV: convection; CND: conduction; IR: infrared radiation)

Interzonal air convection correlation (Barakat, 1987)

$$U_{zn}(T_{z1}, T_{z2}) = \frac{0.3 \cdot \text{Gr}(T_{z1}, T_{z2}, H_{zn})^{0.5} \cdot \text{Pr}_{air} \cdot k_{air}}{H_{zn}} \cdot A_{open} \tag{7.7}$$

where H_{zn} is the effective height of the zone (2.8 m, from the top of workplane partitions to ceiling). It is also used as the characteristic height in the calculation of the Grashof number Gr. T_{z1} and T_{z2} are the air temperatures of the adjacent two zones. k_{air} is the air conductivity. Pr_{air} is the Prandtl number of air (0.71). A_{open} is the area of an imaginary opening between two thermal zones. To account for the fact that the correlation just presented is derived for interzonal convection through an opening between two thermal zones, the value of A_{open} is similar to that of a door (0.8 m × 2.05 m).

Natural ventilation. The outdoor air passing through the typical section is able to mix well with a representative room air temperature, T_{ra}, at 5 air changes per hour (ACH). At 5 ACH, the air velocity of indoor cross-airflow will be about 0.025 m/s across the 18.3 m depth of the building. If the effective thermal capacitance of the room interior contents (other than wall/ceiling mass, which is slow responding) is 50 times that of the room air (a typical value to account for furnishings), and the temperature difference between outdoor and indoor air is 5 °C (say, 25 °C outdoor, and 20 °C indoor), the assumption of air mixing well at 5 ACH means increasing the inlet air by 4.5 °C, and decreasing the room air by 0.5 °C. This is achievable with a convective heat transfer coefficient of 3 W/m²/K, ceiling and floor area for convection, and a mean temperature difference of 4 °C. For 30 ACH, only about one-third of the required energy to warm up the incoming air to the room temperature can be delivered. A mixing effectiveness (ε_{nv}) is introduced into the ventilation heat exchange formula. The ε_{nv} decreases as the ACH increases, and is assumed to be inversely linear with the ACH in this case. The literature (Shaviv, Yezioro, and Capeluto, 2001) indicates that 30 ACH results in the highest potential savings. Hence, ACH ranging from 10 to 30 will be examined in this case study with the calibrated thermal model. The cooling effect from natural ventilation is

$$q_{nv} = (T_{oa} - T_{ra}) \cdot \rho c_{air} \cdot ACH_{nv} \cdot \varepsilon_{nv} \tag{7.8}$$

where $\varepsilon_{nv} = 10/(ACH_{nv} + 5)$. T_{oa} is the exterior air temperature, and T_{ra} is the average temperature of the three thermal zones. ρc_{air} is the volumetric heat capacity of air.

When natural ventilation is employed, heat transfer due to interzonal air convection, infiltration, and mechanical ventilation is set to zero. The natural ventilation heat loss calculated from Eq. (7.8) is assigned to the three thermal zones according to the weights of their effective thermal capacitances, which are equal in this case.

Radiosity Enclosure

In the radiosity enclosure, the workplane (0.9 m above raised floor) is used for radiant heat transfer and daylight distribution calculations, replacing the slab floor in the physical enclosure. The radiant heat

absorbed/lost by the workplane is added to the heat gain/loss of the control volumes of the occupied space.

Transmittances for beam radiation of all windows are functions of the incidence angle, while transmittances for diffuse radiation are constant, but different for different window types. For daylighting windows, it is assumed that 90% of the transmitted solar radiation (including daylight portion) is reflected evenly by the LightLouvers™ to the ceiling surface 6. The remaining 10% is assumed to be inward diffuse radiation from the daylighting glazing/LightLouver™ combination. All transmitted solar radiation through the other windows is assumed to be perfectly diffuse since the windows are designed to avoid direct beam radiation. The reflected solar radiation from surface 6 is also considered to be perfectly diffuse. Assumed surface reflectances are summarized in Table 7.16.

Table 7.16 Reflectance of different surfaces (Figure 7.60) used in radiant heat transfer calculations with radiosity method.

Type of Radiation	Surface Number														
	1	2	3	4	5	6	7	8	9	10	11	12	13	14	15
Visible	0.7	0.7	0.2	0.2	0.2	0.7	0.7	0.7	0.2	0.2	0.2	0.2	0.7	1	1
Solar	0.3	0.3	0.2	0.2	0.2	0.4	0.4	0.4	0.6	0.5	0.5	0.5	0.3	1	1
Long wave	0.1	0.1	0.1	0.1	0.1	0.1	0.1	0.1	0.1	0.1	0.1	0.1	0.1	1	1

Daylighting Model

The Perez model (Perez *et al.*, 1990) is used to estimate the exterior illuminance on façades based on beam and horizontal diffuse radiation. The treatment of transmitted and reflected daylight is the same as described in the preceding paragraph for solar radiation – perfectly diffuse. Using the radiosity enclosure and the initial diffuse luminous exitances on each surface, average workplane illuminance is calculated. Configuration factors have not been used because illuminance at specific points is not considered in this case.

7.4.3.2 Model Validation and Calibration

The measured data (Figure 7.54 to Figure 7.56) are used to calibrate the thermal model. Figure 7.63 compares the simulation results from the calibrated thermal model to the measured data. Comparison indicates that the interzonal convection correlation (Eq. (7.7)) is accurate. The effective thermal capacity of the room control volume is about 50 to 60 times the room air thermal capacity. Acoustic panels are estimated to weaken the heat exchange rate (by about 50%) between the ceiling slab and office space.
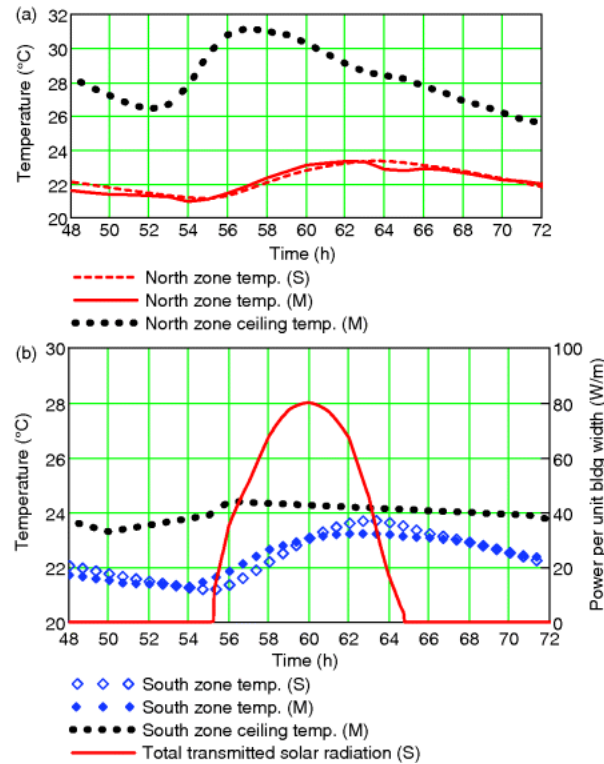
Fig. 7.63 Comparison of measured (M) and simulated (S) thermal performance for Jan. 16. (a) North thermal zone; (b) south zone and the simulated solar heat gain

Based on the measured 24 h slab and room temperature profiles in Figure 7.63 and weather conditions in Figure 7.54, 0.90 kWh/m façade width of heating is required for the south zone, 0.21 kWh/m for the interior zone, and 2.75 kWh/m for the north zone. The energy for warming up the exterior air to supply air temperature is about 1.88 kWh/m of façade width at a ventilation rate of about 0.2 ACH.

The measured daylighting data from Table 7.15 is used to validate the daylighting model. The measurements are taken in the north wing open office area, not the south wing used for modeling. The north wing's south-oriented façade is S13°E. Figure 7.64 shows the simulated average daylight illuminance level on the workplane of each thermal zone. The discrepancies between measured and simulated values are small considering the average illuminances are roughly equal to the illuminances at the centers of the thermal zones. The main potential parameters that cause the discrepancies between measurement and simulation values include the following:

– Cubical and office partitions on the north side are 2 m (80 in.) and 1.4 m (54 in.) high. The partitions in the middle and south zones are 1 m (42 in.) and 1.4 m high. The workplane is taken as 0.9 m high in the radiosity enclosure.

– Cavity effect of workstations and hallways – the bottom plane in the radiosity enclosure is the workplane. This will reduce the actual bottom plane reflectance.

– The structural trusses in the ceiling.

– Adjacent buildings.

– Other approximations and assumptions:

   – Exterior shading blocks 80% of the incident radiation.

   – Reflectance of the RSF LightLouver™ is a constant 0.73, assuming triple bounces between blades for incoming daylight.

   – Assigning 90% of the transmitted solar radiation and daylight from window surface 9 to the ceiling of the south zone (surface 6).

– Perfectly diffuse surfaces.
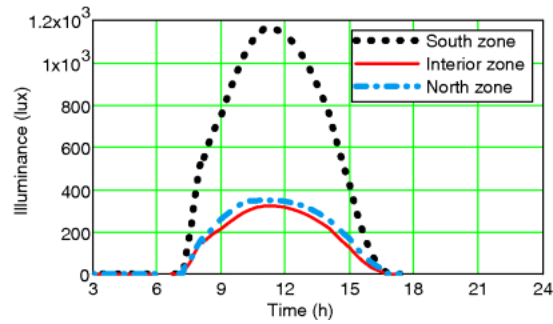
Fig. 7.64 Simulated interior daylight illuminance distribution on the workplane on a clear sunny winter day using radiosity method

7.4.3.3 Integrating Design and Control for Daylighting and Solar Heat Gain – Option with Controlled Shading

During the winter season, the solar altitude angle is low and hence can easily penetrate deeply into perimeter zones and cause glare. Without suitable daylighting and solar heat gain storage measures, blinds will likely block this solar radiation potentially useful for passive space solar heating. On the other hand, in the cooling season, excessive transmitted solar radiation can increase the cooling load. Integrated daylighting and solar heat gain design and control aims to maximize the utilization of solar radiation, not only for daylighting, but for passive solar heating as well. The key design and control elements will be the daylighting portion of the equator-facing window and building-integrated thermal energy storage.

The integrated approach being investigated in this case study is to adopt a Vision Control® (VC) window on the optimally sized equator-oriented windows, and to use it to control the incoming amount of solar radiation to satisfy daylighting and solar heat gain requirements. The VC window has highly reflective blinds between two glass panes. The blinds can be rotated to block direct solar radiation penetration, and reflect the radiation to desired surfaces (normally the ceiling) to allow it to reach deeper into the space. This way, glare from direct sunlight can be avoided, and solar radiation and daylight can be better utilized. Figure 7.65 shows the VC window and its maximum transmittance for different incident solar profile angles.
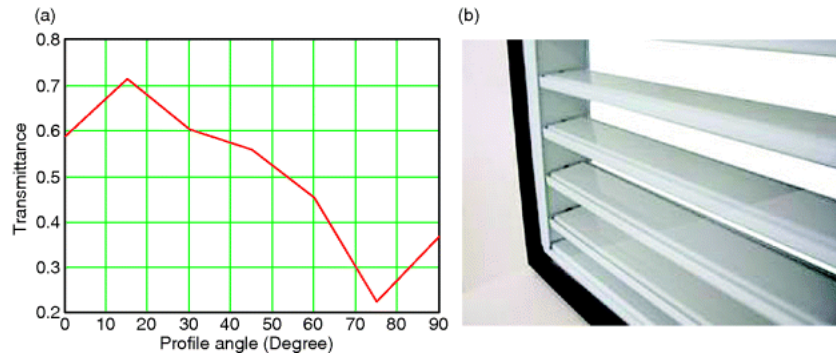
Fig. 7.65 (a) Measured maximum transmittance without direct beam penetration (Peng, 2009) of the (b) Vision Control® window (Photo courtesy of Qian Peng)

In the following subsections, the design and control concepts for different seasons will be investigated using the calibrated integrated thermal and daylighting model. Geographical information for Golden, CO (i.e., latitude and altitude) and selected typical design weather profiles will be used for simulation.

Winter Design Period for Heating-Dominated Climate

High SHGC windows (Table 7.14) are used. Double-glazed window with VC louvers will be used for the daylight window. Triple-glazed windows are used for vision and north façade windows. Figure 7.66

shows the design weather profile. The room temperature setpoint for heating demand is 22 °C between 6 A.M. and 6 P.M., 19 °C for the rest of the time. The effect of acoustic tiles on the radiative and convective heat exchange can be ignored by assuming the acoustic panels are hung vertically instead of horizontally.
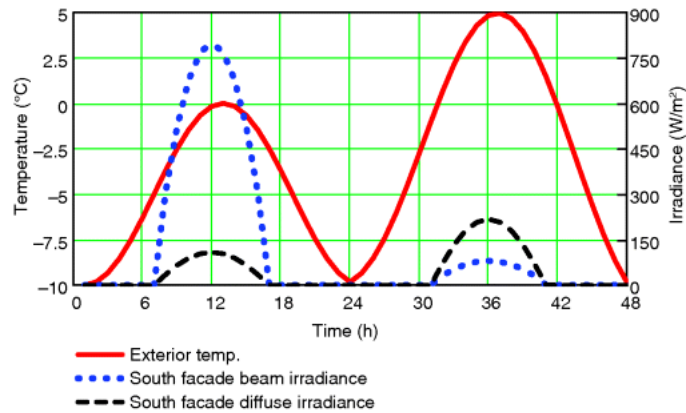
Fig. 7.66 Typical design conditions for heating dominated climate

The heating power to the slab $q_{slb.h}$ is

$$q_{slb.h} = \max\left(T_{spt.h} - T_{rm}, 0\right) \cdot \Delta q_{heating} \tag{7.9}$$

where $\Delta q_{heating}$ = 550 W/K, estimated by assuming the heating power is able to bring the room and slab temperature 1 °C higher in 2 h with 2 °C difference between the setpoint and room air temperatures.

By keeping the daylight window area as it is for the RSF building, the WWR for the daylight window (surface 9) is about 13%. Figure 7.67 shows the thermal and daylighting performance of the typical section. The heating energy consumption for the 2-day study period is 5.74 kWh/m south façade width. The energy is spent in the mornings to heat up the room back to the daytime setpoint after the night setback. The energy for warming up the incoming outdoor air is 5.83 kWh/m south façade width for a 0.2 ACH ventilation rate.
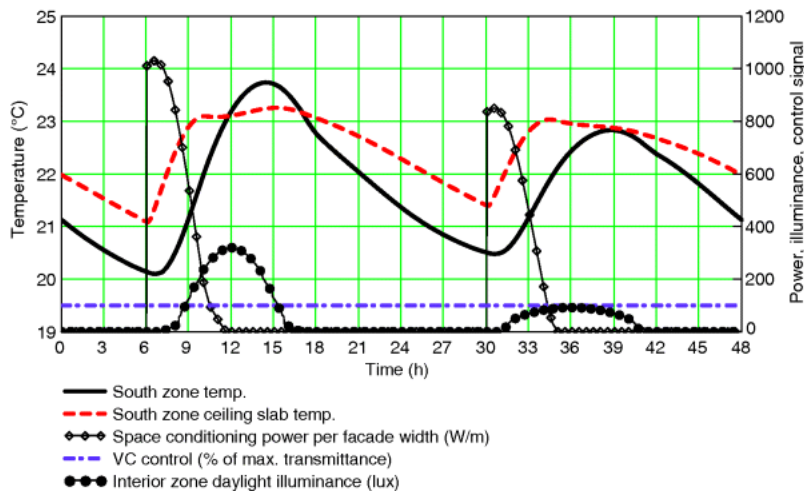
Fig. 7.67 Winter design period performance, with VC on the original daylighting window size

The data indicate that the size of the daylight window can be increased to receive more daylight and passive solar heat gain to reduce the space heating load. Hence, the size of the daylight window is increased to 2.5 times its original size. The WWR of the daylighting window becomes 32%. To avoid space overheating, the control strategy for the VC is if room temperature is 2 °C or more higher than the room heating setpoint (22 °C), then the VC maximum transmittance multiplier, C_r, will be set to

$$C_r = \min\left(\frac{E_{spt}}{E_{zn,i}}, 1\right) \qquad (7.10)$$

where the illuminance set point E_{spt} is set at 300 lux and $E_{zn,i}$ is the average illuminance level of the interior zone.

After enlarging the window size and applying the VC control strategy, the space heating energy consumption is lowered to 5.11 kWh, a reduction of 11% for the 2-day period. Note that the space heating energy consumption is slightly less than that spent on warming supply air. The VC control was activated during the first day when the south zone temperature reached 24 °C to reduce the transmitted amount of solar radiation to avoid space overheating, while daylight illuminance stayed above the illuminance setpoint. As shown in Figure 7.68, the average interior daylight illuminance level is reduced to 350 lux, instead of the illuminance set point of 300 lux. This is because other windows also provide daylight.

South zone temp.
South zone ceiling slab temp.
Space conditioning power per facade width (W/m)
VC control (% of max. transmittance)
Interior zone daylight illuminance (lux)
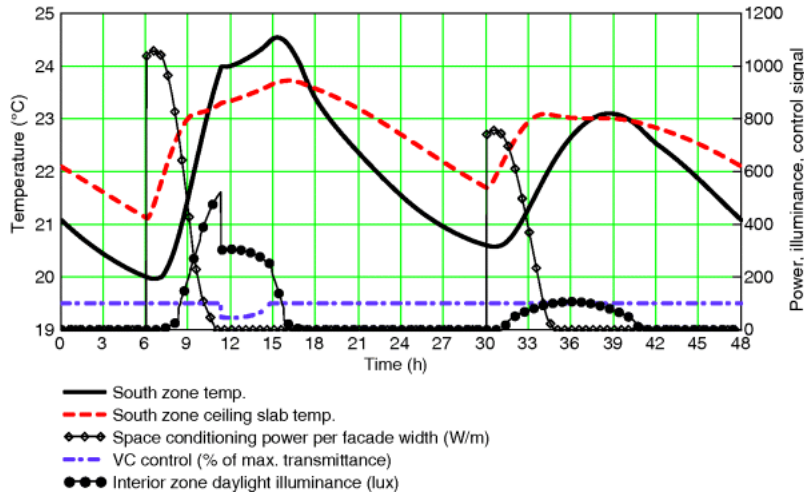
Fig. 7.68 Winter design period performance, daylighting window (VC) size is 2.5 times the original

Even though the transmittance is reduced to avoid space overheating, useful solar heat gains continue to enter the building and warm up the slabs and rooms. The VC reduces the intensity of solar heat gain to a level that matches the heat-absorbing capacity of the room. It is also seen that the room temperature of the north zone is relatively low compared to the south zone. Measures such as ceiling fans can be deployed to enhance the interzonal heat transfer, and hence increase the absorptivity of the entire space. This means more solar heat gain can be utilized. Furthermore, supply air temperature can be set lower to take advantage of abundant passive solar heat gain, and hence lower the energy consumption in warming up the fresh air.

Further potential enhancement in an archetype. Additional improvements that could be explored based on results from the simulations include the following:

– The energy required to warm up outdoor supply air can be reduced by heat recovery ventilation; and,

– Thermal energy collected through solar thermal collectors, such as the transpired collector described earlier, can be used to warm up the supply outdoor air (it has been implemented in RSF, but not considered in the thermal model just presented). This warm air can assist space heating. The collected thermal energy can also be stored in the hydronic slabs/walls, and used later to reduce morning space heating load.

Summer Design Day for Cooling-Dominated Climate

For a cooling-dominated climate case, the room temperature cooling setpoint is 24 °C between 6 A.M. and 6 P.M., and 27 °C for the rest of the time. Double-glazed windows with low SHGC but high visible transmittance are used for all windows including the view windows. The WWR of the daylighting window is kept at 32%. Supply air temperature is kept at 18.9 °C, unchanged as well. The energy for cooling the ventilation air is 2.01 kWh/m façade width for a 0.2 ACH ventilation rate based on the exterior temperature depicted in Figure 7.69. The daylight illuminance setpoint for the interior thermal

zone is 250 lux (300 lux was used in the winter case) to further reduce solar heat gain. The VC louver will be adjusted to reduce transmittance, when room temperature is less than 2 °C lower than the room cooling setpoint and daylight illuminance of the interior zone reaches 250 lux.
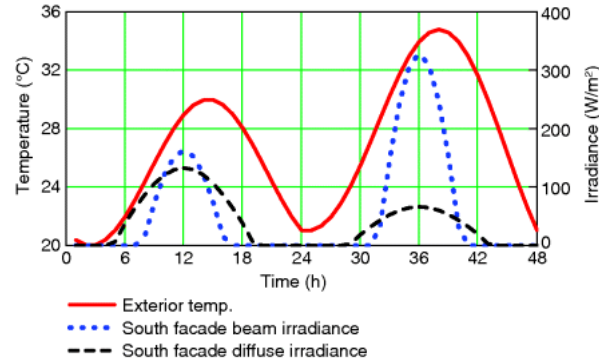
Fig. 7.69 Typical design conditions for cooling dominated climate

Initial simulation indicates that daylighting with the VC louver is not able to satisfy the 250 lux requirement for the interior zone for most of the time, except for the 3 h around noon on a sunny day. This is because the solar altitude angle is high and hence the incidence angle is large. An exterior horizontal reflector with the same area as the daylight window is inserted just below the daylighting window. Natural daylight illuminance on the first design day is able to reach 200 lux between 9 A.M. and 3 P.M., as shown in Figure 7.70. The space cooling load increases slightly as shown in Table 7.17. As seen from Figure 7.70, direct solar radiation can penetrate through the north windows in the early morning and late afternoon.
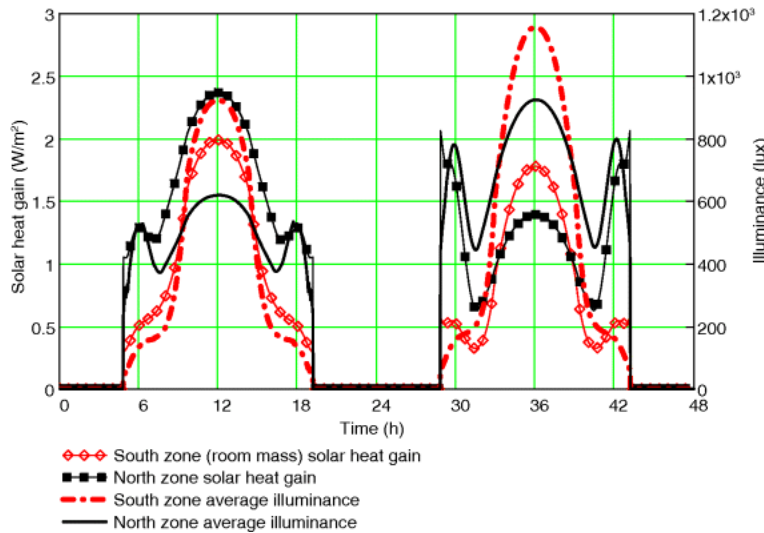
Fig. 7.70 Solar heat gain and daylight illuminance of thermal zones

Table 7.17 Space cooling energy of different design and operation scenarios

Exterior Reflector	Nighttime Ventilation	Space Cooling Energy Consumption per Meter Façade Width (kWh/m)
No	no	7.10
Yes	no	7.20
Yes	10 ACH	4.13
Yes	30 ACH	3.82

Nighttime building free cooling with outdoor cool air is adopted to reduce the space cooling load. Whenever the room temperature is less than 3 °C lower than the daytime room temperature setpoint

and exterior air temperature is lower than room air temperature, free cooling is activated. Increasing the ventilation rate from 10 to 30 ACH results in a marginal reduction (4.3%) in cooling energy consumption. There is also no significant reduction in the peak cooling demand. Figure 7.71 shows the temperature and illuminance profiles of different thermal zones, as well as the control action for the VC, and the space cooling power requirement. The temperature of the north thermal zone is slightly higher than that of the south zone. This is because the north zone has higher overall solar heat gain due to no solar control (e.g., in the early morning and late afternoon). Based on model calibration, the infiltration rate of the north zone is 2.5 times that of the south zone, which is 0.1 ACH based on the south thermal zone volume. That means the north zone also has higher heat gain from exterior hot air.
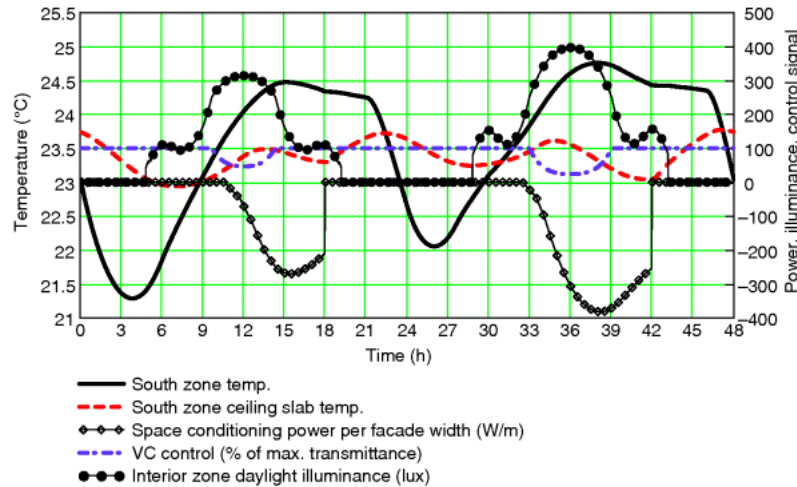
Fig. 7.71 With 30 ACH nighttime natural ventilation and exterior reflector installed

Further potential enhancement in an archetype. The volume of concrete in the ceiling slab of the typical section is about 5.7 m³. A 1 °C change in the slab temperature results in 3.04 kWh of thermal energy storage. Simulation shows that this amount of energy is able to reduce the peak room temperature in free-floating mode (i.e., no space cooling provided) and replace the energy spent on cooling supply outdoor air, which can also be reduced by heat recovery ventilation. Additional temperature drop of the slab can be achieved through increasing the thermal coupling between the room air and the slab, such as in a ventilated concrete slab (Braham, 2000), or in direct slab cooling using outdoor cool air (Chen, Athienitis, and Galal, 2012). Further cooling reduction can be realized by installing exterior shading for the north window to prevent unnecessary solar heat gain in the early morning and late afternoon.

Shoulder Season

The shoulder season (e.g., around September) features mild exterior temperatures and strong solar radiation on the façade resulting from relatively low solar altitude angles. Cooling will dominate the space conditioning energy consumption. Since cool outdoor air is available during the nighttime for free cooling, the measures described in Section 7.4.3.3 on summer design day for cooling-dominated climate can effectively reduce the cooling load and peak demands.

7.4.4 Alternative Design and Operation for Consideration

In addition to the design and operation techniques investigated earlier, here are some others that could also be adopted.

7.4.4.1 Building-Integrated PV: Optimal use of Building Roof and Façade

The current RSF design uses a low 10° roof slope (note that the latitude is 39.7°, so an optimal roof slope would normally be around 40° for solar energy collection), in part to reduce the cost associated with a high ceiling, facilitate roof maintenance, and also use the ceiling for radiant cooling/heating. One possibility in a new design is to optimize the south façade and roof for solar energy collection. For example, using the current building form and orientation, a 1 kW PV system on the façade would be expected to generate about 995 kWh per year as compared to 1253 kWh for the same 1 kW PV system

mounted on the 10° sloped roof.[5] A façade BIPV system could also be combined with heat recovery for solar air heating as described next.

7.4.4.2 Building-Integrated PV/T and Transpired Collector with Air-Source Heat Pump

The building roof and façades can be used as substrates for solar thermal energy collecting systems (e.g., BIPV/T and transpired thermal solar collectors without PV integration). As the building increases in height, the importance of façade surface area increases relative to roof surface area.

The thermal energy collected from the solar thermal energy collecting systems can be used as heat sources for a heat pump. The heat output from the heat pump can be used for space heating through heating a hydronic or air-based BITES.

7.4.4.3 Active Building-Integrated Thermal Energy Storage

Active BITES, such as hydronic or ventilated massive slabs/walls, other than being used solely as the media to provide space heating and cooling, can also be used to store renewable thermal energy for building preconditioning. For example, BITES can be preheated with collected heat from passive solar heat gain and active solar thermal collectors (e.g., transpired collectors and BIPV/T), and precooled with available outdoor cool air, through direct heat exchange or with a heat pump.

With the desired temperature profile and thermal load of the building based on the set temperature profile and weather forecast, frequency domain models of BITES systems can readily provide predictive control information for BITES systems, such as the thermal charging rates and schedule. Frequency domain models also provide insight in optimizing the design of active BITES systems.

7.4.5 Conclusions

The purpose of this case study was to investigate key design features of the RSF and abstract them to an archetype building/cross-section that can inform the design of similar buildings possibly under other climatic conditions and modified function. A key part of the work was modeling of thermal and daylighting performance of a typical zone with a number of design alternatives. The solar utilization of the south façade and roof for electricity and useful heat is also discussed.

The design and performance of the NREL RSF were discussed. An alternative design investigation focused on daylighting and solar heat gain control was conducted. The potential contribution from transpired solar thermal collectors, active building-integrated thermal storage systems, and building precooling with nighttime ventilation were evaluated. This study also demonstrates, in the context of office buildings, how to model similar advanced high-efficiency buildings, and how to perform model-based integrated design and optimization that considers near-optimal operation strategies.

The abstraction to an archetypal office section reveals one of the key elements in façade design: integrated daylighting and solar heat gain control – an energy façade. With optimized energy façades, office buildings can have low energy consumption and high performance. Higher daylighting performance can be reached, and thermal comfort can be maintained without auxiliary space conditioning.

Furthermore, using simulation at the beginning of the design process can help establish factors, such as geometry, that can have a major impact on the energy profile of a building. The analysis of the actual design process followed by the RSF designers showed that building depth, design of fenestration, and ceiling heights were established early in the design.

The design alternatives using motorized venetian blinds integrated in doubled glazed units also showed that by matching window-to-wall ratio to daylighting window shading/daylighting controls, thermal storage, and natural ventilation can also have a major effect on the design of fenestration, making a design link between geometry, thermal storage, and controls. More generally stated, this shows the effect of the window area on daylighting and thermal gains. However, to be effective, this connection must be studied specifically for the climate in which a building is located since each combination of climate and indoor comfort will yield a different optimal window area.

This is significant as well in terms of the design process. As previously mentioned, any changes made to a project – regardless of their reason – late in design development, construction documentation, or even during the construction phase risk adding major cost and time delays to any project. For this reason, often late-stage design changes are not implemented.

Nomenclature

ACH	air change per hour
AHU	air handling unit
BIPV/T	building-integrated photovoltaic/thermal system
BITES	building-integrated thermal energy storage
RSF	Research Support Facility
SHGC	Solar heat gain coefficient
VC	Vision Control®
WWR	window-to-wall ratio

7.5 Enerpos

Aurélie Lenoir, Konstantinos Kapsis, and François Garde

ENERPOS is a two-story, net-zero energy university building, separated into two parallel wings by a green patio (Figure 7.72). The building has a net floor area of 739 m² (with 246 m² of mechanically conditioned floor area) and it is comprised of an administration zone (seven small offices and a meeting room), two computer rooms and five classrooms. The building is located on the Saint-Pierre campus on the south coast of Reunion Island (a territory of France), which is situated in the southern hemisphere, 200 km west of Mauritius island (21.3°S, 55.5°E). The climate is tropical and it is characterized by significant global horizontal radiation (2044 kWh/m²/yr). The weather conditions in Saint-Pierre for 2011 are summarized in Table 7.18. The diurnal (day-to-night) temperature swing in December is about 8 °C.

Fig. 7.72 ENERPOS building on Reunion Island. BIPV roof: 365 m² of PV panels to balance the low consumption of the building (Photo courtesy of Jérôme Balleydier)

Table 7.18 Weather conditions in Saint-Pierre, based on weather station measurements at Saint-Pierre campus (2011)

	Average Temp. (°C)	Min. Temp. (°C)	Max Temp. (°C)	Mean RH (%)	Mean Air Speed (m/s)	Mean Global Horizontal Radiation kWh/(m²·day)
Summer	25.4	16.9	31.9	72.4	2.5	6.3
Winter	21.8	15.1	30.0	72.2	2.5	4.7

The main design objective of ENERPOS was to construct a low-energy building (energy use intensity of 14 kWh$_{FE}$/m²/yr, FE for final energy) using primarily passive design principles, while maintaining visual and thermal comfort for the occupants. Thus, priority was given to indoor environment and energy efficiency measures, natural ventilation, solar shading, and construction materials (Figure 7.73). A PV system on the naturally ventilated PV roof generates electricity and balances the building's energy consumption, while simple active technologies (e.g., ceiling fans) are utilized for the periods of the year when the passive measures alone cannot meet occupancy comfort requirements. The final construction cost of ENERPOS was 3200 €/m² (net floor area) or 1660 €/m² (gross floor area).
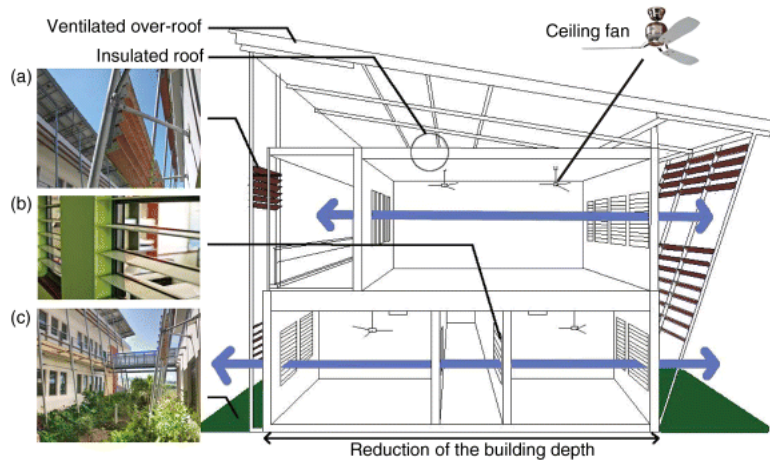
Fig. 7.73 Main features of the Net ZEB design of the ENERPOS building: (a) Exterior fixed solar shading system; (b) Interior frosted glass louvers between the offices and the central corridor; (c) Green patio between the two wings of the building and on top of the parking lot (Photos courtesy of Jérôme Balleydier)

7.5.1 Natural Cross-Ventilation and Ceiling Fans

A major challenge in passive building design in a tropical climate is to maintain thermal comfort using passive means and thus, minimize the cooling energy consumption of the building. ENERPOS' operable windows are located on the north and south building façades, utilizing the sea breeze (south winds) during summer, while minimum openings on the east and west building façades protect the building from the winter prevailing winds (east and southeast winds) and morning and afternoon sun. The long axis of the building is oriented N14°E. The window-to-wall ratio (WWR) of 30% was chosen for cross-ventilation and daylight utilization. Manually operable clear glass louvers (Figure 7.73) were used on the exterior windows to regulate natural cross-ventilation, while providing protection against cyclones and for security against theft. Frosted glass louvers were installed on the interior windows facing the central corridor, also with WWR of 30%, to allow cross-ventilation, while providing privacy to the occupants (Figure 7.73(b)). The building cross-section depth was kept below 10 m for each building wing to permit cross-ventilation and allow daylight to reach the building core. Energy-efficient ceiling fans were installed in all spaces, including those with air conditioning. The use of ceiling fans helps to maintain thermal comfort during warm, windless days.

7.5.2 Solar Shading and Daylighting

An exterior fixed louver shading system (Figure 7.73(a)) was employed on the north and south façades in order to minimize direct solar gains and prevent glare. The solar shading system was designed using 3D simulation tools, providing balance between solar gains and daylighting. Almost no windows were placed on the east and west façades in order to protect the building from the low-altitude morning and afternoon sun that can easily overheat the building. With regard to daylighting, simulations predicted that most spaces are at least 90% daylit during occupied hours (8 A.M. to 5 P.M.) with two classrooms not being equipped with electric lighting, as simulations showed that they could be fully daylit.

7.5.3 Microclimate Measures

The surrounding microclimate has an impact on building energy performance as it directly affects the ground albedo and ground surface temperature, resulting in higher exterior surface and ambient temperatures when, for example, the building surrounding is paved (Givoni, 1998). Thus, ENERPOS is surrounded by a 3 m strip of endemic plants and the parking lot is located underground. In addition, the use of a narrow garden instead of pavement around the building increases the soil permeability that can prevent flooding after heavy tropical storms.

7.5.4 Materials

Regarding the envelope, the walls are made of concrete; the roof is insulated using a 10 cm layer of polystyrene with a ventilated BIPV array over the roof; the solar shading systems are made of wooden strips; the east and west gables are insulated with mineral wool and wooden cladding. The paint used is organic and the wooden components have not undergone any chemical treatment. In order to reduce cost, no insulation is used on the main façades that are shaded by the exterior louver shading systems (Table 7.19).

Table 7.19 Envelope description of the ENERPOS

Roof	BIPV on exterior of roof + 10 cm of polystyrene + 20 cm concrete Overall R-value: 3.4 m² K/W Solar factor (the percentage of solar heat that penetrates the roof to the building's interior): 0.003
Walls	East and West: 18 cm concrete + 8 cm mineral wool, or 18 cm concrete + ventilated air gap + wooden siding Overall R-value: 1.8 m² K/W Solar factor: 0.02
	North and South: 18 cm concrete + solar shading Overall R-value: 0.1 m² K/W/Solar factor: 0.03 Window-to-wall ratio: 30%
Windows	U-value: 1.4 W/m² K Effective solar heat gain coefficient (SHGC) including solar shading: north, 0.10; south, 0.15 Visible transmittance: 0.4

7.5.5 Ergonomics and Interior Design

A particular effort was made for the indoor design of all spaces, ranging from the wall colors to the choice of interior furniture. The building team aimed to prove that a comfortable working space can be designed without extra costs. The offices' ergonomics were studied to achieve a maximum level of comfort for occupants: desks are positioned perpendicularly to the windows, at a 0.5 m distance, to avoid glare and direct solar radiation incident on the desks and chair backs are made from a breathable fabric to allow air circulation.

7.5.6 Energy Efficiency

ENERPOS conserves energy primarily due to its passive design. Energy management strategies are used to decrease the overall energy consumption of active systems (Figure 7.74).
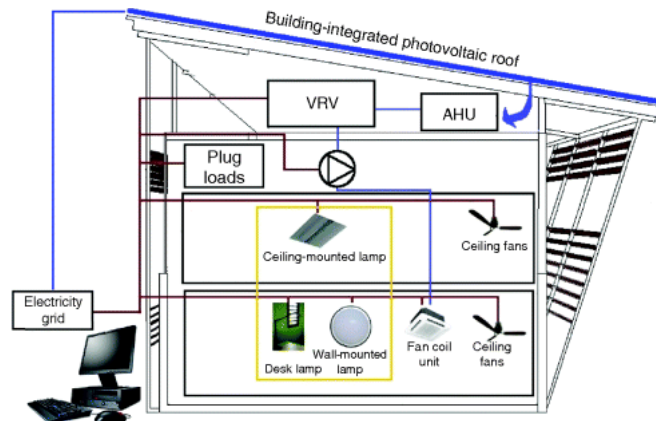
Fig. 7.74 Schematic of the energy efficient systems installed in ENERPOS (VRV is variable refrigerant volume flow; AHU is air handling unit)

7.5.6.1 Artificial Lighting

The installed lighting power density (LPD) is 7 W/m² in the classrooms and 3.7 W/m² in the offices. In the classrooms, ceiling-mounted luminaires provide workplane illuminance of 250 Lux. Timers are used to automatically turn off the lights after 2 h. For the offices, low-energy T-5 luminaires provide indirect ambient lighting (100 lux), while LED desk lamps (task lighting) provide additional lighting (300 lux), if required.

7.5.6.2 Ceiling Fans

Ceiling fans are used in conjunction with a natural ventilation strategy to create air movement and thus, increase thermal comfort. A total of 55 ceiling fans with a 132 cm blade diameter were installed in offices and classrooms. The fans are controlled individually (in offices) or in groups of two or four (classrooms) from wall-mounted switches, using three speed levels. The maximum power used by each ceiling fan is 70 W, which represents 7 W/m² of the area served.

7.5.6.3 Air-Conditioning System

A variable refrigerant flow (VRF) air-conditioning system was installed to cool the offices and computer rooms. The air-conditioning system is composed of several systems:

– A VRV (variable refrigerant volume) system with a cooling capacity of 25.3 kW and energy efficiency ratio of 4.8 (based on manufacturer's datasheets);

– An air handling unit (AHU);

– Twelve ceiling cassette air-conditioning units (one per office and two per computer room and meeting room);

– Two split systems to cool the technical rooms (with a cooling capacity of 700 and 1780 W, respectively).

The air-conditioned area of the building is 246 m², which corresponds to 36% of the net floor area. About 90% of the floor area of the buildings of the University of Reunion Island is air-conditioned with an average cooling capacity of 150 W/m², while the cooling capacity of ENERPOS is 102 W/m² (referring to the floor area of the mechanically conditioned space).

In a standard university building on Reunion Island, the air-conditioning period is usually nine months. During the design phase, a dynamic thermal model of the building was undertaken in the DesignBuilder simulation tool (EnergyPlus with custom interface). Using Givoni's comfort diagram on a psychometric chart, it was possible to predict the operational periods for natural ventilation, ceiling fans, or air-conditioning (Garde *et al.*, 2011). The offices were designed/expected to be air-conditioned for 1.5 months and the computer rooms for three months (15 days on December and from the beginning of February to mid-April, which represents about 42 working days).

Besides reducing the air-conditioning period, the ceiling fans are used to raise the acceptable setpoint temperature during air-conditioning operation hours. In standard buildings, the maximum setpoint temperature to provide thermal comfort is 26 °C. However, with an air velocity on the occupants' skin of 1 m/s (provided by a ceiling fan), the maximum comfort temperature could rise to 30 °C. Energy savings for air-conditioning are about 10% per degree rise of the setpoint temperature. Thus, energy savings in the range of 30 to 40% can be achieved.

7.5.6.4 Computer Network and Plug Loads

The office occupants are encouraged to use laptops and netbooks, which consume much less energy than desktop computers. The computer rooms are equipped only with screens, mice, and keyboards, while all central units are located in an air-conditioned technical room. Thus, thermal loads from the computers are kept outside the computer rooms.

7.5.6.5 Building Management System and Individual Controls

A building management system (BMS) controls the air-conditioning system (operating period, set point temperature), the schedules of exterior lighting and energy consumption by type of end-uses (lighting, ventilation, plug loads, air conditioning, and elevator), and targets the most consuming items through energy management actions. In the offices, the use of ceiling fans and lighting is left to the discretion of the occupants with individual controls. In the classrooms, the controls are grouped for the ceiling fans.

7.5.7 Integration of Renewable Energy Technology

The underlying philosophy of ENERPOS is to balance the final energy consumption of all its uses with its PV production and to reduce the period of time required to reach net-zero energy balance. Thus, the very low consumption of the building is balanced by a 365 m² BIPV roof. The PV panels serve as over-roof system, with half oriented north and half oriented south to allow for an architectural homogeneity of the building (Figure 7.72). Besides electricity production, the BIPV system serves as a ventilated double roof and solar shading for the terrace roof of the building. Because of the BIPV layer, the solar factor (the percentage of solar heat that penetrates the roof to the building's interior) of the roof is 0.003 whereas the PERENE[6] building performance standard requirement is 0.02.

The PV panels used are polycrystalline silicon. The installation is composed of 14 inverters (each 3300 W). Table 7.20 summarizes the main characteristics of the BIPV roof as well as the expected PV production as it was calculated during the design using the PVsyst software. The roof is rented by the university to an independent company who invested in the PV panels.

Table 7.20 Characteristics of the BIPV roofs

	South Wing	North Wing	Total
Area	219 m²	146 m²	365 m²
Peak power	30,240 W	20,160 W	50,400 W
Azimuth	166°SW	−14°NE	
Tilt	9°	9°	
Expected production (PVsyst simulation)	44,612 kWh/yr	32,391 kWh/yr	77,003 kWh/yr

7.5.8 Description of the Design Process

This section provides a brief summary of the design process that was followed on ENERPOS, which was started in 2004. New methods and tools were tested during this design process.

7.5.8.1 Design Objectives and Importance of the Design Brief

The primary design objective of ENERPOS was to demonstrate the use of passive design principles for hot climates and the use of simulation tools and that it is feasible to reduce the energy use of the building by two-thirds, compared to other office and university buildings on Reunion Island. Designing a passive building also meant that a careful consideration was paid to the thermal comfort of the occupants. Buildings in the French tropical regions are often poorly designed where the active systems,

such as the air-conditioning and the artificial lighting, tends to be low-efficiency and oversized, leading to a high annual energy use (e.g., 100 $kWh_{FE}/m^2_{NFA}/yr$ for an office building; NFA: net floor area).

During the ENERPOS design process, a significant effort was put in developing a very detailed design brief in order to achieve the required high energy performance. The brief usually provides a thorough explanation outlining the aims, objectives, and milestones of the project. For the ENERPOS building, a specific section related to energy efficiency and "green" building objectives was added. Some important requirements about the design of buildings in tropical climates were considered:

– A good knowledge of the local climate (e.g., direction of thermal breezes, orientation with respect to the sun, availability of Typical Meteorological Year weather files);

– A good design of the surroundings (e.g., the parking lot was not allowed to be located in front of the main façades of the building, a 4 m strip of vegetation around the building should be planted);

– Priority must be given to the passive design (e.g., roof insulation, solar shading for all openings, cross-natural ventilation, daylight utilization);

– The systems need to be energy efficient (e.g., air-conditioning, artificial lighting); and,

– The building must comply with the local energy standard: PERENE (Garde *et al.*, 2005).

7.5.8.2 Design Team and Timeline

The design team of ENERPOS was rather conventional and composed of an architect supported by several engineering design offices. However, a research project named "ENERPOS" and funded by the French National Research Agency (ANR), whose aim was to develop and test new methods and tools for the design of Net ZEBs in hot climates, was carried out in parallel with the design process. The project involved three French university research laboratories, two design offices and the architect himself. The project was led by Dr. François Garde who provided scientific support throughout the design of ENERPOS (Garde *et al.*, 2011). The ENERPOS building was used as a case study to test the methods and tools developed during the research project. The design team is summarized in Table 7.21 and the main project phases are outlined in Figure 7.75.

Table 7.21 Building team of the ENERPOS building

Building Owner/Representative	University of Reunion Island
Architect	Thierry Faessel-Boehe
General contractor	Léon Grosse
Mechanical, electrical engineer	INSET
Energy modeler	PIMENT Laboratory and Imageen
Environmental design office	Imageen
Structural engineer	RTI
Environmental consultant	TRIBU Paris
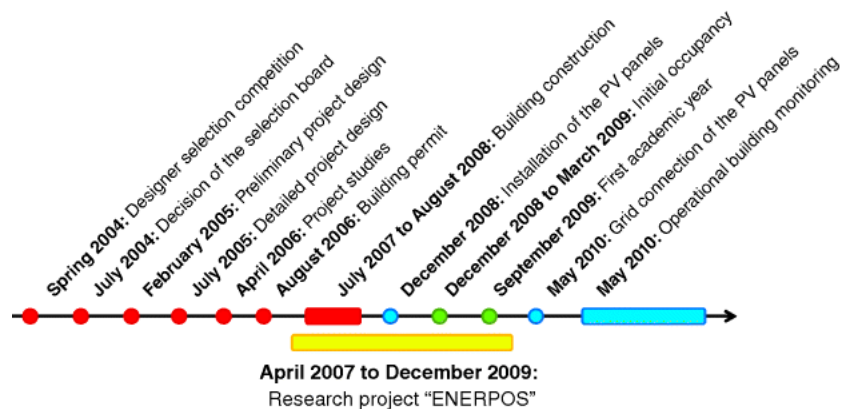
Fig. 7.75 Timeline of the ENERPOS building: from design to occupancy

7.5.8.3 Design Tools

Several software tools were tested in the framework of the ENERPOS research project and during the design of the building to evaluate the thermal performance of the building, such as Codyrun (Boyer *et al.*, 1996) or Design Builder and Dial Europe for daylighting (Garde *et al.*, 2006). However, the models were primarily used to check the passive performance rather than to size the systems.

The design process of ENERPOS identified difficulties and challenges that can arise with the use of simulation tools in the design process. Experience and common sense were more effective in this case, considering the state of research in the field of building simulation at that time (2005). This type of approach is well-suited to simple buildings like ENERPOS. The building has low internal loads. Its location is close to ideal in terms of natural ventilation, with no major noise sources or high buildings in close proximity. Consequently, it was possible to choose an orientation in order to take advantage of the cooling breezes, making the concept of natural ventilation straightforward. Even though the design and the operation of ENERPOS were based on numerous assumptions, its performance in terms of energy and comfort has exceeded predictions.

Regardless, a simulation methodology was proposed at the end of the ENERPOS research project, based on the use of freely available building simulation software. Currently, this methodology is often used for the design of new buildings on Reunion Island. The 3D CAD software SketchUp is the basis of the methodology and is linked to several simulation tools, such as EnergyPlus (for the thermal and energy performance), Daysim (for daylighting), and CattAcoustic (for acoustics). In addition, SketchUp facilitates assessment of the impact of solar shading on the windows of a building (e.g., Figure 7.76) and it is a user-friendly tool for design offices and architects that can be used throughout the design process.
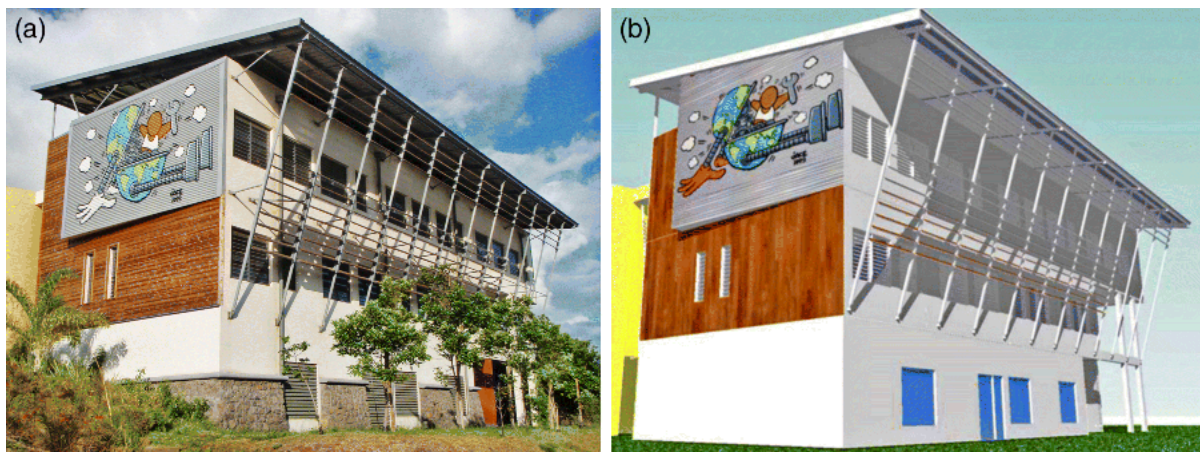
Fig. 7.76 Comparison between (a) a photo of the ENERPOS building (November 26 at 5 P.M.) and (b) the SketchUp Model with projected shadows of shading at the same time

The building performance was assessed including thermal comfort and daylighting. The ENERPOS project suggested the use of the Givoni comfort zones adapted for tropical climates (Givoni, 1976, 1998). The daylight autonomy (DA) or the useful daylight illuminance (UDI) metrics represented satisfactory criteria to evaluate the daylight performance.

7.5.8.4 Human Factors Consideration in the Design

The role of the users and their satisfaction is of prime importance to ensure the success of a building project. In the design process of Net ZEBs in tropical climates, careful consideration of thermal comfort is required. The main idea followed is to offer a range of effective solutions enabling the users to adjust their own thermal comfort rather than controlling the ambiance with automatic systems. In the ENERPOS building, manual louvers and ceiling fans with individual controls are available in the offices and in the classrooms. Information panels in all rooms indicate the procedure to follow when people feel hot.

7.5.9 Monitoring System

The building is closely monitored with data collected every 10 min. This allows for better control of electricity consumption, rapid identification of excessive consumption, and improved understanding of the electrical consumption characteristics of the building. Fifteen energy meters (10 pulses/kWh) measure the consumption of electricity by end-use (interior lighting, exterior lighting, ceiling fans, air-conditioning terminal units, split systems in the two technical rooms, VRV group, air treatment unit, plug loads, and elevator) to identify the most energy-consuming items and take energy management actions, if necessary. There are occupancy sensors to measure the occupancy rate as well as temperature and humidity sensors in all classrooms and offices. An on-site weather station provides outdoor conditions. Portable units measuring environmental conditions (inside air temperature, black globe temperature, air velocity, humidity and illuminance) have been deployed to provide short-term assessment of the indoor environment.

The overall monitoring system cost €72,425, which represents 3% of the overall cost of the building construction. This price includes the fixed instrumentation (energy-meters, temperature and humidity sensors, the wiring, and the commissioning) as well as the portable comfort measuring device.

7.5.10 Monitored Data

7.5.10.1 Measured Performance

The ENERPOS building has been fully monitored since May 2010. The measured data of the second academic year of the building (from September 2011 to August 2012) are given in Figure 7.77. The total energy use of the building was 10,202 kWh, which represents an energy ratio of approximately 14 kWh/m$^2_{NFA}$/yr. Compared to other office and university buildings on Reunion Island (100 kWh/m$^2_{NFA}$/yr), ENERPOS consumes seven times less. By looking at the different end-uses, it should be noted that the plug load consumption represents approximately half of the total energy use of the building and remains more or less constant over the year. The energy end-uses that vary the most are the air-conditioning (particularly the use of the split systems in the technical rooms), ceiling fans, and interior lighting. Furthermore, exterior lighting consumption increases during winter (May to October).

Annual energy tracking sheet of ENERPOS

YEAR 2: September 2011 to August 2012			
Energy use		**Production**	
Annual energy use	10,202 kWh	Annual production	79,440 kWh
Energy index	13.8 kWh/m²$_{NFA}$	**Energy index**	107.5 kWh/m²$_{NFA}$
		Productivity	1,697 kWh/kWp

Energy use in ENERPOS from June 2011 to May 2012 (kWh/month)

Legend: Interior lighting, Exterior lighting, Ceiling fans, Air-conditioning (tech rooms), Air-conditioning (building), Plug loads, Elevator, Outside temperature

Pie chart: 7%, 15%, 9%, 11%, 3%, 2%, 53%
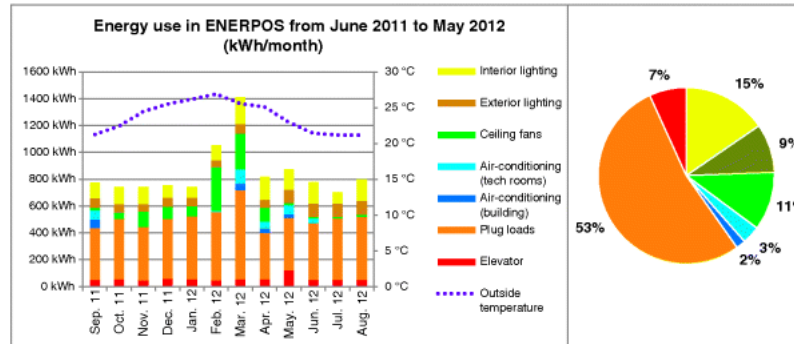
	Sep. 11	Oct. 11	Nov. 11	Dec. 11	Jan. 12	Feb. 12	Mar. 12	Apr. 12	May. 12	Jun. 12	Jul. 12	Aug. 12
Ratio (kWh/m²$_{NFA}$)	1.0	1.0	1.0	1.0	1.0	1.4	1.9	1.1	1.2	1.1	1.0	1.1

	Int. Lighting	Ext. Lighting	Ceiling fans	Air-conditioning	Plug loads	Elevator
Energy use	1575 kWh/y	913 kWh/y	1099 kWh/y	516 kWh/y	5404 kWh/y	694 kWh/y

Legend: Energy use, Production, Standard University Building, Energy use, Production
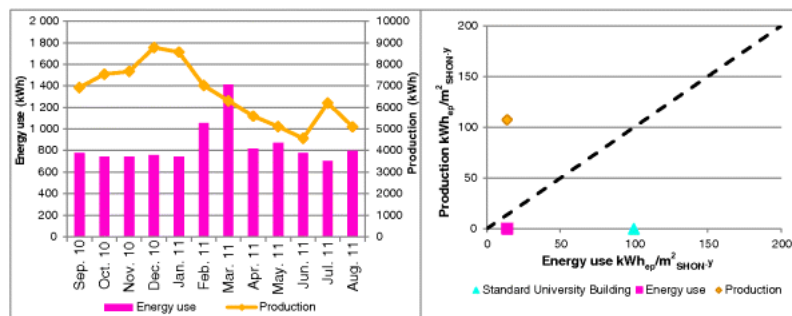
Maximum power load of the building	10.2	W/m²$_{NFA}$ or	11 W/m²$_{UFA}$

Fig. 7.77 Annual performance of ENERPOS for the second academic year of the building (from September 2011 to August 2012)

The ceiling fans are used during summer (November to April). The overall consumption of the fans and the split systems units is 2.2 kWh/m²$_{NFA}$/yr whereas in a standard building, air-conditioning systems usually consume 80 kWh/m²$_{NFA}$/yr. The strategy of using cross-natural-ventilation with ceiling fans represents great potential for energy savings.

The PV production measured over the year was 79,440 kWh compared to an overall consumption of 10,202 kWh. ENERPOS has produced seven times its electrical consumption over the year, making it a Net ZEB on an annual, monthly, and daily basis. The PV system seems oversized, but the design meets the goal of incorporating an architecturally integrated PV roof.

The PV system is not part of the overall cost of the building. It is included in a financial agreement between the University of Reunion Island and a private manufacturer. The terms of the contract specify that the university rent its roof for 15 years. The manufacturer installed the PV system and supports all of the costs and risks (including cyclones and maintenance) during that period, but gets the benefits of the electricity fed into the grid (€0.55/kWh). After 15 years, the university will become the owner of the PV system.

The architect of the building wanted symmetry, with half the over-roof facing north and the other half facing south. Both slopes are 9°, which is not the optimal slope (the optimal orientation is north-facing with a slope of about 21°) in terms of photovoltaic performance for Reunion Island. Comparing the PV

yield of the north roof to the south, it shows that the slight suboptimal orientation does not have a significant impact (about 10% difference).

7.5.11 Comparison of Model Prediction with Measurements for ENERPOS

The example of the ENERPOS building illustrates the uncertainties that can appear in the models developed during the design of a building. As stated in Section 7.5.8.3, several models were developed during the design process of ENERPOS, but those models were used to assess and support the expertise used to design the building rather than to optimize the envelope or the operation of the systems operating within. Two comparisons are presented in this section. The first is a comparison between the energy use predicted during design and the measurements available due to 2 years of monitoring. The second evaluation concerns the thermal comfort in the building with the comparison of the model and the measurements for the annual temperature profile of an office. The use of ceiling fans scheduled during design is also discussed.

7.5.11.1 Energy Use

The methodology used by the design office (Garde *et al.*, 2011) to forecast the energy consumption of the building in the design phase is rather basic and simple to establish. It consists of listing all the equipment, appliances, and systems installed in the building, using an assumed-use scenario (number of hours of use per day and number of days per year) and multiplying by a factor that accounts for the fact that all equipment is not used at the same time and not at the maximum capacity (i.e., diversity factor). In this method, there are several uncertainties associated with the equipment installed, the use scenario, or even the factors used based predominantly on the previous experience of the design office. The aim of this section is to explain uncertainties on energy consumption prediction, during the design phase.

Figure 7.78 and Table 7.22 present a comparison between the energy use that was predicted during design by end-uses and the measurements taken in the building while in operation for 2 years (June 2010 to May 2011 and June 2011 to May 2012). The ratios are given for the net floor area and final energy (electricity). Overall consumption has been largely overestimated during the design stage (45 kWh/m²/yr instead of 13–14 kWh/m²/yr). Major errors made during the design phase to predict the energy consumption of ENERPOS were in relation to the split systems used to cool the two technical rooms, the air-conditioning (AC), the AHU, and the plug loads.
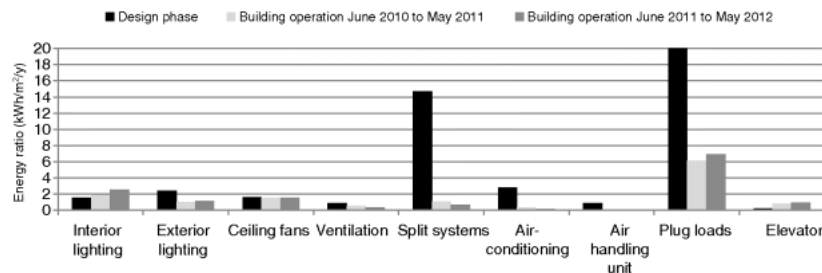
Fig. 7.78 Energy consumption of the ENERPOS building. Comparison between design phase calculations and the measurements for the first two years of operation

Table 7.22 Energy ratio (kWh$_{FE}$/m²/yr) by end-uses: calculation during the design phase and measurements for 2 years

	Interior Lighting	Exterior Lighting	Ceiling Fans	Ventilation	Split Systems	AC	AHU	Plug Loads	Elevator	Tot:
Design phase (kWh$_{FE}$/m²/yr)	1.6	2.4	1.6	0.9	14.7	2.8	0.9	20.0	0.2	45.1
Building operation (June 2010 to May 2011)	1.9	1.0	1.5	0.6	1.1	0.4	0.0	6.2	0.8	13.4
Building operation (June 2011 to May 2012)	2.6	1.2	1.5	0.4	0.7	0.2	0.1	6.9	1.0	14.5

The air conditioning (AC and VRV) and the AHU were installed in the offices and in the two computer rooms. The comfort zones proposed by Givoni (1998) were used to assess the thermal comfort of the rooms when operating under natural ventilation mode. The offices were assumed to be air-conditioned for 1.5 months and the computer rooms for three months (15 days in December and from the start of February to mid-April, which represents 42 working days). The air-conditioning energy was thus predicted to be 2.8 kWh/m²/yr. In fact, it was revealed that after three summer seasons, the air-conditioning in the offices was not used at all. It shows that the hypothesis of the Givoni comfort zones for the assessment of thermal comfort was not completely accurate. Therefore, an extensive field study on thermal comfort was conducted on the ENERPOS building and is presented in Section 7.5.12.

The purpose of the two split system units (one of 1780 W and the second one of 700 W) was to cool the two technical rooms equipped with computer hardware. In fact, only one technical room houses switchgear cubicles, thus only one split system (700 W) is turned on for cooling purposes.

During the design phase, it was proposed to set up an uninterruptible power supply (UPS), particularly for the two computer rooms. Nevertheless, at the current time, there is no UPS in the building. Moreover, up to August 2012, the two computer rooms were not equipped with desktop computers. Students came to the building with their own laptops. The computer rooms are now equipped only with screens, keyboards, and mice. All central units are located in the air-conditioned technical room. With regard to the offices, the use of laptops and netbooks, instead of desktops, has been encouraged, which partially decreases the energy use for plug loads. This change between the design phase and the current situation explains the significant difference in the energy consumption of the plug loads (20 kWh/m²/yr rather than approximately 6–7 kWh/m²/yr for the measurements).

To conclude, the difference between the model predictions and the measurements for the energy use of ENERPOS is not a result of model inaccuracy, but is due to the fact that the actual building operation differs from that expected during design.

7.5.11.2 Thermal Comfort

During the design phase, a dynamic thermal model of the building was undertaken using the DesignBuilder simulation tool. Figure 7.79 shows the annual temperature profile of an office in ENERPOS. Based on the seasonal variations in the temperature of the office, it was possible to predict the different operational periods of natural ventilation, ceiling fans, or air-conditioning, throughout the year. The transition from natural ventilation to ceiling fans was carried out partly based on the experience and knowledge of the site and climate by the design office team, but also on the basis of a maximum average effective room temperature above 28 °C. The transition from ceiling fans to air-conditioning was made when the effective temperature exceeded 30 °C. Design studies indicated that an office required active cooling from January to mid-March and that natural ventilation and ceiling fans were considered sufficient for the rest of the year.

Change in resultant temperature in an office
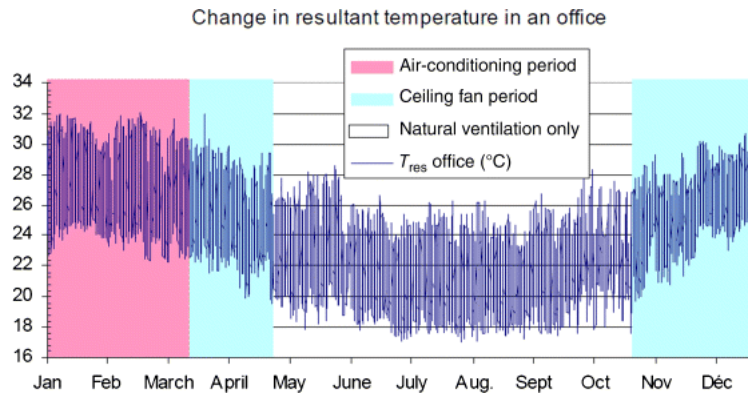
Fig. 7.79 Annual room temperature profile of an ENERPOS office simulated using the DesignBuilder software and the determination of the different operational periods of natural ventilation, ceiling fans or air conditioning. Figure used with permission from ASHRAE (Garde *et al.*, 2011), © 2011 ASHRAE (www.ashrae.org)

Figure 7.80 shows the measurements for the air temperature of an ENERPOS office as well as the energy used by the ceiling fans of the building during the 3-year period, from 2010 to 2012. The comparison between the temperature profiles of the model and the measurements shows that the model was reasonably accurate in terms of maximum temperature during summer (between 30 and 32 °C). However, the minimum temperature in summer was close to 24 °C in the model whereas the measured values do not fall below 28 °C. In the model, it was assumed that the louvers would stay open at night and hence, the building would be cooled down at night. In reality, the users close the louvers when leaving their office in the evening in case of rain.
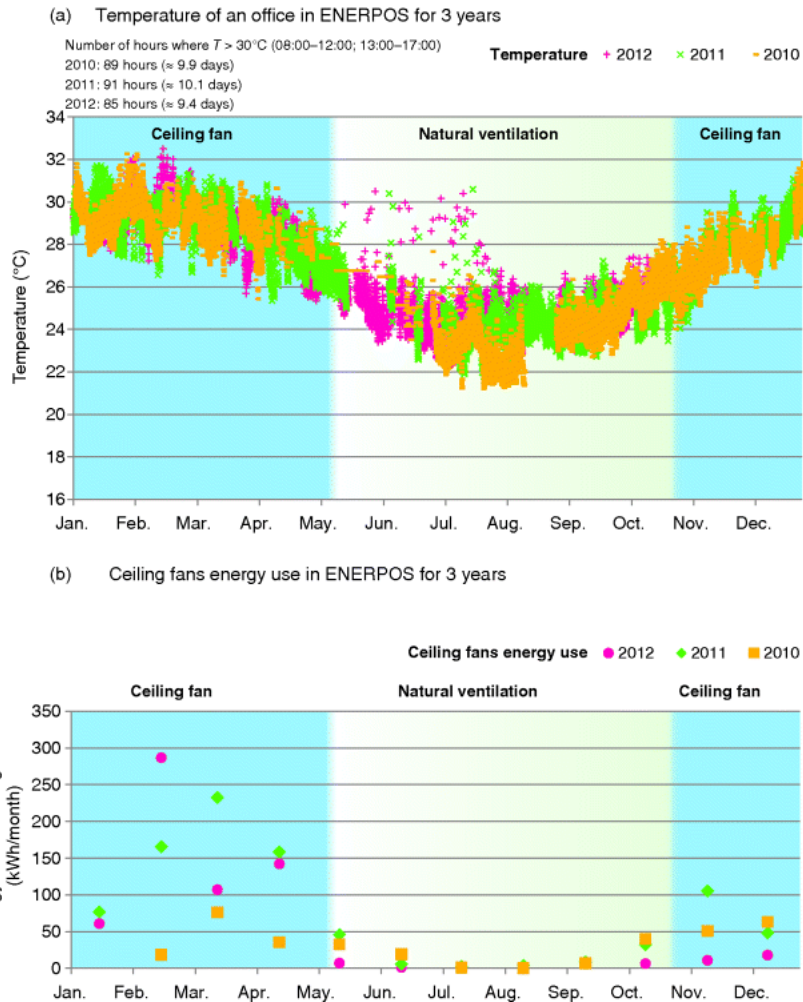
Fig. 7.80 Measurements of (a) the temperature of an office and (b) the energy use for ceiling fans in ENERPOS, for three years

The same observation was made for the winter period where the maximum temperature according to the model was close to 24 °C. The measurements showed that the true temperature of the office was closer to 26 °C. The assumption was also made that the louvers would remain open during winter, which is usually not the case.

These hypotheses should not have a large impact on the determination of the different operational periods as the maximum air temperature of the model in summer is close to the measured values. However, by looking at the energy use for ceiling fans over three years, the real period of use can be identified. As stated previously, the air-conditioning is almost never used in the building. The period of use of the air-conditioning defined during design (January to mid-March) is therefore substituted by a period where ceiling fans are used. It was found that the real period of use of the ceiling fans is a little longer than the one predicted during design (the ceiling fans are still used in early May).

These observations on ENERPOS demonstrate that several uncertainties can appear during design and in the models. User behavior remains the main challenge for the building performance simulations. In order to have a better understanding of the user behavior, particularly with regard to thermal comfort, a field study including a thermal comfort survey has been conducted on the occupants of ENERPOS and is presented in Section 7.5.12.

7.5.12 Thermal Comfort Experimental Study

7.5.12.1 Purpose and Methodology

An extensive field study has been conducted on the ENERPOS building in order to investigate thermal comfort in an energy-efficient building under tropical climate (Lenoir, 2013; Lenoir, Garde, and David, 2011). The purpose was to compare physical measurements with thermal sensation votes in the offices and the classrooms of the building and to compare these results with different approaches, namely the comfort zones proposed by Givoni that were used to assess thermal comfort during the design process of the building.

The methodology followed for this experimental feedback was similar to that of previous studies conducted on the thermal comfort of building occupants (Hwang, Lin, and Kuo, 2006; Kwok and Chun, 2003). The occupants of the building were asked to answer a thermal comfort survey, developed by the PHASE laboratory at the University Paul Sabatier in Toulouse (France), during the course of the ENERPOS research project (Garde *et al.*, 2007). At the same time, a portable unit measuring environmental conditions (air temperature, black globe temperature, air speed, humidity, and illuminance) was placed at a height of 0.8 m above the floor, representing the immediate environment of the seated subjects, during class, automatically collecting the parameters associated with thermal comfort.

The study was carried out during the hot seasons of 2009, 2010, and 2011 (October–April); overall a total of 2092 questionnaires were completed by approximately 700 students and their teachers during 125 two-hour sessions. The gender distribution was 48% males and 52% females. The median age was 21 years and 76% of the interviewees were between the ages of 18 and 22.

The activity level of the students was assumed similar to this on an office (1.2 met). The insulation of the clothing ensembles was estimated on the basis of the answers given in the survey where people were invited to describe what they were wearing. The calculated clothing values averaged in the region of 0.35 clo (0.36 clo for men and 0.34 clo for women). The clothing values were much lower than the assumed summer value of 0.5 given in the ASHRAE Standard 55 (ASHRAE, 2003). This is explained by the fact that most participants were students who wear shorts and open shoes at university rather than pants and closed shoes as the usual summer working clothing.

7.5.12.2 Main Results of the Surveys

The number of votes for each point of the thermal sensation scale is given by temperature ranges in Figure 7.81. It should be noted that based on all the questionnaires, 80% of votes fall between –1 and 1, which corresponds to a comfort situation for the occupants (Fairey, 1981).
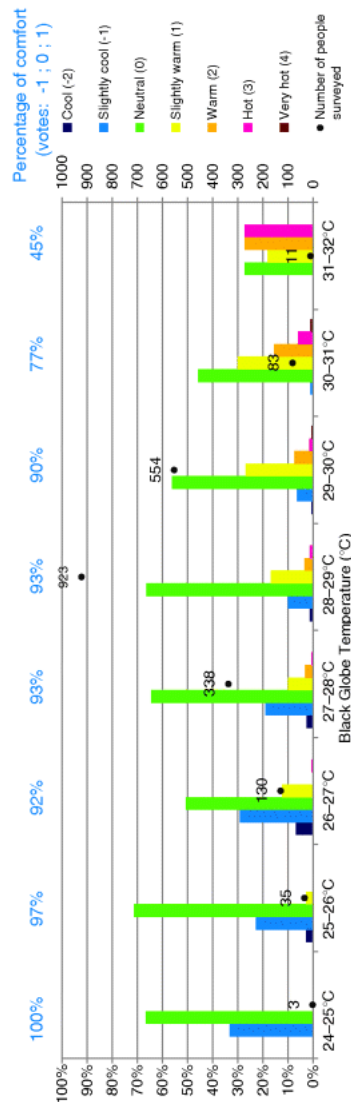
Fig. 7.81 Thermal sensation votes by temperature ranges

Figure 7.81 shows that up to a temperature of 30 °C, at least 80% of the people surveyed express a sensation of comfort. This limit is higher than the level that is generally accepted in comfort standards and used by building designers to assess thermal comfort.

Two main conclusions were drawn from this survey:

1. Thermal comfort can be reached when the operative temperature is up to 30 °C assuming that natural and mechanical ventilation (openings and ceiling fans) are properly sized; and

2. Based on the recorded values (13 to 21 g_{water}/kg_{air}), the humidity level has little effect on thermal comfort. High humidity levels (21 g_{water}/kg_{air}) are not contradictory with thermal comfort and they are much higher than the upper humidity limit of 12 g_{water}/kg_{dryair} recommended by ASHRAE Standard 55 (ASHRAE, 2010).

7.5.12.3 A Comparison between the Experimental Data and the Givoni Comfort Zones

Based on the thermal comfort surveys presented, it is possible to compare the answers given by the occupant of the building with the comfort zones proposed by Givoni on the psychometric chart.

The standard EN 7730 (EN, 2005) gives the relationship between the predicted mean vote (PMV) and the predicted percentage dissatisfied (PPD). When the PMV is between −0.5 and 0.5, the PPD is less

than 10%. For a PPD of 20%, the PMV would be 0.85. As a comfort zone is defined for a maximum percentage of discomfort of 20%, the experimental data represented in Figure 7.81 can be divided into four categories, as shown in Figure 7.82.
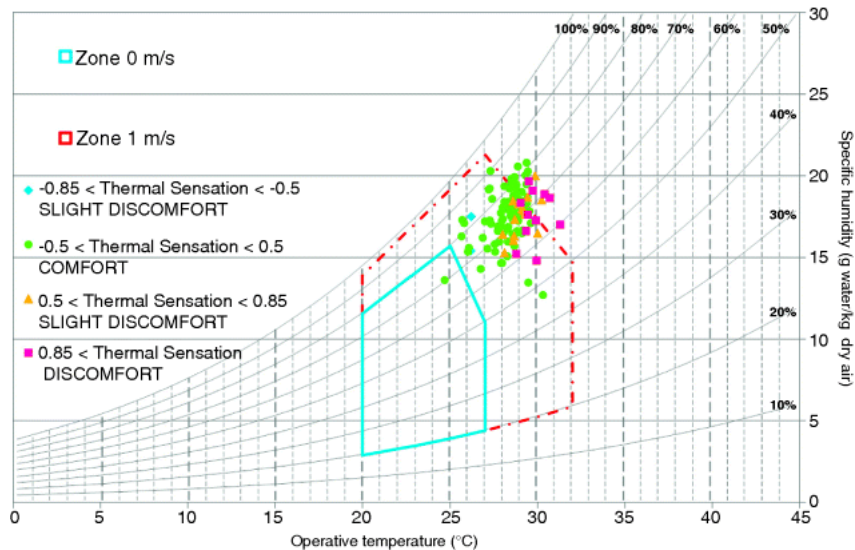
Fig. 7.82 Experimental data from the thermal comfort survey plotted with the Givoni comfort zones

It should be noted that several green dots (corresponding to a comfortable environment) are located outside the Givoni comfort zone for 1 m/s. It was found that people are more tolerant of high humidity than the upper level recommended by Givoni. However, people seem less tolerant of high temperatures.

Based on the conclusions of the survey, a new comfort zone was proposed. It is presented in dark blue in Figure 7.83. The maximum temperature is lowered compared to the Givoni comfort zone, from 32 to 30 °C. The higher limit for humidity is extended to approximately 21 g_{water}/kg_{dryair}.
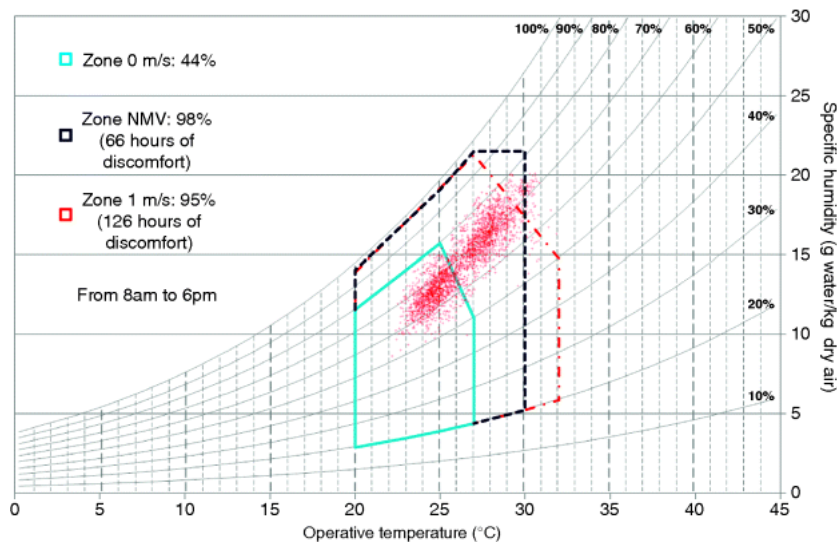
Fig. 7.83 Proposed new comfort zone (dark blue) for a naturally and mechanically ventilated room

Furthermore, taking into account the observations earlier made on air speed, the new zone is not associated with a specific air speed. It is indeed too risky to have discomfort due to air movement when the air speed is in the range of 1 m/s. The new zone proposes temperature and humidity ranges providing thermal comfort assuming that the natural and mechanical ventilation design parameters of the building (openings and ceiling fans) are properly selected. Moreover, it is crucial for the air speed to be under the direct control of the affected occupant and adjustable in relatively low steps of approximately 0.2 m/s. The proposed zone is named NMV (Natural and Mechanical Ventilation).

7.5.13 Lessons Learned for Future Design of Net ZEBs in Tropical Climate

ENERPOS proves that a building can significantly reduce its energy consumption – approximately seven times less than a standard office building on Reunion Island – and thus its environmental impact, while maintaining an acceptable level of comfort for its users (Lenoir, Baird, and Garde, 2012).

The lessons learned from ENERPOS will be useful in the design of future Net ZEBs, especially in tropical climates. The particularly strong link between comfort and energy design was evident in the design of this building. Assumptions about comfort and user behavior had a very high influence on the energy used. Thermal comfort considerations dominated the energy design of the building and they also pointed out the need in further research on this important topic, as well as the need to develop simulation tools that integrate comfort and energy design of buildings in a more systematic way.

7.5.13.1 Interior Lighting

An improvement could be made on the interior lighting switches of the classrooms. Daylighting measurements showed that three parallel areas can be defined. The daylighting is very satisfactory (above 500 lux during the hours of occupancy) near the windows overlooking the exterior, lower (below 300 lux a few hours per day) in the middle, and even lower (below 300 lux several hours per day) on the side of the building overlooking the green patio toward the other building wing. The lights can be controlled with three different switches such that the darkest part of the room can be independently lit.

7.5.13.2 Elevator Energy

Data from the energy monitoring system showed that energy consumption of the elevator accounted for 13% of the overall energy use of the building (which represents 120 kWh/m²·yr). All the inside lights were constantly on. A standby mode was activated, reducing the elevator's energy used by half (reduction of 65 kWh/month).

7.5.13.3 Air-Conditioning

As the air-conditioning of the building is barely used (except for one split system cooling a technical room), its consumption is minimal. However, the VRF system and the ceiling terminal units represent 15% of the overall energy use of the building. In fact, it was discovered that the small display screens installed in the offices and computer rooms consume 7 W, with a monthly consumption of 20 kWh.

7.5.13.4 Occupant Behavior

The ultimate objective is to get active people in a passive building, instead of passive people in an active building. To do this, people need to be educated and adapt their behavior. Signs in the classrooms explain how to properly use the building by operating the louvers or turning on ceiling fans, switching off unnecessary lights, and using the stairs rather than the elevator. Signs also provide suggestions for reducing waste by printing both sides of paper, using reusable cups and glasses, sorting the garbage for recycling, etc.

7.5.13.5 Use of Building Thermal Mass and Night Cooling

The current building design does not use thermal mass to any significant extent to improve comfort. The diurnal temperature swing of 8 °C may enable a cooling of interior thermal mass by a few degrees if high ventilation rates (natural and possibly hybrid ventilation) can be maintained at night. The use of ventilated concrete slabs is another possibility to enhance night cooling of building mass but it will lead to higher fan energy consumption. If thermal mass is to be used to improve thermal comfort and reduce energy consumption, then some exterior insulation needs to be added to the walls.

7.6 Conclusions

In this chapter, four Net ZEB case studies were presented in detail, including their design details, the design process (including the designers and design tools), the measured performance, and finally, systematic assessments of potential improvements to the buildings based on new knowledge and technologies. The buildings represent four very different climates and a diversity of uses. They also demonstrate the differences in building standards and design processes for different building design cultures.

Some of the common conclusions that can be drawn from the case studies include the following:

– Successful Net ZEB design involves energy targets very early in the design process. The case studies are intentionally oriented and shaped to exploit passive design strategies including passive heating and cooling, natural ventilation, and daylighting. Furthermore, considerable effort was taken to ensure that there were adequately sized and oriented surfaces for solar energy collection. The buildings would not have performed nearly as well if the opportunity to exploit the local climate had not been incorporated early into design.

– All design processes involved numerous experts throughout, including both architects and engineers.

– All of the designers paid particular attention to the lighting, equipment, and plug loads. With near-optimal envelopes and HVAC systems, these loads represent both significant energy use and a substantial opportunity for energy savings. While plug loads might normally be neglected or downplayed, they are part of the energy balance for Net ZEB design.

– Most design processes used common BPS tools that were either commercial or government-developed. They were typically selected for a balance of ease of use and available features, sometimes at the cost of accuracy and integrated models.

– Since Net ZEBs tend to use new and custom technologies or design and operational strategies many of the design teams had difficulty in creating models in existing tools that were accurate representations of the buildings as a whole. This issue was addressed by using multiple tools and often creating simplified spreadsheet or customized tools.

– Parametric analysis and formal optimization were used for several of the buildings. One common technique was to examine the predicted performance of short sequences of representative days rather than full-year simulations.

– The design processes revealed that there is a need for at least two categories of design tools: simple tools that facilitate efficient exploratory design in the early design stages and integrated tools that have a greater number of technologies with accurate representations of physics (e.g., thermal mass or solar radiation distribution in rooms). Ideally, these tools are interoperable such that a common model can evolve when using a range of tools from simple to advanced. Because Net ZEBs tend to use advanced and/or custom technologies and other features, ease and flexibility to incorporate new models is important.

– All of the Net ZEB case studies demonstrated the importance of commissioning all buildings. In most cases, the buildings had minor operational issues that resulted in higher energy consumption than predicted. However, these were mostly very straightforward to resolve.

– The case studies demonstrated that monitoring performance using sensors and meters is very valuable for identifying and diagnosing unexpected performance. Ideally, electric circuits should be carefully designed such that categories of electrical loads and spaces can be distinguished. Further monitoring of renewable energy systems, including electrical power and thermal energy outputs, is important. If these systems are unique or customized, then it is particularly important to monitor the systems to ensure they are working as designed. Comparing measured performance to predicted performance, based on simulations, is an invaluable exercise for identifying opportunities for improving performance.

– The case studies demonstrated the value in educating occupants about the proper functioning of their building. They revealed that occupants often used the buildings in ways that were not intended – particularly related to temporary discomfort from passive systems. Most buildings had researchers or operators that used formal or informal educational techniques in order to inform occupants about proper operation (e.g., signs, discussions, and energy dashboards).

Acknowledgment

Notes

1. http://en.openei.org/datasets/dataset/nrel-rsf-measured-data-2011.

2. http://www.nrel.gov/sustainable_nrel/rsf.html.

3. http://www.nrel.gov/publications/.

4. http://en.openei.org/datasets/dataset/nrel-rsf-measured-data-2011.

5. Values estimated for Denver Airport using RETScreen™.

6. PERENE is the energy performance standard for buildings on Reunion Island.

References

American Society of Heating, Refrigerating and Air-Conditioning Engineers (ASHRAE) (2003) Thermal Environmental Conditions for Human Occupancy.

American Society of Heating, Refrigerating and Air-Conditioning Engineers (ASHRAE) (2009) Handbook of fundamentals, in *Ventilation and infiltration*, American Society of Heating, Refrigerating and Air-Conditioning Engineers, Inc., p. 36.

American Society of Heating, Refrigerating and Air-Conditioning Engineers (ASHRAE) (2010) Thermal environmental conditions for human occupancy (Atlanta).

Armstrong, M.M., Swinton, M.C., Ribberink, H., Beausoleil-Morrison, I., and Millette, J. (2009) Synthetically derived profiles for representing occupant-driven electric loads in Canadian housing. *Journal of Building Performance Simulation*, **2**, 15–30.

Athienitis, A.K. (2007) Design of a Solar Home with BIPV-Thermal System and Ground Source Heat Pump. Paper presented at: 2nd SBRN and SESCI 32nd Joint Conference (Calgary, AB).

Barakat, S.A. (1987) Inter-zone convective heat transfer in buildings: a review. *Journal of Solar Energy Engineering, Transactions of the ASME*, **109**, 71–78.

Beausoleil-Morrison, I. (2011) The design of an ESP-r and TRNSYS co-simulator. 12th Conference of International Building Performance Simulation Association (Sydney, Australia), pp. 2333–2340.

Beccali, G., Cellura, M., Brano, V.L., and Orioli, A. (2005a) Is the transfer function method reliable in a European building context? A theoretical analysis and a case study in the south of Italy. *Applied Thermal Engineering*, **25**, 341–357.

Beccali, G., Cellura, M., Brano, V.L., and Orioli, A. (2005b) Single thermal zone balance solved by transfer function method. *Energy and Buildings*, **37**, 1268–1277.

Beccali, G., Cellura, M., Lo Brano, V., and Orioli, A. (2003) An improved algorithm for thermal dynamic simulation of walls using Z-transform coefficients, in *Computational Engineering* (eds C.A. Brebbia, G.M. Carlomagno, and P. Anagnostopoulos), WIT Press, pp. 691–700.

Boyer, H., Chabriat, J.P., Grondin-Perez, B., Tourrand, C., and Brau, J. (1996) Thermal building simulation and computer generation of nodal models. *Building and Environment*, **31**, 207–214.

Bradley, D. and Kummert, M. (2005) New evolutions in TRNSYS – a selection of version 16 features. Paper presented at: IBPSA 2005 – International Building Performance Simulation Association 2005 (Montreal).

Braham, G.D. (2000) Mechanical ventilation and fabric thermal storage. *Indoor and Built Environment*, **9**, 102–110.

Canada Mortgage and Housing Corporation (CMHC) (2010) EQuilibrium™: Healthy Housing for a Healthy Environment.

Cellura, M., Campanella, L., Ciulla, G., Fontana, M., Lo Brano, V., Nardi Cesarini, D., and Spallacci, M. (2010a) The evaluation of the Energy performances of a Net Zero Energy Building: an Italian Case Study. Paper presented at: Eurosun 2010 International Conference on Solar Heating, Cooling and Buildings (Graz, 2010).

Cellura, M., Campanella, L., Ciulla, G., Guarino, F., Brano, V.L., Cesarini, D.N., and Orioli, A. (2011a) A net zero energy building in italy: Design studies to reach the net zero energy target. Paper presented at: Proceedings of Building Simulation 2011: 12th Conference of International Building Performance Simulation Association (Sydney, NSW).

Cellura, M., Campanella, L., Ciulla, G., Guarino, F., Lo Brano, V., Cesarini, D.N., and Orioli, A. (2011b) The redesign of an Italian building to reach net zero energy performances: A case study of the SHC Task 40 - ECBCS Annex 52. Paper presented at: ASHRAE Transactions (Montreal, QC).

Cellura, M., Lo Brano, V., Mistretta, M., and Orioli, A. (2010b) To assess the validity of the transfer function method: A neural model for the optimal choice of conduction transfer functions. Paper presented at: ASHRAE Transactions (Albuquerque, NM).

Chen, Y., Athienitis, A.K., and Galal, K. (2010a) Modeling, design and thermal performance of a BIPV/T system thermally coupled with a ventilated concrete slab in a low energy solar house: Part 1, BIPV/T system and house energy concept. *Solar Energy*, **84**, 1892–1907.

Chen, Y., Athienitis, A.K., and Galal, K. (2012) Thermal performance and charge control strategy of a ventilated concrete slab (VCS) with active cooling using outdoor air. *ASHRAE Transactions*, **118**, 556–568.

Chen, Y., Galal, K., and Athienitis, A.K. (2010b) Modeling, design and thermal performance of a BIPV/T system thermally coupled with a ventilated concrete slab in a low energy solar house: Part 2, ventilated concrete slab. *Solar Energy*, **84**, 1908–1919.

Chetty, M., Tran, D., and Grinter, R. (2008) Getting to green: understanding resource consumption in the home. Paper presented at: Proceedings of the 10th international conference on Ubiquitous computing (Seoul, Korea: ACM).

Department of Energy (DOE) (2009) Getting started with EnergyPlus (Department of Energy).

Department of Energy (DOE) (2013) EnergyPlus Engineering Reference.

Doiron, M., O'Brien, W., and Athienitis, A.K. (2011) Energy performance, comfort and lessons learned from a near Net-Zero energy solar house. *ASHRAE Transactions*, **117**, 1–13.

Doiron, M.A. (2011) Whole-building energy analysis and lessons learned for a near Net-Zero energy solar house, in *Building, Civil, and Environmental Engineering*, Concordia University, Montreal, QC, p. 139.

EN (2005) Analytical determination and interpretation of thermal comfort using calculation of the PMV and PPD indices and local thermal.

Fairey, P.W. (1981) Passive Cooling and Human Comfort (Florida Solar Energy Center).

Garde, F., Bastide, A., Bentaleb, D., and Ottenwelter, E. (2006) The construction of a Zero Energy Building in Reunion Island. Presentation of a new approach to the design studies. Paper presented at: International Mechanical Engineering Congress and Exposition, ASME (Chicago, Illinois, USA).

Garde, F., Bastide, A., Wurtz, E., Thellier, F., Achard, G., Dobre, O., Ottenwelter, E., and Bornarel, A. (2007) ENERPOS: A French Research Program for Developing New Methods for the Design of Zero Energy Buildings in Hot Climates. Paper presented at: CESB Conference (Prague, Czech Republic).

Garde, F., David, M., Adelard, L., and Ottenwelter, E. (2005) Elaboration of Thermal Standard for French Tropical Islands: Presentation of the PERENE Project. Paper presented at: REHVA World Congress CLIMA.

Garde, F., Lenoir, A., David, M., and Ottenwelter, E. (2011) Towards net zero energy buildings in hot climates. Part I: new tools and methods. *ASHRAE Transactions*, **117** (Part 1), 1–8 (Paper No. LV-11-C055).

Givoni, B. (1976) *Man, Climate and Architecture*, Applied Science Publishers Ltd.

Givoni, B. (1998) *Climate Considerations in Building and Urban Design*, John Wiley & Sons, USA.

Gram-Hanssen, K. (2010) Residential heat comfort practices: understanding users. *Building Research & Information*, **38**, 175–186.

Guglielmetti, R., Pless, S., and Torcellini, P. (2010) On the use of integrated daylighting and energy simulations to drive the design of a large net-zero energy office building, in *Proceedings of the Fourth National Conference of IBPSA-USA: SimBuild 2010*, New York, pp. 301–309.

Hirsch, A., Okada, D., Pless, S., and Antia, P. (2011) The role of modeling when designing for absolute energy use intensity requirements in a design-build framework. Paper presented at: ASHRAE winter conference (Las Vegas, US).

Hootman, T. (2012) *Net Zero Energy Design: A Guide for Commercial Architecture*, Wiley.

Hwang, R.-L., Lin, T.-P., and Kuo, N.-J. (2006) Field experiments on thermal comfort in campus classrooms in Taiwan. *Energy and Buildings*, **38**, 53–62.

Kwok, A.G. and Chun, C. (2003) Thermal comfort in Japanese schools. *Solar Energy*, **74**, 245–252.

Lenoir, A. (2013) On comfort in tropical climates. The design and operation of Net Zero energy buildings, in *PIMENT*, University of Reunion Island., Reunion Island, France.

Lenoir, A., Baird, G., and Garde, F. (2012) Post-occupancy evaluation and experimental feedback of a net zero-energy building in a tropical climate. *Architectural Science Review*, **55**(3), 156–168.

Lenoir, A., Garde, F., and David, M. (2011) Towards Net Zero energy buildings in hot climates. Part II: experimental feedback. *ASHRAE Transactions*, **117** (Part 1), 1–8 (Paper No. LV-11-C056).

Natural Resources Canada (NRCan) (2008) *Energy use Data Handbook Tables*, Office of Energy Efficiency (OEE), Canada, ed.

Natural Resources Canada (NRCan) (2010) HOT2000 (Ottawa, Canada).

NREL (2013) NREL RSF Measured Data 2011.

O'Brien, W., Athienitis, A.K., and Kesik, T. (2009) The development of solar house design tool. Paper presented at: 11th International Building Performance Simulation Association (IBPSA) Conference (Glasgow, Scotland, July 27–30, 2009.).

Paulson, B.C. (1976) Designing to reduce construction costs. *Journal of the Construction Division*, **102**, 587–592.

Peng, Q. (2009) *Modeling and Daylighting Design of a New Window with Integrated Controllable Louver System*, Concordia University, Canada, p. 197.

Perez, R., Ineichen, P., Seals, R., Michalsky, J., and Stewart, R. (1990) Modeling daylight availability and irradiance components from direct and global irradiance. *Solar Energy*, **44**, 271–289.

Pogharian, S., Ayoub, J., Candanedo, J.A., and Athienitis, A.K. (2008) Getting to a net zero energy lifestyle in Canada: the Alstonvale net zero energy house. Paper presented at: 3rd European PV Solar Energy Conference (Valencia, Spain).

RETScreen International (2005) Clean Energy Project Analysis (Ministry of Natural Resources Canada).

Salom, J., Widén, J., Candanedo, J.A., Sartori, I., Voss, K., and Marszal, A. (2011) Understanding Net Zero Energy Buildings: Evaluation of Load Matching and Grid Interaction Indicators. 12th International Building Simulation Conference (IBPSA 2011) (Sydney, Australia).

Sartori, I., Napolitano, A., and Voss, K. (2012) Net zero energy buildings: a consistent definition framework. *Energy and Buildings*, **48**, 220–232.

Shaviv, E., Yezioro, A., and Capeluto, I.G. (2001) Thermal mass and night ventilation as passive cooling design strategy. *Renewable Energy*, **24**, 445–452.

Torcellini, P., Pless, S., Lobato, C., and Hootman, T. (2010) Main street net-zero energy buildings: The zero energy method in concept and practice. Paper presented at: ASME 2010 4th International Conference (Phoenix, US).

Torcellini, P.A. and Crawley, D.B. (2006) Understanding zero-energy buildings. *ASHRAE Journal*, **48**, 62–64, 66–69.

TRNSYS (2012) Transient System Simulation Tool.

Tzempelikos, A., Athienitis, A.K., and Karava, P. (2007) Simulation of façade and envelope design options for a new institutional building. *Solar Energy*, **81**, 1088–1103.

Voss, K. and Riley, M. (2009) IEA Joint Project: Towards Net Zero Energy Solar Buildings (NZEBs), pp. 15.

Voss, K., Sartori, I., Napolitano, A., Geier, S., Gonçalves, H., Hall, M., Heiselberg, P., Widén, J., Candanedo, J.A., Musall, E. *et al.* (2010) Load Matching and Grid Interaction of Net Zero Energy Buildings. Paper presented at: EUROSUN 2010 (Graz, Austria).

8
Conclusion, Research Needs, and Future Directions

Andreas Athienitis and William O'Brien

8.1 Net ZEB Modeling, Design, and Simulation

This book has presented the state-of-the-art in terms of modeling, simulation, and design of net-zero energy buildings (Net ZEBs), including a combination of modeling fundamentals and theory, a review of selected technologies, and four in-depth case studies of actual near-net-zero to positive energy buildings in four different climatic regions covering both the residential and commercial/institutional sectors. These case studies have clearly identified that the pathways to reach the net-zero energy target are numerous and diverse, but should be carefully customized for the particular building type, its intended function and operation, and climate. The key to achieving the net-zero energy goal is that it necessarily places energy at the forefront of the design process, along with traditional considerations, such as architectural form, function, and cost, but with comfort at least equally important. Another benefit to the net-zero energy objective (or any absolute performance objective) is that it places greater emphasis on ensuring that the building is performing as expected after occupancy. The case studies demonstrated the importance of having the designers involved in the commissioning and operation during the first months or years of occupancy because many features require some fine tuning and occupants may require some education on the building's proper functions. They also demonstrated the close link between energy performance, comfort, and building operation – both passive and active.

As pointed out in this book, the *efficient* design of net-zero energy buildings (and energy positive ones) requires application of the

following three key concepts:

1. An integrated approach to energy efficiency, passive design, optimization of form, and renewables integration;

2. An integrated approach to building design and operation; optimized net-zero energy buildings need to be designed based on anticipated and realistic operation so as to have a largely predictable and manageable impact on the grid. Smart buildings optimally linked with smart grids will enable a reduction in the need to build new power plants; and,

3. The concept of solar optimization requires optimal design of building form and orientation so as to enable the maximum capture of solar energy from near-equatorial facing facades and roofs for conversion to solar electricity, useful heat, and daylight.

This book has revealed the importance of choosing the right approach and model resolution at different stages of the design. It also identified important gaps in building simulation and design tools as well as methodologies. Some key gaps in building simulation software and design methodologies are listed here:

1. Modeling of building-integrated solar technologies at different stages of the design. For example building-integrated photovoltaic/thermal (BIPV/T) systems and semitransparent PV windows are energy-generating elements that also have a thermal function and possibly a daylighting function. Their proper design requires simultaneous consideration of impact on cooling loads, heating loads, comfort and envelope performance, and durability.

2. Systematic analysis of design options is needed in the early stages of the design when the geometry of the building is not fully fixed. Choice of thermal mass strategies has an important impact on structural design and, accordingly, they need to be assessed in early-stage design tools.

3. Integrated thermal, daylighting, and natural/hybrid ventilation simulation and design of buildings.

4. More accurate prediction of comfort – thermal, visual, and acoustic – at different stages of the design in an integrated

manner with energy simulations. Comfort can be much subtler and complex than merely using indoor air temperature as a metric. Certain common Net ZEB strategies (e.g., open spaces and hard surfaces) can compromise comfort if care is not taken during design. Therefore, detailed models with a comprehensive reporting of occupant comfort conditions (e.g., based on ASHRAE Standard 55) is essential.

5. Integrated study of smart building operating strategies with energy design and comfort studies. As building design and operating strategies become more advanced, demonstration projects and case studies are necessary because such buildings should be tested in the field to evaluate effectiveness with real climate and occupancy.

8.2 Future Directions and Research Needs

Recently, we have seen significant technological developments in key technologies, such as photovoltaics, together with dramatic cost reductions that make it more cost effective to achieve net-zero energy. However, the integration of PV and other technologies, such as heat pumps, with buildings and with other technologies still has a long way to go before similar cost reductions at a system level can be achieved.

The integration of new technologies will lead to the development of new multifunctional building products, such as prefabricated BIPV/T walls and roofs, semitransparent PV windows, windows with integrated automatically controlled shading and daylighting devices, advanced building-integrated thermal storage systems, solar cooling systems integrating PV and heat pumps, and smart building operating strategies.

Human factors in the operation of Net ZEBs are seen as increasingly important as evidenced from the four case studies. Operating strategies need to be designed that take into account the possible scenarios due to human behavior and its impact on comfort and energy performance. The three main approaches to mitigating the uncertainty of occupants are as follows:

1. Carefully selecting building materials and geometry (i.e., passive techniques) that decrease the frequency of discomfort.

2. Smart controls for providing comfort with the possibility of learning controls that learn from occupant preferences and adapt accordingly (e.g., controllers that learn occupant preferences, habits, and schedules).

3. Building performance dashboards and other behavior-shaping design features or strategies. Research has shown that informing occupants of their building's energy performance can have a significant impact on their behavior. For the case of net-zero energy buildings, there is a defined performance target. Occupants should be informed of real-time and annual building performance so they can verify that the target is being achieved.

For Net ZEBs to become widespread the next step is to consider optimal design configurations for clusters of buildings and neighborhoods while considering interaction with electricity grids/microgrids. While net-zero energy buildings place considerable emphasis on individual buildings, we cannot lose sight of the bigger picture. Grid-tied Net ZEBs still have considerable upstream impacts on the environment and energy-supply infrastructure because of their diurnal and/or seasonal dependence on a centralized energy supply. Future research and development must recognize the complex interactions between individual buildings, the community, and the larger scale (e.g., urban and grid-wide).

Through integration, the net-zero energy goal can be achieved at the community level, while allowing significant design flexibility at the individual building level. Different pathways for achieving net-zero energy balance at the community level need to be studied, including solar optimization of building form, density, mix of solar and energy efficiency technologies (e.g., BIPV/T and heat pumps, thermal storage, possibly some district heating). One possible scenario suggests that buildings can be integrated into traditional street patterns while ensuring that one or more large planar surfaces are optimally oriented to capture solar energy. There is also the possibility of integration with seasonal heat storage and district heating systems for cold climates. The optimal mix of technologies, their integrated design, and operation will depend on climatic

conditions and the local conditions, including cost and incentives. Plug-in hybrid and electric vehicles can be integrated into the community energy concept, serving as electrical storage and load management devices, but also providing backup power to the houses during emergency situations such as earthquakes.

In closing, this book has demonstrated that Net ZEBs are a viable design objective for most climates through four detailed, high-quality case studies. Modeling and design issues for the most common and appropriate technologies, systems, and strategies for Net ZEBs were outlined. It is clear from this research and demonstration projects that attention to detail from early-stage design to operation and use of appropriate modeling and simulation tools is essential.

Glossary

a-Si	amorphous silicon
ABC	absorbing, blocking, and covering noise
AC	air-conditioning
ACD	active charge and discharge
ACH	air changes per hour
AEC	architecture, engineering, and construction
AHU	air handling unit
ALD	ASHRAE Likelihood of Dissatisfied
ANR	Agence nationale de la recherche (French National Research Agency)
AR	autoregressive
ARMAX	autoregressive moving-average model with exogenous input
ARX	autoregressive model with exogenous input
ASHRAE	American Society of Heating, Refrigerating and Air Conditioning Engineers
BAPV	building-added photovoltaics
BAS	building automated system
BCVTB	building control virtual test bed
BIM	building information modeling
BIPV	building-integrated photovoltaic
BIPV/T	building-integrated photovoltaic with thermal energy recovery
BITES	building-integrated thermal energy storage
BMS	building management system
BPO	building performance optimization
BPS	building performance simulation
CAD	computer-aided drawing
CaGBC	Canada Green Building Council
CFD	computational fluid dynamics

CHP	combined heat and power generation
CIBSE	Chartered Institution of Building Services Engineers
CLTD	cooling load temperature differential
CM@R	construction management at-risk
CMHC	Canada Mortgage and Housing Corporation
CO$_2$	carbon dioxide
COP	coefficient of performance
CPD	cycles per day
CTF	conduction transfer functions
CTF/QTF	conduction transfer functions with heat source transfer functions
DA	daylight autonomy
DA$_{cont}$	continuous daylight autonomy
DB	design-build
dB	decibels
DCV	demand-controlled ventilation
DE	differential evolution
DF	daylight factor: ratio of the amount of light received in the indoor space from outside to the outdoor illuminance on a horizontal plane
DFT	discrete Fourier transform
DGP	daylight glare probability
DH	district heating
DHW	domestic hot water
Discharge coefficient	a characteristic of openings that takes both the contraction and the friction loss into account. This parameter is required in the calculation of the air flow going through an opening
DLCC	difference in life cycle cost
DOE	design of experiments or Department of Energy (US)
DSO	distribution system operator

EA	evolutionary algorithm
EBC	Energy in Buildings and Communities, group within the IEA
EC	ejector cooling
EH	electrical heating (with electrical radiator)
ELA	equivalent leakage area
ENERPOS	French for ÉNERgie POSitive
EPBD	Energy Performance of Buildings Directive, EU regulation
EPBD-r	European Energy Performance of Buildings Directive recast
ERGEG	European Regulators Group for Electricity and Gas
ERV	energy recovery ventilation
ERVS	energy recovery ventilation system
ESM	energy saving measures
ET	effective temperature
ETFE	ethylene tetrafluoroethylene
EV	electric vehicle
EVA	ethylene vinyl acetate
FR	frequency response
GA	genetic algorithm
gbXML	green building extensible mark-up language
GHG	greenhouse gas
GHP	geothermal heat pump
GP	genetic programming
GSHP	ground source heat pump
GUI	graphical user interface
HB	heat balance method
HDR	high dynamic range
HIT	silicon heterostructures

HJ	Hooke–Jeeves search
HRF	heat removal fluid
HRV	heat recovery ventilation
HVAC	heating, ventilation, and air-conditioning
HX	heat exchanger
IAQ	indoor air quality
IC	initial cost
IDFT	inverse discrete Fourier transform
IDP	integrated design process: design process that consists of involving all project stakeholders at all stages of the design to collaborate in the decision-making process
IEA	International Energy Agency
IEA SHC	International Energy Agency, Solar Heating and Cooling Programme
IEQ	indoor environment quality
IES	Illuminating Engineering Society
IFC	industry foundation classes
ISO	International Organization for Standardization
IT	information technology
JMSB	John Molson School of Business, Concordia University
LBNL	Lawrence Berkeley National Laboratory
LCC	life cycle cost
LD	liquid desiccant
LEED	Leadership in Energy and Environmental Design
LLF	light loss factor
LMGI	load matching and grid interaction
LoI	lines of influence
low-Fe	low iron
LPD	long-term percentage of dissatisfied
LT	Laplace transform

LTI	linear-time invariant
MDF	mean daylight factor: average daylight factor value of a grid of sensors located across the room at workplane height
MIMO	multiple-input, multiple-output
MISO	multiple-input, single-output
MMCF	mismatch compensation factor
MPC	model predictive control
NaOR	Nicol *et al*.'s Overheating Risk
NC	noise criterion
Net ZEB	net-zero energy building
NMV	natural and mechanical ventilation
NRC	noise reduction coefficient
NRCan	Natural Resources Canada
NREL	National Renewable Energy Laboratory
NSERC	National Sciences and Engineering Research Council of Canada
NSGA-II	Non-dominated Sorting Genetic Algorithm-II
NTU	number of transfer units
OB	oil boiler with water radiators
ODE	ordinary differential equations
OECD	Organization for Economic Co-operation and Development
OVA	open cycle vapor absorption
PCM	phase-change material
PEC	primary energy consumption
PERENE	Performance Énergétique des Bâtiments à la Réunion
PHEV	plug-in hybrid electric vehicle
PHPP	Passive House Planning Package
PID	proportional integral derivative
PMV	predicted mean vote: index predicting the mean

	response of a large group of people with regards to thermal comfort (+3 = hot, +2 = warm, +1 = slightly warm, 0 = neutral, −1 = slightly cool, −2 = cool, −3 = cold)
PPD	predicted percentage of dissatisfied
PR_GA	two-step optimization approach
PSO	particle swarm optimization
PV	photovoltaic
PV/T	photovoltaic/thermal
PVB	polyvinyl butyral
PVDF	polyvinylidene fluoride
PVF	polyvinyl fluoride
PW	present worth
QTF	heat source transfer functions
R&D	research and development
RBPC	rule-based predictive control
RC	replacement cost
RES	renewable energy storage/system
RET	renewable energy technology
RSF	Research Support Facility
RSI	R-value, SI units
RTS	radiant time series
SA	sensitivity analysis
SBS	sick building syndrome
SD	solid desiccant
SDD	solar design day
SDHW	solar domestic hot water heating systems
SHC	Solar Heating and Cooling Programme, group within the IEA
SHGC	solar heat gain coefficient
SI	system identification

SISO	single-input, single-output
SPOT	sensor placement and optimization tool
SQL	structured query language
STB	subtask B, part of IEA SHC Task 40
STC	sound transmission class
STPV	semitransparent photovoltaic
STPV/T	semitransparent photovoltaic/thermal
SysID	system identification
TABS	thermoactive building systems or thermally active building systems
TEAM	Technology Early Action Measures
TES	thermal energy storage
TFM	transfer function method
TMY	typical meteorological year
TOU	time-of-use
UDI	useful daylight illuminance
UPS	uninterruptible power supply
US EPA	US Environmental Protection Agency
UTC	unglazed transpired collectors
V2H	vehicle-to-home
VC	vapor compression (Chapter 2) or Vision Control® (Chapter 7)
VCS	ventilated concrete slab
VOC	volatile organic compound
VRF	variable refrigerant flow
VRV	variable refrigerant volume
WWR	window-to-wall area ratio
ZT	z-transfer

Index

A

C

D

distribution system operators (DSOs)

domestic hot water (DHW)

dynamic daylight simulation

dynamic thermal behavior

dynamic window shading devices

E

F

H

hypocaustum

I

International Energy Agency Solar Heating and Cooling Program
(IEA SHC) Task 40

International Solar Energy Society (ISES)

interoperability between multiple tools

inverse discrete Fourier transform (IDFT)

J

JMSB BIPV/T system

L

Laplace transform

latent/sensible heat

M

N

numerical stability

T

WILEY END USER LICENSE AGREEMENT

Go to www.wiley.com/go/eula to access Wiley's ebook EULA.